UNIVERSIDAD DE LEÓN

DEPARTAMENTO DE QUÍMICA Y FÍSICA APLICADAS

CALIDAD DEL AIRE EN LEÓN: FUENTES Y DEPOSICIÓN HÚMEDA DE CONTAMINANTES BIOGÉNICOS Y NO BIOGÉNICOS

AIR QUALITY IN LEÓN: SOURCES AND WET DEPOSITION OF BIOGENIC AND NON-BIOGENIC POLLUTANTS

Fernanda Isabel Oduber Pérez

Doctorado en Ciencia y Tecnología del Medio Ambiente

León, 2020

universidad de león

esDule
Escuela de Doctorado de la Universidad de León

INFORME DEL TUTOR

El Dr. D. Roberto Fraile Laiz como Tutor de la Tesis Doctoral titulada “Calidad del aire en León: fuentes y deposición húmeda de contaminantes biogénicos y no biogénicos” realizada por Dña. Fernanda Isabel Oduber Pérez en el programa de doctorado Ciencia y Tecnología del Medio Ambiente, regulado por el R.D. 99/2011, de 28 de enero, informa favorablemente el depósito de la misma, dado que reúne las condiciones necesarias para su defensa.

Lo que firmo, en León a 14 de abril de 2020

FRAILE LAIZ, ROBERTO (FIRMA)

Firmado digitalmente por FRAILE LAIZ, ROBERTO (FIRMA)
Fecha: 2020.04.14 11:09:22 +02'00'

AGRADECIMIENTOS

La culminación de este trabajo representa el fin de una etapa muy importante de mi vida. Alcanzar los objetivos planteados durante todos estos años no hubiese sido posible sin la ayuda y el apoyo de todas esas personas que de una u otra forma estuvieron a mi lado.

En primer lugar, quiero agradecer a los directores de mi tesis, la Dra. Dña. Amaya Castro, la Dra. Dña. Ana Calvo y el Dr. D. Roberto Fraile, por la oportunidad brindada, por los conocimientos transmitidos, por la confianza depositada y las múltiples horas que dedicaron a mi trabajo. Debo agradecerles el que más que los directores de mi tesis, se hayan convertido en un apoyo muy importante tanto a nivel profesional como a nivel personal.

Al Ministerio de Economía, Industria y Competitividad por la subvención económica BES-2015-074473 sin la que no habría sido posible el desarrollo de esta tesis doctoral. A la Universidad de León por permitirme ser parte del Doctorado de Ciencia y Tecnología del Medio Ambiente.

A todos los miembros del Departamento de Química y Física Aplicadas, de la Universidad de León, por el recibimiento y el apoyo brindado durante todos estos años. A Carlos, por acompañarme y ayudarme durante toda la campaña de muestreo y durante los 4 años de trabajo juntos. A Ely por sus palabras de aliento y su disposición siempre a aclararme las dudas que surgían durante la investigación. Al grupo de Botánica del Departamento de Biodiversidad y Gestión Ambiental de la Universidad de León, en especial a Delia, Rosa, Ana y Alberto, por el tiempo dedicado, la colaboración y la paciencia para explicarme el mundo del polen.

A todo el personal de la Universidad de Aveiro, en especial a Célia, Ana Vicente, Estela y la Prof. Teresa, por su paciencia durante todos los meses de estancia, por su cariñosa acogida y por todos los buenos momentos compartidos. A todo el personal del CESAM, en especial a Joana y a Diana por toda la ayuda prestada.

A todos los expertos en las diferentes disciplinas que aportaron sus conocimientos para que los artículos salieran adelante. Al Prof. Mario Cerqueira de la Universidad de Aveiro (Portugal), a Silvia Nava, Franco Lucarelli y Giulia Calzolai del INF (Florenica, Italia), a Mar Sorribas del INTA (Huelva, España), Veronique Pont del CNRS (Toulouse, Francia), Paulo Fialho del IVAR (Ponta Delgada, Portugal), Esther Coz del CIEMAT (Madrid, España). Al personal de la Universidad de Alcalá por brindarnos la posibilidad de emplear la instrumentación.

A mis padres, que siempre han confiado en mí. Gracias por ir a mi lado en la distancia durante todo este proyecto en el que decidí embarcarme hace tantos años, dándome el ánimo que a veces necesito para continuar, por tantos años de sacrificio para que mis hermanos y yo seamos lo que somos hoy en día. A mis hermanos, porque a pesar de la distancia siempre están conmigo y seguimos celebrando todos nuestros logros juntos. A Rafael, simplemente gracias por la fuerza que me das, por estar a mi lado y por embarcarte conmigo en esta aventura personal y profesional.

A mi familia

ÍNDICE

Se habla de *contaminación atmosférica* para referirse a la presencia en la atmósfera de sustancias provenientes de actividades humanas o de procesos naturales, que tienen un impacto negativo sobre el ser humano y el medio ambiente. Los principales contaminantes atmosféricos son el monóxido de carbono (CO), los óxidos de nitrógeno (NO_x), el dióxido de azufre (SO_2), el ozono (O_3) y el aerosol o material particulado (PM). El término *aerosol atmosférico* se aplica a la suspensión de partículas líquidas y/o sólidas en el aire, que tienen un tamaño típico que va desde unos pocos nanómetros a unos cientos de micras, e incluyen al material biogénico y no biogénico. La composición química del aerosol está determinada principalmente por la fuente que lo emite. Sin embargo, la concentración, composición y distribución de tamaños de las partículas atmosféricas también puede variar temporal y espacialmente, ya que están sometidas a procesos de transporte, transformación y eliminación. Tras su formación o emisión, los aerosoles pueden evolucionar hasta ser eliminados de la atmósfera por deposición seca (sin intervención del agua) o por deposición húmeda (en presencia de hidrometeoros atmosféricos).

Debido a los efectos adversos generados por los contaminantes atmosféricos en la salud humana y en el medio ambiente, se hace cada vez más necesario estudiar la compleja interacción entre el clima y la calidad del aire. El estudio de las fuentes, concentraciones, tendencias, procesos de formación y de eliminación, riesgos en la salud e impacto ambiental de los contaminantes atmosféricos, es una herramienta importante que permite establecer nuevos métodos de monitorización de la contaminación del aire, así como examinar las políticas necesarias para reducir la contaminación. En esta línea, esta tesis aborda una serie de temas relacionados con el estudio de la contaminación atmosférica en León, España, como: *i*) la evolución temporal de los contaminantes atmosféricos y las correlaciones existentes entre la concentración de polen, con los principales contaminantes atmosféricos y ciertos parámetros meteorológicos; *ii*) la contribución de las principales fuentes de emisión de partículas biogénicas (a través del estudio de azúcares) y no biogénicas (mediante la caracterización química del PM_{10}) en León.; *iii*) el impacto de dos casos particulares de contaminación, uno de origen natural (intrusiones de polvo sahariano en invierno) y otro de origen antrópico (tráfico durante la transición verano-otoño) en la calidad del aire y *iv*) la influencia de la composición química de los aerosoles y de las características físicas de la precipitación en el proceso de lavado de diferentes especies químicas, tanto a escala anual como en episodios de corta duración (incendios forestales e intrusión de polvo sahariano).

Esta memoria está dividida en diez Capítulos: los dos primeros presentan una breve introducción teórica y una descripción detallada de la metodología utilizada a lo largo de este estudio. En los **Capítulos 3** al **9** se desarrollan los resultados obtenidos y, finalmente, en el **Capítulo 10** se establecen las conclusiones principales extraídas de esta investigación, así como las aplicaciones y perspectivas futuras.

En el **Capítulo 3** se analiza cómo ha evolucionado la concentración de los contaminantes ambientales gaseosos, CO, SO_2, NO_x y O_3, del PM_{10} y de tres tipos de pólenes, *Fraxinus*, Poaceae y *Populus*, desde 1997 hasta 2016 en la ciudad de León (España). Los resultados principales muestran que hay una tendencia decreciente en la concentración de los contaminantes

atmosféricos estudiados, así como una tendencia creciente en la concentración de *Fraxinus*. Además, se ha observado que el índice polínico estacional (SPIn) del *Fraxinus* está correlacionado negativa y significativamente con los contaminantes atmosféricos, mientras que, el SPIn del tipo polínico Poaceae mostró una correlación significativa con la precipitación antes y durante el período de floración. Por otra parte, la estación polínica principal (MPS) del *Fraxinus* está correlacionada positiva y significativamente con la temperatura, la humedad relativa y la precipitación durante el período de floración. La MPS del Poaceae está correlacionada positivamente con la temperatura mínima durante el período de floración, mientras que la MPS del *Populus* muestra una correlación negativa con dicha temperatura. Los resultados demuestran que los períodos de floración y polinización de los tipos de polen estudiados, dependen en gran medida de las condiciones meteorológicas anteriores a esos períodos y están influenciados por las concentraciones de los contaminantes atmosféricos.

En el **Capítulo 4** se presentan los resultados correspondientes a la caracterización química de los aerosoles muestreados en una zona suburbana de la ciudad de León (España), durante la campaña que se llevó a cabo entre el 9 de marzo de 2016 y el 14 de marzo de 2017. La concentración media anual de PM_{10} en la ciudad de León fue de 23 ± 8 μg m^{-3}, con un valor mínimo de 4 μg m^{-3} y un valor máximo de 59 μg m^{-3}. La fracción carbonosa representa la fracción másica mayoritaria con un 21 ± 7% del PM_{10}. Por otra parte, la caracterización química del PM_{10} permitió determinar las fuentes principales del aerosol en León, a través de la aplicación del modelo de *Factorización de Matriz Positiva* (PMF). En total se observaron seis fuentes principales de aerosoles: el tráfico (29% del PM_{10}), la sal marina envejecida (26% del PM_{10}), los aerosoles secundarios (16% del PM_{10}), el aerosol mineral (13% del PM_{10}), el aerosol marino (7% del PM_{10}) y la quema de biomasa (3% del PM_{10}). Utilizando los resultados obtenidos con el PMF y los parámetros de los tipos de tiempo asociados al flujo geostrófico (SF, WF, ZS y ZW), se construyeron modelos de regresión lineal que permitieron determinar la contribución de cada factor al PM_{10}. El factor marino mostró una dependencia positiva con WF, demostrando que las masas de aire occidentales son responsables del transporte de sales marinas desde el Océano Atlántico hasta León. Los factores de aerosoles secundarios y de tráfico mostraron coeficientes positivos para SF, debido a la contribución de las emisiones antropogénicas del centro de la ciudad y de otras ciudades situadas al sur de León. En el caso de la sal marina envejecida, el coeficiente ZS negativo confirmó que este factor se ve favorecido principalmente por las situaciones anticiclónicas. Los coeficientes de SF negativo y de ZS positivo del factor mineral sugieren que las emisiones de la fábrica de cemento de La Robla, ubicada al norte de la ciudad de León, son una importante fuente de aerosol mineral. El factor de combustión de biomasa no mostró ninguna relación con el flujo geostrófico, probablemente porque se trata de una fuente más local.

El estudio de las fuentes de emisión de bioaerosoles en León se aborda en el **Capítulo 5**, a través del contenido de 17 azúcares presentes en el PM_{10} (arabinosa, fructosa, galactosa, glucosa, ribosa, sucrosa, xilosa, adonitol, arabitol, 2-metileriritol, mio-inositol, manitol, sorbitol, xilitol, galactosano, levoglucosano and manosano), así como de la concentración de los marcadores biológicos (polen y la espora de hongo *Alternaria*), de la composición química de los aerosoles y de las condiciones meteorológicas. Los resultados mostraron que, en primavera, cuando se producen altos niveles de actividad metabólica de las plantas y aumentan las temperaturas, la glucosa, la sacarosa, el 2-metil-eritritol, el manitol, el arabitol y el inositol, están significativamente correlacionados con la concentración de polen en el aire. Entre la primavera y el otoño, las

concentraciones de *Alternaria* en el aire están significativamente correlacionadas con las temperaturas, las concentraciones de arabitol y sorbitol + adonitol. Además, durante los días de lluvia, la *Alternaria* también está correlacionada con el manitol. En otoño, las temperaturas más bajas provocan un aumento de las concentraciones de levoglucosano, manosano y galactosano, probablemente debido al incremento en el uso de aparatos de calefacción doméstica. Estos anhídridos azúcares y la arabinosa, la fructosa y la glucosa, están significativamente correlacionados con el K, NO_3^-, OC, EC, Cu, Zn, Se, Pb, V y el Ni, mientras que el manosano también se correlaciona con As, lo que demuestra que estos anhídridos sacáridos pueden ser emitidos desde diferentes fuentes antropogénicas. La precipitación puede provocar un aumento de la concentración de glucosa y sacarosa, debido a que la rotura de las partículas de polen hidratado libera los azúcares unidos a los fragmentos más pequeños. Además, la precipitación también puede causar un incremento de la concentración de arabitol (trazador de esporas fúngicas aerotransportadas).

En el **Capítulo 6** se analiza la variación temporal de la distribución del tamaño de los aerosoles en una zona urbana de León, entre agosto y octubre de 2012, con el fin de identificar los cambios asociados a la transición del verano al otoño. Se observó que, a medida que avanza el verano, la concentración total de partículas aumenta de 1000 ± 600 partículas cm^{-3} en agosto a 1500 ± 1000 partículas cm^{-3} en octubre, debido principalmente a un aumento en el flujo del tráfico después de las vacaciones de verano y al comienzo del nuevo año académico, en septiembre. La concentración de partículas fue mayor entre semana que durante los fines de semana en los meses de septiembre y octubre. Sin embargo, en agosto no se observó una variación apreciable en la concentración de partículas, debida a la menor actividad en la ciudad, causada por el descanso vacacional. Se registró una distribución bimodal de los tamaños de los aerosoles, con la mayor concentración de partículas y el menor diámetro medio en la moda fina durante el mes de octubre. Los valores más altos de la fracción respirable estimada en adultos sanos, se obtienen en los días laborables entre las 0600 y 1000 UTC (alrededor de 15 $\mu g\ m^{-3}$) y por la tarde, entre las 1700 y 2000 UTC (alrededor de 12 $\mu g\ m^{-3}$), coincidiendo con las horas punta.

Corresponde al **Capítulo 7** el estudio descriptivo de dos eventos de intrusión de polvo sahariano que afectaron a la calidad del aire en León, en el mes de febrero de 2016 y de 2017. Durante el invierno, las intrusiones de polvo sahariano no son muy frecuentes y cuando ocurren, no suelen llegar al noroeste de la Península. El estudio se llevó a cabo con un enfoque integrador que comprende: *i*) las condiciones sinópticas típicas; *ii*) la composición química de los aerosoles; *iii*) la distribución del tamaño de las partículas; *iv*) la concentración del polen; *v*) el espesor óptico de los aerosoles (AOD); *vi*) el forzamiento radiativo, y *vii*) la estimación del impacto de los aerosoles en el tracto respiratorio. En la caracterización global de estos eventos de intrusión de polvo, se observó: la superación del valor límite diario de PM_{10}, un aumento de las partículas en la moda gruesa y un incremento de la concentración de hierro. En el evento de 2016, se registró un valor del AOD y del exponente de Ångström característicos del aerosol del desierto (1.1 y 0.05, respectivamente). Además, se identificaron granos de polen que no son típicos de León durante este período. El análisis químico del aerosol del evento de 2017, permitió confirmar la presencia de los principales elementos asociados a las fuentes minerales (Al, Ca, Si). Los forzamientos radiativos atmosféricos indican que las dos intrusiones de polvo sahariano causaron un efecto de enfriamiento en la atmósfera, con valores medios de -15.6 K $día^{-1}$ y -12.4 K $día^{-1}$ durante las intrusiones de polvo de febrero de 2016 y de 2017, respectivamente. La masa de partículas de las

fracciones inhalable y respirable alcanzó unos valores nueve veces superiores a los obtenidos durante los días sin intrusiones de polvo en León.

Finalmente, los Capítulos 8 y 9 investigan el proceso de eliminación del aerosol por la lluvia, a partir de los datos obtenidos durante la campaña de muestreo simultáneo de aerosoles y precipitación, de un año de duración, que se presentó en el Capítulo 4.

Los resultados sobre la caracterización química del agua de lluvia recogida durante el periodo de muestreo, se presentan en el **Capítulo 8**. En general, se observó que el agua de lluvia está dominada por los iones NH_4^+, seguido de SO_4^{2-} y NO_3^- en todas las estaciones del año. En verano se registró una mayor concentración de iones, así como una conductividad mayor y un pH más bajo, probablemente debido al bajo volumen de precipitación registrado. En invierno, los altos valores de Na^+ y Cl^- en el agua de lluvia muestran una contribución de aerosoles marinos, mientras que en verano las altas concentraciones de Ca^{2+}, Mg^{2+}, SO_4^{2-}, NH_4^+ y NO_3^- reflejan la contribución de aerosoles minerales y de fuentes antropogénicas. Por otra parte, se realizó un estudio para establecer modelos lineales de predicción de la composición química del agua de lluvia y los coeficientes de *scavenging*, a partir de los parámetros físicos de las gotas de lluvia (obtenidos por medio de datos de un disdrómetro óptico) y de las propiedades químicas de los aerosoles. Los modelos lineales muestran que, en el agua de lluvia, la concentración de carbono orgánico disuelto y de los iones inorgánicos solubles en agua Ca^{2+}, SO_4^2 y NO_3^- aumenta con el volumen barrido por las gotas de lluvia. Sin embargo, la fracción de carbono insoluble tiene una dependencia negativa con el volumen barrido y positiva con el diámetro de la gota de lluvia. Los coeficientes de *scavenging* se ven afectados por la concentración en el aire de cada especie antes de la precipitación, por la duración del evento y por el tiempo transcurrido entre dos eventos de precipitación.

Por otra parte, en el **Capítulo 9** se estudia el impacto en la composición del agua de lluvia de dos eventos de transporte de aerosoles que afectaron a la calidad del aire en el norte de España: *i*) un episodio de incendios forestales masivos que se produjo en el noroeste de la Península Ibérica en agosto de 2016; y *ii*) una intrusión de polvo sahariano invernal que llegó a León en febrero de 2017. Los incendios forestales ocurridos en el norte de Portugal y el noroeste de España en agosto de 2016 afectaron a la composición química de la precipitación registrada en León el 15 de agosto de 2016. Así, se registró un aumento de las concentraciones de K^+, NH_4^+, SO_4^{2-}, Cl^-, NO_3^- y de carbono orgánico, tanto soluble como insoluble y, en consecuencia, una acidificación del agua de lluvia (pH = 4.8), en comparación con las muestras de precipitación recogidas en días sin influencia de emisiones de quema de biomasa. El segundo evento de precipitación estudiado tuvo lugar entre el 11 y el 14 de febrero de 2017. Se recogieron cuatro muestras de lluvia diarias (P_1, P_2, P_3 y P_4). La muestra de lluvia del 12 de febrero (P_2) coincidió con una intrusión de polvo sahariano que alcanzó el norte de la península Ibérica. La composición química de P_2 mostró un aumento en las concentraciones de Ca^{2+} (>800%), Mg^{2+} (71%), Cl^- (62%), y SO_4^{2-} (33%), con respecto a la muestra P_1. El aporte de elementos minerales a la atmósfera ayudó a neutralizar el agua de lluvia de la muestra P_2, causando valores de pH superiores a 6.5. Una vez que la intrusión de polvo abandonó el norte de la Península, la composición del agua de lluvia de las muestras P_3 y P_4 reveló una mezcla de contribución de aerosol marino con emisiones antropogénicas locales, así como una disminución de las concentraciones de los iones y de la conductividad, y un aumento de los valores de pH.

Air pollution refers to the presence in the atmosphere of substances resulting from human activities or natural processes, which have a negative impact on humans and the environment. The main atmospheric pollutants are carbon monoxide (CO), nitrogen oxides (NO_x), sulphur dioxide (SO_2), ozone (O_3) and aerosol or particulate matter (PM). The term atmospheric aerosol applies to the suspension of liquid and/or solid particles in the air, which have a typical size ranging from a few nanometers to a few hundred microns, and include both biogenic and non-biogenic material. The aerosol chemical composition is mainly determined by the source of the aerosol. However, the concentration, composition and size distribution of atmospheric particles can also vary temporally and spatially, as they are subject to transport, transformation and removal processes. After their formation or emission, aerosols can evolve to be removed from the atmosphere by dry deposition (without the intervention of water) or by wet deposition (in the presence of atmospheric hydrometeors).

Due to the adverse effects of air pollutants on human health and the environment, there is an increasing need to study the complex interaction between climate and air quality. The study of sources, concentrations, trends, formation and removal processes, health risks and environmental impact of air pollutants is an important tool for establishing new methods of monitoring air pollution, as well as examining the policies needed to reduce pollution. In this line, this thesis addresses a series of topics related to the study of air pollution in León, Spain, such as: *i*) the temporal evolution of atmospheric pollutants and the existing correlations between pollen concentration, with the main atmospheric pollutants and certain meteorological parameters; *ii*) the contribution of the main sources of biogenic (through the study of sugar compounds) and non-biogenic (through the chemical characterization of PM_{10}) particle emissions in León. ; iii) the impact of two particular cases of pollution, one of natural origin (Saharan dust intrusions in winter) and the other of anthropic origin (traffic during the summer-autumn transition) on the air quality and *iv*) the influence of the chemical composition of aerosols and the physical characteristics of precipitation on the scavenging of different chemical species, both on an annual scale and in short-term episodes (forest fires and Saharan dust intrusion).

This work is divided into ten Chapters: the first two present a brief theoretical introduction and a detailed description of the methodology used throughout this study. **Chapters 3 to 9** develop the results obtained and, finally, **Chapter 10** sets out the main conclusions drawn from this research, as well as the applications and future perspectives.

Chapter 3 presents the evolution of the concentration of several gaseous air pollutants (CO, SO_2, NO_x and O_3) of PM_{10} and of three types of pollens, *Fraxinus*, Poaceae and *Populus*, from 1997 to 2016 in León city (Spain). The main results show that there is a decreasing trend in the concentration of the air pollutants studied, as well as an increasing trend in the concentration of *Fraxinus*. Furthermore, it has been observed that the seasonal pollen index (SPIn) of *Fraxinus* is negatively and significantly correlated with atmospheric pollutants, while the SPIn of the pollen type Poaceae showed a significant correlation with precipitation before and during the flowering period. Moreover, the *Fraxinus* main pollen season (MPS) is positively and significantly correlated

with temperature, relative humidity and precipitation during the flowering period. Poaceae MPS is positively correlated with minimum temperature during the flowering period, while *Populus* MPS shows a negative correlation with minimum temperature. The results show that the flowering and pollination periods of the studied pollen types depend largely on the meteorological conditions before these periods and are influenced by the concentrations of air pollutants.

Chapter 4 shows the results corresponding to the chemical characterization of the aerosols sampled in a suburban area of León city (Spain), during the campaign carried out between 9 March 2016 and 14 March 2017. The annual mean concentration of PM_{10} in León city was 23 ± 8 μg m^{-3}, with a minimum value of 4 μg m^{-3} and a maximum value of 59 μg m^{-3}. The carbonaceous fraction represents the majority mass fraction with 21 ± 7% of PM_{10}. Furthermore, the chemical characterization of PM_{10} allowed the determination of the main sources of aerosols in León, through the application of the Positive Matrix Factorization (PMF) model. In total, six main aerosol sources were observed: traffic (29% of PM_{10}), aged sea salt (26% of PM_{10}), secondary aerosols (16% of PM_{10}), mineral aerosol (13% of PM_{10}), marine aerosol (7% of PM_{10}) and biomass burning (3% of PM_{10}). Using the results obtained with the PMF and the parameters of the weather types associated to the geostrophic flows (SF, WF, ZS and ZW), linear regression models that allowed to determine the contribution of each factor to the PM_{10} were constructed. The marine factor showed a positive dependence with WF, demonstrating that the western air masses are responsible for the transport of sea salts from the Atlantic Ocean to León. The secondary aerosol and traffic factors showed positive correlations with SF, due to the contribution of anthropogenic emissions from the city centre and other cities located south of León. In the case of aged sea salt, the negative correlation with ZS confirmed that this factor is mainly favored by anticyclonic situations. The correlations of the mineral factor with SF (negative) and ZS (positive) suggest that La Robla cement factory, located north of the city of León, is an important source of mineral aerosol. The biomass combustion factor showed no relationship with geostrophic flow, probably because it is a more local source.

The study of bioaerosol emission sources in León is addressed in **Chapter 5**, through the content of 17 sugar compounds in PM_{10} (arabinose, fructose, galactose, glucose, ribose, sucrose, xylose, adonitol, arabitol, 2-methyleriritol, myo-inositol, mannitol, sorbitol, xylitol, galactose, levoglucosan and mannosan), as well as the concentration of biological markers (pollen and *Alternaria* fungal spore), chemical composition of aerosols and meteorological conditions. The results showed that, in spring, when high levels of metabolic activity of plants occurs and temperatures increase, glucose, sucrose, 2-methyl-erythritol, mannitol, arabitol and inositol are significantly correlated with the airborne pollen concentration. Between spring and autumn, airborne *Alternaria* concentrations are significantly correlated with temperatures, arabitol and sorbitol + adonitol concentrations. In addition, during rainy days, *Alternaria* is also correlated with mannitol. In autumn, lower temperatures lead to increased concentrations of levoglucosan, mannitol and galactose, probably due to the increasing use of domestic heating appliances. These anhydrosugars and arabinose, fructose and glucose are significantly correlated with K, NO_3^-, OC, EC, Cu, Zn, Se, Pb, V and Ni, while mannosan is also correlated with As, which shows that these anhydrosaccharide can be emitted from different anthropogenic sources. Precipitation can cause an increase in the concentration of glucose and sucrose, due to the hydrated pollen particles

rupture releases the sugar compounds contained in the smallest fragments. In addition, precipitation causes an increase in the concentration of arabitol (airborne fungal spore tracer).

Chapter 6 presents an analysis of the temporal variation of the aerosol size distribution in an urban area of León, between August and October 2012, in order to identify the changes associated with the summer-autumn transition. It was observed that, as the summer progresses, the total concentration of particles increases from 1000 ± 600 particles cm^{-3} in August to 1500 ± 1000 particles cm^{-3} in October, mainly due to an increase in traffic flow after the summer holidays and at the beginning of the new academic year in September. Particle concentration was higher during weekdays than during weekends in the months of September and October. However, in August there was no substantial variation in the particle concentration, due to the lower activity in the city, caused by the holidays. A bimodal size distribution of aerosol particles was recorded, with the highest concentration of particles and the smallest average diameter in the fine mode during October. The highest values of the estimated respirable fraction in healthy adults were obtained for working days between 0600 and 1000 UTC (about 15 µg m^{-3}) and in the afternoon between 1700 and 2000 UTC (about 12 µg m^{-3}), coinciding with peak hours.

Chapter 7 shows a descriptive study of two Saharan dust intrusion events that affected air quality in León, in February 2016 and 2017. During winter, Saharan dust intrusions are not frequent and when occur, they usually do not reach the northwest of the Peninsula. The study was carried out with an integrative approach that includes: *i*) typical synoptic conditions; *ii*) aerosol chemical composition; *iii*) particle size distribution; *iv*) pollen concentration; *v*) aerosol optical depth (AOD); *vi*) radiative forcing and *vii*) estimation of the impact of aerosols on the respiratory tract. In the overall characterization of these dust intrusion events, it was found: the exceedance of the daily limit value for PM_{10}, an increase in coarse-mode of particles and an increase in iron concentration. In the 2016 event, a value of AOD and Ångström exponent characteristic of desert aerosol was recorded (1.1 and 0.05, respectively). In addition, pollen grains not typical of León during this period were identified. The chemical analysis of the aerosol of the 2017 event, allowed to confirm the presence of the main elements associated to the mineral sources (Al, Ca, Si). Atmospheric radiative forcing indicates that the two Saharan dust intrusions caused a cooling effect in the atmosphere, with average values of -15.6 K day^{-1} and -12.4 K day^{-1} during the dust intrusions of February 2016 and 2017, respectively. The inhalable and respirable mass fractions reached values nine times higher than those obtained during the days without dust intrusions in León.

Finally, **Chapters 8 and 9** deal with the process of aerosol scavenging by rain, based on data obtained during the one-year simultaneous aerosol and precipitation sampling campaign presented in **Chapter 4**.

The results on the chemical characterisation of rainwater collected during the sampling period are presented in **Chapter 8**. In general, it was observed that rainwater is dominated by NH_4^+, followed by SO_4^{2-} and NO_3^- in all seasons. A higher concentration of ions was recorded in summer, as well as higher conductivity and lower pH, probably due to the low volume of precipitation recorded. In winter, high values of Na^+ and Cl^- in rainwater show a contribution from marine aerosols, while in summer high concentrations of Ca^{2+}, Mg^{2+}, SO_4^{2-}, NH_4^+ and NO_3^- reflect the contribution of mineral aerosols and anthropogenic sources. Moreover, a study was

carried out to establish multilinear models to predict the chemical composition of rainwater and scavenging coefficients, from the physical parameters of raindrops (obtained by means of data from an optical disdrometer) and the chemical properties of aerosols. Linear models show that in rainwater, the concentration of dissolved organic carbon and water-soluble inorganic ions Ca^{2+}, SO_4^{2-} and NO_3^- increases with the volume swept by raindrops. However, the fraction of insoluble carbon has a negative dependence with the swept volume and positive dependence with the diameter of the raindrop. The scavenging coefficients are affected by the concentration in the air of each species before precipitation, by the duration of the event and by the time elapsed between two precipitation events.

In addition, **Chapter 9** addresses the impact on rainwater composition of two aerosol transport events that affected the air quality in northern Spain: *i*) a massive forest fire episode that occurred in the northwest of the Iberian Peninsula in August 2016; and *ii*) a winter Saharan dust intrusion that reached León in February 2017. The forest fires that occurred in northern Portugal and northwestern Spain in August 2016 affected the chemical composition of the precipitation recorded in León on 15 August 2016. Thus, there was an increase in the concentrations of K^+, NH_4^+, SO_4^{2-}, Cl^-, NO_3^- and organic carbon, both soluble and insoluble, and consequently an acidification of rainwater (pH = 4.8), compared to the precipitation samples collected on days without the influence of biomass burning emissions. The second precipitation event studied took place between 11 and 14 February 2017. Four daily rainfall samples were collected (P_1, P_2, P_3 and P_4). The rainwater sample of 12 February (P_2) coincided with a Saharan dust intrusion that reached the north of the Iberian Peninsula. The chemical composition of P_2 showed an increase in the concentrations of Ca^{2+} (>800%), Mg^{2+} (71%), Cl^- (62%), and SO_4^{2-} (33%), with respect to the P_1 sample. The contribution of mineral elements to the atmosphere helped neutralize the P_2 rainwater sample, causing pH values above 6.5. Once the dust intrusion left the north of the Peninsula, the composition of P_3 and P_4 rainwater samples revealed a mixture of marine aerosol contribution with local anthropogenic emissions, as well as a decrease in the ion concentrations and conductivity, and an increase in pH.

A	Anticiclónico, *Anticyclonic*
ACP	Análisis de Componentes Principales, *Principal Component Analysis*
AE	Exponente de Ämstrong, *Ämstrong Exponent*
AEMET	Agencia Estatal de Meteorología
AERONET	*AErosol Robotic NETwork*
AGL	Sobre el nivel de superficie, *Above Ground Level*
AOD	Espesor óptico de los aerosoles, *Aerosol Optical Depth*
APIn	Índice polínico anual, *Annual Pollen Integral*
BC	Carbono negro, *Black Carbon*
BCS	Lavado por debajo de la nube, *Below-Cloud Scavenging*
BOA	Parte baja de la atmósfera, *Bottom Of Atmosphere*
BrC	Carbono marrón, *Brown carbon*
CI	Cromatografía Iónica, *Ionic Chromatography*
CMD	Diámetro de la mediana de la distribución del número de partículas, *Count Median Diameter*
CNN	Núcleos de condensación de nubes, *Cloud Condensation Nuclei*
CPC	Contador de partículas, *Condensation Particle Counter*
CWT	Tipos de Tiempo, *Circulation Weather Types*
DGT	Dirección General de Tráfico
DLV	Valor límite diario, *Daily Limit Value*
DMA	Analizador de Movilidad Diferencial, *Diferencial Mobility Analyzer*
DOC	Carbono Orgánico Disuelto, *Dissolve Organic Carbon*
EC	Carbono elemental, *Elemental Carbon*
EF	Factor de enriquecimiento, *Enrichtment Factor*
ELISA	*Enzyme Linked Inmuno Sorbent Assay*
EPA	*Environmental Protection Agency*
FE-SEM	Microscopía de Barrido por Emisión de Campo, *Field Emission Scanning Electron Microscopy*
GAME	*Global Atmospheric ModEL*
RH	Humedad Relativa, *Relative Humidity*
HYSPLIT	*Hybrid Single-Particle Lagrangian Integral Trayectory*
ICS	Lavado dentro de la nube, *In-Cloud Scavenging*
INE	Instituto Nacional de Estadística
IPCC	*Intergovernmental Panel on Climate Change*
ISO	*International Organization for Standardization*
LPM	Monitor Láser de Precipitación, *Laser Precipitation Monitor*
MODIS	*MODerate Resolution Imaging Spectroradiometer*
MPS	Estación polínica principal, *Main Pollen Season*
NAAPS	*Navy Aerosol Analysis and Prediction System*
NCAR	*National Center for Atmospheric Research*
NDIR	Infrarrojo no dispersivo, *Non-Dispersive Infrared*

NF	Factor de neutralización, *Neutralization Factor*
NOAA	*National Oceanic and Atmospheric Administration*
NRL	*Naval Research Laboratory*
OC	Carbono Orgánico, *Organic Carbon*
OCP	Contador óptico de partículas, *Optical Particle Counter*
OMS	Organización Mundial de la Salud
ONU	Organización de Naciones Unidas
PAD	Detección Amperométrica Pulsada, *Pulsed Amperometric Detection*
PBA	Aerosoles biogénicos primarios, *Primary Biological Aerosols*
PC	Carbono orgánico pirolizado, *Pyrolyzed organic Carbon*
PCASP	*Passive Cavity Aerosol Spectrometer Probe*
PIXE	Emisión de Rayos X Inducida por Partículas, *Particle-Induced X-ray Emission*
PM	Material Particulado, *Particulate Matter*
PM_1	Material Particulado de menos de 1 µm, *Particulate Matter less than 1 µm*
PM_{10}	Material Particulado de menos de 10 µm, *Particulate Matter less than 10 µm*
$PM_{2.5}$	Material Particulado de menos de 2.5 µm, *Particulate Matter less than 2.5 µm*
PMF	Factorización de Matriz Positiva, *Positive Matrix Factorization*
POM	Materia orgánica particulada, *Particulate Organic Matter*
REA	Red Española de Aerobiología
RTM	*Radiative Transfer Model*
SDD	*Silicon Drift Detectors*
SLP	Presión a nivel del mar, *Sea-Level Pressure*
SMD	Diámetro de la mediana de la distribución de superficie de las partículas, *Surface Median Diameter*)
SMPS	*Scanning Mobility Particle Sizer*
SPIn	Índice polínico estacional, *Seasonal Pollen Integral*
SSA	*Single Scattering Albedo*
TOA	Techo de la atmósfera, *Top Of Atmosphere*
VMD	Diámetro de la mediana de la distribución del volumen de las partículas (*Volume Median Diameter*)
VOCs	Compuestos Orgánicos Volátiles, *Volatile Organic Compounds*
VWM	Concentración media volumétrica, *Volume Weighted Mean concentration*
VWSD	Desviación estándar de la media volumétrica, *Volume Weighted Standard Deviation*
WIEC	Carbono Elemental Insoluble en agua, *Water Insoluble Elemental Carbon*
WIOC	Carbono Orgánico Insoluble en agua, *Water Insoluble Organic Carbon*
ΔFATM	Forzamiento radiativo atmosférico, *Atmospheric radiative forcing*
ΔFBOA	Forzamiento radiativo en superficie, *Radiative forcing on surface*
ΔFTOA	Forzamiento radiativo para el sistema superficie + atmósfera, *Radiative forcing for the surface + atmosphere system*
σ_g	Desviación geométrica, *Geometric deviation*

1

INTRODUCCIÓN

En los últimos años se ha observado un creciente interés en el estudio de los contaminantes atmosféricos y sus fuentes, debido a los múltiples efectos que tienen en la salud humana y en el medio ambiente. La contaminación atmosférica se define como la presencia de sustancias en la atmósfera, provenientes de actividades humanas o de procesos naturales, que causan efectos adversos al ser humano y al medio ambiente (Weber, 1982). Por otra parte, en la Directiva (2008/50/CE) se establece que un contaminante atmosférico es "toda sustancia presente en el aire ambiente que pueda tener efectos nocivos para la salud humana y el medio ambiente en su conjunto". Los principales contaminantes atmosféricos son: el monóxido de carbono (CO), los óxidos de nitrógeno (NO_x), el dióxido de azufre (SO_2), el ozono (O_3) y el material particulado atmosférico (PM, en inglés *Particulate Matter*), que incluye a las partículas biogénicas (polen, esporas de hongos, bacterias, virus, etc.) y a las partículas no biogénicas (polvo mineral, cenizas, sales marinas, etc.). Estos contaminantes coexisten en la atmósfera, con la posibilidad de interactuar entre sí y aumentar su impacto adverso debido al efecto sinérgico.

La exposición a altos niveles de contaminantes atmosféricos puede causar enfermedades cardíacas, cáncer de pulmón y enfermedades respiratorias crónicas (Analitis et al., 2006; Bernstein et al., 2004; Brunekreef and Holgate, 2002; Kim et al., 2015; Lelieveld et al., 2015). La *Organización Mundial de la Salud* (OMS) estima que 9 de cada 10 personas respiran aire con altas concentraciones de contaminantes y que más del 80% de las personas que viven en zonas urbanas están expuestas a niveles de calidad del aire que superan los valores límite recomendados para la salud humana. Además, la OMS señala que la contaminación atmosférica causa alrededor de 4.2[1] millones de muertes al año en todo el mundo.

Las principales fuentes de contaminación en zonas urbanas son el tráfico, la generación de energía, los sistemas de calefacción, la incineración de desechos y las industrias. El alto consumo de energía, especialmente en ciudades muy pobladas, es una de las principales causas de los altos niveles de contaminación atmosférica. En Delhi, India, la segunda ciudad más poblada del mundo según la *Organización de las Naciones Unidas* (ONU), se estiman unas emisiones anuales de 13.8 kt de CO, 4.3 kt de CO_2, 37.4 kt de SO_2, 12 kt de NO_x y 10.2 kt de PM (Venkitasamy and Bhaskar,

[1] Con el fin de unificar el formato utilizado a lo largo de la memoria y considerando que algunos capítulos han sido redactados en inglés, hemos establecido el uso del punto como separador decimal en todo el texto.

2016), donde un 68% de las emisiones de SO_2 provienen de la generación de energía eléctrica y entre un 66 y un 74% de las emisiones de NO_x provienen del tráfico (Gurjar et al., 2016). Por otra parte, en China la generación de energía eléctrica a base de carbón es responsable de más del 23%, 45% y 64% de las emisiones nacionales de PM, de SO_2 y de NO_x, respectivamente (Yuan et al., 2018). Más concretamente, en la ciudad de Weinan, China, con 5.5 millones de habitantes, las emisiones anuales de SO_2, NO_x y CO se estiman en aproximadamente 42 kt, 85 kt y 13 kt, respectivamente (Y. Xu et al., 2017). En España, el Ministerio para la Transición Ecológica y el Reto Demográfico, en el Inventario Nacional de Contaminantes Atmosféricos de 2018, muestra que se emiten anualmente 492 kt de CO, 74 kt de SO_x, 120 kt de NO_2 por actividades industriales, mientras que por el sector del transporte se emiten aproximadamente 172 kt de CO, 0.4 kt de SO_x y 237 kt de NO_2, siendo las actividades industriales la mayor fuente de SO_2 y CO, y el tráfico la mayor fuente de NO_2.

Con el incremento de las áreas urbanas a escala mundial, y dado que los contaminantes atmosféricos pueden viajar entre ciudades e incluso entre continentes (ej. Cerón-Bretón et al., 2013; Escudero et al., 2007; Maring et al., 2003; Perfumo and Marchant, 2010), causando impactos importantes sobre la salud humana y el medio ambiente, se hace cada vez más necesario estudiar la compleja interacción clima-calidad del aire. Este tipo de estudios permite establecer nuevos métodos de monitorización de la contaminación del aire, así como examinar las políticas necesarias para reducir la contaminación. De este modo, se pretende mitigar el cambio climático a corto y a largo plazo y el número de enfermedades relacionadas con la contaminación atmosférica. Por todo ello, resulta esencial conocer las fuentes, concentraciones, tendencias, transformaciones, procesos de formación y eliminación, riesgo en la salud e impacto ambiental que tienen los contaminantes atmosféricos en una localidad determinada.

Los apartados siguientes se dedican a exponer los aspectos teóricos más relevantes sobre las fuentes de emisión de los aerosoles, su composición química, la distribución de tamaños de las partículas, los mecanismos de formación y eliminación de las mismas, las propiedades ópticas del aerosol y el impacto que suponen los contaminantes atmosféricos en el ambiente y en la salud humana. Finalmente, se hace mención al marco normativo referente a la calidad del aire ambiente en Europa y España.

1.1. FUENTES DEL MATERIAL PARTICULADO

Los aerosoles atmosféricos son definidos como una suspensión de partículas líquidas y/o sólidas en el aire, que tienen un tamaño típico que va desde unos pocos nanómetros a unos cientos de micras y que residen en la atmósfera durante al menos varias horas (Seinfeld and Pandis, 2016). Los aerosoles atmosféricos o material particulado (PM) suelen ser categorizados de acuerdo con su tamaño como PM_{10}, $PM_{2.5}$ o PM_1, nomenclatura que hace referencia a las partículas en el aire que pasan a través de un cabezal de muestreo para un diámetro aerodinámico de 10 µm, 2.5 µm y 1 µm, respectivamente, con una eficiencia de corte del 50%. Esto significa que, de las partículas recogidas en el filtro de muestreo, al menos el 50% debe corresponder a la fracción de PM_{10}, $PM_{2.5}$ y PM_1, respectivamente. Se define diámetro aerodinámico como el diámetro de una partícula esférica de densidad 1 g cm^{-3}, que presenta la misma velocidad de sedimentación que la partícula en cuestión (Hinds, 2012).

El origen de los aerosoles puede ser primario o secundario, y de fuentes naturales o antropogénicas. El PM de origen primario es aquel que es emitido directamente hacia la atmósfera, mientras que el aerosol secundario es aquel que se forma *in situ* por procesos de conversión de gases a partículas (Colbeck and Lazaridis, 2014; Seinfeld and Pandis, 2016). Las fuentes naturales son aquellas en las que el material particulado es emitido debido a diferentes procesos que ocurren en la naturaleza, mientras que las fuentes antropogénicas están ligadas a las actividades humanas.

1.1.1. Fuentes naturales de origen primario

Los aerosoles procedentes de las fuentes naturales de origen primario son principalmente el polvo mineral, el aerosol marino y los aerosoles biogénicos primarios. A continuación, se hace una breve descripción de las fuentes más importantes de estos aerosoles.

- **Polvo mineral**

Las partículas pertenecientes a la fracción mineral, conocida como fracción *crustal* (del inglés *crust*, corteza), se generan principalmente por la acción del viento sobre la superficie terrestre. El polvo mineral es arrastrado por el viento procedente de las regiones desérticas y semiáridas, y una vez en la atmósfera las partículas de polvo pueden ser transportadas largas distancias (Choobari et al., 2014; Schütz and Sebert, 1987). Las fuentes más importantes de polvo mineral se encuentran en el hemisferio norte, principalmente sobre el desierto del Sahara y el Sahel, al norte de África. Otros desiertos, como el Rub al-Jalí, ubicado en la Península Arábiga, el Gobi y el Taklamakan en China, también son una fuente importante de aerosol mineral a escala mundial (Calvo et al., 2013; Choobari et al., 2014; Goudie, 2014).

En general, el aerosol mineral está compuesto por cuarzo, calcita, feldespato potásico, caolinita, clorita, lilita y montmorillonita (Schütz y Sebert, 1987). Los elementos que constituyen esta fracción son principalmente Si, Al, Ca, Fe y Ti en forma de óxidos y carbonatos (Hewitt and Jackson, 2008; Kandler et al., 2009). El tamaño de las partículas provenientes de fuentes minerales es variable y puede cubrir un rango de entre 0.01 a 1000 μm (D'Almeida y Schütz, 1983; Schütz y Sebert, 1987). Cerca de las fuentes de emisión, el tamaño medio de la partícula mineral varía entre 30 y 50 μm. A medida que son transportadas por la acción del viento, la distribución de tamaños de las partículas puede encontrarse entre 1 y 2 μm (Choobari et al., 2014).

- **Aerosol marino**

Las partículas de aerosol marino son aquellas que se producen por la ruptura de las burbujas, formadas por la acción del viento y las olas en la superficie de las masas de agua marítimas y oceánicas (Calvo et al., 2013), como se muestra en la Figura 1.1.

El aerosol marino está principalmente compuesto por sales marinas (NaCl, KCl, $CaSO_4$ y Na_2SO_4), sulfato no marino, polvo mineral y en menor proporción, nitratos. La concentración de las sales marinas depende principalmente de la velocidad del viento (Fitzgerald, 1991). El espectro de tamaño del aerosol marino abarca más de cinco ordenes de magnitud, moviéndose principalmente entre 0.02 μm y 8 μm (Fitzgerald, 1991; Hewitt and Jackson, 2008).

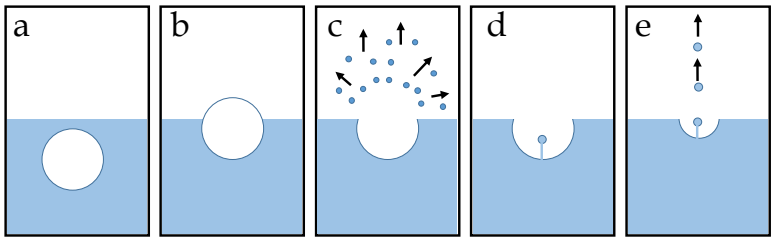

FIG. 1.1. Secuencia esquemática de la formación de las partículas de aerosol marino por ruptura de burbujas de aire: a-b) la burbuja de aire asciende hacia la superficie del mar, c) la parte superior de la película de la burbuja se rompe y se forman pequeñas gotas que comienzan a evaporarse, d-e) ocurre la contracción de la cavidad dejada por la burbuja y se forman gotas de chorro desde el centro de la cavidad (adaptado de Lewis et al., 2004).

- **Emisiones volcánicas**

Aunque la actividad volcánica ocurre de forma esporádica, cuando ocurre produce importantes emisiones hacia la atmósfera. Las emisiones están compuestas principalmente por cenizas (SiO_2, Al_2O_3 y Fe_2O_3, mayormente), gases (SO_2, H_2S, CO_2, HCl y HF) y vapor de agua. Las emisiones volcánicas pueden introducir a la atmósfera aproximadamente 33 toneladas al año de cenizas, mientras que las emisiones de azufre debido a las erupciones volcánicas representan entre un 10 y un 20% de las emisiones totales de azufre natural inyectadas a la atmósfera (Hewitt and Jackson, 2008).

- **Emisiones biogénicas**

Esta categoría incluye los aerosoles biogénicos primarios (PBA, en inglés *Primary Biological Aerosols*) o bioaerosoles, que provienen de la vegetación (fragmentos de plantas, polen, esporas, hongos, etc.), del material orgánico en descomposición, bacterias, etc. Por ello, la mayor fuente de bioaerosoles son los ecosistemas terrestres. Las partículas biológicas tienen morfologías y distribuciones de tamaño muy diversas. Los tamaños pueden estar comprendidos entre algunos nanómetros (virus, fragmentos de células) y unos pocos cientos de micrómetros (polen, restos vegetales, etc.) (Cox and Wathes, 1995; Després et al., 2012; Fröhlich-Nowoisky et al., 2016; Matthias-Maser, 1998; Polymenakou et al., 2008).

Los aerosoles biogénicos primarios se componen principalmente de carbono orgánico (OC, del inglés *Organic Carbon*) biogénico, por lo que en su composición representan una parte importante los azúcares. Así, los compuestos como el arabitol o el manitol, responsables del almacenamiento de energía en los hongos, o la fructosa y la glucosa, presentes en tejidos vegetales, son ampliamente utilizados para la identificación de bioaerosoles (Bauer et al., 2008; Burshtein et al., 2011; Fu et al., 2012; Medeiros et al., 2006; Simoneit et al., 2004).

1.1.2. Fuentes naturales de origen secundario

Los aerosoles naturales de origen secundario son aquellos que se forman por la conversión gas-partícula, a partir de las emisiones de gases precursores provenientes de fuentes naturales. La liberación de sulfuro de dimetilo o DMS (CH_3SCH_3) por los océanos a partir de la actividad

biológica del fitoplancton, es una de las principales fuentes naturales de sulfato de origen secundario en el aerosol (Hewitt and Jackson, 2008). Por otra parte, la formación de nitrato secundario tiene principalmente dos fuentes naturales: el NO_2 formado *in situ* en la tropósfera por acción de los rayos y el N_2O proveniente de la actividad bacteriana en suelos y océanos.

Los aerosoles orgánicos secundarios se forman a partir de los compuestos orgánicos volátiles (VOCs, del inglés *Volatile Organic Compounds*) oxidados en la atmósfera. Entre las fuentes naturales de VOCs se encuentran las plantas, los suelos, los océanos y el agua dulce. Los terpenos, emitidos principalmente por las plantas, son considerados los VOCs biogénicos más abundantes y con mayor potencial de formación de aerosoles orgánicos secundarios (Colbeck, 2008; Hewitt and Jackson, 2008).

1.1.3. Fuentes antropogénicas de origen primario

A continuación se realiza una breve descripción de las principales fuentes antropogénicas de origen primario, entre las que se destacan la quema de biomasa, las actividades industriales, el tráfico y la quema de carbón (Calvo et al., 2013).

- **Quema de biomasa**

La quema de biomasa abarca los incendios forestales y las actividades antropogénicas como la quema de rastrojos o residuos vegetales y el encendido de chimeneas para uso doméstico. Los principales productos de la quema de biomasa son el hollín, los sulfatos, nitratos y los productos de combustión incompleta que contienen compuestos carbonosos, además de los productos gaseosos como CO_2, CO, CH_4 y VOCs (Alves et al., 2011; Hewitt and Jackson, 2008).

La biomasa se compone principalmente de celulosa, hemicelulosa y lignina. La alteración térmica de la celulosa y hemicelulosa produce diferentes compuestos como el levoglucosano (1,6-anhídrido-β-D-glucopiranosa), manosano (1,6-anhídrido-β-D-manopiranosa) y galactosano (1,6-anhídrido-β-D-galactopiranosa), diterpenoides, triterpenoides, metoxifenoles, derivados del furano, etc. (Simoneit et al., 1999). Por otra parte, los aerosoles emitidos por la quema de biomasa además de estar constituidos por carbono orgánico (entre un 10 y 20%), también se caracterizan por estar compuestos de carbono negro (BC, del inglés *Black Carbon*) y de iones inorgánicos como K^+ y Cl^- (Urban et al., 2012). Las distribuciones del tamaño de las partículas provenientes de las emisiones de quema de biomasa varían en función del tipo de combustible y la fase de combustión (Castro et al., 2018). Las partículas de humo fresco pueden tener tamaños medios de entre 0.10 y 0.16 μm (Alonso-Blanco et al., 2012; Vu et al., 2015).

- **Actividad industrial**

Los contaminantes provenientes de actividades industriales son liberados durante las distintas etapas de los procesos industriales. El tipo de contaminante depende principalmente del tipo de proceso de producción, de la tecnología y de la materia prima utilizada. Las mayores fuentes industriales de aerosoles incluyen: minería, quema de combustibles fósiles, fabricación de cemento, fundición de metales, petroquímicas, etc. (Hewitt and Jackson, 2008). En general, los aerosoles de las zonas industrializadas presentan niveles relativamente altos de As, Cu, Cr, Mn,

Ni, Zn, Mo, Cd, Se, Pb, Sn, V y Ni (Querol et al., 2007). Además, las actividades industriales y, en particular, la producción de energía a partir de combustibles fósiles, son también una fuente importante de gases que actúan como precursores de aerosoles secundarios (Calvo et al., 2013). La emisión por procesos industriales contribuye principalmente a las partículas con tamaños de entre 40 y 50 nm (Vu et al., 2015).

- **Tráfico**

El tráfico rodado constituye la mayor fuente de aerosoles primarios y secundarios en zonas urbanas. Las partículas emitidas por el tráfico presentan un amplio rango de tamaños y composición química y pueden proceder de los tubos de escape (en inglés *exhaust*) y de otras fuentes distintas de los tubos de escape (en inglés *non-exhaust*).

Entre las fuentes *non-exhaust* de partículas se encuentran el desgaste de los frenos, de los neumáticos y del pavimento y la resuspensión de polvo del pavimento. En general, la composición química de estas partículas incluye elementos como el Cu, Sb, Zn, As, Pb y elementos asociados al material mineral como el Al, Ca, Fe, Mg, Mn y Ti (Thorpe and Harrison, 2008). Las partículas emitidas por fuentes de tráfico *non-exhaust* presentan mayormente diámetros de entre 1 y 10 μm (Thorpe and Harrison, 2008).

Las partículas provenientes de emisiones *exhaust* pueden generarse directamente en el motor durante la combustión del combustible, o pueden formarse en el aire por nucleación y condensación durante la dilución y el enfriamiento de las emisiones de gases calientes del tubo de escape. Las partículas generadas por la combustión de combustibles fósiles consisten principalmente en carbono negro y en una menor cantidad de metales (como V y Ni), hidrocarburos y compuestos de azufre. Adicionalmente, las emisiones debidas a la quema de combustible en los vehículos incluyen gases como CO, CO_2 y NO_x, siendo el tráfico una de las mayores fuentes de óxidos de nitrógeno en áreas urbanas, así como de una gran cantidad de VOCs (benceno, tolueno, xileno, etc.) (Alves et al., 2015; Reşitoğlu et al., 2015).

- **Quema de carbón**

El carbón se utiliza como combustible para la generación de energía eléctrica y para los sistemas de calefacción domésticos. Está compuesto principalmente por C, H, O, N y S, y, en una menor proporción, por Si, Al, Ca, Mg, K, Na, Fe, Mn, Ti, halógenos y elementos traza (Xu et al., 2004). La quema de carbón es una de las principales fuentes antropogénicas de As y Se (utilizados como marcadores para este tipo de emisiones), y además libera a la atmósfera gases como SO_x, NO_x, CO_2 y VOCs (Chen et al., 2013; Xie et al., 2006). El rango de tamaños de las partículas emitidas por la quema de carbón oscila entre 50 nm y 100 nm (Bond et al., 2002; Chang et al., 2004; Tiwari et al., 2014).

1.1.4. Fuentes antropogénicas de origen secundario

La quema de combustibles fósiles representa una de las mayores fuentes antropogénicas de aerosol secundario. Sus emisiones pueden liberar a la atmósfera importantes cantidades de VOCs, óxidos de nitrógeno y azufre (Alastuey et al., 2004; Qin et al., 2017). La oxidación de SO_2 y NO_x

en fase gaseosa o condensada en la atmósfera es la mayor fuente de partículas secundarias. En la fase gaseosa la oxidación para la formación de ácido sulfúrico (H_2SO_4) y ácido nítrico (HNO_3) es dominada por la presencia de hidroxilos, mientras que en la fase condensada cerca del 50% de NO_x y más del 80% de SO_2 son oxidados mediante reacciones heterogéneas (Atkinson, 2000; Jenkin and Clemitshaw, 2000). Por otra parte, el NO_x y los VOCs son precursores para la formación de ozono en la tropósfera a partir de reacciones de radicales libres (Atkinson, 2000; Jenkin and Clemitshaw, 2000; Sillman, 1999).

1.2. COMPOSICIÓN QUÍMICA DEL AEROSOL

La composición química del aerosol está determinada principalmente por la fuente que lo emite en el caso de los aerosoles primarios y, en el caso de las partículas secundarias, por los procesos que las forman (Calvo et al., 2013; Viana et al., 2008). Sin embargo, la concentración, composición y distribución de tamaño de las partículas atmosféricas también varían temporal y espacialmente, a causa de los procesos de transporte, transformación y eliminación (Denjean et al., 2016; Vu et al., 2015) a los que está sometido el aerosol.

Las circunstancias meteorológicas también constituyen un aspecto importante que puede influenciar la composición química del aerosol. La velocidad del viento, la procedencia de las masas de aire, así como ciertos escenarios sinópticos, pueden influir en el aporte de contaminantes regionales y/o continentales, favoreciendo su transporte a largas distancias (Elminir, 2005; Fernández-Camacho et al., 2016; Rodríguez et al., 2002). Por otra parte, la humedad relativa y la temperatura pueden afectar los niveles de contaminantes locales, especialmente en los meses de invierno, cuando el descenso en las temperaturas y el aumento en la humedad relativa conducen a un incremento en el uso de sistemas de calefacción y en la densidad del tráfico, aumentando las emisiones de origen antropogénico local (Elminir, 2005; Titos et al., 2017).

En general, el material particulado está compuesto mayoritariamente por compuestos orgánicos, BC o carbono elemental (EC, del inglés *Elemental Carbon*), sulfato, nitrato, amonio, sal marina y polvo mineral. Las partículas gruesas, formadas por procesos mecánicos, son ricas en Al, Ca, Fe, Si y NaCl (Alastuey et al., 2016; Formenti et al., 2003; Koulouri et al., 2008), mientras que las partículas finas, formadas por procesos de combustión o por la conversión gas-partícula, suelen ser ricas en sulfato, amonio y nitrato y, en menor proporción, por compuestos orgánicos volátiles y por otras especies tóxicas como As, Cd, Cs, Sr, Zn y Se (Colbeck, 2008; Samek et al., 2017; Tian et al., 2010; Vicente and Alves, 2018).

La fracción carbonosa, conformada por el OC y el EC, generalmente contribuye entre un 20 y un 70% del total de partículas en la atmósfera (ej. Calvo et al., 2008; Gonçalves et al., 2016; Gugamsetty et al., 2012; Theodosi et al., 2010). El carbono elemental o carbono negro es el componente carbonoso inorgánico formado durante la combustión a alta temperatura de los combustibles fósiles y de la quema de biomasa. El término de carbono negro suele asignarse a la fracción de carbono inorgánico particulado que es determinado por métodos ópticos, mientras que el término de carbono elemental corresponde a la fase más degradada del BC, que es determinada por métodos térmicos. El EC tiene una estructura química similar al grafito impuro, con una ratio másica H/C cercana a cero y una aromaticidad máxima (Colbeck, 2008; Seinfeld and Pandis, 2016). Por otra parte, el OC engloba una mezcla compleja de miles de compuestos

orgánicos diferentes, que pueden ser emitidos en grandes cantidades por fuentes antropogénicas o por fuentes naturales, como se explicó en el apartado 1.1.

El sulfato en la atmósfera se forma principalmente por la foto-oxidación del SO_2 en presencia de O_2. Esta reacción fotoquímica produce trióxido de azufre (SO_3), que reacciona rápidamente con el vapor de agua para formar H_2SO_4 (Cox, 1974). Las partículas de H_2SO_4 pueden ser neutralizadas parcial o totalmente por el amoníaco (NH_3) presente en condiciones atmosféricas normales. En condiciones de altas concentraciones de carbonato de calcio ($CaCO_3$) o de cloruro de sodio (NaCl), el H_2SO_4 reacciona con estas especies para formar sulfato de calcio ($CaSO_4$) o sulfato de sodio (Na_2SO_4), respectivamente (Colbeck, 2008; Seinfeld and Pandis, 2016), como se indica en las reacciones 1.1 y 1.2.

$$CaCO_{3\,(s)} + H_2SO_{4\,(g+ac)} \rightarrow CaSO_{4\,(s)} + CO_{2\,(g)} + H_2O_{\,(ac)} \qquad \text{Reacción 1.1}$$

$$2NaCl_{\,(s)} + H_2SO_{4\,(g+ac)} \rightarrow 2HCl_{\,(g)} + Na_2SO_{4\,(s)} \qquad \text{Reacción 1.2}$$

El nitrato se encuentra presente en la atmósfera principalmente en dos formas, como nitrato de amonio (NH_4NO_3) y como nitrato de sodio ($NaNO_3$). La primera se forma a partir de la reacción de neutralización del HNO_3 en fase vapor, con el NH_3 (Reacción 1.3), mientras que la segunda resulta del desplazamiento del NaCl por el HNO_3 en fase vapor (Reacción 1.4) (Colbeck, 2008).

Como se observa en la reacción 1.3, la formación de NH_4NO_3 es un proceso reversible. Esto se debe a la alta presión de vapor del NH_3 y del HNO_3, lo que causa que el nitrato de amonio formado sea una especie inestable que se volatiliza parcialmente a una temperatura de 20 ^oC y totalmente a más de 25 ^oC, para formar de nuevo NH_3 y HNO_3 (EPA, 2004a).

$$NH_{3\,(g)} + HNO_{3\,(g)} \rightleftharpoons NH_4NO_{3\,(s)} \qquad \text{Reacción 1.3}$$

$$NaCl_{\,(s)} + HNO_{3\,(g)} \rightarrow HCl_{\,(g)} + NaNO_{3\,(s)} \qquad \text{Reacción 1.4}$$

Una fracción minoritaria del aerosol está compuesta principalmente por metales traza como el Cr, As, Se, V, Ni, Pb, Cd, Hg, Ni, Cd, Zn, etc. Las concentraciones de estos elementos en el aerosol atmosférico están relacionadas con las fuentes de emisión. La resuspensión del polvo y la erosión de los suelos por la acción del viento, contribuyen a escala mundial a la emisión natural total de metales traza a la atmósfera, mientras que los aerosoles de sal marina pueden contribuir a alrededor del 10% del total de las emisiones de metales traza (Colbeck, 2008). Por otra parte, la quema de combustibles fósiles es la fuente antropogénica más importante de elementos como el V, Ni, Cd, Pb, Cu, Mn, entre otros, mientras que la abrasión de la goma de los neumáticos es otra fuente importante que contribuye al Zn atmosférico. La quema de carbón es una de las fuentes principales de emisión a la atmósfera de As y Se (Chen et al., 2013; Lin et al., 2005) y los procesos metalúrgicos industriales emiten grandes cantidades de As, Cd, Cu, Ni y Zn.

1.3. DISTRIBUCIÓN DE TAMAÑO DE LOS AEROSOLES

El tamaño de las partículas es un parámetro que está relacionado con la composición química, las propiedades ópticas, la evolución y eliminación de los aerosoles, así como el impacto

en el tracto respiratorio humano. Los diámetros de las partículas atmosféricas varían desde 1 nm hasta más de 1000 µm y están determinados por los procesos de formación y las subsecuentes reacciones químicas y físicas que sufren dichas partículas en la atmósfera. La Fig. 1.2 muestra los rangos de tamaño típicos para algunos aerosoles.

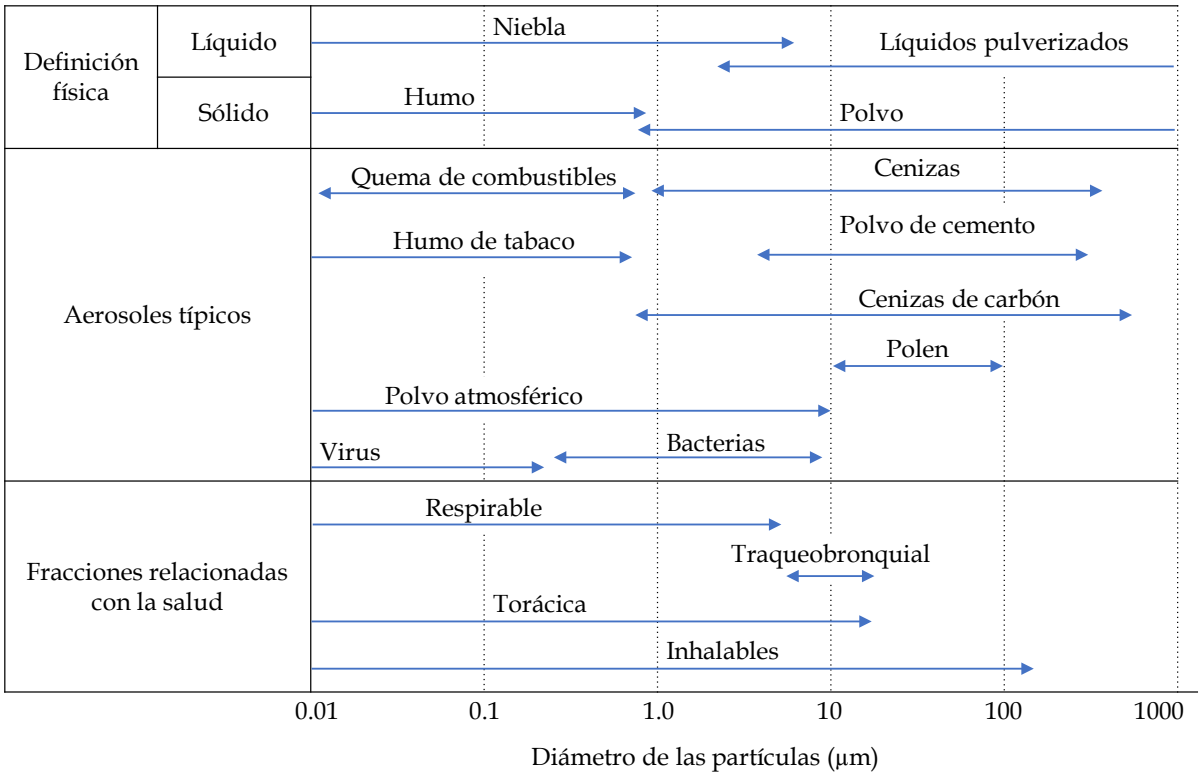

FIG. 1.2. Rangos típicos de tamaños de aerosoles (adaptado de Colbeck and Lazaridis, 2014).

En general, el material particulado atmosférico es polidisperso, es decir, las distribuciones de los tamaños de las partículas presentan un amplio rango. Por ello, las partículas se clasifican según su tamaño basándose en la distribución modal observada. Las modas se definen principalmente en términos de los rangos de tamaños de las partículas asociados a sus mecanismos de formación, fuentes, composición y transporte (Colbeck and Lazaridis, 2014; EPA, 2004a). En la distribución modal se pueden observar varias subcategorías: moda de nucleación, moda Aitken, moda de acumulación y moda gruesa (Fig. 1.3):

- *Moda de nucleación*: Son partículas con diámetros (D_p) menores a 0.1 µm, recién formadas por procesos de nucleación (condensación de un gas sobre sí mismo para formar un núcleo) de precursores gaseosos. La nucleación depende de la concentración del gas precursor, de la humedad relativa y de la temperatura. El límite inferior de tamaño de esta categoría no está muy bien definido, pero está cerca de los 3 nm (Colbeck and Lazaridis, 2014).

- *Moda Aitken*: Son partículas que se originan a partir de la nucleación del vapor o del crecimiento de partículas preexistentes como resultado de un proceso de condensación. Las partículas en la moda Aitken tienen diámetros de entre 0.01 µm y 0.1 µm. Las *partículas ultrafinas* incluyen la moda de nucleación y gran parte son de la moda Aitken (Colbeck and Lazaridis, 2014).

- *Moda de acumulación*: Esta moda incluye a las partículas con diámetros desde 0.1 hasta 3 µm. Las partículas en esta moda se forman por coagulación de partículas más pequeñas o por condensación de los componentes gaseosos como consecuencia de reacciones en fase líquida, que pueden tener lugar en las gotas de agua de las nubes. Durante condiciones de alta humedad relativa, las partículas higroscópicas en la moda de acumulación crecen en tamaño, aumentando la superposición de partículas finas y gruesas (Colbeck and Lazaridis, 2014).

  Las *partículas finas* incluyen las modas de nucleación, Aitken y acumulación. Se forman por procesos de combustión o por reacciones químicas de gases que generan productos con bajas presiones de vapor. Las partículas finas están compuestas por metales (y óxidos de metales), carbono negro o elemental, compuestos orgánicos primarios y secundarios, y iones de sulfato, nitrato, amonio e hidrógeno (Koulouri et al., 2008).

- *Moda gruesa*: Las partículas de esta moda tienen tamaños superiores a 1 µm y se forman por la descomposición mecánica de minerales, material de la corteza terrestre y desechos orgánicos. Además, la moda gruesa puede incluir a la sal marina, el nitrato formado por la reacción del ácido nítrico con el cloruro de sodio, y el sulfato formado por la reacción del dióxido de azufre con partículas básicas (Querol et al., 1998).

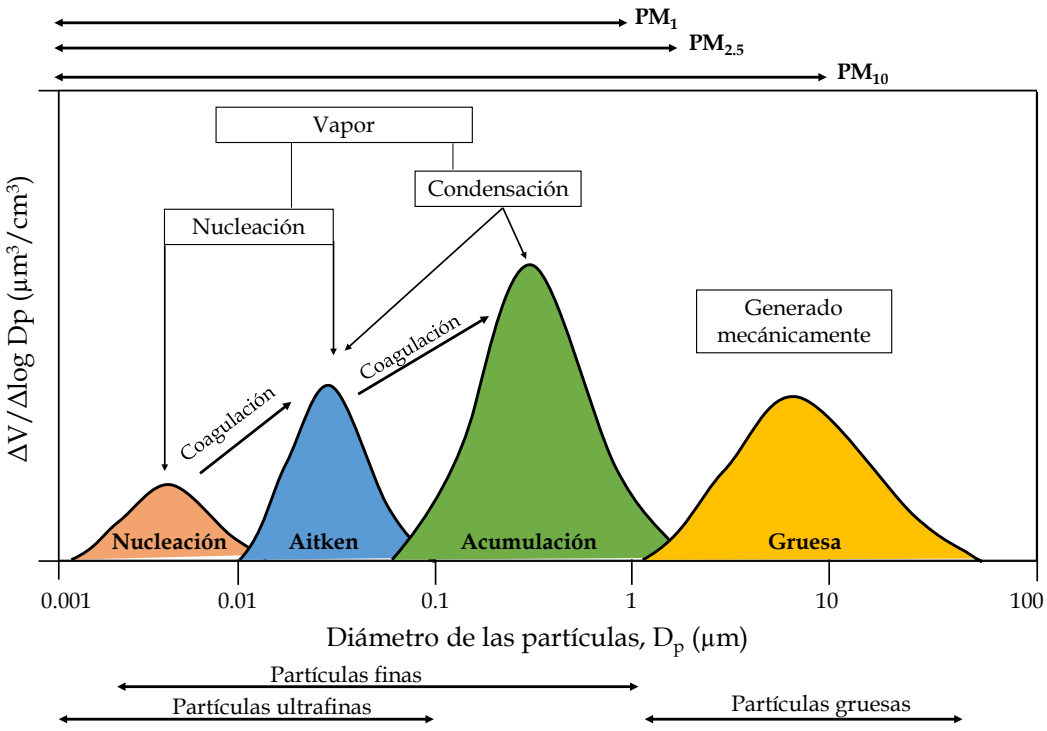

FIG. 1.3. Distribución del tamaño de partículas en función del tamaño, identificación de las modas y diferentes clasificaciones por tamaños. También se muestran los principales mecanismos de formación y crecimiento de las cuatro modas de partículas atmosféricas (adaptado de EPA, 2004).

Las distribuciones modales observadas suelen describirse mediante distribuciones lognormales (Hinds, 2012). Las distribuciones individuales se caracterizan por tres parámetros, como se muestra en la Ecuación 1.1: la concentración numérica, N (cm^{-3}); la desviación geométrica σ_g (adimensional), y el diámetro geométrico medio D_g (µm).

$$\frac{dN}{dlogD} = \frac{N}{\sqrt{2\pi}\, log\, \sigma_g} exp\left[-\frac{(\log D_g - \log D)^2}{2\,(\log \sigma_g)^2}\right] \quad \text{Ecuación 1.1}$$

donde D_g y σ_g están definidos por las Ecuaciones 1.2 y 1.3, respectivamente:

$$D_g = exp\left[\frac{\sum_i (\log D_i n_i)}{N}\right] \quad \text{Ecuación 1.2}$$

donde n_i es el número de partículas del tamaño D_i.

$$\sigma_g = exp\left[\frac{\sum_i n_i (\log D_g - \log D_i)^2}{N-1}\right]^{1/2} \quad \text{Ecuación 1.3}$$

Las distribuciones de las partículas ambientales generalmente corresponden a la suma de m distribuciones lognormales, como se muestra en la Ecuación 1.4.

$$\frac{dN}{dlogD} = \sum_{j=1}^{m} \frac{N_j}{\sqrt{2\pi}\, log \sigma_{g,j}} exp\left[-\frac{(log\, D_{g,j} - \log D)^2}{2(\log \sigma_{g,j})^2}\right] \quad \text{Ecuación 1.4}$$

Las distribuciones de superficie y volumen también se consideran distribuciones lognormales si se admite que las partículas son aproximadamente esféricas. En ese caso, las distribuciones se obtienen al sustituir de la Ecuación 1.4 el número de partículas N_j, por la superficie S_j y el volumen V_j, respectivamente, y el diámetro geométrico medio de la moda $D_{g,j}$ (o el diámetro de la mediana del número de partículas, CMD[2]), por el diámetro de la mediana de la superficie (SMD) y del volumen (VMD), respectivamente.

1.4. MECANISMOS DE FORMACIÓN Y ELIMINACIÓN DE LAS PARTÍCULAS

Las partículas pueden formarse por *nucleación* a partir de material en fase gaseosa y crecer, bien sea por *condensación*, a medida que el material en fase gaseosa se condensa en las partículas existentes, o por *coagulación*, en la que dos partículas se combinan para formar una sola.

La nucleación puede ser de dos tipos: *homogénea* o *heterogénea*. La nucleación homogénea consiste en la formación de nuevas partículas por condensación de gases en ausencia de partículas preexistentes. Debido a que en la atmósfera existen diferentes vapores condensables en bajas concentraciones, el mecanismo predominante de formación de partículas es la nucleación binaria (de dos componentes) o multicomponente (Seinfeld and Pandis, 2016). La nucleación heterogénea o *condensación* tiene lugar cuando las moléculas gaseosas condensan sobre partículas insolubles.

[2] CMD: La media geométrica de la distribución del número de partículas es la media aritmética de la distribución de ln *dp*, que es una distribución normal simétrica y, por lo tanto, la media y la mediana son iguales (siendo *dp* el diámetro de la partícula). Por lo tanto, para la distribución lognormal del número de partículas, D_g es igual a la mediana del diámetro de la distribución del número de partículas (CMD, en inglés *Count Median Diameter*).

El proceso contrario se denomina *evaporación*. Previo a estos procesos se producen frecuentemente los fenómenos de *adsorción* y *desorción,* que implican la retención y expulsión, respectivamente, de los átomos, iones o moléculas en la superficie de las partículas. Estos dos procesos no implican un cambio en el número, pero sí en la superficie, volumen y en la masa de la población de aerosoles.

Los aerosoles en la atmósfera pueden colisionar como resultado del movimiento browniano o de fuerzas hidrodinámicas, eléctricas o gravitacionales. Estas colisiones originan la *coagulación* de partículas, donde las partículas primarias que colisionan se fusionan y pierden su identidad, o en la *aglomeración*, donde retienen su identidad y forma, creando estructuras complejas (Colbeck and Lazaridis, 2014).

Tras su formación y evolución, los aerosoles pueden ser eliminados de la atmósfera principalmente mediante dos mecanismos: *deposición seca y deposición húmeda*.

- **Deposición seca**

La deposición seca ocurre cuando las especies gaseosas y/o particuladas son transportadas desde la atmósfera hacia las superficies (suelos, monumentos, lagos, etc.), sin la intervención del agua. La deposición seca depende principalmente de la turbulencia atmosférica, las propiedades químicas de las especies y la naturaleza de la superficie en sí. El proceso de deposición seca, tanto de gases como de partículas, es generalmente descrito en tres pasos: *i*) el transporte aerodinámico a través de la atmósfera hasta una capa muy delgada de aire estancado adyacente a la superficie; *ii*) el transporte molecular (gases) o Browniano (partículas) a través de la capa delgada de aire estancado o *subcapa cuasi-laminar* hacia la superficie, y *iii*) la captación en la superficie (Seinfeld and Pandis, 2016).

En la subcapa cuasi-laminar, el transporte ocurre por *difusión* (gases) y *sedimentación* (partículas) (Seinfeld and Pandis, 2016). La sedimentación es la forma más simple de deposición seca. En general, la deposición de partículas gruesas está dominada por la sedimentación gravitacional, mientras que las partículas finas se asientan lentamente, y son transportadas por el movimiento Browniano.

- **Deposición húmeda**

La deposición húmeda se refiere al proceso natural por el cual el material atmosférico es barrido (*scavenging*) por hidrometeoros atmosféricos (gotas de nubes, neblina, lluvia, nieve) y, como consecuencia, depositado en la superficie de la Tierra. Los términos *in-cloud* y *below-cloud* son generalmente utilizados para referirse a los procesos de *scavenging*. *In-cloud scavenging* hace referencia a la eliminación del aerosol en el interior de la nube, mientras que *below-cloud scavenging* se refiere a los procesos de remoción por debajo de la nube debido a la lluvia, nieve, etc. (Celle-Jeanton et al., 2009; D. Xu et al., 2017).

Durante la formación de las nubes (*in-cloud*), la concentración del aerosol se ve afectada principalmente por dos mecanismos de *scavenging*: nucleación e impactación. El proceso por el que una fracción del aerosol, que actúa como núcleo de condensación (CNN, del inglés *Cloud Condensation Nuclei*), se activa y crece libremente por difusión del vapor se denomina s*cavenging*

por nucleación. Este proceso determina la composición inicial de las nubes (Levin et al., 2003). Posteriormente, ocurren una serie de procesos adicionales como reacciones químicas en la fase acuosa, colisiones entre los aerosoles intersticiales y las gotas de las nubes y unión de las gotas de las nubes, que pueden modificar la composición de la nube. Los gases solubles como el HNO_3, el NH_3 y el SO_2, pueden disolverse dentro de las gotas, creando un medio para una serie de reacciones en fase acuosa (Kumar, 1986; Seinfeld and Pandis, 2016).

A medida que las gotas de lluvia caen a la superficie terrestre (*below-cloud*), se producen una serie de interacciones adicionales entre las gotas de lluvia y el aerosol, causando la eliminación de material de la atmósfera. Por ello, la composición química del agua de lluvia proporciona información sobre la contribución relativa de las diferentes fuentes de contaminantes atmosféricos en una localidad específica (ej. Arsene et al., 2007; Godoy-Silva et al., 2017; Martins et al., 2019; Nadzir et al., 2017; Uchiyama et al., 2017; Xu et al., 2015).

El proceso de lavado *below-cloud* está influenciado por la distribución de tamaño de las gotas de lluvia y del aerosol, la intensidad y duración del episodio de lluvia y la eficiencia de las colisiones entre las gotas y del aerosol atmosférico (Blanco-Alegre et al., 2018; Fredericks and Saylor, 2019; Roy et al., 2019; X. Xu et al., 2017).

La eficacia de los procesos de *below-cloud scavenging* se estudia mediante el cálculo de diferentes parámetros. Dos de los más utilizados son el *coeficiente de scavenging*, λ [s^{-1}], que indica el cambio relativo por segundo, de la concentración C de partículas de un diámetro determinado (Ecuación 1.5) (Blanco-Alegre et al., 2018; Seinfeld and Pandis, 2016; Zikova and Zdimal, 2016); y el *scavenging ratio W*, que expresa la relación entre la concentración de los contaminantes en el agua de lluvia y en el aire (Ecuación 1.6) (Cerqueira et al., 2010; Jaffrezo and Colin, 1988; Kasper-Giebl et al., 1999; Kulshrestha et al., 2009).

$$\lambda = \frac{1}{t_1 - t_0} ln \frac{C_1}{C_0} \qquad \text{Ecuación 1.5}$$

donde C_1 y C_0 representan la concentración de partículas de determinado diámetro en los instantes t_1 y t_0, respectivamente.

$$W = \frac{[C]_{lluvia}}{[C]_{aire}} \times \rho \qquad \text{Ecuación 1.6}$$

donde $[C]_{lluvia}$ y $[C]_{aire}$ hacen referencia a la concentración de la especie objeto de estudio en el agua de lluvia y en el aire, respectivamente, y ρ es la densidad del aire.

1.5. PROPIEDADES ÓPTICAS DE LOS AEROSOLES

Si un campo de partículas atmosféricas es atravesado por radiación electromagnética, parte de esa radiación es transmitida, otra parte es absorbida y parte sufre *scattering* (dispersión) debido a las partículas presentes. La luz dispersada por una partícula depende de su tamaño y forma, de la longitud de onda incidente, del índice de refracción de la partícula y del medio que lo rodea (Ebert et al., 2002; Kandler et al., 2007; Wang and Rood, 2008). Los procesos de *scattering* y

absorción no son independientes entre sí y son utilizados para describir las propiedades ópticas de las partículas a través del índice de refracción complejo, *m* (Ecuación 1.7).

$$m = n - ki \qquad \text{Ecuación 1.7}$$

donde la parte real del índice, *n*, representa el *scattering* y la parte imaginaria, *k*, determina la capacidad de absorción de la radiación por parte de la partícula. El índice de refracción es una magnitud dependiente de la composición química del aerosol y de la longitud de onda incidente.

La dispersión de la luz causada por partículas de tamaños mucho menores que la longitud de onda incidente, es descrita mediante la teoría de dispersión de Rayleigh. La magnitud de la dispersión de Rayleigh, medida con el coeficiente de *scattering*, depende de la densidad del gas y de la partícula en la atmósfera y puede variar entre 9 Mm^{-1} y 11 Mm^{-1}, dependiendo principalmente de la altura del lugar de muestreo (EPA, 2004a). Por otra parte, la teoría de Mie permite calcular la dispersión y absorción de la radiación causada por las partículas con tamaños del orden de la longitud de onda incidente.

La dispersión y absorción de la radiación dependen del parámetro de tamaño (x), que establece la relación entre el radio de la partícula y la longitud de onda de la radiación incidente ($2\pi r/\lambda$), así como del índice de refracción (m). La dispersión de la radiación depende también del ángulo de *scattering* Θ (formado por la dirección de propagación del rayo incidente y la de un determinado haz dispersado) y de la función de fase $P(\Theta; \lambda)$, que es una función adimensional que describe su distribución angular.

Los aerosoles pueden influenciar el balance radiativo atmosférico mediante la dispersión y absorción de la radiación (Calvo et al., 2010; Obregón et al., 2015; Streets et al., 2013). El efecto radiativo de los aerosoles en la atmósfera se estima mediante el uso de modelos, que utilizan propiedades ópticas como el albedo de *scattering* simple *SSA*, el espesor óptico de aerosoles $\delta(\lambda)$ (AOD, del inglés *Aerosol Optical Depth*) y el parámetro de asimetría g. El SSA determina el signo del forzamiento radiativo, mientras que el parámetro de asimetría y el espesor óptico determinan la intensidad del forzamiento (Dubovik et al., 2002).

La contribución de la absorción más el *scattering* (es decir, la extinción) se determina a través del SSA, que depende de la longitud de onda incidente y del índice de refracción de las partículas (Bohren and Huffman, 1983; Calvo et al., 2010). El parámetro de asimetría es una estimación de la direccionalidad de la función de fase, es decir, de la asimetría de la radiación redistribuida y toma valores entre -1 y 1. El AOD representa la masa total de aerosoles en la columna atmosférica y su dependencia espectral es parametrizada utilizando la ley de Ångström (1964):

$$\delta = \beta\lambda^{-\alpha} \qquad \text{Ecuación 1.8}$$

donde α es el exponente de Ångström, relacionado con el tamaño de las partículas, que define las características espectrales de los aerosoles, mientras que β es el parámetro de turbiedad, que está relacionado con la concentración de partículas en la columna vertical atmosférica y representa el AOD a 1 μm. El parámetro α toma valores entre 0 y 4, donde 0 indica el predominio de partículas de tamaño grande y un valor de 4 indica el predominio de partículas de tamaño pequeño. Por

otra parte, los valores de β pueden variar en 0 (atmósfera absolutamente limpia) y 0.5 (atmósfera con una gran carga de aerosoles).

1.6. IMPACTO DE LOS CONTAMINANTES ATMOSFÉRICOS SOBRE EL CLIMA

Los efectos que tienen los contaminantes atmosféricos sobre el clima son complejos y varían dependiendo de las diferentes actividades humanas y los procesos naturales, del nivel total de emisiones y de su composición. El ozono troposférico, originado por las emisiones de óxidos de nitrógeno y diversas formas de carbono incompletamente oxidado, y los aerosoles como el carbono negro y el carbono orgánico secundario, que tienen un impacto relativamente rápido sobre el clima (IPCC, 2014a).

El PM puede tener efectos directos e indirectos sobre el clima. La extinción de la luz, como consecuencia de la dispersión múltiple y/o la absorción de la radiación solar por los aerosoles atmosféricos, es un efecto directo del aerosol sobre el clima. En algunos casos, la presencia de partículas puede aumentar la reflectancia de la energía solar que escapa de la parte superior de la atmósfera, causando un enfriamiento neto de la tierra. En otros casos, los aerosoles absorbentes como el BC y el polvo mineral, pueden aumentar la absorción de la radiación, provocando un efecto de calentamiento neto. Según un informe del IPCC (2014b), los aerosoles aportan un forzamiento radiativo neto negativo estimado entre – 1.9 y – 0.1 W m^{-2}. Adicionalmente, la extinción de la luz provocada por los aerosoles también puede causar la reducción de la visibilidad, lo que acarrea graves problemas para el transporte.

Los efectos indirectos están relacionados con los cambios en las nubes, causados por las partículas que sirven como núcleos de condensación. Las características de las nubes en sí mismas también pueden verse afectadas por las emisiones de contaminantes atmosféricos.

1.7. IMPACTO DE LOS CONTAMINANTES ATMOSFÉRICOS SOBRE EL MEDIO AMBIENTE

Ciertas reacciones químicas que ocurren en la atmósfera provocan cambios en las características físicas y químicas de los aerosoles atmosféricos, lo que puede causar una serie de problemas medioambientales como la degradación de la calidad del aire y la destrucción de la capa de ozono, entre otros. Las emisiones de SO_2 y NO_x y su posterior conversión durante el transporte en ácidos sulfúrico y nítrico, respectivamente, así como la emisión de especies ácidas orgánicas, pueden ser incorporadas a la nube y a las gotas que precipitan, causando la disminución del pH del agua de lluvia a valores por debajo de 5.6 (lluvia ácida) (Akpo et al., 2015; Charlson and Rodhe, 1982; Custódio et al., 2014; Radojevic and Tan, 2000). La deposición ácida trae como consecuencia la acidificación del agua terrestre y el subsecuente daño al ecosistema acuático, daños en la vegetación y en los materiales de construcción y estructuras (Seinfeld and Pandis, 2016).

Los bioaerosoles también pueden causar daños importantes en el medio ambiente. Los patógenos de las plantas dispersados a través del aire son responsables de grandes pérdidas económicas en la agricultura, debido al daño que causan a los cultivos.

1.8. IMPACTO DE LOS CONTAMINANTES ATMOSFÉRICOS SOBRE LA SALUD

Los efectos de los aerosoles sobre la salud dependen principalmente del tamaño, composición y concentración de las partículas. En ciudades con altos niveles de contaminación, debido a las emisiones de tráfico e industriales, los niveles de PM_{10}, $PM_{2.5}$, O_3, CO, SO_2 y NO_2 se asocian a una mayor tasa de admisiones hospitalarias por asma, a un mayor riesgo de sufrir problemas neurológicos y psiquiátricos, así como una mayor tasa de mortalidad y morbilidad cardíaca, cardiovascular y pulmonar (Curtis et al., 2006; Díaz et al., 1999; Pascal et al., 2014). Además, diversos estudios sugieren que altos niveles de partículas atmosféricas pueden provocar hipertensión gestacional, preeclampsia, nacimientos prematuros, bajo peso al nacer en los bebés y, posiblemente, muertes fetales e infantiles (Curtis et al., 2006; Kampa and Castanas, 2008; Kim et al., 2015). Los contaminantes atmosféricos, incluidos el PM y los gases procedentes de los motores diésel, se asocian también al cáncer de pulmón (Curtis et al., 2006; Hooper and Kaufman, 2018).

Los bioaerosoles pueden tener efectos infecciosos, alérgicos o tóxicos, causando impactos en la salud humana. Los niveles altos de hongos y polen suelen asociarse a problemas respiratorios como el asma y la rinitis (D'Amato et al., 2007; Fukutomi and Taniguchi, 2015). Por otra parte, varias enfermedades infecciosas de los humanos y de los animales, como la tuberculosis, legionelosis, gripe, sarampión y otras, podrían propagarse por medio de bacterias y virus transportados por el aire. La inhalación de hongos patógenos dispersados por el aire como el *Aspergillus*, el *Cyptococcus* y el *Pneumocystis* spp., pueden causar infecciones asociadas con la mortalidad, especialmente en personas con una función inmunológica deficiente (Fröhlich-Nowoisky et al., 2016).

La inhalación de material particulado induce a respuestas inflamatorias en las vías respiratorias, ocasionando problemas como la falta de aliento (disnea), malestar y dolor en el pecho, tos y sibilancias (Hamanaka and Mutlu, 2018; Kim et al., 2015). Por otra parte, la exposición prolongada a altas concentraciones de partículas finas y ultrafinas en el ambiente está relacionada con un mayor número de partículas retenidas en el pulmón (Brauer et al., 2001). Sin embargo, la respuesta biológica a las partículas es función de la dosis depositada en la región específica de las vías respiratorias, lo que depende de la deposición inicial y la subsiguiente retención de partículas dentro del tracto respiratorio (EPA, 2004b).

El tracto respiratorio humano puede dividirse en tres regiones principales: región extratorácica, región traqueobronquial y región alveolar (Fig. 1.4). La fracción de partículas inhaladas que se depositan en las distintas regiones de las vías respiratorias es determinada principalmente por el tamaño de las partículas. Las partículas con diámetros superiores a 10 μm son retenidas en la región extratorácica, mientras que las de diámetros inferiores a 10 μm son capaces de pasar a la región traqueobronquial. Las partículas con diámetros inferiores a 2.5 μm representan un mayor riesgo para la salud, ya que son capaces de llegar a los alveolos y a la sangre (EPA, 2004b).

La deposición de partículas en el tracto respiratorio puede ser estimada tomando en cuenta el modelo desarrollado por la Organización Internacional de Normalización (ISO, del inglés *International Organization for Standardization*), en el que se establecen diferentes definiciones para

las partículas relacionadas con la región del tracto respiratorio donde se depositan: *i*) la fracción inhalable, que corresponde a la fracción de masa de partículas inhaladas por la nariz y la boca; *ii*) la fracción torácica, definida por la fracción de partículas que penetran más allá de la laringe; *iii*) la fracción extra-torácica, es la fracción de partículas retenidas en la región respiratoria anterior a la laringe y *iv*) la fracción respirable, que corresponde a la fracción de masa de partículas inhaladas que penetra en las vías respiratorias no ciliadas.

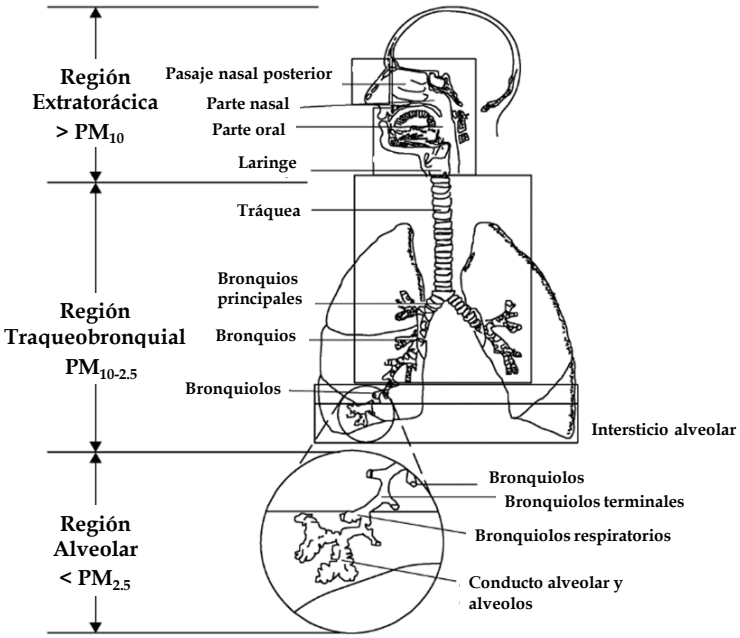

FIG. 1.4. Regiones del tracto respiratorio humano en relación con el acceso del material particulado según su tamaño (adaptado de EPA, 2004b).

1.9. MARCO NORMATIVO

En 1996 se aprobó en Europa la Directiva 96/62/CE sobre *la Evaluación y Gestión de la Calidad del Aire Ambiente*. Esta Directiva es la primera en implementar criterios fijos, objetivos y técnicas de evaluación de la calidad del aire. Durante los años posteriores se desarrollaron diferentes Directivas entre las que se encuentran las 1999/30/CE, 2000/69/CE y 2002/3/CE. En la actualidad, las regulaciones relativas a la calidad del aire en Europa se recogen en dos Directivas:

- Directiva 2008/50/EC del Parlamento Europeo y del Consejo, de 21 de mayo de 2008, relativo a la *Calidad del Aire Ambiente y a una Atmósfera más Limpia en Europa*.

- Directiva 2004/107/EC del Parlamento Europeo y del Consejo, de 15 de diciembre 2004, relativo a *Arsénico, Cadmio, Mercurio, Níquel e Hidrocarburos Aromáticos en Aire Ambiente.*

En España, la base jurídica relativa a la *Protección del Medio Ambiente Atmosférico* data de 1972, año en que se aprobó la Ley 38/1972. Posteriormente, esta ley se adaptó a las necesidades medioambientales europeas para una mejor prevención de los efectos nocivos de los contaminantes atmosféricos sobre la salud humana y el medio ambiente y se integró en los Reales

Decretos 833/1975, 1073/2002, 1796/2003 y 812/2007. Estos Reales Decretos fueron derogados e integrados en la Ley 34/2007 del 15 de noviembre de 2007, referente a la *Protección de la Calidad del Aire y de la Atmósfera*, y del Real Decreto 102/2011 del 28 de enero 2011, relativo a *Mejora de la Calidad del Aire*.

Las directivas y decretos antes mencionados establecen una serie de valores límite permitidos de los contaminantes atmosféricos para la protección de la salud humana. En la Tabla 1.1 se muestran los valores límite para el SO_2, NO_x, NO_2, PM_{10}, $PM_{2.5}$, CO y O_3 establecidos en la Directiva 2008/50/EC y en el Real Decreto 102/2011.

TABLA 1.1. Valores límite para el SO_2, NO_x, NO_2, PM_{10}, $PM_{2.5}$, CO y O_3, para la protección de la salud humana.

Contaminante atmosférico	Valor límite
SO_2	Media horaria: 350 μg m^{-3}. No podrá superarse más de 24 veces por año civil
	Media diaria: 125 μg m^{-3}. No podrá superarse más de 3 veces por año civil
NO_2 y NO_x	Media horaria: 200 μg m^{-3}. No podrá superarse más de 18 veces por año civil
	Media anual: 40 μg m^{-3}
PM_{10}	Media diaria: 50 μg m^{-3}. No podrá superarse más de 35 veces por año civil
	Media anual: 40 μg m^{-3}
CO	Máximo diario de las medias móviles octohorarias: 10 mg m^{-3}
O_3	Máximo diario de las medias móviles octohorarias: 120 μg m^{-3}. No podrá superarse más de 25 días por año civil, promediados en un período de 3 años

En el Artículo 3 del Real Decreto 102/2011, se establece que, tanto las Comunidades Autónomas como las autoridades locales deberán tomar las medidas necesarias para garantizar que las concentraciones de los contaminantes regulados no superen los objetivos establecidos. Asimismo, en el Artículo 24 relativo a los *Planes de Calidad del Aire*, se establece que cuando en determinadas zonas se supere algún valor límite de contaminantes en el aire ambiente, las Comunidades Autónomas españolas aprobarán planes de calidad del aire que permitan respetar el valor límite correspondiente. En este sentido, en la Comunidad Autónoma de Castilla y León aprobó en 2002 la *Estrategia de Control de la Calidad del Aire de Castilla y León 2001-2010*, que tiene como principal objetivo prevenir y reducir la concentración de contaminantes atmosféricos nocivos, en orden a proteger el medio ambiente y la salud humana. Las acciones adoptadas en dicha *Estrategia* son:

- La elaboración de un inventario de emisiones a escala regional, actualizado cada cuatro años.
- La evaluación de las emisiones industriales.
- Promover el uso del transporte público.
- El control de las emisiones de los vehículos.
- Tomar acciones sobre las emisiones de las actividades de producción agropecuaria.
- Tomar acciones preventivas sobre la producción de las instalaciones con mayor capacidad contaminante.
- Realizar programas de asesoramiento y subvenciones a empresas para la reducción de emisiones.
- Realizar campañas de promoción del ahorro energético.

- Promover el uso de energías alternativas.

En cuanto a la normativa de carácter local, debemos señalar que en 2012 se aprobó en León (España) la *Ordenanza Municipal de Protección de la Atmósfera*, que tiene como objetivo regular todas las actividades e instalaciones que puedan producir humo, polvo, gases, vapores y olores en el ámbito municipal, para evitar la contaminación del aire.

La evaluación de las concentraciones de los contaminantes atmosféricos se realiza en León a partir de las mediciones realizadas por la *Red de Calidad del Aire de la Junta de Castilla y León*. De esta forma, desde 1997 la ciudad de León ha contado con cuatro estaciones fijas (Tabla 1.2), donde se realiza la evaluación continua de las concentraciones de cada contaminante según lo según lo estipulado en el Anexo VII del Real Decreto 102/2011 (Tabla 1.3).

TABLA 1.2. Estaciones de la Red de Calidad del Aire de la ciudad de León.

Estación	Ubicación	Tipo	Período	Contaminantes analizados
1	Avenida de San Ignacio de Loyola (05° 35' 14" W 42° 36' 14" N)	Tráfico	enero 1997- actualidad	CO, NO, NO_2, O_3, PM_{10}, SO_2.
2	Plaza de toros de León (05º 34' 17" W 42º 35' 19" N)	Tráfico	enero 1997- agosto 2009	
3	Calle de San Juan de Sahagún (05° 33' 53" W 42° 36' 32" N)	Tráfico + Industrial	enero 2001- mayo 2013	NO, NO_2, O_3, PM_{10}, SO_2.
4	Coto Escolar (05° 33' 59" W 42° 34' 31" N)	Fondo	enero 2010- actualidad	

TABLA 1.3. Métodos de referencia para la evaluación de la concentración de los contaminantes atmosféricos.

Contaminante atmosférico	Método
SO_2	UNE-EN 14212:2013 *Calidad del aire ambiente-Método estándar para medir la concentración de dióxido de azufre por fluorescencia ultravioleta*
NO_2 and NO_x	UNE-EN 14211:2013 *Calidad del aire ambiente-Método estándar para medir la concentración de dióxido de nitrógeno y monóxido de nitrógeno por quimioluminiscencia*
PM_{10}	UNE-EN 12341:1999 *Calidad del aire ambiente-Determinación de la fracción de PM_{10} de las partículas en suspensión - Método de referencia y procedimiento de ensayo sobre el terreno para demostrar la equivalencia de los métodos de medición con el método de referencia*
$PM_{2.5}$	UNE-EN 14907:2006 *Calidad del aire ambiente - Método gravimétrico de medición para la determinación de la fracción de masa $PM_{2.5}$ de las partículas en suspensión*
CO	UNE-EN 14626:2013 *Calidad del aire ambiente-Método estándar para la medición de la concentración de monóxido de carbono por espectrometría infrarroja no dispersiva*
O_3	UNE-EN 14625:2013 *Calidad del aire ambiente-Método estándar para medir la concentración de ozono por fotometría ultravioleta*

Las estaciones 1 y 3 son estaciones de tráfico situadas en una zona residencial urbana con un tráfico medio. En estas zonas, las principales fuentes de contaminación son las emisiones de los vehículos y los dispositivos residenciales que se utilizan para la calefacción y el agua caliente, especialmente en los meses más fríos. La estación 2 estaba situada en una intersección de tráfico

intenso en una zona urbana. Esta estación fue retirada en 2009 por no cumplir los criterios de clasificación y localización de los puntos de evaluación para el muestreo establecidos en el Anexo III del Real Decreto 102/2011. En 2010 el Ayuntamiento de León colocó un cuarto punto de muestreo en el Coto Escolar, que permite cumplir con los criterios de macro y micro implantación establecidos en la legislación vigente. Este último punto está situado en una zona suburbana que no tiene influencia directa de las emisiones vehiculares, industriales o residenciales de la ciudad.

1.10. OBJETIVOS

El desarrollo de esta Memoria de Tesis Doctoral tiene planteados como objetivos principales:

1. Estudiar la evolución temporal de la concentración de contaminantes atmosféricos en la ciudad de León (España), así como su correlación con la concentración de algunos pólenes alergénicos y con ciertos parámetros meteorológicos.

2. Determinar la contribución de las principales fuentes de emisión de partículas biogénicas (a través del estudio de azúcares) y no biogénicas mediante la caracterización química del PM_{10} en León.

3. Analizar el impacto de dos casos particulares de contaminación, uno de origen natural (intrusiones de polvo sahariano en invierno) y otro de origen antrópico (tráfico, durante la transición verano-otoño) en la calidad del aire.

4. Examinar la influencia de la composición química de los aerosoles y de las características físicas de la precipitación en las propiedades físico-químicas del agua de lluvia y, por consiguiente, en el proceso de lavado de diferentes especies químicas, tanto a escala anual como en episodios de corta duración (incendios forestales e intrusión de polvo sahariano).

1.11. ESTRUCTURA DE LA MEMORIA

Esta Tesis Doctoral se estructura de la siguiente manera: en el **Capítulo 1** se presenta una breve introducción teórica, donde se señalan los conceptos más importantes referentes a la contaminación atmosférica, los principales contaminantes y sus fuentes, así como los efectos en el medio ambiente y en la salud humana. En este Capítulo se han introducido los objetivos de esta Memoria y la relevancia de la investigación realizada.

El **Capítulo 2** describe con detalle la metodología utilizada a lo largo de este estudio. Incluye, por un lado, la instrumentación utilizada durante el muestreo del aerosol y bioaerosol (como son los captadores de PM_{10} y polen, y los espectrómetros para determinar las distribuciones de tamaño de las partículas) y, por otro lado, la instrumentación empleada para el estudio de la precipitación (como son el captador de lluvia y el disdrómetro). Además, se recoge información sobre las bases de datos empleadas para el estudio de las variables meteorológicas. También se describen los métodos analíticos y estadísticos utilizados.

Los resultados obtenidos en esta Memoria de Tesis Doctoral se desarrollan entre los Capítulos 3 y 9 de la siguiente forma:

En el **Capítulo 3** se aborda el *Objetivo 1* de esta Tesis a través de un estudio sobre la evolución de la concentración de los contaminantes ambientales gaseosos, CO, SO_2, NO_x y O_3, del PM_{10} y de tres tipos de pólenes, *Fraxinus*, Poaceae y *Populus*, durante las últimas dos décadas en la ciudad de León (España). De esta forma, se pretende evaluar el estado actual de la calidad del aire en León y el impacto que ha tenido a lo largo de las últimas décadas el desarrollo de diferentes normativas europeas y españolas sobre la contaminación atmosférica. El estudio también explora la correlación entre la concentración de diferentes tipos de pólenes y los principales contaminantes atmosféricos y parámetros meteorológicos, lo que permite identificar los principales factores que afectan a la concentración de polen en la atmósfera. Estos resultados se encuentran publicados en la revista *Agricultural and Forest Meteorology (2019), 264, 16–26*.

El *Objetivo 2* se trata en los Capítulos 4 y 5, donde se presenta una descripción detallada de las fuentes de aerosoles y bioaerosoles en la ciudad de León durante la campaña de muestreo realizada entre marzo de 2016 y marzo de 2017. El **Capítulo 4** se dedica a la caracterización química de los aerosoles y al estudio de la contribución de las fuentes de emisión, a través del software *Positive Matrix Factorization* (PMF). También se analiza la relación entre las contribuciones de cada fuente, los tipos de tiempo y las condiciones meteorológicas. Por otra parte, en el **Capítulo 5** se ofrece un estudio detallado de las fuentes de emisión de bioaerosoles, a través del análisis de 17 azúcares presentes en el PM_{10} (arabinosa, fructosa, galactosa, glucosa, ribosa, sucrosa, xilosa, adonitol, arabitol, 2-metileritritol, mioinositol, manitol, sorbitol, xilitol, galactano, levoglucosano y manosano), explorando su relación con los parámetros meteorológicos, con marcadores biológicos (polen y esporas de hongos) y con la composición química de los aerosoles. Ambos capítulos se han redactado en forma de artículos y se han enviado a revistas científicas para su publicación.

Los Capítulos 6 y 7 estudian el impacto en la calidad del aire y en la salud humana de dos fuentes específicas de aerosoles en León: el tráfico, como fuente antropogénica, y la intrusión de polvo sahariano, como fuente natural, a fin de cumplimentar el *Objetivo 3*. En el **Capítulo 6** se analiza la variación temporal de la distribución de tamaño de los aerosoles en León entre agosto y octubre de 2012 en una zona urbana, con el fin de identificar los cambios asociados a la transición del verano al otoño. Este período incluye el fin de las vacaciones de verano y el reinicio de las actividades en la ciudad, por lo que se investiga principalmente el impacto de las emisiones de tráfico en la ciudad de León. Los resultados de este estudio se encuentran publicados en *Air Quality, Atmosphere & Health (2018), 11, 505–520*. Por otra parte, en el **Capítulo 7** se realiza un estudio descriptivo de dos eventos inusuales de intrusión de polvo sahariano, que afectaron a la calidad del aire en León, en los meses de febrero de 2016 y de 2017. Estos eventos se estudiaron teniendo en cuenta diferentes aspectos, entre los que se incluyen: condiciones sinópticas típicas, composición química de los aerosoles, distribución del tamaño de las partículas, concentración de polen, espesor óptico y forzamiento radiativo (mediante el modelo GAME, *Global Atmospheric ModEl*). Este estudio se encuentra publicado en *Science of the Total Environment (2019), 669, 213–228*. Asimismo, en ambos capítulos se analizó la penetración de las partículas en las vías respiratorias estudiando las fracciones inhalables, torácicas, traqueobronquiales y respirables, de acuerdo con la Norma ISO 7708:1995.

Para cumplir con el *Objetivo 4*, en los Capítulos 8 y 9 se examina el proceso de lavado de los aerosoles por la lluvia, a partir de los datos obtenidos durante la campaña de muestreo simultánea de aerosoles y precipitación, de un año de duración (marzo 2016- marzo 2017) en León (España). En el **Capítulo 8**, se presenta un estudio para establecer modelos lineales de predicción de la composición química del agua de lluvia, de la ratio de *scavenging* y de los coeficientes de *scavenging*, mediante los parámetros físicos de las gotas de lluvia obtenidos por medio del disdrómetro, y mediante las propiedades químicas de los aerosoles. Este estudio se encuentra en fase de revisión en la revista *Environmental Research*. Por otra parte, en el **Capítulo 9**, se estudia el impacto en la composición del agua de lluvia de dos eventos de transporte de aerosoles: *i*) un episodio de incendios forestales masivos que se produjo en el oeste de la Península Ibérica en agosto de 2016, cuyos penachos alcanzaron a la ciudad de León; y *ii*) una intrusión de polvo sahariano invernal que llegó a León en febrero de 2017. Este estudio se ha remitido para su posible publicación y se encuentra en fase avanzada de revisión en la revista *Science of the Total Environment*.

El **Capítulo 10** se glosan las conclusiones principales extraídas de este trabajo, así como las posibles aplicaciones y perspectivas futuras, que perfilan un panorama de potenciales líneas de investigación enlazadas con las materias que se han discutido en esta tesis.

Por último, en la sección de anexos, se recoge el material suplementario correspondiente a los Capítulos 3, 7 y 8.

1.12. REFERENCIAS

Akpo, A.B., Galy-Lacaux, C., Laouali, D., Delon, C., Liousse, C., Adon, M., Gardrat, E., Mariscal, A., Darakpa, C., 2015. Precipitation chemistry and wet deposition in a remote wet savanna site in West Africa: Djougou (Benin). Atmos. Environ. 115, 110–123. doi:10.1016/j.atmosenv.2015.04.064

Alastuey, A., Querol, X., Aas, W., Lucarelli, F., Pérez, N., Moreno, T., Cavalli, F., Areskoug, H., Balan, V., Catrambone, M., Ceburnis, D., Cerro, J.C., Conil, S., Gevorgyan, L., Hueglin, C., Imre, K., Jaffrezo, J.-L., Leeson, S.R., Mihalopoulos, N., Mitosinkova, M., Dowd, C.D., Pey, J., Putaud, J.-P., Riffault, V., Ripoll, A., Sciare, J., Sellegri, K., Spindler, G., Yttri, K.E., 2016. Geochemistry of PM10 over Europe during the EMEP intensive measurement periods in summer 2012 and winter 2013. Atmos. Chem. Phys. 16, 6107–6129. doi:10.5194/acp-16-6107-2016

Alastuey, A., Querol, X., Rodríguez, S., Plana, F., Lopez-Soler, A., Ruiz, C., Mantilla, E., 2004. Monitoring of atmospheric particulate matter around sources of secondary inorganic aerosol. Atmos. Environ. 38, 4979–4992. doi:10.1016/j.atmosenv.2004.06.026

Alonso-Blanco, E., Calvo, A.I., Fraile, R., Castro, A., 2012. The Influence of Wildfires on Aerosol Size Distributions in Rural Areas. Sci. World J. 2012, 1–13. doi:10.1100/2012/735697

Alves, C.A., Lopes, D.J., Calvo, A.I., Evtyugina, M., Rocha, S., Nunes, T., 2015. Emissions from Light-Duty Diesel and Gasoline in-use Vehicles Measured on Chassis Dynamometer Test Cycles. Aerosol Air Qual. Res. 15, 99–116. doi:10.4209/aaqr.2014.01.0006

Alves, C.A., Vicente, A., Monteiro, C., Gonçalves, C., Evtyugina, M., Pio, C., 2011. Emission of

trace gases and organic components in smoke particles from a wildfire in a mixed-evergreen forest in Portugal. Sci. Total Environ. 409, 1466–1475. doi:10.1016/j.scitotenv.2010.12.025

Analitis, A., Katsouyanni, K., Dimakopoulou, K., Samoli, E., Nikoloulopoulos, A.K., Petasakis, Y., Touloumi, G., Schwartz, J., Anderson, H.R., Cambra, K., Forastiere, F., Zmirou, D., Vonk, J.M., Clancy, L., Kriz, B., Bobvos, J., Pekkanen, J., 2006. Short-Term Effects of Ambient Particles on Cardiovascular and Respiratory Mortality. Epidemiology 17, 230–233. doi:10.1097/01.ede.0000199439.57655.6b

Ångström, A., 1964. The parameters of atmospheric turbidity. Tellus 16, 64–75. doi:10.3402/tellusa.v16i1.8885

Arsene, C., Olariu, R.I., Mihalopoulos, N., 2007. Chemical composition of rainwater in the northeastern Romania, Iasi region (2003–2006). Atmos. Environ. 41, 9452–9467. doi:10.1016/j.atmosenv.2007.08.046

Atkinson, R., 2000. Atmospheric chemistry of VOCs and NOx. Atmos. Environ. 34, 2063–2101. doi:10.1016/S1352-2310(99)00460-4

Bauer, H., Claeys, M., Vermeylen, R., Schueller, E., Weinke, G., Berger, A., Puxbaum, H., 2008. Arabitol and mannitol as tracers for the quantification of airborne fungal spores. Atmos. Environ. 42, 588–593. doi:10.1016/j.atmosenv.2007.10.013

Bernstein, J.A., Alexis, N., Barnes, C., Bernstein, I.L., Nel, A., Peden, D., Diaz-Sanchez, D., Tarlo, S.M., Williams, P.B., Bernstein, J.A., 2004. Health effects of air pollution. J. Allergy Clin. Immunol. 114, 1116–1123. doi:10.1016/j.jaci.2004.08.030

Blanco-Alegre, C., Castro, A., Calvo, A.I., Oduber, F., Alonso-Blanco, E., Fernández-González, D., Valencia-Barrera, R.M., Vega-Maray, A.M., Fraile, R., 2018. Below-cloud scavenging of fine and coarse aerosol particles by rain: The role of raindrop size. Q. J. R. Meteorol. Soc. 144, 2715–2726. doi:10.1002/qj.3399

Bohren, C.F., Huffman, D.R., 1983. Absorption and Scattering of Light by Small Particles. Wiley, Weinheim, Germany. doi:10.1002/9783527618156

Bond, T.C., Covert, D.S., Kramlich, J.C., Larson, T. V, Charlson, R.J., 2002. Primary particle emissions from residential coal burning: Optical properties and size distributions. J. Geophys. Res. Atmos. 107, ICC 9-1-ICC 9-14. doi:10.1029/2001JD000571

Brauer, M., Avila-Casado, C., Fortoul, T.I., Vedal, S., Stevens, B., Churg, A., 2001. Air pollution and retained particles in the lung. Environ. Health Perspect. 109, 1039–1043. doi:10.1289/ehp.011091039

Brunekreef, B., Holgate, S.T., 2002. Air pollution and health. Lancet 360, 1233–1242. doi:10.1016/S0140-6736(02)11274-8

Burshtein, N., Lang-Yona, N., Rudich, Y., 2011. Ergosterol, arabitol and mannitol as tracers for biogenic aerosols in the eastern Mediterranean. Atmos. Chem. Phys. 11, 829–839. doi:10.5194/acp-11-829-2011

Calvo, A.I., Alves, C., Castro, A., Pont, V., Vicente, A.M., Fraile, R., 2013. Research on aerosol sources and chemical composition: Past, current and emerging issues. Atmos. Res. 120–121, 1–28. doi:10.1016/j.atmosres.2012.09.021

Calvo, A.I., Pont, V., Castro, A., Mallet, M., Palencia, C., Roger, J.C., Dubuisson, P., Fraile, R., 2010. Radiative forcing of haze during a forest fire in Spain. J. Geophys. Res. 115, D08206. doi:10.1029/2009JD012172

Calvo, A.I., Pont, V., Liousse, C., Dupré, B., Mariscal, A., Zouiten, C., Gardrat, E., Castera, P., Lacaux, C.G., Castro, A., Fraile, R., 2008. Chemical composition of urban aerosols in Toulouse, France during CAPITOUL experiment. Meteorol. Atmos. Phys. 102, 307–323. doi:10.1007/s00703-008-0319-2

Castro, A., Calvo, A.I., Blanco-Alegre, C., Oduber, F., Alves, C., Coz, E., Amato, F., Querol, X., Fraile, R., 2018. Impact of the wood combustion in an open fireplace on the air quality of a living room: Estimation of the respirable fraction. Sci. Total Environ. 628–629, 169–176. doi:10.1016/j.scitotenv.2018.02.001

Celle-Jeanton, H., Travi, Y., Loÿe-Pilot, M.-D., Huneau, F., Bertrand, G., 2009. Rainwater chemistry at a Mediterranean inland station (Avignon, France): Local contribution versus long-range supply. Atmos. Res. 91, 118–126. doi:10.1016/j.atmosres.2008.06.003

Cerón-Bretón, J.G., Cerón-Bretón, R.M., Ramírez-Lara, E., Rojas-Domínguez, L., Vadillo-Saénz, M.S., Guzmán-Mar, J.L., 2013. Measurements of Atmospheric Pollutants (Aromatic Hydrocarbons , O3, NOx, NO, NO2, CO, and SO2) in ambient air of a site located at the northeast of Mexico during summer 2011. WSEAS Trans. Syst. 12.

Cerqueira, M., Pio, C., Legrand, M., Puxbaum, H., Kasper-Giebl, A., Afonso, J., Preunkert, S., Gelencsér, A., Fialho, P., 2010. Particulate carbon in precipitation at European background sites. J. Aerosol Sci. 41, 51–61. doi:10.1016/j.jaerosci.2009.08.002

Chang, M.C.O., Chow, J.C., Watson, J.G., Hopke, P.K., Yi, S.M., England, G.C., 2004. Measurement of ultrafine particle size distributions from coal-, oil-, and gas-fired stationary combustion sources. J. Air Waste Manag. Assoc. 54, 1494–1505. doi:10.1080/10473289.2004.10471010

Charlson, R.J., Rodhe, H., 1982. Factors controlling the acidity of natural rainwater. Nature 295, 683–685. doi:10.1038/295683a0

Chen, J., Liu, G., Kang, Y., Wu, B., Sun, R., Zhou, C., Wu, D., 2013. Atmospheric emissions of F, As, Se, Hg, and Sb from coal-fired power and heat generation in China. Chemosphere 90, 1925–1932. doi:10.1016/j.chemosphere.2012.10.032

Choobari, O.A., Zawar-Reza, P., Sturman, A., 2014. The global distribution of mineral dust and its impacts on the climate system: A review. Atmos. Res. 138, 152–165. doi:10.1016/j.atmosres.2013.11.007

Colbeck, I., 2008. Environmental Chemistry of Aerosols. Blackwell Publishing Ltd.

Colbeck, I., Lazaridis, M., 2014. Aerosol Science: Technology and Applications. John Wiley & Sons Ltd.

Cox, C.S., Wathes, C.M., 1995. Bioaerosols Handbook. Lewis Publishers.

Cox, R.A., 1974. Particle formation from homogeneous reactions of sulphur dioxide and nitrogen dioxide. Tellus 26, 235–240. doi:10.3402/tellusa.v26i1-2.9782

Curtis, L., Rea, W., Smith-Willis, P., Fenyves, E., Pan, Y., 2006. Adverse health effects of outdoor air pollutants. Environ. Int. 32, 815–830. doi:10.1016/j.envint.2006.03.012

Custódio, D., Cerqueira, M., Fialho, P., Nunes, T., Pio, C., Henriques, D., 2014. Wet deposition of particulate carbon to the Central North Atlantic Ocean. Sci. Total Environ. 496, 92–99. doi:10.1016/j.scitotenv.2014.06.103

d'Almeida, G.A., Schütz, L., 1983. Number, Mass and Volume Distributions of Mineral Aerosol and Soils of the Sahara. J. Clim. Appl. Meteorol. 22, 233–243. doi:10.1175/1520-0450(1983)022<0233:NMAVDO>2.0.CO;2

D'Amato, G., Cecchi, L., Bonini, S., Nunes, C., Annesi-Maesano, I., Behrendt, H., Liccardi, G., Popov, T., van Cauwenberge, P., 2007. Allergenic pollen and pollen allergy in Europe. Allergy 62, 976–990. doi:10.1111/j.1398-9995.2007.01393.x

Denjean, C., Cassola, F., Mazzino, A., Triquet, S., Chevaillier, S., Grand, N., Bourrianne, T., Momboisse, G., Sellegri, K., Schwarzenbock, A., Freney, E., Mallet, M., Formenti, P., 2016. Size distribution and optical properties of mineral dust aerosols transported in the western Mediterranean. Atmos. Chem. Phys. 16, 1081–1104. doi:10.5194/acp-16-1081-2016

Després, V.R., Alex Huffman, J., Burrows, S.M., Hoose, C., Safatov, A.S., Buryak, G., Fröhlich-Nowoisky, J., Elbert, W., Andreae, M.O., Pöschl, U., Jaenicke, R., 2012. Primary biological aerosol particles in the atmosphere: A review. Tellus, Ser. B Chem. Phys. Meteorol. 64. doi:10.3402/tellusb.v64i0.15598

Díaz, J., García, R., Ribera, P., Alberdi, J.C., Hernández, E., Pajares, M.S., Otero, A., 1999. Modeling of air pollution and its relationship with mortality and morbidity in Madrid, Spain. Int. Arch. Occup. Environ. Health 72, 366–376. doi:10.1007/s004200050388

Dubovik, O., Holben, B., Eck, T.F., Smirnov, A., Kaufman, Y.J., King, M.D., Tanré, D., Slutsker, I., 2002. Variability of Absorption and Optical Properties of Key Aerosol Types Observed in Worldwide Locations. J. Atmos. Sci. 59, 590–608. doi:10.1175/1520-0469(2002)059<0590:VOAAOP>2.0.CO;2

Ebert, M., Weinbruch, S., Rausch, A., Gorzawski, G., Hoffmann, P., Wex, H., Helas, G., 2002. Complex refractive index of aerosols during LACE 98 as derived from the analysis of individual particles. J. Geophys. Res. Atmos. 107, 1–15. doi:10.1029/2000JD000195

Elminir, H.K., 2005. Dependence of urban air pollutants on meteorology. Sci. Total Environ. 350, 225–237. doi:10.1016/j.scitotenv.2005.01.043

EPA, 2004a. Air Quality Criteria for Particulate Matter. Volume I.

EPA, 2004b. Air Quality Criteria for Particulate Matter. Volume II.

Escudero, M., Querol, X., Ávila, A., Cuevas, E., 2007. Origin of the exceedances of the European daily PM limit value in regional background areas of Spain. Atmos. Environ. 41, 730–744. doi:10.1016/j.atmosenv.2006.09.014

Fernández-Camacho, R., de la Rosa, J.D., Sánchez de la Campa, A.M., 2016. Trends and sources vs air mass origins in a major city in South-western Europe: Implications for air quality management. Sci. Total Environ. 553, 305–315. doi:10.1016/j.scitotenv.2016.02.079

Fitzgerald, J.W., 1991. Marine aerosols: A review. Atmos. Environ. Part A. Gen. Top. 25, 533–545. doi:10.1016/0960-1686(91)90050-H

Formenti, P., Elbert, W., Maenhaut, W., Haywood, J., Andreae, M.O., 2003. Chemical composition

of mineral dust aerosol during the Saharan Dust Experiment (SHADE) airborne campaign in the Cape Verde region, September 2000. J. Geophys. Res. 108, 8576. doi:10.1029/2002JD002648

Fredericks, S., Saylor, J.R., 2019. Experimental study of drop shape and wake effects on particle scavenging for non-evaporating drops using ultrasonic levitation. J. Aerosol Sci. 127, 1–17. doi:10.1016/j.jaerosci.2018.10.001

Fröhlich-Nowoisky, J., Kampf, C.J., Weber, B., Huffman, J.A., Pöhlker, C., Andreae, M.O., Lang-Yona, N., Burrows, S.M., Gunthe, S.S., Elbert, W., Su, H., Hoor, P., Thines, E., Hoffmann, T., Després, V.R., Pöschl, U., 2016. Bioaerosols in the Earth system: Climate, health, and ecosystem interactions. Atmos. Res. 182, 346–376. doi:10.1016/j.atmosres.2016.07.018

Fu, P., Kawamura, K., Kobayashi, M., Simoneit, B.R.T., 2012. Seasonal variations of sugars in atmospheric particulate matter from Gosan, Jeju Island: Significant contributions of airborne pollen and Asian dust in spring. Atmos. Environ. 55, 234–239. doi:10.1016/j.atmosenv.2012.02.061

Fukutomi, Y., Taniguchi, M., 2015. Sensitization to fungal allergens: Resolved and unresolved issues. Allergol. Int. 64, 321–331. doi:10.1016/j.alit.2015.05.007

Godoy-Silva, D., Nogueira, R.F.P., Campos, M.L.A.M., 2017. A 13-year study of dissolved organic carbon in rainwater of an agro-industrial region of São Paulo state (Brazil) heavily impacted by biomass burning. Sci. Total Environ. 609, 476–483. doi:10.1016/j.scitotenv.2017.07.145

Gonçalves, C., Figueiredo, B.R., Alves, C.A., Cardoso, A.A., da Silva, R., Kanzawa, S.H., Vicente, A.M., 2016. Chemical characterisation of total suspended particulate matter from a remote area in Amazonia. Atmos. Res. 182, 102–113. doi:10.1016/j.atmosres.2016.07.027

Goudie, A.S., 2014. Desert dust and human health disorders. Environ. Int. 63, 101–113. doi:10.1016/j.envint.2013.10.011

Gugamsetty, B., Wei, H., Liu, C.-N., Awasthi, A., Hsu, S.-C., Tsai, C.-J., Roam, G.-D., Wu, Y.-C., Chen, C.-F., 2012. Source Characterization and Apportionment of PM10, PM2.5 and PM0.1 by Using Positive Matrix Factorization. Aerosol Air Qual. Res. 12, 476–491. doi:10.4209/aaqr.2012.04.0084

Gurjar, B.R., Ravindra, K., Nagpure, A.S., 2016. Air pollution trends over Indian megacities and their local-to-global implications. Atmos. Environ. 142, 475–495. doi:10.1016/j.atmosenv.2016.06.030

Hamanaka, R.B., Mutlu, G.M., 2018. Particulate Matter Air Pollution: Effects on the Cardiovascular System. Front. Endocrinol. (Lausanne). 9, 1–15. doi:10.3389/fendo.2018.00680

Hewitt, C.N., Jackson, A. V., 2008. Handbook of Atmospheric Science, Handbook of Atmospheric Science: Principles and Applications. Blackwell Science Ltd, Malden, MA, USA. doi:10.1002/9780470999318

Hinds, W.C., 2012. Aerosol Technology: Properties, Behavior, and Measurement of Airborne Particles. Wiley.

Hooper, L.G., Kaufman, J.D., 2018. Ambient air pollution and clinical implications for susceptible populations. Ann. Am. Thorac. Soc. 15, S64–S68. doi:10.1513/AnnalsATS.201707-574MG

International Organization for Standardization, 1995. ISO 7708: 1995 Air quality -Particle size

fraction definitions for health-related sampling. ISO Publications, 1st edition, 1995-04-01.

IPCC, 2014a. Climate Change 2014 Part A: Global and Sectoral Aspects. Working group II contribution to the fifth assessment report of the intergovernmental panel on climate change, Climate Change 2014: Impacts, Adaptation, and Vulnerability: Part A: Global and Sectorial Aspects.

IPCC, 2014b. Climate Change 2014: Working Group III Contribution to the Fifth Assessment Report of the Intergovernmental Panel on Climate Change, Climate Change 2014 Mitigation of Climate Change. Cambridge University Press. doi:10.1017/CBO9780511546013

Jaffrezo, J.-L., Colin, J.-L., 1988. Rain-aerosol coupling in urban area: Scavenging ratio measurement and identification of some transfer processes. Atmos. Environ. 22, 929–935. doi:10.1016/0004-6981(88)90270-3

Jenkin, M.E., Clemitshaw, K.C., 2000. Ozone and other secondary photochemical pollutants: chemical processes governing their formation in the planetary boundary layer. Atmos. Environ. 34, 2499–2527. doi:10.1016/S1352-2310(99)00478-1

Kampa, M., Castanas, E., 2008. Human health effects of air pollution. Environ. Pollut. 151, 362–367. doi:10.1016/j.envpol.2007.06.012

Kandler, K., Benker, N., Bundke, U., Cuevas, E., Ebert, M., Knippertz, P., Rodríguez, S., Schütz, L., Weinbruch, S., 2007. Chemical composition and complex refractive index of Saharan Mineral Dust at Izaña, Tenerife (Spain) derived by electron microscopy. Atmos. Environ. 41, 8058–8074. doi:10.1016/j.atmosenv.2007.06.047

Kandler, K., Schütz, L., Deutscher, C., Ebert, M., Hofmann, H., Jäckel, S., Jaenicke, R., Knippertz, P., Lieke, K., Massling, A., Petzold, A., Schladitz, A., Weinzierl, B., Wiedensohler, A., Zorn, S., Weinbruch, S., 2009. Size distribution, mass concentration, chemical and mineralogical composition and derived optical parameters of the boundary layer aerosol at Tinfou, Morocco, during SAMUM 2006. Tellus, Ser. B Chem. Phys. Meteorol. 61, 32–50. doi:10.1111/j.1600-0889.2008.00385.x

Kasper-Giebl, A., Kalina, M.F., Puxbaum, H., 1999. Scavenging ratios for sulfate, ammonium and nitrate determined at Mt. Sonnblick (3106m a.s.l.). Atmos. Environ. 33, 895–906. doi:10.1016/S1352-2310(98)00279-9

Kim, K., Kabir, E., Kabir, S., 2015. A review on the human health impact of airborne particulate matter. Environ. Int. 74, 136–143. doi:10.1016/j.envint.2014.10.005

Koulouri, E., Saarikoski, S., Theodosi, C., Markaki, Z., Gerasopoulos, E., Kouvarakis, G., Mäkelä, T., Hillamo, R., Mihalopoulos, N., 2008. Chemical composition and sources of fine and coarse aerosol particles in the Eastern Mediterranean. Atmos. Environ. 42, 6542–6550. doi:10.1016/j.atmosenv.2008.04.010

Kulshrestha, U.C., Reddy, L.A.K., Satyanarayana, J., Kulshrestha, M.J., 2009. Real-time wet scavenging of major chemical constituents of aerosols and role of rain intensity in Indian region. Atmos. Environ. 43, 5123–5127. doi:10.1016/j.atmosenv.2009.07.025

Kumar, S., 1986. Reactive scavenging of pollutants by rain: a modeling approach. Atmos. Environ. 20, 1015–1024. doi:10.1016/0004-6981(86)90287-8

Lelieveld, J., Evans, J.S., Fnais, M., Giannadaki, D., Pozzer, A., 2015. The contribution of outdoor air pollution sources to premature mortality on a global scale. Nature 525, 367–371. doi:10.1038/nature15371

Levin, Z., Teller, A., Ganor, E., Graham, B., Andreae, M.O., Maenhaut, W., Falkovich, A.H., Rudich, Y., 2003. Role of aerosol size and composition in nucleation scavenging within clouds in a shallow cold front. J. Geophys. Res. Atmos. 108, 2003JD003647. doi:10.1029/2003JD003647

Lewis, E.R., Lewis, E.R., Lewis, R., Sparks, R.S.J., Karlstrom, K.E., Schwartz, S.E., Hawkesworth, C.J., Union, A.G., 2004. Sea Salt Aerosol Production: Mechanisms, Methods, Measurements, and Models, Geophysical Monograph Series. Wiley.

Lin, C.-C., Chen, S.-J., Huang, K.-L., Hwang, W.-I., Chang-Chien, G.-P., Lin, W.-Y., 2005. Characteristics of Metals in Nano/Ultrafine/Fine/Coarse Particles Collected Beside a Heavily Trafficked Road. Environ. Sci. Technol. 39, 8113–8122. doi:10.1021/es048182a

Maring, H., Savoie, D.L., Izaguirre, M.A., Custals, L., 2003. Mineral dust aerosol size distribution change during atmospheric transport. J. Geophys. Res. 108, 8592. doi:10.1029/2002JD002536

Martins, E.H., Nogarotto, D.C., Mortatti, J., Pozza, S.A., 2019. Chemical composition of rainwater in an urban area of the southeast of Brazil. Atmos. Pollut. Res. 10, 520–530. doi:10.1016/j.apr.2018.10.003

Matthias-Maser, S., 1998. Primary biological aerosol particles: their significance, sources, sampling methods and size distribution in the atmosphere. Atmos. Part. 349–368.

Medeiros, P.M., Conte, M.H., Weber, J.C., Simoneit, B.R.T., 2006. Sugars as source indicators of biogenic organic carbon in aerosols collected above the Howland Experimental Forest, Maine. Atmos. Environ. 40, 1694–1705. doi:10.1016/j.atmosenv.2005.11.001

Nadzir, M.S.M., Lin, C.Y., Khan, M.F., Latif, M.T., Dominick, D., Hamid, H.H.A., Mohamad, N., Maulud, K.N.A., Wahab, M.I.A., Kamaludin, N.F., Lazim, M.A.S.M., 2017. Characterization of rainwater chemical composition after a Southeast Asia haze event: insight of transboundary pollutant transport during the northeast monsoon. Environ. Sci. Pollut. Res. 24, 15278–15290. doi:10.1007/s11356-017-9131-1

Obregón, M.A., Pereira, S., Salgueiro, V., Costa, M.J., Silva, A.M., Serrano, A., Bortoli, D., 2015. Aerosol radiative effects during two desert dust events in August 2012 over the southwestern Iberian Peninsula. Atmos. Res. 153, 404–415. doi:10.1016/j.atmosres.2014.10.007

Organización de las Naciones Unidas, 2018. Las ciudades seguirán creciendo, sobre todo en los países en desarrollo [WWW Document]. URL https://www.un.org/development/desa/es/news/population/2018-world-urbanization-prospects.html (accessed 2.12.20).

Organización Mundial de la Salud, 2018. Ambient (outdoor) air pollution [WWW Document]. URL https://www.who.int/news-room/fact-sheets/detail/ambient-(outdoor)-air-quality-and-health (accessed 2.12.20).

Parlamento Europeo y del Consejo, 2008. Directiva 2008/50/CE: relativa a la calidad del aire ambiente y a una atmósfera más limpia en Europa, Diario Oficial de la Unión Europea.

Pascal, M., Falq, G., Wagner, V., Chatignoux, E., Corso, M., Blanchard, M., Host, S., Pascal, L.,

Larrieu, S., 2014. Short-term impacts of particulate matter (PM10, PM10–2.5, PM2.5) on mortality in nine French cities. Atmos. Environ. 95, 175–184. doi:10.1016/j.atmosenv.2014.06.030

Perfumo, A., Marchant, R., 2010. Global transport of thermophilic bacteria in atmospheric dust. Environ. Microbiol. Rep. 2, 333–339. doi:10.1111/j.1758-2229.2010.00143.x

Polymenakou, P.N., Mandalakis, M., Stephanou, E.G., Tselepides, A., 2008. Particle size distribution of airborne microorganisms and pathogens during an intense African dust event in the eastern Mediterranean. Environ. Health Perspect. 116, 292–296. doi:10.1289/ehp.10684

Qin, Y.M., Tan, H.B., Li, Y.J., Schurman, M.I., Li, F., Canonaco, F., Prévôt, A.S.H., Chan, C.K., 2017. Impacts of traffic emissions on atmospheric particulate nitrate and organics at a downwind site on the periphery of Guangzhou, China. Atmos. Chem. Phys. 17, 10245–10258. doi:10.5194/acp-17-10245-2017

Querol, X., Alastuey, A., Puicercus, J.A., Mantilla, E., Miro, J. V., Lopez-Soler, A., Plana, F., Artiñano, B., 1998. Seasonal evolution of suspended particles around a large coal-fired power station: Particulate levels and sources. Atmos. Environ. 32, 1963–1978. doi:10.1016/S1352-2310(97)00504-9

Querol, X., Viana, M., Alastuey, A., Amato, F., Moreno, T., Castillo, S., Pey, J., de la Rosa, J., Sánchez de la Campa, A., Artíñano, B., Salvador, P., García Dos Santos, S., Fernández-Patier, R., Moreno-Grau, S., Negral, L., Minguillón, M.C., Monfort, E., Gil, J.I., Inza, A., Ortega, L.A., Santamaría, J.M., Zabalza, J., 2007. Source origin of trace elements in PM from regional background, urban and industrial sites of Spain. Atmos. Environ. 41, 7219–7231. doi:10.1016/j.atmosenv.2007.05.022

Radojevic, M., Tan, K.., 2000. Impacts of biomass burning and regional haze on the pH of rainwater in Brunei Darussalam. Atmos. Environ. 34, 2739–2744. doi:10.1016/S1352-2310(99)00339-8

Real Decreto 102/2011, 2011. Real Decreto 102/2011, de 28 de enero, relativo a la mejora de la calidad del aire. Boletín Of. del estado 25, 9574–9626.

Reşitoğlu, İ.A., Altinişik, K., Keskin, A., 2015. The pollutant emissions from diesel-engine vehicles and exhaust aftertreatment systems. Clean Technol. Environ. Policy 17, 15–27. doi:10.1007/s10098-014-0793-9

Rodríguez, S., Querol, X., Alastuey, A., Plana, F., 2002. Sources and processes affecting levels and composition of atmospheric aerosol in the western Mediterranean. J. Geophys. Res. 107, 4777. doi:10.1029/2001JD001488

Roy, A., Chatterjee, A., Ghosh, A., Das, S.K., Ghosh, S.K., Raha, S., 2019. Below-cloud scavenging of size-segregated aerosols and its effect on rainwater acidity and nutrient deposition: A long-term (2009–2018) and real-time observation over eastern Himalaya. Sci. Total Environ. 674, 223–233. doi:10.1016/j.scitotenv.2019.04.165

Samek, L., Stegowski, Z., Furman, L., Fiedor, J., 2017. Chemical content and estimated sources of fine fraction of particulate matter collected in Krakow. Air Qual. Atmos. Heal. 10, 47–52. doi:10.1007/s11869-016-0407-2

Schütz, L., Sebert, M., 1987. Mineral aerosols and source identification. J. Aerosol Sci. 18, 1–10.

doi:10.1016/0021-8502(87)90002-4

Seinfeld, J.H., Pandis, S.N., 2016. Atmospheric Chemistry and Physics: From Air Pollution to Climate Change, 3rd ed. John Wiley & Sons.

Sillman, S., 1999. The relation between ozone, NOx and hydrocarbons in urban and polluted rural environments. Atmos. Environ. 33, 1821–1845. doi:10.1016/S1352-2310(98)00345-8

Simoneit, B.R.T., Elias, V.O., Kobayashi, M., Kawamura, K., Rushdi, A.I., Medeiros, P.M., Rogge, W.F., Didyk, B.M., 2004. Sugars Dominant Water-Soluble Organic Compounds in Soils and Characterization as Tracers in Atmospheric Particulate Matter. Environ. Sci. Technol. 38, 5939–5949. doi:10.1021/es0403099

Simoneit, B.R.T., Schauer, J.J., Nolte, C.G., Oros, D.R., Elias, V.O., Fraser, M.P., Rogge, W.F., Cass, G.R., 1999. Levoglucosan, a tracer for cellulose in biomass burning and atmospheric particles. Atmos. Environ. 33, 173–182.

Streets, D.G., Shindell, D.T., Lu, Z., Faluvegi, G., 2013. Radiative forcing due to major aerosol emitting sectors in China and India. Geophys. Res. Lett. 40, 4409–4414. doi:10.1002/grl.50805

Theodosi, C., Im, U., Bougiatioti, A., Zarmpas, P., Yenigun, O., Mihalopoulos, N., 2010. Aerosol chemical composition over Istanbul. Sci. Total Environ. 408, 2482–2491. doi:10.1016/j.scitotenv.2010.02.039

Thorpe, A., Harrison, R.M., 2008. Sources and properties of non-exhaust particulate matter from road traffic: A review. Sci. Total Environ. 400, 270–282. doi:10.1016/j.scitotenv.2008.06.007

Tian, H.Z., Wang, Y., Xue, Z.G., Cheng, K., Qu, Y.P., Chai, F.H., Hao, J.M., 2010. Trend and characteristics of atmospheric emissions of Hg, As, and Se from coal combustion in China, 1980-2007. Atmos. Chem. Phys. 10, 11905–11919. doi:10.5194/acp-10-11905-2010

Titos, G., del Águila, A., Cazorla, A., Lyamani, H., Casquero-Vera, J.A., Colombi, C., Cuccia, E., Gianelle, V., Močnik, G., Alastuey, A., Olmo, F.J., Alados-Arboledas, L., 2017. Spatial and temporal variability of carbonaceous aerosols: Assessing the impact of biomass burning in the urban environment. Sci. Total Environ. 578, 613–625. doi:10.1016/j.scitotenv.2016.11.007

Tiwari, M., Sahu, S.K., Bhangare, R.C., Yousaf, A., Pandit, G.G., 2014. Particle size distributions of ultrafine combustion aerosols generated from household fuels. Atmos. Pollut. Res. 5, 145–150. doi:10.5094/APR.2014.018

Uchiyama, R., Okochi, H., Katsumi, N., Ogata, H., 2017. The impact of air pollutants on rainwater chemistry during "urban-induced heavy rainfall" in downtown Tokyo, Japan. J. Geophys. Res. Atmos. 122, 6502–6519. doi:10.1002/2017JD026803

Urban, R.C., Lima-Souza, M., Caetano-Silva, L., Queiroz, M.E.C., Nogueira, R.F.P., Allen, A.G., Cardoso, A.A., Held, G., Campos, M.L.A.M., 2012. Use of levoglucosan, potassium, and water-soluble organic carbon to characterize the origins of biomass-burning aerosols. Atmos. Environ. 61, 562–569. doi:10.1016/j.atmosenv.2012.07.082

Venkitasamy, S., Bhaskar, B.V., 2016. Emission inventory – a preliminary approach to primary pollutants. Curr. Sci. 111, 1831–1835.

Viana, M., Kuhlbusch, T.A.J., Querol, X., Alastuey, A., Harrison, R.M., Hopke, P.K., Winiwarter, W., Vallius, M., Szidat, S., Prévôt, A.S.H., Hueglin, C., Bloemen, H., Wåhlin, P., Vecchi, R.,

Miranda, A.I., Kasper-Giebl, A., Maenhaut, W., Hitzenberger, R., 2008. Source apportionment of particulate matter in Europe: A review of methods and results. J. Aerosol Sci. 39, 827–849. doi:10.1016/j.jaerosci.2008.05.007

Vicente, E.D., Alves, C.A., 2018. An overview of particulate emissions from residential biomass combustion. Atmos. Res. 199, 159–185. doi:10.1016/j.atmosres.2017.08.027

Vu, T. V., Delgado-Saborit, J.M., Harrison, R.M., 2015. Review: Particle number size distributions from seven major sources and implications for source apportionment studies. Atmos. Environ. 122, 114–132. doi:10.1016/j.atmosenv.2015.09.027

Wang, W., Rood, M.J., 2008. Real refractive index: Dependence on relative humidity and solute composition with relevancy to atmospheric aerosol particles. J. Geophys. Res. 113, D23305. doi:10.1029/2008JD010165

Weber, E., 1982. Air Pollution: Assessment Methodology and Modeling, Volume 2. Plenun Press, New York.

Xie, R., Seip, H.M., Wibetoe, G., Nori, S., McLeod, C.W., 2006. Heavy coal combustion as the dominant source of particulate pollution in Taiyuan, China, corroborated by high concentrations of arsenic and selenium in PM10. Sci. Total Environ. 370, 409–415. doi:10.1016/j.scitotenv.2006.07.004

Xu, D., Ge, B., Wang, Z., Sun, Y., Chen, Y., Ji, D., Yang, T., Ma, Z., Cheng, N., Hao, J., Yao, X., 2017. Below-cloud wet scavenging of soluble inorganic ions by rain in Beijing during the summer of 2014. Environ. Pollut. 230, 963–973. doi:10.1016/j.envpol.2017.07.033

Xu, M., Yan, R., Zheng, C., Qiao, Y., Han, J., Sheng, C., 2004. Status of trace element emission in a coal combustion process: A review. Fuel Process. Technol. 85, 215–237. doi:10.1016/S0378-3820(03)00174-7

Xu, X., Zhang, Z., Bao, L., Mo, L., Yu, X., Fan, D., Lun, X., 2017. Influence of rainfall duration and intensity on particulate matter removal from plant leaves. Sci. Total Environ. 609, 11–16. doi:10.1016/j.scitotenv.2017.07.141

Xu, Y., Hu, J., Ying, Q., Hao, H., Wang, D., Zhang, H., 2017. Current and future emissions of primary pollutants from coal-fired power plants in Shaanxi, China. Sci. Total Environ. 595, 505–514. doi:10.1016/j.scitotenv.2017.03.267

Xu, Z., Wu, Y., Liu, W., Liang, C., Ji, J., Zhao, T., Zhang, X., 2015. Chemical composition of rainwater and the acid neutralizing effect at Beijing and Chizhou city, China. Atmos. Res. 164–165, 278–285. doi:10.1016/j.atmosres.2015.05.009

Yuan, J., Na, C., Lei, Q., Xiong, M., Guo, J., Hu, Z., 2018. Coal use for power generation in China. Resour. Conserv. Recycl. 129, 443–453. doi:10.1016/j.resconrec.2016.03.021

Zikova, N., Zdimal, V., 2016. Precipitation scavenging of aerosol particles at a rural site in the Czech Republic. Tellus B Chem. Phys. Meteorol. 68, 27343. doi:10.3402/tellusb.v68.27343

2

METODOLOGÍA

2.1. ZONA DE ESTUDIO

La ciudad de León se encuentra situada al noroeste de la Península Ibérica (42º 36' N, 05º 35' O) a 838 m sobre el nivel del mar (Fig. 2.1). Según los datos ofrecidos por el *Instituto Nacional de Estadística* (INE), la población de la ciudad de León y los municipios cercanos (San Andrés del Rabanedo, Villaquilambre, Valverde de la Virgen y Onzonilla), se ha incrementado gradualmente desde el año 1998, pasando de 176 333 habitantes a 185 393 habitantes en 2016.

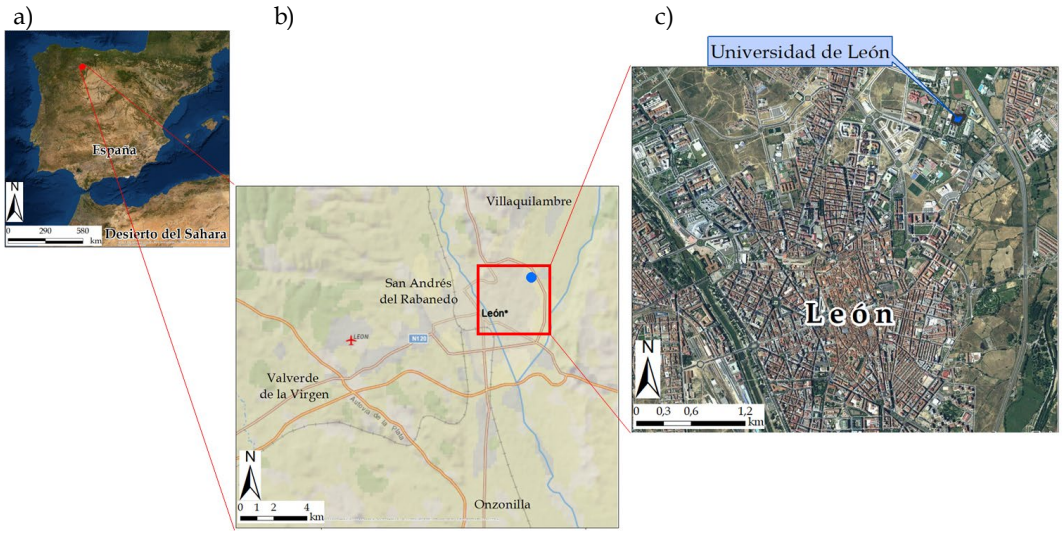

FIG. 2.1. a) Mapa de la península Ibérica, b) localización de la ciudad de León y c) mapa de la ciudad de León y localización del punto de muestreo en azul.

El clima es de tipo Mediterráneo con características continentales debido a la proximidad con la Cordillera Cantábrica (Castro et al., 2010). Según la *Agencia Estatal de Meteorología* (AEMET), la temperatura media anual de León es de 11 ºC. Los veranos son cálidos con temperaturas mínimas y máximas de alrededor de 12 y 26 ºC, respectivamente (Tabla 2.1). Las temperaturas mínimas suelen registrarse en los meses de enero y febrero, con valores medios de -0.7 y 0 ºC, respectivamente. La media anual de días con nieve es de 13, de los cuales 4 se registran en el mes

de enero, 3 en el mes de febrero, 2 en los meses de marzo y diciembre y 1 en los meses de abril y noviembre. Los eventos de lluvia se distribuyen irregularmente durante todo el año, con una media anual de 75 episodios y 515 mm, y con valores mínimos entre los meses de julio y agosto (42 mm en total) y máximos entre los meses de octubre a diciembre (186 mm en total).

Tabla 2.1. Valores medios estacionales en la ciudad de León, de temperatura (T), temperatura mínima ($T_{Mín}$), temperatura máxima (T_{Max}), humedad relativa (HR), días con precipitación (DP), días con nieve (DN) y días con heladas (DH) (Fuente: AEMET).

Estación	Meses	T (ºC)	$T_{Mín}$ (ºC)	T_{Max} (ºC)	HR (%)	DP (precipitación media, mm)	DN	DH
Invierno	diciembre, enero, febrero	4.0	-0.1	8.2	80	22 (150)	9	48
Primavera	marzo, abril, mayo	9.7	3.9	15.6	64	22 (133)	3	15
Verano	junio, julio, agosto	18.8	11.6	26.1	54	10 (73)	0	0
Otoño	septiembre, octubre, noviembre	11.7	6.5	16.9	72	20 (159)	1	8
Anual		11.1	5.5	16.7	68	75 (515)	13	71

La ciudad de León se caracteriza por la ausencia de grandes industrias, y se considera que las principales fuentes de emisión de partículas son el tráfico y los sistemas de calefacción doméstica (Blanco-Alegre et al., 2019; Oduber et al., 2018). En el año 2017, el parque de vehículos en la provincia de León se componía de 354,748 vehículos, según los datos publicados por el gobierno regional de la *Junta de Castilla y León*. Por otra parte, según la *Dirección General de Tráfico* (DGT), los vehículos registrados se agrupan aproximadamente de la siguiente manera: autobuses (0.2%), camiones (8.1%), ciclomotores (4.6%), camionetas (8.0%), motocicletas (6.3%), automóviles particulares (68.4%) y otros (4.3%). En cuanto a las fuentes de energía, la Junta de Castilla y León informó en el año 2008 de que los hogares en la provincia de León utilizan en mayor proporción diésel (37%) y gas (30%) como fuente de energía. Sin embargo, y a pesar de los esfuerzos realizados por el gobierno local para eliminar las instalaciones de carbón, en 2008 aproximadamente el 6% de los hogares usaban todavía carbón para la calefacción y en muchos de ellos estos sistemas permanecen actualmente en funcionamiento.

Las zonas montañosas ubicadas al norte de la provincia (a unos 30 km de la ciudad), conforman una fuente importante de bioaerosoles debido a la presencia de numerosos bosques con diversos tipos de vegetación, cuya polinización contribuye a una alta concentración de polen en la atmósfera. El género *Quercus* y muchos taxones híbridos, comúnmente conocidos como robles y encinas, son predominantes y se distribuyen por toda la provincia. En prados y praderas, hay una gran variedad de gramíneas y otras herbáceas (*Bromus sp.*, *Dactylis sp.*, *Holcus lanatus*, *Phleum pratense*, *Poa sp.*, *Plantago sp.*, *Chenopodium sp.*, etc.). El polen de una gran cantidad de especies de cipreses y arizonicas (*Cupressaceae*), cedros (*Cedrus deodora*), plátanos de sombra (*Platanus acerifolia*), oleaceae (*Ligustrum sp.*), castaños (*Aesculus hippocastanum*), arces (*Acer negundo*), es muy abundante en León, ya que generalmente se usan como árboles ornamentales debido a su resistencia a las condiciones climáticas extremas que se registran en la provincia (Del Río González, 2005; Oduber et al., 2019). Otras fuentes de emisión son las esporas fúngicas que se desarrollan en los tejidos vegetales en descomposición y los restos vegetales de la frecuente poda del césped (Calvo et al., 2018).

2.2. MUESTREO

La presente Tesis Doctoral se encuentra enmarcada en el proyecto AERORAIN, para el que se llevó a cabo una campaña de muestreo entre el 9 de marzo del 2016 y el 14 de marzo del 2017, en la terraza de la Facultad de Veterinaria (aproximadamente a 12 m del suelo) de la Universidad de León (Fig. 2.1). Durante la campaña, se realizó un muestreo diario y simultáneo de material particulado (PM_{10}) y precipitación, recogiéndose un total de 712 muestras de PM_{10} (354 filtros de cuarzo y 354 de teflón) y 74 muestras de precipitación. Además, se midió en continuo tanto el tamaño de las gotas de lluvia como la distribución de tamaños del aerosol y su contenido en carbono negro.

Adicionalmente, se llevó a cabo un muestreo horario de polen y diario de la fracción alergénica del aerosol atmosférico, realizado por el grupo de Botánica del Departamento de Biodiversidad y Gestión Ambiental de la Universidad de León (España), en el punto de muestreo perteneciente a la Red Española de Aerobiología, ubicado también en la misma terraza de la Facultad de Veterinaria de la Universidad de León.

A continuación, se recoge una descripción detallada de los equipos utilizados durante el periodo de muestreo.

2.2.1. Material particulado atmosférico (PM_{10})

Las muestras de PM_{10} se recolectaron utilizado tres captadores de partículas: uno de alto volumen y dos de bajo volumen; siguiendo los procedimientos establecidos en la normativa EN 12341: 2014. Antes y después del muestreo, los filtros de cuarzo y teflón se acondicionaron durante aproximadamente 24 horas, en una habitación con humedad relativa (< 50%) y temperatura controladas (20 ºC), para ser pesados en una *balanza semi-micro electrónica* (Mettler Toledo, XPE105DR) de precisión 0.00001 g (Fig. 2.2).

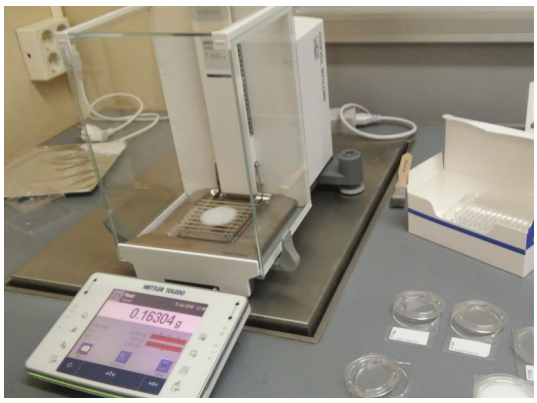

FIG. 2.2. Balanza semi-micro electrónica, marca Mettler Toledo (XPE105DR), utilizada para el pesaje de los filtros de teflón y cuarzo.

Los captadores utilizados para el muestreo de PM_{10} funcionan mediante la aspiración de un caudal de aire específico, gracias a una bomba de vacío. El caudal de aire cargado con partículas pasa a través de un cabezal de muestreo que permite la selección de las partículas según

su tamaño. Finalmente, se depositan sobre un filtro (de cuarzo, teflón o policarbonato), para su posterior análisis. Los captadores utilizados fueron:

- *Captador de alto volumen* (CAV- A/Mb): con un volumen de muestreo de 30 m^3 h^{-1} y provisto de filtros de cuarzo de 150 mm de diámetro (poro de 0.45 µm) (Fig. 2.3a). Antes del muestreo, los filtros de cuarzo fueron calcinados en una mufla a 600 ºC durante 6 horas, con el fin de eliminar cualquier contaminante orgánico y, tras el muestreo, se doblaron y almacenaron en papel de aluminio (también calcinado), hasta el momento del pesaje. Una vez muestreados, los filtros de cuarzo fueron almacenados a -18 ºC hasta el momento del análisis.

- *Captador de bajo volumen* (TECORA, ECHOPM): provisto de filtros de teflón de 47 mm de diámetro (poro de 0.2 µm), y con un volumen de muestreo de 2.3 m^3 h^{-1} (Fig. 2.3b). Una vez muestreados, los filtros de teflón se almacenaron dentro de placas de Petri en el congelador a -18 ºC.

- *Captador de bajo volumen* (Gent): con un volumen de muestreo de 10 L min^{-1} (que equivale a 0.6 m^3 h^{-1}), provisto de filtros de policarbonato de 47 mm de diámetro (poro de 0.2 µm) (Fig. 2.3c). Los filtros fueron almacenados en placas de Petri, provistas de una lámina de papel de aluminio previamente calcinada, y refrigerados hasta su posterior análisis.

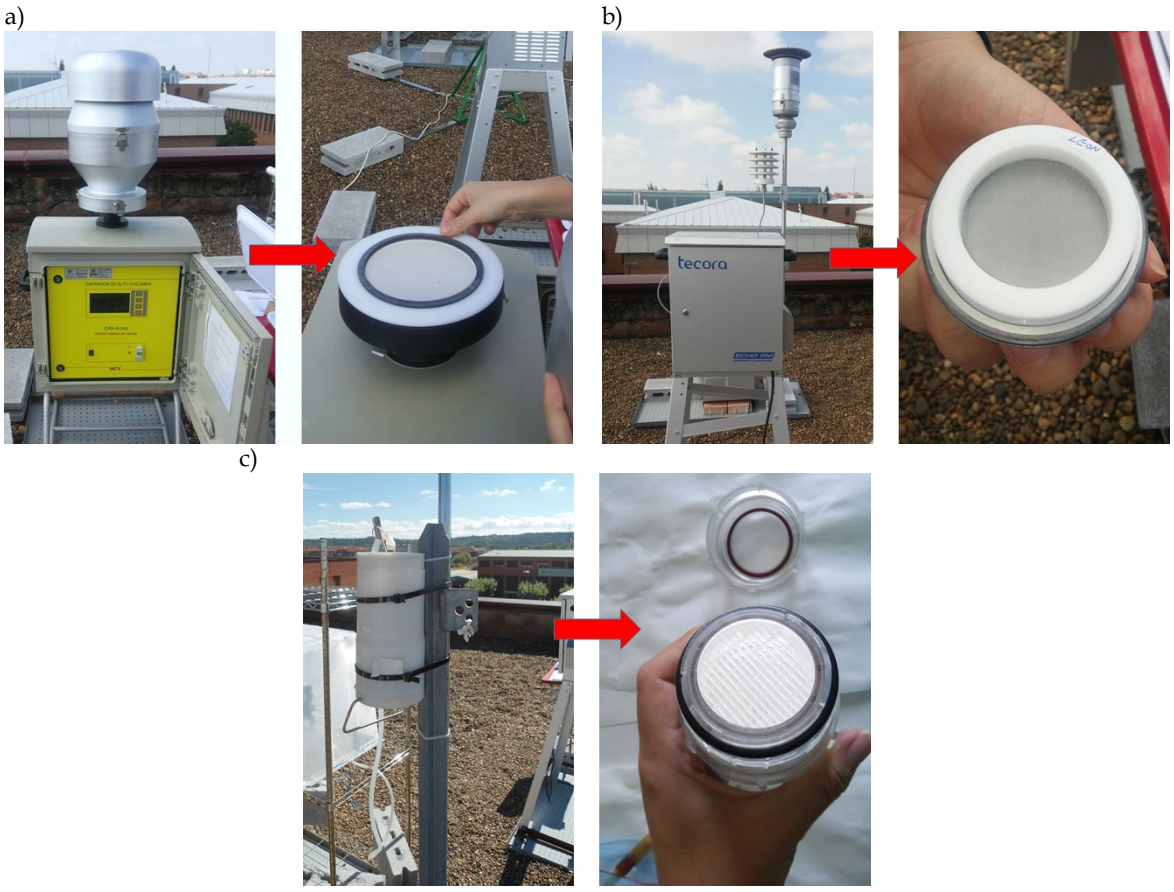

FIG. 2.3. a) Captador de alto volumen (CAV- A/Mb) y filtro de cuarzo de 150 mm de diámetro, b) captador de bajo volumen (TECORA, ECHOPM) y filtro de teflón de 47 mm de diámetro y c) captador de bajo volumen (Gent) con filtro de policarbonato de 47 mm de diámetro.

2.2.2. Precipitación

Las muestras de agua de lluvia se recogieron utilizando un colector marca Eigenbrodt UNS 130/E (Fig. 2.4a). El equipo de muestreo cuenta con un sensor, que permite que la cubierta se abra al comienzo de la precipitación y se cierre una vez la precipitación ha cesado. El agua de lluvia muestreada fluye hacia una botella de vidrio de 3.5 L, colocada en el interior del colector.

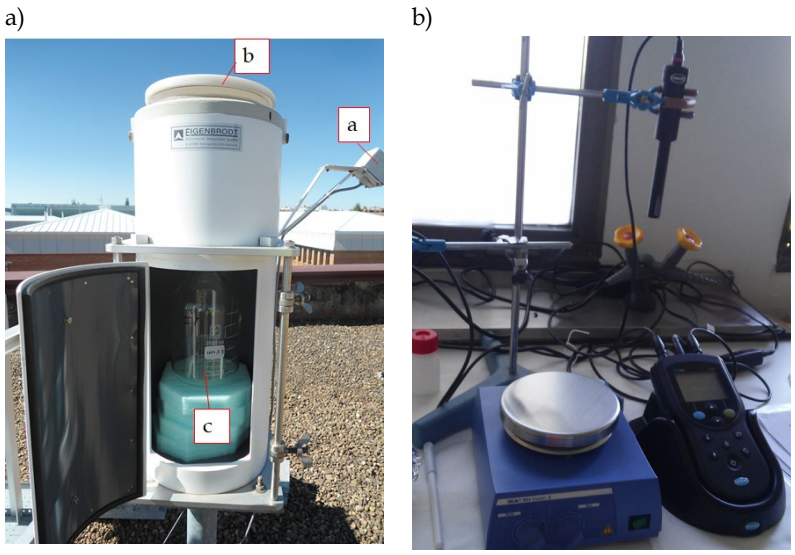

FIG. 2.4. a) Colector de precipitación (Eigenbrodt UNS 130/E) utilizado para el muestreo (a: sensor de lluvia; b: cubierta; c: botella para recoger la precipitación), y b) medidor de pH y conductividad (Hach, HQ 40d multi).

Inmediatamente después de la recogida de las muestras de agua de lluvia, se determinó su conductividad y pH utilizando un medidor marca Hach, HQ 40d multi (Fig. 2.4b). Posteriormente, las muestras de agua de lluvia se filtraron a través de filtros de cuarzo de 15 mm de diámetro (tamaño de poro de 0.45 µm) para separar la materia soluble e insoluble (Fig. 2.5). La fracción líquida filtrada, que contiene el material soluble, se almacenó en botellas de vidrio en el congelador a -18 ^{o}C hasta su análisis. Los filtros, que contenían la fracción insoluble, se colocaron dentro de un desecador durante 24 horas, tras lo que se almacenaron en el congelador hasta su posterior análisis.

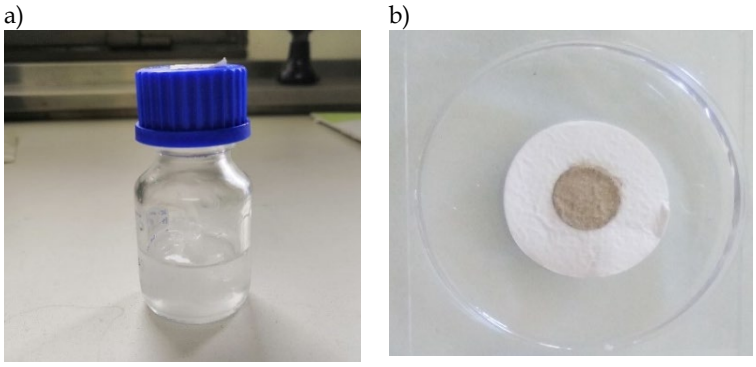

FIG. 2.5. a) Fracción líquida filtrada y b) filtro de cuarzo con la fracción insoluble del agua de lluvia muestreada.

2.2.3. Polen y fracción alergénica

El polen atmosférico se muestreó utilizando una *trampa volumétrica Hirst* (Hirst, 1952), ubicada en la terraza de la Facultad de Veterinaria (Fig. 2.6a), con un flujo de succión de 10 L min^{-1}. Los recuentos horarios y diarios, llevados a cabo con el microscopio óptico, se hicieron de acuerdo con el método recomendado por la Red Aerobiológica Española (Galán Soldevilla et al., 2007).

Para la cuantificación de la fracción alergénica del aerosol atmosférico, se recogieron muestras con un *captador ciclónico de bajo volumen* (Fig. 2.6b), ubicado en el punto de muestreo y con un caudal de succión de 16.5 L min^{-1} (Burkard Manufacturing Co. Ltd.). Las partículas atmosféricas se recogieron en seco directamente en un vial Eppendorf de 1.5 ml, cada 24 horas. Las muestras recogidas cada día se almacenaron a -20 ºC.

a) b)

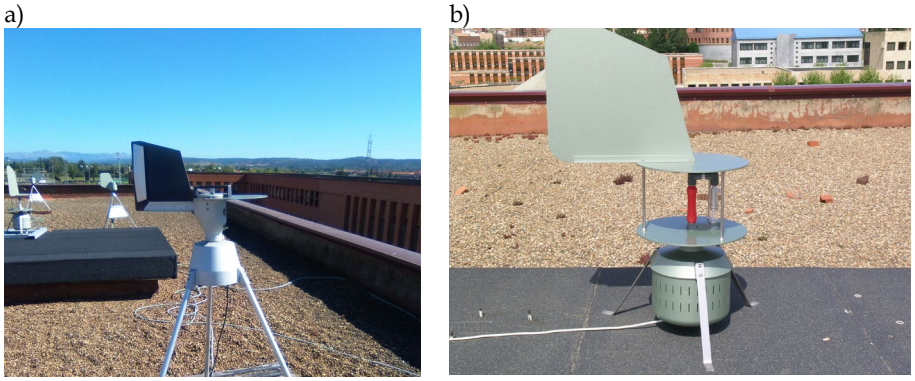

FIG. 2.6. a) Trampa volumétrica Hirst y b) Captador ciclónico de bajo volumen.

2.3. INSTRUMENTACIÓN Y METODOLOGÍA ANALÍTICA

El siguiente apartado tiene como objetivo realizar una descripción detallada de los equipos de medida y de la metodología analítica utilizados para la caracterización físico-química del aerosol y de la precipitación durante la campaña de muestreo.

2.3.1. Caracterización física del aerosol y de la precipitación

2.3.1.1. Distribución de tamaño de las partículas

La distribución de tamaño de las partículas se midió continuamente durante toda la campaña utilizando un *espectrómetro láser* (PCASP, en inglés *Passive Cavity Aerosol Spectrometer Probe*) y un *espectrómetro SMPS* (del inglés *Scanning Mobility Particle Sizer*). Ambos equipos estaban instalados en el sitio de muestreo. A continuación, se hace una descripción más detallada del funcionamiento de ambos espectrómetros.

- **Espectrómetro óptico PCASP**

Las distribuciones del tamaño de las partículas se midieron continuamente cada minuto usando un espectrómetro láser PCASP-X, fabricado por Particle Measuring Systems, Inc., PMS

(Fig. 2.7). El PCASP es un contador óptico de partículas (OPC, del inglés *Optical Particle Counter*) que permite obtener la distribución de tamaño de las partículas de diámetros ópticos nominales entre 0.1 y 10 µm (equivalente a esferas de látex) en 31 canales discretos, es decir, 31 intervalos de tamaños (Tabla 2.2). Adicionalmente se dispone de un canal 32 donde se incluye todas las partículas de tamaño superior a 10 µm.

El PCASP muestrea un volumen de aire ajustable de entre 1.0 a 3.0 $cm^3\ s^{-1}$, que debe ser conocido en cada medida. Las partículas muestreadas pasan a través de un rayo láser de He-Ne y su tamaño es estimado según el grado en que dispersan la luz de 632.8 nm de longitud de onda entre ángulos de dispersión de 45º y 135º. La luz dispersada es recogida por el sistema óptico y dirigida hacia el fotodiodo. Calvo (2009) ofrece una descripción más detallada.

FIG. 2.7. Espectrómetro láser PCASP-X (*Particle Measuring Systems*, Inc., PMS).

Tabla 2.2. Intervalos de tamaño de partículas (diámetros) medidos con la PCASP-X, equivalente a esferas de látex de índice de refracción de 1,58-0i (Calvo, 2009).

Canal	Tamaño (µm)	Intervalo (µm)	Canal	Tamaño (µm)	Intervalo (µm)
1	0.10 – 0.12	0.02	17	0.90 – 1.00	0.10
2	0.12 – 0.14	0.02	18	1.00 – 1.20	0.20
3	0.14 – 0.16	0.02	19	1.20 – 1.40	0.20
4	0.16 – 0.18	0.02	20	1.40 – 1.60	0.20
5	0.18 – 0.20	0.02	21	1.60 – 1.80	0.20
6	0.20 – 0.23	0.03	22	1.80 – 2.00	0.20
7	0.23 – 0.26	0.03	23	2.00 – 2.30	0.30
8	0.26 – 0.30	0.04	24	2.30 – 2.60	0.30
9	0.30 – 0.35	0.05	25	2.60 – 3.00	0.40
10	0.35 – 0.40	0.05	26	3.00 – 3.50	0.50
11	0.40 – 0.45	0.05	27	3,50 – 4,00	0,50
12	0.45 – 0.50	0.05	28	4.00 – 5.00	1.00
13	0.50 – 0.60	0.10	29	5.00 – 6.50	1.50
14	0.60 – 0.70	0.10	30	6.50 – 8.00	1.50
15	0.70 – 0.80	0.10	31	8.00 – 10.00	2.00
16	0.80 – 0.90	0.10	32	> 10.00	

El número exacto de partículas por unidad de volumen muestreado en cada canal se determina realizando una serie de correcciones sobre el número de cuentas indicado por el espectrómetro. Entre estas correcciones se encuentran:

- Ajuste del volumen muestreado en función de la altitud del punto de muestreo. Esta corrección se realiza según las indicaciones dadas por el fabricante.

- Ajuste de cada medida según la *actividad*. Una vez que la partícula pasa a través del láser la información sobre su tamaño es transferida al sistema de datos. Esto supone un período fijo de retardo en el cual la electrónica debe ser reajustada para la llegada de la siguiente partícula, lo que impide temporalmente una nueva medida. La lectura de la *actividad* aparece como un número de 0 a 100, que indica el porcentaje total de tiempo en el que la sonda contabiliza partículas activamente durante la toma de datos. Teóricamente, el espectrómetro láser es capaz de medir 10 000 partículas por segundo, lo que corresponde a un valor del 100% de *actividad*.

- Corrección de las distribuciones de tamaño en función del índice de refracción de las partículas. El PCASP está calibrado con partículas de látex que son fuertemente dispersoras de la radiación. Sin embargo, las partículas ambientales son generalmente menos dispersoras y muestran ciertas propiedades absorbentes, por lo que los diámetros de las partículas suelen subestimarse. Debido a esto, se deben realizar correcciones a los diámetros de los distintos canales teniendo en cuenta un índice de refracción medio característico del tipo de aerosol muestreado.

Debido a que durante la campaña de muestreo fue posible obtener la composición química diaria del aerosol atmosférico, el índice de refracción ($m = n - Ki$) y la densidad media, $\bar{\rho}$, fueron calculados a partir de las ecuaciones 2.1 y 2.2 (Alves et al., 2014; Calvo et al., 2013; Levin et al., 2010), asumiendo que las partículas se encuentran en forma anhidra y que los compuestos químicos están mezclados internamente:

$$\bar{\rho}^{-1} = \sum_i \frac{X_i}{\rho_i} \qquad \text{Ecuación 2.1}$$

$$m = \bar{\rho} \sum_i \frac{X_i n_i}{\rho_i} - \bar{\rho} \sum_i \frac{X_i k_i}{\rho_i} i \qquad \text{Ecuación 2.2}$$

donde X_i es la fracción másica de cada componente y ρ_i, n_i y k_i son la densidad e índices de refracción reales e imaginarios de cada componente, respectivamente. Finalmente, los diámetros corregidos correspondientes a los diferentes canales, fueron obtenidos usando este índice de refracción en un modelo basado en la Teoría de Mie (Bohren and Huffman, 1983).

- **Espectrómetro de movilidad diferencial SMPS**

Las distribuciones del tamaño de las partículas sub-micrométricas se midieron continuamente, cada 6 minutos, usando un espectrómetro de movilidad diferencial (SMPS, del inglés *Scaning Mobility Particle Sizer*), marca TSI-SMPS Modelo 3938, un analizador de movilidad diferencial (DMA, del inglés *Differential Mobility Analyser*) Modelo 3081 y un contador de partículas (CPC, del inglés *Condensation Particle Counter*) Modelo 3772 (Fig. 2.8). El SMPS permite obtener la distribución de tamaño de las partículas de diámetros entre 14.6 a 791.5 nm, en 112 canales. El SMPS se compone de un clasificador electrostático cuya función es discriminar el tamaño del aerosol, un DMA y un CPC que indica el número de partículas que hay por cada intervalo de tamaños.

La muestra de aire con aerosol polidisperso (de varios tamaños) entra en el clasificador electrostático y a continuación pasa a través del impactador. En el impactador las partículas se separan en dos rangos, de acuerdo con sus diámetros aerodinámicos. El aerosol polidisperso, en el rango de tamaño seleccionado, atraviesa el neutralizador de partículas (rayos X), en el que las partículas adquieren una distribución de carga eléctrica conocida. El aerosol cargado llega al DMA donde, en función del voltaje aplicado, se seleccionan las partículas de una determinada movilidad eléctrica (propiedad de la partícula que depende tanto de su tamaño como de su estado de carga). Las partículas con diámetros correspondientes a la movilidad eléctrica seleccionada, constituyen un aerosol monodisperso que logra alcanzar la salida del DMA.

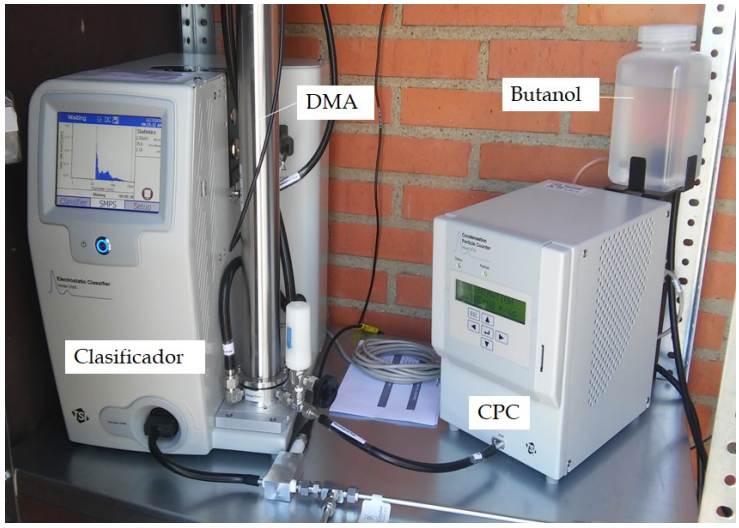

FIG. 2.8. Espectrómetro de partículas sub-micrométricas SMPS.

El aerosol monodisperso accede al CPC, que contabiliza el número de partículas clasificadas en el DMA. En el CPC las partículas aumentan su tamaño debido al butanol que actúa como líquido condensable sobre las partículas, ya que de esta forma pueden ser detectadas ópticamente. El aerosol entra en la cámara óptica, compuesta fundamentalmente por un láser y un fotodetector, produciendo la dispersión de la luz y generando un impulso eléctrico en el detector. Una descripción más detallada de los principios de esta técnica y del funcionamiento del SMPS se encuentra en Alonso-Blanco (2019) y Sorribas Panero (2007).

El software permite obtener la distribución del tamaño de las partículas seleccionadas en el DMA, y la concentración de partículas correspondientes a cada tamaño registradas en el CPC. Para determinar el número de partículas que hay en cada intervalo de tamaño es necesario aplicar también una serie de correcciones descritas por Wiedensohler et al. (2012), entre las que se encuentran:

- *Corrección de pérdidas por difusión:* en el sistema se puede producir una deposición de las partículas más pequeñas (< 0.3 µm) sobre la superficie sólida, causada por movimientos de difusión Browniana (Hinds, 2012). En consecuencia, se registrará un número menor de partículas, que depende del caudal de arrastre y del tamaño de la partícula, y es menor a medida que el tiempo de residencia en el sistema es menor (cuando son mayores los caudales y los tamaños de las partículas) (Flagan, 1999).

- *Corrección por carga múltiple:* las partículas de tamaños superiores a 100 nm pueden adquirir cargas múltiples (Wiedensohler, 1988), lo que supone un aumento de su movilidad eléctrica. Esto implica que la clasificación de estas partículas puede ser errónea si se considera que la partícula tiene una única carga, subestimando su diámetro. La corrección del error de la medida asociado a las partículas con carga múltiple se realiza mediante la aplicación de un algoritmo basado en la teoría de aproximación de distribución bipolar de carga (Wiedensohler, 1988). Esta corrección se encuentra incorporada al software de medición.

2.3.1.2. Carbono negro y contenido de hierro del aerosol mineral

Para la determinación del carbono negro se utilizó un *Aethalometer AE-31* (Magee Scientific, EE. UU.) (Fig. 2.9a) con una resolución temporal de 2 minutos. Este equipo se encontraba instalado en el punto de muestreo y realizaba mediciones de forma continua durante toda la campaña.

El *etalómetro* mide continuamente la atenuación de la luz causada por el aerosol atmosférico depositado en una cinta de filtro de cuarzo (Fig. 2.9b), a siete longitudes de onda: 370, 470, 520, 590, 660, 880 y 950 nm. El instrumento dispone de dos fotodetectores: uno mide la intensidad $I_R(\lambda)$ de la luz que atraviesa un punto del filtro de cuarzo sin muestra de aerosol (llamado punto de referencia), mientras que el otro mide la intensidad $I_S(\lambda)$ de la luz que atraviesa un punto del filtro de cuarzo donde el aerosol se acumula continuamente. Fialho et al. (2005) y Weingartner et al. (2003) ofrecen una explicación más detallada.

a) b)

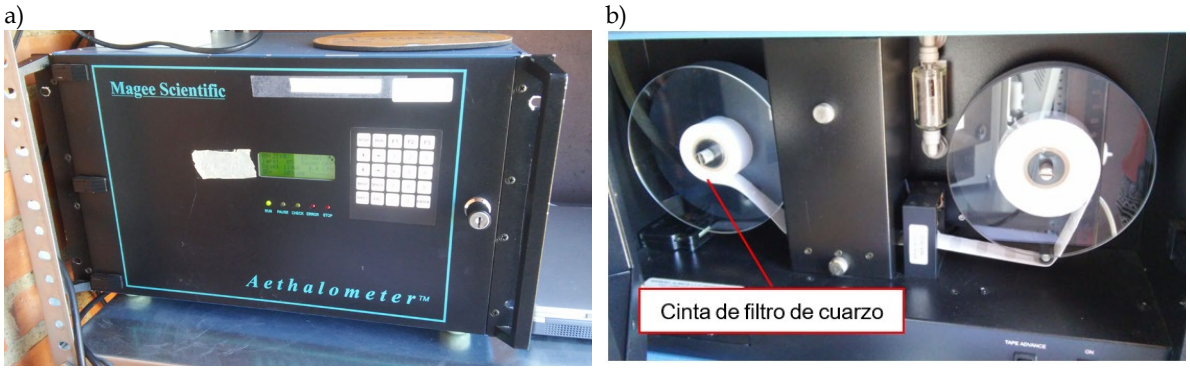

FIG. 2.9. a) *Etalómetro AE-31* (Magee Scientific, EE. UU.), b) interior del etalómetro con la cinta de filtro de cuarzo.

La concentración másica de carbono negro (BC) se determina a partir del cambio en la atenuación óptica a 880 nm. A esta longitud de onda, otras partículas carbonosas o minerales del aerosol absorben significativamente menos que el carbono negro, por lo que la absorción puede ser atribuida exclusivamente al efecto del BC (Fialho et al., 2005; Sandradewi et al., 2008; Yang et al., 2009).

Por otra parte, las partículas de polvo mineral también son capaces de absorber la luz a longitudes de onda del visible, por lo que, si están presentes, ambos -el BC y el polvo mineral- contribuyen al coeficiente de absorción del aerosol medido [$\sigma_{aerosol}(\lambda, t)$], como se muestra en la Ecuación 2.3 (Fialho et al., 2005).

$$\sigma_{aerosol}(\lambda, t) = \sigma_{BC}(\lambda, t) + \sigma_{dust}(\lambda, t) \quad \text{Ecuación 2.3}$$

donde $\sigma_{BC}(\lambda, t)$ y $\sigma_{dust}(\lambda, t)$ son los coeficientes de absorción del BC y del aerosol mineral, respectivamente. Las muestras con alto contenido de aerosol mineral, proveniente principalmente de intrusiones de polvo sahariano, se caracterizan por tener un color marrón-rojizo. Esta coloración se asocia a altas concentraciones de hierro en forma de óxidos (Fe_2O_3). El modelo de dos componentes (Ecuación 2.3), desarrollado posteriormente por Fialho et al. (2006), permite determinar la concentración de hierro asociada al polvo mineral en suelos con bajas concentraciones de materia orgánica:

$$\sigma_{aerosol}(\lambda, t) = K_{BC} \times \lambda^{-1} \times C_{BC}(t) + K_{Fe} \times \lambda^{-4} \times C_{Fe}(t) \quad \text{Ecuación 2.4}$$

donde C_{BC} y C_{Fe} son las concentraciones de carbono negro y hierro, respectivamente; y K_{BC} y K_{Fe} son constantes con valores de 14,625 μm m^2 g^{-1} y 0,234 μm m^4 g^{-1}, respectivamente.

2.3.1.3. Parámetros físicos de las gotas de lluvia

El espectro de tamaños de las gotas de lluvia se obtuvo con un *disdrómetro láser* (LPM, del inglés *Laser Precipitation Monitor*) de Thies Clima (Fig. 2.10), que registró gotas de entre 0.125 y 8 mm de tamaño en 22 rangos con una frecuencia de un minuto. Este disdrómetro detecta los hidrometeoros que atraviesan un área de muestra de 228 × 20 mm^2 y determina su velocidad de caída y su volumen de a partir de la duración y la cantidad de pérdida de señal de un láser de 780 nm de longitud de onda.

FIG. 2.10. *Disdrómetro láser* (LPM) de Thies Clima, ubicado en la terraza de la Facultad de Veterinaria de la Universidad de León (España).

A partir de los datos proporcionados por el LPM, se obtuvieron las siguientes variables de precipitación: intensidad de precipitación, precipitación acumulada, número de gotas, volumen barrido por las gotas que caen, media y desviación estándar de los tamaños de las gotas de lluvia. La distribución del volumen de precipitación, el número de gotas de lluvia y las distribuciones de tamaño de gota se pueden ajustar a una función de densidad de probabilidad gamma f(x), que se define como:

$$f(x) = \frac{\beta^{\alpha} x^{\alpha-1} \exp(-\beta x)}{\Gamma(\alpha)}$$ Ecuación 2.5

donde Γ es la función gamma de Euler, definida como:

$$\Gamma(s) = \int_0^{\infty} t^{s-1} \exp(-t) dt$$ Ecuación 2.6

La distribución gamma (Ecuación 2.5), que depende del parámetro de forma α, se convierte en una distribución exponencial cuando α = 1. La distribución también varía con el parámetro de escala β, que está relacionado con la velocidad de caída de la curva a cero. La función se define para cualquier valor no negativo de x, y los parámetros α y β tienen que ser reales positivos. Cuando α > 1, la distribución gamma tiene forma de campana asimétrica, con un máximo en (α -1)/β. El método de los momentos se utilizó para determinar los valores de α y β (Marques et al., 2014). Esta información puede ampliarse en Fernández-Raga et al. (2017) y (2009).

2.3.2. Caracterización química del aerosol y de la precipitación

La caracterización química del aerosol y de la precipitación se llevó a cabo siguiendo los siguientes procesos (Fig. 2.11):

- *Filtros de cuarzo*: se utilizaron para la determinación de la concentración de: a) PM_{10} mediante el método gravimétrico; b) carbono orgánico (OC) y elemental (EC) mediante el método termo-óptico, y c) azúcares solubles en agua mediante cromatografía iónica.

- *Filtros de teflón*: se determinó la concentración másica de PM_{10} mediante el método gravimétrico. Por otra parte, los filtros de teflón se dividieron en dos mitades (Fig. 2.12), utilizando una de ellas para la determinación de metales traza por el método PIXE, mientras que la otra mitad se utilizó para el análisis de iones inorgánicos solubles en agua mediante la técnica de cromatografía iónica.

- *Filtros de policarbonato*: se emplearon para el análisis de la morfología y la composición elemental de las partículas de aerosol individuales, mediante *Microscopía Electrónica de Barrido por Emisión de Campo* (FE-SEM).

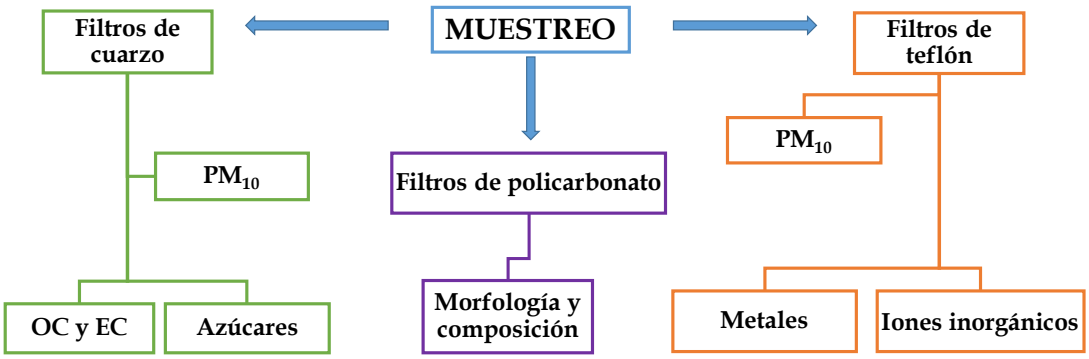

FIG. 2.11. Determinaciones químicas realizadas con los filtros de cuarzo, teflón y policarbonato recogidos durante la campaña de muestreo.

FIG. 2.12. Corte de los filtros de teflón para su posterior análisis.

En cuanto a las muestras de precipitación (Fig. 2.13), la fracción soluble fue utilizada para la determinación del carbono orgánico disuelto (DOC, en inglés *Dissolved Organic Carbon*) mediante un análisis termo-óptico, y para la determinación de los iones solubles en agua por cromatografía iónica. La fracción insoluble fue utilizada para la determinación de carbono orgánico (WIOC, en inglés *Water Insoluble Organic Carbon*) y elemental (WIEC, en inglés *Water Insoluble Elemental Carbon*) insolubles en agua. Las caracterizaciones químicas se realizaron posteriormente al muestreo y mediante técnicas analíticas diversas, que se describen en detalle en los apartados siguientes.

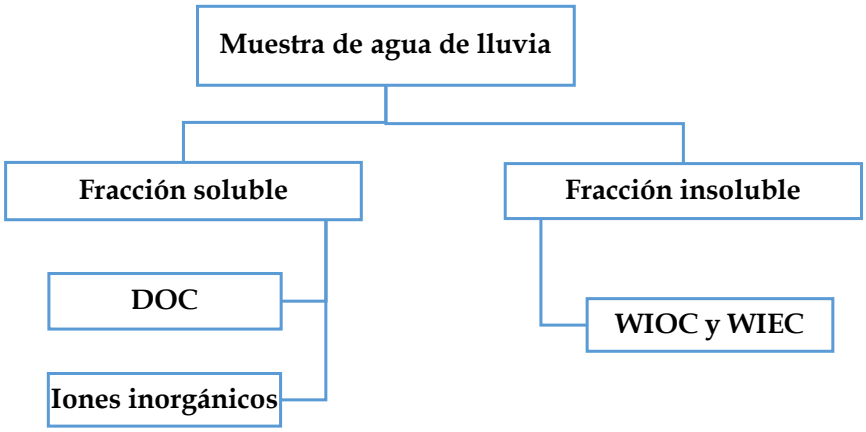

FIG. 2.13. Determinaciones realizadas con las fracciones solubles e insolubles de las muestras de agua de lluvia recogidas durante la campaña de muestreo.

2.3.2.1. Determinación del carbono orgánico y elemental

La determinación del carbono orgánico y elemental, tanto en los filtros de cuarzo del PM_{10} como en la fracción insoluble de las muestras de precipitación, se llevó a cabo mediante una *técnica termo-óptica*, utilizado un equipo fabricado por el Departamento de Medio Ambiente de la Universidad de Aveiro (Portugal). Este equipo consta de un tubo de cuarzo con dos zonas de calentamiento, un láser (Fig. 2.14a) y un analizador de CO_2 por infrarrojo no dispersivo (Fig. 2.14b). En ambos casos se tomaron dos porciones de 9 mm de diámetro cada una y las curvas de calibración se realizaron utilizando corrientes de CH_4 a 45.81 y 349.5 ppm.

La determinación de la fracción carbonosa se realiza inicialmente con un calentamiento controlado en condiciones anóxicas para separar el OC en dos fracciones de volatilidad creciente. La primera fracción corresponde a la volatilización de compuestos orgánicos de bajo peso molecular (OC1), a una temperatura menor a 200 °C. La segunda fracción está relacionada con la descomposición y oxidación de especies de mayor peso molecular a temperaturas que oscilan entre 200 y 600 °C (OC2). La última fracción de OC se identifica por transmitancia y corresponde al carbono orgánico pirolizado (PC) producido en los pasos de calentamiento anteriores. La fracción restante se evapora/quema en un segundo paso bajo un flujo de gas que contiene O_2. Esta última fracción de carbono contiene EC inicial más OC que se ha pirolizado durante el calentamiento en atmósfera inerte. La interferencia entre PC y EC es controlada mediante la evaluación continua del oscurecimiento del filtro utilizando un haz de láser He-Ne de 632 nm y un fotodetector que mide la transmitancia de luz del filtro. El OC y EC se volatilizan como CO_2, que se cuantifica continuamente mediante un analizador infrarrojo no dispersivo.

Las comprobaciones de la precisión de la medida se realizaron con el análisis de filtros de cuarzo calcinados impregnados con una solución patrón de Hidrogenoftalato de Potasio ($C_8H_5KO_4$) con una concentración equivalente a entre 40 y 50 µg de C.

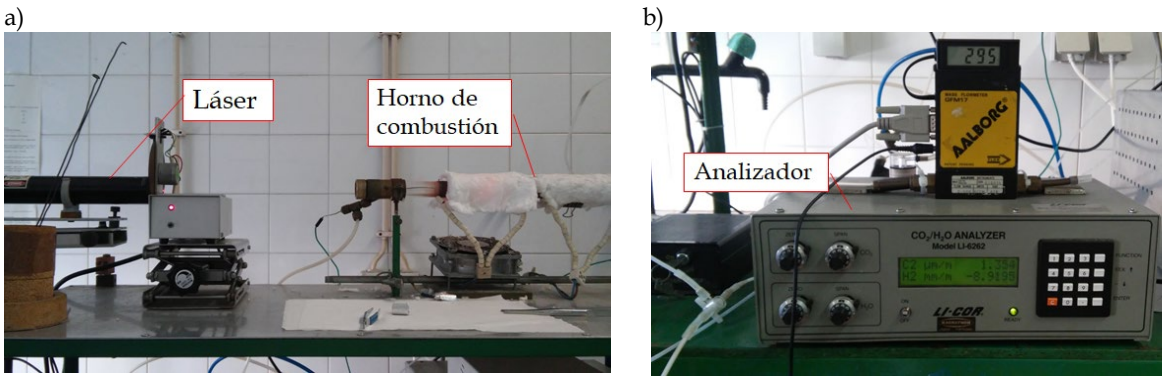

FIG. 2.14. Sistema para la determinación de carbono orgánico (OC) y elemental (EC): a) láser y horno de combustión, b) analizador infrarrojo no dispersivo. Departamento de Medio Ambiente de la Universidad de Aveiro (Portugal).

2.3.2.2. Determinación de azúcares

Los azúcares se determinaron a partir de las muestras de PM_{10} de los filtros de cuarzo. Los azúcares solubles en agua se extrajeron tomando un área equivalente a 14.14 cm^2 de los filtros de cuarzo, en 3 ml de agua ultra pura Mili-Q y en agitación ultrasónica durante 15 min. Los extractos fueron filtrados con jeringas de PTFE (Politetrafluoroetileno) con filtros de poro de 0.2 µm y transferidos a viales de vidrio para su posterior análisis en el mismo día.

El análisis de los 17 azúcares listados en la Tabla 2.3 se llevó a cabo mediante la técnica de *Cromatografía Iónica (CI)*, utilizando un cromatógrafo Thermo Scientific Dionex™ ICS-5000 (Fig. 2.15), provisto de una columna analítica de intercambio iónico CarboPac® PA-1 (2 × 250 mm), ubicado en el Centro de Estudios Ambientales y Marinos, CESAM, de la Universidad de Aveiro (Portugal). La cromatografía iónica es una técnica físico-química de separación, utilizada para realizar análisis cuantitativos de iones orgánicos e inorgánicos en muestras de mezclas complejas.

Tabla 2.3. Azúcares analizados y sus fórmulas moleculares.

Compuesto	Fórmula molecular	Marca (% de pureza)
Sacáridos		
L – (+) - arabinosa	$C_5H_{10}O_5$	Sigma-Aldrich (99%)
D – (-) - fructosa	$C_6H_{12}O_6$	Sigma-Aldrich (99%)
D – (+) - galactosa	$C_6H_{12}O_6$	Sigma-Aldrich (99%)
D (-)+(-) glucosa	$C_6H_{12}O_6$	Sigma-Aldrich (99.5%)
D – (-) - ribosa	$C_5H_{10}O_5$	Alfa Aesar (99%)
Sucrosa	$C_{12}H_{22}O_{11}$	Sigma-Aldrich (99.5%)
D- (+) - xilosa	$C_5H_{10}O_5$	Alfa Aesar (98%)
Alcohol-sacáridos		
Adonitol	$C_5H_{12}O_5$	Alfa Aesar (99%)
L – (-) - arabitol	$C_5H_{12}O_5$	Sigma-Aldrich (98%)
2-metileritritol	$C_4H_{10}O_4$	Alfa Aesar (99%)
myo-inositol	$C_6H_{12}O_6$	Sigma-Aldrich (99%)
D-manitol	$C_6H_{14}O_6$	Sigma-Aldrich (98%)
D-sorbitol	$C_6H_{14}O_6$	Alfa Aesar (98%)
Xilitol	$C_5H_{12}O_5$	Sigma-Aldrich (99%)
Anhidro-sacáridos		
Galactosano	$C_6H_{10}O_5$	Sigma-Aldrich (99%)
Levoglucosano (1,6-Anidro-β-glucosa)	$C_6H_{10}O_5$	Sigma-Aldrich (99%)
Mannosano	$C_6H_{10}O_5$	Sigma-Aldrich (99%)

FIG. 2.15. Cromatógrafo iónico Thermo Scientific Dionex™ ICS-5000, ubicado en el Departamento de Medio Ambiente de la Universidad de Aveiro (Portugal).

Durante el análisis, una alícuota de la muestra se mezcla con la corriente del eluyente, a través de la válvula de inyección. La mezcla es transportada hacia la columna de separación con la ayuda de un sistema de bombas. En la columna de separación los iones de la muestra son convertidos en su correspondiente forma acida o básica, según sea el caso, para la posterior detección. Cada ion es identificado por su tiempo de retención en la columna de intercambio iónico (Creatchman and Landsberger, 1999).

El cromatógrafo está equipado con un inyector automático a 13 ± 2 ºC y con una bomba cuaternaria con un volumen de muestra de 10 µl. El sistema de detección consta de un detector amperométrico (Dionex ED50), equipado con una celda electroquímica con un electrodo de oro y

un electrodo de pH como referencia (ambos Dionex), funcionando en el modo de Detección Amperométrica Pulsada (*PAD*, del inglés *Pulsed Amperometric Detection*).

Se prepararon soluciones estándar de 1000 μg ml^{-1} para cada uno de los diecisiete compuestos, a partir de reactivos con pureza mayor del 98% (Tabla 2.3). A partir de estas soluciones estándar individuales en agua Milli-Q ultra pura, se prepararon 5 patrones con concentraciones de todos los azúcares en el rango de 0.5 y 5 μg ml^{-1}, para las curvas de calibración.

La metodología utilizada se basa en la descrita por Caseiro et al. (2007) y Piazzalunga et al. (2010), utilizando gradientes en múltiples pasos (Tabla 2.4) con agua ultra pura Mili-Q y dos soluciones hidróxido de sodio (NaOH) de 200 mM y 5 mM. Para la fase móvil, las soluciones de NaOH diluido se prepararon a partir de una solución de NaOH al 50 - 52% en agua (eluyente para CI Sigma-Aldrich). Para evitar la absorción de CO_2 y la consiguiente contaminación de carbonato del eluyente, los tanques de eluyente fueron purgados con un flujo de N_2 durante 10 - 15 minutos.

Tabla 2.4. Condiciones del gradiente en múltiples pasos con agua ultra pura Mili-Q (A), NaOH 200 mM (B) y NaOH 5 mM (C).

Tiempo (min)	Flujo	% A	% B	% C
0	0.25	90	0	10
10	0.25	90	0	10
15	0.25	85	15	0
35	0.25	85	15	0
45	0.25	0	100	0
55	0.25	90	0	10
70	0.25	90	0	10

La identificación de cada uno de los azúcares se realizó por comparación del tiempo de retención de los picos obtenidos en las muestras con los picos observados con las soluciones patrones individuales. Finalmente, la concentración de cada uno de los azúcares se obtuvo por la integración del área de los picos y su interpolación en las curvas de calibración.

2.3.2.3. Determinación de metales traza

Para la determinación de metales traza se utilizó la técnica de *Emisión de Rayos X Inducida por Partículas* (PIXE, del inglés *Particle-Induced X-ray Emission*). PIXE es una técnica de análisis no destructivo, que permite la cuantificación simultánea de los 72 elementos con número atómico mayor a 10 (de sodio a uranio en la tabla periódica). La ventaja del PIXE es que las muestras pueden ser analizadas sin necesidad de aplicar ningún tratamiento previo. Los espectros de rayos X se obtienen por la excitación de los electrones de las capas internas de los átomos, por protones energéticos. Las energías de los rayos X emitidos cuando se vuelven a llenar las vacantes creadas, son características únicas de los elementos de los que proceden y el número de rayos X emitidos es proporcional a la masa de ese elemento en la muestra analizada.

Los análisis se realizaron en el acelerador Tandetron 3MV del laboratorio del Instituto Nacional de Física Nuclear (INFN-LABEC) de Florencia (Italia) (Fig. 2.16), utilizando una de las

mitades de los filtros de teflón. El acelerador está configurado con un haz externo de protones y dos detectores SDD (en inglés *Silicon Drift Detectors*). El tiempo total de medición es de 90 s por muestra. Cada muestra se irradia con un haz de protones de 3.0 MeV extraído a través de una ventana de Si_3N_4 de 500 nm de espesor. Las muestras de aerosol se colocan a una distancia de aproximadamente 1 cm de la ventana, perpendicular al haz. Tanto el escaneo de los filtros como el cambio de la muestra son controlados automáticamente por el sistema de adquisición.

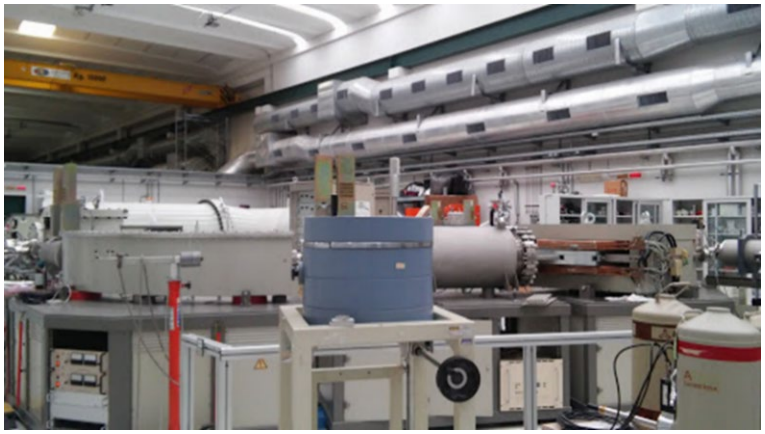

FIG. 2.16. Instalaciones del equipo para el análisis a través de la técnica PIXE en el Instituto Nacional de Física Nuclear (INFN) de Florencia (Italia).

El SDD utilizado para detectar los rayos X de los elementos de bajo número atómico se coloca a aproximadamente 145° con respecto a la dirección del haz, a una distancia de 6 cm del objetivo. Los rayos X de baja energía (hasta ± 1 keV) son detectados a través de una ventana ultra-delgada de berilio de 8 µm, bajo atmósfera inerte de helio. Para la detección de los elementos de números atómicos medio-altos se utiliza el SDD, suministrado por KETEK GmbH. El detector se coloca a 135° con respecto a la dirección del haz, a una distancia de aproximadamente 2 a 2.5 cm del objetivo. Una descripción más detallada sobre el equipo y la técnica puede encontrarse en Lucarelli et al. (2014, 2015).

Los espectros PIXE se ajustan utilizando el código *GUPIX* y las concentraciones elementales se obtienen mediante una curva de calibración a partir de un conjunto de estándares de densidad de área conocida (Micromatter Inc.).

2.3.2.4. Determinación de iones inorgánicos solubles en agua

Los iones inorgánicos solubles en agua se determinaron tanto en las muestras de precipitación como en la mitad sobrante de los filtros de teflón, utilizando la técnica de *Cromatografía Iónica* mencionada en el apartado 2.3.2.2 y el equipo mostrado en la Figura 2.15. La determinación de los cationes Li^+, Na^+, K^+, NH_4^+, Mg^{2+} y Ca^{2+} se realizó utilizando una columna IonPac® CS16 (4 × 250 mm) a 20 °C, con una solución de 30 mM de ácido metanosulfónico (MSA) como eluyente a 0.36 ml min^{-1}. Los aniones Br^-, Cl^-, F^-, SO_4^{2-}, PO_4^{2-}, NO_2^-, y NO_3^-, fueron determinados utilizando una columna IonPac® AS11 (4 × 250 mm) a 20 °C, con una solución de 30 mM de Hidróxido de Potasio (KOH) como eluyente y un flujo constante de 0.20 ml min^{-1}.

Los iones inorgánicos solubles en agua se extrajeron de los filtros de teflón mediante agitación ultrasónica durante 15 minutos, en 6 ml de agua ultrapura Mili-Q. Tanto los extractos de los filtros de teflón como las muestras de precipitación se filtraron con jeringas de PTFE con filtros de poro de 0.2 μm y transferidos a viales de vidrio para su posterior análisis. La cuantificación de los iones analizados se realizó mediante curvas de calibración obtenidas a partir de las concentraciones de las soluciones patrones mostradas en la Tabla 2.5.

Tabla 2.5. Reactivos de partida y concentraciones de las soluciones madres y soluciones patrones utilizadas para las curvas de calibración de los iones inorgánicos analizados.

Sal	Ion analizado	Concentración del ion en la solución madre (mg L^{-1})	Rango de concentraciones del ion en las soluciones patrones (mg L^{-1})
NaCl	Cl^-	648.46	0.03 a 7.20
KNO_3	NO_3^-	630.57	0.10 a 24.00
KH_2PO_4	PO_4^{2-}	411.68	0.15 a 36.00
$NaNO_2$	NO_2^-	534.58	0.10 a 24.00
KBr	Br^-	529.04	0.10 a 24.00
NaF	F^-	1210.12	0.02 a 4.80
Na_2SO_4	SO_4^{2-}	478.64	0.15 a 36.00
NaCl	Na^+	1542.12	0.05 a 8.00
LiCl	Li^+	5107.77	0.0125 a 2.0000
$MgSO_4.7H_2O$	Mg^{2+}	3952.38	0.06 a 9.60
$(NH_4)_2SO_4$	NH_4^+	2662.12	0.06 a 9.60
KBr	K^+	1890.21	0.125 a 20.000
$CaCl_2.2H_2O$	Ca^{2+}	1769.20	0.125 a 20.000

2.3.2.5. Análisis morfológico y químico

El análisis morfológico y químico de algunas muestras se llevó a cabo a través de la técnica de *Microscopía Electrónica de Barrido* (MEB), utilizando un Microscopio Electrónico Hitachi TM-100 (Fig. 2.17a) y un Microscopio Digital de Barrido (DSM950) (Fig. 2.17b), ambos ubicados en la Universidad de Alcalá, en Alcalá de Henares (España).

a) b)

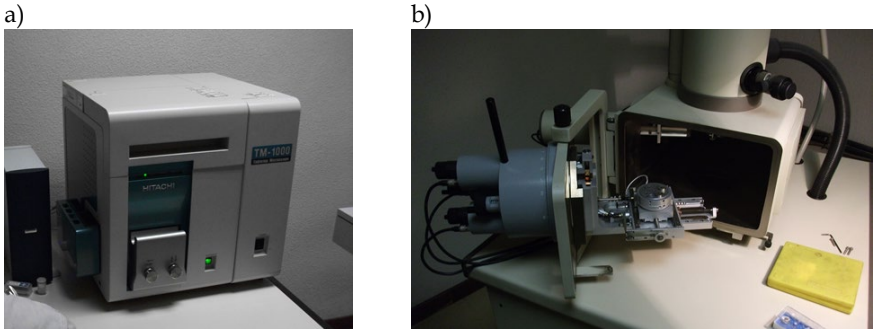

FIG. 2.17. a) Microscopio Electrónico Hitachi TM-100 y b) Microscopio Digital de Barrido (DSM950), ubicados en la Universidad de Alcalá, en Alcalá de Henares (España).

En el microscopio electrónico de barrido la muestra es recorrida por un haz concentrado de electrones. Los electrones son dispersados por la muestra, creando así una imagen ampliada de

la superficie del objeto. Para llevar a cabo este análisis se deben cumplir dos condiciones: las muestras tienen que estar secas y ser conductoras de la corriente eléctrica. La preparación de las muestras consistió en la colocación de una pequeña fracción del filtro en un portamuestras de composición grafítica, que posteriormente fue recubierto con oro para lograr que la muestra fuera conductora.

El microscopio electrónico permite realizar un análisis cualitativo y cuantitativo de los elementos químicos (desde el carbono al uranio) que se encuentran presentes en la muestra. La técnica se basa en la excitación de los átomos de la muestra, causada por los electrones incidentes, lo que provoca la emisión de rayos X a una longitud de onda característica de los elementos presentes. El análisis se realiza eligiendo uno o varios puntos de interés en la muestra y obteniendo espectros de rayos X mediante software. Finalmente, el software proporciona la identificación y la concentración de los diferentes elementos presentes en la sección analizada.

2.3.2.6. Determinación de carbono orgánico soluble en agua

El carbono orgánico soluble en agua fue determinado utilizando las fracciones líquidas de las muestras de precipitación. Este análisis se realizó por combustión y detección infrarroja en un analizador de carbono orgánico total Shimadzu (TOC-VCPH) (Fig. 2.18), ubicado en el Departamento de Química de la Universidad de Aveiro (Portugal).

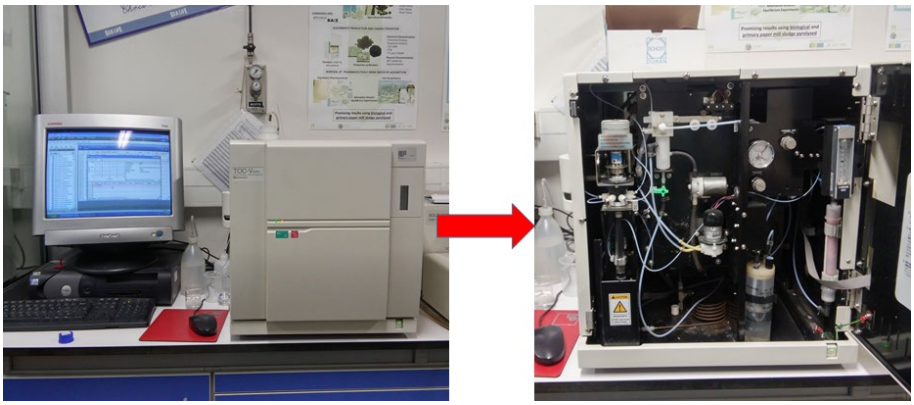

FIG. 2.18. Analizador de Carbono Orgánico Total (TOC-VCPH) ubicado en el Departamento de Química de la Universidad de Aveiro (Portugal).

Para la determinación del DOC, primero se agrega una pequeña cantidad de ácido clorhídrico (HCl) disuelto, para acidificar la muestra, a la vez que se burbujea con N_2. Esto convierte todo el carbono inorgánico de la muestra en dióxido de carbono y lo expulsa de la solución de la muestra. De esta forma, la concentración de carbono total analizado posteriormente corresponde exclusivamente a la concentración de carbono orgánico disuelto. La solución resultante, ahora libre de carbono inorgánico, entra a través de un tubo de combustión a 600 ^{o}C, lleno de Pt como catalizador, con la ayuda de una corriente de O_2 a 150 ml min^{-1}. Una vez entra la muestra en el tubo de combustión, esta se oxida o se descompone para crear dióxido de carbono. El O_2 transporta los productos de combustión desde el tubo de combustión a la celda de muestra del detector infrarrojo no dispersivo (NDIR, en inglés *Non-Dispersive Infrared*), donde se detecta el dióxido de carbono. La señal analógica del NDIR forma un pico y el procesador de datos calcula

el área del pico. Las curvas de calibración para la cuantificación del DOC se realizaron a partir de una solución patrón de hidrogenoftalato de potasio ($C_8H_5KO_4$) con una concentración entre 0.10 y 0.50 μg ml^{-1} de C.

2.3.3. Determinación de la fracción alergénica

La determinación de la fracción alergénica del aerosol se realizó siguiendo el procedimiento descrito por Fernández-González et al. (2010, 2019), que supone modificaciones de los métodos anteriormente descritos por Moreno-Grau et al. (2006) y Takahashi et al. (2001). La metodología para la determinación de la fracción alergénica relacionada con la proteína *Alt a 1*, consta de dos etapas: extracción y cuantificación.

En la fase de extracción, las muestras de partículas atmosféricas, previamente recogidas en los tubos Eppendorf, fueron centrifugadas a 14000 r.p.m. y posteriormente extraídas con una solución de buffer fosfato (50 mM pH 7.0), NaCl 150 mM, EDTA 3 mM, Tween 20 al 0.005% y NH_4HCO_3 125 mM. El extracto se separó por centrifugación a 4000 r.p.m. durante 10 minutos y tanto el sobrenadante como el sedimento, fueron almacenados por separado a -20 ° C.

El contenido de la proteína *Alt a 1* en las muestras extraídas, se cuantificó utilizando un método ELISA (en inglés *Enzyme Linked Inmuno Sorbent Assay*) doble Sándwich. Las placas ELISA (Greiner, Frickenhausen, Alemania) se recubrieron con el anticuerpo correspondiente a la *Alt a 1* en una solución salina de búfer fosfato (PBS). Una vez superado el periodo de incubación, se vació el contenido de las placas y se añadió una solución de PBS con Albúmina de Suero Bovino (BSA) al 1% y Tween-20 al 0.05% (PBS-BSA-T). Las placas se incubaron durante 1 hora y, posteriormente se vació su contenido para realizar 3 lavados sucesivos con una solución de PBS con 0.1% de BSA y 0.1% de Tween-20 (PBS-B-T). Finalmente, la actividad enzimática se determinó agregando o-fenilendiamina y midiendo la absorbancia de las soluciones resultantes con un lector de placas. La cuantificación del alérgeno se realizó mediante la interpolación de los valores de absorbancia en una curva de calibración lineal.

2.4. HERRAMIENTAS ESTADÍSTICAS

Las principales determinaciones estadísticas se realizaron utilizando el *software* SPSS Statistics (IBM V.24). Las herramientas estadísticas utilizadas a lo largo del estudio fueron principalmente: los test no-paramétricos de *Kruskall-Wallis* y de *Mann-Withney*, el coeficiente de correlación lineal de *Pearson* y el *Análisis de Componentes Principales* (ACP).

Los test no-paramétricos de *Kruskall-Wallis* y de *Mann-Withney* permiten evaluar la significación estadística de los diferentes resultados tanto químicos como físicos, obtenidos en el estudio. El test de *Kruskall-Wallis* permite decidir si *K* muestras independientes proceden o no de la misma población. En el caso de que las muestras provengan de diferentes poblaciones, la prueba *U* de *Mann-Whitney* permite comprobar si tal diferencia se produce por los resultados de uno o de varios grupos.

Con el coeficiente lineal de *Pearson* se determina la relación lineal entre dos variables. Para la determinación del coeficiente de Pearson se requiere que la variable sea continua y que la

relación sea lineal. La hipótesis nula del contraste es que no existe ninguna relación entre las variables. Si el coeficiente tiene un valor de +1 indica que la relación es perfecta y directa, y si tiene un valor de -1 indica que la relación es perfecta e inversa.

El *Análisis de Componentes Principales* permite la asociación de los diferentes componentes químicos a diferentes fuentes de aerosol, mediante la reducción del número de variables. Los factores o componentes principales obtenidos después de aplicar el ACP, serán el resultado de una combinación lineal de las variables originales, independientes entre sí. Durante el análisis se utilizó la rotación *Varimax*, que permite que cada componente rotado en vertical (en la matriz de cargas factoriales) presente altas correlaciones aunque se utilicen unas cuantas variables. La interpretación de los factores debe ser deducida tras observar la relación de los factores con las variables iniciales, evaluando tanto el signo como la magnitud de las correlaciones.

2.4.1. Factorización de Matriz Positiva

El análisis de la contribución de las fuentes de aerosoles se llevó a cabo utilizando el modelo PMF (*Positive Matrix Factorization*). Se trata de una herramienta de análisis de factores multivariados desarrollada por la Agencia de Protección Ambiental de EE. UU. (EPA), que descompone una matriz de cada dato de muestra en dos matrices: contribuciones de factores (*g*) y perfiles de factores (*f*). El objetivo de este modelo es resolver el balance de masa química entre las concentraciones de cada especie medida y los perfiles de origen (Ecuación 2.6), utilizando el número *p* de factores, el perfil de especie *f* y la masa *g* aportada por cada factor a cada muestra:

$$x_{ij} = \sum_{k=1}^{p} g_{ik} f_{kj} + e_{ij} \qquad \text{Ecuación 2.6}$$

donde e_{ij} es el residuo de cada muestra/especie.

Los valores g_{ik} y f_{kj} son ajustados hasta que se encuentra un valor mínimo de *Q*, definido como:

$$Q = \sum_{j=1}^{m} \sum_{i=1}^{n} \frac{e_{ij}^2}{s_{ij}^2} \qquad \text{Ecuación 2.7}$$

donde s_{ij} es la incertidumbre de la concentración de cada muestra/especie, *n* es el número de muestras y *m* es el número de especies.

El modelo muestra dos valores de *Q*: *Q* (verdadero) y *Q* (robusto). La diferencia entre esos dos parámetros permite medir el impacto de los puntos de datos con residuos de alta escala. *Q* (verdadero) es el parámetro de bondad de ajuste que se calcula incluyendo todos los puntos y *Q* (robusto) se calcula excluyendo los puntos que el modelo no ajusta. *Q* (robusto) se utiliza para elegir la ejecución óptima de las múltiples ejecuciones, debido a que este parámetro no está influenciado por los puntos que el PMF no ajusta. Por lo tanto, la mejor solución es la que proporciona la *Q* más baja (robusta). Los perfiles de los factores obtenidos tienen que ser interpretados por los usuarios para identificar los tipos de fuente, utilizando la información de perfiles de fuentes (Paatero, 1997; Paatero et al., 2014; Paatero and Tapper, 1994).

Para ejecutar PMF, se utilizaron concentraciones e incertidumbres de las propiedades químicas de 355 muestras de PM_{10}. Los datos que faltaban fueron sustituidos por el valor medio de los valores registrados y sus incertidumbres fueron reemplazadas por cuatro veces el valor medio. Los valores por debajo de los límites de detección se reemplazaron por la mitad del valor mínimo registrado y sus incertidumbres se reemplazaron por 5/6 veces el valor del límite de detección (Polissar et al., 1998).

2.5. HERRAMIENTAS ADICIONALES

2.5.1. Parámetros meteorológicos

Los parámetros meteorológicos utilizados (presión, temperatura media, temperatura mínima, temperatura máxima, humedad relativa, precipitación acumulada, velocidad y dirección del viento) a lo largo del estudio se obtuvieron de dos fuentes distintas: i) mediante la estación meteorológica ubicada en el punto de muestreo, y ii) utilizando los datos proporcionados por la AEMET.

La estación meteorológica se encontraba ubicada a 2 m de los equipos de muestreo de aerosol y precipitación, y registraba datos minutales. Por otra parte, la estación meteorológica de la AEMET se encuentra ubicada en el Aeropuerto de León (Virgen del Camino) (Fig. 2.1), a aproximadamente 8 km de la Universidad de León, y proporciona datos medios diarios.

2.5.2. Origen de las masas de aire

Para determinar el origen de las masas de aire que afectaban la zona de estudio se utilizaron:

- Retro-trayectorias calculadas a 500 m, 1500 m, 3000 m (agl) empleando el modelo HYSPLIT (*Hybrid Single-Particle Lagrangian Integrated Trayectory*) de la NOAA (*National Oceanic and Atmospheric Administration*, Maryland, EEUU) (Draxler and Rolph, 2012; Draxler, 2011; Stein et al., 2015), que permite realizar un amplio rango de simulaciones relacionadas con el transporte a gran escala, dispersión y depósito de contaminantes.

- Mapas de aerosoles de la *Marine Meteorology Division* del *Naval Research Laboratory* (NRL), EEUU. Los cálculos del *Navy Aerosol Analysis and Prediction System* (NAAPS) muestran mapas de distribución de espesor óptico y de concentración en superficie de polvo mineral, sulfato y materia carbonosa proveniente de la quema de biomasa.

2.5.3. Tipos de tiempo

Se realizó una clasificación de los tipos de tiempo (CWT, en inglés *Circulation Weather Types*) basada en los trabajos de Jenkinson y Collison (1977) y Jones et al. (1993), para identificar el tipo de tiempo asociado con una situación sinóptica particular. La circulación diaria que afecta a la Península Ibérica se describe utilizando un conjunto de índices asociados con la dirección y la vorticidad del flujo geostrófico: flujo del sur (SF), flujo del oeste (WF), flujo total (F), vorticidad de corte del sur (ZS), vorticidad de corte del oeste (ZW) y vorticidad de corte total (Z). Estos

índices se calculan utilizando los valores de presión a nivel del mar (SLP) obtenidos para los 16 puntos de la cuadrícula distribuidos en la Península Ibérica (Fig. 2.19). Esta base de datos está disponible para la mayor parte del hemisferio norte en intervalos de 5° de latitud por 5° de longitud, a través del Centro Nacional de Investigación Atmosférica (NCAR, del inglés *National Center for Atmospheric Research*). Se utilizó la misma cuadrícula que en el estudio realizado por Trigo y DaCamara (2000). Este método permite un máximo de 26 CWT diferentes, mostrados en la Tabla 2.6.

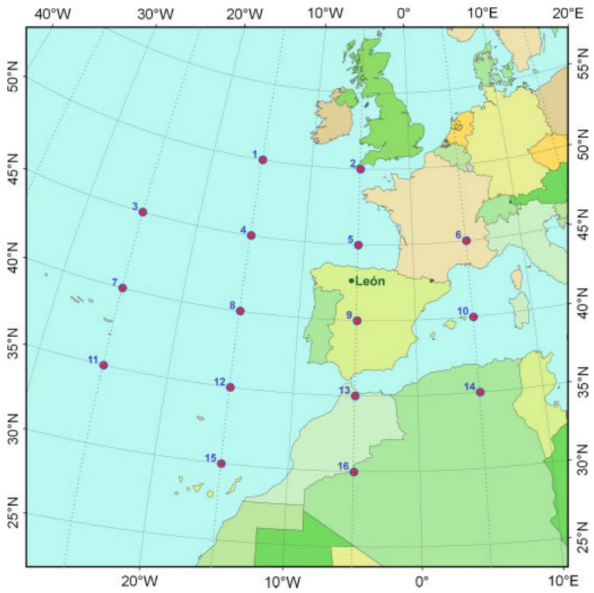

FIG. 2.19. Cuadrícula de 16 puntos a partir de los cuales se obtienen los valores de los índices asociados con la dirección y la vorticidad del flujo geostrófico de presión a nivel del mar (tomado de Fernández-González et al., 2012).

Tabla 2.6. Tipos de tiempo originales (CWTs, en inglés *Circulation Weather Types*), con 2 tipos puros controlados por la vorticidad geostrófica, 8 tipos direccionales y 16 tipos híbridos (Fuente: Fernández-Raga et al., 2017; Trigo and DaCamara, 2000).

Tipos de tiempo de Lamb							
Puros		**Tipos direccionales**		**Híbridos ciclónicos**		**Híbridos anticiclónicos**	
C	Ciclónico	NE	Nordeste	CNE	Ciclónico del nordeste	ANE	Anticiclónico del nordeste
A	Anticiclónico	E	Este	CE	Ciclónico del este	AE	Anticiclónico del este
		SE	Sureste	CSE	Ciclónico del sureste	ASE	Anticiclónico del sureste
		S	Sur	CS	Ciclónico del sur	AS	Anticiclónico del sur
		SW	Suroeste	CSW	Ciclónico del suroeste	ASW	Anticiclónico del suroeste
		W	Oeste	CW	Ciclónico del oeste	AW	Anticiclónico del oeste
		NW	Noroeste	CNW	Ciclónico del noroeste	ANW	Anticiclónico del noroeste
		N	Norte	CN	Ciclónico del norte	AN	Anticiclónico del norte

2.5.4. Forzamiento Radiativo

El forzamiento radiativo de los aerosoles en cielo despejado se ha estimado utilizando el *Modelo de Transferencia Radiativa* (RTM) GAME (*Global Atmospheric ModEl*) (Dubuisson et al., 2004, 1996). Para la aplicación de este modelo es necesario tener en cuenta los siguientes parámetros:

- Parámetros ópticos: la estimación del albedo de *scattering* simple (SSA, en inglés *Single Scattering Albedo*) y del parámetro de asimetría (*g*), se basan en la Teoría de Mie, calculados a partir del espectro de tamaño del aerosol y el índice de refracción, para las siete longitudes de onda empleadas en el Modelo GAME (330, 440, 550, 670, 870, 1020 y 2000 nm).

- Distribución de tamaño de las partículas: se obtienen como medidas de campo durante el período de muestreo, utilizando los espectrómetros SMPS y/o PCASP.

- Parámetro del espesor óptico de los aerosoles (AOD, en inglés *Aerosol Optical Depth*): es obtenido de los datos del sensor MODIS (*Moderate Resolution Imaging Spectroradiometer*) a una longitud de onda de 550 nm.

- Perfiles verticales de propiedades atmosféricas: tales como humedad relativa, temperatura, presión y las concentraciones de ozono se han estimado a través de modelos disponibles en la NOAA.

Los flujos radiativos netos hacia arriba y hacia abajo se calculan sobre toda la región de onda corta y se realizan en cada intervalo de 3 h y durante todo el período de estudio, con y sin aerosoles. A partir de estos flujos, se calcula el forzamiento directo diario del aerosol a cielo despejado en la parte baja de la atmósfera (BOA), ΔFBOA (Ecuación 2.8) y en el techo de la atmósfera (TOA, 20 km en este caso), ΔFTOA (Ecuación 2.9). El ΔFBOA y el ΔFTOA representan el efecto de las partículas en los flujos netos de radiación de onda corta que alcanzan la superficie y los reflejados hacia el espacio por los aerosoles, respectivamente.

$$\Delta FBOA = FBOA(w)\downarrow - FBOA(o)\downarrow \qquad \text{Ecuación 2.8}$$

$$\Delta FTOA = -(FTOA(w)\uparrow - FTOA(o)\uparrow) \qquad \text{Ecuación 2.9}$$

donde FBOA(w)↓ y FBOA(o)↓ representan los flujos radiativos netos descendentes simulados en la superficie con (w) y sin (o) aerosoles, respectivamente; y FTOA(w)↑ y FTOA(o) ↑ son los flujos radiativos netos ascendentes simulados en el techo de la atmósfera, con (w) y sin (o) aerosoles (Calvo et al., 2010).

Con la convención considerada aquí, un signo positivo de ΔFBOA y ΔFTOA indica un efecto de calentamiento de aerosoles. El forzamiento atmosférico ΔFATM se estimó a través de la diferencia entre el forzamiento directo de aerosol en el techo y en la parte baja de la atmósfera (Ecuación 2.10) y representa la posible absorción de la radiación solar por las partículas dentro de las capas atmosféricas de aerosol especificadas. Una descripción más detallada se encuentra en Calvo et al. (2010).

$$\Delta FATM = \Delta FTOA - \Delta FBOA \qquad \text{Ecuación 2.10}$$

2.5.5. Fotómetro solar CIMEL

Las propiedades ópticas de los aerosoles a lo largo del recorrido vertical atmosférico se midieron con un *fotómetro Cimel* CE318 Sun/Sky (Fig. 2.20). El Cimel es un instrumento que trabaja de forma autónoma y permite determinar la irradiancia solar directa y la radiancia del cielo. Está conformado por una cabeza sensora compuesta por dos fotodiodos de silicio que actúan como detectores, y siete filtros interferenciales con longitudes de onda nominales de 340, 380, 440, 670, 870, 936 y 1020 nm, colocados en una rueda provista de un motor paso a paso. La cabeza sensora es dirigida en las direcciones del acimut y del cenit (movimientos horizontal y vertical) por medio de un robot, provisto de una montura altacimutal con dos motores de transmisión directa paso a paso. La posición del Sol es calculada a través del software que controla el sistema de seguimiento, según el lugar de observación.

FIG. 2.20. Fotómetro Cimel CE318 Sun/Sky.

Las medidas de radiancia del cielo siguen dos configuraciones distintas: el *almucántar solar* y el *plano principal* (Fig. 2.21):

- *Almucántar solar*: el instrumento realiza una medida de irradiancia solar directa, manteniendo constante el ángulo de elevación y, posteriormente, realiza las medidas barriendo ángulos acimutales hasta 180º a ambos lados del disco solar. Las medidas son utilizadas para comprobar la homogeneidad de la atmósfera.

- *Plano principal*: mide la radiancia del cielo para cada longitud de onda, a un ángulo acimutal constante, variando el ángulo cenital.

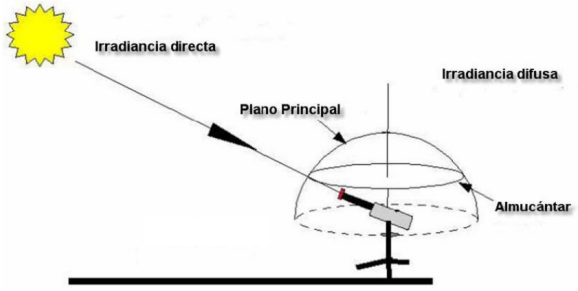

FIG. 2.21. Esquema ilustrativo de las medidas llevadas a cabo por el fotómetro Cimel CE318 Sun/Sky (tomado de Calvo, 2009).

2.5.6. Fracciones de tamaño de aerosol depositadas en el tracto respiratorio

La estimación de la deposición de partículas en el tracto respiratorio humano se realizó siguiendo la metodología establecida por la Norma ISO 7708:1995 *Air quality: particle size fractions definitions for health-related sampling* (International Organization for Standardization, 1995). Esta normativa establece las siguientes definiciones para las partículas relacionadas con la región del tracto respiratorio donde se depositan:

- La fracción inhalable es la fracción de masa de partículas atmosféricas que se inhalan por la nariz y la boca.
- La fracción extra-torácica es la fracción de masa de partículas inhaladas que se retienen en la región respiratoria anterior a la laringe.
- La fracción torácica es la fracción de masa de partículas inhaladas capaces de penetrar más allá de la laringe. Numéricamente, es equivalente al porcentaje de la fracción inhalable dada por una distribución log-normal acumulativa con una mediana de 11.64 µm con una desviación estándar geométrica de 1.5.
- La fracción traqueobronquial corresponde a la fracción másica de partículas inhaladas que pueden atravesar la laringe, pero no pueden atravesar las vías respiratorias no ciliadas.
- La fracción respirable es la fracción de masa de partículas inhaladas que penetra en las vías respiratorias no ciliadas. En individuos sanos y de alto riesgo está representada por el porcentaje de la fracción inhalable dada por una distribución log-normal acumulativa con una mediana de 4.25 y 2.5 µm, respectivamente.

Las diferentes fracciones másicas de aerosoles se evaluaron teniendo en cuenta la densidad estimada de las partículas, los diámetros aerodinámicos de los canales del espectrómetro y el número de partículas en cada canal, obtenidos por el PCASP y/o el SMPS.

2.6. REFERENCIAS

Agencia Estatal de Meteorología. Valores climatológicos normales. León, Virgen del Camino. URL http://www.aemet.es (accessed 2.20).

Alonso-Blanco, E., 2019. Caracterización de la distribución de tamaños y propiedades higroscópicas del aerosol atmosférico en España mediante Analizadores de Movilidad Diferencial (DMA). Universidad de Alcalá de Henares.

Alves, C.A., Calvo, A.I., Marques, L., Castro, A., Nunes, T., Coz, E., Fraile, R., 2014. Particulate matter in the indoor and outdoor air of a gymnasium and a fronton. Environ. Sci. Pollut. Res. 21, 12390–12402. doi:10.1007/s11356-014-3168-1

Blanco-Alegre, C., Calvo, A.I., Coz, E., Castro, A., Oduber, F., Prévôt, A.S.H., Močnik, G., Fraile, R., 2019. Quantification of source specific black carbon scavenging using an aethalometer and a disdrometer. Environ. Pollut. 246, 336–345. doi:10.1016/j.envpol.2018.11.102

Bohren, C.F., Huffman, D.R., 1983. Absorption and Scattering of Light by Small Particles. Wiley, Weinheim, Germany. doi:10.1002/9783527618156

Calvo, A.I., 2009. Caracterización y transporte del aerosol atmosférico: medio urbano, rural y quema de biomasa. Universidad de León.

Calvo, A.I., Baumgardner, D., Castro, A., Fernández-González, D., Vega-Maray, A.M., Valencia-Barrera, R.M., Oduber, F., Blanco-Alegre, C., Fraile, R., 2018. Daily behavior of urban Fluorescing Aerosol Particles in northwest Spain. Atmos. Environ. 184, 262–277. doi:10.1016/j.atmosenv.2018.04.027

Calvo, A.I., Pont, V., Castro, A., Mallet, M., Palencia, C., Roger, J.C., Dubuisson, P., Fraile, R., 2010. Radiative forcing of haze during a forest fire in Spain. J. Geophys. Res. 115, D08206. doi:10.1029/2009JD012172

Calvo, A.I., Tarelho, L.A.C., Teixeira, E.R., Alves, C., Nunes, T., Duarte, M., Coz, E., Custodio, D., Castro, A., Artiñano, B., Fraile, R., 2013. Particulate emissions from the co-combustion of forest biomass and sewage sludge in a bubbling fluidised bed reactor. Fuel Process. Technol. 114, 58–68. doi:10.1016/j.fuproc.2013.03.021

Caseiro, A., Marr, I.L., Claeys, M., Kasper-Giebl, A., Puxbaum, H., Pio, C.A., 2007. Determination of saccharides in atmospheric aerosol using anion-exchange high-performance liquid chromatography and pulsed-amperometric detection. J. Chromatogr. A 1171, 37–45. doi:10.1016/j.chroma.2007.09.038

Castro, A., Alonso-Blanco, E., González-Colino, M., Calvo, A.I., Fernández-Raga, M., Fraile, R., 2010. Aerosol size distribution in precipitation events in León, Spain. Atmos. Res. 96, 421–435. doi:10.1016/j.atmosres.2010.01.014

Creatchman, M., Landsberger, S., 1999. Elemental Analysis of Airborne Particles, Advances in environmental, industrial, and process control technologies. Gordon and Breach Science Publishers, Amsterdan, The Netherlands.

Del Río González, S., 2005. El cambio climático y su influencia en la vegetación de Castilla y León (España). Itinera Geobot. 5–534.

Dirección General de Tráfico. Parque distribuido por tipo de vehículo y año de matriculación. URL https://sedeapl.dgt.gob.es/WEB_IEST_CONSULTA/ (accessed 2.20).

Draxler, R., Rolph, G., 2012. Hysplit (Hybrid Single-Particle Lagrangian Integrated Trajectory). Silver Spring. NOAA Air Resour. Lab.

Draxler, R.R., 2011. Hysplit (hybrid single-particle lagrangian integrated trajectory) model access via NOAA ARL ready website. http//ready. arl. noaa. gov/HYSPLIT. php.

Dubuisson, P., Buriez, J.C., Fouquart, Y., 1996. High spectral resolution solar radiative transfer in absorbing and scattering media: Application to the satellite simulation. J. Quant. Spectrosc. Radiat. Transf. 55, 103–126. doi:10.1016/0022-4073(95)00134-4

Dubuisson, P., Dessailly, D., Vesperini, M., Frouin, R., 2004. Water vapor retrieval over ocean using near-infrared radiometry. J. Geophys. Res. 109, D19106. doi:10.1029/2004JD004516

European, C. for S., 2014. EN 12341: 2014 Ambient air - Standard gravimetric measurement method for the determination of the PM_{10} or $PM_{2.5}$ mass concentration of suspended particulate matter.

Fernández-González, D., González-Parrado, Z., Vega-Maray, A.M., Valencia-Barrera, R.M., Camazón-Izquierdo, B., De Nuntiis, P., Mandrioli, P., 2010. Platanus pollen allergen, Pla a 1: Quantification in the atmosphere and influence on a sensitizing population. Clin. Exp. Allergy 40, 1701–1708. doi:10.1111/j.1365-2222.2010.03595.x

Fernández-González, D., Vega Maray, A.M., González Parrado, Z., Valencia Barrera, R.M., Gutiérrez, P., De Nuntiis, P., Mandrioli, P., 2019. Are the profilins an important component in the atmosphere? Ole e 2-like panallergen. Aerobiologia (Bologna). 35, 165–175. doi:10.1007/s10453-018-9548-0

Fernández-González, S., Del Río, S., Castro, A., Penas, A., Fernández-Raga, M., Calvo, A.I., Fraile, R., 2012. Connection between NAO, weather types and precipitation in León, Spain (1948-2008). Int. J. Climatol. 32, 2181–2196. doi:10.1002/joc.2431

Fernández-Raga, M., Castro, A., Marcos, E., Palencia, C., Fraile, R., 2017. Weather types and rainfall microstructure in Leon, Spain. Int. J. Climatol. 37, 1834–1842. doi:10.1002/joc.4816

Fernández-Raga, M., Castro, A., Palencia, C., Calvo, A.I., Fraile, R., 2009. Rain events on 22 October 2006 in León (Spain): Drop size spectra. Atmos. Res. 93, 619–635. doi:10.1016/j.atmosres.2008.09.035

Fialho, P., Freitas, M.C., Barata, F., Vieira, B., Hansen, A.D.A., Honrath, R.E., 2006. The Aethalometer calibration and determination of iron concentration in dust aerosols. J. Aerosol Sci. 37, 1497–1506. doi:10.1016/j.jaerosci.2006.03.002

Fialho, P., Hansen, A.D.A., Honrath, R.E., 2005. Absorption coefficients by aerosols in remote areas: A new approach to decouple dust and black carbon absorption coefficients using seven-wavelength Aethalometer data. J. Aerosol Sci. 36, 267–282. doi:10.1016/j.jaerosci.2004.09.004

Flagan, R.C., 1999. On Differential Mobility Analyzer Resolution. Aerosol Sci. Technol. 30, 556–570. doi:10.1080/027868299304417

Galán Soldevilla, C., Cariñanos González, P., Alcázar Teno, P., Domínguez Vilches, E., 2007. Spanish aerobiology network (REA): management and quality manual. Universidad de Córdoba.

Hinds, W.C., 2012. Aerosol Technology: Properties, Behavior, and Measurement of Airborne Particles. Wiley.

Hirst, J.M., 1952. An automatic volumetric spore trap. Ann. Appl. Biol. 39, 257–265. doi:10.1111/j.1744-7348.1952.tb00904.x

Instituto Nacional de Estadística, 2016. Cifras de población. URL http://www.ine.es (accessed 2.20).

International Organization for Standardization, 1995. ISO 7708: 1995 Air quality -Particle size fraction definitions for health-related sampling. ISO Publications, 1st edition, 1995-04-01.

Jenkinson, A.F., Collison, F.P., 1977. An initial climatology of gales over the North Sea. Synop. Climatol. branch Memo. 62, 18.

Jones, P.D., Hulme, M., Briffa, K.R., 1993. A comparison of Lamb circulation types with an objective classification scheme. Int. J. Climatol. 13, 655–663. doi:10.1002/joc.3370130606

Junta de Castilla y León, 2017. Matriculaciones de vehículos. URL https://estadistica.jcyl.es/web/es/estadisticas-temas/matriculaciones-vehiculos-anios-anteriores.html (accessed 2.20).

Levin, E.J.T., McMeeking, G.R., Carrico, C.M., Mack, L.E., Kreidenweis, S.M., Wold, C.E., Moosmüller, H., Arnott, W.P., Hao, W.M., Collett, J.L., Malm, W.C., 2010. Biomass burning smoke aerosol properties measured during Fire Laboratory at Missoula Experiments (FLAME). J. Geophys. Res. 115, D18210. doi:10.1029/2009JD013601

Lucarelli, F., Calzolai, G., Chiari, M., Giannoni, M., Mochi, D., Nava, S., Carraresi, L., 2014. The upgraded external-beam PIXE/PIGE set-up at LABEC for very fast measurements on aerosol samples. Nucl. Instruments Methods Phys. Res. Sect. B Beam Interact. with Mater. Atoms 318, 55–59. doi:10.1016/j.nimb.2013.05.099

Lucarelli, F., Chiari, M., Calzolai, G., Giannoni, M., Nava, S., Udisti, R., Severi, M., Querol, X., Amato, F., Alves, C., Eleftheriadis, K., 2015. The role of PIXE in the AIRUSE project "testing and development of air quality mitigation measures in Southern Europe." Nucl. Instruments Methods Phys. Res. Sect. B Beam Interact. with Mater. Atoms 363, 92–98. doi:10.1016/j.nimb.2015.08.023

Marques, R.F. de P.V., Mello, C.R. de, Silva, A.M. da, Franco, C.S., Oliveira, A.S. de, 2014. Performance of the probability distribution models applied to heavy rainfall daily events. Ciência e Agrotecnologia 38, 335–342. doi:10.1590/s1413-70542014000400003

Moreno-Grau, S., Elvira-Rendueles, B., Moreno, J., García-Sánchez, A., Vergara, N., Asturias, J.A., Arilla, M.C., Ibarrola, I., Seoane-Camba, J.A., Suárez-Cervera, M., 2006. Correlation between Olea europaea and Parietaria judaica pollen counts and quantification of their major allergens Ole e 1 and Par j 1-Par j 2. Ann. Allergy, Asthma Immunol. 96, 858–864. doi:https://doi.org/10.1016/S1081-1206(10)61350-6

Oduber, F., Calvo, A.I., Blanco-Alegre, C., Castro, A., Vega-Maray, A.M., Valencia-Barrera, R.M., Fernández-González, D., Fraile, R., 2019. Links between recent trends in airborne pollen concentration, meteorological parameters and air pollutants. Agric. For. Meteorol. 264, 16–26. doi:10.1016/j.agrformet.2018.09.023

Oduber, F., Castro, A., Calvo, A.I., Blanco-Alegre, C., Alonso-Blanco, E., Belmonte, P., Fraile, R., 2018. Summer-autumn air pollution in León, Spain: Changes in aerosol size distribution and expected effects on the respiratory tract. Air Qual. Atmos. Heal. 11, 505–520. doi:10.1007/s11869-018-0556-6

Paatero, P., 1997. Least squares formulation of robust non-negative factor analysis. Chemom. Intell. Lab. Syst. 37, 23–35. doi:10.1016/S0169-7439(96)00044-5

Paatero, P., Eberly, S., Brown, S.G., Norris, G.A., 2014. Methods for estimating uncertainty in factor analytic solutions. Atmos. Meas. Tech. 7, 781–797. doi:10.5194/amt-7-781-2014

Paatero, P., Tapper, U., 1994. Positive matrix factorization: A non-negative factor model with optimal utilization of error estimates of data values. Environmetrics 5, 111–126. doi:10.1002/env.3170050203

Piazzalunga, A., Fermo, P., Bernardoni, V., Vecchi, R., Valli, G., de Gregorio, M.A., 2010. A simplified method for levoglucosan quantification in wintertime atmospheric particulate

matter by high performance anion-exchange chromatography coupled with pulsed amperometric detection. Int. J. Environ. Anal. Chem. doi:10.1080/03067310903023619

Polissar, A. V., Hopke, P.K., Paatero, P., Malm, W.C., Sisler, J.F., 1998. Atmospheric aerosol over Alaska 2. Elemental composition and sources. J. Geophys. Res. Atmos. 103, 19045–19057. doi:10.1029/98JD01212

Sandradewi, J., Prévôt, A.S.H., Szidat, S., Perron, N., Alfarra, M.R., Lanz, V.A., Weingartner, E., Baltensperger, U., 2008. Using Aerosol Light Absorption Measurements for the Quantitative Determination of Wood Burning and Traffic Emission Contributions to Particulate Matter. Environ. Sci. Technol. 42, 3316–3323. doi:10.1021/es702253m

Sorribas Panero, M. del M., 2007. Medida y Caracterización del Aerosol Atmosférico en un Ambiente Rural y Costero del Suroeste de Europa. La Distribución Numérica de Tamaños en el Rango Sub-Micrométrico. Universidad de Valladolid.

Stein, A.F., Draxler, R.R., Rolph, G.D., Stunder, B.J.B., Cohen, M.D., Ngan, F., 2015. NOAA's HYSPLIT Atmospheric Transport and Dispersion Modeling System. Bull. Am. Meteorol. Soc. 96, 2059–2077. doi:10.1175/BAMS-D-14-00110.1

Takahashi, Y., Ohashi, T., Nagoya, T., Sakaguchi, M., Yasueda, H., Nitta, H., 2001. Possibility of real-time measurement of an airborne Cryptomeria japonica pollen allergen based on the principle of surface plasmon resonance. Aerobiologia (Bologna). 17, 313–318. doi:10.1023/A:1013002001583

Trigo, R.M., DaCamara, C.C., 2000. Circulation weather types and their influence on the precipitation regime in Portugal. Int. J. Climatol. 20, 1559–1581. doi:10.1002/1097-0088(20001115)20:13<1559::AID-JOC555>3.0.CO;2-5

Weingartner, E., Saathoff, H., Schnaiter, M., Streit, N., Bitnar, B., Baltensperger, U., 2003. Absorption of light by soot particles: Determination of the absorption coefficient by means of aethalometers. J. Aerosol Sci. 34, 1445–1463. doi:10.1016/S0021-8502(03)00359-8

Wiedensohler, A., 1988. An approximation of the bipolar charge distribution for particles in the submicron size range. J. Aerosol Sci. 19, 387–389. doi:10.1016/0021-8502(88)90278-9

Wiedensohler, A., Birmili, W., Nowak, A., Sonntag, A., Weinhold, K., Merkel, M., Wehner, B., Tuch, T., Pfeifer, S., Fiebig, M., Fjäraa, A.M., Asmi, E., Sellegri, K., Depuy, R., Venzac, H., Villani, P., Laj, P., Aalto, P., Ogren, J.A., Swietlicki, E., Williams, P., Roldin, P., Quincey, P., Hüglin, C., Fierz-Schmidhauser, R., Gysel, M., Weingartner, E., Riccobono, F., Santos, S., Grüning, C., Faloon, K., Beddows, D., Harrison, R., Monahan, C., Jennings, S.G., O'Dowd, C.D., Marinoni, A., Horn, H.G., Keck, L., Jiang, J., Scheckman, J., McMurry, P.H., Deng, Z., Zhao, C.S., Moerman, M., Henzing, B., De Leeuw, G., Löschau, G., Bastian, S., 2012. Mobility particle size spectrometers: Harmonization of technical standards and data structure to facilitate high quality long-term observations of atmospheric particle number size distributions. Atmos. Meas. Tech. 5, 657–685. doi:10.5194/amt-5-657-2012

Yang, M., Howell, S.G., Zhuang, J., Huebert, B.J., 2009. Attribution of aerosol light absorption to black carbon, brown carbon, and dust in China - Interpretations of atmospheric measurements during EAST-AIRE. Atmos. Chem. Phys. 9, 2035–2050. doi:10.5194/acp-9-2035-2009

3

LINKS BETWEEN RECENT TRENDS IN AIRBORNE POLLEN CONCENTRATION, METEOROLOGICAL PARAMETERS AND AIR POLLUTANTS

Published in: Agricultural and Forest Meteorology 264(2019)16–26

3.1. INTRODUCTION

In the atmosphere there are several pollutants that cause a negative impact on human health and the environment. The main air pollutants are carbon monoxide (CO), nitrogen oxides (NO_x), particulate matter (PM), which includes bioaerosols (pollen, fungal spore, bacteria, viruses, etc.) and non-biological particles, sulfur dioxide (SO_2) and ozone (O_3). These pollutants, gases and particles, coexist in the same medium, the atmosphere, with the possibility of interacting with each other and increasing their adverse impact due to synergistic effects (Monsalve et al., 2013). Thus, the exposure to O_3 is related to inflammatory effects in the respiratory tract, and the exposure to CO, NO_2, PM and SO_2 has been associated with cardiopulmonary mortality, pulmonary edema, problems in the central nervous system, and respiratory and cardiovascular hospital admissions (Bernstein et al., 2004; Brunekreef and Holgate, 2002; Curtis et al., 2006; Kampa and Castanas, 2008). The presence of high levels of bioaerosols in the atmosphere is usually linked to allergic respiratory diseases (Buters et al., 2012, 2015).

On the other hand, the presence of high levels of air pollutants may also affect the environment. For example, aerosols may scatter or absorb solar and infrared radiation (Calvo et al., 2010; Ren-Jian et al., 2012) and NO_x is the main precursor of acid rain, which may cause the acidification of soils, lakes, and streams, and accelerate the corrosion of buildings and monuments (Tang et al., 2005).

For many years, efforts have been made in Europe to reduce the levels of emission of air pollutants. In 1996 the Directive 96/62/CE about the Evaluation and Management of Ambient Air Quality was passed. This was the first standard adopting fixed criteria, objectives and evaluation techniques for air quality. From this one, in the following years, different Directives have been developed including Directives 1999/30/CE, 2000/69/CE, 2002/3/CE and 2004/107/CE. All these Directives were incorporated to the one currently in force, Directive 2008/50/EC relative to Ambient Air Quality and a Cleaner Atmosphere in Europe.

In Spain, the legal basis relative to the Protection of the Atmospheric Environment dates from 1972, when the Law 38/1972 was passed. Subsequently, this law was adapted to the European environmental needs for better prevention of the harmful effects of atmospheric pollutants over human health and the environment, and was integrated into the Royal Decrees 833/1975, 1073/2002, 1796/2003 and 812/2007. These Royal Decrees were derogated and integrated into the current Spanish regulation about Air Quality and Atmosphere Protection (Law 34/2007) and Improvement of Air Quality (Royal Decree 102/2011).

Long-term studies of air pollutants are essential to evaluate the effectiveness of the implementation of national and/or international environmental policies. In the past decade, several authors have reported a general and progressive decrease in air pollutant concentrations, attributable to different actions taken by local governments and international organizations to reduce emissions (Aziz et al., 2016; Ebelt et al., 2001; Guerreiro et al., 2014; Karanasiou et al., 2014; Querol et al., 2014). Studies focusing on the long-term trend of airborne pollen concentrations have been of great interest in recent years due to the increase in allergies, especially in urban and industrialized areas. In addition, airborne pollen is considered a sensitive indicator of plants to climate change (Clot, 2003; D'Amato et al., 2015, 2016; Oteros et al., 2015).

Although there are many studies on air pollutant concentration trends, there are few on pollen concentration trends (e.g. Galán et al., 2016; Sofiev et al., 2015) and those relating both topics are scarce. Atmospheric pollution has a direct effect on the physical, chemical and biological properties of pollen grains, and the change registered in the concentrations of air pollutants in the past decade and the impact of environmental regulations on the levels of air pollutants can be related to pollen concentrations and allergenic proteins which are potentially responsible for the increase in allergic diseases. According to Sénéchal et al. (2015), atmospheric pollutants may have several effects on pollen: i) increasing their potential health hazards; ii) alteration of the physicochemical characteristics of the pollen surface, iii) change in the allergenic potential, and iv) decrease in viability and germination. For example, high levels of CO_2 may be related to an increase in the airborne pollen concentration in large cities and, as a consequence, to an increase in respiratory allergies (Albertine et al., 2014; Rogers et al., 2006; Schmidt, 2016; Sharma et al., 2014). Evidence demonstrates that there is an interaction between air pollution and plant-derived respiratory disorders (Beggs, 2010; Bielory et al., 2012; D'Amato et al., 2000, 2014,2015). This interaction is influenced by several factors such as the type of air pollutants, plant species, climatic factors, chemical interactions, etc. (Beggs, 2004; D'Amato et al., 2007; Reinmuth-Selzle et al., 2017).

Due to the different levels of air pollutant concentrations and the numerous types of vegetation in different regions of Spain, and because of the lack of data on the connection between air pollutants and pollen concentration in the northwest of the Iberian Peninsula, it is interesting to assess this connection on the basis of long-term trends in the city of León. León, situated in the NW of the Peninsula, is an ideal place for this study because of its unique characteristics: it has a wide variety of vegetation associated with respiratory allergies and there is a Spanish Aerobiology Network (REA) station, with a historical database of pollen levels of several species in the city, together with an extensive database on air quality.

The aim of this study is to evaluate the trend in *Fraxinus*, Poaceae and *Populus* pollen concentration (related to allergies) as well as atmospheric pollutants in León (Spain) over the last

two decades. The study also seeks to explore the correlation between the concentration of pollen and both the main atmospheric pollutants and the meteorological parameters. Additionally, the location of the main sources of atmospheric pollutants and pollen from the selected taxa in León will also be investigated.

3.2. MATERIAL AND METHOD

3.2.1. Study zone

The study was carried out in the city of León, located in the northwest of the Iberian Peninsula (42° 36′ N, 05° 35′ W and 838 m above sea level), between 1997 and 2016. The climate is Mediterranean with continental features. The mean seasonal weather conditions obtained from the National Agency for Meteorology (www.aemet.es) are presented in Table 3.1.

TABLE 3.1. Maximum, minimum and mean values of temperature (T), relative humidity (RH), days with precipitation (DP) and days with snow (DS) by season in the city of León.

Season	Months	T (°C)	T_{Min} (°C)	T_{Max} (°C)	RH (%)	DP (mean precipitation)	DS
Winter	January, February, March	5.2	0.4	10.0	74	6.4 (39 mm)	2.9
Spring	April, May, June	12.9	6.7	19.1	61	4 (44 mm)	0.3
Summer	July, August, September	18.6	11.5	25.7	56	3.3 (27 mm)	0
Autumn	October, November, December	7.6	3.3	12.0	79	8.1 (62 mm)	1

The population of the city of León and the nearby municipalities (San Andrés del Rabanedo, Villaquilambre, Valverde de la Virgen and Onzonilla) has grown, according to the data presented by the National Institute for Statistics (www.ine.es), from 176,333 inhabitants in 1998 to 185,393 inhabitants in 2016. With regard to the number of cars, the regional government of the Junta de Castilla y León registered an increase in the province of León from 301,365 vehicles in 2005 to 347,174 vehicles in 2015 (www.estadistica.jcyl.es). Besides, the General Agency for Traffic (www.dgt.es) reports that the vehicles registered are grouped as follows: buses (0.2%), trucks (8.1%), mopeds (4.6%), vans (8.0%), motorcycles (6.3%), private cars (68.4%) and others (4.3%). Fig. 3.1 shows the classification of these vehicles by type of fuel (diesel, gasoline and electric) from 2010 to 2016.

The mountains located north of the province (about 30 km far from the city) are an important area of origin of bioaerosols because of their numerous forests, with many types of vegetation, whose pollination contributes to a high pollen concentration. In addition, deciduous forests, with poplars (*Populus* L.) and ash trees (*Fraxinus* Tourn. ex L.), are present in numerous valleys and as ornamental flora. A variety of grasses (Poaceae Barnhart) and other herbaceous plants are also found in grasslands and meadows (Del Río González, 2005).

These pollen types (*Fraxinus*, Poaceae and *Populus*) have been chosen for analysis because grass pollen (16–40 µm size) is the main cause of respiratory allergies in the world (D'Amato et al., 2010) and also in León. The other two pollen types correspond to pre-spring flowering species with high incidence in pollinosis in the area. *Fraxinus* (pollen size: 15–24 µm) belongs to the Oleaceae family, one of the most allergenic types in Mediterranean regions and whose incidence is increasing in the city of León due to cross-reactivity with the rest of the family's species (Lombardero et al., 2002). *Populus* (pollen size: 22–30 µm) is a taxon not always well identified as responsible for pollinosis, as its symptoms coincide with those from viral conditions characteristic of this season.

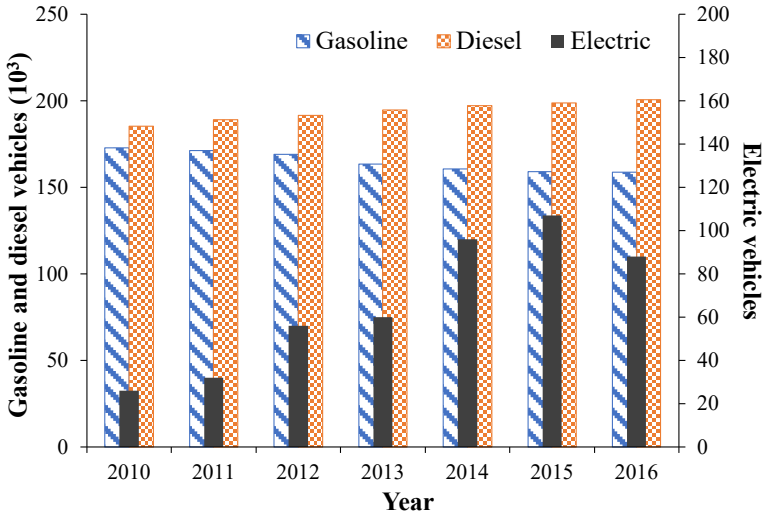

FIG. 3.1. Number of electric, gasoline and diesel vehicles in the province of León (data from the Spanish General Agency for Traffic -DGT).

3.2.2. Sampling and data bases

Atmospheric pollen concentration was analyzed using a Hirst volumetric trap (Hirst, 1952), placed on the terrace of the Faculty of Veterinary Sciences of the University of León (42° 36′ 50″ N, 5° 33′ 38″ W, 846 m) from 1994 to 2016 (Fig. 3.2). The daily and hourly optical microscopic counts were carried out using the method recommended by the Spanish Aerobiological Network (Galán Soldevilla et al., 2007). The average daily and hourly pollen concentrations for *Fraxinus*, Poaceae and *Populus* were expressed as pollen grains per cubic meter of air. The Main Pollen Season (MPS) was defined by Galán et al. (2017) as the period when the atmosphere contains significant concentrations of pollen and the Seasonal Pollen Integral (SPIn) as the integral over time of pollen concentration expressed as pollen day m^{-3}. There are different methods to define the main season start and end (Jato et al., 2006; Pfaar et al., 2017), depending on the main goal of the study. For our work, the consecutive days representing 95% of the SPIn, were selected to establish the MPS, starting on the day on which the accumulated value reaches 2.5% and ending on the day when 97.5% of the SPIn is reached (Andersen, 1991). This criterion has been widely used in many works (Chiesa and Toletti, 2004; Recio et al., 2010; Rojo et al., 2015).

The study of the evolution of pollen concentration was carried out in three periods of four months each (January–April, May–August, and September–December). These three groups will

allow us to define for each species the flowering period. The other two periods will be considered as previous to the flowering period.

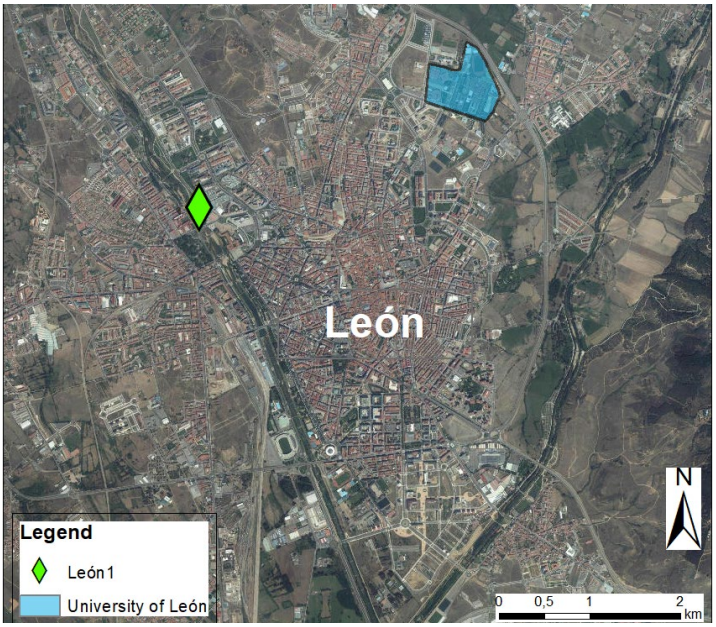

FIG. 3.2. Map of the city of León.

For this study, we have used the data provided by the Air Quality Network of the Junta de Castilla y León (www.servicios.jcyl.es/esco/), from January 1997 to December 2016 for the traffic station León1, located in San Ignacio de Loyola Avenue (05° 35′ 14″ W 42° 36′ 14″ N), for the air pollutants CO, NO, NO_2, PM_{10}, SO_2 and O_3 (Fig. 3.2). This station is located in an urban residential area with medium traffic. The main sources of pollution in León are vehicular emissions and residential devices used for heating, especially in the cold months (Oduber et al., 2018).

The meteorological parameters (mean temperature, relative humidity, minimum temperature, maximum temperature, wind direction, wind speed and accumulated precipitation) during the study period (1994–2016) were obtained from the database of the National Agency for Meteorology (www.aemet.es). The atmospheric pollutant emission levels were drawn from the National Emissions Inventory of the Spanish Ministry of Agriculture, Nature and Food Quality (MAGRAMA- www.magrama.gob.es) and the data on the production and consumption of energy in the province of León were taken from the website of the regional government Junta de Castilla y León (www.energia.jcyl.es).

3.2.3. Statistics treatment

The statistical treatment has been carried out using R software (www.R-project.org) with the Openair package (Carslaw, 2015; Carslaw and Ropkins, 2012) and SPSS (IBM Statistics Software V. 24). The trend calculations were carried out using Theil-Sen methodology and non-parametric Mann-Kendall tests (Hipel and McLeod, 2005; Kendall and Gibbons, 1990) for a significance level of $p < 0.001$. The correlation among pollen concentrations, pollutant

concentrations and meteorological parameters (temperature, relative humidity and rain) was made using the nonparametric Spearman's rank correlation method.

3.3. RESULTS AND DISCUSSION

3.3.1. Trends in air pollutant concentrations and meteorological parameters

The Mann Kendall Trend test was applied to the meteorological parameters and the pollutant concentrations registered by the traffic station León1. Regarding the meteorological parameters, no significant trends were observed during the study period.

The application of the Mann Kendall Trend test to pollutant concentrations showed the following results (Fig. 3.3):

- A significant decreasing trend of CO concentrations beginning around 2006 (-0.07 mg m^{-3} $year^{-1}$).
- The NO concentrations show a significant decrease (-1.73 µg m^{-3} $year^{-1}$), and the Man-Kendall test shows that this trend begins around 2007.
- The NO_2 concentrations show a significant decrease (-1.78 µg m^{-3} $year^{-1}$), from 2002.
- A significant decreasing trend of PM_{10} concentrations in the study period (2.35 µg m^{-3} $year^{-1}$) beginning around 2004.
- A statistically significant decrease in SO_2 concentrations (-2.08 µg m^{-3} $year^{-1}$), beginning around 2007.
- O_3 concentrations show a significant decrease beginning around 2000 (-1.38 µg m^{-3} $year^{-1}$).

The general decrease in air pollutant emissions is probably the result of a series of measures taken in different sectors such as industrial, public electricity and road transport, so that from 2008 the recorded values were within the permissible limit values. The CO and SO_2 concentrations decreased by 85% each, NO and NO_2 concentrations dropped by 66 and 55%, respectively, PM_{10} decreased by 76% and O_3 by 31%. Several papers have found similar results in other cities. For example, in Germany, Ebelt et al. (2001) reported a reduction in the NO and SO_2 concentrations between 1990–1999 (91% and up to -50%, respectively). Aziz et al. (2016) showed a decreasing trend in SO_2 levels (-70%), CO (-32%), NO_x (-39%) and PM_{10} (-48%), but an increasing trend in O_3 (+79%), in Bangkok between 2000 and 2015. The same pattern was found by Guerreiro et al. (2014) in the study of 38 European cities between 2002 to 2011, with a general decrease of SO_2 (between 34 and 50%), NO_x (between 23 and 27%) and CO (between 27 and 32%) concentrations. In different cities of Spain, Querol et al. (2014) reported a decrease in the CO (up to −6.4% $year^{-1}$), SO_2 (up to -7.7% $year^{-1}$), NO_2 (up to -3.7% $year^{-1}$) and PM_{10} (up to -5.1% $year^{-1}$) concentrations between 2001 to 2012, which are comparable to those found in this study (-5.01, -5.32, -3.39 and -4.11% $year^{-1}$, respectively). Karanasiou et al. (2014) also reported a decreasing trend in SO_2, NO_2, PM_{10} and CO concentrations in Barcelona (-0.21, -0.65, -2.2 µg m^{-3} $year^{-1}$, -0.02 mg m^{-3} $year^{-1}$, respectively) during the period of 2003–2010, a decrease of the SO_2 and CO concentrations (−0.97 µg m^{-3} $year^{-1}$ and -0.11 mg m^{-3} $year^{-1}$, respectively) in Madrid between 2001 and 2009, and a decrease in PM_{10} concentrations (-2.11 µg m^{-3} $year^{-1}$) in Huelva (2003–2010). A more detailed analysis of each sector can be found as supplementary material in Annex 1.

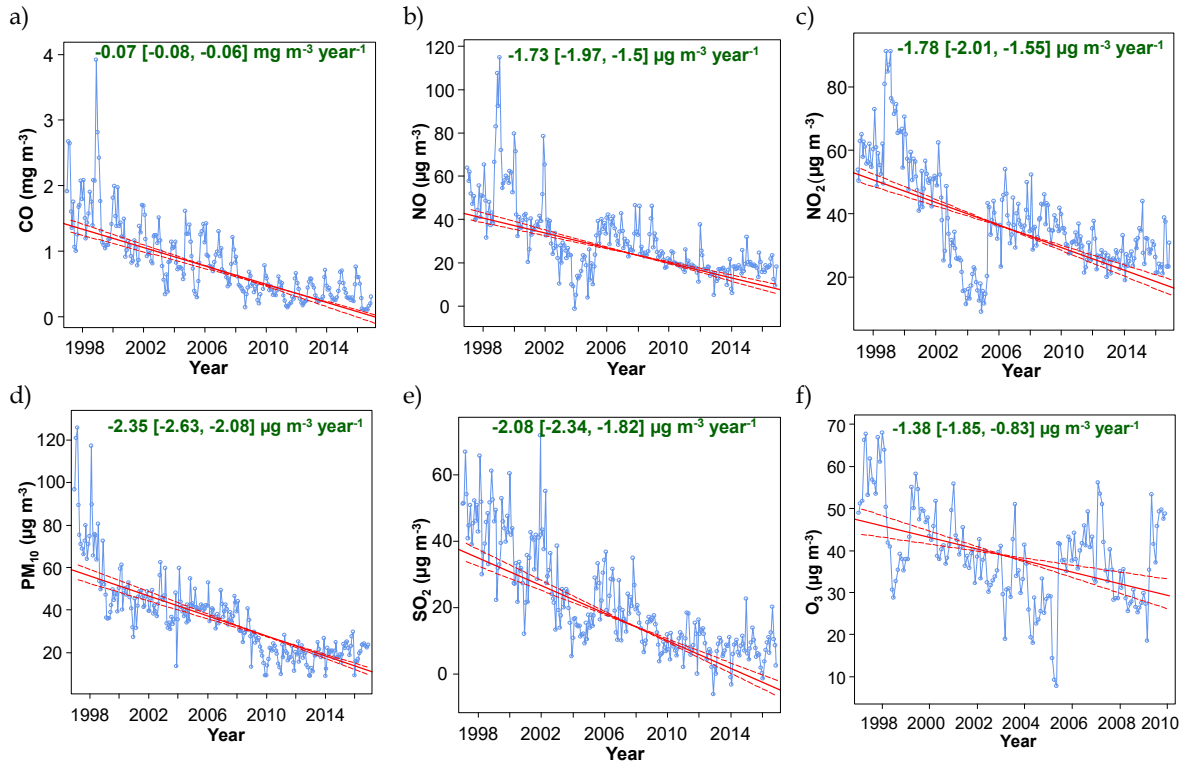

FIG. 3.3. Long-term trends of a) CO, b) NO, c) NO_2, d) PM_{10}, e) SO_2 and f) O_3 concentrations, in the traffic station León1. The solid red line shows the estimated lineal trend and the dashed red lines show the 95% confidence intervals for the trend. The overall trend is shown at the top and the 95% confidence intervals in the slope.

3.3.2. Long-Term trends SPIn and MPS

The seasonal pollen integral, SPIn, varied between 38 (year 2000) and 732 (year 2015) pollen day m^{-3} for *Fraxinus*, between 1625 (year 2009) and 7072 (year 2000) pollen day m^{-3} for Poaceae and between 296 (year 2004) and 2992 (year 2012) pollen day m^{-3} for *Populus*. The Mann Kendall trend test was applied to the SPIn. The results showed that only *Fraxinus* had a statistically significant increasing trend in pollen concentration (beginning in 2006), with an increase of 10 pollen day m^{-3} $year^{-1}$ ($p < 0.01$).

In a previous study carried out in different cities of Spain (Córdoba, Granada, Barcelona and Orense) between 1994–2013, Galán et al. (2016) reported similar results. They found that the *Fraxinus* SPIn had a positive significant trend in all cases. In some European cities, the increasing trend observed for SPIn of several pollen has been attributed to the increase in temperatures in the past decade (Ziello et al., 2012). However, in León we observed a significant decreasing trend in the minimum temperatures (-0.07 °C $year^{-1}$, $p < 0.01$) from 1994 to 2016, and no significant trend in the mean or maximum temperatures that can be linked to the trend observed in the *Fraxinus* SPIn. The increasing trend in the pollen concentrations may be due to the fact that many ornamental trees planted in the city in the past two decades have reached maturity and therefore their floral and pollen production is very abundant. The decrease in the minimum temperatures also allowed for a more suitable vernalization and, in consequence, optimum flowering.

In the case of Poaceae and *Populus* SPIn, they have a non-significant positive and negative trend, respectively. Some authors report different trends for these two pollen types SPIn in other cities. Damialis et al. (2007) observed a significant positive trend for Poaceae and a significant negative trend for *Populus* SPIn in Greece. These trends are linked to a rise in the temperatures and changes in the local pollen due to the urbanization in the area of study. In Spain, Galán et al. (2016) show that Poaceae SPIn has a significant negative trend in Santiago, Badajoz and León and a positive one in Orense and Cartagena, showing clear differences due to the geographical distribution of species. The different trends observed could be mainly attributed to local human activities, and changes in rainfall patterns. These behaviors suggest different endogenous processes of adaptation to the local climate for the different taxa.

Fig. 3.4 shows the monthly evolution of pollen concentration during the study period. This allows us to identify the pollination period for each species and its changes over the years. The MPS of the *Fraxinus* starts at the end of January and ends in mid-April (average duration of 77 days, minimum of 32 days in 2005 and 2015 and maximum of 136 days in 2016); the MPS of Poaceae starts at the end of March and ends in the first days of August (average duration of 136 days, minimum of 89 days in 2015 and maximum of 195 days in 1997).

Regarding *Populus*, the flowering season begins in the first days of March and ends in April (average duration of 37 days, minimum of 17 days in 1994 and maximum of 89 days in 2000). No trends in the advance or in the delay of the main pollen season and in the number of days with presence of pollen have been observed in any of the three taxa analyzed. However, some authors, such as Recio et al. (2010), reported an advance of 2 days year^{-1} and a delay of 7 days year^{-1} in the study of the MPS trend, between 1992–2007, of Poaceae in Malaga, Spain. These authors reported that the increase in rainfall at the beginning of spring delays the start of MPS, most probably because the water content of the soil favors vegetative development and inhibits early flowering. Moreover, the end of pollination is affected by the increase in the minimum temperature in spring due to the withering of the flowers and dehydration, especially, of the herbaceous plants, which can dry quickly when there is low availability of water. The meteorological conditions before the flowering period have an important influence on this process and in the release of pollen. The beginning of the main pollen season in these plants is related to changes in temperatures, which must reach a level that allows the end of the vernalization period of the plants (Galán et al., 2016; Puc and Bosiacka, 2011).

In Toledo, Spain, García-Mozo et al. (2006) reported that the flowering period for *Fraxinus*, Poaceae and *Populus* started in February, April and January, respectively. In Córdoba Velasco-Jiménez et al. (2013) observed that the flowering period of Poaceae and *Populus* started in April and February and ended in June and April, respectively, coinciding with the results found in this study. García-Mozo et al. (2006) found in Toledo that the start of the summer and the increase in the temperatures coincide with the decreasing pollen concentration (most abundant taxas Cupressaceae, *Quercus*, Poaceae, *Populus*, *Olea*, Urticaceae, *Platanus*, *Pinus* and *Ulmus*). They observed that in Toledo the autumn is the season with lowest pollen concentrations, as very few species flower in this season and rainfall cleans the atmosphere (scavenging). The same behavior was observed in the present study in the city of León.

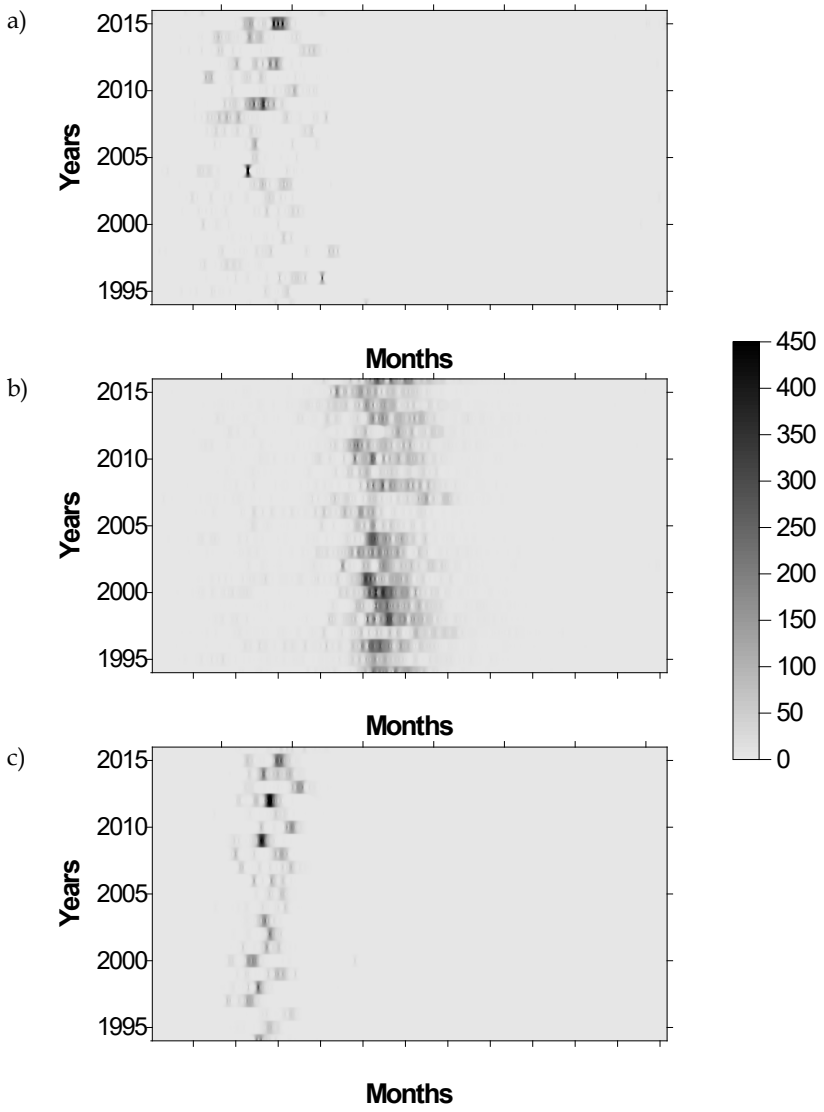

FIG. 3.4. Evolution of the daily pollen concentration between the years 1994 and 2016 for a) *Fraxinus* (concentrations × 5), b) Poaceae and c) *Populus*.

3.3.3. Correlation of pollen concentration with meteorological parameters and air pollutants

3.3.3.1. *Correlations between pollen concentration and meteorological parameters*

The Spearman coefficients were computed between pollen concentration parameters (SPIn and MPS) and meteorological parameters (mean temperature, relative humidity, minimum temperature, maximum temperature and accumulated precipitation) for *Fraxinus*, Poaceae and *Populus*, following previous studies: Grinn-Gofroń and Bosiacka, (2015); Plaza et al. (2016); Puc, (2012); Rathnayake et al. (2017); Rojo et al. (2015); Sabo et al. (2015); Tassan-Mazzocco et al. (2015); Vara et al. (2016). The calculations were made on an annual and a four-month basis. This way we obtained the correlation coefficients before and during the flowering period (Table 3.2).

In León, the SPIn of *Fraxinus* and *Populus* have not a significant correlation with the meteorological parameters. However, previous studies carried out in Northern Serbia and in the

city of León have reported a significant correlation between different types of APIn (Annual Pollen Integral) pollen and relative humidity (Fernández-González et al., 1993; Sabo et al., 2015). Variations in relative humidity affect the physiology of plants and, consequently, their phenology. These variations can also influence the emission and dispersion of grains of pollen to the atmosphere, either because the anthers are not dry enough to release the pollen or because the pollen, once in the air, becomes partially hydrated and scatters hardly. Consequently, the correlation between relative humidity and SPIn depends mainly on the plant phenology. The morphology of pollen, that is, the shape and characteristics of its wall, hardly influence these correlations. In addition, Makra et al. (2014) have reported that the relative humidity has an important influence on dry climate conditions, where the low availability of groundwater is replaced in part by relative humidity.

TABLE 3.2. Spearman coefficients between pollen concentration parameters (SPIn and MPS) and meteorological parameters (mean temperature (T), relative humidity (RH), minimum temperature (T_{Min}), maximum temperature (T_{Max}), and accumulated precipitation (P)) for *Fraxinus*, Poaceae and *Populus*.

	Fraxinus		**Poaceae**		***Populus***	
	SPIn	**MPS**	**SPIn**	**MPS**	**SPIn**	**MPS**
Annual						
T	0.02	-0.02	-0.08	0.21	0.03	**-0.45***
T_{Min}	-0.36	0.06	-0.20	0.06	-0.20	**-0.44***
T_{Max}	0.31	-0.03	0.11	0.24	0.08	-0.11
RH	-0.16	0.19	0.38	-0.20	-0.29	0.08
P	-0.38	0.14	0.36	-0.05	0.00	-0.17
January-April						
T	-0.05	0.19	0.08	0.17	-0.05	-0.20
T_{Min}	-0.21	**0.44***	0.28	0.12	-0.23	-0.08
T_{Max}	0.28	-0.13	-0.25	0.26	0.23	-0.15
RH	-0.10	**0.51***	0.27	-0.23	-0.28	0.30
P	-0.15	**0.59****	**0.52***	-0.23	-0.16	0.19
May- August						
T	-0.07	-0.17	0.04	-0.17	0.00	-0.34
T_{Min}	-0.33	-0.13	0.04	-0.17	-0.14	-0.37
T_{Max}	0.15	-0.09	-0.01	-0.26	0.04	-0.17
RH	-0.12	0.13	0.32	-0.04	-0.34	0.14
P	-0.13	0.15	**0.44***	-0.22	-0.17	-0.14
September-December						
T	-0.04	-0.11	-0.39	0.41	0.01	-0.14
T_{Min}	-0.20	-0.33	-0.30	**0.42***	0.04	**-0.45***
T_{Max}	0.24	0.09	-0.37	0.32	0.05	0.20
RH	-0.02	-0.38	0.06	-0.17	0.20	-0.41
P	-0.24	-0.40	-0.15	0.14	0.24	-0.26

** $p < 0.01$, * $p < 0.05$

The *Fraxinus* MPS was positively correlated with relative humidity, minimum temperature and accumulate precipitation during the flowering period (January–April) (0.51, 0.44, 0.59, $p < 0.05$ and $p < 0.01$, respectively). Thus, the duration of the main pollen season is favored by

cold and wet conditions, typical of autumn and winter in León. Other authors have reported the influence of minimum temperatures and rainfall on the *Fraxinus* pollination period (Jato et al., 2004; Peeters, 2000; Tsai et al., 2016), and observed that the main pollen season is longer if there are low temperatures and heavy rain when the first pollen grains are present in the air.

The Spearman correlation coefficients show that the *Populus* MPS has a significant negative correlation with the minimum temperature before flowering (−0.45, $p < 0.05$). Makra et al. (2012) report an opposite behavior for *Populus* in southern Hungary and conclude that the main pollen season is extended in a warm and dry climate, promoting pollen release. In contrast, in León, the extension of the flowering period of *Populus* is favored by low temperatures. As a result, it has been observed that the *Populus* shows a great tolerance to climate change with extensions of the MPS favored in both warm and cold conditions.

The Poaceae MPS correlates with the minimum temperature before the flowering period (0.42, $p < 0.05$) and SPIn shows a significant positive correlation with the rainfall before and during the flowering period (0.52, 0.44, respectively, $p < 0.05$). Authors like Cariñanos et al. (2004) have observed in different regions of Spain a more intense flowering if there was a period of rain in the 2–4 weeks previous to the flowering season. García-Mozo et al. (2016) and Makra et al. (2012) have reported the same behavior in studies carried out in Córdoba (Spain) and in Szeged (Hungary), respectively. Moreover, Recio et al. (2010) found a significant correlation between Poaceae SPIn and the total annual rainfall and the minimum temperature in Málaga (Spain). These four cities (León, Córdoba, Málaga and Szeged) are located between latitudes of 36° and 46 °N, with a population between 130,000 and 570,000 inhabitants, are characterized by low rainfall, hot summers and cold winters, with the exception of Málaga, which has mild winters due to its location in the southern coast of the Iberian Peninsula. In contrast to León, Córdoba and Málaga have average temperatures during spring that are higher than 10 °C; however, the average annual precipitation is similar to that observed in León. These studies show that, if there is enough water available, pollen concentrations during the late spring can be high, even in cases where the early spring temperatures are higher. If the spring is cold and the precipitation at the beginning of summer is high, pollen grains can be removed from the air and the pollen concentration can be reduced to a minimum, shortening the MPS.

3.3.3.2. *Correlations between pollen concentration and air pollutants*

The Spearman coefficients were also computed for SPIn and MPS and the air pollutant concentrations (CO, NO, NO_2, O_3, PM_{10}, SO_2) recorded by the traffic station León1 (Table 3.3). Significant correlations were only observed for *Fraxinus*.

Spearman correlation shows that the *Fraxinus* SPIn are negatively correlated with the concentration of several contaminants. However, the Poaceae and *Populus* SPIn and MPS do not show a clear correlation with air pollutant concentrations. In studies carried out in Oporto, Portugal, Sousa et al. (2008) found a non-significant correlation of *Fraxinus* and Poaceae pollen with O_3 and PM_{10} concentrations.

As mentioned above, the flowering period of *Fraxinus* is from January to April. The O_3 concentrations before the flowering period are negatively correlated with the *Fraxinus* pollination

season (MPS). Consequently, high levels of O_3 may inhibit the plant development and cause a shortening of the pollination period. In some urban areas, where the O_3 levels are low, an improvement in plant growth has been reported (Ziello et al., 2012).

The *Fraxinus* SPIn also shows a significant negative correlation with SO_2 concentrations before the pollination season. Air pollutants such as SO_2 and NO_2 can negatively affect the development of the plant and the flowering phenology and, consequently, reduce the pollen production. Moreover, in vitro studies have demonstrated that the exposition of pollen to SO_2 and NO_2, even under safe values for human health, cause a general drop of the soluble protein content released by pollen including allergen (Bist et al., 2004; Cuinica et al., 2013, 2014; Sousa et al., 2012).

TABLE 3.3. Spearman coefficients between pollen concentration parameters (SPIn and MPS) and atmospheric pollutant concentrations (CO, NO, NO_2, PM_{10}, SO_2, and O_3) for *Fraxinus*, Poaceae and *Populus*.

	Fraxinus		**Poaceae**		***Populus***	
	SPIn	**MPS**	**SPIn**	**MPS**	**SPIn**	**MPS**
Annual						
CO	**-0.484***	-0.096	0.262	-0.080	-0.186	-0.337
NO	**-0.468***	-0.223	0.194	-0.121	-0.056	-0.338
NO_2	-0.436	-0.233	0.134	-0.105	0.023	-0.181
O_3	-0.533	-0.209	0.231	0.061	0.258	-0.069
PM_{10}	**-0.553***	-0.084	0.292	-0.111	-0.313	-0.243
SO_2	**-0.531***	-0.105	0.248	-0.028	-0.287	-0.361
January-April						
CO	**-0.598****	-0.138	0.313	-0.177	-0.215	-0.377
NO	-0.379	**-**0.210	0.182	-0.056	0.086	-0.321
NO_2	-0.238	-0.175	0.230	-0.147	0.229	-0.156
O_3	-0.302	-0.302	0.401	0.019	0.071	0.127
PM_{10}	-0.376	-0.155	0.189	0.110	-0.241	-0.399
SO_2	-0.383	-0.133	0.179	0.031	-0.075	-0.438
May- August						
CO	**-0.450***	-0.041	0.338	-0.088	-0.144	-0.272
NO	**-0.600****	-0.154	0.239	-0.096	-0.274	-0.319
NO_2	**-0.532***	-0.318	0.029	-0.041	0.027	-0.274
O_3	-0.291	-0.390	-0.104	0.283	0.258	-0.228
PM_{10}	**-0.555***	-0.090	0.286	-0.098	-0.245	-0.279
SO_2	**-0.641****	-0.005	0.317	-0.120	-0.418	-0.252
September- December						
CO	**-0.484***	-0.086	0.111	0.042	-0.214	-0.418
NO	**-0.502***	-0.138	0.135	-0.175	-0.107	-0.132
NO_2	-0.438	-0.151	0.141	-0.126	0.042	-0.114
O_3	-0.533	**-0.637***	-0.170	0.217	0.159	-0.228
PM_{10}	**-0.576****	0.067	0.323	-0.184	-0.409	-0.205
SO_2	**-0.644****	0.128	0.340	-0.087	-0.430	-0.196

*** p< 0.01, *p< 0.05*

The significant correlation observed for both the *Fraxinus* pollen and the air pollutant concentrations coincides with the long-term trends described in sections 3.3.2 and 3.3.3. Even though the correlation may simply indicate unrelated trends in time, we speculate that the statistically significant increase on pollen concentrations of *Fraxinus* in León, may have been influenced by the decrease in the air pollutant concentrations in León since 1997.

Table 3.3 shows a negative correlation between the particulate matter and the pollen concentrations. Several authors have demonstrated that the particulate matter in the atmosphere adheres to the pollen surface of different species (Bellanger et al., 2012; Chehregani et al., 2004; Majd et al., 2004; Okuyama et al., 2007; Rezanejad, 2007; Rezanejad et al., 2003), causing morphological modifications and anomalies in the pollen structure (Majd et al., 2004; Majd and Mohamadi, 1992; Molfino, 1992; Rezanejad, 2007; Ruffin et al., 1983). In this study we have not found an influence of the particulate matter onto the pollen MPS.

3.3.4. Location of the main sources

For the identification of the pollen and pollutant sources, Spearman correlation between pollutant concentrations, correlation between SO_2 with T_{Min} and polar plots were carried out. The Spearman correlation coefficients were computed for the pollutants measured in the traffic station León1. There is a significant correlation between PM_{10} and NO_x (0.6, $p < 0.01$) which points towards road traffic emissions as a common origin. The high correlation between PM_{10} and CO (0.74, $p < 0.01$) shows the relationship with the primary emissions from combustion processes. The PM_{10} also correlates with SO_2 (0.75, $p < 0.01$) due the contribution of fossil fuel combustion (Calvo et al., 2013). This behavior was also reported by Karanasiou et al. (2014) in Spanish cities like Madrid, Barcelona and Huelva.

It was observed that there is a negative correlation between SO_2 concentrations and minimum temperatures in León (-0.17, $p< 0.01$). This behavior may be associated to the noteworthy contribution of coal combustion devices (emitting high amounts of SO_2) still in use in León during cold months, as evidenced by the increase of SO_2 (19 ± 20 and 24 ± 23 μg m^{-3} in summer and winter, respectively).

The polar plots in Fig. 3.5 show the variation of the air pollutant concentrations with wind direction and speed, using the concentration data for the entire study period.

In general, a decrease in the air pollutant concentrations was observed with the increase of wind speed (except for ozone). The main emission sources of NO, NO_2 and SO_2 come from the residential areas around the sampling point, which may include heating systems, industrial areas and road traffic emissions.

Daily variation of the pollen concentration with the wind direction and speed during the pollination seasons over the entire study period is represented in Fig. 3.6. Polar plots show that the main source of pollen is located close to the sampling point and towards NE. In general, a decrease in the pollen concentration is observed when wind speed increases.

The origin of the pollen from the NE and its high concentration in the case of *Fraxinus* is a consequence of the fact that the largest plant mass is found on the Torío riverside, less than 3 km

from the sampling station. The prevailing pollen types come from native species characteristic of these habitats and in very small numbers from species grown for ornamental purposes next to the sampling collector. Something similar happens with *Populus*, but the scarce concentration (in spite of the large pollen production of this species) shows that most of the trees of this species are further away from the sampling station, although they are also part of the riverside. A smaller amount comes from the SE, where there are also plantations of this tree for logging, about 12–20 km far from the sampling point. The ways of dispersion for arboreal species in relation to the wind were analyzed in some areas of Spain (Maya-Manzano et al., 2017) and Europe (Skjøth et al., 2013). Regarding grasses, the distribution observed in Fig. 3.6 clearly shows that the pollen comes from the surroundings of the sampling station, as expected from these herbaceous plants widely distributed in meadows and gardens (Peel et al., 2014).

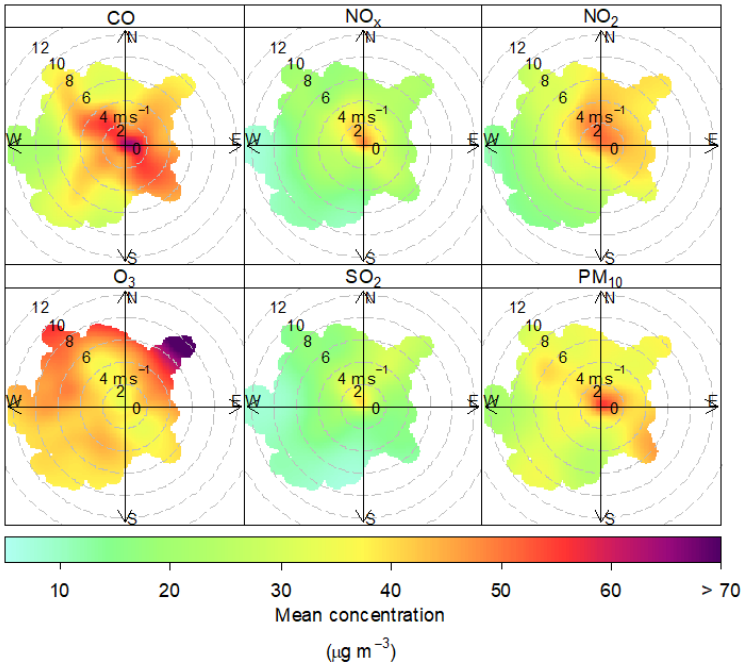

FIG. 3.5. Polar plots (daily variation of the pollutant concentrations as a function of wind speed and direction) for CO (concentration × 5 ·10⁴ µg m⁻³), NO_x, NO_2, O_3, SO_2 and PM_{10} concentrations of the entire study period.

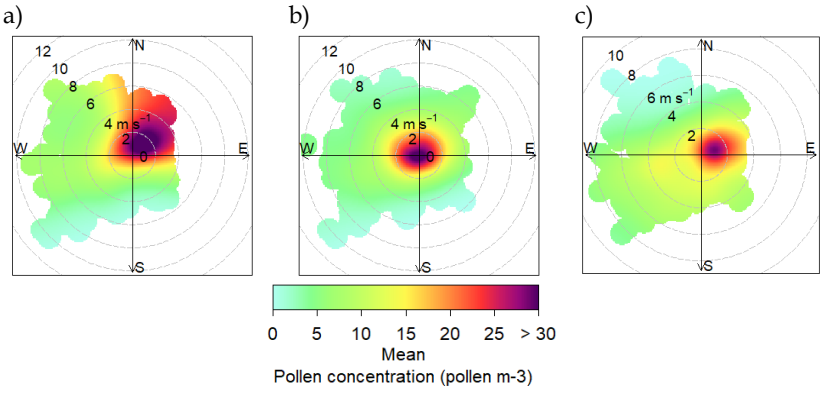

FIG. 3.6. Polar Plots (variation of the pollen concentration during the pollination period as a function of wind speed and direction) for a) *Fraxinus* (concentration × 5), b) Poaceae and c) *Populus*, with concentrations of the entire study period.

3.4. CONCLUSIONS

The evolution of two decades of data on air pollutants, meteorological parameters and pollen concentration of *Fraxinus*, Poaceae and *Populus*, was analyzed in this study. In general, a significant decreasing trend in the atmospheric pollutant concentrations in the city of León was observed, probably due to the efficiency of international and national policies, and to the local measures taken for reducing emissions from road traffic, industrial activities and public electricity. However, no trend was detected in any of the meteorological parameters studied. Likewise, no trends in the advance or in the delay of the main pollen season, as well as in the number of days with presence of pollen were recorded in any of the three taxa analyzed. The observed correlations of the air pollutant concentrations with both the seasonal pollen integral and the main pollen season for *Fraxinus*, mainly in the months before the pollination period, could suggest a relationship between the increasing trend in *Fraxinus* pollen concentrations and the decreasing trend in air pollutant concentrations. Moreover, the evolution of the concentrations of the three studied pollen taxa also depends on the changes in the urbanization of the city of León. The localization of the main sources of the three studied taxa is close to the sampling point and in the NE sector, where the main plant mass is located. Another minor contribution comes from the ornamental plants next to the sampling collector. The Spearman correlation shows that the flowering and pollination periods depend largely on the weather conditions before these periods.

This type of interdisciplinary analysis is essential for a better understanding of the intricate interactions between biosphere, atmosphere and lithosphere. This study is a first step towards a better characterization of the multifaceted nature of the topic, which will help policy makers develop measures to further reduce the impact of pollen on human health.

3.5. REFERENCES

Albertine, J.M., Manning, W.J., DaCosta, M., Stinson, K.A., Muilenberg, M.L., Rogers, C.A., 2014. Projected carbon dioxide to increase grass pollen and allergen exposure despite higher ozone levels. PLoS One 9. https://doi.org/10.1371/journal.pone.0111712. e111712.

Andersen, T.B., 1991. A model to predict the beginning of the pollen season. Grana 30, 269–275. https://doi.org/10.1080/00173139109427810.

Aziz, T.A., Xu, R., Fan, C., Shah, M., Boonman, T., Thao, P., Bonnet, S., Garivait, S., 2016. Analysis of spatial and temporal variation of criteria air pollutants in Bangkok metropolitan region (BMR) during 2000–2015. Proceedings of The 1st International Electronic Conference on Atmospheric Sciences. https://doi.org/10.3390/ecas2016- B006. B006.

Beggs, P.J., 2004. Impacts of climate change on aeroallergens: past and future. Clin. Exp. Allergy 34, 1507–1513. https://doi.org/10.1111/j.1365-2222.2004.02061.x.

Beggs, P.J., 2010. Adaptation to impacts of climate change on aeroallergens and allergic respiratory diseases. Int. J. Environ. Res. Public Health 7, 3006–3021. https://doi.org/10.3390/ijerph7083006.

Bellanger, A.-P., Bosch-Cano, F., Millon, L., Ruffaldi, P., Franchi, M., Bernard, N., 2012. Reactions of airway epithelial cells to birch pollen grains previously exposed to in situ atmospheric Pb

concentrations: a preliminary assay of allergenicity. Biol. Trace Elem. Res. 150, 391–395. https://doi.org/10.1007/s12011-012-9485-7.

Bernstein, J.A., Alexis, N., Barnes, C., Bernstein, I.L., Nel, A., Peden, D., Diaz-Sanchez, D., Tarlo, S.M., Williams, P.B., Bernstein, J.A., 2004. Health effects of air pollution. J. Allergy Clin. Immunol. 114, 1116–1123. https://doi.org/10.1016/j.jaci.2004.08.030.

Bielory, L., Lyons, K., Goldberg, R., 2012. Climate change and allergic disease. Curr. Allergy Asthma Rep. 12, 485–494. https://doi.org/10.1007/s11882-012-0314-z.

Bist, A., Pandit, T., Bhatnagar, A.K., Singh, A.B., 2004. Variability in protein content of pollen of Castor bean (Ricinus communis) before and after exposure to the air pollutants SO_2 and NO_2. Grana 43, 94–100. https://doi.org/10.1080/ 00173130410019316.

Brunekreef, B., Holgate, S.T., 2002. Air pollution and health. Air Pollut. Rev. 360, 1233–1242.

Buters, J.T.M., Thibaudon, M., Smith, M., Kennedy, R., Rantio-Lehtimäki, A., Albertini, R., Reese, G., Weber, B., Galan, C., Brandao, R., Antunes, C.M., Jäger, S., Berger, U., Celenk, S., Grewling, Ł., Jackowiak, B., Sauliene, I., Weichenmeier, I., Pusch, G., Sarioglu, H., Ueffing, M., Behrendt, H., Prank, M., Sofiev, M., Cecchi, L., 2012. Release of Bet v 1 from birch pollen from 5 European countries. Results from the HIALINE study. Atmos. Environ. 55, 496–505. https://doi.org/10.1016/j.atmosenv. 2012.01.054.

Buters, J., Prank, M., Sofiev, M., Pusch, G., Albertini, R., Annesi-Maesano, I., Antunes, C., Behrendt, H., Berger, U., Brandao, R., Celenk, S., Galan, C., Grewling, Ł., Jackowiak, B., Kennedy, R., Rantio-Lehtimäki, A., Reese, G., Sauliene, I., Smith, M., Thibaudon, M., Weber, B., Cecchi, L., 2015. Variation of the group 5 grass pollen allergen content of airborne pollen in relation to geographic location and time in season the HIALINE working group. J. Allergy Clin. Immunol. 136, 87–95. https://doi.org/10.1016/j.jaci. 2015.01.049. e6.

Calvo, A.I., Pont, V., Castro, A., Mallet, M., Palencia, C., Roger, J.C., Dubuisson, P., Fraile, R., 2010. Radiative forcing of haze during a forest fire in Spain. J. Geophys. Res. 115https://doi.org/10.1029/2009JD012172. D08206.

Calvo, A.I., Alves, C., Castro, A., Pont, V., Vicente, A.M., Fraile, R., 2013. Research on aerosol sources and chemical composition: past, current and emerging issues. Atmos. Res. 1–28. https://doi.org/10.1016/j.atmosres.2012.09.021. 120–121.

Cariñanos, P., Galan, C., Alcázar, P., Domıńguez, E., 2004. Airborne pollen records response to climatic conditions in arid areas of the Iberian Peninsula. Environ. Exp. Bot. 52, 11–22. https://doi.org/10.1016/j.envexpbot.2003.11.008.

Carslaw, D., 2015. The Openair Manual Open-Source Tools for Analysing Air Pollution Data. King's Coll., London, pp. 287.

Carslaw, D.C., Ropkins, K., 2012. Openair—an R package for air quality data analysis. Environ. Model. Softw. 27–28, 52–61. https://doi.org/10.1016/j.envsoft.2011.09.008.

Chehregani, A.H., Majde, A., Moin, M., Golami, M., Shariatzadeh, S.M., Mohsenzae, F., 2004. Effect of Air Pollution on Some Cytogenetic Characteristics, Structure, Viability and Proteins of Zinnia elegans Pollen Grains. Pak. J. Biol. Sci. 7, 118–122. https:// doi.org/10.3923/pjbs.2004.118.122.

Chiesa, V., Toletti, G., 2004. Network of collaborations for innovation: the case of biotechnology. Technol. Anal. Strateg. Manag. 16, 73–96. https://doi.org/10.1080/ 0953732032000175517.

Clot, B., 2003. Trends in airborne pollen: an overview of 21 years of data in Neuchâtel (Switzerland). Aerobiologia (Bologna) 19, 227–234. https://doi.org/10.1023/ B:AERO.0000006572.53105.17.

Cuinica, L.G., Abreu, I., Gomes, C.R., Esteves da Silva, J.C.G., 2013. Exposure of Betula pendula Roth pollen to atmospheric pollutants CO, O_3 and SO_2. Grana 52, 299–304. https://doi.org/10.1080/00173134.2013.830145.

Cuinica, L.G., Abreu, I., da Silva, J.C.G.E., 2014. In vitro exposure of Ostrya carpinifolia and Carpinus betulus pollen to atmospheric levels of CO, O_3 and SO_2. Environ. Sci. Pollut. Res. 21, 2256–2262. https://doi.org/10.1007/s11356-013-2108-9.

Curtis, L., Rea, W., Smith-Willis, P., Fenyves, E., Pan, Y., 2006. Adverse health effects of outdoor air pollutants. Environ. Int. 32, 815–830. https://doi.org/10.1016/j.envint. 2006.03.012.

D'Amato, G., 2000. Urban air pollution and plant-derived respiratory allergy. Clin. Exp. Allergy 30, 628–636. https://doi.org/10.1046/j.1365-2222.2000.00798.x.

D'Amato, G., Cecchi, L., Bonini, S., Nunes, C., Annesi-Maesano, I., Behrendt, H., Liccardi, G., Popov, T., van Cauwenberge, P., 2007. Allergenic pollen and pollen allergy in Europe. Allergy 62, 976–990. https://doi.org/10.1111/j.1398-9995.2007.01393.x.

D'Amato, G., Cecchi, L., D'Amato, M., Liccardi, G., 2010. Urban air pollution and climate change as environmental risk factors of respiratory allergy: an update. J. Investig. Allergol. Clin. Immunol. 20, 95–102 quiz following 102.

D'Amato, G., Bergmann, K.C., Cecchi, L., Annesi-Maesano, I., Sanduzzi, A., Liccardi, G., Vitale, C., Stanziola, A., D'Amato, M., 2014. Climate change and air pollution. Allergo J. 23, 32–38. https://doi.org/10.1007/s15007-014-0484-1.

D'Amato, G., Holgate, S.T., Pawankar, R., Ledford, D.K., Cecchi, L., Al-Ahmad, M., Al- Enezi, F., Al-Muhsen, S., Ansotegui, I., Baena-Cagnani, C.E., Baker, D.J., Bayram, H., Bergmann, K.C., Boulet, L.P., Buters, J.T.M., D'Amato, M., Dorsano, S., Douwes, J., Finlay, S.E., Garrasi, D., Gómez, M., Haahtela, T., Halwani, R., Hassani, Y., Mahboub, B., Marks, G., Michelozzi, P., Montagni, M., Nunes, C., Oh, J.J.W., Popov, T.A., Portnoy, J., Ridolo, E., Rosário, N., Rottem, M., Sánchez-Borges, M., Sibanda, E., Sienra-Monge, J.J., Vitale, C., Annesi-Maesano, I., 2015. Meteorological conditions, climate change, new emerging factors, and asthma and related allergic disorders. A statement of the World Allergy Organization. World Allergy Organ. J. 8. https://doi. org/10.1186/s40413-015-0073-0.

D'Amato, G., Vitale, C., Lanza, M., Molino, A., D'amato, M., 2016. Climate change, air pollution, and allergic respiratory diseases: an update. Curr. Opin. Allergy Clin. Immunol. 16, 434–440.

Damialis, A., Halley, J.M., Gioulekas, D., Vokou, D., 2007. Long-term trends in atmospheric pollen levels in the city of Thessaloniki, Greece. Atmos. Environ. 41, 7011–7021. https://doi.org/10.1016/j.atmosenv.2007.05.009.

Del Río González, S., 2005. El cambio climático y su influencia en la vegetación de Castilla y León (España). Itinera Geobot. 5–534.

Ebelt, S., Brauer, M., Cyrys, J., Tuch, T., Kreyling, W.G., Wichmann, H.-E., Heinrich, J., 2001. Air quality in Postunification Erfurt, east Germany: associating changes in pollutant concentrations with changes in emissions. Environ. Health Perspect. 109, 325–333. https://doi.org/10.1289/ehp.01109325.

Fernández-González, D., Suarez-Cervera, M., Díaz-González, T., Valencia- Barrera, R.M., 1993. Airborne pollen and spores of Leon (Spain). Int. J. Biometeorol. 27, 89–95.

Galán, C., Alcázar, P., Oteros, J., García-Mozo, H., Aira, M.J., Belmonte, J., Diaz de la Guardia, C., Fernández-González, D., Gutierrez-Bustillo, M., Moreno-Grau, S., Pérez- Badía, R., Rodríguez-Rajo, J., Ruiz-Valenzuela, L., Tormo, R., Trigo, M.M., Domínguez-Vilches, E., 2016. Airborne pollen trends in the Iberian Peninsula. Sci. Total Environ. 550, 53–59. https://doi.org/10.1016/j.scitotenv.2016.01.069.

Galán, C., Ariatti, A., Bonini, M., Clot, B., Crouzy, B., Dahl, A., Fernandez-González, D., Frenguelli, G., Gehrig, R., Isard, S., Levetin, E., Li, D.W., Mandrioli, P., Rogers, C.A., Thibaudon, M., Sauliene, I., Skjoth, C., Smith, M., Sofiev, M., 2017. Recommended terminology for aerobiological studies. Aerobiologia (Bologna) 33, 293–295. https://doi.org/10.1007/s10453-017-9496-0.

García-Mozo, H., Pérez-Badia, R., Fernández-González, F., Galán, C., 2006. Airborne pollen sampling in Toledo, Central Spain. Aerobiologia (Bologna) 22, 55–66. https://doi.org/10.1007/s10453-005-9015-6.

García-Mozo, H., Oteros, J.A., Galán, C., 2016. Impact of land cover changes and climate on the main airborne pollen types in Southern Spain. Sci. Total Environ. 548–549, 221–228. https://doi.org/10.1016/j.scitotenv.2016.01.005.

Grinn-Gofroń, A., Bosiacka, B., 2015. Effects of meteorological factors on the composition of selected fungal spores in the air. Aerobiologia (Bologna). 31, 63–72. https://doi.org/10.1007/s10453-014-9347-1.

Guerreiro, C.B.B., Foltescu, V., de Leeuw, F., 2014. Air quality status and trends in Europe. Atmos. Environ. 98, 376–384. https://doi.org/10.1016/j.atmosenv.2014.09.017.

Hipel, K.W., McLeod, A.I., 2005. Time Series Modelling of Water Resources and Environmental Systems. Elsevier, Amsterdam.

Hirst, J.M., 1952. An automatic volumetric spore trap. Ann. Appl. Biol. 39, 257–265. https://doi.org/10.1111/j.1744-7348.1952.tb00904.x.

Jato, V., Rodríguez-Rajo, J., Dacosta, N., Aira, M., 2004. Heat and chill requirements of Fraxinus flowering in Galicia (NW Spain). Grana 43, 217–223. https://doi.org/10.1080/00173130410016274.

Jato, V., Rodríguez-Rajo, F.J., Alcázar, P., De Nuntiis, P., Galán, C., Mandrioli, P., 2006. May the definition of pollen season influence aerobiological results? Aerobiologia (Bologna) 22, 13–25. https://doi.org/10.1007/s10453-005-9011-x.

Kampa, M., Castanas, E., 2008. Human health effects of air pollution. Environ. Pollut. 151, 362–367. https://doi.org/10.1016/j.envpol.2007.06.012.

Karanasiou, A., Querol, X., Alastuey, A., Perez, N., Pey, J., Perrino, C., Berti, G., Gandini, M., Poluzzi, V., Ferrari, S., de la Rosa, J., Pascal, M., Samoli, E., Kelessis, A., Sunyer, J., Alessandrini, E., Stafoggia, M., Forastiere, F., 2014. Particulate matter and gaseous pollutants in the Mediterranean Basin: results from the MED-PARTICLES project. Sci. Total Environ. 488–489, 297–315. https://doi.org/10.1016/j.scitotenv.2014.04.096.

Kendall, M., Gibbons, D.J., 1990. Rank Correlation Methods. London Griffin. Lombardero, M., Obispo, T., Calabozo, B., Lezaun, A., Polo, F., Barber, D., 2002. Cross-reactivity between olive and other species. Role of Ole e 1-related proteins. Allergy 57, 29–34. https://doi.org/10.1034/j.1398-9995.2002.057s71029.x.

Majd, A., Mohamadi, S., 1992. Effect of certain toxins and air pollution on pollen development of Glycine max. J. Islam. Azad Univ. 649–651.

Majd, A., Chehregani, A., Moin, M., Gholami, M., Kohno, S., Nabe, T., Shariatzade, M.A., 2004. The effects of air pollution on structures, proteins and allergenicity of pollen grains. Aerobiologia (Bologna) 20, 111–118. https://doi.org/10.1023/B:AERO.0000032950.12169. 38.

Makra, L., Matyasovszky, I., Páldy, A., Deák, Á.J., 2012. The influence of extreme high and low temperatures and precipitation totals on pollen seasons of Ambrosia, Poaceae and *Populus* in Szeged, southern Hungary. Grana 51, 215–227. https://doi. org/10.1080/00173134.2012. 661764.

Makra, L., Csépe, Z., Matyasovszky, I., Deák, Á.J., Sümeghy, Z., Tusnády, G., 2014. The effects of the current and past meteorological elements influencing the current pollen concentrations for different taxa. Bot. Stud. 55 (43). https://doi.org/10.1186/ s40529-014-0043-9.

Maya-Manzano, J.M., Sadyś, M., Tormo-Molina, R., Fernández-Rodríguez, S., Oteros, J., Silva-Palacios, I., Gonzalo-Garijo, A., 2017. Relationships between airborne pollen grains, wind direction and land cover using GIS and circular statistics. Sci. Total Environ. 584–585, 603–613. https://doi.org/10.1016/j.scitotenv.2017.01.085.

Molfino, N.A., 1992. The effects of air pollution on atopic asthma. Medicina (B. Aires).52, 363–367.

Monsalve, F., Tomás, C., Fraile, R., 2013. Influence of meteorological parameters and air pollutants onto the morbidity due to respiratory diseases in Castilla-La Mancha.

Spain. Aerosol Air Qual. Res. 13, 1297–1312. https://doi.org/10.4209/aaqr.2012.12. 0348.

Oduber, F., Castro, A., Calvo, A.I., Blanco-Alegre, C., Alonso-Blanco, E., Belmonte, P., Fraile, R., 2018. Summer-autumn air pollution in León, Spain: changes in aerosol size distribution and expected effects on the respiratory tract. Air Qual. Atmos. Heal. 11, 505–520. https://doi.org/10.1007/s11869-018-0556-6.

Okuyama, Y., Matsumoto, K., Okochi, H., Igawa, M., 2007. Adsorption of air pollutants on the grain surface of Japanese cedar pollen. Atmos. Environ. 41, 253–260. https://doi. org/10.1016/j.atmosenv.2006.08.009.

Oteros, J., García-Mozo, H., Alcázar, P., Belmonte, J., Bermejo, D., Boi, M., Cariñanos, P., Díaz de la Guardia, C., Fernández-González, D., González-Minero, F., Gutiérrez- Bustillo, A.M., Moreno-Grau, S., Pérez-Badía, R., Rodríguez-Rajo, F.J., Ruíz- Valenzuela, L., Suárez-Pérez, J., Trigo, M.M., Domínguez-Vilches, E., Galán, C., 2015. A new method for determining the

sources of airborne particles. J. Environ. Manage. 155, 212–218. https://doi.org/10.1016/j.jenvman.2015.03.037.

Peel, R.G., Ørby, P.V., Skjøth, C.A., Kennedy, R., Schlünssen, V., Smith, M., Sommer, J., Hertel, O., 2014. Seasonal variation in diurnal atmospheric grass pollen concentration profiles. Biogeosciences 11, 821–832. https://doi.org/10.5194/bg-11-821-2014.

Peeters, A.G., 2000. Frost periods and beginning of the ash (*Fraxinus excelsior* L.) pollen season in Basel (Switzerland). Aerobiologia (Bologna) 16, 353–359. https://doi.org/ 10.1023/A:1026566625568.

Pfaar, O., Bastl, K., Berger, U., Buters, J., Calderon, M.A., Clot, B., Darsow, U., Demoly, P., Durham, S.R., Galán, C., Gehrig, R., Gerth van Wijk, R., Jacobsen, L., Klimek, L., Sofiev, M., Thibaudon, M., Bergmann, K.C., 2017. Defining pollen exposure times for clinical trials of allergen immunotherapy for pollen-induced rhino conjunctivitis – an EAACI position paper. Allergy Eur. J. Allergy Clin. Immunol 72, 713–722. https:// doi.org/10.1111/all.13092.

Plaza, M.P., Alcázar, P., Galán, C., 2016. Correlation between airborne Olea europaea pollen concentrations and levels of the major allergen Ole e 1 in Córdoba, Spain, 2012–2014. Int. J. Biometeorol. 60, 1841–1847. https://doi.org/10.1007/s00484-016-1171-6.

Puc, M., 2012. Influence of meteorological parameters and air pollution on hourly fluctuation of birch (*Betula L.*) and ash (*Fraxinus L.*) airborne pollen. Ann. Agric. Environ. Med. 19, 660–665.

Puc, M., Bosiacka, B., 2011. Effects of meteorological factors and air pollution on urban pollen concentrations. Polish J. Environ. Stud. 20, 611–618.

Querol, X., Alastuey, A., Pandolfi, M., Reche, C., Pérez, N., Minguillón, M.C., Moreno, T., Viana, M., Escudero, M., Orio, A., Pallarés, M., Reina, F., 2014. 2001–2012 trends on air quality in Spain. Sci. Total Environ. 490, 957–969. https://doi.org/10.1016/j. scitotenv.2014.05.074.

Rathnayake, C.M., Metwali, N., Jayarathne, T., Kettler, J., Huang, Y., Thorne, P.S., O'Shaughnessy, P.T., Stone, E.A., 2017. Influence of rain on the abundance of bioaerosols in fine and coarse particles. Atmos. Chem. Phys. 17, 2459–2475. https:// doi.org/10.5194/acp-17-2459-2017.

Recio, M., Docampo, S., García-Sánchez, J., Trigo, M.M., Melgar, M., Cabezudo, B., 2010. Influence of temperature, rainfall and wind trends on grass pollination in Malaga (western Mediterranean coast). Agric. For. Meteorol. 150, 931–940. https://doi.org/ 10.1016/j.agrformet.2010.02.012.

Reinmuth-Selzle, K., Kampf, C.J., Lucas, K., Lang-Yona, N., Fröhlich-Nowoisky, J., Shiraiwa, M., Lakey, P.S.J., Lai, S., Liu, F., Kunert, A.T., Ziegler, K., Shen, F., Sgarbanti, R., Weber, B., Bellinghausen, I., Saloga, J., Weller, M.G., Duschl, A., Schuppan, D., Pöschl, U., 2017. Air pollution and climate change effects on allergies in the Anthropocene: abundance, interaction, and modification of allergens and adjuvants. Environ. Sci. Technol. 51, 4119–4141. https://doi.org/10.1021/acs.est.6b04908.

Ren-Jian, Z., Kin-Fai, H., Zhen-Xing, S., 2012. The role of aerosol in climate change, the environment, and human health. Atmos. Ocean. Sci. Lett. 5, 156–161. https://doi. org/10.1080/16742834.2012.11446983.

Rezanejad, F., 2007. The effect of air pollution on microsporogenesis, pollen development and soluble pollen proteins in Spartium junceum L. (Fabaceae). Turk. J. Bot. 31, 183–191.

Rezanejad, F., Majd, A., Shariatzadeh, S.M.A., Moein, M., Aminzadeh, M., Mirzaeian, M., 2003. Effect of air pollution on soluble proteins, structure and cellular material release in pollen of Lagerstroemia indica L. (Lytraceae). Acta Biol. Cracoviensia Ser. Bot. 45, 129–132.

Rogers, C.A., Wayne, P.M., Macklin, E.A., Muilenberg, M.L., Wagner, C.J., Epstein, P.R., Bazzaz, F.A., 2006. Interaction of the onset of spring and elevated atmospheric CO_2 on Ragweed (Ambrosia artemisiifolia L.) pollen production. Environ. Health Perspect. 114, 865–869. https://doi.org/10.1289/ehp.8549.

Rojo, J., Rapp, A., Lara, B., Fernández-González, F., Pérez-Badia, R., 2015. Effect of land uses and wind direction on the contribution of local sources to airborne pollen. Sci. Total Environ. 538, 672–682. https://doi.org/10.1016/j.scitotenv.2015.08.074.

Ruffin, J., Williams, D., Banerjee, U., Pinnix, K., 1983. The effects of some environmental gaseous pollutants on pollen-wall proteins of certain airborne pollen grains: a preliminary study. Grana 22, 171–175. https://doi.org/10.1080/00173138309427703.

Sabo, N.Č., Popović, A., Đorđević, D., 2015. Air pollution by pollen grains of Anemophilous species: influence of chemical and meteorological parameters. Water Air Soil Pollut. 226, 292. https://doi.org/10.1007/s11270-015-2549-5.

Schmidt, C.W., 2016. Pollen overload: seasonal allergies in a changing climate. Environ. Health Perspect. 124, A70–A75. https://doi.org/10.1289/ehp.124-A70.

Sénéchal, H., Visez, N., Charpin, D., Shahali, Y., Peltre, G., Biolley, J.-P., Lhuissier, F., Couderc, R., Yamada, O., Malrat-Domenge, A., Pham-Thi, N., Poncet, P., Sutra, J.-P., 2015. A review of the effects of major atmospheric pollutants on pollen grains, pollen content, and allergenicity. Transfus. Apher. Sci. 2015, 1–29. https://doi.org/10.1155/2015/940243.

Sharma, N., Sinha, P.G., Bhatnagar, A.K., 2014. Effect of elevated CO_2 on cell structure and function in seed plants. Clim. Chang. Environ. Sustain. 2, 69. https://doi.org/10. 5958/2320-642X.2014.00001.5.

Skjøth, C.A., Ørby, P.V., Becker, T., Geels, C., Schlünssen, V., Sigsgaard, T., Bønløkke, J.H., Sommer, J., Søgaard, P., Hertel, O., 2013. Identifying urban sources as cause of elevated grass pollen concentrations using GIS and remote sensing. Biogeosciences 10, 541–554. https://doi.org/10.5194/bg-10-541-2013.

Sofiev, M., Berger, U., Prank, M., Vira, J., Arteta, J., Belmonte, J., Bergmann, K.-C., Chéroux, F., Elbern, H., Friese, E., Galan, C., Gehrig, R., Khvorostyanov, D., Kranenburg, R., Kumar, U., Marécal, V., Meleux, F., Menut, L., Pessi, A.-M., Robertson, L., Ritenberga, O., Rodinkova, V., Saarto, A., Segers, A., Severova, E., Sauliene, I., Siljamo, P., Steensen, B.M., Teinemaa, E., Thibaudon, M., Peuch, V.-H., 2015. MACC regional multi-model ensemble simulations of birch pollen dispersion in Europe. Atmos. Chem. Phys. 15, 8115–8130. https://doi.org/10.5194/acp-15-8115- 2015.

Galán Soldevilla, C., Cariñanos González, P., Alcázar Teno, P., Domínguez Vilches, E., 2007. Spanish Aerobiology Network (REA): Management and Quality Manual.

Sousa, S.I.V., Martins, F.G., Pereira, M.C., Alvim-Ferraz, M.C.M., Ribeiro, H., Oliveira, M., Abreu, I., 2008. Influence of atmospheric ozone, PM_{10} and meteorological factors on the concentration

of airborne pollen and fungal spores. Atmos. Environ. 42, 7452–7464. https://doi.org/10.1016/j.atmosenv.2008.06.004.

Sousa, R., Duque, L., Duarte, A.J., Gomes, C.R., Ribeiro, H., Cruz, A., Esteves da Silva, J.C.G., Abreu, I., 2012. In vitro exposure of acer negundo pollen to atmospheric levels of SO_2 and NO_2: effects on allergenicity and germination. Environ. Sci. Technol. 46, 2406–2412. https://doi.org/10.1021/es2034685.

Tang, A., Zhuang, G., Wang, Y., Yuan, H., Sun, Y., 2005. The chemistry of precipitation and its relation to aerosol in Beijing. Atmos. Environ. 39, 3397–3406. https://doi. org/10.1016/j.atmosenv.2005.02.001.

Tassan-Mazzocco, F., Felluga, A., Verardo, P., 2015. Prediction of wind-carried Gramineae and Urticaceae pollen occurrence in the Friuli Venezia Giulia region (Italy). Aerobiologia (Bologna) 31, 559–574. https://doi.org/10.1007/s10453-015-9386-2.

Tsai, C.-W., Young, T., Warren, P.H., Maltby, L., 2016. Phenological responses of ash (*Fraxinus excelsior*) and sycamore (*Acer pseudoplatanus*) to riparian thermal conditions. Urban For. Urban Green. 16, 95–102. https://doi.org/10.1016/j.ufug.2016. 02.001.

Vara, A., Fernández-González, M., Aira, M.J., Rodríguez-Rajo, F.J., 2016. *Fraxinus* pollen and allergen concentrations in Ourense (South-western Europe). Environ. Res. 147, 241–248. https://doi.org/10.1016/j.envres.2016.02.014.

Velasco-Jiménez, M.J., Alcázar, P., Domínguez-Vilches, E., Galán, C., 2013. Comparative study of airborne pollen counts located in different areas of the city of Córdoba (south-western Spain). Aerobiologia (Bologna) 29, 113–120. https://doi.org/10.1007/s10453-012-9267-x.

Ziello, C., Sparks, T.H., Estrella, N., Belmonte, J., Bergmann, K.C., Bucher, E., Brighetti, M.A., Damialis, A., Detandt, M., Galán, C., Gehrig, R., Grewling, L., Gutiérrez Bustillo, A.M., Hallsdóttir, M., Kockhans-Bieda, M.-C., De Linares, C., Myszkowska, D., Pàldy, A., Sánchez, A., Smith, M., Thibaudon, M., Travaglini, A., Uruska, A., Valencia- Barrera, R.M., Vokou, D., Wachter, R., de Weger, L.A., Menzel, A., 2012. Changes to airborne pollen counts across Europe. PLoS One 7https://doi.org/10.1371/journal. pone.0034076. e34076.

4

POSITIVE MATRIX FACTORIZATION AND WEATHER TYPES: A USEFUL DUAL TOOL FOR AEROSOL SOURCE APPORTIONMENT

Sent to Science of the Total Environment, April 2020

4.1. INTRODUCTION

Aerosols are important components of the atmosphere and are defined as particles in solid or liquid state which are suspended in the air (Mészáros, 1999). Physical, chemical and optical characteristics of atmospheric aerosols depend largely on their sources and formation processes. Several authors have reported that depending of these characteristics, atmospheric aerosol can cause a high impact on the local and regional deterioration of air quality (Paraskevopoulou et al., 2015), visibility reduction and health (Kanakidou et al., 2005; Ren-Jian et al., 2012). Atmospheric aerosol sources can be divided into: *i*) natural, which include seas, volcanoes, vegetation, wildfires, deserts and soil resuspension and *ii*) anthropogenic, which are caused by human activities, mainly in urban and industrial areas, such as exhaust and non-exhaust traffic related emissions, industrial activities, fossil fuel combustion, cooking, and biomass burning (Calvo et al., 2013).

At a specific location, aerosol concentrations depend on several factors such as meteorological conditions, regional background, local and regional sources, etc. Thus, the study of the distribution of sources is essential in the field of atmospheric science since it allows the reconstruction of the patterns of pollution sources that influence the composition and concentration of atmospheric pollutants in a specific area, with the objective of devising mitigation strategies to improve air quality.

The role of meteorological conditions in the atmospheric processes of dilution, transformation, transport and removal of pollutants has been widely studied in recent years (e.g. Baltaci et al., 2019; Gvozdić et al., 2011; Kuzu and Saral, 2017). These studies have allowed a better understanding of the atmospheric factors affecting the air quality, becoming an important area of research. The concentrations of pollutants in the atmosphere are also linked to the occurrence of specific weather features (including wind speed and velocity) induced by mesoscale processes (e.g. Baltaci et al., 2019; Calvo et al., 2012; Kwok et al., 2017; Russo et al., 2014; Weissert et al.,

2018), which are specific to a given region. Thus, the weather types and the origin of air masses provide valuable information on the influence of polluting sources at a given study area (Calvo et al., 2012).

Different source apportionment models are available to identify ambient air pollution sources and quantify their contribution to measured levels. Viana et al. (2008) described three main groups of source apportionment techniques: *i*) methods based on the evaluation of monitoring data (including correlations between wind direction and particulate matter (PM) components); *ii*) methods based on emission inventories and/or dispersion models; *iii*) receptor models to quantify the contribution of sources to PM from its chemical composition (Paatero and Tapper, 1994), which include models such as principal component analysis (PCA), positive matrix factorization (PMF), regression models, chemical mass balance (CMB), among others. Receptor models are widely used due to the availability of software that allows the identification of the sources. PMF is one of the most used and useful models, especially where detailed data do not exist on the composition of the main emission sources, but where large numbers of sampled data are available on ambient concentrations (Norris et al., 2014; Paatero and Tapper, 1994).

Throughout the years, authors have studied and identified the contribution of aerosol sources in different environments (e.g. Amato et al., 2016; Cesari et al., 2016; Mazzei et al., 2008; Paraskevopoulou et al., 2015). In Spain, several aerosol source apportionment have been carried out using PMF (Aldabe et al., 2011; Cusack et al., 2013; Pindado and Perez, 2011; Titos et al., 2014; Yubero et al., 2011) or other techniques (Artiñano et al., 2003; Pey et al., 2009; Querol et al., 2002, 2001), especially in large urban centers such as Barcelona and Madrid, where the main primary sources are involved (traffic, industrial activities, fossil fuel combustion, etc.) or at rural sites highly impacted by biomass burning.

Previous studies carried out in León city (NW of Spain), described it as a city mainly affected by fossil fuel and biomass burning emissions, due to road traffic and domestic heating devices (Blanco-Alegre et al., 2019; Oduber et al., 2018) specially in autumn and winter. Moreover, the northwest of the Iberian Peninsula is often affected by long-range transport events, such as Saharan dust intrusions and wildfires, which can cause an increase in the particulate concentrations and changes in the aerosol chemical composition (Alonso-Blanco et al., 2018, 2012; Oduber et al., 2019). However, until now no previous studies described in depth the aerosol chemical composition and their possible sources in León city.

As discussed above, both meteorological characteristics (regional state of the atmosphere) and source apportionment methods are useful tools in air quality studies. However, studies combining these approaches and taking advantage of potential synergies between them are scarce. This study aims to fill this gap with the analysis of the link between the source contributions and the circulation weather types in a suburban area of León city, Spain. For this purpose, attempts were made to establish linear regression models integrating the daily contribution of each source to PM_{10} and the parameters of weather types associated with the geostrophic flow: southerly flow (SF), westerly flow (WF), southerly shear vorticity (ZS) and westerly shear vorticity (ZW). Besides, the main influence of the sources during the different circulation weather type and the relationship with the meteorological conditions, were also

analyzed. As far as we know, this kind of research is inexistent and will represent a step forward in the studies on aerosol source apportionment.

4.2. EXPERIMENTAL BACKGROUND

4.2.1. Sampling site

Atmospheric aerosols were sampled between 09 March 2016 and 14 March 2017, on the terrace of the Faculty of Veterinary Sciences at the University of León (42° 36′ 50″ N, 5° 33′ 38″ W, 846 m), in a suburban area located in the NE of the urban center of León city, Spain (Fig. 4.1). In 2017, the National Institute for Statistics (www.ine.es) reported a population of 125,317 inhabitants. The city is characterized by the absence of large emitting industries, except for some pharmaceutical industries located around the city within a radius of 5 km. 30 km north of the city, in La Robla, there is also a cement factory.

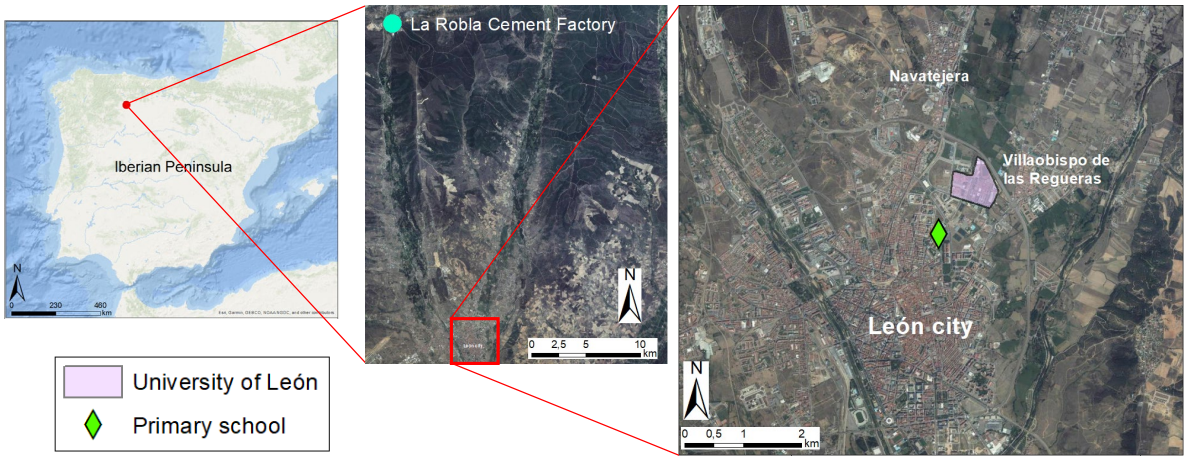

FIG. 4.1. Map of the Iberian Peninsula and location of the sampling site.

The climate in León is Continental type with great influence of the Mediterranean climate, with long and cold winters and warm summers. The mean annual temperature is 11 °C, influenced by the proximity of the Cantabrian Mountain Range to the north. Minimum precipitation values are registered in summer, when droughts are very common, while spring is the season with maximum precipitation values (Table 4.1). In winter there are frequent frosts (74 frost days per year, on average) and, on average, 16 snow days are registered per year, but large snowfalls are not frequent (Castro et al., 2010).

TABLE 4.1. Annual and seasonal mean temperatures (T), relative humidity (RH), accumulated precipitation (P) and wind speed (ws) in León during the study period.

	Annual	Winter	Spring	Summer	Autumn
T (°C)	11 ± 7	5 ± 3	10 ± 4	20 ± 4	10 ± 4
RH (%)	63 ± 14	70 ± 12	64 ± 11	48 ± 7	70 ± 11
P (mm)	485	150	229	31	75
ws (m/s)	0.8 ± 0.7	0.8 ± 0.7	1.2 ± 0.8	0.6 ± 0.3	0.7 ± 0.5

4.2.2. Materials and methods

4.2.2.1. Aerosol sampling and chemical analysis

The sampling of PM_{10} was carried out by using a low volume sampler (TECORA, ECHOPM) equipped with 47 mm diameter teflon filters and a high-volume sampler (CAV-Mb) equipped with 150 mm diameter quartz filters. The filter samples were collected every 24 h, starting at 1200 UTC every day.

Quartz filters

Quartz filters were used for the determination of PM_{10} mass by gravimetry, weighing the filters before and after sampling (± 0.00001 g) on an electronic semi-microbalance (Mettler Toledo, XPE105DR).

The determination of organic and elemental carbon (OC and EC, respectively) was carried out using the thermal-optical technique, following the procedure described in Alves et al. (2015) and Pio et al. (2011). To account for elements such as oxygen, hydrogen and nitrogen, the amount of particulate organic matter (POM) has been estimated by multiplying the average OC concentration by a factor of 1.6 (Liousse et al., 1996).

A portion of the quartz filters was extracted with 3 ml of ultra-pure deionized water and filtered through a 0.2 µm PTFE syringe filter for the determination of levoglucosan. The extracts were analyzed in a Thermo Scientific Dionex™ ICS-5000 ion chromatograph equipped with amperometric detector and a CarboPac® PA-1 column (2 × 250 mm), and quantified through a calibration curve made from a levoglucosan standard (SIGMA Aldrich, 99% purity).

Teflon filters

Teflon filters were first cut in half. One half was used for the analysis of water-soluble inorganic ions by ion chromatography. This portion was extracted with 6 ml of ultra-pure deionized water and filtered through a 0.2 µm PTFE syringe filter. The chromatographic analysis was performed on a Thermo Scientific DionexTM ICS-5000 equipment provided with an IonPac® CS16 column (4 × 250 mm) and an IonPac® AS11 column (4 × 250 mm) for the analysis of cations (Li^+, Na^+, K^+, Ca^{2+}, Mg^{2+}, NH_4^+) and anions (F^-, Cl^-, SO_4^{2-}, NO_3^-, NO_2^-), respectively. The other half was used for the determination of the major trace elements (Na, Mg, Al, Si, P, S, Cl, K, Ca, Ti, V, Cr, Mn, Fe, Ni, Cu, Zn, As, Se, Br, Rb, Sr, Pb), using the Particle-Induced X-ray Emission (PIXE) technique described by Lucarelli et al. (2015).

4.2.2.2. Circulation weather types

In order to study the relationship between the aerosol composition and the weather types, a circulation weather type (CWT) classification, based on Lamb (1972), was carried out. The direction and vorticity of the geostrophic flow (southerly flow SF, westerly flow WF, southerly shear vorticity ZS and westerly shear vorticity ZW), obtained from the atmospheric pressure at sea level in 16 grid points distributed over the Iberian Peninsula (Trigo and DaCamara, 2000),

have been used to establish each one of the 26 different CWTs: *i*) 8 "pure" weather types, (N, S, E, W, NW, SW, SE and NE); *ii*) 2 "non-directional" (anticyclonic-A and cyclonic-C); *iii*) 16 "hybrid" types, as a result of the combination between "non-directional" and "pure" types: AN, ANE, ANW, AS, ASE, ASW, AE, AW and CN, CNE, CNW, CS, CSE, CSW, CE, CW (Table A2.1 in Annex 2). More information about this classification can be found in Fernández-Raga et al. (2017) and Trigo and DaCamara (2000).

4.2.2.3. PMF model

The analysis of the aerosol source contribution was carried out using the Positive Matrix Factorization (PMF) model, by using the PMF 5.0.14 software, developed by the U.S. Environmental Protection Agency (EPA) (Paatero, 1997; Paatero et al., 2014; Paatero and Tapper, 1994). To run PMF, concentrations and uncertainties of the chemical properties of 364 PM_{10} samples were used. Missing data were substituted by the median value and their uncertainties were replaced by four times the median value. The values below detection limits (BDL) were replaced by half of the minimum value reported and their uncertainties were replaced by 5/6 times the detection limit value, according to the methodology used by Polissar et al. (1998).

4.2.2.4. Additional data and data analysis

Seasons have been defined as follows: *i*) winter: from 21 December to 20 March; *ii*) spring: from 21 March to 20 June; *iii*) summer: from 21 June to 20 September; and *iv*) autumn: from 21 September to 20 December. Temperature, wind speed and direction, relative humidity and precipitation data, were recorded by an automatic weather station located in the sampling site.

For the statistical treatment, SPSS software (IBM Statistics Software V. 24) and R software with the Openair package (Carslaw, 2015; Carslaw and Ropkins, 2012) were used. The Kruskal-Wallis non-parametric test (Kruskal and Wallis, 1952) followed by Dunn test (Dunn, 1964) were applied to obtain the statistically significant differences. An automatic linear modelling (IBM SPSS Statistics 24) by step-wise with a significance of 0.05 and a removal probability of 0.1 was also used

4.3. RESULTS AND DISCUSSION

4.3.1. PM_{10} mass concentrations and chemical composition

During the sampling period, the mean annual PM_{10} mass concentration was 23 ± 8 μg/m^3. This value is similar to those reported in other suburban stations, during one-year sampling campaigns, by Waked et al. (2014) in Lens, France (22 ± 13 μg/m^3) and by Amato et al. (2016) in Barcelona, Spain (22.5 μg/m^3) and in Athens, Greece (19.8 μg/m^3). The minimum value of 4 μg/m^3 was recorded between 12 and 13 March 2017, after a precipitation event. The maximum concentration (59 μg/m^3) was reached between 23 and 24 February 2017, during an intense Saharan dust intrusion (Oduber et al., 2019). It was the only day in which the air quality daily limit value (DLV) for PM_{10} (50 μg/m^3, Directive 2008/50/CE) was exceeded. The lowest mean seasonal PM_{10} value was registered in spring with 19 ± 6 μg/m^3 (Table A2.2). This season is

characterized by low mean temperatures and high relative humidity (Table 4.1) and is usually very rainy, which helps scavenge the atmosphere.

Carbonaceous constituents (POM + EC), represented the highest PM_{10} mass fraction in all seasons, with an annual mean percentage of 22 ± 7%. Winter showed the highest carbonaceous fraction with 21 ± 7% of PM_{10}, and presented statistical significant differences compared to summer and autumn ($p < 0.05$). Calvo et al. (2013) describe that the primary anthropogenic OC and EC are mainly emitted by combustion processes, such as those involving road traffic and domestic heating devices. Levoglucosan (a tracer of biomass burning) concentrations were higher in winter and autumn than in summer, showing statistically significant differences between seasons ($p < 0.01$), indicating that, in summer, OC values are more closely related to bioaerosol sources and forest fires, while in winter and autumn biomass burning is a major contributor to this carbonaceous component.

The concentration of the elements related to the mineral fraction (Si, Fe, Ca, Al) was higher in summer than in the other seasons (Table A2.2), due to the Saharan dust intrusions that reach the Peninsula during the warm months (Díaz et al., 2017). A significant correlation between NH_4^+ and both SO_4^{2-} and NO_3^- ($r = 0.69$ and 0.80, respectively, $p < 0.01$) was observed, suggesting that the ammonium acts as neutralizer of sulfate and nitrate aerosols. The highest values of sulfate were observed in summer and spring, mainly due to the increase in the SO_2 oxidation rate under high insolation conditions (Galindo et al., 2008; Seinfeld and Pandis, 2016). Moreover, the highest concentrations of nitrate were recorded in winter (1.3 ± 1.5 µg/m^3) (Table A2.2), due to the thermal stability of ammonium nitrate (Querol et al., 2004). Additionally, nitrate concentrations are affected by the NO_x emissions from residential combustion devices (Vicente et al., 2013), and from exhaust systems of motor vehicles (Alves et al., 2015).

4.3.2. PMF source apportionment

Aerosol source apportionment was carried out by PMF analysis. The best adjustment was provided by a 6-factor solution. The patterns obtained allowed to identify the following sources in the city of León (Fig. A2.1 in Annex 2): traffic, aged sea salt, secondary aerosol, mineral, marine, and biomass burning (B.B.). In addition, approximately 6% of the PM_{10} mass cannot be explained by any of the factors and was mentioned as an unknown fraction (Fig. 4.2).

Traffic source

Traffic, which includes exhaust and non-exhaust emissions, was the prevailing aerosol source in León city during the entire year, representing 29% of PM_{10} (Fig. 4.2). Alleman et al. (2010) and Amato et al. (2016) also reported road transport as the main aerosol source in urban stations in France (15% of PM_{10}) and Portugal (23% of PM_{10}), respectively, while in background stations, the traffic contribution to PM_{10} ranged between 18 and 22% in the study of Amato et al. (2016) (Table 4.2). This factor is characterized by high contributions of EC, OC, NO_3^-, Cu, Cr, Zn and Se, which can be associated with fossil fuel emissions (Lin et al., 2005). Between autumn and winter a significant increase in the contribution of this aerosol source was observed, probably due to the academic activities of the study site. Additionally, near the sampling site there is a bus stop with high traffic flow during the academic period, which may contribute to the increase of this

factor. In summer, the traffic flow decreases considerably, due to the vacation period of the University of León and the primary school in the vicinity of the sampling point (Fig. 4.1) (Oduber et al., 2018).

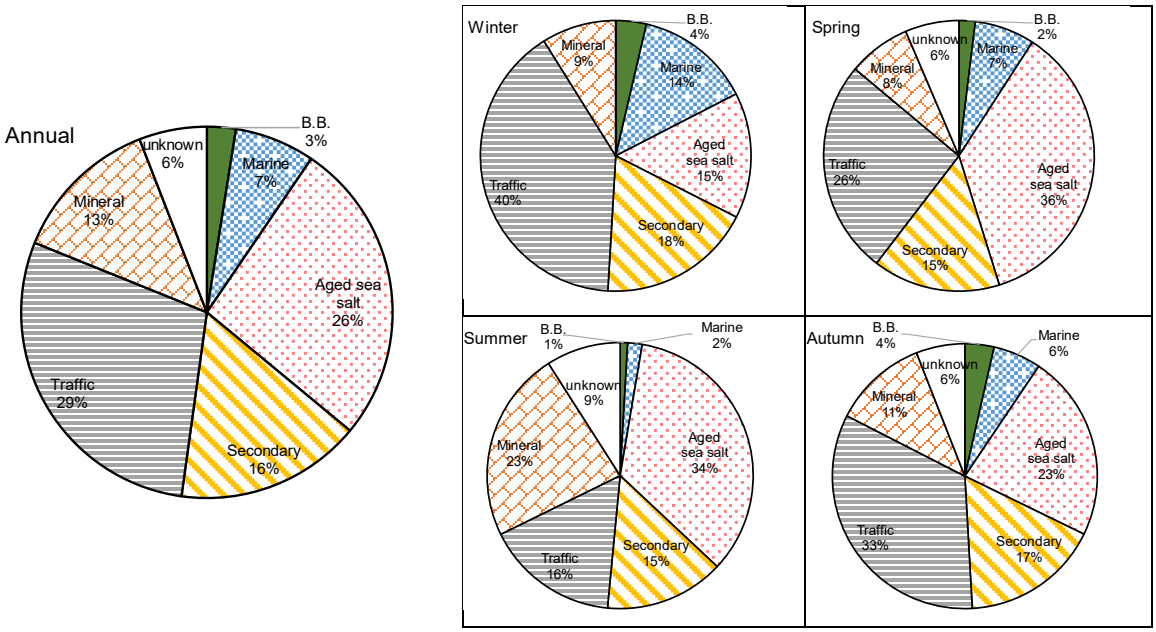

FIG. 4.2. Annual and seasonal contributions, in % of PM_{10}, of the identified sources: traffic, aged sea salt, secondary, mineral, marine and biomass burning (B.B.).

Aged sea salt source

Aged sea salt was the second most important factor contributing to the annual PM_{10} with 26%, summer and spring being the seasons with the highest contribution (Fig. 4.2). Waked et al. (2014) reported a contribution of 19% of PM_{10} from aged sea salt aerosol in Lens, France, while Amato et al. (2016) reported contribution of 11% in Barcelona, Spain, 5% in Florence and 2% in Milan, Italy (Table 4.2), coinciding in all cases with an increase in the contribution during the summer. This factor is characterized by high levels of crustal-related elements (Si, Mg, Al, Fe), Na, S, NO_3^-, OC and EC, and the absence of Cl^- and NH_4^+. The depletion in Cl^- and NH_4^+ levels is caused by the reaction of both SO_2 and sulfuric acid (H_2SO_4) with sea salt particles (Hsu et al., 2007; Song and Carmichael, 1999). Moreover, due to Mg^{2+} and Na^+ are considered as tracers of sea salt, the Mg^{2+}/Na^+ mass ratio was evaluated taking into account days with an aged sea salt contribution higher than 50% of PM_{10}, obtaining a mean value of 0.22 ± 0.06. Beuck et al. (2011) and Yao et al. (2003) reported for aged sea salt aerosols, a ratio close to 0.12, which agrees with the theoretical value reported by Seinfeld and Pandis (2016). The difference observed between our results and these studies may be due to the contribution of mineral particles to this factor.

Secondary aerosols source

The third factor is dominated by the presence of S, NO_3^- and NH_4^+, which represent the formation of secondary inorganic aerosols (Salvador et al., 2004). This is the predominant source of aerosol in suburban stations studied by Amato et al. (2016) and Waked et al. (2014), with contributions to PM_{10} from 28 to 40% and where the traffic contribution does not exceed 20%

(Table 4.2). Secondary aerosols are formed from chemical and photochemical processes that occur between pollutants, generally released to the atmosphere by anthropogenic sources (Gugamsetty et al., 2012). The contribution from this source to PM_{10} in León was similar in the four seasons (Fig. 4.2). During summer and spring, the formation of secondary sulfates is promoted by the solar radiation, while in winter and autumn, the secondary nitrates are more important (Querol et al., 2004).

Mineral source

This factor is dominated by crustal elements as Si, Al, Ti, Fe, Ca, K and Mg. The arrival of dust from Saharan outbreaks and soil resuspension are the main sources contributing to this factor. Besides, the cement factory located in La Robla, at approximately 20 km north of the sampling site, is probably another important source of mineral particles, due to it works mainly with clinker, which is a material consisting of CaO, SiO_2, Al_2O_3, Fe_2O_3, among others. Regarding the annual contribution to PM_{10} mass concentration, this factor represents 13% (Fig. 4.2), with seasonal percentages ranging between 8% (in spring) and 23% (in summer). Amato et al. (2016) reported values ranging between 1 and 14% of PM_{10} in other cities also affected by Saharan dust intrusions, while Manousakas et al. (2015) observed a contribution of 33% of soil dust in Megalopolis, Greece (Table 4.2). Moreover, Gugamsetty et al. (2012) and Hsu et al. (2016) observed contributions of 44 and 34%, respectively, from soil dust to PM_{10}, due to local activities.

Marine source

Due to the significant loading of Cl, Na and Mg, the fifth factor is defined as marine (Borbély-Kiss et al., 1999; Salvador et al., 2004). The highest contribution from this factor was obtained in winter, followed by spring (14% and 7%, respectively). Although León is not in the coastal region, the marine contribution seems important in winter, when the highest Na and Cl concentrations were registered (0.26 ± 0.23 μg/m^3 and 0.46 ± 0.37 μg/m^3, respectively). It can be attributed to the Atlantic frontal system, that is more frequent in winter and spring, and which generally reaches the city of León when penetrating from the Atlantic Ocean, approximately 200 km far from the city.

Biomass burning source

This factor is characterized by high amounts of levoglucosan, which is a biomass burning tracer (Vicente and Alves, 2018). Constituents such as K, NO_3^- and OC, which are also related to biomass burning (Sharma et al., 2016), were also present in small proportions. The highest contribution of this factor was obtained in winter and autumn (Fig. 4.2), when the emissions from residential heating devices are more frequent and intense. Moreover, in summer and spring, a small contribution of biomass burning emissions to the aerosol loads, probably due to wildfire events, which are more often in the northwest of the Peninsula in the warmer months (Alonso-Blanco et al., 2012, 2018).

Unknown sources

The unknown factor represents approximately 6% of the PM_{10} mass concentration. This last source could represent a sum of small sources of atmospheric aerosol, among which some

pharmaceutical industries, coal combustion emissions and / or primary biogenic emissions, etc. Waked et al. (2014) reported in Lens, France, an annual contribution of primary biogenic emissions to PM_{10} of 9% (Table 4.2), which reaches up to 20% in summer, due to an increase in the concentration of fungal spores, fern spores, pollen grains and fragments of plants in the air, in addition to the presence of large agricultural activities near the sampling site. The increase in the contribution of this unknown source, especially during the summer (9%), is probably due to a large contribution of primary biogenic emissions during the warmer months. Fernández-González et al. (1993) showed that the pollen season in León mainly occurs between late spring and summer. Therefore, in these months, aerosol concentrations may be affected by primary biogenic emissions due to high levels of pollen spores in the atmosphere.

TABLE 4.2. Source contributions of PM_{10} obtained with PMF by different studies.

Study	Location	PM_{10} ($\mu g/m^3$)	Sources (contribution to PM_{10})
Amato et al. (2016)	Barcelona, Spain (urban background)	22.5	Secondary sulfate and organics (27%), secondary nitrate (13%), vehicle exhaust (14%), vehicle non-exhaust (12%), aged sea salt (11%), local dust (11%), industrial (7%), heavy oil combustion (4%), Saharan dust (1%)
	Porto, Portugal (urban traffic)	34.5	Vehicle exhaust (23%), mineral (18%), marine (16%), biomass burning (12%), heavy oil and secondary sulfate (10%), secondary nitrate (9%), vehicle non-exhaust (8%), industrial (4%)
	Florence, Italy (urban background)	18.9	Secondary sulfate and organics (21%), biomass burning (15%), vehicle exhaust (13%), local dust (12%), secondary nitrate (11%), vehicle non-exhaust (9%), heavy oil combustion (5%), aged sea salt (5%), Saharan dust (4%), marine (4%)
	Milan, Italy (urban background)	38.1	Secondary nitrate (26%), biomass burning (17%), vehicle non-exhaust (14%), secondary sulfate and organics (13%), local dust (8%), industrial (8%), vehicle exhaust (7%), aged sea salt (2%)
	Athens, Greece (suburban background)	19.8	Secondary sulfate and organics (19%), secondary nitrate (15%), Saharan dust (14%), local dust (11%), vehicle exhaust (10%), vehicle non-exhaust (8%), biomass burning (7%), marine (5%), heavy oil combustion (4%)
Hsu et al. (2016)	Changhua County, Taiwan (residential area)	52.4 ± 27.2	Soil dust and crustal metals (44%), coal combustion (25%), oil combustion (23%), traffic (8%)
Manousakas et al. (2015)	Megalopolis, Greece (urban)	24.3	Soil dust (33%), biomass burning (19%), road dust (15%), power plant emissions (13%), traffic (12%), marine (8%)
Waked et al. (2014)	Lens, France (urban background)	22 ± 15	Secondary (28%), aged sea salt (19%), biomass burning (13%), mineral (13%), primary biogenic (9%), marine (8%), primary traffic (6%), heavy oil combustion (4%)
Gugamsetty et al. (2012)	Shinjung station, New Taipei City, Taiwan (urban)	39.45 ± 11.58	Soil dust (34%), vehicle emissions (25%), secondary aerosols (24%), sea salt (8%), industrial (8%)
Alleman et al. (2010)	Dunkirk, France (industrial)	Ranging from 14 to 36	Road transport (15%), dust resuspension (13%), metallurgical coke plant (13%), marine (12%), crustal dust (11%), petrochemical activities (9%), metallurgical sintering plant (9%), ferromanganese plant (7%)

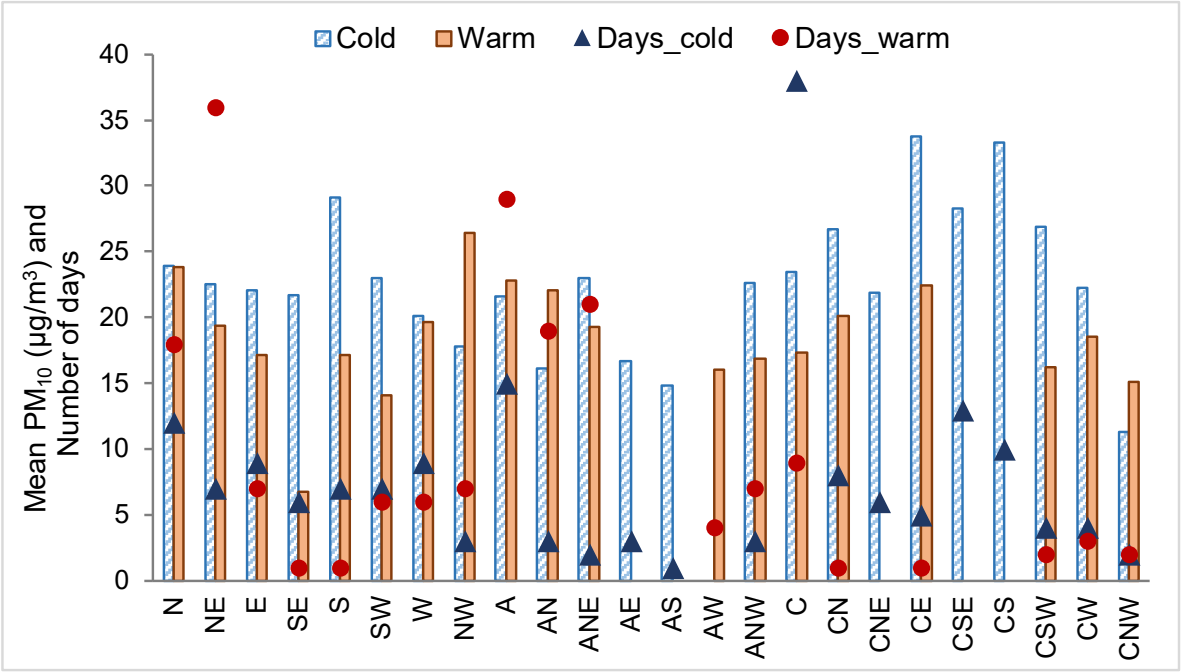

FIG. 4.3. Mean PM_{10} and number of days for the different circulation weather types (CWTs) during the cold and warm periods.

4.3.3. Relationship between source contributions and circulation weather types

In order to characterize the daily contribution of each source and the influence of CWTs on these emissions, a seasonal analysis was carried out taking into account two periods: cold (winter and autumn) and warm (spring and summer).

During the sampling period, the more frequent weather types were pure cyclonic (C), with 13% of the days, followed by pure anticyclonic (A) and NE both with 12% of the sampling days. NE weather type was most frequent in the warm period with 20% of the days, followed by A with 16%. In the cold period, the most frequent weather type was pure cyclonic with a frequency of 22% of the days, followed by A with 9% (Fig. 4.3).

In general, the mean PM_{10} values were higher for all the CWTs during the cold period than in the warm period, except for NW, A, AN and CNW (Fig. 4.3). Furthermore, Figures 4.4a and 4.4b show that, in the cold period, the largest contribution to PM_{10} came from traffic and secondary aerosol factors, while in the warm period a higher share was registered for mineral and aged sea salt factors.

During the cold period, the highest mean values of PM_{10} were observed for the hybrid cyclonic types with S and E components, CE (34 µg/m³), CSE (28 µg/m³), CS (33 µg/m³) and S (29 µg/m³). Traffic and secondary aerosol factors have a major contribution during these weather types (Fig. 4.4a), due to the increased emissions from heating devices and from road traffic in winter and autumn. Moreover, the lowest PM_{10} values in the cold period are associated with CNW (11 µg/m³) and AS (15 µg/m³), encompassing higher contributions from traffic and aged sea salt. Nevertheless, these CWTs in the cold period lasted only 2 days, in the case of AS, and 1 day, for CNW.

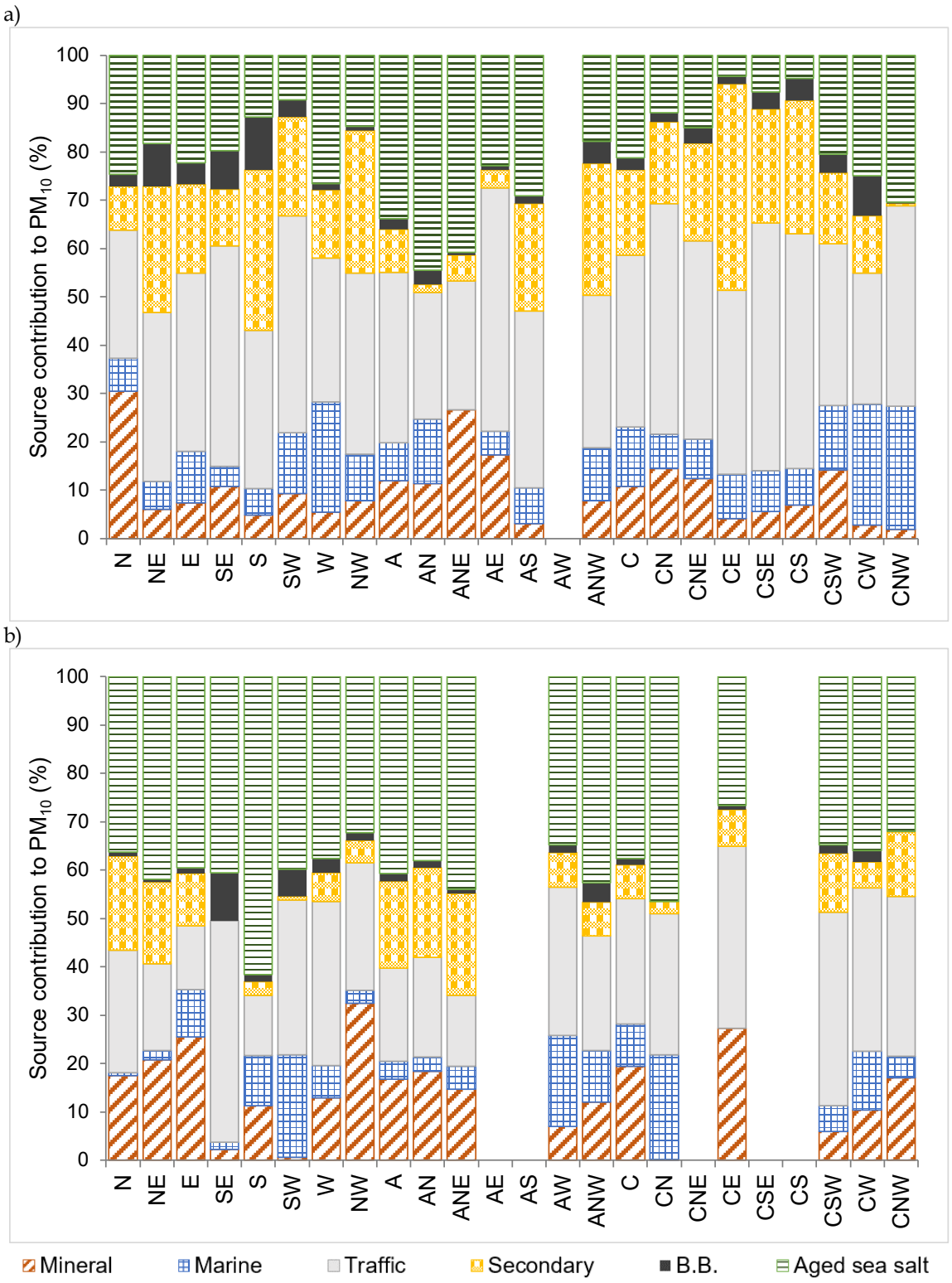

FIG. 4.4. Source contribution to PM_{10} (%) for the different circulation weather types (CWT) in the: a) cold period and b) warm period.

During the warm period, the weather types with north component, NW, N, AN, and the pure anticyclonic, A, showed the highest mean PM_{10} values (between 22 and 26 $\mu g/m^3$). Anticyclonic types, A and AN, exhibited high contribution of aged sea salt (41 and 38%,

respectively), secondary (18% for both) and mineral (17 and 18%, respectively) factors (Fig. 4.4b). These weather types are more frequent in summer, when the high pressure system of the Azores during the days with northerly weather types favor a high photochemical activity (Santurtún et al., 2015). Fernández-Raga et al. (2017) reported that the atmospheric stability conditions of the anticyclonic type causes a greater local dust resuspension and an inhibition of the dispersion. In addition, the Saharan dust intrusions are frequently related to anticyclonic situations (Díaz et al., 2017). Besides, N and NW weather types showed a high contribution from aged sea salt (36 and 32%, respectively) and mineral (17 and 32%, respectively) factors.

Cyclonic types CW and CNW accounted for 25% of the PM_{10} contribution from marine source in the cold period (Fig. 4.4a), whereas in the warm period the highest contribution from this source was associated with SW weather type (Fig 4.4b). Westerly weather types are characterized by being humid air masses loaded with marine salts from the Atlantic Ocean. In León, westerly weather types are more frequent in winter and spring (with a frequency of 19% and 21% of the winter and spring days, respectively) than in summer and autumn (2% and 8% of days, respectively). Due to their instability, these CWTs are associated with significant rainfall events (Fernández-Raga et al., 2017; Santos et al., 2005). Moreover, the main PM_{10} contribution from biomass burning was recorded for the directional S type, with 11% in the cold period, and SE, with 10% of the PM_{10} contribution in the warm period. These CWTs are more frequent in spring and autumn, when the use of domestic heating devices is frequent.

4.3.4. Aerosol composition and geostrophic flow

In order to determinate the association between each aerosol source contribution and the geostrophic flow, an automatic linear modelling (IBM SPSS Statistics 24) by stepwise, was used. For the construction of the linear models, all the elements analyzed in the PMF model, the PM_{10} source contribution from PMF and the geostrophic flow were introduced in the models. The dependent and independent variables as well as the coefficients of the models that are statistically significant ($p < 0.05$) are shown in Table 4.3.

TABLE 4.3. Intercept (β), (coefficients ± σ) and variance (R^2) of multi-linear regression models of PM_{10} for each source contribution. Each summand in the equations are expressed in $\mu g/m^3$.

PM_{10} Source ($\mu g/m^3$)	Multi-linear regression models		R^2
	β ($\mu g/m^3$)	(Coefficients ± σ)	
Traffic =	-2.6 ± 0.3	[EC] (10.1 ± 0.4) + [Se] (368 ± 96) + (SF) ($1.0\times10^{-3} \pm 0.2\times10^{-3}$) + [Cu] (352 ± 74)	0.91
Aged sea salt =	2.2 ± 0.2	$[SO_4^{2-}]$ (3.2 ± 0.2) - $[NH_4^+]$ (4.2 ± 0.4) + [Na] (21.0 ± 1.2) - [Cl] (11.8 ± 0.8) + $[NO_3^-]$ (0.6 ± 0.2) -(ZS) ($3.13\times10^{-4} \pm 1.5\times10^{-4}$)	0.81
Secondary =	-0.32 ± 0.09	$[NH_4^+]$ (8.16 ± 0.19) - $[NO_3^-]$ (0.74 ± 0.08) + $[SO_4^{2-}]$ (0.35 ± 0.08) + (SF) ($1.95\times10^{-4} \pm 0.88\times10^{-4}$)	0.97
Mineral =	-0.70 ± 0.06	[Al] (10.35 ± 0.41) + [Ca] (3.41 ± 0.39) - (SF) ($3.36\times10^{-4} \pm 0.56\times10^{-4}$) + (ZS) ($2.39\times10^{-4} \pm 0.51\times10^{-4}$) + [Si] (0.46 ± 0.19)	0.98
Marine =	-0.44 ± 0.03	[Cl] (5.53 ± 0.13) + [Na] (3.32 ± 0.21) + (WF) ($8.22\times10^{-5} \pm 3.20\times10^{-5}$)	0.98
Biomass burning =	-0.077 ± 0.012	[Levoglucosan] (58.740 ± 0.441)	0.99

The linear models showed a clear dependence on the main tracer elements for each factor. Regarding the geostrophic flow, a positive coefficient for westerly flows (WF) in marine factor

concentrations was observed. This result is in line with the fact that the western air masses are responsible for transporting large amounts of sea salts from the Atlantic Ocean to León. Moreover, secondary and traffic factors had positive coefficients for southerly flows (SF). This may be due to the significant contribution of anthropogenic emissions from the city center, which include traffic, heating devices and pharmaceutical industries (located at about 8 km south of the sampling site) added to the anthropogenic emissions of other cities located in the southern of León such as Zamora, Segovia and Valladolid.

The southerly shear vorticity (ZS) appears with a significant coefficient only in aged sea salt and mineral factors. In the case of aged sea salt, the negative ZS coefficient confirms that this factor is mainly favored by anticyclonic situations, as discussed in section 4.3.3. The SF negative and ZS positive coefficients obtained for the mineral factor deserve attention, suggesting that this input is favored by cyclonic and northern conditions. However, Saharan dust intrusions, which can be considered as the main mineral source, are mainly associated with anticyclonic situations and southern flows in the Iberian Peninsula (Díaz et al., 2017; Oduber et al., 2019; Titos et al., 2017). These results, along with those observed for the CWTs, for which the highest PM_{10} contribution from the mineral factor is associated with northerly types, confirm that the emissions from the cement factory in La Robla could be an important source of mineral aerosol that must be considered.

Finally, the biomass burning factor shows no relation with geostrophic flow, probably because it is a more local source.

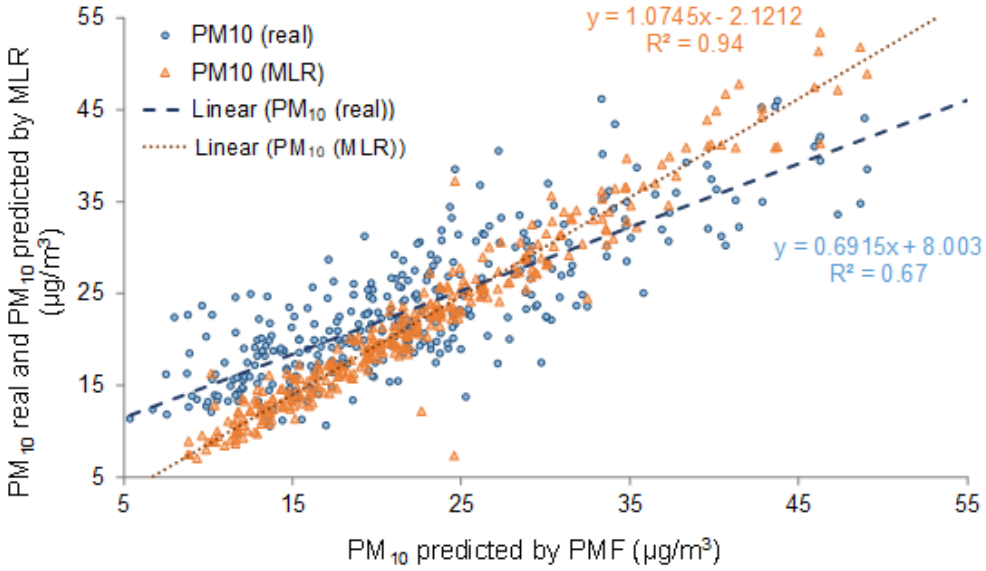

FIG. 4.5. Linear relationship between PM_{10} real and PM_{10} predicted with multi-linear regression models (MLR) vs PM_{10} predicted with PMF.

Assuming that the six factors described in Table 4.3 are the only sources of PM_{10} in León, and applying each linear regression model to calculate the individual contribution of each source, it is possible to calculate the total daily mass concentration of PM_{10}. This allows comparing the results obtained by the PMF model and those derived from the linear models presented in this

work. The linear fit of Figure 4.5 shows a R^2= 0.94, which indicates that the results obtained through the application of the linear models are similar to those obtained by PMF for the PM_{10} daily reconstruction. The Kruskal-Wallis test shows that there are no significant differences between the PM_{10} concentrations obtained by PMF and those estimated by the multi-linear model ($p < 0.05$).

These linear models (Table 4.3) can be very useful to determine the contribution of a specific source to PM_{10} in León, only by knowing the geostrophic flow and the concentration of the elements involved in the model.

4.4. CONCLUSIONS

A PM_{10} sampling campaign was carried out in a suburban area of León city, Spain, between May 2016 and May 2017, with the aim of determining aerosol sources and their association with air masses and circulation weather types. The positive matrix factorization (PMF) analysis allowed to identify 6 main aerosol sources: traffic, aged sea salt, secondary aerosols, mineral, marine and biomass burning, with an annual contribution to PM_{10} of 29%, 26%, 16%, 13%, 14% and 3%, respectively. Traffic and secondary aerosols factors showed the highest PM_{10} contribution for the hybrid cyclonic weather types CE, CS and CSE. Anticyclonic types A, AN and ANE, exhibited high values of secondary aerosols (15%), aged sea salt (20%) and mineral (17%) factors. Besides, the mineral factor showed the highest contributions for northerly types, N (23%) and NW (27%).

Based on both the PMF results and the parameters of weather types associated with the geostrophic flow (SF, WF, ZS and ZW), it was possible to construct multi-linear regression models for each aerosol source. This allowed to describe locally the relationship of the circulation weather types and the emissions from each source to the daily concentration of PM_{10}. The results showed that the contribution of each factor to PM_{10} depends on the main tracer elements of each source and on the geostrophic flow.

The daily mass concentration of PM_{10}, estimated from the multilinear models, agreed with the results obtained by the PMF model, leading to a coefficient of determination of 0.94. Unlike the PMF method, these linear models can be applied to determine the contribution of PM_{10} sources in León only by knowing the geostrophic flow and the concentration of the elements involved in the model.

The results show that the combination of PMF models and circulation weather types can be a useful dual tool in the local analysis of source apportionment. The application of these results in local air quality models can provide helpful information for formulating mitigation measures.

4.5. REFERENCES

Aldabe, J., Elustondo, D., Santamaría, C., Lasheras, E., Pandolfi, M., Alastuey, A., Querol, X., Santamaría, J.M., 2011. Chemical characterisation and source apportionment of $PM_{2.5}$ and PM_{10} at rural, urban and traffic sites in Navarra (North of Spain). Atmos. Res. 102, 191–205. doi:10.1016/j.atmosres.2011.07.003

Alleman, L.Y., Lamaison, L., Perdrix, E., Robache, A., Galloo, J., 2010. PM_{10} metal concentrations and source identification using positive matrix factorization and wind sectoring in a French industrial zone. Atmos. Res. 96, 612–625. doi:10.1016/j.atmosres.2010.02.008

Alonso-Blanco, E., Calvo, A.I., Fraile, R., Castro, A., 2012. The Influence of Wildfires on Aerosol Size Distributions in Rural Areas. Sci. World J. 2012, 1–13. doi:10.1100/2012/735697

Alonso-Blanco, E., Castro, A., Calvo, A.I., Pont, V., Mallet, M., Fraile, R., 2018. Wildfire smoke plumes transport under a subsidence inversion: Climate and health implications in a distant urban area. Sci. Total Environ. 619–620, 988–1002. doi:10.1016/j.scitotenv.2017.11.142

Alves, C.A., Lopes, D.J., Calvo, A.I., Evtyugina, M., Rocha, S., Nunes, T., 2015. Emissions from Light-Duty Diesel and Gasoline in-use Vehicles Measured on Chassis Dynamometer Test Cycles. Aerosol Air Qual. Res. 15, 99–116. doi:10.4209/aaqr.2014.01.0006

Amato, F., Alastuey, A., Karanasiou, A., Lucarelli, F., Nava, S., Calzolai, G., Severi, M., Becagli, S., Gianelle, V.L., Colombi, C., Alves, C., Custódio, D., Nunes, T., Cerqueira, M., Pio, C., Eleftheriadis, K., Diapouli, E., Reche, C., Minguillón, M.C., Manousakas, M., Maggos, T., Vratolis, S., Harrison, R.M., Querol, X., 2016. AIRUSE-LIFE+: a harmonized PM speciation and source apportionment in five southern European cities. Atmos. Chem. Phys. 16, 3289–3309. doi:10.5194/acp-16-3289-2016

Artiñano, B., Salvador, P., Alonso, D.G., Querol, X., Alastuey, A., 2003. Anthropogenic and natural influence on the PM_{10} and $PM_{2.5}$ aerosol in Madrid (Spain). Analysis of high concentration episodes. Environ. Pollut. 125, 453–465. doi:10.1016/S0269-7491(03)00078-2

Baltaci, H., Akkoyunlu, B.O., Arslan, H., Yetemen, O., Ozdemir, E.T., 2019. The influence of meteorological conditions and atmospheric circulation types on PM_{10} levels in western Turkey. Environ. Monit. Assess. 191, 606–619. doi:10.1007/s10661-019-7609-7

Beuck, H., Quass, U., Klemm, O., Kuhlbusch, T.A.J., 2011. Assessment of sea salt and mineral dust contributions to PM_{10} in NW Germany using tracer models and positive matrix factorization. Atmos. Environ. 45, 5813–5821. doi:10.1016/j.atmosenv.2011.07.010

Blanco-Alegre, C., Calvo, A.I., Coz, E., Castro, A., Oduber, F., Prévôt, A.S.H., Močnik, G., Fraile, R., 2019. Quantification of source specific black carbon scavenging using an aethalometer and a disdrometer. Environ. Pollut. 246, 336–345. doi:10.1016/j.envpol.2018.11.102

Borbély-Kiss, I., Koltay, E., Szabó, G.Y., Bozó, L., Tar, K., 1999. Composition and sources of urban and rural atmospheric aerosol in eastern Hungary. J. Aerosol Sci. 30, 369–391. doi:10.1016/S0021-8502(98)00051-2

Calvo, A.I., Alves, C., Castro, A., Pont, V., Vicente, A.M., Fraile, R., 2013. Research on aerosol sources and chemical composition: Past, current and emerging issues. Atmos. Res. 120–121, 1–28. doi:10.1016/j.atmosres.2012.09.021

Calvo, A.I., Pont, V., Olmo, F.J., Castro, A., Alados-Arboledas, L., Vicente, A.M., Fernández-Raga, M., Fraile, R., 2012. Air Masses and Weather Types: A Useful Tool for Characterizing Precipitation Chemistry and Wet Deposition. Aerosol Air Qual. Res. 12, 856–878. doi:10.4209/aaqr.2012.03.0068

Carslaw, D.C., 2015. The openair manual–open-source tools for analysing air pollution data.

Carslaw, D.C., Ropkins, K., 2012. Openair - An r package for air quality data analysis. Environ. Model. Softw. 27–28, 52–61. doi:10.1016/j.envsoft.2011.09.008

Castro, A., Alonso-Blanco, E., González-Colino, M., Calvo, A.I., Fernández-Raga, M., Fraile, R., 2010. Aerosol size distribution in precipitation events in León, Spain. Atmos. Res. 96, 421–435. doi:10.1016/j.atmosres.2010.01.014

Cesari, D., Donateo, A., Conte, M., Merico, E., Giangreco, A., Giangreco, F., Contini, D., 2016. An inter-comparison of $PM_{2.5}$ at urban and urban background sites: Chemical characterization and source apportionment. Atmos. Res. 174–175, 106–119. doi:10.1016/j.atmosres.2016.02.004

Cusack, M., Pérez, N., Pey, J., Alastuey, A., Querol, X., 2013. Source apportionment of fine PM and sub-micron particle number concentrations at a regional background site in the western Mediterranean: A 2.5 year study. Atmos. Chem. Phys. 13, 5173–5187. doi:10.5194/acp-13-5173-2013

Díaz, J., Linares, C., Carmona, R., Russo, A., Ortiz, C., Salvador, P., Trigo, R.M., 2017. Saharan dust intrusions in Spain: Health impacts and associated synoptic conditions. Environ. Res. 156, 455–467. doi:10.1016/j.envres.2017.03.047

Dunn, O.J., 1964. Multiple Comparisons Using Rank Sums. Technometrics 6, 241–252. doi:10.1080/00401706.1964.10490181

Fernández-González, D., Suarez-Cervera, M., Díaz-González, T., Valencia-Barrera, R.M., 1993. Airborne pollen and spores of León (Spain). Int. J. Biometeorol. 37, 89–95. doi:10.1007/BF01214387

Fernández-Raga, M., Castro, A., Marcos, E., Palencia, C., Fraile, R., 2017. Weather types and rainfall microstructure in Leon, Spain. Int. J. Climatol. 37, 1834–1842. doi:10.1002/joc.4816

Galindo, N., Nicolás, J.F., Yubero, E., Caballero, S., Pastor, C., Crespo, J., 2008. Factors affecting levels of aerosol sulfate and nitrate on the Western Mediterranean coast. Atmos. Res. 88, 305–313. doi:10.1016/j.atmosres.2007.11.024

Gugamsetty, B., Wei, H., Liu, C.-N., Awasthi, A., Hsu, S.-C., Tsai, C.-J., Roam, G.-D., Wu, Y.-C., Chen, C.-F., 2012. Source Characterization and Apportionment of PM_{10}, $PM_{2.5}$ and $PM_{0.1}$ by Using Positive Matrix Factorization. Aerosol Air Qual. Res. 12, 476–491. doi:10.4209/aaqr.2012.04.0084

Gvozdić, V., Kovač-Andrić, E., Brana, J., 2011. Influence of Meteorological Factors NO_2, SO_2, CO and PM_{10} on the Concentration of O_3 in the Urban Atmosphere of Eastern Croatia. Environ. Model. Assess. 16, 491–501. doi:10.1007/s10666-011-9256-4

Hsu, C.Y., Chiang, H.C., Lin, S.L., Chen, M.J., Lin, T.Y., Chen, Y.C., 2016. Elemental characterization and source apportionment of PM_{10} and $PM_{2.5}$ in the western coastal area of central Taiwan. Sci. Total Environ. 541, 1139–1150. doi:10.1016/j.scitotenv.2015.09.122

Hsu, S., Liu, S.C., Kao, S., Jeng, W., Huang, Y., Tseng, C., Tsai, F., Tu, J., Yang, Y., 2007. Water-soluble species in the marine aerosol from the northern South China Sea: High chloride depletion related to air pollution. J. Geophys. Res. 112, D19304. doi:10.1029/2007JD008844

Kanakidou, M., Seinfeld, J.H., Pandis, S.N., Barnes, I., Dentener, F.J., Facchini, M.C., Van Dingenen, R., Ervens, B., Nenes, A., Nielsen, C.J., Swietlicki, E., Putaud, J.P., Balkanski, Y.,

Fuzzi, S., Horth, J., Moortgat, G.K., Winterhalter, R., Myhre, C.E.L., Tsigaridis, K., Vignati, E., Stephanou, E.G., Wilson, J., 2005. Organic aerosol and global climate modelling: a review. Atmos. Chem. Phys. 5, 1053–1123. doi:10.5194/acp-5-1053-2005

Kruskal, W.H., Wallis, W.A., 1952. Use of Ranks in One-Criterion Variance Analysis. J. Am. Stat. Assoc. 47, 583–621. doi:10.1080/01621459.1952.10483441

Kuzu, S.L., Saral, A., 2017. The effect of meteorological conditions on aerosol size distribution in Istanbul. Air Qual. Atmos. Heal. 10, 1029–1038. doi:10.1007/s11869-017-0491-y

Kwok, L.K., Lam, Y.F., Tam, C.Y., 2017. Developing a statistical based approach for predicting local air quality in complex terrain area. Atmos. Pollut. Res. doi:10.1016/j.apr.2016.08.001

Lamb, H.H., 1972. British Isles weather types and a register of daily sequence of circulation patterns, Geophysical Memoir, HMSO, London. Her Majesty's stationery office.

Lin, C.-C., Chen, S.-J., Huang, K.-L., Hwang, W.-I., Chang-Chien, G.-P., Lin, W.-Y., 2005. Characteristics of Metals in Nano/Ultrafine/Fine/Coarse Particles Collected Beside a Heavily Trafficked Road. Environ. Sci. Technol. 39, 8113–8122. doi:10.1021/es048182a

Liousse, C., Penner, J.E., Chuang, C., Walton, J.J., Eddleman, H., Cachier, H., 1996. A global three-dimensional model study of carbonaceous aerosols. J. Geophys. Res. Atmos. 101, 19411–19432. doi:10.1029/95JD03426

Lucarelli, F., Chiari, M., Calzolai, G., Giannoni, M., Nava, S., Udisti, R., Severi, M., Querol, X., Amato, F., Alves, C., Eleftheriadis, K., 2015. The role of PIXE in the AIRUSE project "testing and development of air quality mitigation measures in Southern Europe." Nucl. Instruments Methods Phys. Res. Sect. B Beam Interact. with Mater. Atoms 363, 92–98. doi:10.1016/j.nimb.2015.08.023

Manousakas, M., Diapouli, E., Papaefthymiou, H., Migliori, A., Karydas, A.G., Padilla-Alvarez, R., Bogovac, M., Kaiser, R.B., Jaksic, M., Bogdanovic-Radovic, I., Eleftheriadis, K., 2015. Source apportionment by PMF on elemental concentrations obtained by PIXE analysis of PM_{10} samples collected at the vicinity of lignite power plants and mines in Megalopolis, Greece. Nucl. Instruments Methods Phys. Res. Sect. B Beam Interact. with Mater. Atoms 349, 114–124. doi:10.1016/j.nimb.2015.02.037

Mazzei, F., D'Alessandro, A., Lucarelli, F., Nava, S., Prati, P., Valli, G., Vecchi, R., 2008. Characterization of particulate matter sources in an urban environment. Sci. Total Environ. 401, 81–89. doi:10.1016/j.scitotenv.2008.03.008

Mészáros, E., 1999. Fundamentals of atmospheric aerosol chemistry. Acad. Kiado Budapest.

Norris, G., Duvall, R., Brown, S., Bai, S., 2014. EPA Positive Matrix Factorization (PMF) 5.0 Fundamentals and User Guide. U.S. Environmental Protection Agency.

Oduber, F., Calvo, A.I., Blanco-Alegre, C., Castro, A., Nunes, T., Alves, C., Sorribas, M., Fernández-González, D., Vega-Maray, A.M., Valencia-Barrera, R.M., Lucarelli, F., Nava, S., Calzolai, G., Alonso-Blanco, E., Fraile, B., Fialho, P., Coz, E., Prevot, A.S.H., Pont, V., Fraile, R., 2019. Unusual winter Saharan dust intrusions at Northwest Spain: Air quality, radiative and health impacts. Sci. Total Environ. 669, 213–228. doi:10.1016/j.scitotenv.2019.02.305

Oduber, F., Castro, A., Calvo, A.I., Blanco-Alegre, C., Alonso-Blanco, E., Belmonte, P., Fraile, R., 2018. Summer-autumn air pollution in león, Spain: Changes in aerosol size distribution and expected effects on the respiratory tract. Air Qual. Atmos. Heal. 11, 505–520. doi:10.1007/s11869-018-0556-6

Paatero, P., 1997. Least squares formulation of robust non-negative factor analysis. Chemom. Intell. Lab. Syst. 37, 23–35. doi:10.1016/S0169-7439(96)00044-5

Paatero, P., Eberly, S., Brown, S.G., Norris, G.A., 2014. Methods for estimating uncertainty in factor analytic solutions. Atmos. Meas. Tech. 7, 781–797. doi:10.5194/amt-7-781-2014

Paatero, P., Tapper, U., 1994. Positive matrix factorization: A non-negative factor model with optimal utilization of error estimates of data values. Environmetrics 5, 111–126. doi:10.1002/env.3170050203

Paraskevopoulou, D., Liakakou, E., Gerasopoulos, E., Mihalopoulos, N., 2015. Sources of atmospheric aerosol from long-term measurements (5years) of chemical composition in Athens, Greece. Sci. Total Environ. 527–528, 165–178. doi:10.1016/j.scitotenv.2015.04.022

Pey, J., Querol, X., Alastuey, A., Rodríguez, S., Putaud, J.P., Van Dingenen, R., 2009. Source apportionment of urban fine and ultra-fine particle number concentration in a Western Mediterranean city. Atmos. Environ. 43, 4407–4415. doi:10.1016/j.atmosenv.2009.05.024

Pindado, O., Perez, R.M., 2011. Source apportionment of particulate organic compounds in a rural area of Spain by positive matrix factorization. Atmos. Pollut. Res. 2, 492–505. doi:10.5094/APR.2011.056

Pio, C., Cerqueira, M., Harrison, R.M., Nunes, T., Mirante, F., Alves, C., Oliveira, C., Sanchez de la Campa, A., Artiñano, B., Matos, M., 2011. OC/EC ratio observations in Europe: Re-thinking the approach for apportionment between primary and secondary organic carbon. Atmos. Environ. 45, 6121–6132. doi:10.1016/j.atmosenv.2011.08.045

Polissar, A. V., Hopke, P.K., Paatero, P., Malm, W.C., Sisler, J.F., 1998. Atmospheric aerosol over Alaska 2. Elemental composition and sources. J. Geophys. Res. Atmos. 103, 19045–19057. doi:10.1029/98JD01212

Querol, X., Alastuey, A., Rodriguez, S., Plana, F., Ruiz, C.R., Cots, N., Massagué, G., Puig, O., 2001. PM_{10} and $PM_{2.5}$ source apportionment in the Barcelona Metropolitan area, Catalonia, Spain. Atmos. Environ. 35, 6407–6419. doi:10.1016/S1352-2310(01)00361-2

Querol, X., Alastuey, A., Rosa, J. de la, Sánchez-de-la-Campa, A., Plana, F., Ruiz, C.R., 2002. Source apportionment analysis of atmospheric particulates in an industrialised urban site in southwestern Spain. Atmos. Environ. 36, 3113–3125. doi:10.1016/S1352-2310(02)00257-1

Querol, X., Alastuey, A., Viana, M.M., Rodriguez, S., Artiñano, B., Salvador, P., Garcia do Santos, S., Fernández Patier, R., Ruiz, C.R., de la Rosa, J., Sanchez de la Campa, A., Menendez, M., Gil, J.I., 2004. Speciation and origin of PM_{10} and $PM_{2.5}$ in Spain. J. Aerosol Sci. 35, 1151–1172. doi:10.1016/j.jaerosci.2004.04.002

Ren-Jian, Z., Kin-Fai, H., Zhen-Xing, S., 2012. The Role of Aerosol in Climate Change, the Environment, and Human Health. Atmos. Ocean. Sci. Lett. 5, 156–161. doi:10.1080/16742834.2012.11446983

Russo, A., Trigo, R.M., Martins, H., Mendes, M.T., 2014. NO_2, PM_{10} and O_3 urban concentrations and its association with circulation weather types in Portugal. Atmos. Environ. 89, 768–785. doi:10.1016/j.atmosenv.2014.02.010

Salvador, P., Artiñano, B., Alonso, D.G., Querol, X., Alastuey, A., 2004. Identification and characterisation of sources of PM_{10} in Madrid (Spain) by statistical methods. Atmos. Environ. 38, 435–447. doi:10.1016/j.atmosenv.2003.09.070

Santos, J.A., Corte-Real, J., Leite, S.M., 2005. Weather regimes and their connection to the winter rainfall in Portugal. Int. J. Climatol. 25, 33–50. doi:10.1002/joc.1101

Santurtún, A., González-Hidalgo, J.C., Sanchez-Lorenzo, A., Zarrabeitia, M.T., 2015. Surface ozone concentration trends and its relationship with weather types in Spain (2001–2010). Atmos. Environ. 101, 10–22. doi:10.1016/j.atmosenv.2014.11.005

Seinfeld, J.H., Pandis, S.N., 2016. Atmospheric Chemistry and Physics: From Air Pollution to Climate Change, 3rd Ed. John Wiley & Sons.

Sharma, S.K., Sharma, A., Saxena, M., Choudhary, N., Masiwal, R., Mandal, T.K., Sharma, C., 2016. Chemical characterization and source apportionment of aerosol at an urban area of Central Delhi, India. Atmos. Pollut. Res. 7, 110–121. doi:10.1016/j.apr.2015.08.002

Song, C.H., Carmichael, G.R., 1999. The aging process of naturally emitted aerosol (sea-salt and mineral aerosol) during long range transport. Atmos. Environ. 33, 2203–2218. doi:10.1016/S1352-2310(98)00301-X

Titos, G., Ealo, M., Pandolfi, M., Pérez, N., Sola, Y., Sicard, M., Comerón, A., Querol, X., Alastuey, A., 2017. Spatiotemporal evolution of a severe winter dust event in the western Mediterranean: Aerosol optical and physical properties. J. Geophys. Res. Atmos. 122, 4052–4069. doi:10.1002/2016JD026252

Titos, G., Lyamani, H., Pandolfi, M., Alastuey, A., Alados-Arboledas, L., 2014. Identification of fine (PM_1) and coarse (PM_{10-1}) sources of particulate matter in an urban environment. Atmos. Environ. 89, 593–602. doi:10.1016/j.atmosenv.2014.03.001

Trigo, R.M., DaCamara, C.C., 2000. Circulation weather types and their influence on the precipitation regime in Portugal. Int. J. Climatol. 20, 1559–1581. doi:10.1002/1097-0088(20001115)20:13<1559::AID-JOC555>3.0.CO;2-5

Viana, M., Kuhlbusch, T.A.J., Querol, X., Alastuey, A., Harrison, R.M., Hopke, P.K., Winiwarter, W., Vallius, M., Szidat, S., Prévôt, A.S.H., Hueglin, C., Bloemen, H., Wåhlin, P., Vecchi, R., Miranda, A.I., Kasper-Giebl, A., Maenhaut, W., Hitzenberger, R., 2008. Source apportionment of particulate matter in Europe: A review of methods and results. J. Aerosol Sci. 39, 827–849. doi:10.1016/j.jaerosci.2008.05.007

Vicente, A., Alves, C., Calvo, A.I., Fernandes, A.P., Nunes, T., Monteiro, C., Almeida, S.M., Pio, C., 2013. Emission factors and detailed chemical composition of smoke particles from the 2010 wildfire season. Atmos. Environ. 71, 295–303. doi:10.1016/j.atmosenv.2013.01.062

Vicente, E.D., Alves, C.A., 2018. An overview of particulate emissions from residential biomass combustion. Atmos. Res. 199, 159–185. doi:10.1016/j.atmosres.2017.08.027

Waked, A., Favez, O., Alleman, L.Y., Piot, C., Petit, J.-E., Delaunay, T., Verlinden, E., Golly, B., Besombes, J.-L., Jaffrezo, J.-L., Leoz-Garziandia, E., 2014. Source apportionment of PM_{10} in a north-western Europe regional urban background site (Lens, France) using positive matrix factorization and including primary biogenic emissions. Atmos. Chem. Phys. 14, 3325–3346. doi:10.5194/acp-14-3325-2014

Weissert, L.F., Salmond, J.A., Miskell, G., Alavi-Shoshtari, M., Williams, D.E., 2018. Development of a microscale land use regression model for predicting NO_2 concentrations at a heavy trafficked suburban area in Auckland, NZ. Sci. Total Environ. doi:10.1016/j.scitotenv.2017.11.028

Yao, X., Fang, M., Chan, C.K., 2003. The size dependence of chloride depletion in fine and coarse sea-salt particles. Atmos. Environ. 37, 743–751. doi:10.1016/S1352-2310(02)00955-X

Yubero, E., Carratalá, A., Crespo, J., Nicolás, J., Santacatalina, M., Nava, S., Lucarelli, F., Chiari, M., 2011. PM_{10} source apportionment in the surroundings of the San Vicente del Raspeig cement plant complex in southeastern Spain. Environ. Sci. Pollut. Res. 18, 64–74. doi:10.1007/s11356-010-0352-9.

5

ONE-YEAR STUDY OF AIRBORNE SUGAR COMPOUNDS: CROSS-INTERPRETATION WITH OTHER CHEMICAL SPECIES AND METEOROLOGICAL CONDITIONS

Sent to Agricultural and Forest Meteorology , April 2020

5.1. INTRODUCTION

Atmospheric bioaerosols comprise a variety of biological particles that include bacteria, fungi, fungal spores, pollen and allergenic pollens, arthropod allergens (e.g., from mites and cockroaches), pet allergens, algae, amoebae and viruses (Després et al., 2012; Douwes et al., 2008; Fröhlich-Nowoisky et al., 2016). They play an important role in human health and atmospheric processes. Pollen allergens are considered to be primarily glycoproteins that are released into the atmosphere in the form of exudates. Thus, it is the glucidic fraction that triggers the allergic responses, so an interaction of sugars with other particles, biotic or not, can clearly increase the symptoms of respiratory allergies (Dall'Antonia et al., 2014). The presence of high levels of pollen in the atmosphere has been related to allergic respiratory diseases, such as asthma, rhinitis, and atopic dermatitis (D'Amato et al., 2007; Fröhlich-Nowoisky et al., 2016; Fukutomi and Taniguchi, 2015). In particular, among fungal spores, the specie Alternaria alternata can be considered one of the most allergenic species. The main allergen produced by this fungal spore is the Alt a 1 acid glycoprotein (16.4 kDa and 15.3 kDa band), which is found in the cytoplasm and cellular wall of mold and mycelial spores. It is related to the development of asthma and rhinitis, as well as to epidemics of asthma exacerbation (Armentia et al., 2019; Fukutomi and Taniguchi, 2015), although its true biological function remains unknown.

Sugar compounds (saccharides, alcohol-saccharides and anhydrosaccharides) represent an important part of the water-soluble organic fraction in the atmospheric aerosol (Barbaro et al., 2019; Burshtein et al., 2011; Simoneit et al., 2004; Wang et al., 2018; Yttri et al., 2007). These organic compounds can have their origin in different anthropogenic and natural sources, including biomass combustion and/or biogenic primary emissions (Table A3.1 in Annex 3).

Anhydrosaccharides, levoglucosan, galactosan and mannosan, which originate from the pyrolysis of cellulose and hemicellulose, and potassium, located in the cytoplasm of plants, are used as biomass burning tracers (Vicente and Alves, 2018). Arabitol and mannitol, responsible for

the energy storage in fungi, have been pointed out as biomarkers of fungal spores in the air (Bauer et al., 2008; Burshtein et al., 2011; Medeiros et al., 2006). Nevertheless, high concentrations of alcohol-saccharides have also been observed in plant tissues. Mannitol is found in more than 70 different families of plants, as well as bacteria. Similarly, sorbitol is the primary photosynthetic metabolite of sucrose in many species, for example of the Rosaceae family, including all of the genus Malus, Pyrus and Prunus (apples, pears and stone fruits, respectively) (Dumschott et al., 2017). Sucrose, fructose and glucose are free sugars found in high concentrations in plant tissues and are major contributors to pollen (Fu et al., 2012; Medeiros et al., 2006; Simoneit et al., 2004; Speranza et al., 1997). Besides, a small fraction of fructose, glucose and other less studied saccharides, such as arabinose, galactose, xylose, xylitol and ribose, has been observed in smoke samples from biomass burning (Alves et al., 2011; Medeiros et al., 2006; Vicente et al., 2013).

The atmospheric concentrations of bioaerosols are also affected by meteorological conditions. Temperature, wind speed, relative humidity and precipitation are parameters that influence the airborne concentration of fungal spores, plants flowering and pollination periods (Fernández-González et al., 1993; Filali Ben Sidel et al., 2015; Grinn-Gofroń et al., 2019; Makra et al., 2014; Oduber et al., 2019a; Sabo et al., 2015). Although the impact of precipitation on different sugar compounds have not been examined in detail until now, to better understand atmospheric processes, it may be important to assess the behaviour of these constituents after a rain event. For example, the below-cloud scavenging (BCS) process has a direct impact on the aerosol concentration in the air. This process depends on several features of rainfall, such as raindrop size distribution and rainfall rate, and on the local/regional concentration of the particles and gases in the atmosphere (Celle-Jeanton et al., 2009; Xu et al., 2017). The scavenging of different species, mainly inorganic, and the relationship with the intensity and volume of precipitation, has been studied by several authors in different regions of the world (i.e. Blanco-Alegre et al., 2019; Calvo et al., 2012; Custódio et al., 2014; Pan and Wang, 2015; Uchiyama et al., 2017). Even though a washing effect by rain has been observed for several aerosols, certain particles as pollen can swell and rupture producing hundreds of fine-size particles (D'Amato et al., 2007), increasing the concentration of sugar compounds in the atmosphere.

It is important to know under what meteorological conditions sugar compounds are emitted and what chemical and biological markers are well correlated with them. This will allow to determine the natural and/or anthropogenic origin of these compounds. This type of studies is only possible if a long-term study is carried out, taking into account the meteorological parameters, chemical composition and biogenic contribution of atmospheric particles. Thus, this study aims to: *i*) evaluate, between March 2016 and March 2017 in León (Spain), the daily and seasonal evolution of seventeen sugar compounds in the PM_{10} fraction: arabinose, fructose, galactose, glucose, ribose, sucrose, xylose, adonitol, arabitol, 2-methyleryritol, myoinositol, mannitol, sorbitol, xylitol, galactosan, levoglucosan and mannosan; *ii*) establish the correlation with meteorological parameters, with some biological markers (pollen and fungal spore concentrations) and with chemical markers (K, As, Se, SO_4^{2-}, NO_3^-, Pb, Zn, etc.); *iii*) finally, estimate the impact of precipitation on the concentration of sugar compounds.

To our knowledge, only a few studies have evaluated the temporal evolution of the main sugar compounds in particulate matter and much less have related their concentrations in the

environment to meteorological conditions, mainly under rain weather, to some biological tracers and to other chemical species.

5.2. EXPERIMENTAL

5.2.1. Sampling

5.2.1.1. Site

The city of León is located in the northwest of the Iberian Peninsula (42º 36′ N, 05º 35′ W and 838 m a.s.l.) and is characterised by a continental type climate with influence of the Mediterranean. Winters are cold and long, with average temperatures of 5 ± 3 ºC, while summers are warm with average temperatures of 20 ± 4 ºC. Spring is the season with the highest amount of rain, while summer is usually a dry season with frequent storms (Castro et al., 2010; Fernández-Raga et al., 2017).

The sampling campaign was carried out in a suburban area located in the northeast of León city, Spain (Fig. A3.1 in Annex 3). The sampling site is characterised by the absence of large emitting industries and a high contribution of biomass burning and fossil fuel emissions, due to the high traffic flow in the vicinity of the sampling area and the use of domestic heating devices in the city centre and in nearby towns (Blanco-Alegre et al., 2019; Oduber et al., 2018). In addition, León is greatly affected by primary biological emissions from the surroundings. Furthermore, numerous forests with many types of vegetation, whose pollination contributes to a high concentration of pollen, are about 30 km north from the city (Calvo et al., 2018; Oduber et al., 2019a). Approximately 30 km south of the city, extensive agricultural areas are located, which can represent a significant source of fungi due to rotting fruits or when crops are harvested.

5.2.1.2. PM_{10}

PM_{10} samples were collected every 24 hours, beginning at 1200 UTC every day between 9 March 2016 and 14 March 2017 by using a low volume sampler (TECORA, ECHOPM), equipped with 47 mm diameter Teflon filters and a high-volume sampler (CAV-Mb), equipped with 150 mm diameter quartz filters.

Quartz filters were used for the determination of the PM_{10} mass by the gravimetric method, weighing the filters in an electronic semi-micro balance (Mettler Toledo, XPE105DR). A total of 325 samples of each, Teflon and quartz filters, were collected throughout the sampling campaign. The time period for each season was considered as follows: winter from 21 December to 20 March, spring from 21 March to 20 June, summer from 21 June to 20 October and autumn from 21 October to 20 December.

5.2.1.3. Bioaerosols and allergenic fraction

Atmospheric bioaerosol sampling was performed continuously by using a Hirst volumetric trap (Hirst, 1952), placed in the same sampling location. The daily analysis of the samples was carried out according to the Standard 2018 CEN Ref. No.FprEN 16868:2018E.

The atmospheric aerosol for the quantification of the allergenic fraction was sampled with a low-volume sampler Burkard Multi-Vial Cyclone (Burkard Manufacturing Co. Ltd.). Atmospheric particles were collected dry directly into a 1.5 mL Eppendorf vial every 24 h and stored at -20 ºC. The quantification of the aeroallergen Alt a 1 was carried out following the method described by Fernández-González et al. (2019, 2010).

5.2.1.4. Rainfall parameters

Rain variables were measured by a laser disdrometer (Laser Precipitation Monitor, LPM) of *Thies Clima*, which registered raindrops between 0.125 and 8 mm in 22 drop size ranges, on a 1-minute basis (Fernández-Raga et al., 2009). From the data provided by the LPM, the following rainfall variables were obtained: precipitation intensity, accumulated precipitation, number of drops, volume swept by falling drops, mean and standard deviation of raindrop sizes.

5.2.2. Analytical techniques

5.2.2.1. Particulate sugar compounds

A portion of each quartz filter, with an area of about 14.14 cm^2, was used for the determination of 17 sugar compounds: 7 saccharides (arabinose, fructose, galactose, glucose, ribose, sucrose and xylose), 7 alcohol-saccharides (adonitol, arabitol, 2- methylerythritol, myo-inositol, mannitol, sorbitol and xylitol) and 3 anhydrosaccharides (galactosan, levoglucosan and mannosan).

Sugar compounds were extracted with 3 mL of ultra-pure Milli-Q water with ultrasonic agitation. The extracts were filtered with a 0.2 µm pore PTFE syringe filter and transferred to glass vials for injection into the chromatograph on the same day. The analysis of the 17 sugar compounds was carried out by means of a Thermo Scientific DionexTM ICS-5000 ion chromatograph equipped with a CarboPac® PA-1 (2 × 250 mm) anion-exchange analytical column. The methodology is based on Caseiro et al. (2007) and Piazzalunga et al. (2010), using multi-step gradient conditions with ultra-pure Milli-Q water and two solutions of NaOH (200 mM and 5 mM). The methodology allowed a good separation of sixteen of the seventeen sugars analysed. The alcohol-sugars, sorbitol and adonitol co-eluted in the same retention time, so the results obtained for these two compounds are shown as a sum of both as SA.

5.2.2.2. Organic and elemental carbon analysis

Two quartz filter punches, 9 mm in diameter each, were used to determine organic carbon (OC) and elemental carbon (EC) by using the thermal-optical system developed by the University of Aveiro (Portugal), following the methodology described by Alves et al. (2015) and Pio et al. (2011).

5.2.2.3. Water-soluble ions

Half of each Teflon filter was used to extract water-soluble ions with 6 mL ultra-pure Milli-Q water with ultrasonic agitation. The extracts were filtered with a 0.2 µm pore size PTFE syringe

filter and stored in glass vials in the refrigerator until analysis. The determination of water-soluble ions was carried out by means of a Thermo Scientific DionexTM ICS-5000 ion chromatograph. Cations (Na^+, K^+, NH_4^+, Mg^{2+} and Ca^{2+}) were separated with an IonPac® CS16 (4 × 250 mm) column and using a solution of 30 mM of methanesulphonic (MSA) as mobile phase. Anions (Cl^-, NO_3^- and SO_4^{2-}) were separated with an IonPac® AS11 (4 × 250 mm) column and with a solution of 30 mM of potassium hydroxide (KOH) as mobile phase.

5.2.2.4. Trace elements

The other half of the Teflon filters was used for the determination of major trace elements (Na, Mg, Al, Si, P, S, Cl, K, Ca, Ti, V, Cr, Mn, Fe, Ni, Cu, Zn, As, Se, Br, Rb, Sr, Pb), using the PIXE technique (Particle-Induced X-ray Emission) described by Lucarelli et al. (2015).

5.2.3. Scavenging coefficients

The scavenging coefficient was evaluated through the following equation:

$$\Delta C = \frac{C_2 - C_1}{C_1} \times 100 \qquad \text{Equation 5.1}$$

where C_2 and C_1 are the concentration of the studied sugar compound after and before the precipitation event, respectively. Sugar compound concentrations before and after the precipitation event were obtained as a mean value, calculated from the concentrations registered 2 days before and 2 days after the event, respectively. Consequently, a negative ΔC indicates effective scavenging.

5.2.4. Additional data

Weather information (temperature, precipitation and relative humidity) was recorded in the sampling location with an automatic meteorological station. Additional weather information (insolation and wind) was obtained from the database of the National Agency for Meteorology (www.aemet.es). For the statistical treatment, SPSS software (IBM Statistics Software V. 24) was used. The Kruskal-Wallis non-parametric test (Kruskal and Wallis, 1952) followed by Dunn test (Dunn, 1964) was applied in order to determine the eventual statistically significant differences ($p < 0.05$).

5.3. RESULTS AND DISCUSSION

5.3.1. Annual evolution of sugar compounds in PM_{10}

During the sampling campaign, the total sugar concentrations in PM_{10} ranged between 1.3 and 1052 ng m^{-3}, with an annual mean of 64 ± 108 ng m^{-3} (Table A3.2 in Annex 3), which represents 0.3% of PM_{10}. Spring was the season with the highest daily and mean total sugar concentrations (1052 and 122 ± 193 ng m^{-3}, respectively), with statistically significant differences with the rest of the seasons. In contrast, winter was the season with the lowest total sugar concentration (41 ± 47 ng m^{-3}). Theodosi et al. (2018) reported similar annual values, in a rural site in Greece, with a total

mean concentration of 57.7 ng m^{-3}. Shahid et al. (2019) showed a total mean concentration of 2100 ng m^{-3}, in a study carried out in an urban site of Pakistan in December. Emygdio et al. (2018) reported a total mean sugar concentration of 363.2 ng m^{-3}, in Brazil, between autumn and winter. Moreover, Liu et al. (2016) documented a total sugar concentration of 792 ng m^{-3} in Beijing, China, between 2010 and 2011. The differences are probably due to the quantification of compounds not entirely coincident, the variety of sources, the period of sampling, the weather conditions and the impact of long-range and local events that may affect sugar levels at each location. Besides, in temperate regions, early spring is the period of greatest plant activity, when most species restart vegetative growth and flowering occurs. All this implies important movements of cellulose during plant development. In León, high levels of sugar compounds in the atmosphere, caused by anthropogenic and biogenic emissions, is common throughout the year. Between autumn and winter, biomass burning emissions are frequent due to the use of domestic heating devices (Blanco-Alegre et al., 2019). In spring and summer, pollen and airborne spores are present because of the flowering and pollination of the large mass of plants and sporulation of fungi surrounding the city (Calvo et al., 2018; Fernández-González et al., 1993; Oduber et al., 2019a).

The monthly evolution of the sugar compounds shows higher concentrations of arabinose, fructose, glucose, ribose, sucrose, xylose, arabitol, 2-methylerythritol and myo-inositol between May and July (Fig. 5.1). All these saccharides, except ribose and xylose, are significantly correlated ($r > 0.6$), indicating a common origin. These saccharides can be abundantly emitted as primary biogenic aerosol particles (fungal spores, pollen, bacteria, and plant fragments) (Medeiros et al., 2006; Rathnayake et al., 2017; Theodosi et al., 2018). Therefore, the higher concentrations of these saccharides between May and July could be linked to the main pollen season in León (Fernández-González et al., 1993; Oduber et al., 2019a) and to the continuous lawn mowing around the sampling point, which implies the breakage of the vegetal tissues of numerous herbaceous plants, with the release of sugars to the atmosphere.

Between October and February, galactose, mannitol, SA, galactosan, levoglucosan and mannosan, showed the highest concentrations, while arabitol and xylitol also exhibited an important contribution during these months. Levoglucosan, mannosan and galactosan (significantly correlated, $r > 0.5$) are usually related to biomass burning emissions (Vicente and Alves, 2018), which are frequent between autumn and early spring, due to wood burning for domestic heating purposes in León. Moreover, during summer, the Iberian Peninsula is often affected by forest fires. Thus, emissions from wildfires may contribute to the enhancement of anhydrosugar levels in the atmosphere during this season.

Higher concentrations of fructose, sucrose and glucose during summer, and higher concentrations of anhydrosugars during winter, were also reported by Wang et al. (2018) in an urban station of Xi'an, China. The same behaviour was observed by Yttri et al. (2007) in a suburban station of Norway, showing concentrations of sucrose, levoglucosan, mannosan and galactosan in winter of 5.3, 605, 167 and 4 ng m^{-3}, respectively, and 20, 47, 10 and 3 ng m^{-3}, respectively, in summer. Both studies found that the increase in the anhydrosugar concentrations during cold seasons can be due to an increase in the use of domestic heating devices, together with the stagnation caused by the low boundary layer.

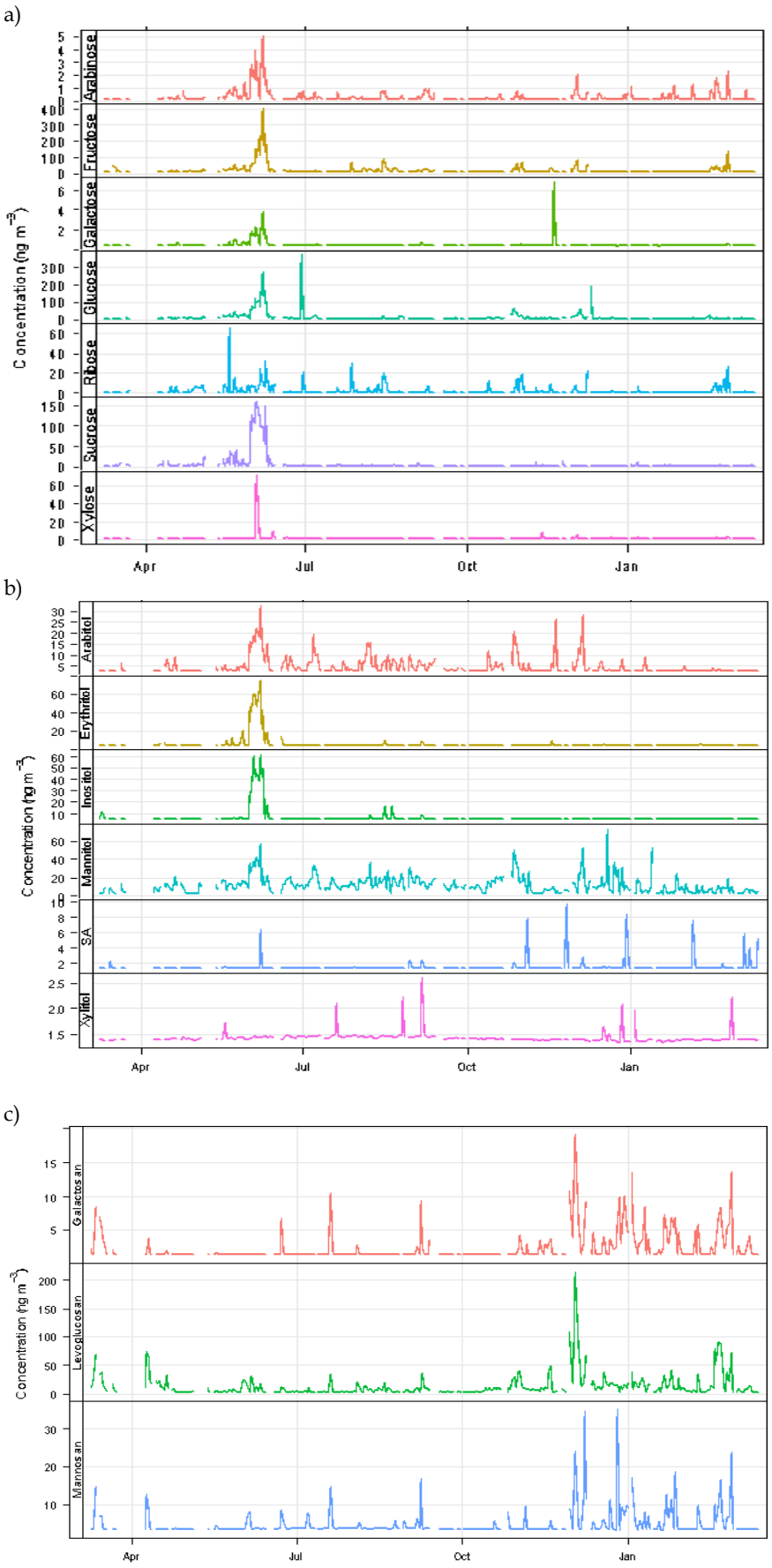

FIG. 5.1. Evolution of daily concentrations of: a) saccharides, b) alcohol-saccharides, c) anhydrosaccharides.

5.3.2. Sugar compounds vs meteorological parameters

The anhydrosaccharides displayed a negative significant correlation with T_{Min} in spring (levoglucosan and mannosan) and with T_{Max} in autumn (galactosan). Due to the low temperatures and high relative humidity between late-autumn and early-spring in León (Table 5.1), the use of heating devices is very common, causing increased levels of anhydrosugars due to emissions from biomass-based domestic heating devices.

Wind speed affected air sugar concentrations particularly in spring, when winds are at their strongest in León (Table 5.1). In this season, arabinose, glucose, sucrose, arabitol, 2-metylerythritol and mannitol are negatively correlated with wind speed ($0.3 < r < 0.6$, Table 5.2). However, during summer, the concentration of sucrose and mannitol increase with increasing wind speed. This fact could be related with the location of the source. Airborne particles emitted far from the sampling location need high wind speeds to reach the monitoring site, so aerosol concentrations increase with wind speed. Nevertheless, a decrease in concentrations with increasing wind speed suggests sources close to the sampling site, with the greatest impact in stagnant atmospheric conditions (Carslaw et al., 2006; Yu et al., 2004).

TABLE 5.1. Seasonal mean values for insolation, wind speed (ws), temperature (T), minimum temperature (T_{Min}), maximum temperature (T_{Max}), relative humidity (RH), total accumulated precipitation and rain days in León (Spain) during the sampling period.

	Winter	**Spring**	**Summer**	**Autumn**
Insolation (h day^{-1})	6 ± 4	9 ± 4	13 ± 2	6 ± 4
ws (m s^{-1})	0.9 ± 0.7	1.1 ± 0.8	0.6 ± 0.3	0.6 ± 0.4
T (°C)	5 ± 3	11 ± 5	21 ± 3	10 ± 4
T_{Min} (°C)	0 ± 3	5 ± 4	12 ± 3	4 ± 4
T_{Max} (°C)	12 ± 4	17 ± 5	30 ± 3	16 ± 6
RH (%)	70 ± 12	63 ± 11	48 ± 8	71 ± 11
Precipitation (mm)	131.5	155.1	15.3	69.4
Rain days	31	24	6	23

Insolation showed a significant correlation with glucose ($r = 0.1$, Table 5.2). However, when evaluated by season, it is observed that this correlation increases up to 0.3, also showing a correlation with arabinose ($r = 0.4$) and arabitol ($r = 0.5$) in spring. Glucose, sucrose, 2-metylerythritol and mannitol revealed a significant positive correlation with mean temperatures (T), with r between 0.1 and 0.5. The same behaviour was observed for these sugar compounds and minimum and maximum temperatures (T_{Min}, T_{Max}, respectively). In spring, arabinose, fructose, galactose, glucose, sucrose, arabitol, 2-metylethritol, inositol and mannitol are positively correlated with T and T_{Max}. Fernández-González et al. (1993) observed that the airborne pollen concentration in León is greatly affected by temperatures and reported that pollen concentrations have maximum values with temperatures between 20 and 25 ^{o}C, which are usual between spring and summer in León. Furthermore, Calvo et al. (2018) and Fernández-González et al. (1993) also reported that in León the maximum pollen concentration is reached between late-spring and early-summer, due to the high concentration of several pollen types (Quercus, Pinus, Salix, Plantago, Ericaceae, Leguminosae, Urticaceae and Poaceae).

TABLE 5.2. Pearson correlations between sugar compounds and meteorological parameters: insolation, wind speed (ws), temperature (T), minimum (T_{Min}) and maximum (T_{Max}) temperature, relative humidity (RH) and precipitation.

	Arabinose	Fructose	Galactose	Glucose	Ribose	Sucrose	Xylose	Arabitol	Erythritol	Inositol	Mannitol	SA	Xylitol	Galactosan	Levoglucosan	Mannosan
Annual																
Insolation	0.16	0.06	-0.22	**0.12***	0.13	0.16	0.21	0.03	0.34	0.00	0.03	-0.35	0.42	-0.10	-0.11	-0.16
ws	-0.06	-0.15	0.20	-0.05	0.06	-0.12	0.06	-0.10	**-0.47***	-0.37	**-0.21****	0.36	**0.88***	-0.05	-0.10	0.06
T	0.05	0.10	-0.03	**0.14***	0.11	**0.24***	0.41	0.09	**0.48***	0.44	**0.18****	-0.30	0.43	0.01	**-0.21****	-0.14
T_{Min}	-0.02	0.09	0.09	**0.13***	0.08	**0.20***	0.40	0.10	0.32	0.39	**0.21****	-0.18	0.34	0.05	**-0.19****	-0.08
T_{Max}	0.07	0.09	-0.11	**0.12***	0.11	**0.23***	0.38	0.07	**0.51***	0.40	**0.15***	-0.45	0.47	-0.03	**-0.20****	-0.19
HR	-0.08	0.01	0.31	-0.05	-0.13	-0.16	-0.15	0.00	-0.28	0.15	-0.02	0.18	-0.48	0.05	**0.14***	**0.41****
Spring																
Insolation	**0.37***	0.24	0.42	**0.29***	0.18	0.22		**0.45***	0.26	0.08	0.21			0.53	0.01	0.07
ws	**-0.39***	-0.28	-0.34	**-0.26***	-0.04	**-0.37****		**-0.56****	**-0.60***	-0.47	**-0.33***			-0.40	0.11	0.20
T	**0.50****	**0.51****	**0.52***	**0.61****	0.36	**0.58****		**0.58****	**0.49***	**0.75****	**0.55****			**-0.72***	**-0.30***	-0.29
T_{Min}	0.29	**0.39****	0.23	**0.47****	0.30	**0.44****		0.31	0.30	**0.68****	**0.43****			-0.67	**-0.32***	-0.23
T_{Max}	**0.53****	**0.53****	**0.57***	**0.60****	0.31	**0.60****		**0.63****	**0.55***	**0.76****	**0.56****			-0.01	-0.24	-0.28
HR	**-0.39***	-0.19	-0.31	**-0.27***	-0.15	**-0.30***		**-0.48***	-0.25	-0.07	-0.20			-0.43	0.00	0.27
Summer																
Insolation	-0.18	-0.20		0.04	-0.13	-0.12		-0.07		-0.58	**-0.26***			0.132	0.034	-0.218
ws	0.36	-0.07		0.12	-0.10	**0.64****		0.07		0.22	**0.25***			0.236	-0.149	0.303
T	-0.42	0.07		-0.03	0.08	0.01		0.17		-0.52	**0.24***			0.481	-0.241	-0.405
T_{Min}	-0.26	0.08		0.01	0.05	0.09		0.24		0.01	**0.38****			0.661	-0.102	-0.061
T_{Max}	-0.43	0.03		-0.06	0.07	-0.07		0.11		-0.52	0.10			0.209	-0.189	-0.591
HR	0.26	-0.15		0.04	-0.07	0.01		0.07		0.75	0.11			-0.215	0.175	0.173
Autumn																
Insolation	0.20	0.49		0.07	0.23	0.12	0.90	-0.16			-0.11	-0.61		-0.27	-0.13	0.10
ws	0.53	-0.10		-0.19	0.03	0.30	-0.79	0.09			**-0.28***	0.82		-0.13	-0.06	0.01
T	-0.21	-0.02		-0.07	-0.26	**-0.56***	-0.23	-0.01			0.14	-0.75		-0.17	-0.16	-0.35
T_{Min}	-0.25	0.02		-0.09	-0.26	**-0.55***	-0.36	0.10			**0.29***	-0.87		0.14	-0.05	-0.29
T_{Max}	-0.23	0.15		0.02	-0.04	-0.48	0.92	-0.07			0.07	-0.69		**-0.44***	-0.22	-0.24
HR	-0.07	-0.09		0.10	-0.23	0.14	0.35	0.28			0.17	0.24		0.24	0.11	0.32
Winter																
Insolation	-0.16	-0.52		0.05	-0.33	0.19	-0.65	0.05			-0.03	-0.44	0.33	-0.15	0.102	-0.19
ws	0.50	**0.81***		-0.16	**0.74***	-0.15	0.59	0.19			-0.25	0.53	0.88	0.11	**-0.34****	0.08
T	0.30	-0.51		**0.38****	-0.06	-0.15	-0.52	**-0.90***			-0.21	-0.45	0.76	-0.07	-0.05	0.01
T_{Min}	0.30	-0.45		**0.30****	-0.20	-0.23	-0.28	-0.69			-0.19	-0.25	-0.12	-0.11	-0.18	0.13
T_{Max}	0.11	-0.43		**0.25***	-0.22	0.27	-0.56	-0.53			-0.14	-0.63	0.60	-0.02	0.10	-0.12
HR	0.26	0.44		0.11	0.12	-0.05	0.29	-0.18			0.04	0.10	-0.41	0.05	-0.04	**0.48****

*$p < 0.05$, **$p < 0.01$

5.3.3. Sugar compounds vs precipitation

In order to evaluate the effect of precipitation on the concentrations of sugar compounds, a total of 41 precipitation events were studied during the sampling campaign. Table 5.3 shows the main characteristics of these events.

TABLE 5.3. Mean monthly intensity, accumulated precipitation and duration of precipitation events in León during the sampling period.

Month	Number of events	Intensity (mm h^{-1})	Precipitation (mm)	Duration (h)
January	5	0.4 ± 0.2	21	12 ± 8
February	6	1.1 ± 0.4	97	14 ± 2
March	1	0.2	1	5
April	11	0.7 ± 0.4	93	9 ± 6
May	4	1.1 ± 0.4	38	10 ± 6
June				
July				
August	3	2 ± 2	6	5 ± 4
September				
October	3	0.61 ± 0.07	15	10 ± 2
November	3	0.5 ± 0.3	10	9 ± 5
December	5	0.5 ± 0.3	20	9 ± 5

Although for some of the sugar compounds, a decrease in the concentration after a precipitation event is observed (Fig. 5.2), there are some cases (glucose, mannosan, fructose, sucrose, ribose, SA, mannitol and arabitol) in which an increase is registered. As D'Amato et al., (2007) pointed out that, during periods of rain, pollen particles can swell and break, producing hundreds of fine-size particles, and increasing the population of the airborne modes, which may persist in the atmosphere for weeks after precipitation (Bigg et al., 2015; Morris et al., 2017). This can be due to the hydration of the pollen grains and to the release of glycidic molecules (associated or not with proteins) from the cytoplasm or to the rupture of some pollen spores and / or bacteria walls, if there are very strong pressure changes (Fernández-González et al., 2010).

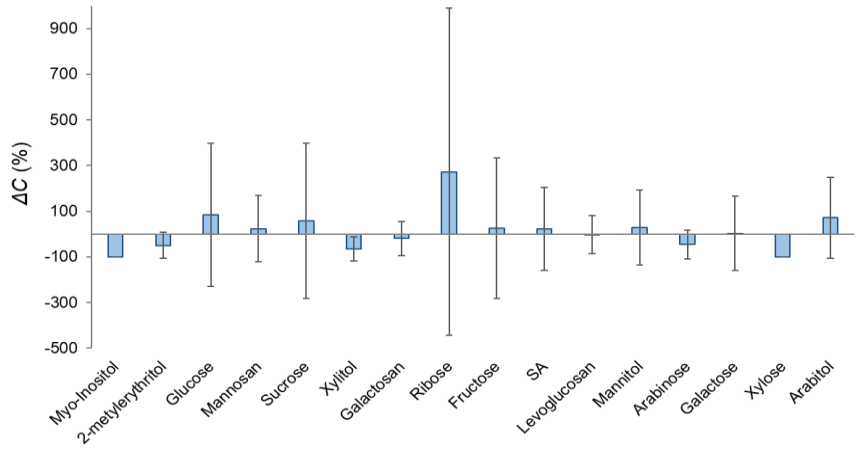

FIG. 5.2. Mean scavenging coefficients (boxes) and standard deviations (whiskers) for each sugar compound during the sampling campaign in León.

Arabitol, SA and mannitol also showed a substantial increase in their concentrations after a rain event. These saccharides are used as tracers for airborne fungal spores, and rain could trigger mechanisms of passive and/or active release and/or promote the growth of fungi, germination and growth of hyphae (Schulthess and Faeth, 1998). Wet conditions that follow rainfall events are favourable for the active release of fungal spores, causing an increase in their concentrations in the air (Rodríguez-Rajo et al., 2005; Van Osdol et al., 2004).

Significant positive correlations between ΔC of glucose and several rain parameters (mean intensity, swept volume and drop mean size) were observed (Table 5.4). Furthermore, raindrops larger than 3 mm correlated significantly with ΔC for this sugar, while for smaller raindrops, the correlation shows a (non-significant) washing effect. A similar pattern is observed for fructose for raindrops larger than 4 mm. Mannosan concentration raises significantly after rain with increasing mean rain intensities, accumulated precipitations and drop mean sizes. For larger raindrop sizes, a positive correlation with ΔC is also registered. These results could support the existence of a threshold raindrop size above which the release of sugar compounds prevails over the scavenging process.

5.3.4. Sugar compounds vs biomarkers

The total pollen concentration was positively correlated with arabinose, fructose, glucose, ribose, sucrose, arabitol and myo-inositol ($r > 0.2$, Table 5.5). Graham et al. (2003) also reported higher glucose, fructose and sucrose concentrations coinciding with higher pollen, fern spores and insect counts, in Amazonia in 2001. Medeiros et al. (2006) observed that, in Howland Forest, United States, glucose was the most abundant monosaccharide during the growing season, while galactose and arabinose increased between spring and mid-summer, as observed in this study (Fig. 5.1), reflecting the synthesis of primary sugars at the beginning of the plant growing season. The Pearson correlation of total pollen concentration with fructose, glucose and sucrose increases in spring ($r > 0.4$), coinciding with the main pollen season (Fig. 5.3).

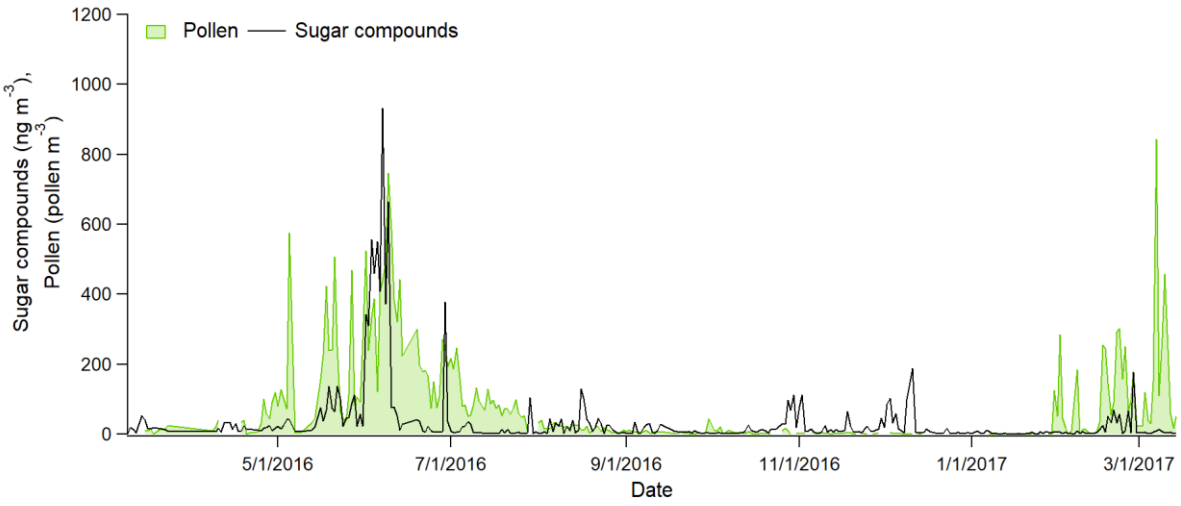

FIG. 5.3. Daily evolution of the total pollen concentration and sum of concentrations of sugar compounds: myo-inositol, 2-methylerythritol, arabitol, arabinose, fructose, galactose, glucose, mannitol, ribose, and sucrose, in León during the sampling campaign.

Table 5.4. Pearson correlations between ΔC of each sugar compound and physical characteristics of precipitation: intensity, accumulated precipitation, number of raindrops, volume swept by the raindrops and raindrop size.

	Methylerythritol	**Xylitol**	**Arabitol**	**Levoglucosan**	**SA**	**Mannitol**	**Mannosan**	**Galactosan**	**Arabinose**	**Galactose**	**Glucose**	**Fructose**	**Ribose**	**Sucrose**
Intensity (mm h^{-1})	-0.46	-0.60	0.04	-0.05	0.18	0.03	**0.43****	0.13	0.11	-0.33	**0.71****	0.18	0.38	0.21
Precipitation (mm)	-0.40	-0.36	-0.18	0.05	-0.04	-0.07	**0.31***	0.29	0.39	-0.30	-0.16	-0.18	-0.19	**0.42***
Number of raindrops min^{-1}	-0.12	-0.24	0.21	0.21	0.25	**0.40***	-0.15	0.09	0.22	-0.33	-0.07	-0.18	-0.17	0.28
Total volume swept (mm^3 m^{-3})	-0.75	**-0.72***	0.06	0.19	0.20	0.16	0.25	0.12	0.14	-0.40	**0.45****	0.05	-0.01	0.36
Mean raindrop size (mm)	-0.82	-0.27	-0.02	-0.27	-0.02	-0.16	**0.39***	-0.11	**-0.53***	0.13	**0.58****	0.17	0.38	-0.13
Raindrop size (mm)														
0.125	0.34	0.24	0.19	0.20	0.29	**0.41***	-0.16	0.09	0.30	-0.22	-0.04	-0.15	-0.24	0.21
0.25	0.18	-0.17	0.29	0.19	0.28	**0.47****	-0.18	0.10	0.18	-0.26	-0.02	-0.12	-0.20	0.22
0.375	-0.55	-0.35	0.27	0.19	0.23	**0.45****	-0.14	0.04	0.05	-0.28	-0.06	-0.18	-0.04	0.27
0.5	-0.83	-0.52	-0.05	0.10	0.02	0.14	0.10	-0.02	-0.12	-0.22	-0.23	-0.33	0.20	0.33
0.75	**-0.93***	-0.40	-0.24	0.01	-0.12	-0.12	0.19	0.03	-0.17	-0.21	-0.26	-0.30	0.29	0.30
1	**-0.97****	-0.38	-0.28	0.01	-0.15	-0.16	0.16	0.11	-0.11	-0.21	-0.25	-0.26	0.14	0.34
1.25	-0.87	-0.37	-0.32	0.02	-0.12	-0.20	0.17	0.18	0.01	-0.17	-0.25	-0.22	0.04	0.33
1.5	-0.70	-0.30	**-0.35***	0.03	-0.06	-0.23	0.17	0.22	0.16	-0.19	-0.24	-0.21	0.02	0.31
1.75	-0.54	-0.17	**-0.35***	0.04	-0.02	-0.25	0.19	0.24	0.29	-0.22	-0.23	-0.18	0.03	0.28
2	-0.38	-0.03	-0.31	0.06	0.01	-0.24	0.21	0.28	0.36	-0.21	-0.15	-0.15	0.07	0.27
2.5	-0.20	0.12	-0.24	0.10	0.03	-0.22	0.23	0.25	0.48	-0.24	0.10	0.07	0.16	0.19
3	-0.17	0.11	-0.11	0.18	0.07	-0.15	0.25	0.24	**0.55***	-0.26	**0.37***	0.31	0.13	0.09
3.5	-0.01	0.17	-0.04	0.21	0.08	-0.09	0.26	0.20	0.46	-0.25	**0.49****	0.34	0.02	0.01
4	0.12	0.11	0.02	0.22	0.07	-0.05	0.26	0.15	0.43	-0.29	**0.54****	**0.42***		
4.5	0.04	0.01	0.10	0.24	0.08	0.01	0.29	0.09	0.31	-0.27	**0.69****	**0.51****	-0.19	-0.01
5	-0.26	-0.07	0.11	0.24	0.09	0.03	0.31	0.07	0.27	-0.25	**0.69****	**0.50****	-0.03	-0.02
5.5		-0.04	0.10	0.24	0.08	0.02	0.31	0.10	0.30	-0.25	**0.64****	**0.47***	-0.17	-0.01
6	0.52	-0.09	0.15	0.24	0.11	0.06	**0.33***	0.07	0.27	-0.20	**0.74****	**0.50****	-0.15	-0.01
6.5		-0.02	0.07	0.22	0.10	0.01	0.31	0.13	0.30	-0.21	**0.56****	**0.38***	-0.25	-0.01
7		-0.07	0.14	0.24	0.10	0.05	**0.33***	0.08	0.27	-0.21	**0.73****	**0.48****	-0.19	-0.01
7.5		0.05	0.06	0.22	0.08		0.30	0.14	0.31	-0.19	**0.53****	**0.39***	-0.19	-0.01

* $p < 0.05$, ** $p < 0.01$

Table 5.5. Pearson correlations between sugar compounds and organic (OC) and elemental (EC) carbon, inorganic ions, trace elements, pollen, allergen (Alt a1) and *Alternaria* concentrations.

	Arabinose	Fructose	Galactose	Glucose	Ribose	Sucrose	Xylose	Arabitol	Erythritol	Inositol	Mannitol	SA	Xylitol	Galactosan	Levoglucosan	Mannosan
Annual																
NH_4^+	**0.25***	**0.20***	0.19	0.11	-0.02	0.04	-0.14	0.15	0.33	0.47	**0.26****	-0.12	-0.80	0.16	**0.19****	**0.55****
SO_4^{2-}	**0.26***	**0.23***	0.14	**0.14***	0.01	0.18	0.00	0.07	0.29	0.33	**0.28****	-0.05	-0.84	0.04	-0.07	**0.44****
NO_3^-	0.13	0.01	-0.15	-0.01	-0.06	-0.14	-0.27	-0.03	-0.11	-0.34	0.11	-0.13	-0.69	**0.33****	**0.32****	**0.43****
Na	-0.03	-0.17	0.28	**-0.12***	-0.07	-0.17	-0.36	-0.11	**-0.52***	**-0.65****	**-0.16****	0.17	-0.53	0.03	0.00	-0.22
Al	-0.07	-0.05	-0.22	-0.03	0.02	0.02	0.00	-0.01	0.07	0.03	0.07	0.09	0.61	-0.03	-0.10	0.00
Si	-0.07	-0.06	-0.20	0.00	-0.04	0.01	0.01	0.00	0.06	0.05	0.09	-0.03	0.67	-0.07	-0.10	-0.03
P	-0.01	0.07	-0.10	**0.15****	-0.01	0.06	0.02	0.16	**0.60****	**0.62****	**0.40****	-0.10	0.04	0.12	-0.01	0.09
Cl	-0.02	-0.10	0.40	**-0.12***	-0.12	**-0.19***	-0.39	-0.06	**-0.47***	**-0.59****	**-0.17****	0.17	-0.73	0.11	0.10	0.02
K	0.02	0.01	-0.16	-0.04	0.02	-0.09	-0.32	-0.01	-0.09	0.10	0.05	0.10	-0.17	**0.29****	0.12	**0.38****
V	-0.04	0.05	-0.35	0.07	0.10	-0.16	-0.46	-0.09	-0.33	-0.39	-0.02	-0.03	-0.23	0.22	**0.23***	**0.30***
Ni	**0.44***	0.16	0.45	0.01	0.24	-0.02	0.22	0.16	0.31	-0.42	-0.06	0.77	-0.42	0.27	0.02	**0.51****
Cu	0.02	-0.01	-0.31	-0.02	0.04	-0.08	-0.35	-0.05	0.01	0.21	0.08	-0.01	-0.63	0.21	**0.23****	0.08
Zn	0.14	0.18	-0.16	0.01	0.03	0.11	-0.24	0.07	0.18	**0.52***	**0.13***	0.30	-0.62	**0.35****	0.08	**0.54****
As	0.27	0.19	-0.29	-0.09	0.15	-0.23	**0.92****	0.07	-0.78		-0.04	-0.36	-0.67	0.24	0.06	**0.41***
Se	-0.11	-0.07	**0.50***	-0.05	-0.08	-0.18	-0.37	0.01	-0.20	0.02	-0.07	-0.08	-0.55	0.06	0.10	**0.58****
Pb	0.03	0.06	0.24	0.00	0.03	-0.02	-0.43	0.04	0.28	0.17	0.05	0.19	-0.96	0.22	**0.18***	0.21
OC	**0.38****	**0.52****	-0.11	**0.20****	**0.32****	**0.28****	-0.34	**0.24***	**0.47***	**0.72****	**0.23****	0.17	-0.60	**0.53****	**0.24****	**0.46****
EC	**0.26***	**0.32****	-0.03	0.09	0.15	0.11	-0.37	0.10	**0.57****	**0.69****	0.07	0.11	-0.62	**0.29****	**0.18****	0.21
Pollen	**0.40****	**0.41****	0.04	**0.36****	**0.34****	**0.59****	0.52	**0.23***	0.31	**0.55***	0.11	0.17	0.57	0.00	-0.02	0.05
Alt a1	0.03	0.09	0.55	-0.12	-0.05	0.00	**0.99***	-0.03	0.29	-0.34	-0.06			-0.52	0.13	
Alternaria	-0.14	-0.15	-0.31	-0.10	-0.10	-0.20	-0.28	-0.13	0.03	-0.22	0.02	-0.38	0.65	-0.02	-0.06	-0.14
Spring																
NH_4^+	0.38	0.15	**0.77****	0.11	0.18	0.11		**0.47***	0.44	**0.66***	**0.31***			0.65	**0.39***	-0.55
SO_4^{2-}	**0.48****	**0.43****	**0.69****	**0.44****	0.23	**0.36****		**0.49***	0.47	**0.68****	**0.52****			0.15	-0.12	-0.61
NO_3^-	-0.07	-0.17	-0.40	-0.15	-0.18	-0.16		-0.16	0.03	-0.05	-0.08			0.36	0.09	-0.44
Na	-0.17	-0.25	-0.51	-0.23	-0.09	**-0.29***		-0.37	**-0.51***	**-0.71****	**-0.31***			0.22	0.22	0.65
Al	0.29	0.29	0.27	**0.39****	0.13	**0.36***		**0.38***	0.27	**0.76****	**0.31***			0.11	-0.18	-0.72
Si	0.22	0.19	0.23	**0.30***	0.07	0.27		0.32	0.21	**0.72****	**0.26***			0.26	-0.19	**-0.86***
P	**0.48****	**0.48****	**0.58***	**0.50****	0.14	**0.42****		0.35	**0.76****	**0.85****	**0.57****			0.01	**-0.39****	-0.57
Cl	-0.18	-0.23	-0.40	**-0.24***	-0.17	**-0.28***		-0.38	**-0.49***	**-0.69****	**-0.36****			0.32	0.23	0.53
K	0.22	0.17	0.09	**0.27***	0.13	0.24		0.28	0.16	**0.68****	**0.28***			0.18	-0.08	**-0.76***
V	-0.19	-0.25	-0.22	-0.17	0.11	-0.33		-0.21	-0.26	-0.44	-0.04			-0.11	0.25	0.96
Ni	0.77	-0.06	0.40	0.27	-0.26	0.50		0.50	0.28	-0.88	0.70				0.07	
Cu	0.29	-0.07	0.22	0.10	0.08	0.18		0.21	**0.53***	**0.54***	0.17			0.17	-0.07	-0.37
Zn	0.26	0.21	0.39	0.21	-0.07	**0.32***		**0.48***	0.21	**0.55***	**0.29***			0.20	0.00	-0.57

As	-0.57	-0.31	-0.85	-0.25	-0.34	-0.36		-0.03	-0.86		-0.49		-0.10	0.19	
Se	-0.32	-0.22	-0.12	-0.24	-0.15	-0.27		-0.37	-0.01	0.03	-0.19		**0.80***	0.10	-0.30
Pb	0.25	0.05	0.37	0.04	-0.06	0.06		0.26	0.50	0.14	0.15		0.73	0.22	-0.51
OC	**0.64****	**0.75****	0.48	**0.69****	**0.427***	**0.60****		**0.62****	**0.52***	**0.74****	**0.57****		0.03	-0.05	-0.53
EC	**0.64****	**0.53****	**0.61***	**0.52****	0.23	**0.33***		**0.50****	**0.62****	**0.72****	**0.46****		-0.02	0.18	0.11
Pollen	0.33	**0.44****	0.48	**0.54****	0.35	**0.55****		0.32	0.02	0.26	**0.38****		0.36	-0.10	-0.45
Alt a1	0.49	0.00	0.52	0.29	-0.20	0.48		0.18	0.25	-0.34	0.39			0.26	
Alternaria	0.20	0.40	0.28	0.35	-0.03	0.06		0.24	0.10	0.24	0.29		0.75	0.08	-0.39
Summer															
NH_4^+	-0.08	-0.05		0.12	0.01	0.37		0.05		0.88	0.16		0.33	-0.24	-0.49
SO_4^{2-}	0.19	-0.04		0.09	0.00	0.35		-0.04		0.84	0.21		0.09	-0.16	-0.17
NO_3^-	0.37	-0.08		-0.09	-0.12	0.31		-0.04		0.71	**0.25***		-0.08	-0.05	0.11
Na	0.37	-0.07		-0.07	-0.17	0.22		-0.10		0.26	0.02		0.30	-0.09	-0.15
Al	0.10	-0.09		-0.04	0.03	0.39		0.07		-0.05	**0.28***		0.29	-0.02	0.55
Si	0.09	-0.11		-0.05	0.02	0.38		0.07		-0.09	**0.28***		0.34	-0.02	0.59
P	0.13	-0.29		0.04	-0.11	0.00		**0.40****		0.25	**0.55****		0.13	-0.09	-0.15
Cl	**0.47***	-0.07		-0.07	-0.13	0.10		-0.11		0.12	-0.12		0.21	-0.03	0.18
K	0.32	-0.02		-0.03	-0.17	0.32		0.07		0.24	**0.27***		0.11	0.03	0.58
V	-0.05	-0.25		0.11	-0.43	0.35		0.19			0.04		-0.19	0.09	0.14
Ni	0.43	0.47		-0.13	0.77	-0.21		-0.10			-0.24		-0.72	-0.15	-0.08
Cu	0.32	0.00		-0.02	0.23	0.07		-0.07		0.17	**0.27***		0.32	-0.18	**0.70***
Zn	**0.48***	-0.17		0.06	-0.15	0.13		-0.03		0.57	**0.24***		0.36	-0.05	0.63
As				-0.43				0.85			0.70				
Se	0.36	-0.05		0.09	0.12	0.42		-0.15		0.69	0.13		0.45	0.01	-0.23
Pb	0.44	-0.03		0.18	0.11	0.41		0.02		**0.99***	0.24		0.62	-0.24	-0.07
OC	0.31	0.00		0.10	-0.08	0.13		0.15		0.48	**0.27***		0.74	0.12	**0.76***
EC	**0.47***	-0.01		0.02	-0.03	0.08		-0.13		0.32	0.10		0.70	0.17	**0.71***
Pollen	-0.03	**-0.36***		**0.30****	0.13	-0.02		-0.10		-0.65	-0.16		0.39	-0.19	-0.16
Alt a1	-0.48	**0.99****		-0.15		-0.52		-0.14			0.04			0.45	
Alternaria	-0.11	-0.28		-0.11	-0.41	0.01		0.20		-0.46	0.14		0.33	-0.12	0.03
Autumn															
NH_4^+	**0.80****	**0.56***		**0.25***	-0.02	-0.07		-0.06			0.16	0.51	0.35	**0.27***	**0.88****
SO_4^{2-}	0.45	0.29		-0.10	-0.32	-0.20	0.90	-0.32			-0.09	0.33	0.11	-0.03	**0.74****
NO_3^-	**0.93****	**0.61***		**0.34****	0.16	-0.11	0.12	0.01			0.08	0.54	**0.69****	**0.58****	**0.77****
Na	0.23	-0.30		-0.11	-0.41	0.12	-0.81	0.04			-0.18	-0.05	0.07	0.08	-0.18
Al	0.09	0.35		-0.07	0.25	-0.36	-0.93	-0.08			0.02	0.34	-0.09	0.00	0.04
Si	0.07	0.32		0.19	-0.03	-0.18	**0.96***	-0.09			-0.01	0.20	-0.25	-0.06	-0.02
P	0.02	0.39		**0.26***	0.26	-0.41	0.46	0.07			**0.50****	-0.18	0.06	0.09	0.14
Cl	0.43	-0.23		0.06	-0.12	0.26	-0.03	0.08			-0.11	0.00	0.15	**0.27***	0.12
K	**0.72****	**0.79****		0.19	0.40	-0.24	0.01	-0.04			0.12	0.35	**0.49***	**0.42****	**0.78****

V	0.05	0.56	0.21	0.86	-	0.12	-0.07	-0.13			0.09	0.14	0.46
Ni	0.32	0.56	0.19	**0.74***	0.23	0.27	0.03	-0.09			0.15	0.23	0.57
Cu	0.29	0.21	**0.23***	0.45	-0.25	-0.55	-0.09	0.12	0.21		0.38	**0.43****	0.27
Zn	**0.58***	0.53	0.00	**0.58***	-0.34	-0.21	-0.16	0.11	0.44		0.31	0.06	**0.88****
As	**0.84***	0.58	0.30	0.09	-0.20	0.91	0.05	0.04			0.21	0.25	**0.95****
Se	0.13	-0.22	0.23	0.20	0.30	**0.96***	0.39	-0.07	-0.51		-0.15	0.17	**0.73****
Pb	0.17	0.28	0.10	**0.56***	0.19	-0.66	0.11	0.12	0.31		0.16	**0.29***	0.34
OC	0.56	**0.85****	**0.27***	**0.61****	-0.31	0.17	-0.07	**0.27***	0.32		**0.46***	**0.41****	**0.70****
EC	0.43	0.44	0.20	0.42	-0.44	-0.52	-0.11	0.06	0.20		0.33	**0.32***	**0.69****
Pollen	0.61	0.11	-0.07	0.09	-0.40		-0.07	0.02			0.14	-0.02	-0.32
Alt a1			-0.44	-0.88	-0.56		-0.57	-0.48			-0.52	-0.16	
Alternaria	-0.16	-0.24	-0.13	0.05	-0.26		**-0.39***	-0.06	**-0.99***		-0.25	-0.11	-0.35
Winter													
NH_4^+	0.21	0.56	0.17	-0.23	0.32	0.16	0.13	**0.40****	-0.18	-0.90	0.08	0.09	**0.57****
SO_4^{2-}	0.28	0.59	0.13	-0.26	0.44	0.16	-0.07	**0.40****	-0.26	-0.99	-0.04	0.04	**0.70****
NO_3^-	0.26	0.49	0.21	-0.11	0.09	0.13	-0.04	**0.27***	-0.18	-0.71	0.14	0.06	0.30
Na	-0.01	0.38	-0.09	0.33	-0.44	-0.09	-0.52	-0.07	0.33	-0.43	0.02	-0.18	**-0.47****
Al	0.03	**0.78***	-0.14	-0.03	0.04	0.05	0.73	-0.10	-0.27	0.95	-0.11	-0.09	-0.04
Si	0.07	0.65	-0.01	-0.11	-0.06	-0.15	0.67	-0.02	-0.31	0.94	-0.13	-0.08	-0.05
P	-0.18	0.39	0.15	-0.23	0.01	-0.32	-0.09	0.17	0.01	-0.41	0.02	-0.03	0.26
Cl	-0.11	0.28	-0.21	0.08	-0.36	0.05	0.40	-0.02	0.28	-0.95	0.14	-0.17	-0.24
K	0.32	**0.93****	-0.16	0.18	0.04	0.33	**0.90***	-0.11	-0.17	0.54	0.23	-0.01	0.25
V	-0.21	0.19	0.19	0.04	0.34	0.08	0.53	0.13	-0.04	-0.23	0.13	-0.02	-0.12
Ni	-0.25		0.01	0.40	0.27	0.12		0.25		-0.42	0.28	0.25	0.26
Cu	-0.19	0.09	-0.08	-0.07	-0.28	-0.13	0.67	0.07	-0.20	-0.64	0.10	0.08	-0.14
Zn	0.11	0.50	-0.10	0.14	-0.14	0.56	0.67	0.10	-0.19	-0.66	**0.42****	0.16	0.24
As	0.13	**0.91***	-0.26	0.62	0.02	**0.93***		0.01	-0.93	-0.53	0.33	-0.05	0.36
Se	0.01	-0.02	-0.15	-0.50	0.20	-0.58	0.71	0.05	-0.28	-0.50	0.12	-0.04	**0.63****
Pb	0.19	0.08	-0.08	-0.43	0.25	0.48	-0.41	-0.01	0.64		0.20	-0.02	0.12
OC	0.37	**0.94****	-0.13	**0.64***	-0.12	0.54	**0.91***	0.03	-0.01	-0.52	**0.60****	0.20	**0.42***
EC	-0.05	0.33	-0.13	0.26	-0.32	-0.25	**0.97****	-0.05	-0.04	-0.49	0.28	0.03	0.00
Pollen	0.24	0.07	**0.39****	0.24	0.01	-0.08	-0.71	-0.10	**-0.88***	0.89	-0.07	0.08	**0.41***
Alt a1													
Alternaria	0.18	0.63	-0.03	0.80	0.52	0.88		-0.11	-0.69		0.17	**0.36***	0.01

* $p < 0.05$, ** $p < 0.01$

Mannitol was also significantly correlated with pollen concentration in spring (r = 0.4). Burshtein et al. (2011) explained that, although mannitol is common in fungi, it is also abundant in various families of plants. Therefore, the correlations observed could be attributed to high levels of metabolic activity of plants during the flowering period. Moreover, in winter only glucose and mannosan showed a correlation with pollen. According to Fernández-González et al. (1993), the pollen calendar of León displays high levels of three types (*Crupessaceae*, *Alnus glutinosa* and *Corylus avellane*) in winter. This result probably indicates that these pollen types can emit higher concentrations of glucose than fructose and sucrose, compared to the emissions of typical spring-summer pollens.

The fungal spore, *Alternaria*, showed significant positive correlations with T, T_{Min} and T_{Max} (~ 0.4) and a negative relationship with RH (-0.3) between spring and autumn. Fernández et al. (1998) described that the *Alternaria* fungal spore has an optimal growth with mean temperatures between 22 and 28 ^{o}C. Furthermore, Rathnayake et al. (2016) reported high positive correlations between fungal spore tracers and mean temperature, confirming that the proliferation of fungi is favoured by high temperatures (around 23 and 27 ^{o}C). Besides, Filali Ben Sidel et al. (2015) found that this fungal spore is released under high temperature and low relative humidity conditions, corroborating the correlation observed in this study. However, *Alternaria* only correlated significantly with some of the sugars, such as arabitol and SA (in autumn), and levoglucosan (in winter), which probably indicates the presence of these sugars in the spore walls, and their release once the sporangia have decomposed.

Considering only rainy days, *Alternaria* was significantly correlated only with mannitol (r = 0.50, Table 5.6), and with Alt a 1 (r = 0.90), which is the most important allergen of spores of this genus and that can be released under different environmental conditions (Hong et al., 2005; Skóra et al., 2015; Twaroch et al., 2012). Several authors indicated that relative humidity and rainfall in previous days could favour the release and/or growth of fungal spores (Gosselin et al., 2016; Rodríguez-Rajo et al., 2005; Van Osdol et al., 2004). Moreover, during rainy days, ribose and sucrose also showed a significant correlation with pollen concentrations. This result indicates that the release of these saccharides is assisted by rain.

5.3.5. Sugar compounds vs other chemical species

Species related to biomass burning emissions, such as K, NO_3^- and OC (Reche et al., 2012; Urban et al., 2012; Zhang et al., 2010) were significantly correlated with levoglucosan, mannosan and galactosan ($0.3 < r < 0.5$), suggesting a common origin. These correlations are even higher when analysed during autumn, when the Pearson coefficients ranged between 0.4 and 0.8, while in spring and summer the anhydrosaccharides do not present a significant relationship with these species (Table 5.5)

TABLE 5.6. Pearson correlations on days with precipitation between sugar compounds and organic (OC) and elemental (EC) carbon, inorganic ions, trace elements, pollen, allergen (Alt a1) and *Alternaria* concentrations.

	Arabinose	**Fructose**	**Galactose**	**Glucose**	**Ribose**	**Sucrose**	**Xylose**	**Arabitol**	**Erythritol**	**Inositol**	**Mannitol**	**SA**	**Xylitol**	**Galactosan**	**Levoglucosan**	**Mannosan**
Days with precipitation																
NH_4^+	0.43	0.24	-0.42	0.12	-0.10	-0.07	0.62	0.05	0.92		0.18	0.18		-0.03	0.09	**0.64***
SO_4^{2-}	**0.42***	0.40	-0.25	0.06	-0.05	0.12	0.92	0.18	**0.90***		**0.32****	0.24		-0.02	-0.08	**0.65****
NO_3^-	**0.48***	0.20	-0.12	0.18	0.00	-0.12	-0.40	-0.01	0.54		0.11	0.35		0.09	0.09	0.27
Na	0.23	0.11	0.72	-0.11	-0.02	-0.15	-0.78	0.08	-0.48		**-0.28***	0.01		0.12	-0.08	-0.49
Al	-0.04	-0.10	-0.34	-0.03	-0.03	0.11	-0.59	0.01	0.77		0.07	0.54		0.05	-0.10	-0.24
Si	-0.05	-0.12	-0.26	0.18	-0.18	0.09		-0.02	0.79		0.07	0.38		-0.08	-0.11	-0.31
P	-0.20	-0.21	-0.22	0.19	-0.18	0.01	0.84	0.14	**0.91***		**0.44****	0.12		-0.19	-0.07	-0.05
Cl	0.21	0.08	**0.87***	-0.08	-0.22	-0.22	0.87	0.16	-0.58		**-0.30***	-0.04		0.14	-0.07	0.23
K	0.33	0.36	-0.15	0.07	0.21	0.04	0.00	0.02	0.82		0.04	0.48		0.33	0.02	0.47
V	**0.86****	**0.76***		0.23	0.29	0.06		0.46			-0.24			-0.04	0.04	0.28
Ni	0.61	0.66		0.17	0.67	-0.04		0.20			-0.30			-0.01	0.12	0.57
Cu	0.32	0.27	-0.42	0.12	-0.06	0.17	-0.83	-0.13	**0.95***		0.08	0.40		-0.08	0.07	-0.12
Zn	0.27	0.32	-0.26	-0.01	0.03	0.12	-0.69	-0.05	-0.14		0.09	0.54		0.29	0.01	**0.64****
As	0.60	**0.94****	-0.59	0.00	0.25	-0.34	1.00	-0.07			-0.19			0.20	0.00	0.52
Se	0.11	0.48	**0.87***	0.03	-0.26	-0.01	0.80	0.30	0.24		-0.15	-0.40		0.06	0.03	**0.72****
Pb	0.42	0.25	0.40	-0.04	-0.06	0.10		-0.01	0.66		-0.02	0.71		0.25	0.02	0.23
OC	**0.70****	**0.78****	-0.39	0.18	**0.55***	0.28	0.06	0.05	0.72		0.16	0.51		**0.49***	0.06	**0.63****
EC	**0.41***	**0.62****	-0.62	0.13	**0.76****	**0.37***	-0.82	-0.13	**0.92***		0.07	0.50		0.01	0.02	0.17
Pollen	0.26	0.35	-0.40	0.13	**0.89****	**0.65****		0.10	0.77		0.05	0.21		0.47	0.05	0.18
Alt a1	0.59	-0.13	-0.82	-0.15	-0.87	-0.21		-0.37	-0.34		-0.06				-0.02	
Alternaria	-0.02	-0.32	-0.66	0.02	-0.01	-0.18		0.10			**0.50****	-1.00		0.36	-0.03	-0.21

* $p < 0.05$, ** $p < 0.01$

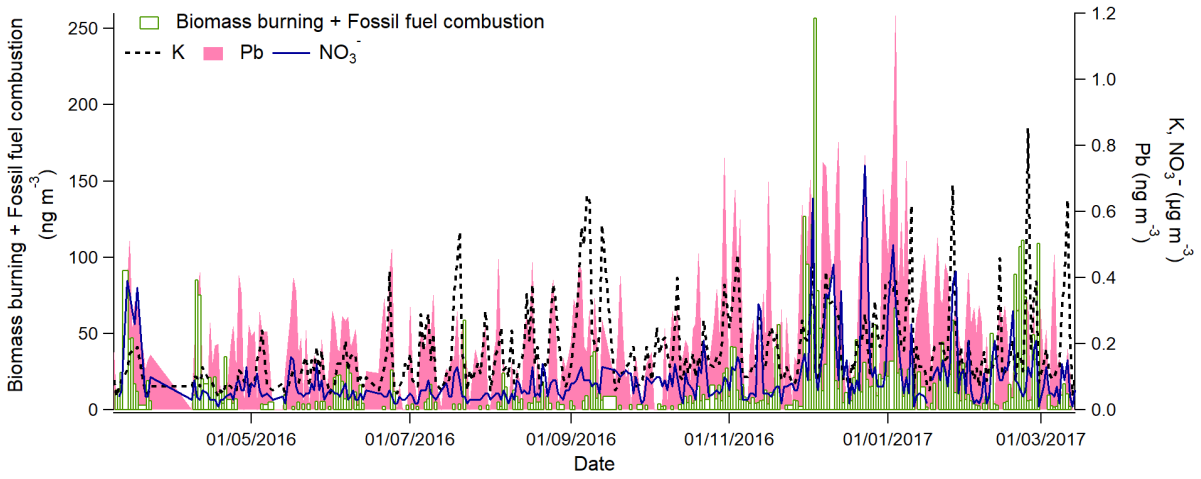

FIG. 5.4. Daily evolution of K, Pb, NO_3^- (concentration × 0.1) and the sum of concentrations of sugar compounds: levoglucosan, mannosan and galactosan, represented as biomass burning + fossil fuel, in León during the sampling campaign.

Fig. 5.4 shows that the concentrations of levoglucosan, mannosan and galactosan, as well as NO_3^-, K and Pb, peak between December and March, when an increase in the use of residential heating appliances take place in León. Arabinose, fructose and glucose are also correlated with K, NO_3^- and OC in autumn. Biomass burning emissions can cause an increase in several sugar compounds, such as glucose, arabinose, ribose, arabitol, etc. (Medeiros et al., 2006; Vicente et al., 2013). The glucose-to-levoglucosan ratio can be used to determine the major source of glucose, since levoglucosan is used as a biomass burning tracer. In this study an annual mean of 1.7 and a considerable decrease of this ratio in autumn (1.3) and winter (0.5) was observed. Previous studies have proposed a value of approximately 4.5 for smoke-free samples, and close to 0.9 for smoke samples (Barbaro et al., 2015; Medeiros et al., 2006). In the city of León, the glucose/levoglucosan ratios only exceeded the value of 4.5 in 11 days: 8 in spring, 1 in summer and 2 in autumn, suggesting that smoke particles are an important source of glucose in the remaining days.

Anhydrosaccharides, mannosan and levoglucosan, are also correlated with some traffic emission tracers such as EC, OC, Cu, Zn, Se, Pb, V and Ni (Calvo et al., 2013; Manousakas et al., 2017), with $r > 0.2$. These correlations are even better when only the autumn is analysed ($r > 0.4$), whereas in the other seasons no significant relationships between these species and anhydrosaccharides were obtained. Although levoglucosan and mannosan are usually associated with biomass burning emissions, these results show that they can also be related to fossil fuel combustion and/or traffic emissions. Alves et al. (2020) reported that both the shredded tiny tyre chips and the wear particles that form from the interaction between tyres and pavement, can release appreciable amounts of levoglucosan. Cellulose fibres are mixed with rubber compounds in the tyre vulcanisation process. The temperatures reached in the friction between the tyres and the pavements during vehicle running are probably enough to convert part of the cellulose fibres into sugars. In autumn, mannosan was correlated with As, which is a coal combustion marker (Vejahati et al., 2010). León has a coal-fired power station (located 30 km north of the city) and domestic coal-fired devices are still used in the province, so coal burning can be a significant source of particulate matter in the region. On rainy days, it was also observed that mannosan,

mannitol, arabinose and fructose correlated with some of the fossil fuel tracers, probably due to an increase in traffic flow and/or use of residential heating devices in those days.

Sulphate and ammonium were significantly correlated with some sugar compounds: arabitol, fructose, mannitol, mannosan and levoglucosan ($r > 0.2$) in all seasons except summer, suggesting a common origin. Ammonium-sulphate is formed from the photo-oxidation of SO_2 from fossil fuel combustion (Alastuey et al., 2004; Qin et al., 2017). In addition, SO_4^{2-} and NH_4^+ are formed by the progressive gas-to-particle conversion of the components emitted by biomass burning (Balasubramanian et al., 1999).

Mineral-related elements (Al, Si, K) showed a positive correlation with glucose, sucrose, arabitol, myo-inositol and mannitol ($0.3 < r < 0.8$) in spring. As already mentioned, in spring high levels of pollen are registered in León. Thus, the observed correlation is probably related to soil resuspension and/or dust intrusions, which can transport high amounts of biological particles (Oduber et al., 2019b).

5.4. CONCLUSIONS

The daily evolution of seventeen sugar compounds in aerosol samples, collected between 9 March 2016 and 14 March 2017 was analysed. The concentration database of the sugar compounds has allowed to determine its natural and/or anthropogenic origin, based on the association with other variables, such as several other chemical species, pollen, fungal spores and meteorological conditions. During the sampling campaign, the total sugar concentrations in PM_{10} ranged between 1.3 and 1052 ng m^{-3}, with an annual mean of 64 ± 108 ng m^{-3}, accounting for 0.3% of the PM_{10} mass concentration.

Pearson correlations between the analysed sugar compounds, meteorological parameters, other chemical species and biological tracers (pollen and *Alternaria* concentrations), showed that:

- In spring, when a high metabolic activity of plants occurs and temperature increases, sugar compounds (glucose, sucrose, 2-methyl-erithritol, mannitol, arabitol and inositol) correlated with airborne pollen concentrations. Glucose, sucrose, arabitol, myo-inositol and mannitol were also correlated with Al, Si and K, pointing to soil resuspension and/or dust intrusions as emission sources in this season. However, the use of glucose and arabinose as a pollen tracer should be done with great care, because they can also be related to biomass burning emissions.

- Between spring and autumn, *Alternaria* air concentrations increased with rising temperatures and decreasing relative humidity, due to the proliferation of fungi. In autumn, arabitol and sorbitol + adonitol can be used as tracers for this fungal spore. Moreover, on rainy days, mannitol and the allergen Alt a 1, were correlated with *Alternaria*, which probably indicates that mannitol is a good tracer for *Alternaria* in wet periods.

- In autumn, lower temperatures cause an increase in the concentrations of levoglucosan, mannosan and galactosan, due to the increasing use of residential heating devices. In this season, these anhydrosugars and arabinose, fructose and glucose, presented significant relationships with K, NO_3^- and OC (biomass burning tracers). Furthermore, mannosan and

levoglucosan were correlated with EC, OC, Cu, Zn, Se, Pb, V and Ni, which are traffic and fossil fuel combustion markers. In autumn, mannosan was also correlated with As, a coal combustion marker. Thus, the selection of these anhydrosaccharides as tracers of biomass burning during the cold season, may be overestimating the contribution of that source, due to the contribution from other anthropogenic emissions.

Precipitation can cause an increase in glucose and sucrose concentrations, due to the breakage of pollen particles that can release sugar compounds bonded to hundreds of fine size grains. Rainfall can also cause an increase in arabitol concentrations owing to the release and growth of fungi. The increase of glucose concentration after rain showed a significant positive correlation with mean rainfall intensity, swept volume and drop mean size. Concretely, raindrops larger than 3 mm increased glucose concentration, while smaller raindrops produced a (non-significant) washing effect. The behaviour of fructose was similar for raindrops larger than 4 mm. This fact could suggest the existence of a threshold raindrop size that split both processes: washing and release of sugar compounds. Nevertheless, further studies are needed in order to validate this hypothesis.

The study of concentrations and origin of atmospheric bioaerosols is increasingly necessary of their health consequences. This work reveals that the association of sugar compounds with biological and non-biological tracers and with meteorological conditions is a necessary tool to assign the origin of water-soluble organic compounds, helping to assess the bioaerosol levels in the air. To avoid overestimating or wrongly assigning a source, monitoring of multiple parameters and the combined assessment of all of them must be made.

5.5. REFERENCES

Alastuey, A., Querol, X., Rodríguez, S., Plana, F., Lopez-Soler, A., Ruiz, C., Mantilla, E., 2004. Monitoring of atmospheric particulate matter around sources of secondary inorganic aerosol. Atmos. Environ. 38, 4979–4992. doi:10.1016/j.atmosenv.2004.06.026

Alves, C.A., Lopes, D.J., Calvo, A.I., Evtyugina, M., Rocha, S., Nunes, T., 2015. Emissions from Light-Duty Diesel and Gasoline in-use Vehicles Measured on Chassis Dynamometer Test Cycles. Aerosol Air Qual. Res. 15, 99–116. doi:10.4209/aaqr.2014.01.0006

Alves, C.A., Vicente, A., Monteiro, C., Gonçalves, C., Evtyugina, M., Pio, C., 2011. Emission of trace gases and organic components in smoke particles from a wildfire in a mixed-evergreen forest in Portugal. Sci. Total Environ. 409, 1466–1475. doi:10.1016/j.scitotenv.2010.12.025

Alves, C.A., Vicente, A.M.P., Calvo, A.I., Baumgardner, D., Amato, F., Querol, X., Pio, C., Gustafsson, M., 2020. Physical and chemical properties of non-exhaust particles generated from wear between pavements and tyres. Atmos. Environ. 224, 117252. doi:10.1016/j.atmosenv.2019.117252

Armentia, A., Martín-Armentia, S., Moral, A., Montejo, D., Martin-Armentia, B., Sastre, R., Fernández, S., Corell, A., Fernandez, D., 2019. Molecular study of hypersensitivity to spores in adults and children from Castile & Leon. Allergol. Immunopathol. (Madr). 47, 350–356. doi:10.1016/J.ALLER.2018.10.002

Balasubramanian, R., Victor, T., Begum, R., 1999. Impact of biomass burning on rainwater acidity and composition in Singapore. J. Geophys. Res. Atmos. 104, 26881–26890. doi:10.1029/1999JD900247

Barbaro, E., Feltracco, M., Cesari, D., Padoan, S., Zangrando, R., Contini, D., Barbante, C., Gambaro, A., 2019. Characterization of the water soluble fraction in ultrafine, fine, and coarse atmospheric aerosol. Sci. Total Environ. 658, 1423–1439. doi:10.1016/j.scitotenv.2018.12.298

Barbaro, E., Kirchgeorg, T., Zangrando, R., Vecchiato, M., Piazza, R., Barbante, C., Gambaro, A., 2015. Sugars in Antarctic aerosol. Atmos. Environ. 118, 135–144. doi:10.1016/j.atmosenv.2015.07.047

Bauer, H., Claeys, M., Vermeylen, R., Schueller, E., Weinke, G., Berger, A., Puxbaum, H., 2008. Arabitol and mannitol as tracers for the quantification of airborne fungal spores. Atmos. Environ. 42, 588–593. doi:10.1016/j.atmosenv.2007.10.013

Bigg, E.K., Soubeyrand, S., Morris, C.E., 2015. Persistent after-effects of heavy rain on concentrations of ice nuclei and rainfall suggest a biological cause. Atmos. Chem. Phys. 15, 2313–2326. doi:10.5194/acp-15-2313-2015

Blanco-Alegre, C., Calvo, A.I., Coz, E., Castro, A., Oduber, F., Prévôt, A.S.H., Močnik, G., Fraile, R., 2019. Quantification of source specific black carbon scavenging using an aethalometer and a disdrometer. Environ. Pollut. 246, 336–345. doi:10.1016/j.envpol.2018.11.102

Burshtein, N., Lang-Yona, N., Rudich, Y., 2011. Ergosterol, arabitol and mannitol as tracers for biogenic aerosols in the eastern Mediterranean. Atmos. Chem. Phys. 11, 829–839. doi:10.5194/acp-11-829-2011

Calvo, A.I., Alves, C., Castro, A., Pont, V., Vicente, A.M., Fraile, R., 2013. Research on aerosol sources and chemical composition: Past, current and emerging issues. Atmos. Res. 120–121, 1–28. doi:10.1016/j.atmosres.2012.09.021

Calvo, A.I., Baumgardner, D., Castro, A., Fernández-González, D., Vega-Maray, A.M., Valencia-Barrera, R.M., Oduber, F., Blanco-Alegre, C., Fraile, R., 2018. Daily behavior of urban Fluorescing Aerosol Particles in northwest Spain. Atmos. Environ. 184, 262–277. doi:10.1016/j.atmosenv.2018.04.027

Calvo, A.I., Pont, V., Olmo, F.J., Castro, A., Alados-Arboledas, L., Vicente, A.M., Fernández-Raga, M., Fraile, R., 2012. Air Masses and Weather Types: A Useful Tool for Characterizing Precipitation Chemistry and Wet Deposition. Aerosol Air Qual. Res. 12, 856–878. doi:10.4209/aaqr.2012.03.0068

Carslaw, D.C., Beevers, S.D., Ropkins, K., Bell, M.C., 2006. Detecting and quantifying aircraft and other on-airport contributions to ambient nitrogen oxides in the vicinity of a large international airport. Atmos. Environ. 40, 5424–5434. doi:10.1016/j.atmosenv.2006.04.062

Caseiro, A., Marr, I.L., Claeys, M., Kasper-Giebl, A., Puxbaum, H., Pio, C.A., 2007. Determination of saccharides in atmospheric aerosol using anion-exchange high-performance liquid chromatography and pulsed-amperometric detection. J. Chromatogr. A 1171, 37–45. doi:10.1016/j.chroma.2007.09.038

Castro, A., Alonso-Blanco, E., González-Colino, M., Calvo, A.I., Fernández-Raga, M., Fraile, R., 2010. Aerosol size distribution in precipitation events in León, Spain. Atmos. Res. 96, 421–435. doi:10.1016/j.atmosres.2010.01.014

Celle-Jeanton, H., Travi, Y., Loÿe-Pilot, M.-D., Huneau, F., Bertrand, G., 2009. Rainwater chemistry at a Mediterranean inland station (Avignon, France): Local contribution versus long-range supply. Atmos. Res. 91, 118–126. doi:10.1016/j.atmosres.2008.06.003

Custódio, D., Cerqueira, M., Fialho, P., Nunes, T., Pio, C., Henriques, D., 2014. Wet deposition of particulate carbon to the Central North Atlantic Ocean. Sci. Total Environ. 496, 92–99. doi:10.1016/j.scitotenv.2014.06.103

Dall'Antonia, F., Pavkov-Keller, T., Zangger, K., Keller, W., 2014. Structure of allergens and structure based epitope predictions. Methods 66, 3–21. doi:10.1016/j.ymeth.2013.07.024

D'Amato, G., Liccardi, G., Frenguelli, G., 2007. Thunderstorm-asthma and pollen allergy. Allergy 62, 11–16. doi:10.1111/j.1398-9995.2006.01271.x

Després, V., Huffman, J.A., Burrows, S.M., Hoose, C., Safatov, A., Buryak, G., Fröhlich-Nowoisky, J., Elbert, W., Andreae, M., Pöschl, U., Jaenicke, R., 2012. Primary biological aerosol particles in the atmosphere: a review. Tellus B Chem. Phys. Meteorol. 64, 15598. doi:10.3402/tellusb.v64i0.15598

Douwes, J., Eduard, W., Thorne, P.S., 2008. Bioaerosols, in: Heggenhougen, H.K. (Kris) (Ed.), International Encyclopedia of Public Health. Academic Press, Oxford, pp. 287–297. doi:https://doi.org/10.1016/B978-012373960-5.00281-1

Dumschott, K., Richter, A., Loescher, W., Merchant, A., 2017. Post photosynthetic carbon partitioning to sugar alcohols and consequences for plant growth. Phytochemistry 144, 243–252. doi:10.1016/j.phytochem.2017.09.019

Dunn, O.J., 1964. Multiple Comparisons Using Rank Sums. Technometrics 6, 241–252. doi:10.1080/00401706.1964.10490181

Emygdio, A.P.M., Andrade, M. de F., Gonçalves, F.L.T., Engling, G., Zanetti, R.H. de S., Kumar, P., 2018. Biomarkers as indicators of fungal biomass in the atmosphere of São Paulo, Brazil. Sci. Total Environ. 612, 809–821. doi:10.1016/j.scitotenv.2017.08.153

Fernández-González, D., González-Parrado, Z., Vega-Maray, A.M., Valencia-Barrera, R.M., Camazón-Izquierdo, B., De Nuntiis, P., Mandrioli, P., 2010. Platanus pollen allergen, Pla a 1: Quantification in the atmosphere and influence on a sensitizing population. Clin. Exp. Allergy 40, 1701–1708. doi:10.1111/j.1365-2222.2010.03595.x

Fernández-González, D, Suarez-Cervera, M., Díaz-Gonzáles, T., Valencia- Barrera, R.M., 1993. Airborne pollen and spores of Leon (Spain). Int. J. Biometeorol. 27, 89–95. doi:10.1007/BF01214387

Fernández-González, D., Vega Maray, A.M., González Parrado, Z., Valencia Barrera, R.M., Gutiérrez, P., De Nuntiis, P., Mandrioli, P., 2019. Are the profilins an important component in the atmosphere? Ole e 2-like panallergen. Aerobiologia (Bologna). 35, 165–175. doi:10.1007/s10453-018-9548-0

Fernández-Raga, M., Castro, A., Marcos, E., Palencia, C., Fraile, R., 2017. Weather types and rainfall microstructure in Leon, Spain. Int. J. Climatol. 37, 1834–1842. doi:10.1002/joc.4816

Fernández-Raga, M., Castro, A., Palencia, C., Calvo, A.I., Fraile, R., 2009. Rain events on 22 October 2006 in León (Spain): Drop size spectra. Atmos. Res. 93, 619–635. doi:10.1016/j.atmosres.2008.09.035

Fernández, D., Valencia, R.M., Molnár, T., Vega, A., Sagüés, E., 1998. Daily and seasonal variations of Alternaria and Cladosporium airborne spores in León (North-West, Spain). Aerobiologia (Bologna). 14, 215–220. doi:10.1007/BF02694209

Filali Ben Sidel, F., Bouziane, H., del Mar Trigo, M., El Haskouri, F., Bardei, F., Redouane, A., Kadiri, M., Riadi, H., Kazzaz, M., 2015. Airborne fungal spores of Alternaria, meteorological parameters and predicting variables. Int. J. Biometeorol. 59, 339–346. doi:10.1007/s00484-014-0845-1

Fröhlich-Nowoisky, J., Kampf, C.J., Weber, B., Huffman, J.A., Pöhlker, C., Andreae, M.O., Lang-Yona, N., Burrows, S.M., Gunthe, S.S., Elbert, W., Su, H., Hoor, P., Thines, E., Hoffmann, T., Després, V.R., Pöschl, U., 2016. Bioaerosols in the Earth system: Climate, health, and ecosystem interactions. Atmos. Res. 182, 346–376. doi:10.1016/j.atmosres.2016.07.018

Fu, P., Kawamura, K., Kobayashi, M., Simoneit, B.R.T., 2012. Seasonal variations of sugars in atmospheric particulate matter from Gosan, Jeju Island: Significant contributions of airborne pollen and Asian dust in spring. Atmos. Environ. 55, 234–239. doi:10.1016/j.atmosenv.2012.02.061

Fukutomi, Y., Taniguchi, M., 2015. Sensitization to fungal allergens: Resolved and unresolved issues. Allergol. Int. 64, 321–331. doi:10.1016/j.alit.2015.05.007

Gosselin, M.I., Rathnayake, C.M., Crawford, I., Pöhlker, C., Fröhlich-Nowoisky, J., Schmer, B., Després, V.R., Engling, G., Gallagher, M., Stone, E., Pöschl, U., Huffman, J.A., 2016. Fluorescent bioaerosol particle, molecular tracer, and fungal spore concentrations during dry and rainy periods in a semi-arid forest. Atmos. Chem. Phys. 16, 15165–15184. doi:10.5194/acp-16-15165-2016

Graham, B., Guyon, P., Taylor, P.E., Artaxo, P., Maenhaut, W., Glovsky, M.M., Flagan, R.C., Andreae, M.O., 2003. Organic compounds present in the natural Amazonian aerosol: Characterization by gas chromatography-mass spectrometry. J. Geophys. Res. Atmos. 108, n/a-n/a. doi:10.1029/2003JD003990

Grinn-Gofroń, A., Nowosad, J., Bosiacka, B., Camacho, I., Pashley, C., Belmonte, J., De Linares, C., Ianovici, N., Manzano, J.M.M., Sadyś, M., Skjøth, C., Rodinkova, V., Tormo-Molina, R., Vokou, D., Fernández-Rodríguez, S., Damialis, A., 2019. Airborne Alternaria and Cladosporium fungal spores in Europe: Forecasting possibilities and relationships with meteorological parameters. Sci. Total Environ. 653, 938–946. doi:10.1016/j.scitotenv.2018.10.419

Hirst, J.M., 1952. An automatic volumetric spore trap. Ann. Appl. Biol. 39, 257–265. doi:10.1111/j.1744-7348.1952.tb00904.x

Hong, S.G., Cramer, R.A., Lawrence, C.B., Pryor, B.M., 2005. Alt a 1 allergen homologs from Alternaria and related taxa: Analysis of phylogenetic content and secondary structure. Fungal Genet. Biol. 42, 119–129. doi:10.1016/j.fgb.2004.10.009

Kruskal, W.H., Wallis, W.A., 1952. Use of Ranks in One-Criterion Variance Analysis. J. Am. Stat. Assoc. 47, 583–621. doi:10.1080/01621459.1952.10483441

Liu, X., Du, Z., Cheng, Y., Liang, L., Engling, G., Duan, F., He, K., 2016. Seasonal variations and source estimation of saccharides in atmospheric particulate matter in Beijing, China. Chemosphere 150, 365–377. doi:10.1016/j.chemosphere.2016.02.002

Lucarelli, F., Chiari, M., Calzolai, G., Giannoni, M., Nava, S., Udisti, R., Severi, M., Querol, X., Amato, F., Alves, C., Eleftheriadis, K., 2015. The role of PIXE in the AIRUSE project "testing and development of air quality mitigation measures in Southern Europe." Nucl. Instruments Methods Phys. Res. Sect. B Beam Interact. with Mater. Atoms 363, 92–98. doi:10.1016/j.nimb.2015.08.023

Makra, L., Csépe, Z., Matyasovszky, I., Tusnády, G., Deák, Á., 2014. Separation of the current and past meteorological parameters in influencing the current pollen concentrations. Acta Climatol. Chorol. 47.48, 85–98.

Manousakas, M., Papaefthymiou, H., Diapouli, E., Migliori, A., Karydas, A.G., Bogdanovic-Radovic, I., Eleftheriadis, K., 2017. Assessment of $PM_{2.5}$ sources and their corresponding level of uncertainty in a coastal urban area using EPA PMF 5.0 enhanced diagnostics. Sci. Total Environ. 574, 155–164. doi:10.1016/j.scitotenv.2016.09.047

Medeiros, P.M., Conte, M.H., Weber, J.C., Simoneit, B.R.T., 2006. Sugars as source indicators of biogenic organic carbon in aerosols collected above the Howland Experimental Forest, Maine. Atmos. Environ. 40, 1694–1705. doi:10.1016/j.atmosenv.2005.11.001

Morris, C.E., Soubeyrand, S., Bigg, E.K., Creamean, J.M., Sands, D.C., 2017. Mapping Rainfall Feedback to Reveal the Potential Sensitivity of Precipitation to Biological Aerosols. Bull. Am. Meteorol. Soc. 98, 1109–1118. doi:10.1175/BAMS-D-15-00293.1

Oduber, F., Calvo, A.I., Blanco-Alegre, C., Castro, A., Nunes, T., Alves, C., Sorribas, M., Fernández-González, D., Vega-Maray, A.M., Valencia-Barrera, R.M., Lucarelli, F., Nava, S., Calzolai, G., Alonso-Blanco, E., Fraile, B., Fialho, P., Coz, E., Prevot, A.S.H., Pont, V., Fraile, R., 2019b. Unusual winter Saharan dust intrusions at Northwest Spain: Air quality, radiative and health impacts. Sci. Total Environ. 669, 213–228. doi:10.1016/j.scitotenv.2019.02.305

Oduber, F., Calvo, A.I., Blanco-Alegre, C., Castro, A., Vega-Maray, A.M., Valencia-Barrera, R.M., Fernández-González, D., Fraile, R., 2019a. Links between recent trends in airborne pollen concentration, meteorological parameters and air pollutants. Agric. For. Meteorol. 264, 16–26. doi:10.1016/j.agrformet.2018.09.023

Oduber, F., Castro, A., Calvo, A.I., Blanco-Alegre, C., Alonso-Blanco, E., Belmonte, P., Fraile, R., 2018. Summer-autumn air pollution in león, Spain: Changes in aerosol size distribution and expected effects on the respiratory tract. Air Qual. Atmos. Heal. 11, 505–520. doi:10.1007/s11869-018-0556-6

Pan, Y.P., Wang, Y.S., 2015. Atmospheric wet and dry deposition of trace elements at 10 sites in Northern China. Atmos. Chem. Phys. 15, 951–972. doi:10.5194/acp-15-951-2015

Piazzalunga, A., Fermo, P., Bernardoni, V., Vecchi, R., Valli, G., de Gregorio, M.A., 2010. A simplified method for levoglucosan quantification in wintertime atmospheric particulate matter by high performance anion-exchange chromatography coupled with pulsed amperometric detection. Int. J. Environ. Anal. Chem. doi:10.1080/03067310903023619

Pio, C., Cerqueira, M., Harrison, R.M., Nunes, T., Mirante, F., Alves, C., Oliveira, C., Sanchez de la Campa, A., Artíñano, B., Matos, M., 2011. OC/EC ratio observations in Europe: Re-thinking the approach for apportionment between primary and secondary organic carbon. Atmos. Environ. 45, 6121–6132. doi:10.1016/j.atmosenv.2011.08.045

Qin, Y.M., Tan, H.B., Li, Y.J., Schurman, M.I., Li, F., Canonaco, F., Prévôt, A.S.H., Chan, C.K., 2017. Impacts of traffic emissions on atmospheric particulate nitrate and organics at a downwind site on the periphery of Guangzhou, China. Atmos. Chem. Phys. 17, 10245–10258. doi:10.5194/acp-17-10245-2017

Rathnayake, C.M., Metwali, N., Baker, Z., Jayarathne, T., Kostle, P.A., Thorne, P.S., O'Shaughnessy, P.T., Stone, E.A., O'Shaughnessy, P.T., Stone, E.A., 2016. Urban enhancement of PM10 bioaerosol tracers relative to background locations in the Midwestern United States. J. Geophys. Res. Atmos. 121, 5071–5089. doi:10.1002/2015JD024538

Rathnayake, C.M., Metwali, N., Jayarathne, T., Kettler, J., Huang, Y., Thorne, P.S., O'Shaughnessy, P.T., Stone, E.A., 2017. Influence of rain on the abundance of bioaerosols in fine and coarse particles. Atmos. Chem. Phys. 17, 2459–2475. doi:10.5194/acp-17-2459-2017

Reche, C., Viana, M., Amato, F., Alastuey, A., Moreno, T., Hillamo, R., Teinilä, K., Saarnio, K., Seco, R., Peñuelas, J., Mohr, C., Prévôt, A.S.H., Querol, X., 2012. Biomass burning contributions to urban aerosols in a coastal Mediterranean City. Sci. Total Environ. 427–428, 175–190. doi:10.1016/j.scitotenv.2012.04.012

Rodríguez-Rajo, F.J., Iglesias, I., Jato, V., 2005. Variation assessment of airborne Alternaria and Cladosporium spores at different bioclimatical conditions. Mycol. Res. 109, 497–507. doi:10.1017/S0953756204001777

Sabo, N.Č., Popović, A., Đorđević, D., 2015. Air Pollution by Pollen Grains of Anemophilous Species: Influence of Chemical and Meteorological Parameters. Water, Air, Soil Pollut. 226, 292. doi:10.1007/s11270-015-2549-5

Schulthess, F.M., Faeth, S.H., 1998. Distribution, Abundances, and Associations of the Endophytic Fungal Community of Arizona Fescue (Festuca arizonica). Mycologia 90, 569. doi:10.2307/3761215

Shahid, I., Kistler, M., Shahid, M.Z., Puxbaum, H., 2019. Aerosol Chemical Characterization and Contribution of Biomass Burning to Particulate Matter at a Residential Site in Islamabad, Pakistan. Aerosol Air Qual. Res. 19, 148–162. doi:10.4209/aaqr.2017.12.0573

Simoneit, B.R.T., Elias, V.O., Kobayashi, M., Kawamura, K., Rushdi, A.I., Medeiros, P.M., Rogge, W.F., Didyk, B.M., 2004. Sugars Dominant Water-Soluble Organic Compounds in Soils and Characterization as Tracers in Atmospheric Particulate Matter. Environ. Sci. Technol. 38, 5939–5949. doi:10.1021/es0403099

Skóra, J., Otlewska, A., Gutarowska, B., Leszczyńska, J., Majak, I., Stępień, Ł., 2015. Production of the allergenic protein alt a 1 by Alternaria isolates from working environments. Int. J. Environ. Res. Public Health 12, 2164–2183. doi:10.3390/ijerph120202164

Speranza, A., Calzoni, G.L., Pacini, E., 1997. Occurrence of mono- or disaccharides and polysaccharide reserves in mature pollen grains. Sex. Plant Reprod. 10, 110–115. doi:10.1007/s004970050076

Theodosi, C., Panagiotopoulos, C., Nouara, A., Zarmpas, P., Nicolaou, P., Violaki, K., Kanakidou, M., Sempéré, R., Mihalopoulos, N., 2018. Sugars in atmospheric aerosols over the Eastern Mediterranean. Prog. Oceanogr. 163, 70–81. doi:10.1016/j.pocean.2017.09.001

Twaroch, T.E., Arcalís, E., Sterflinger, K., Stöger, E., Swoboda, I., Valenta, R., 2012. Predominant localization of the major Alternaria allergen Alt a 1 in the cell wall of airborne spores. J. Allergy Clin. Immunol. 129, 1148–1149. doi:10.1016/j.jaci.2011.10.008

Uchiyama, R., Okochi, H., Katsumi, N., Ogata, H., 2017. The impact of air pollutants on rainwater chemistry during "urban-induced heavy rainfall" in downtown Tokyo, Japan. J. Geophys. Res. Atmos. 122, 6502–6519. doi:10.1002/2017JD026803

Urban, R.C., Lima-Souza, M., Caetano-Silva, L., Queiroz, M.E.C., Nogueira, R.F.P., Allen, A.G., Cardoso, A.A., Held, G., Campos, M.L.A.M., 2012. Use of levoglucosan, potassium, and water-soluble organic carbon to characterize the origins of biomass-burning aerosols. Atmos. Environ. 61, 562–569. doi:10.1016/j.atmosenv.2012.07.082

Van Osdol, T.J., Hu, F., Barnes, C.S., Portnoy, J., 2004. The relationship between airborne ascospores, cladosporium and rainfall events. J. Allergy Clin. Immunol. 113, S62. doi:10.1016/J.JACI.2003.12.192

Vejahati, F., Xu, Z., Gupta, R., 2010. Trace elements in coal: Associations with coal and minerals and their behavior during coal utilization - A review. Fuel 89, 904–911. doi:10.1016/j.fuel.2009.06.013

Vicente, A., Alves, C., Calvo, A.I., Fernandes, A.P., Nunes, T., Monteiro, C., Almeida, S.M., Pio, C., 2013. Emission factors and detailed chemical composition of smoke particles from the 2010 wildfire season. Atmos. Environ. 71, 295–303. doi:10.1016/j.atmosenv.2013.01.062

Vicente, E.D., Alves, C.A., 2018. An overview of particulate emissions from residential biomass combustion. Atmos. Res. 199, 159–185. doi:10.1016/j.atmosres.2017.08.027

Wang, X., Shen, Z., Liu, F., Lu, D., Tao, J., Lei, Y., Zhang, Q., Zeng, Y., Xu, H., Wu, Y., Zhang, R., Cao, J., 2018. Saccharides in summer and winter PM2.5 over Xi'an, Northwestern China: Sources, and yearly variations of biomass burning contribution to PM2.5. Atmos. Res. 214, 410–417. doi:10.1016/j.atmosres.2018.08.024

Xu, X., Zhang, Z., Bao, L., Mo, L., Yu, X., Fan, D., Lun, X., 2017. Influence of rainfall duration and intensity on particulate matter removal from plant leaves. Sci. Total Environ. 609, 11–16. doi:10.1016/j.scitotenv.2017.07.141

Yttri, K.E., Dye, C., Kiss, G., 2007. Ambient aerosol concentrations of sugars and sugar-alcohols at four different sites in Norway. Atmos. Chem. Phys. 7, 4267–4279. doi:10.5194/acp-7-4267-2007

Yu, K.N., Cheung, Y.P., Cheung, T., Henry, R.C., 2004. Identifying the impact of large urban airports on local air quality by nonparametric regression. Atmos. Environ. 38, 4501–4507. doi:10.1016/j.atmosenv.2004.05.034

Zhang, Z., Engling, G., Lin, C.Y., Chou, C.C.K., Lung, S.C.C., Chang, S.Y., Fan, S., Chan, C.Y., Zhang, Y.H., 2010. Chemical speciation, transport and contribution of biomass burning smoke to ambient aerosol in Guangzhou, a mega city of China. Atmos. Environ. 44, 3187–3195. doi:10.1016/j.atmosenv.2010.05.024

6

SUMMER-AUTUMN AIR POLLUTION IN LEÓN, SPAIN: CHANGES IN AEROSOL SIZE DISTRIBUTION AND EXPECTED EFFECTS ON THE RESPIRATORY TRACT

Published in: Air Quality, Atmosphere & Health (2018) 11:505–520

6.1. INTRODUCTION

In recent years, there has been a growing interest in the study of atmospheric aerosol and its sources because of the multiple effects that this air pollutant has on human health and on the environment. Evidence shows that, depending on the size, atmospheric particles can reach different regions of the respiratory tract, and long- or short-term exposure may cause serious respiratory and cardiovascular disease and even death (Monsalve et al. 2013; Goudie 2014; Pascal et al. 2014; Lelieveld et al. 2015). Several studies confirm that there is a relationship between the increase of PM_{10} levels and the death rate from cardiovascular and respiratory causes. Samet et al. (2000) tried to relate the fine particle concentration with the mortality in 20 US cities during the period 1987–1994. They found an increase of 0.68% in the number of deaths from cardiovascular and respiratory causes for each 10 μg m^{-3} of increase in PM_{10}. The same increase in PM_{10} may cause an increase of 0.8% in respiratory deaths in some European cities (Analitis et al. 2006). Fine and ultrafine particles receive more attention because they hardly sediment due to their small size, so they remain suspended longer than larger particles (Jacob 1999) and they may penetrate deeply into the respiratory system (Wilson and Suh 1997; Pope and Dockery 2006; Ren-Jian et al. 2012; Kim et al. 2015). It has been shown that long-term residence in an area of high particle concentration is associated with a greater number of ultrafine particles retained in the lung (Tan et al. 2000).

In urban areas there are important sources of fine and ultrafine particles; one of them is traffic. Gugamsetty et al. (2012) have found that in urban areas of Asian regions vehicle emission was the main source of $PM_{2.5}$ (33%). In addition, studies carried out by Kim Oanh et al. (2006) in traffic areas of Bangkok, Beijing, and Manila show high $PM_{2.5}$ concentrations (50, 168, and 44 μg m^{-3}, respectively) and high PM_{10} concentrations (76, 262, and 54 μg m^{-3}, respectively) during the dry season, reflecting a high contribution from traffic. In Spain, different studies in urban sites have shown that road traffic is an important contributor to particulate matter. This is the case of the study carried out by Querol et al. (2004) in Las Palmas, Barcelona, Llodio, and Madrid, which

found that traffic contributes about 30–50% of PM_{10} mass, depending on the sampling site location. Another important source of aerosol affecting some areas of Spain and the Mediterranean is the Saharan Desert. Artíñano et al. (2003), Kuzu (2016) and Lyamani et al. (2005) have indicated that aerosol size distributions and particle concentrations are affected by the long-range transport of dust particles from the Saharan Desert, particularly in the summer months.

León is a city located in the northwest of Spain characterized by the absence of large emitting industries. The main source of atmospheric particulate emissions is considered to be road traffic during the whole year (Castro et al. 2010). Besides, the emissions produced by the domestic heating devices, especially during the cold months, are remarkable. Because of that, it is important to analyze the temporal variation of particulate matter in León from August to October in order to characterize the evolution of aerosol size distribution associated with the change of season, which represents the transition from a situation with low human activity in the holiday period to one characterized by the hectic rhythm of the city, and its influence on the respiratory system.

Due to the lack of information regarding air quality in the northwest of the Iberian Peninsula, it seems necessary to carry out detailed studies in this region to provide valuable information for completing the map of air quality in the Peninsula.

The aim of this study is to analyze the temporal variation of aerosol size distribution in León from August to October 2012 in order to identify changes associated with the summer-autumn transition. This period includes the end of the summer holidays and the re-start of the activities in the city. Furthermore, the influence of these aerosols in the respiratory tract was analyzed studying of inhalable, thoracic, respirable, and tracheobronchial fractions.

The study of this transitional time will enable us to identify and quantify any changes associated with the contribution of different sources in different months of the year. The result will be a powerful tool for the establishment of appropriate aerosol mitigation measures.

6.2. STUDY ZONE

León is a city in northwestern Iberia (42° 36′ N, 05° 35′ W, and 838 m above sea level) with a population of more than 135,000 inhabitants. The climate is of the Mediterranean type with continental features. Rain events are scattered irregularly over the year, with minimum precipitation values in summer (80 mm) and maximum values in fall (190 mm) and spring (130 mm). The temperatures are cool, with an annual mean of 10.9 °C. The summer is warm, but tempered by the altitude of the city, with minimum and maximum temperatures around 12 and 27 °C, respectively. In fall, the minimum temperatures are around 3 °C and the maximum around 12 °C (Castro et al. 2010). Due to these low temperatures, domestic heating systems are turned on even in the early months of autumn. In León, most buildings use gasoil, natural gas, biomass, or coal for heating and hot water. As a consequence, the emissions produced by these sources, especially during the cold months, are remarkable.

The aerosol sampling was carried out at the Secondary School IES Ordoño II (León, Spain), in the NE of the urban center of León. The measuring probe was installed at 1.5 m above the

ground, directed towards a street with less activity in summer during the school holidays. This street is one of the entrances to the university campus, with continuous traffic and a bus stop nearby. The houses around are occupied by students during the semester, but are mostly uninhabited during the summer. Next to the secondary school, there is an elementary school (about 300 m) and a health center (100 m), with continuous entrances and exits of pedestrians and vehicles, but with no activity at weekends (Saturdays and Sundays). The University of León, the elementary school and the health center are situated to the northeast of the sampling point. The city center is to the southwest and the ring road of the city and other access roads are to the southeast (Fig. 6.1).

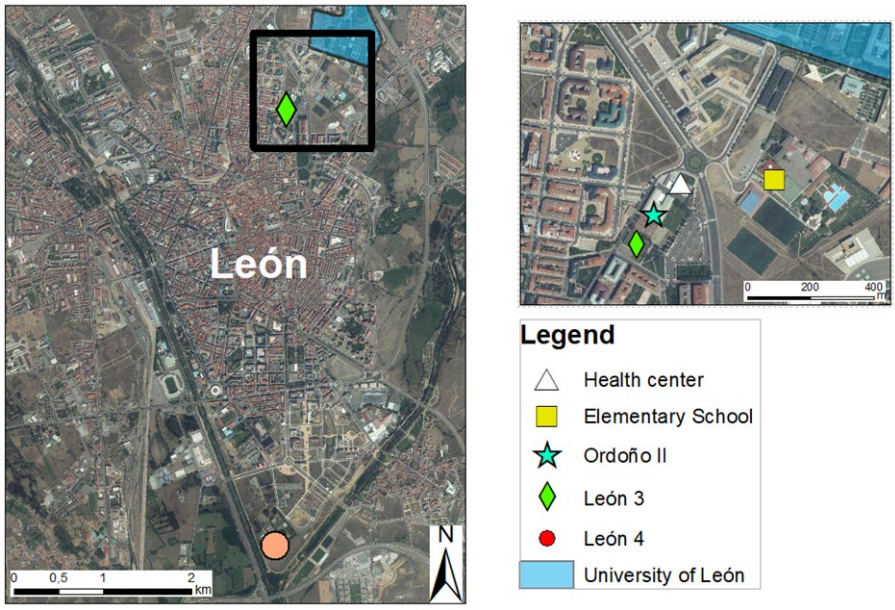

FIG. 6.1. Map of the city of León, Spain.

6.3. MATERIALS AND METHODS

The study period covered between 1 August and 23 October, 2012. The particle number size distributions were measured using a passive cavity aerosol spectrometer probe (PCASP-X, manufactured by Particle Measuring Systems, Inc., PMS). These aerosol size distributions were measured in a range between 0.1 and 10 µm (latex equivalent) in 31 channels, on the basis of the light-scattering properties of the particles at a wavelength of 633 nm between angles of 35° and 135°. A detailed description of the PCASP-X, as well as the necessary corrections and uncertainty of measurements can be found in Calvo et al. (2010, 2013b).

For each particle size range, the diameters corresponding to the different channels were corrected with a mean refractive index typical of the type of aerosol sampled, in this case, urban particles. To do this, the refractive indices depending on the relative humidity corresponding to a wavelength of 632.8 nm (laser He-Ne) (Kim and Boatman 1990) were used (Table 6.1). In order to obtain a representative refractive index for each measurement, an interpolation was performed for the real and the imaginary part depending on the relative humidity at the time of measurement (values between 10 and 96%). After these corrections, particle sizes ranged between 0.08 and 12 µm.

TABLE 6.1. Refractive index of atmospheric aerosol corresponding to a wavelength of 632.8 nm (laser He-Ne) according to the model of urban aerosol by Kim and Boatman (1990).

Relative humidity (%)	Refractive index of urban aerosol
0	$1.574 - 9.13 \times 10^{-2} i$
50	$1.557 - 8.48 \times 10^{-2} i$
70	$1.485 - 5.78 \times 10^{-2} i$
80	$1.419 - 3.29 \times 10^{-2} i$
90	$1.384 - 1.94 \times 10^{-2} i$
99	$1.344 - 4.44 \times 10^{-3} i$

The daily and hourly concentrations were studied. The time variation of the particle numbers during the day, for each hour and day of the week were analyzed. Five hourly intervals (0000–0500 UTC, 0500–1000 UTC, 1000–1500 UTC, 1500–2000 UTC, and 2000–0000 UTC) were established and compared.

In addition, an automatic weather station located on the terrace of the Faculty of Veterinary Science (University of León), located 700 m from the aerosols sampling site, recorded temperature, wind speed and direction, relative humidity, and precipitation data.

To complete the present study, the data reported by the Air Quality Control Network of León were used (http://servicios. jcyl.es/esco). NO_2, NO, O_3, SO_2, and PM_{10} concentrations were obtained from the León3 Station (urban + traffic), located at 05° 33′ 53″ W 42° 36′ 32″ N, nearby the measurement point. Additionally, $PM_{2.5}$ concentrations were provided by the León4 Station (suburban, background), located at 05° 33′ 59″ W 42° 34′ 31″ N (Fig. 6.1).

The Kruskal-Wallis non-parametric test (Kruskal and Wallis 1952) followed by the Dunn (1964) test were applied to the data in order to find statistically significant differences at the 0.05 level of significance.

Finally, we used the International Organization for Standarization (1995), about *Air quality: particle size fractions definitions for health-related sampling*. Using the methodology described in this standard, the inhalable, thoracic, tracheobronchial, and respirable fractions were estimated. The different mass fractions of aerosols were evaluated taking into account the estimated density of the particles, the aerodynamic diameters of the channels of the spectrometer, and the number of particles in each channel. This methodology has been previously applied in other studies (Castro et al. 2015; Alonso-Blanco et al. 2018).

6.4. RESULTS

6.4.1. Meteorological study and preliminary considerations

Table 6.2 shows the extreme values and means of temperature and relative humidity, as well as the accumulated precipitation in each month of the sampling campaign. Figure 6.2 shows

the frequency of each wind direction recorded in the sampling period and the wind speed average for each direction. As usual, the winds come predominantly from the NW and SSW. The most intense winds blow from these directions, whereas those from the first quadrant are remarkably light.

TABLE 6.2. Minimum, maximum, and mean values of temperature (T, °C), relative humidity (HR, %), and accumulated precipitation (mm) for August, September, and October 2012.

	August	**September**	**October**
T_{Min} (°C)	3	2	2
T_{Max} (°C)	35	31	26
T_{mean} (°C)	19	17	14
HR_{min} (%)	10	15	1
HR_{max} (%)	92	93	17
HR_{mean} (%)	49	57	70
Rain days (accumulated precip.)	3 days (5 mm)	4 days (15 mm)	7 days (48 mm)

During the study period, important episodes that may have affected the particle levels in northwestern Iberia were reported by the CALIMA Network, a Commission by the Spanish Ministry of Agriculture, Food and the Environment (http:// www.calima.ws). The CALIMA database includes monthly reports on Saharan dust outbreaks and 24-h forecasts of biomass combustion and European sulfate events in nine Spanish regions. The report for our study period and region showed three biomass combustion events (August 20–22; September 1–6 and 14–17) and three African intrusions (August 8–10; September 10–12 and October 6–7). Additionally, the regional government (Junta de Castilla y León), in the Annual Report on Air Quality in Castilla y León for 2012 (http://www.medioambiente.jcyl.es), presented some episodes that affected the particle levels in the region. Specifically, a forest fire was recorded in August in the municipality of Castrocontrigo (province of León) located at about 70 km southwest of León (straight line). This forest fire was detected on 19 August and became extinct on 6 September. The fire burned 11,768 ha and produced an episode of intense atmospheric pollution over León during 19, 20, and 21 August, which was aggravated by an intense and persistent subsidence thermal inversion. This was the largest wildfire ever recorded in Castilla y León. The episodes are identified in Table 6.3.

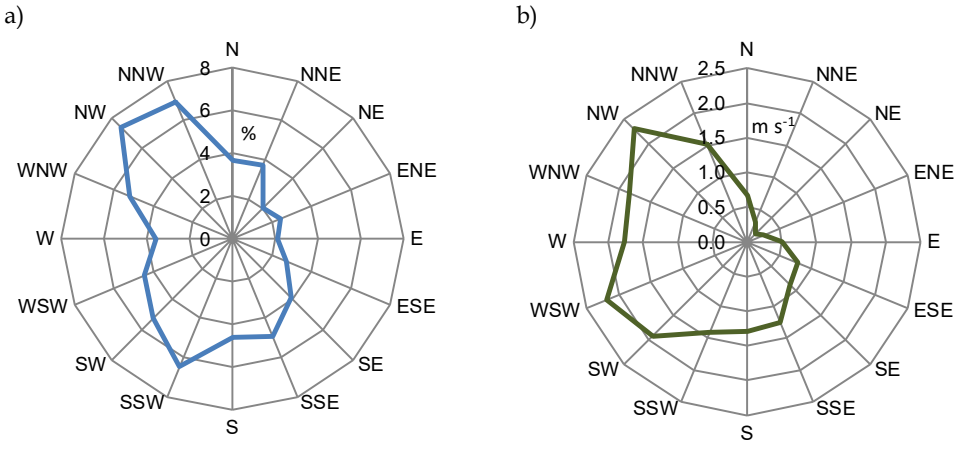

FIG. 6.2. a) Frequencies of wind direction and b) mean wind speed.

TABLE 6.3. Episodes during August, September, and October 2012 in northwestern Iberia reported by the CALIMA Network and Annual Report on Air Quality in Castilla y León for 2012.

Month	Date	Event
August	01 to 05	African intrusion
	07 to 12	
	16 to 23	
	20 to 22	Biomass combustion
September	01 to 06	Biomass combustion
	14 to 17	
	07 to 12	African intrusion
	17 to 22	
October	06 to 08	African intrusion

6.4.2. Aerosol Size Distribution

The monthly, daily, and hourly variation of number and size of particles were studied. The following parameters were studied: numeric (N_T), surface (S_T) and volume (V_T) concentrations, mean diameter of the particle number (CMD), surface (SMD), and volume (VMD) distributions, and the respective geometric standard deviations (σ_g) from August to October.

6.4.2.1. Evolution of particle number concentration

Table 6.4 shows the monthly, weekly, daily, and hourly particle number, surface and volume distributions. The total particle number increased from August to October (from 1000 ± 600 to 1500 ± 1000 particles cm^{-3}, respectively) probably due to reduced road traffic during the summer holidays and to the absence of heating emissions. In addition, in summer, the lower concentrations of particles could be attributed to a higher boundary layer thickness enhancing pollutant dispersion (Johansson et al. 2007; Calvo et al. 2008). During the second week of September, the new academic year began in the elementary school and in the secondary school. In the University Campus, the academic activity started later, in the last week of September. This always causes an intensification of the road traffic, private vehicles, and bus lines in the campus and surroundings of the sampling point. Furthermore, the temperature drops at the beginning of autumn caused a progressive increase in the use of domestic heating devices and a growth in vehicle use within the city, triggering a higher particle concentration in October.

The mean particle size was similar in August, September, and October (CMD of 0.14 µm). Figure 6.3 shows great variability in the total particle number and their sizes throughout the day. The intervals 0500–1000 and 1500–2000 show statistically significant differences with the rest of the intervals considered (Kruskal-Wallis test, $p \leq 0.05$). The largest particle sizes were registered at night, at weekends and on weekdays, reaching maximum values (CMD of 0.16 µm) between 0200 and 0400 UTC, and minimum values (CMD of 0.13 µm) between 1600 and 1800 UTC (Table 6.4). This may be related to an increase in humidity and a decrease in temperature that allows for the condensation of semi-volatile species (Zhang and Wexler 2004; Zhang et al. 2004). There was a greater number of particles between 0600 and 1000 UTC (with an average of 1850 particles cm^{-3} and a maximum of 5422 particles cm^{-3}) and between 1700 and 1900 UTC (with an average of 1400

particles cm^{-3} and a maximum of 4880 particles cm^{-3}), which may be due to increased road traffic in both intervals. The number of particles was higher on weekdays (between 700 and 1900 particles cm^{-3}) than at weekends (between 800 and 1500 particles cm^{-3}) with maximum values of 1868 particles cm^{-3} in the morning, between 0500 and 1000 UTC.

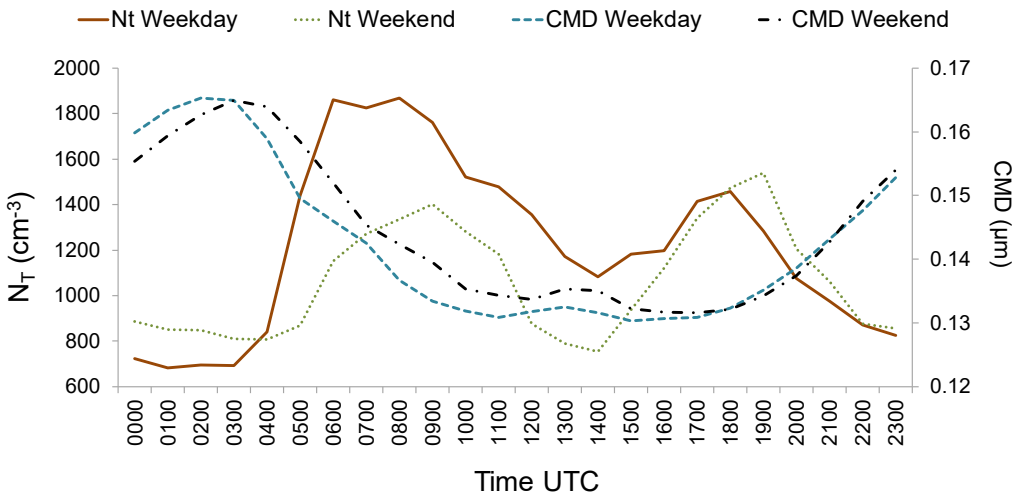

FIG. 6.3. Hourly variation of the total number of particles (N_T) and count median diameter of the particle number (CMD).

For particle number concentration, there were significant differences between Saturday and Sunday, and between Sunday and the rest of the days of the week (except Wednesdays) ($p \leq 0.05$). The highest mean concentration of particles was found on Mondays and Tuesdays at 0600 UTC, with 2300 ± 1000 particles cm^{-3} and 2100 ± 1400 particles cm^{-3}, respectively. On Sundays, the maximum number of particles per unit volume occurred during the afternoon, between 1800 and 1900 UTC, reaching a mean of 1500 ± 1300 particles cm^{-3}. This may be due to an intensification of traffic at the end of the weekend when people return to the city, and the influx of the population near the city of León who come to the city to spend the Sunday afternoon.

During the period studied, the typical evolution of the urban aerosol particle concentration was altered by the occurrence of three main events that affected the air quality of León: (i) two Saharan dust intrusions (Table 6.3) took place between 8 and 10 August and between 10 and 12 September, with an increase in the total particle number and CMD (maximum of 1673 particles cm^{-3}, 0.14 µm, and 2448 particles cm^{-3}, 0.16 µm, respectively) accompanied by an increase in temperature and a decrease in relative humidity (Fig. 6.4); and (ii) a forest fire occurred in Castrocontrigo, between 19 and 27 August, resulting in an increase in the total particle number, in CMD (maximum of 1634 particles cm^{-3}, 0.15 µm), and in the relative humidity (Alonso-Blanco et al. 2018). The different behavior of both Saharan dust intrusions may be due to the varying origin of the dust and air mass trajectory before arriving in León. Furthermore, the local (meteorological and pollution) conditions might lead to different aerosol load and characteristics, such as aerosol size distribution, among others.

TABLE 6.4. Numeric (N_T, particles cm^{-3}), surface (S_T, µm^2 cm^{-3}), and volume (V_T, µm^3 cm^{-3}) concentrations, count median diameter of the particle number (CMD), surface (SMD), and volume (VMD) distributions and the respective geometric standard deviations (σ_g) for months, weekday/weekend, day of week, and for weekdays/weekend time intervals.

	Particle number distribution			**Surface distribution**			**Volume distribution**		
	N_T (cm^{-3})	**CMD (µm)**	**σ_g**	**S_T (µm^2 cm^{-3})**	**SMD (µm)**	**σ_g**	**V_T (µm^3 cm^{-3})**	**VMD (µm)**	**σ_g**
August	1000 ± 600	0.14 ± 0.02	1.4 ± 0.1	100 ± 70	0.5 ± 0.3	4.4 ± 1.0	30 ± 30	4.5 ± 1.7	3.4 ± 2.0
September	1200 ± 700	0.14 ± 0.02	1.4 ± 0.1	120 ± 70	0.4 ± 0.2	4.3 ± 0.9	30 ± 20	4.6 ± 1.7	3.4 ± 0.8
October	1500 ± 1000	0.14 ± 0.02	1.4 ± 0.0	140 ± 90	0.3 ± 0.1	3.1 ± 0.8	18 ± 13	3.1 ± 1.6	5.0 ± 1.3
Weekdays	1200 ± 800	0.14 ± 0.02	1.4 ± 0.1	120 ± 70	0.4 ± 0.3	4.0 ± 1.0	30 ± 30	4.3 ± 1.8	3.8 ± 1.7
Weekend	1100 ± 700	0.14 ± 0.02	1.4 ± 0.0	110 ± 70	0.4 ± 0.2	4.0 ± 1.1	20 ± 19	4.1 ± 1.8	3.7 ± 1.2
Monday	1300 ± 900	0.14 ± 0.02	1.4 ± 0.0	130 ± 80	0.4 ± 0.2	4.1 ± 0.9	30 ± 20	4.3 ± 1.6	3.7 ± 1.0
Tuesday	1300 ± 800	0.14 ± 0.02	1.4 ± 0.0	130 ± 80	0.4 ± 0.1	4.0 ± 1.0	30 ± 17	4.4 ± 1.7	3.8 ± 1.0
Wednesday	1100 ± 700	0.14 ± 0.02	1.4 ± 0.1	110 ± 60	0.5 ± 0.4	4.0 ± 1.1	20 ± 20	4.3 ± 2.0	3.8 ± 1.3
Thursday	1200 ± 800	0.14 ± 0.02	1.4 ± 0.1	120 ± 70	0.5 ± 0.4	4.0 ± 1.1	30 ± 30	4.3 ± 2.0	3.8 ± 1.3
Friday	1200 ± 700	0.14 ± 0.02	1.4 ± 0.1	120 ± 70	0.5 ± 0.4	4.1 ± 1.0	30 ± 40	4.2 ± 1.6	3.8 ± 3.0
Saturday	1200 ± 800	0.14 ± 0.02	1.4 ± 0.0	120 ± 80	0.5 ± 0.4	4.0 ± 1.1	30 ± 20	4.0 ± 1.8	3.8 ± 1.2
Sunday	1000 ± 600	0.14 ± 0.02	1.4 ± 0.0	100 ± 50	0.4 ± 0.2	4.1 ± 1.0	20 ± 13	4.2 ± 1.9	3.8 ± 1.2
Weekdays									
0000-0500	700 ± 500	0.16 ± 0.02	1.4 ± 0.0	100 ± 60	0.5 ± 0.3	3.9 ± 1.1	30 ± 30	4.9 ± 2.0	4.0 ± 1.2
0500-1000	1800 ± 900	0.14 ± 0.01	1.4 ± 0.0	170 ± 90	0.4 ± 0.2	3.9 ± 1.1	30 ± 30	4.4 ± 2.0	4.0 ± 1.4
1000-1500	1300 ± 700	0.13 ± 0.01	1.4 ± 0.0	120 ± 70	0.4 ± 0.4	4.1 ± 1.0	20 ± 19	3.8 ± 1.5	3.6 ± 1.2
1500-2000	1300 ± 800	0.13 ± 0.01	1.4 ± 0.1	120 ± 70	0.5 ± 0.4	4.2 ± 1.0	30 ± 30	4.0 ± 1.4	3.5 ± 1.0
2000-0000	900 ± 500	0.15 ± 0.01	1.4 ± 0.0	110 ± 60	0.5 ± 0.2	4.2 ± 1.0	30 ± 20	4.5 ± 1.5	3.8 ± 3.0
Weekend									
0000-0500	800 ± 500	0.16 ± 0.02	1.4 ± 0.0	110 ± 70	0.4 ± 0.1	3.9 ± 1.1	30 ± 20	4.8 ± 2.0	4.0 ± 1.3
0500-1000	1200 ± 700	0.15 ± 0.01	1.4 ± 0.0	130 ± 70	0.4 ± 0.2	3.8 ± 1.1	30 ± 30	4.1 ± 1.9	4.0 ± 1.4
1000-1500	1000 ± 600	0.13 ± 0.01	1.4 ± 0.0	90 ± 60	0.4 ± 0.2	4.0 ± 0.9	20 ± 10	3.4 ± 1.2	3.5 ± 1.1
1500-2000	1300 ± 1000	0.13 ± 0.01	1.4 ± 0.0	110 ± 90	0.4 ± 0.2	4.2 ± 1.0	20 ± 10	3.7 ± 1.5	3.5 ± 1.0
2000-0000	1000 ± 500	0.15 ± 0.02	1.4 ± 0.0	110 ± 50	0.4 ± 0.1	4.2 ± 1.1	20 ± 10	4.7 ± 2.0	3.6 ± 1.0

(*) When the deviation is represented with 0.0 its mean that is inferior to 0.005

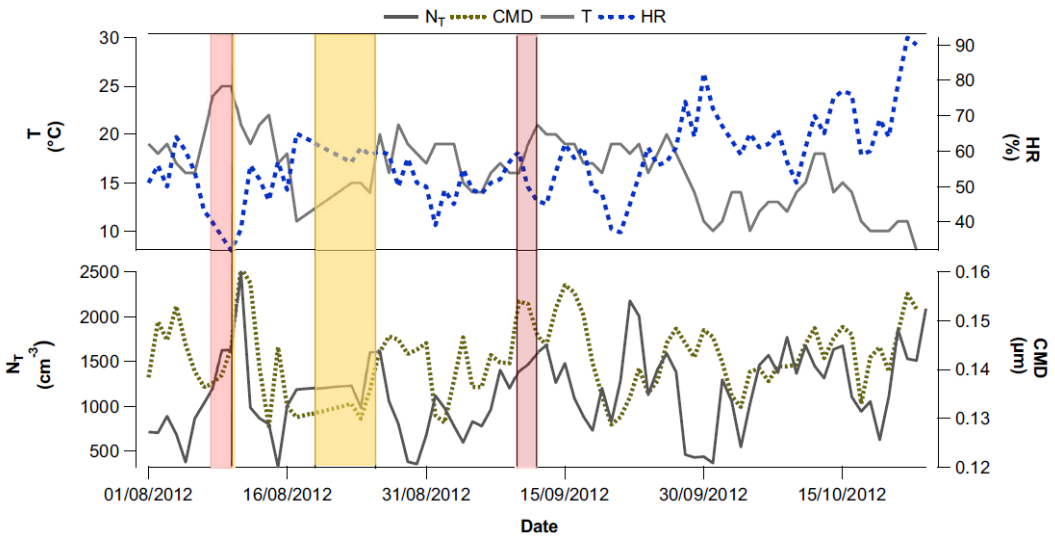

FIG. 6.4. Daily variation of temperature (T) and relative humidity (HR) and the total number of particles (N_T), count median diameter of the particle number (CMD). The dark red bars show the Saharan intrusion events and the light yellow bar shows the forest fire event.

6.4.2.2. Modes of aerosol size distribution

The particle size distribution showed a bimodal profile, with a fine mode or accumulation mode (CMD < 1 µm) and a small fraction corresponding to a coarse mode (CMD ≥ 1 µm).

The monthly evolution of the particle number showed an increase in the number of particles with diameters smaller than 0.1 µm from August to October (22 and 25%, respectively), which may indicate that road traffic was the main source of aerosol, even more important than the contribution of resuspension, which generates larger particles (Calvo et al. 2013a).

As summer progressed to autumn, the mean particle number corresponding to the fine mode increased (from 303 in August to 573 particles cm^{-3} in October) and the CMD decreased (from 0.09 to 0.08 µm) (Table 6.5). The main reason for this increase can be the traffic intensification after the holidays, the lower dispersion caused by the thinner boundary layer and/or the use of the heating devices in autumn. Besides, the contribution of particles from the forest fire and the Saharan dust intrusions in the summer prompted an increase in the CMD (Lyamani et al. 2005; Alonso-Blanco et al. 2012, 2018). These events did not occur in autumn and this could explain the CMD decrease observed.

On weekdays, Monday and Tuesday registered the highest number of particles, with around 465 particles cm^{-3} with a CMD of 0.08 µm in the fine mode. As the week progressed, a steady decrease in the particle number was observed, reaching 312 particles cm^{-3} on Sunday (Table 6.5).

The study showed a higher concentration of particles during weekdays compared to the weekend, registering a decrease of 27%. On weekdays, the highest particle number of the fine mode was observed during the daytime with a maximum between 0500 and 1000 UTC, with 657 particles cm^{-3}. The lowest number of particles was registered at night between 0000 and

0500 UTC, with 180 particles cm^{-3}, suggesting that most of the particles originated from human activities. During the weekend, the maximum particle number of the fine mode was found between 1500 and 2000 UTC. This may be due to the increase in road traffic that occurs especially on Sundays, due to the return of people who spend the weekend outside León. The coarse mode was almost negligible (Table 6.5 and Fig. 6.5).

TABLE 6.5. Mean particle number, CMD and geometric standard deviation (σ_g) of the particle size distribution, for different intervals of time for fine mode (CMD < 1 μm) and coarse mode (for CMD ≥ 1 μm).

		First Mode			Second Mode			
		Fine			Fine		Coarse	
		N_T (cm^{-3})	CMD (μm)	σ_g	N_T (cm^{-3})	CMD (μm)	CMD (μm)	σ_g
August		303	0.09	1.74	0.22		1.65	1.83
September		407	0.08	1.80	0.38		1.06	2.07
October		573	0.08	1.71	0.76	0.59		1.94
Monday		465	0.08	1.74	0.21		1.57	1.82
Tuesday		466	0.08	1.76	0.55	0.81		2.06
Wednesday		406	0.08	1.79	0.75	0.49		2.68
Thursday		423	0.08	1.76	0.77	0.56		2.59
Friday		393	0.08	1.73	0.26		1.58	1.93
Saturday		318	0.09	1.70	0.34	0.93		2.29
Sunday		312	0.08	1.77	0.16		1.61	1.80
Weekdays		431	0.08	1.76	0.60	0.73		2.30
Weekend		314	0.09	1.73	0.23		1.08	1.65
Weekdays	0000-0500 UTC	180	0.10	1.76	0.12		1.81	1.63
	0500-1000 UTC	657	0.08	1.74	0.95	0.56		2.47
	1000-1500 UTC	474	0.08	1.71	1.16	0.41		2.76
	1500-2000 UTC	456	0.08	1.69	1.06	0.42		2.82
	2000-0000 UTC	290	0.09	1.78	0.20		1.59	1.84
Weekend	0000-0500 UTC	193	0.11	1.72	0.25		1.30	1.85
	0500-1000 UTC	363	0.09	1.73	0.27		1.15	1.75
	1000-1500 UTC	293	0.09	1.72	0.51	0.49		3.36
	1500-2000 UTC	410	0.08	1.71	0.27		1.02	1.74
	2000-0000 UTC	314	0.09	1.76	0.45	0.86		2.09

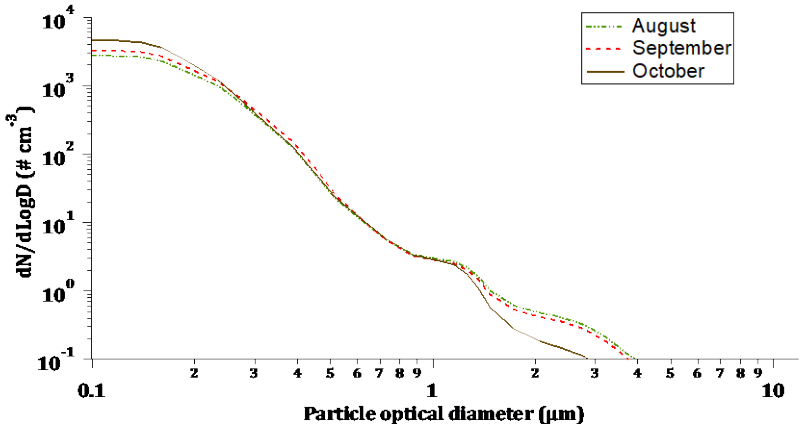

FIG. 6.5. Monthly averaged aerosol size distributions.

6.4.3. Analysis of air pollutants

The Saharan intrusions reported in Table 6.3 are reflected in the increase of PM_{10} and $PM_{2.5}$ observed in Fig. 6.6. One of these episodes was recorded between 8 and 11 August, with a daily maximum concentration of PM_{10} of 55 μg m^{-3} (exceeding the daily threshold of 50 μg m^{-3} established by *Directive 2008/50/EC*) and 16 μg m^{-3} of $PM_{2.5}$ (10 August). In September, during the Saharan intrusions, there were three increases of PM_{10} and $PM_{2.5}$ in León: (i) between 8 and 12 of September, with a daily maximum concentration of $PM_{2.5}$ and PM_{10} of 16 and 36 μg m^{-3}, respectively (8 September); (ii) between 17 and 18 September, with maximum daily concentrations of 10 and 38 μg m^{-3} (17 September); and (iii) between 20 and 21 September, with a maximum of 11 and 37 μg m^{-3} (21 September). Similarly, a PM increase was observed during the forest fire of Castrocontrigo (from 19 August to 6 September). The daily peaks during this episode were reached on 21 August with 32 and 13 μg m^{-3} for PM_{10} and $PM_{2.5}$, respectively (Alonso-Blanco et al. 2018).

Changes in the concentrations of pollutants were detected during the summer-autumn transition with the study of the slope of the linear regression, with a value of $r \geq 0.21$ for 83 degrees of freedom (d.o.f.) and $\alpha = 0.05$. Thus, when analyzing the daily evolution of the air pollutant concentrations during the sampling period, we observed that $PM_{2.5}$, PM_{10}, and O_3 concentrations showed a significant decrease as the autumn set in (−0.06, −0.08, and −0.43 μg m^{-3} day^{-1}, respectively, $p < 0.05$), while NO and NO_2 concentrations showed a significant positive trend (0.05 and 0.08 μg m^{-3} day^{-1}, respectively, $p < 0.05$). SO_2 concentrations did not show a significant trend and remained practically constant (slope = 0.002 μg m^{-3} day^{-1}). The SO_2 concentration did not reveal any significant changes between August and October, although some SO_2 peaks were recorded in September, associated to a temperature decrease (Fig. 6.6); this may be due to the beginning of the domestic heating season.

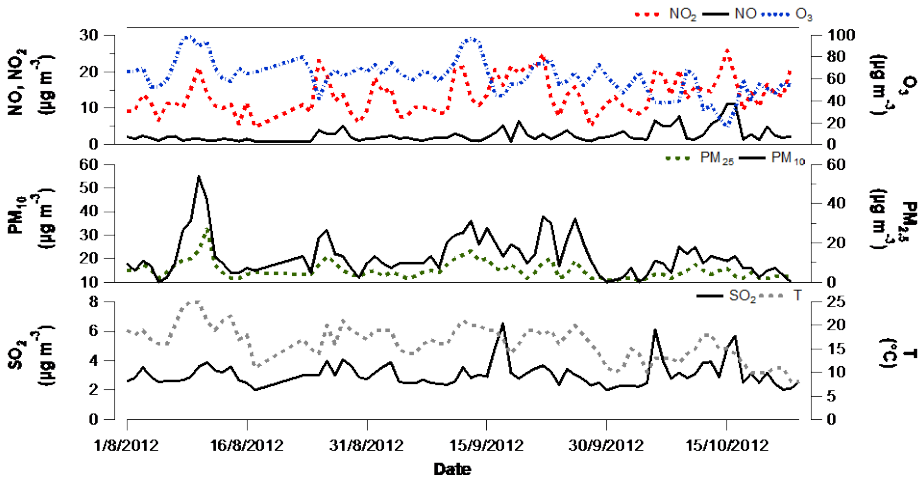

FIG. 6.6. Daily evolution of NO, NO_2, O_3; PM_{10}, $PM_{2.5}$; SO_2; and daily mean temperature (T), during August, September, and October in the study area.

The crucial influence of traffic emissions on aerosol concentration in León was also confirmed by the significant Pearson correlation coefficient ($r \geq 0.062$, d.o.f. = 1831 and $\alpha = 0.05$) observed between N_T and PM_{10}, $PM_{2.5}$, NO_2, and NO (Table 6.6). Thus, aerosol mass and number

concentrations (PM_{10}, $PM_{2.5}$, and N_T) were correlated with NO_2, evidencing the common source (traffic), and with SO_2, probably due to the influence of the emissions from the heating systems, especially in the cold months and/or the emissions from traffic. Authors like Khanum et al. (2017) have reported this behavior in metropolitan areas, where the main source of particles was traffic.

TABLE 6.6. Pearson correlation coefficients between N_T, $PM_{2.5}$, PM_{10}, NO, NO_2 and SO_2.

	$PM_{2.5}$	**PM_{10}**	**NO**	**NO_2**	**SO_2**
N_T	0.296**	0.294**	0.361**	0.338**	0.067**
$PM_{2.5}$	1	0.652**	0.009	0.156**	0.075**
PM_{10}		1	0.085**	0.270**	0.137**
NO			1	0.453**	0.199**
NO_2				1	0.247**

** $p < 0.01$

6.4.4. Analysis of particulate sources

Figure 6.7 shows the daily variation of the particle number concentrations, with the wind direction and speed during the months of August to October. The main source of particles was located to the southeast of the sampling point: the access road to the north of the city (Fig. 6.1). There was also an important contribution of particles coming from the city center (SW sector).

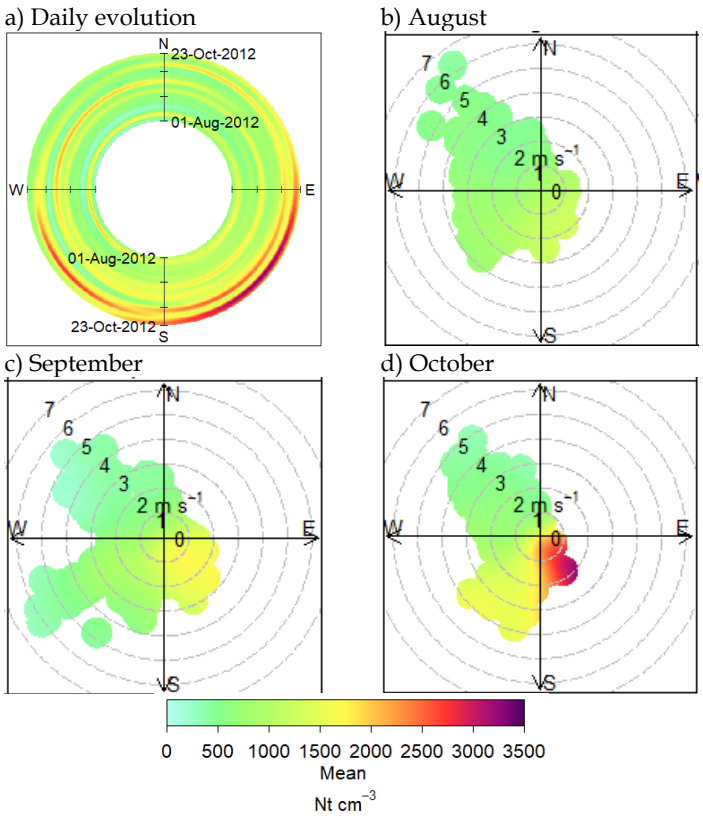

FIG. 6.7. a) Annulus plot (daily evolution of particle number concentration N_T as a function of wind direction) and polar plots (daily particle number concentration N_T as a function of wind speed and direction) for b) August, c) September, and d) October 2012.

During the summer days analyzed (1 August to 21 September), the particle concentration did not exceed 1600 particles cm^{-3}. However, from September, there was an increase of the particle concentration reaching a maximum at the end of October with 2500 particles cm^{-3}. In addition, the polar plots show that when the wind had a western component, there was a decrease in particle concentration and an increase in the speed. In contrast, with the SE wind, there appears to be no link between concentration and wind speed. This fact could be related to the proximity of the sources to the sampling point. Thus, in the SE sector, the main (and almost the only) aerosol source was the road traffic associated with the ring road. Regarding NO_2, the mean concentrations did not exceed 11 µg m^{-3} in August, but in October there was an increase and the mean concentrations reached 18 µg m^{-3}. This is consistent with the traffic intensification in the city, and especially in the vicinity of the sampling point, due to the increase of the activities in the area after the summer holidays (Fig. 6.8).

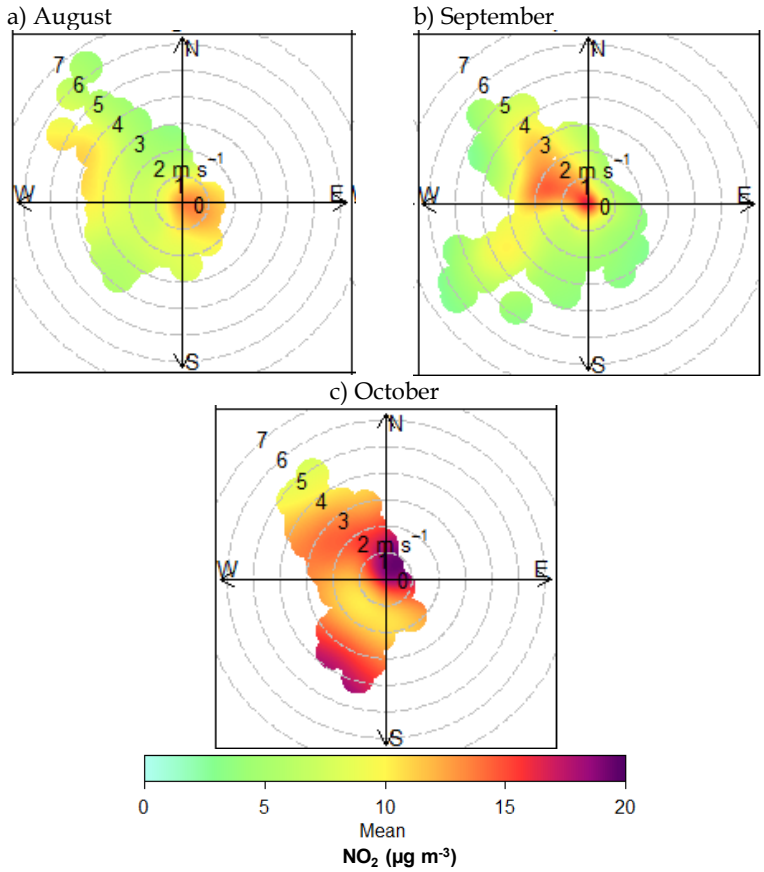

FIG. 6.8. Polar plots (daily NO_2 concentrations as a function of wind speed and direction) for a) August, b) September, and c) October 2012.

6.4.5. Inhalable, thoracic, tracheobronchial and respirable fractions

The ISO 7708 (1995) establishes the following definitions for particles related to the respiratory tract region where they are deposited: (i) The inhalable fraction is the mass fraction of atmospheric particles that are inhaled through the nose and mouth; (ii) the thoracic fraction is the mass fraction of inhaled particles capable of penetrating beyond the larynx. Numerically, it is equivalent to the percentage of the inhalable convention given by a cumulative log-normal

distribution with a median of 11.64 µm; (iii) The extrathoracic fraction is the mass fraction of inhaled particles that are retained in the respiratory region anterior to the larynx; (iv) the respirable fraction is the mass fraction of inhaled particles that penetrates the nonciliated airways in healthy and high-risk individuals (represented by the percentage of the inhalable convention given by a cumulative log-normal distribution with a median of 4.25 and 2.5 µm, respectively). More details can be found in Morawska and Salthammer (2004). Besides, Brown et al. (2013) provided estimates of thoracic and respirable fractions for a variety of activities and breathing habits useful for other experimental studies, as well as in the search for relationships between particle size and their impact on respiratory health.

The results showed that for the inhalable fraction, the percentage of the particles inhaled through the nose and mouth varied slightly between 75 and 83% (for monthly, daily, and hourly studies) (Fig. 6.9). This means that there were no significant differences between months, between days of the week, or between hours of the day. However, the values of the inhaled mass of aerosols were higher in August and September (41 and 45 µg m^{-3} on average, respectively) than in October (28 µg m^{-3}), peaking on Thursdays and Fridays (45 and 53 µg m^{-3}, respectively). On weekdays, the most critical periods were 0600–0900 UTC and 1700–1800 UTC with more than 50 µg m^{-3} (maximum reached between 0600 and 0700 UTC, with 63 µg m^{-3}), while during the weekends the highest values of the inhaled mass were registered at 0000–0200 UTC (45 µg m^{-3}) and at 0700–0900 UTC (56 µg m^{-3}).

For the tracheobronchial fraction in healthy adults, the percentage of particles that could not pass through a nonciliated airway and were deposited in the trachea and bronchi varied between 20 and 38%. October was the month with the lowest value. Regarding the mass deposited, the maximum was in August and September with 17 and 18 µg m^{-3}, respectively, decreasing in October with 7 µg m^{-3}. Fridays, with 22 µg m^{-3} of particles that came up to the trachea and bronchi, should be highlighted. In general, there were no differences between weekdays and weekends, but there were differences between the time intervals. On weekdays, the maximum was observed between 0600 and 1000 and 1700–1900 UTC (18 and 19 µg m^{-3}, respectively) and at weekends, between 0700 and 0800 UTC (22 µg m^{-3}).

For the respirable fraction in healthy adults, the behavior is always complementary to what was observed in the tracheobronchial fraction: the greater the mass deposited in the tracheobronchial area, the smaller the mass deposited in the alveolar area. It has been observed that the percentage of particles that could pass through the nonciliated airway and reach the alveolar zone (where bronchioles and alveoli are located) was higher in October (34%) and lowest in August and September (20% in both months), and the highest percentages were reached from Saturday to Tuesday (23%). On weekdays, the percentage of particles that came to the alveolar zone showed higher values during the morning (between 22 and 25% of 0800–1400 UTC). At weekends, the percentage of atmospheric particles deposited was significantly higher during most of the daytime (values of 25–29% between 0900 and 2000 UTC). Concerning the deposited mass, the lowest values were obtained in August (10 µg m^{-3}), and on Wednesdays and Sundays (9 µg m^{-3}). On weekdays, the highest values were obtained between 0600 and 1000 UTC (around 15 µg m^{-3}) and in the afternoon, between 1700 and 2000 UTC (around 12 µg m^{-3}). However, at weekends, the time intervals that registered the highest values of mass deposited in the alveolar area were 0700–0800 (14 µg m^{-3}) and 1900–2000 UTC (13 µg m^{-3}).

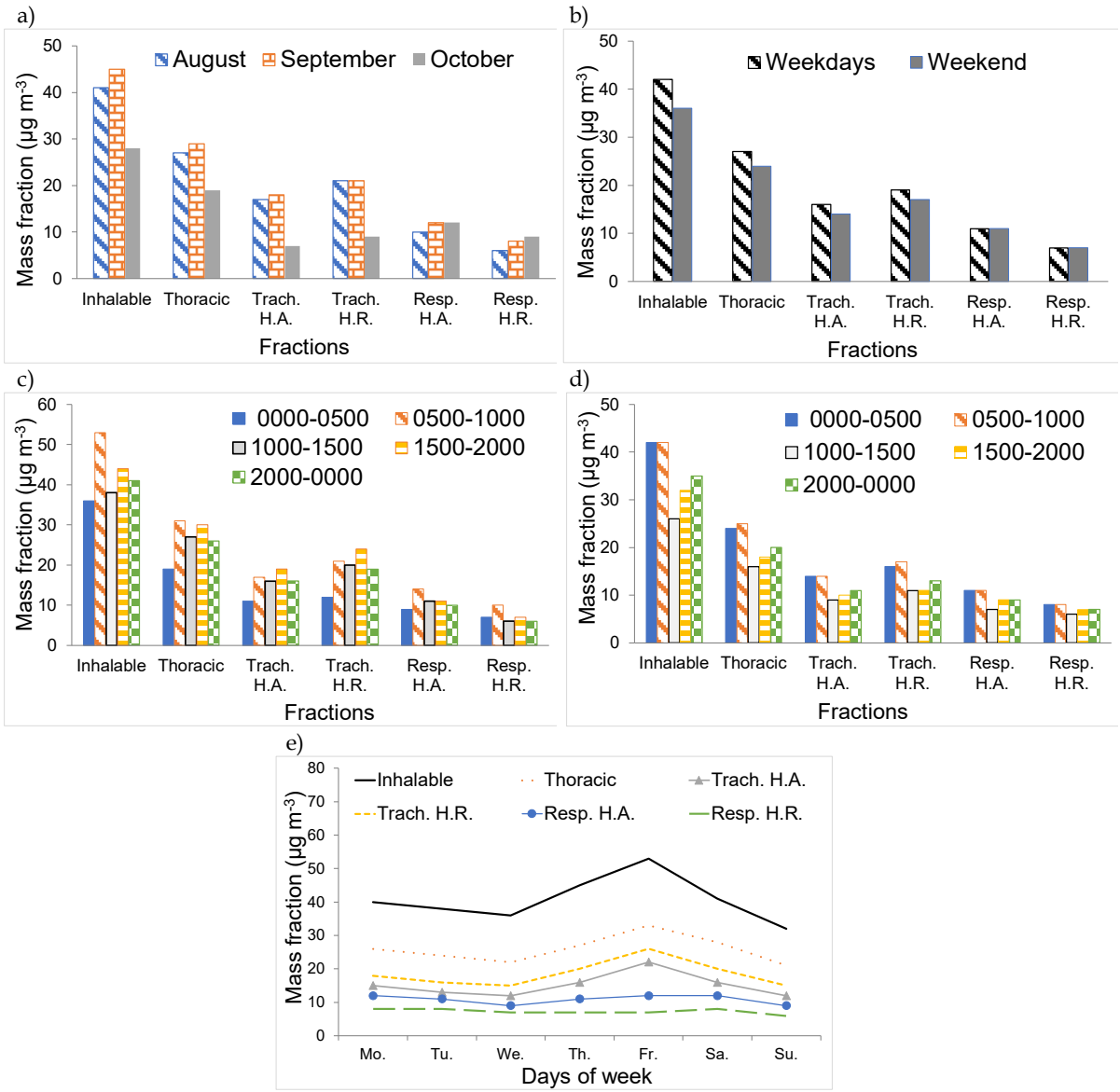

FIG. 6.9. Inhalable, thoracic, tracheobronquial (trach.), and respirable (resp.) mass fractions (µg m^{-3}) in healthy adults and high-risk population (children, frail, or sick people) in the respiratory tract for different time intervals: a) months, b) weekdays/weekend, c) hourly intervals for week- days, d) hourly intervals for weekends, e) days of the week.

For the respirable fraction, in high-risk population like children, elderly and weak people, it was observed that the best month was August with 6 µg m^{-3} and the worst was October with 9 µg m^{-3} particles that reach the alveolar zone. There were no significant differences between weekdays, Sundays being the most favorable days. On weekdays, the more critical hours were between 0600 and 0900 UTC with an average of 11 µg m^{-3}, and at weekends throughout the day the value of 9 µg m^{-3} was not exceeded.

6.4.6. Comparison with other cities

A comparative study has been carried out with other cities. After a bibliographic review, only the cities with data about number and mass concentration have been retained. This

information is compiled in Tables 6.7 and 6.8. Table 6.7 shows the pollution levels registered in this study and those registered in other cities. As in the present study, in cities like Zabrze (Poland), Milan (Italy), Augsburg (Germany), and Leipzig (Germany), the particle number concentration was higher in the cold seasons (autumn and winter) than in the warm ones (summer and spring) (Wehner and Wiedensohler 2002; Cyrys et al. 2008; Lonati et al. 2011; Klejnowski et al. 2013). This is not the case in other places, with more rural characteristics, such as Hohenpeissenberg (Germany). The higher concentrations in the summer can be attributed to the special characteristics of the place: according to Held et al. (2008), a stable layer of thermal inversion is usually recorded during the winter. On the other hand, Aalto et al. (2005) and Wehner and Wiedensohler (2002) found that the numeric concentration was higher on weekdays than at weekends, and that there were differences between the weekdays and weekends of the cold and the warm months, as has been observed in the present study.

When comparing the general results obtained in this study with those observed in other cities, it can be seen that the aerosol pollution is lower in León (Table 6.7). The main cause could be the relatively small size of the city (less than 200,000 inhabitants) with few industries and whose pollution in summer is mainly caused by traffic, forest fires, and Saharan dust outbreaks, and in autumn by road traffic and heating devices. In other studies, conducted in urban areas, a trimodal aerosol size distribution was found (Wehner and Wiedensohler 2002; Hussein et al. 2003; Stanier et al. 2004; Wu et al. 2008; Lonati et al. 2011). In the study carried out by Woo et al. (2001) in Atlanta, the three modes obtained were described as (*i*) nucleation mode, with a range of diameters between 3 and 10 nm and a total number of 5564 particles cm^{-3}; (*ii*) Aitken mode, with a range of diameters between 10 and 100 nm and 13,482 particles cm^{-3}; (*iii*) accumulation mode, between 100 and 2000 nm, and 1690 particles cm^{-3}. Lonati et al. (2011) found that in Milan, in peak traffic hours, Aitken mode particles dominate the size distribution (38 nm in the cold season and 39.8 nm in the warm season), indicating that traffic exhaust emissions are the main source of ultrafine particles in the urban environment. In the present study, only two modes were identified due to the size interval measured by the PCASP, with a narrower size range.

Table 6.8 shows a compilation of $PM_{2.5}$ and PM_{10} concentrations found in other studies in different cities of the world. There are important differences between the cities and the study period, with $PM_{2.5}$ values between 17.5 and 43.1 μg m^{-3} and PM_{10} values between 26. 1 and 79.7 μg m^{-3}. During the sampling period in León, the month with the lowest concentration was October (16 μg m^{-3}), while August and September showed values of 21 and 22 μg m^{-3}, respectively. However, in Athens (Greece), during the same period in 1999, Chaloulakou et al. (2003) found that the highest concentration of PM_{10} occurred in October with a value of 79.7 μg m^{-3} and the lowest concentration (67.0 μg m^{-3}) was registered in August.

In León, the lowest $PM_{2.5}/PM_{10}$ daily ratio was found in summer (0.12) due to the contribution of coarse particles from a dust intrusion. Similar behavior has been found by Hieu and Lee (2010), Deshmukh et al. (2013) and Rashki et al. (2013). The $PM_{2.5}/PM_{10}$ mean ratio decreases progressively from August to October (0.33 and 0.25, respectively). Studies conducted in Istanbul by Kuzu and Saral (2017) show that during the winter there is a higher concentration of coarse particles, which can be attributed to an increase in human activities like domestic heating and diesel vehicle emissions because of an increase of relative humidity and the consequent particle growth. Other authors corroborate that during the colder months, there is an increase in

the PM concentration due to the use of heating devices (Reizer and Juda-Rezler 2016; Samek et al. 2017).

TABLE 6.7. Mean values of the number concentration of particles cm^{-3} for different cities (adapted from Klejnowski et al. 2013).

Location	Study period	Numeric concentration (cm^{-3})	Reference
León, Spain	August-October 2012	Summer: Weekdays: $1.09 \cdot 10^3$ Weekend: $0.98 \cdot 10^3$ Autumn: Weekdays: $1.59 \cdot 10^3$ Weekend: $1.36 \cdot 10^3$	This study
Zabrze, Poland	January-October 2010	Summer: $4.95 \cdot 10^3$ Winter: $8.80 \cdot 10^3$	Klejnowski et al. 2013
Milan, Italy	September 2003-August 2004	Cold station: $2.5 \cdot 10^4$ Warm station: $1.3 \cdot 10^4$	Lonati et al. 2011
Bourgesplatz, Augsburg, Germany	December 2003, May 2004	Winter: $2.03 \cdot 10^4$ Spring: $1.69 \cdot 10^4$	Cyrys et al. 2008
Fachhochschule, Augsburg, Germany		Winter: $2.40 \cdot 10^4$ Spring: $1.84 \cdot 10^4$	
Hohenpeissenberg, Germany	2003-2004	Summer: $3.1 \cdot 10^3$ Winter: $1.8 \cdot 10^3$	Held et al. 2008
Amsterdan, Netherlands	October 2002-March 2004	Background: $1.81 \cdot 10^4$	Puustinen et al. 2007
Birmingham, United Kindom		Urban background: $1.88 \cdot 10^4$	
Athens,Greece		Urban background: $2.03 \cdot 10^4$	
Helsinki,Finland	October 2002-March 2004	Urban background: $1.25 \cdot 10^4$	Puustinen et al. 2007
	2001-2003	Weekdays: $1.1 \cdot 10^4$ Weekend: $0.69 \cdot 10^4$	Aalto et al. 2005
Augsburg, Germany	2001-2003	Weekdays: $1.0 \cdot 10^4$ Weekend: $0.82 \cdot 10^4$	Aalto et al. 2005
Barcelona, Spain	2001-2003	Weekdays: $3.9 \cdot 10^4$ Weekend: $2.76 \cdot 10^4$	Aalto et al. 2005
Stockholm, Sweden	2001-2003	Weekdays: $1.0 \cdot 10^4$ Weekend: $0.8 \cdot 10^4$	
Leipzig, Germany	1997-2001	Winter: Weekdays: $2.14 \cdot 10^4$ Sundays: $1.40 \cdot 10^4$ Summer: Weekdays: $1.47 \cdot 10^4$ Sundays: $1.16 \cdot 10^4$	Wehner and Wiedensohler, 2002

TABLE 6.8. Mean values (μg m^{-3}) and standard deviation (σ) of the mass concentration of $PM_{2.5}$ and PM_{10} for different cities.

Location	Study period	Type	$PM_{2.5}$(σ)	PM_{10}(σ)	Reference
León, Spain	August 2012	Urban	7	21	Air Quality Control Network of the León city
	September 2012		6	22	
	October 2012		4	16	
Hong Kong	October 2004-September 2005	Urban	55.5(25.5)	-	Cheng et al. 2015
Taiwan (New Taipei City)	May-November 2011	Urban	21.82(7.50)	39.45(11.58)	Gugamsetty et al. 2012
Spain (Madrid)	1999-2000	Urban	34.1(13.3)	47.7(20.8)	Salvador et al. 2011
Spain (Madrid)	2007-2008	Urban	20.7 (9.2)	41.4(19.4)	
Spain (Alcobendas)	2001	Urban	24.9(15.3)	32.2(19.2)	
Spain (Chapinería)	2004-2005	Rural	16.8(10.7)	31.6(21.7)	
Spain (Barcelona)	2005-2006	Urban	29	45	Pérez et al. 2008
Austria (location 1 of Project AUPHEP)	June-September 1999	Urban	17.5(7.3)	26.1(10.5)	Gomišček et al. 2004
Greece (Heraklion)	November 2000-September 2005	Urban	-	51(33)	Gerasopoulos et al. 2006
Greece (Finokalia)	2004- 2005	Background	-	28(30)	
Greece (Athens)	July 1999	Urban	39.6(8.4)	73.6 (11.2)	Chaloulakou et al. 2003
	August 1999		38.4(13.7)	67.0 (23.0)	
	September 1999		43.1(13.3)	76.6(22.9)	
	October 1999		42.5(14.7)	79.7 (25.9)	

6.5. CONCLUSIONS

A detailed knowledge of the characteristic variables of aerosol size distribution is essential to determine the sources and the impacts of particulate matter on human health. This subject is of special relevance when air quality compromises human well- being, for example under Saharan dust outbreaks or forest fires. This study has enabled us to gain more in-depth knowledge about changes in air quality associated with the summer-autumn transition, when dust intrusions and biomass burning are prevailing in León. The city is also affected by low temperatures by the beginning of autumn. As a consequence, the study of the summer-autumn transition becomes essential due to the important contribution of domestic heating devices. Obviously, the pollution due to road traffic increases as the autumn progresses. In León, during the summer-autumn transition, the particle number increased from 1000 ± 600 in August to 1500 ± 1000 particles cm^{-3} in October and around of 25% of the particles had sizes lower than 0.1 μm. The main reasons for the increase in the particle number could be the traffic intensification after the summer holidays, the lower dispersion caused by the low boundary layer thickness and the beginning of the use of domestic heating devices in autumn. August was the only month with no differences between the particle concentrations registered on weekdays and at weekends. This is probably due to the decrease of the activity in the city during the summer holidays. The weekly pattern showed a progressive decrease of particle concentration from Mondays to Sundays during the study period. Regarding the hourly distribution, two daily peaks in the particle concentration were observed: between 0500 and 0800 UTC (with 1751 particles cm^{-3}) and between 1700 and 2000 UTC (with

1307 particles cm^{-3}). Sunday registered a maximum concentration of particles during the afternoon, possibly due to increased road traffic caused by the return to the city after the weekend. In the global study, the size distribution showed a fine mode with hourly CMD between 0.08 and 0.10 µm, without a well-defined coarse mode. When analyzing the relationship between wind speed and particle number concentration, it was found that the main contribution comes from the SE, probably due to the pollution from the ring road traffic. Furthermore, the particle concentration seemed not to depend on the wind speed in this direction. For the respirable fraction in healthy adults, the highest values were obtained in September and October (12 µg m^{-3}), and on Monday, Friday, and Saturday (12 µg m^{-3}). On weekdays, the highest values were obtained between 0600 and 1000 UTC (around 15 µg m^{-3}) and in the afternoon, between 1700 and 2000 UTC (around 12 µg m^{-3}). At weekends, the periods in which more mass could be deposited in the alveolar area were 0700–0800 (14 µg m^{-3}) and 1900–2000 UTC (13 µg m^{-3}). León, with mean concentrations of total particle number of 1200 ± 800 particle cm^{-3} and PM_{10} of 20 ± 3 µg m^{-3} during the study period, presents low pollution levels when compared with other cities in the world.

6.6. REFERENCES

Aalto P, Hämeri K, Paatero P, Kulmala M, Bellander T, Berglind N, Bouso L, Castaño-Vinyals G, Sunyer J, Cattani G, Marconi A, Cyrys J, Klot S, Peters A, Zetzsche K, Lanki T, Pekkanen J, Nyberg F, Sjövall B, Forastiere F (2005) Aerosol particle number concentration measurements in five European cities using TSI-3022 condensation particle counter over a three-year period during health effects of air pollution on susceptible subpopulations. J Air Waste Manage Assoc 55:1064–1076. https://doi.org/10.1080/10473289. 2005.10464702

Alonso-Blanco E, Calvo AI, Fraile R, Castro A (2012) The influence of wildfires on aerosol size distributions in rural areas. Sci World J 2012:1–13. https://doi.org/10.1100/2012/735697

Alonso-Blanco E, Castro A, Calvo AI, Pont V, Mallet M, Fraile R (2018) Wildfire smoke plumes transport under a subsidence inversion: climate and health implications in a distant urban area. Sci Total Environ 619–620:988–1002. https://doi.org/10.1016/j.scitotenv.2017.11.142

Analitis A, Katsouyanni K, Dimakopoulou K, Samoli E, Nikoloulopoulos AK, Petasakis Y, Touloumi G, Schwartz J, Anderson HR, Cambra K, Forastiere F, Zmirou D, Vonk JM, Clancy L, Kriz B, Bobvos J, Pekkanen J (2006) Short-term effects of ambient particles on cardiovascular and respiratory mortality. Epidemiology 17:230–233. https://doi.org/10.1097/01.ede. 0000199439.57655.6b

Artíñano B, Salvador P, Alonso DG et al (2003) Anthropogenic and natural influence on the PM_{10} and $PM_{2.5}$ aerosol in Madrid (Spain). Analysis of high concentration episodes. Environ Pollut 125:453–465. https://doi.org/10.1016/S0269-7491(03)00078-2

Brown J, Gordon T, Price O, Asgharian B (2013) Thoracic and respirable particle definitions for human health risk assessment. Part Fibre Toxicol 10(1):12.

Calvo AI, Alves C, Castro A, Pont V, Vicente AM, Fraile R (2013a) Research on aerosol sources and chemical composition: past, current and emerging issues. Atmos Res 120–121:1–28. https://doi.org/10. 1016/j.atmosres.2012.09.021

Calvo AI, Pont V, Castro A, Mallet M, Palencia C, Roger JC, Dubuisson P, Fraile R (2010) Radiative forcing of haze during a forest fire in Spain. J Geophys Res Atmos 115:1–10. https://doi.org/10.1029/ 2009JD012172

Calvo AI, Pont V, Liousse C, Dupré B, Mariscal A, Zouiten C, Gardrat E, Castera P, Lacaux CG, Castro A, Fraile R (2008) Chemical composition of urban aerosols in Toulouse, France during CAPITOUL experiment. Meteorol Atmos Phys 102:307–323. https://doi.org/ 10.1007/s00703-008-0319-2

Calvo AI, Tarelho LAC, Teixeira ER, Alves C, Nunes T, Duarte M, Coz E, Custodio D, Castro A, Artiñano B, Fraile R (2013b) Particulate emissions from the co-combustion of forest biomass and sewage sludge in a bubbling fluidised bed reactor. Fuel Process Technol 114:58–68. https://doi.org/10.1016/j.fuproc.2013.03.021

Castro A, Alonso-Blanco E, González-Colino M, Calvo AI, Fernández-Raga M, Fraile R (2010) Aerosol size distribution in precipitation events in León, Spain. Atmos Res 96:421–435. https://doi.org/10. 1016/j.atmosres.2010.01.014

Castro A, Calvo AI, Alves C, Alonso-Blanco E, Coz E, Marques L, Nunes T, Fernández-Guisuraga JM, Fraile R (2015) Indoor aerosol size distributions in a gymnasium. Sci Total Environ 524–525:178– 186. https://doi.org/10.1016/j.scitotenv.2015.03.118

Chaloulakou A, Kassomenos P, Spyrellis N, Demokritou P, Koutrakis P (2003) Measurements of PM_{10} and $PM_{2.5}$ particle concentrations in Athens, Greece. Atmos Environ 37:649–660

Cheng Y, Lee S, Gu Z, Ho K, Zhang Y, Huang Y, Chow JC, Watson JG, Cao J, Zhang R (2015) $PM_{2.5}$ and $PM_{10\text{-}2.5}$ chemical composition and source apportionment near a Hong Kong roadway. Particuology 18:96–104. https://doi.org/10.1016/j.partic.2013.10.003

Cyrys J, Pitz M, Heinrich J, Wichmann HE, Peters A (2008) Spatial and temporal variation of particle number concentration in Augsburg, Germany. Sci Total Environ 401:168–175. https://doi.org/10.1016/ j.scitotenv.2008.03.043

Deshmukh DK, Deb MK, Mkoma SL (2013) Size distribution and seasonal variation of size-segregated particulate matter in the ambient air of Raipur city, India. Air Qual Atmos Heal 6:259–276. https:// doi.org/10.1007/s11869-011-0169-9

Dunn OJ (1964) Multiple comparisons using rank sums. Technometrics 6:241–252. https://doi.org/10.1080/00401706.1964.10490181

Gerasopoulos E, Kouvarakis G, Babasakalis P et al (2006) Origin and variability of particulate matter (PM_{10}) mass concentrations over the Eastern Mediterranean. Atmos Environ 40:4679–4690. https:// doi.org/10.1016/j.atmosenv.2006.04.020

Gomišček B, Hauck H, Stopper S, Preining O (2004) Spatial and temporal variations of PM1, PM2.5, PM10 and particle number concentration during the AUPHEP—project. Atmos Environ 38:3917–3934. https://doi.org/10.1016/j.atmosenv.2004.03.056

Goudie A (2014) Desert dust and human health disorders. Environ Int 63: 101–113. https://doi.org/10.1016/j.envint.2013.10.011

Gugamsetty B, Wei H, Liu CN et al (2012) Source characterization and apportionment of PM_{10}, $PM_{2.5}$ and $PM_{0.1}$ by using positive matrix factorization. Aerosol Air Qual Res 12:476–491. https://doi.org/10. 4209/aaqr.2012.04.0084

Held A, Zerrath A, Mckeon U et al (2008) Aerosol size distributions measured in urban, rural and high-alpine air with an electrical low pressure impactor (ELPI). Atmos Environ 42:8502–8512. https:// doi.org/10.1016/j.atmosenv.2008.06.015

Hieu NT, Lee BK (2010) Characteristics of particulate matter and metals in the ambient air from a residential area in the largest industrial city in Korea. Atmos Res 98:526–537. https://doi.org/10.1016/j. atmosres.2010.08.019

Hussein T, Puustinen A, Aalto PP, Mäkelä JM, Hämeri K, Kulmala M (2003) Urban aerosol number size distributions. Atmos Chem Phys Discuss 3:5139–5184. https://doi.org/10.5194/acpd-3-5139-2003

International Organization for Standarization (ISO) (1995) ISO 7708: 1995 (E): air quality—particle size fraction definitions for health related sampling. ISO publications, 1st edition, 1995-04-01

Jacob D (1999) Introduction to atmospheric chemistry. Princeton University Press

Johansson C, Norman M, Gidhagen L (2007) Spatial & temporal variations of PM_{10} and particle number concentrations in urban air. Environ Monit Assess 127:477–487. https://doi.org/10.1007/ s10661-006-9296-4

Khanum F, Chaudhry MN, Kumar P (2017) Characterization of five-year observation data of fine particulate matter in the metropolitan area of Lahore. Air Qual Atmos Heal 10:725–736. https://doi.org/10.1007/ s11869-017-0464-1

Kim KH, Kabir E, Kabir S (2015) A review on the human health impact of airborne particulate matter. Environ Int 74:136–143. https://doi. org/10.1016/j.envint.2014.10.005

Kim YJ, Boatman JF (1990) Size calibration corrections for the active scattering aerosol spectrometer probe (ASASP-100X). Aerosol Sci Technol 12:665–672. https://doi.org/10.1080/02786829008959381

Kim Oanh NT, Upadhyay N, Zhuang YH, Hao ZP, Murthy DVS, Lestari P, Villarin JT, Chengchua K, Co HX, Dung NT (2006) Particulate air pollution in six Asian cities: spatial and temporal distributions, and associated sources. Atmos Environ 40:3367–3380. https://doi.org/ 10.1016/j.atmosenv.2006.01.050

Klejnowski K, Krasa A, Rogula-Kozłowska W, Błaszczak B (2013) Number size distribution of ambient particles in a typical urban site: the first polish assessment based on long-term (9 months) measurements. Sci World J 2013:1–13. https://doi.org/10.1155/2013/539568

Kruskal WH, Wallis WA (1952) Use of ranks in one-criterion variance analysis. J Am Stat Assoc 47:583–621. https://doi.org/10.1080/ 01621459.1952.10483441

Kuzu SL (2016) Compositional variation of PCBs, PAHs, and OCPs at gas phase and size segregated particle phase during dust incursion from the Saharan Desert in the Northwestern Anatolian Peninsula. Adv Meteorol 2016:1–12. https://doi.org/10.1155/2016/7153286

Kuzu SL, Saral A (2017) The effect of meteorological conditions on aerosol size distribution in Istanbul. Air Qual Atmos Heal 10: 1029–1038. https://doi.org/10.1007/s11869-017-0491-y

Lelieveld J, Evans JS, Fnais M, Giannadaki D, Pozzer A (2015) The contribution of outdoor air pollution sources to premature mortality on a global scale. Nature 525:367–371. https://doi.org/10.1038/ nature15371

Lonati G, Crippa M, Gianelle V, Van Dingenen R (2011) Daily patterns of the multi-modal structure of the particle number size distribution in Milan, Italy. Atmos Environ 45:2434–2442. https://doi.org/10.1016/ j.atmosenv.2011.02.003

Lyamani H, Olmo FJ, Alados-Arboledas L (2005) Saharan dust outbreak over southeastern Spain as detected by sun photometer. Atmos Environ 39:7276–7284. https://doi.org/10.1016/j.atmosenv.2005.09.011

Monsalve F, Tomás C, Fraile R (2013) Influence of meteorological parameters and air pollutants onto the morbidity due to respiratory diseases in Castilla-La Mancha, Spain. Aerosol Air Qual Res 13: 1297–1312. https://doi.org/10.4209/aaqr.2012.12.0348

Morawska L, Salthammer T (2004) Indoor environment: airborne particles and settled dust. Wiley-VCH Verlag GmbH & Co. KGaA, Weinhelim

Pascal M, Falq G, Wagner V, Chatignoux E, Corso M, Blanchard M, Host S, Pascal L, Larrieu S (2014) Short-term impacts of particulate matter (PM_{10}, $PM_{10-2.5}$, $PM_{2.5}$) on mortality in nine French cities. Atmos Environ 95:175–184. https://doi.org/10.1016/j.atmosenv. 2014.06.030

Pérez N, Pey J, Querol X, Alastuey A, López JM, Viana M (2008) Partitioning of major and trace components in PM_{10}–$PM_{2.5}$– PM_1 at an urban site in Southern Europe. Atmos Environ 42: 1677–1691. https://doi.org/10.1016/j.atmosenv.2007.11.034

Pope CA, Dockery DW (2006) Health effects of fine particulate air pollution: lines that connect. J Air Waste Manage Assoc 56:709–742. https://doi.org/10.1080/10473289.2006.10464485

Puustinen A, Hämeri K, Pekkanen J, Kulmala M, de Hartog J, Meliefste K, ten Brink H, Kos G, Katsouyanni K, Karakatsani A, Kotronarou A, Kavouras I, Meddings C, Thomas S, Harrison R, Ayres JG, van der Zee S, Hoek G (2007) Spatial variation of particle number and mass over four European cities. Atmos Environ 41:6622–6636. https://doi.org/10.1016/j.atmosenv.2007.04.020

Querol X, Alastuey A, Viana MM, Rodriguez S, Artiñano B, Salvador P, Garcia do Santos S, Fernandez Patier R, Ruiz CR, de la Rosa J, Sanchez de la Campa A, Menendez M, Gil JI (2004) Speciation and origin of PM_{10} and $PM_{2.5}$ in Spain. J Aerosol Sci 35:1151–1172. https://doi.org/10.1016/j. jaerosci.2004.04.002

Rashki A, Rautenbach CJ d W, Eriksson PG, Kaskaoutis DG, Gupta P (2013) Temporal changes of particulate concentration in the ambient air over the city of Zahedan, Iran. Air Qual Atmos Heal 6:123–135. https://doi.org/10.1007/s11869-011-0152-5

Reizer M, Juda-Rezler K (2016) Explaining the high PM_{10} concentrations observed in Polish urban areas. Air Qual Atmos Heal 9:517–531. https://doi.org/10.1007/s11869-015-0358-z

Ren-Jian Z, Kin-Fai H, Zhen-Xing S (2012) The role of aerosol in climate change, the environment, and human health. Atmos Ocean Sci Lett 5:156–161. https://doi.org/10.1080/16742834.2012.11446983

Salvador P, Artíñano B, Viana MM, Querol X, Alastuey A, González- Fernández I, Alonso R (2011) Spatial and temporal variations in PM_{10} and $PM_{2.5}$ across Madrid metropolitan area in 1999-2008. Procedia Environ Sci 4:198–208. https://doi.org/10.1016/j.proenv. 2011.03.024

Samek L, Stegowski Z, Furman L, Fiedor J (2017) Chemical content and estimated sources of fine fraction of particulate matter collected in Krakow. Air Qual Atmos Heal 10:47–52. https://doi.org/10.1007/ s11869-016-0407-2

Samet J, Dominici F, Curriero F et al (2000) Fine particulate air pollution and mortality in 20 U.S. cities, 1987-1994. N Engl J Med 343:1742–1749

Stanier CO, Khlystov AYAY, Pandis SN (2004) Ambient aerosol size distributions and number concentrations measured during the Pittsburgh Air Quality Study (PAQS). Atmos Environ 38:3275–3284. https://doi.org/10.1016/j.atmosenv.2004.03.020

Tan WC, Qiu D, Liam BL et al (2000) The human bone marrow response to acute air pollution caused by forest fires. Am J Respir Crit Care Med 161:1213–1217. https://doi.org/10.1164/ajrccm.161.4.9904084

Wehner B, Wiedensohler A (2002) Long term measurements of submicrometer urban aerosols: statistical analysis for correlations with meteorological conditions and trace gases. Atmos Chem Phys Discuss 2:1699–1733. https://doi.org/10.5194/acpd-2-1699-2002

Wilson WE, Suh HH (1997) Fine particles and coarse particles: concentration relationships relevant to epidemiologic studies. J Air Waste Manage Assoc 47:1238–1249. https://doi.org/10.1080/10473289. 1997.10464074

Woo KS, Chen DR, Pui DYH, McMurry PH (2001) Measurement of Atlanta aerosol size distributions: observations of ultrafine particle events. Aerosol Sci Technol 34:75–87. https://doi.org/10.1080/ 027868201300082049

Wu Z, Hu M, Lin P, Liu S, Wehner B, Wiedensohler A (2008) Particle number size distribution in the urban atmosphere of Beijing, China. Atmos Environ 42:7967–7980. https://doi.org/10.1016/j.atmosenv. 2008.06.022

Zhang KM, Wexler AS (2004) Evolution of particle number distribution near roadways—Part I: analysis of aerosol dynamics and its implications for engine emission measurement. Atmos Environ 38:6643– 6653. https://doi.org/10.1016/j.atmosenv.2004.06.043

Zhang KM, Wexler AS, Zhu YF, Hinds WC, Sioutas C (2004) Evolution of particle number distribution near roadways. Part II: the "Road-to- Ambient" process. Atmos Environ 38:6655–6665. https://doi.org/10.1016/j.atmosenv.2004.06.044

7

UNUSUAL WINTER SAHARAN DUST INTRUSIONS AT NORTHWEST SPAIN: AIR QUALITY, RADIATIVE AND HEALTH IMPACTS

Published in: Science of the Total Environment 669 (2019) 213–228

7.1. INTRODUCTION

The Intergovernmental Panel on Climate Change (IPCC) fourth assessment report suggests that one of the major natural sources of particles is mineral dust, which comes from dry continental areas. Moreover, the acceleration of the desertification process in arid regions, due to climate change, can result in a rise of dust outbreaks (IPCC, 2014).

Desert dust outbreaks represent a high risk to human health and can cause respiratory and cardiovascular disorders (Goudie, 2014; Jiménez et al., 2010; Stafoggia et al., 2015; Tobías et al., 2011). The effect of particles from mineral dust is related to their chemical composition and size (Díaz et al., 2017; Griffin, 2007; López-Villarrubia et al., 2012; Perez et al., 2008). Depending on their size, they can reach different parts of the respiratory system (ISO, 1995) and, consequently, cause different effects on the human health (Fubini and Otero Areán, 1999). Besides, desert dust is mainly composed of calcite ($CaCO_3$), dolomite ($CaMg(CO_3)_2$), quartz (SiO_2) and clay minerals (Calvo et al., 2013; Caquineau et al., 1998; Coz et al., 2009; Glaccum and Prospero, 1980; Guerzoni et al., 1997; Schütz and Sebert, 1987), which are related to asthma and silicosis (Fubini and Otero Areán, 1999).

The high exposure risk during outbreaks is also associated with the biological material mixed with the dust (Garrison et al., 2006; Griffin, 2007; Griffin et al., 2001; Polymenakou et al., 2007). Dust storms can transport bacteria, pollen spores, fungi and viruses, which are capable of surviving long-range transport (Tomadin et al., 1989). The presence of this biological material in small size particles have a potential implication on human health, and may have direct incidence in diseases as meningococcal meningitis and coccidioidomycosis (Goudie, 2014; Polymenakou et al., 2007).

African dust is one of the natural causes of the exceedances of the PM_{10} daily limit value (DLV, 50 μg m^{-3} set by the Directive 2008/50/ EC) in the Iberian Peninsula (Escudero et al., 2007;

Nicolás et al., 2008; Querol et al., 2004a; Salvador et al., 2013). Studies carried out by Alastuey et al. (2016) between 2012 and 2013 in different European cities show that, during dust outbreaks, southern and eastern countries have the most elevated concentrations of mineral dust (20–40% of PM_{10}), due to the proximity to the dust sources. The magnitude of these events depends on several factors (surface wind speed, vegetation cover, soil texture and moisture).

Spain is frequently affected by Saharan dust outbreaks, due to its proximity to large emitting areas (Sahara and Sahel desert) and the meteorological and dynamical characteristics of the atmosphere (Alastuey et al., 2016; Escudero et al., 2007; Querol et al., 2014; Rodríguez et al., 2001). Southern cities are more affected than northern ones (Viana et al., 2014). Stafoggia et al. (2015) and Nicolás et al. (2008) reported an increase in the PM_{10} mass concentrations during dust outbreak episodes in southern and southeastern Spain, with a contribution of mineral dust between 5 and 40% of the total PM_{10} mass. Moreover, Querol et al. (2004a) showed that the African dust outbreaks are less frequent in the north of Spain than in the south, with an average of 6 and 17 episodes per year, respectively. Most of these events occur between spring and summer, when the dust transportation is governed by the anticyclonic activities over the east or southeast of Iberian Peninsula (Lyamani et al., 2015; Rodríguez et al., 2001; Salvador et al., 2013), with a mean duration of 5–19 days in the south and < 4 days in the north of Spain (Querol et al., 2004a). In winter, Saharan dust intrusions are scarce and usually do not reach the northwest of the peninsula. Furthermore, they are governed by the cyclonic activities over the west or south of Portugal (Díaz et al., 2017; Rodríguez et al., 2001). These episodes are characterized by a short duration (between 2 and 5 and < 4 days in the south and the north of Spain, respectively) (Querol et al., 2004a). The MAPAMA (Ministry of Agriculture and Fisheries, Food and Environment) network reported that between 2005 and 2017 there was an average of 14 events of dust intrusion per year that could have reached the north of the peninsula. Most of these events are registered in summer and spring (average of 5 per year), with a mean duration of 3 days in both seasons. Winter is the season that registers the fewest number of events (average of 2 per year) with a mean duration of 3 days. Regarding to the Saharan dust intrusions that could have reached León between 2005 and 2017, the air quality network of Castilla and León (http://www.medioambiente.jcyl.es/) shows that, approximately, 11% of these events caused an exceedance of the PM_{10} DLV, and on average the PM_{10} levels during the dust outbreaks were between 29 ± 10 μg m^{-3} in summer and 39 ± 13 μg m^{-3} in winter.

There are many studies about the harmful effects of the Saharan intrusions on the Iberian Peninsula, especially in southern cities, but most of them are focused on summer events. However, the studies of winter intrusions and their effects on human health in the north of Spain are scarce. The identification of African events allows determining the contribution of Saharan episodes to the total PM_{10} mass, and the study of these episodes through different disciplines leads to a more comprehensive characterization and a better understanding for the establishment of future mitigation measures. Thus, based on the analyzes of two African dust intrusions in winter 2016 and 2017, which reached the north of Spain, we focus our study on a descriptive understanding of these events including: i) typical synoptic conditions; ii) aerosol chemical composition; iii) particle size distribution; iv) pollen concentration; v) aerosol optical depth; vi) radiative impact and vii) estimation of the impact of aerosols on respiratory tract.

7.2. STUDY AREA

The study was carried out in León city, Spain, located in the northwest of the Iberian Peninsula, at the University of León (42° 36′ 50″ N, 5° 33′ 38″ W, 846 m asl) (Fig. 7.1) in two different periods: i) between 20 and 23 February 2016 and ii) between 21 and 24 February 2017. The city is characterized by the absence of large industries, whilst traffic is considered the main source of particles. The climate in this region is Mediterranean type with continental features, with annual mean temperature of 10.9 °C. Rain events occur irregularly over the year, with minimum precipitation values in summer (80 mm) and maximum values in fall (190 mm). Winters are cold with frequent frosts (74 frost days per year, on average) (Castro et al., 2010).

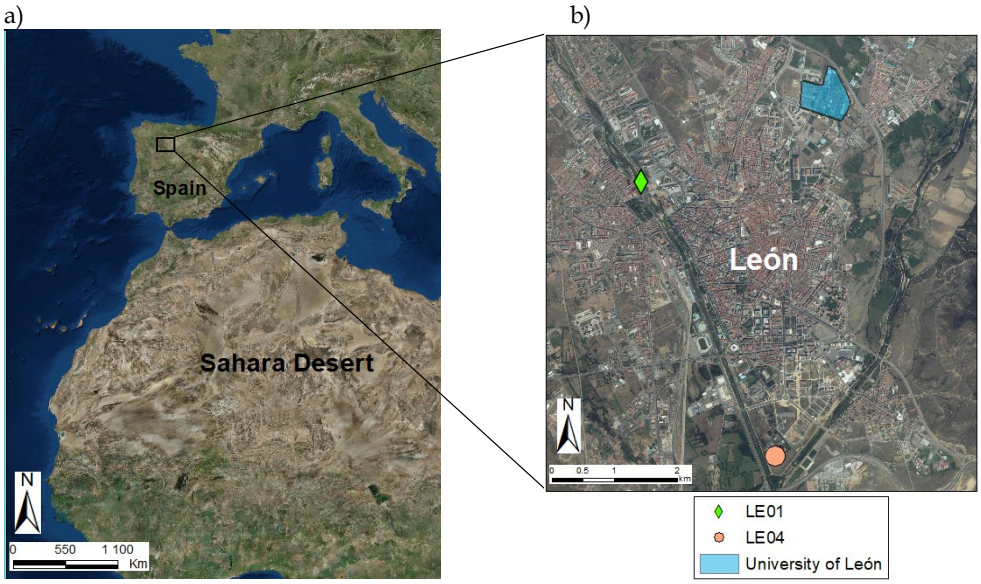

FIG. 7.1. a) Sahara Desert and region of León (Spain) identified by a black square box; b) León city with the location of the sampling sites and the University of León.

In February, due to the climatic and floristic characteristics of León city, there are a few pollen types present in the atmosphere, which come from the release of arboreal plants flowering in winter and pre-spring, such as *Alnus*, *Corylus*, *Cupressaceae*, *Fraxinus* and Poaceae (residual). Alder (*Alnus glutinosa*) and hazel (*Corylus avellana*) are part of the natural vegetation of deciduous forest that is about 30 km north of the city. Pollens from these species can be scarce in the atmosphere. The presence of pollen of a large number of species of cypresses and arizonicas (*Cupressaceae*) is very abundant in León, because they are usually used as ornamental trees due to their resistance to extreme climatic conditions. In addition, at the end of February the ash (*Fraxinus excelsior*) pollen begins to appear, which come from the natural vegetation of riverbanks and some parks of León (Oduber et al., 2019).

7.3. MATERIALS AND METHODS

7.3.1. Sampling instruments

During both sampling campaigns, several continuous measurements were made using different instruments:

- The particle size distributions were measured continuously every minute using a passive cavity aerosol spectrometer probe (PCASP-X, manufactured by Particle Measuring Systems, Inc., PMS) in a range between 0.1 and 10 µm (latex equivalent) in 31 channels. The corrections related to the refractive index and relative humidity were made as explained in previous works (Calvo et al., 2010; Castro et al., 2015, 2018). The accuracy for PCASP measurements is between 16% (concentration) and 20% (diameter)[1]. Additionally, a scanning mobility particle sizer (TSI-SMPS Model 3938: DMA 3081 and CPC 3772) for the continuous sampling (on a 6-min basis) of the submicrometer particles ranging from 14.6 to 791.5 nm, in 112 channels, was used, taking into account the corrections according to Wiedensohler et al. (2012). The uncertainties in the concentration of the measured size distributions are assumed to be 10% from 20 to 200 nm, while above this size range it increases to 30% (Wiedensohler et al., 2012).

- Data from an AE-31 aethalometer (Magee Scientific) with a precision of 10^{-3} µg m^{-3} (Blanco-Alegre et al., 2019) were used to estimate the iron content from aerosol dust (on a 2-minute basis) by the two component model detailed in Fialho et al. (2006). The load correction model proposed by Weingartner et al. (2003) was used. Considering scattering measurements were not available for the experiment, the best approximation for *f* (describing the shadowing effect) were taken from the winter values proposed in Sandradewi et al. (2008).

- For pollen monitoring, a volumetric Hirst-type spore-trap (Lanzoni VPPS 2000) was used. Daily and hourly pollen counts were made using optical microscopy for the identification of pollen and spores, following the method recommended by the Spanish Aerobiological Network and fulfilling the aerobiological quality requirements of the European Aerobiology Society (Galán Soldevilla et al., 2007). The estimated uncertainties associated with the pollen measurements, under the working conditions, was about 10% (Oteros et al., 2017; UNI 11108:2004, 2004).

Furthermore, for the event of 2016, the optical properties of aerosols along the atmospheric vertical path, were measured with a Cimel CE318 Sun/Sky Photometer. The calibration of the direct component was performed using the Langley method during a period with stable and low atmospheric turbidity conditions. The irradiance calibration uncertainty is 1–2%, depending on the channel (Holben et al., 1998). The aerosol optical depth (AOD) was retrieved by ESR.PACK code, which is based on the SKYRAD.PACK algorithm (Takamura and Nakajima, 2004). The AOD retrieved by ESR.PACK is comparable to the retrieval of the Aerosol Robotic Network (AERONET) of NASA, with mean deviation values between −0.0030 and +0.0041 (0.012 in the case of AOD at 340 nm) (Estellés et al., 2012). The absolute error for AOD retrieval with the Cimel sun photometer within AERONET protocols is 0.01–0.02 (Holben et al., 1998). The Ångström exponent (AE, dimensionless), as indicator of the average particle size, was calculated using AOD at 440 and 870 nm.

During the event of February 2017, three simultaneous 24 h samplings of PM_{10} were carried out, starting at 1200 UTC. Two of them, by means of two low volume samplers, TECORA ECHOPM operated with 47 mm diameter teflon filters and a Gent PM_{10} stacked filter unit sampler operating with 47 mm diameter polycarbonate filters (0.2 µm pore size). The third sample was

[1] https://www.esrl.noaa.gov/gmd/aero/instrumentation/pcasp100.html (accessed 12.12.18)

taken by a high-volume sampler (CAV-A/Mb) equipped with a 150 mm diameter quartz filter. The dates of the filters refer to the beginning of the sampling (from 1200 UTC of that day to 1200 UTC of the next day).

7.3.2. Analytical methodologies

Quartz filters were used for the quantification of PM_{10} by gravimetry using an electronic microbalance (Mettler Toledo, XPE105DR) and for the determination of organic and elemental carbon (OC and EC, respectively) by a thermo-optical technique developed by the University of Aveiro, Portugal (Alves et al., 2015; Pio et al., 2011). The calculated uncertainties of concentrations measured by this analytical method ranged between 5 and 10%.

The quantification of water-soluble inorganic ions (Na^+, K^+, Ca^{2+}, Mg^{2+}, NH^+, Cl^-, SO_4^{2-}, NO_3^- and NO_2^-) was carried out using the solution obtained after extracting half of the teflon filters with 6 mL of ultrapure deionized water, and subsequently analyzed in a Thermo Scientific Dionex™ ICS-5000 Ion Chromatograph. The other half of the teflon filters were used for the determination of the major trace elements by PIXE (Particle-Induced X-ray Emission), following the methodology described by Lucarelli et al. (2015). The estimated uncertainties for the ion chromatography and PIXE measurements are dependent on the analyzed element and their limits of detection. These uncertainties can range from 2% to 20% in PIXE and between 5 and 10% in ion chromatography (Lucarelli et al., 2015).

The morphology and elemental composition of individual aerosol particles collected on the polycarbonate filters were investigated by Field Emission Scanning Electron Microscopy (FE-SEM) using a Tabletop Microscope Hitachi TM-100 and a Digital Scanning Microscope DSM950.

7.3.3. Additional databases and statistical treatment

Additional data (PM_{10} and SO_2) from two air quality stations belonging to the regional air quality network (http://www.medioambiente. jcyl.es/) were used: the urban traffic station LE01 is located in an urban residential area in San Ignacio de Loyola Avenue (05° 35' 14" W 42° 36' 14" N) and the suburban/background station LE04, located in Coto escolar (05° 33' 59" W 42° 34' 31" N) (Fig. 7.1), which is not directly influenced by vehicular, industrial or residential emissions. The data were recorded from 0000 UTC of the sampling day to 0000 UTC of the next day.

Furthermore, meteorological parameters such as temperature, relative humidity, precipitation, wind speed and direction were recorded by an automatic weather station located in the sampling site.

The origin of air masses during the study period was interpreted by the determination of daily 3-day back trajectories (at 500, 1500 and 3000 m agl) using the HYSPLIT model (Draxler and Rolph, 2012; Rolph et al., 2017; Stein et al., 2015). The Spanish Meteorological Agency (AEMET) provided visibility and diffuse and direct radiation data for the studied period.

The statistical treatment has been carried out using the SPSS software (IBM Statistics Software V. 24). The correlation between pollutant concentrations was made using the

nonparametric Pearson correlation method. The Kruskal-Wallis non-parametric test (Kruskal and Wallis, 1952), followed by the Dunn, 1964 test, was applied to the data in order to find statistically significant differences.

7.3.4. Estimation of the aerosol clear sky radiative forcing

The aerosol clear sky radiative forcing has been estimated using the discrete ordinate Radiative Transfer Model Global Atmospheric ModEl (RTM GAME) (Dubuisson et al., 2004, 1996). Upward and downward net radiative fluxes are calculated over the entire short-wave region and are performed at every 3 h interval and for the whole study period with and without aerosols. From these fluxes, we computed the aerosol clear sky daily direct forcing at the bottom of atmosphere (ΔF_{BOA}) and at the top of the atmosphere (ΔF_{TOA} - 20 km in this case). With the considered convention here, a positive sign of ΔF_{BOA} and ΔF_{TOA} indicates an aerosol warming effect. The atmospheric forcing ΔF_{ATM} was estimated through the difference between the top and bottom aerosol direct forcing; it represents the possible absorption of solar radiation due to absorbing particles within the atmospheric specified aerosol layers. An important point for estimating the direct forcing of aerosols is their vertical profile within the atmosphere and associated optical properties. The single scattering albedo (*SSA*), asymmetry parameter (*g*) and extinction coefficient profiles were also determined with the same methodology as described by Calvo et al., (2010). Vertical profiles of atmospheric properties such as relative humidity, temperature, pressure and ozone concentrations have been measured through radiosoundings available at National Oceanic and Atmospheric Administration (NOAA) for the whole study period.

7.3.5. Estimation of the health impacts: deposition of particles in respiratory tract regions

Following the Spanish standard UNE (1997) (equivalent to ISO, 1995), the aerosol size fractions deposited in respiratory tract regions (inhalable, thoracic, tracheobronchial and respirable) were estimated considering the following parameters: i) the number of particles in each channel of the PCASP-X and SMPS; ii) the aerodynamic diameter corresponding to these channels and iii) the estimated aerosol density (Alonso-Blanco et al., 2018; Castro et al., 2015, 2018; Morawska and Salthammer, 2003).

7.4. RESULTS AND DISCUSSIONS

7.4.1. Synoptic conditions and meteorological considerations

On 19 February 2016, the anticyclone of the Azores extended its influence on the Iberian Peninsula, with isobars up to 1028 hPa on the area of study. The peninsular south started to be affected by the relative low pressures from North Africa. At 500 hPa (charts not shown here), a trough centered on the peninsula was observed. On 20 February (Fig. 7.2a) African air continued entering the peninsular south, both at ground (isobars of 1024 hPa) and at 500 hPa, and there was a parcel of colder air coming from the rupture of the previous day trough. The Atlantic anticyclone influenced the rest of the Peninsula with a center of high pressure (1032 hPa) very close to the study area. This center was intensified (up to 1034 hPa) and moved towards northeast on the next

day, allowing the mass of African air to advance from the south, and reaching the peninsular latitude. At 500 hPa level, the air parcel located in the NE of the Canary Islands favored this African air intake.

The surface map on 22 February 2016 (Fig. 7.2b), presents the temporary retreat of the Atlantic anticyclone, together with the connection of a center of high pressures on the Northern Peninsula with a center of relative low-pressure placed on the Gulf of Cadiz. The same situation is observed at 500 hPa. As a result, African air continued entering directly into Iberia and towards higher latitudes. Finally, from 23 February, the peninsular high-pressure system moved towards the south, up to the north of Africa, and the influence of the Azores Anticyclone affected again the whole Peninsula, causing winds from north or northeast that opposed the entry of African air, hence the disappearance of the air parcel located to the SW of the Peninsula.

On 21 February 2017 (Fig. 7.2c) a clear influence of the anticyclone of the Azores on the northern half of the peninsula was observed, while the southern half became affected by the airflow caused by the low pressures located to the north of Africa, which is also observed at 500 hPa level (chart not shown here). This situation remained almost unchanged in the surface chart of the next day, although the anticyclonic influence had weakened, and the relative low-pressure system had moved towards the Gulf of Cadiz, thus maintaining the entry of African air into the peninsular South.

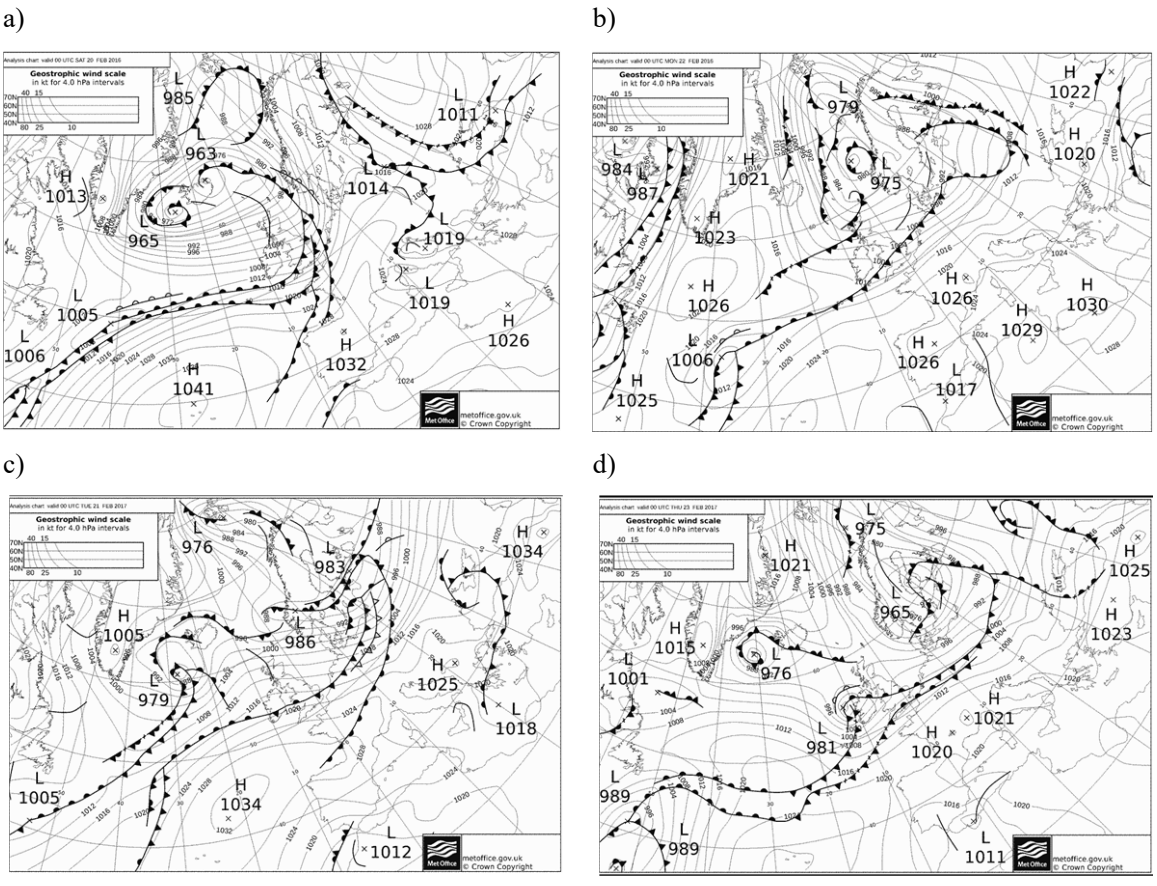

FIG. 7.2. Synoptic charts (surface pressure) for 20 and 22 February 2016 a) and b), 21 and 23 February 2017 c) and d).

The isobaric configuration of Thursday, 23 February 2017 (Fig. 7.2d), evidences the rupture of the anticyclonic influence as a result of a barometric swamp (or flat low) located in the peninsular North that facilitated the movement of the Saharan air towards higher latitudes, pushed by the air movement around the low of the North African. Therefore, the airflow from North Africa continued both in surface and in height. Nevertheless, this lack of definition in the isobars did not last long: the day after, the Atlantic anticyclone advanced on the Bay of Biscay and the anticyclonic influence returned to the peninsula, with wind flow from northeast. Simultaneously, a cold front advanced from north, resulting in a change in the air mass arriving to the study area. This situation became stable on the following day, when an anticyclone center appeared on the Bay of Biscay, with a wide influence over the entire Iberian Peninsula, thus preventing the entrance of African air from south.

The HYSPLIT model allows evidencing the arrival of air masses coming from North Africa in both events (Fig. 7.3) and the NAAPs model shows the dust load over Iberia on 22 February 2016 (Fig. 7.3c) and 23 February 2017 (Fig. 7.3d). Furthermore, an increase in the temperature and a decrease in the relative humidity, on 22 February 2016 (+1 °C and −10%, respectively) and on 23 February 2017 (+3 °C and −23%, respectively), were registered. The meteorological data recorded at the sampling point showed that the mean temperature and relative humidity for February 2016 and 2017 in León were 5 ± 4 °C and 76 ± 16%, respectively.

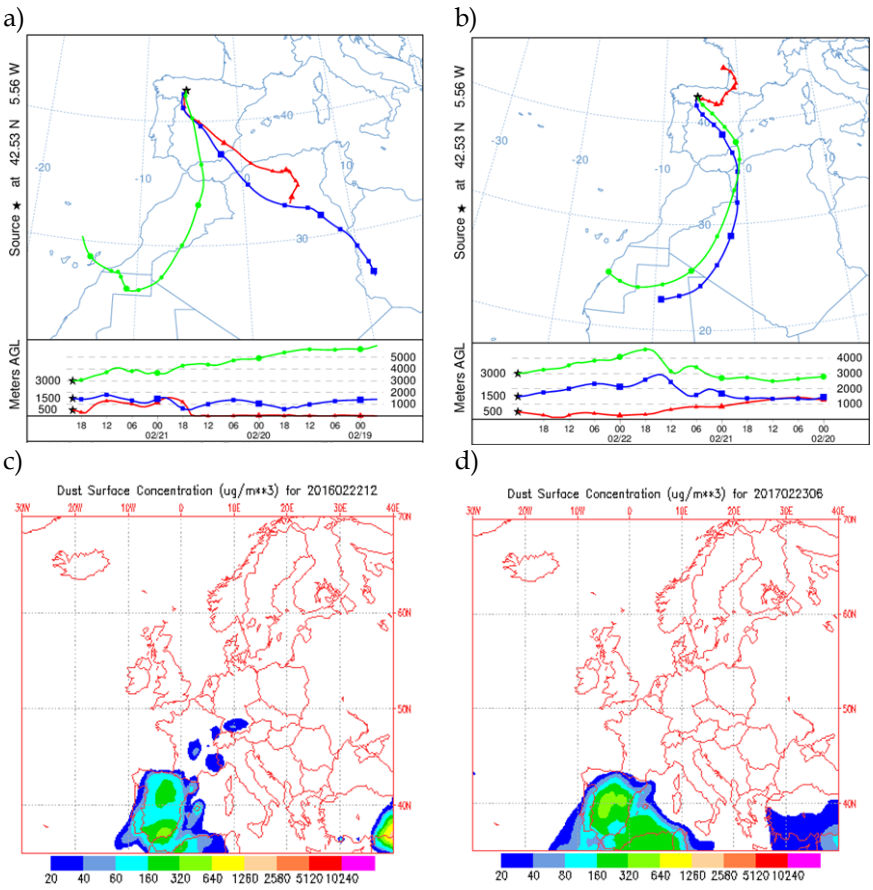

FIG. 7.3. a) HYSPLIT back trajectories at 500, 1500 and 3000 m agl on a) 22 February 2016 at 2000 UTC and c) 21 February 2017 at 0000 UTC, and NAAPs images of dust concentration on c) 22 February 2016 at 1200 UTC and d) 23 February 2017 at 0600 UTC.

7.4.2. Impact on particulate matter

7.4.2.1. PM_{10}

Over the course of 21 and 22 February 2016, a progressive increase in the PM_{10} concentration was observed in the stations LE01 and LE04, reaching the maximum hourly value on 22 February between 1200 and 1400 UTC, with 113 μg m^{-3} and 75 μg m^{-3}, respectively. The DLV was exceeded on 22 February 2016 (daily mean of 52 μg m^{-3} in station LE01). The Kruskal-Wallis test (Kruskal and Wallis, 1952) shows that there were significant differences ($p < 0.05$) between mean PM_{10} values in the previous days (mean hourly concentration between 20 at 0000 UTC and 21 at 0800 UTC of 22 ± 18 μg m^{-3}) and during (mean hourly concentration between 21 at 0900 UTC and 23 at 0900 UTC of 41 ± 27 μg m^{-3}) the Saharan dust intrusion. This unusual episode was also studied by Titos et al. (2017) in Northeastern Spain. They reported an exceedance of PM_{10} DLV in 90% of the 250 air quality stations across Iberia and Balearic Islands on 22 February, as in this work. Also, from the gravimetric analysis, they registered a daily PM_{10} mass concentration of 97 μg m^{-3} on 23 February 2016 in Montsec, in the NE of the peninsula, and found that 80% of the PM_{10} mass was from mineral origin.

Regarding the dust intrusion event of February 2017, an increase in the PM_{10} level was observed between 22 February at 2000 UTC and 24 February 2017 at 0900 UTC in both air quality stations, LE01 and LE04 (Fig. 7.4), reaching a maximum value of 156 μg m^{-3} on 23 February at 1200 UTC (data from station LE01). On 23 February, the PM_{10} DLV was exceeded (daily mean 86 μg m^{-3} was recorded at station LE01). This concentration was more than three times the value measured in days without intrusion (26 ± 14 μg m^{-3}). The Kruskal and Wallis test showed significant differences ($p < 0.05$) between PM_{10} values in days before and during the Saharan dust intrusion.

On 20 February 2016, and 21 February 2017, before the Saharan dust plumes reached León city, important increases in PM_{10}, accompanied by an increase in the SO_2 concentrations (Fig. 7.4a and c), were observed. However, these peaks were not registered by the station LE04 (Fig. 7.4b and d). The station LE01 is located in an urban area, where the emissions from traffic and domestic heating devices (including coal combustion appliances, emitting SO_2) are important and can trigger the PM_{10} levels causing the exceedance of the DLV.

Due to the particularity of both studied events, and in order to establish the differences and similarities between those and other dust events that reached the Iberian Peninsula, a brief comparison and analysis has been carried out in this section. Table 7.1 shows several dust episodes, which may have affected the air quality of different cities in Spain.

As observed in Table 7.1, the PM_{10} DLV is not usually exceeded during intrusion events in the city of León. This fact gives more importance to the extremely unusual behavior observed during the dusty period of February 2016 and 2017, which reached PM_{10} values even more higher than those observed in summer or spring Saharan outbreaks in this city. The intrusion event of 2017 also showed a higher intensity compared with that of 2016, showing a PM_{10} similar to that reported by Artíñano et al. (2003), Escudero et al. (2007) and Rodríguez et al. (2001) during summer and spring dust intrusions. Due to the proximity of the dust source, southern regions of Spain are more affected than northern regions by dust outbreaks (about 200 km and 800 km far

from North Africa, respectively), as observed by Rodríguez et al. (2001) and Titos et al. (2017), who reported values of PM_{10} higher than 100 µg m^{-3} in different winter Saharan dust intrusions in contrast with those observed in northern locations were the PM_{10} levels do not reach such concentration.

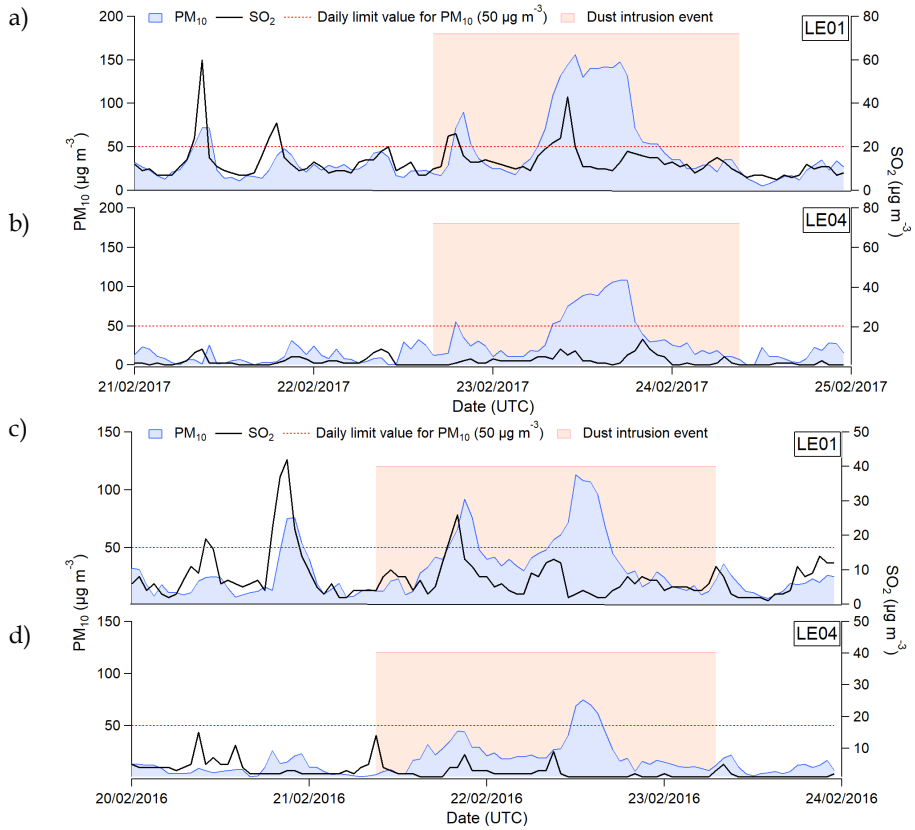

FIG. 7.4. Hourly evolution of PM_{10} and SO_2 during the 2016 and 2017 Saharan dust outbreaks at LE01 [a) and c)] and LE04 [b) and d)].

7.4.2.2. OC and EC

The evolution of the carbonaceous fraction before and during Saharan dust intrusions of 2017, is not well defined. Taken into account the quartz filters samples between 18 and 21 February as before the intrusion, and between 23 and 24 as during the Saharan dust intrusion, the following results were observed: the carbonaceous (OC + EC) fraction barely change during the dust intrusion, going from 16 ± 4% to 8% of PM_{10} mass; organic carbon (OC) concentration slightly increase, from mean concentrations of 2.3 ± 0.6 to 4.2 µg m^{-3}, before and during the dust event, respectively; elemental carbon (EC) concentration do not show a significant change during the Saharan intrusion (0.7 ± 0.3 and 0.8 µg m^{-3} in days without and with Saharan dust outbreaks, respectively). Some authors as Aymoz et al. (2004) and Putaud et al., (2000) reported an increase in the OC concentration associated with mineral dust, during summer Saharan dust outbreaks in France in 2000 and Tenerife Island in 1997, respectively. This increase is probably due to the contribution of hundreds of organic compounds transported during these events. The low variability of EC concentration during the dust outbreak may indicate that the dust cloud was not mixed with anthropogenic sources during the transport (Fig. 7.3), which could have caused an increase in EC concentrations. Thus, the EC signature is linked to the influence of local sources.

TABLE 7.1. Maximum PM_{10} concentration and duration in days of different Saharan dust events that affected the Iberian Peninsula. Values not exceeding DLV are in bold.

Reference	Study zone	Station	Study period	Season	Duration (days)	PM_{10} ($\mu g\ m^{-3}$)
This work (PM_{10} data from air quality network)	León (NW)	Urban, traffic	20-24 February 2016	Winter	2	52
			21-25 February 2017		1	86
PM_{10} data from air quality network	León (NW)	Urban, traffic	21 March 2014	Spring	1	21
			12-17 April 2015		5	51
			29-30 August 2015		2	31
			19-20 July 2016	Summer	2	43
			26-27 August 2017		1	38
Escudero et al. (2007)	Peñausende (NW)	Background	21-29 March 2002	Spring	3	62
	O Saviñao (NW)					88
			16-28 June 2003	Summer	4	43
Rodríguez et al. (2001)	Carboneras (SE)	Rural	22- 23 January 1997	Winter	2	147
	Monagrega (NE)	Rural	4-5 June 1998	Summer	2	71
Nicolás et al. (2008)	Elche (SE)	Urban, background	16 July 2005	Summer	1	58
Titos et al. (2017)	Southwest		20-25 February 2016	Winter	2	> 200
	Southeast					> 150
	East					> 50
	Centre					> 150
	North					< 50
	Northeast					> 50
Cachorro et al. (2008)	Peñasuende (N)	Background	22 July- 3 August 2004	Summer	5	200
	Campisablos (Centre)					100
Coz et al. (2010)	Casa de Campo, Madrid (Centre)	Suburban	16 March 2004	Spring		98
	CIEMAT, Madrid (Centre)	Suburban background				92
Artíñano et al. (2003)	Escuelas Aguirre, Madrid (Centre)	Urban	29 June- 2 July 1999	Summer	3	63
			11-12 July 1999		2	53
			24-26 July 1999		3	63
			19 August 1999		1	54
			24-25 August 1999		2	80
			27-29 October 1999	Autumn	3	88
			5-13 March 2000	Spring	8	70
			15-17 May 2000		3	47

7.4.2.3. Trace elements

The chemical composition of the 24 h teflon filters, sampled during the intrusion, between 23 and 24 February, shows that the increase in the PM_{10} mass concentrations was due to an increase in the mass concentration of Al, Ca, Si, Fe, Mg and Ti (Table 7.2). These elements are generally associated with a crustal source (Alastuey et al., 2016; Aymoz et al., 2004; Caquineau et al., 1998; Viana et al., 2002). The statistically significant correlation between PM_{10} and each crustal element ($r = 0.9$, $p < 0.01$), confirmed the important contribution from crustal material to PM_{10}. Si, Ca, Al, Fe and Mg represent up to 5.5% of the PM_{10} during the dust intrusion, while on the remaining days, the contribution did not reach 3% of the PM_{10} mass. This behavior was also reported by Viana et al., (2002) for winter intrusion events in the Canary Islands, located west of the Saharan Desert, between 1998 and 2000, with a significant increase in the Si, Al, K, Ti, Ca, Fe, Mn, Mg and Ba concentrations.

TABLE 7.2. Mass ratio (element/PM_{10}) (%) and mean concentration (mean ± standard deviation) for the crustal elements present in the four filters sampled between 18 and 22 February (before the Saharan dust) and in the filter sampled during the Saharan dust event (23 February 2017).

	% of PM_{10} mass		**Concentration (µg m^{-3})**	
	Before	**During**	**Before**	**During**
PM_{10}			19 ± 3	59
Al	0.5 ± 0.2	5.6	0.10 ± 0.04	3.31
Ca	1.0 ± 0.5	3.4	0.20 ± 0.10	2.04
Si	1.3 ± 0.6	11.1	0.25 ± 0.11	6.53
Fe	0.9 ± 0.4	3.3	0.18 ± 0.07	1.96
K	0.7 ± 0.2	1.4	0.13 ± 0.03	0.852
Mg	0.12 ± 0.04	1.05	0.022 ± 0.008	0.619
Mn	0.015 ± 0.006	0.054	0.0028 ± 0.0010	0.0316
Na	0.8 ± 0.3	0.6	0.16 ± 0.06	0.36
Ti	0.04 ± 0.02	0.34	0.008 ± 0.004	0.204

The total mineral fraction ($\sum Al_2O_3$, SiO_2, Ca, Mg, Fe and K) represents 44% of the PM_{10} mass during the dust outbreak and only 7% for the period before the outbreak. The SEM analysis also showed the presence of coarse particles mainly with Si, Al and Fe composition (Fig. 7.5). The mineral mass concentration reached 27 µg m^{-3} during the Saharan dust intrusion versus 3.2 µg m^{-3} and 2.2 µg m^{-3} registered in the days before and after the event, respectively. These results are coincident with the typical levels of mineral dust reported by other authors in Spain. In a study conducted in Elche, Spain, between 2004 and 2005, Nicolás et al. (2008) showed that the mean African dust contribution to PM_{10} mass concentration during normal days were 3.3 and 1.2 µg m^{-3} in summer and winter, respectively. Querol et al. (2004b), in a study carried out in the Iberian Peninsula between 1998 and 2002, reported that the mean mineral contribution to PM_{10} ranged between 5.5 and 2 µg m^{-3} in the south and east, and in the remaining areas, respectively. Additionally, Viana et al. (2014) showed that, in Spain, in 2008 and 2009, the main source of natural aerosol was African dust, even more than sea spray, and the contributions of mineral source to PM_{10} levels in 2008 and 2009, ranged between 1 and 4 µg m^{-3} from north to south, through the year. Alastuey et al. (2016) reported higher concentrations of mineral dust in summer

compared to winter (up to 10 µg m^{-3} and < 2 µg m^{-3}, respectively) in a study carried out in several European cities between 2012 and 2013, due to the high frequency of dust events during summer.

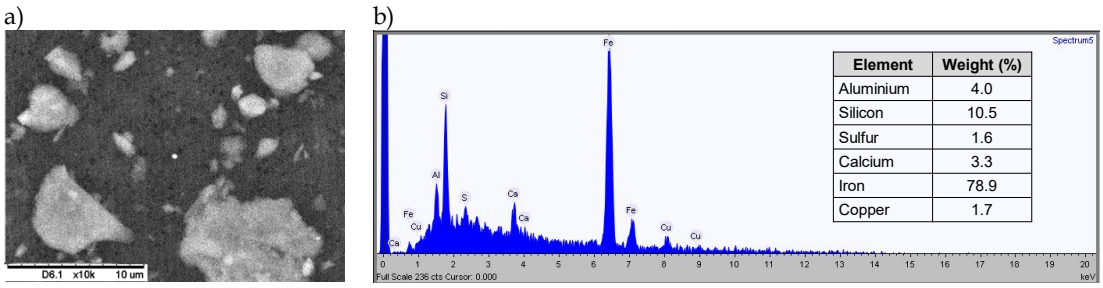

Element	Weight (%)
Aluminium	4.0
Silicon	10.5
Sulfur	1.6
Calcium	3.3
Iron	78.9
Copper	1.7

FIG. 7.5. a) SEM image and b) elemental composition of individual aerosol particles collected on the polycarbonate filter from 23 to 24 February 2017.

7.4.2.4. Water soluble inorganic ions

An increase in the SO_4^{2-}, Cl^- and NO_3^- concentrations associated with the increase of PM_{10} concentration was also observed (Fig. 7.6). Dentener et al. (1996) and Liao et al. (2003) showed that, in areas close to the source regions of mineral dust, sulfate and nitrate can be associated with the coarse mode of the aerosol. Galindo et al. (2008) also reported an increase in sulfate and nitrate concentrations in coarse size fractions in a study carried out in southern Spain between 2003 and 2004, during summer Saharan dust outbreaks, compared to normal days.

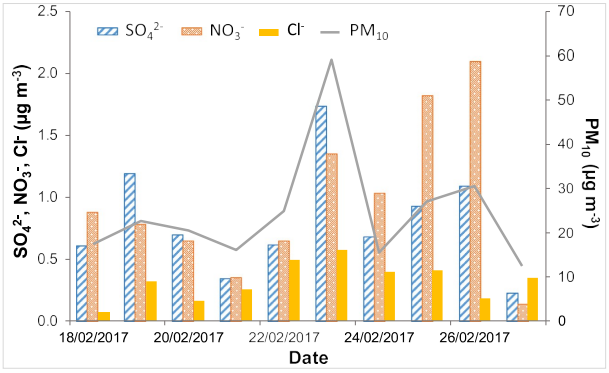

FIG. 7.6. Daily evolution of SO_4^{2-}, NO_3^-, Cl^- and PM_{10} concentrations during the intrusion of February 2017.

The SO_4^{2-}/Ca^{2+} mass ratio on 23 February to 24 February 2017 was 1.4, while for previous (between 18 and 21) and subsequent days (between 24 and 28) the mean value was 3.9 ± 1.4. Putaud et al. (2000) reported a SO_4^{2-}/Ca^{2+} mass ratio between 1.8 and 2.9 for Tenerife Island (Spain) during a Saharan outbreak in summer 1997. They also suggested that a pure Saharan dust mass ratio should be about 0.4–0.6, according to the ion chromatographic analysis carried out on samples of fine grains of sand from the Sahara Desert. The difference observed between the pure dust mass ratio and our results could be attributable to the contribution from anthropogenic sources that could increase the SO_4^{2-} levels. Moreover, the Cl^-/Na^+ ratio obtained during the dust outbreak was 1.6, while in days before and after the event the mean value was 1.3 ± 0.3. These relationships are very close to the one reported by Aymoz et al. (2004) for halite (1.5), which suggests an enrichment of the mineral fraction of the aerosol during the dust outbreaks.

7.4.2.5. Estimation of iron concentration from aethalometer data

The time series of the aethalometer data for black carbon (BC) and the estimated iron dust after the application of two-component model (Fialho et al., 2006, 2014) is consistent with the presence of high quantities of dust during Saharan intrusions. Fig. 7.7a shows a first peak on 20 February 2016. As mentioned in the previous section, this peak registered before the intrusion is probably due to a local pollution episode related to coal combustion and/or biomass burning. The emission of brown carbon (BrC, light-absorbing organic carbon) during these activities (Bond, 2001; Olson et al., 2015; Yang et al., 2009) enhances the aethalometer attenuation signal (Fialho et al., 2014), giving rise to a "false Fe peak". When the Saharan dust plume reached León on 21 February, an increase in the iron concentration was observed, attaining a maximum of 4.1 μg m^{-3} and a mean value of 0.8 ± 0.7 μg m^{-3} during the dusty period between 0900 UTC 21 and 0900 UTC 23, while before and after the event (between 0000 UTC 21 and 0800 UTC 21, and between 1000 UTC 23 and 0000 UTC 24, respectively), the mean iron value was 0.7 ± 0.7 μg m^{-3}, confirming the high contribution from this natural source during the outbreak (Guerzoni et al., 1997; Guieu et al., 2002).

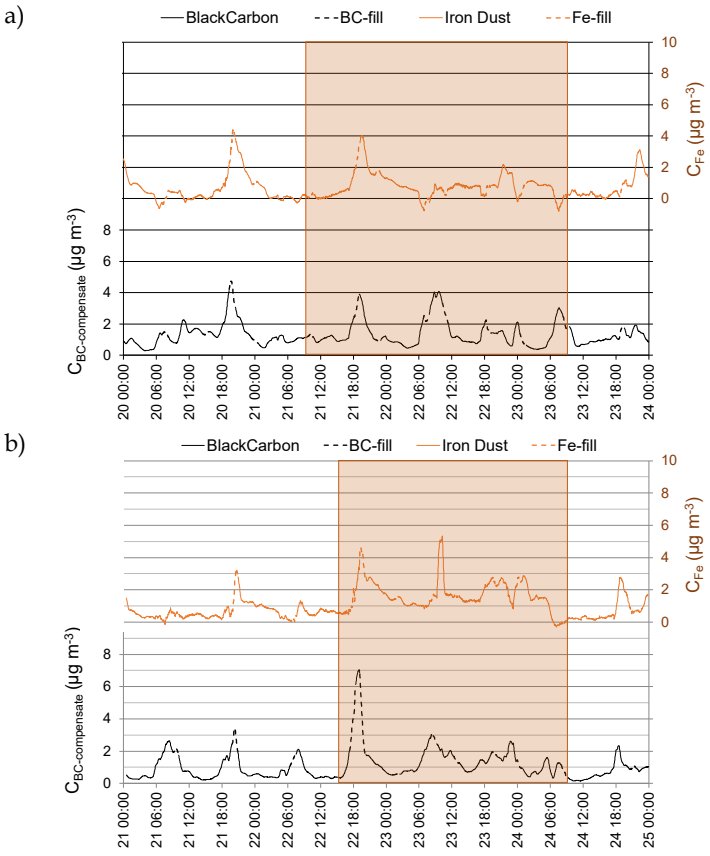

FIG. 7.7. Two-minute moving average of iron dust (red) and black carbon (black) concentrations between a) 20 and 24 February 2016 and b) 21 and 25 February 2017. The orange shadow shows the dust intrusion period.

On 23 February 2017, an important increase in both black carbon and iron concentrations is also observed (Fig. 7.7b), reaching a maximum value of Fe on 23 February at 10:16 (UTC) of 5.3 μg m^{-3}. The Fe concentration estimated by the aethalometer during the Saharan dust outbreak (23

to 24 February 2017) was 1.3 ± 0.8 μg m^{-3}. The value obtained from PIXE for one-day sampled filter during the same period was 2.0 μg m^{-3}, which falls within the range of values provided by the aethalometer.

7.4.2.6. Aerosol size distribution

The evolution of the aerosol size distributions, total particle number concentration (N_t) and particles concentration belonging to each of the three modes (nucleation, Aitken and accumulation) was also investigated through the data obtained from the PCASP and SMPS. The corrections corresponding to the data from the PCASP were carried out using a refractive index and a density for the days without intrusions (1.645–0.01016*i* and 2.086 g cm^{-3}, respectively) and for the days with intrusion (1.601–0.00755*i* and 2.295 g cm^{-3}, respectively), which were calculated from the aerosol composition (Alves et al. (2014), following the methodology described by Levin et al. (2010). Fig. 7.8a shows a first peak in the particle number concentrations of the three modes (nucleation, Aitken and accumulation) at 1900 UTC on 20 February 2016 (37 × 10^3 particles cm^{-3}), with maxima in the aerodynamic diameter interval 30–100 nm, suggesting emissions from anthropogenic sources (Charron and Harrison, 2003; Wehner and Wiedensohler, 2002) and confirming the contribution from domestic heating devices and traffic observed in Fig. 7.4a. Dust intrusion events were evidenced by the increase in the total particle number concentrations, reaching a maximum of 25 × 10^3 particles cm^{-3} on 21 February 2016 at 1900 UTC (Fig. 7.8a) and 11 × 10^3 particles cm^{-3} on 22 February 2017 at 1900 UTC (Fig. 7.8b). Additionally, there was an important increase of particles with aerodynamic diameters > 100 nm, reaching the maximum of 3.9 × 10^3 particles cm^{-3} on 22 February 2016 and 4.4 × 10^3 particles cm^{-3} on 23 February 2017.

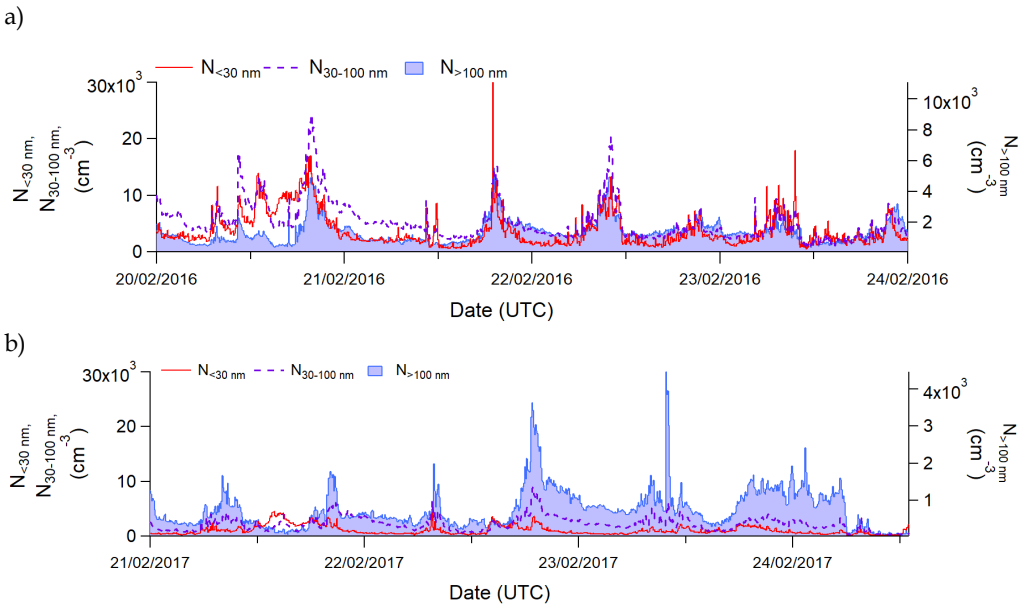

FIG. 7.8. Evolution of the aerosol size distributions and particles concentration for each of the three modes: nucleation ($N_{<30\ nm}$), Aitken ($N_{30–100\ nm}$) and accumulation ($N_{>100\ nm}$) during the study period of a) 2016 and b) 2017.

The day before the Saharan dust intrusion of 2016, the particle size distribution showed a unimodal profile (Fig. 7.9a), with one fine mode (~0.1 μm), which indicates a contribution from

road traffic (Calvo et al., 2013). When the dust plumes arrived in León, a small fraction corresponding to a coarse mode (~2 µm) confirmed the presence of dust particles (Ansmann et al., 2003; Córdoba-Jabonero et al., 2011; Struckmeier et al., 2016). This behavior was also detected by Titos et al. (2017). They reported the existence of a coarse mode (~3 µm) during their study of the event of February 2016 in Montsec, Spain. Moreover, before the dust event of 2017, a bimodal profile was observed (Fig. 7.9b) with modal diameter of the number size distribution at about 0.1 and 0.6 µm, indicating the contribution of anthropogenic sources. On 23 February 2017 a small fraction corresponding to a coarse mode (particle diameter Dp ~3 µm) attributable to dust particles (Denjean et al., 2016) was registered, which was also recorded the next day. The high concentration of coarse particles during the event of 2017 was confirmed by the morphological analysis. Thus, Fig. 7.10 shows a high number of particles larger than 1 µm on 23 February 2017, compared with the filter sampled on 23 March 2017 (day without dust intrusion) in León.

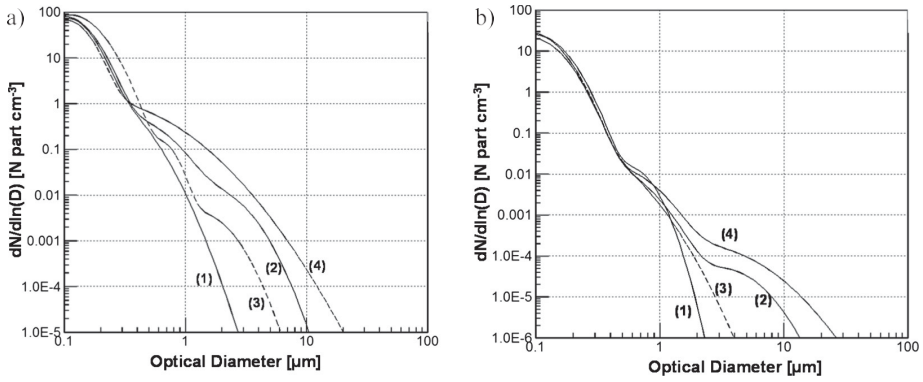

FIG. 7.9. Theoretical aerosol size number for the intrusion of 2016 (a), and for 2017 (b). The lines corresponding to days before (1), during (2) and after (3) of the intrusion, and the time when the maximum PM_{10} level was reached (4) during the intrusion.

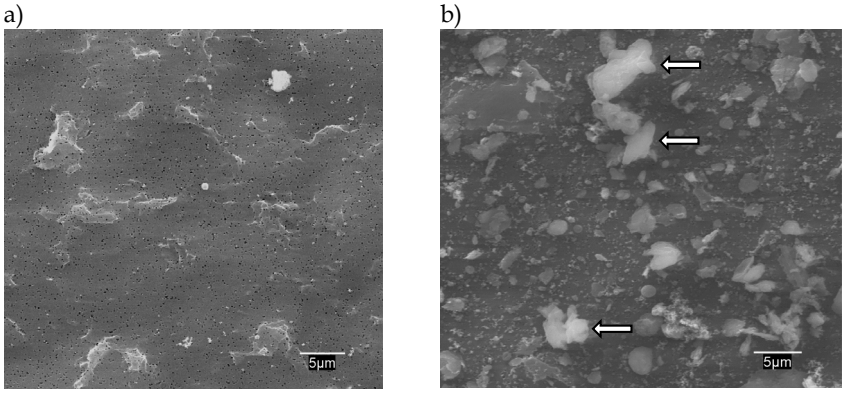

FIG. 7.10. SEM images of a) day without Saharan dust intrusion and b) on 23 February 2017. The withe arrows point to some of the dust particles.

7.4.3. Impact on columnar properties

7.4.3.1. Optical depth

Following the information of the temporal evolution of the aerosol optical depth (AOD) and the Ångström exponent (AE) over León, the intensity of the desert dust outbreak of the event

of 2016 was quantified. The criteria conditions used for dusty and background conditions at León during this episode are the following: low AOD ≤ 0.1 and high AE ≥1 correspond to background conditions, a Saharan dust episode is detected with values of high AOD and low AE ≤ 0.5, and periods of transition between these two patterns are characterized by moderate AOD and 0.5 ≤ AE ≤ 1. The rapid arrival of the desert dust plume is observed with the increase of AOD and the decrease of AE during the early morning of 21 February. The following day, 22 February, shows a clear desert aerosol character, registering at 0950 UTC the highest AOD with a value of 1.1 and the lowest AE with 0.05. The desert dust aerosol quickly moved away, which dropped back to background levels on 23 February, confirming the results previously analyzed (Fig. 7.11).

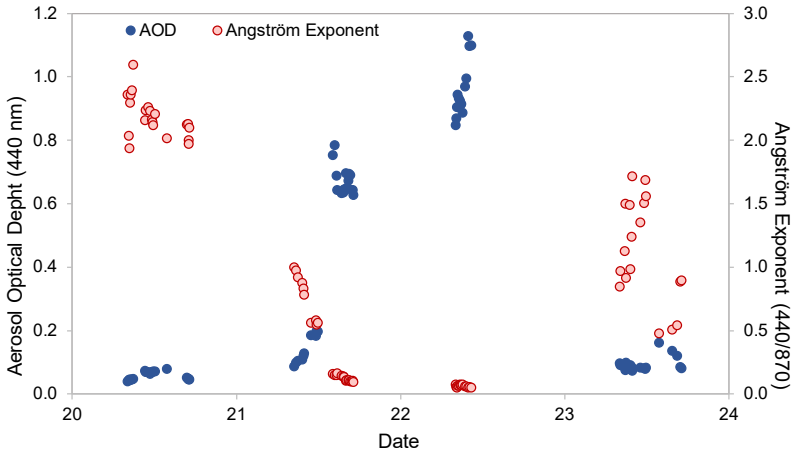

FIG. 7.11. Time series of AOD (440 nm) and Ångström exponent (440/870) at León from 20 to 23 of February 2016.

The particular feature of the desert dust episode during February 2016 has also been shown by Sorribas et al. (2017), who studied the same event from historical datasets of meteorological variables, aerosol properties and ozone concentration at El Arenosillo observatory (southwestern Spain). In this work, a historical dataset (2006–2015) of February meteorological scenarios over North Africa evidenced the existence of airflows from the Sahel to Algeria and consequently temperature increases from the surface to 700 hPa by up to 7–9 °C relative to the last decade. This phenomenon transports particles to the Iberian Peninsula at ground level and higher altitudes as Titos et al. (2017) and Cazorla et al. (2017) showed in their studies carried out in different cities of Spain, between 20 and 24 February 2016. Similar episodes over the peninsula with AOD higher than 1 have been detected before, as the one in the summer of 2004, reaching an AOD of 2.7 (Cachorro et al., 2008). In this case, the desert dust was also mixed with smoke particles from concurrent forest fires in the Iberian Peninsula. Other extreme Saharan events were detected during September 2007 with AOD reaching 1.5 (Guerrero-Rascado et al., 2009). Nevertheless, the episodes were observed during warm seasons, not in the middle of winter, which illustrates the particularity of the present study.

7.4.3.2. Radiative forcing

One of the main effects of Saharan intrusions is the change in radiative forcing (Perrone and Bergamo, 2011). To underline the radiative forcing of these dust episodes we have computed

mean aerosol daily radiative forcing over three specific periods (before, during and after the dust episode). These three periods are listed in the first column of the Table A4.1 (Annex 4). Concerning the Saharan dust event in 2016 mean ΔF_{TOA} values vary from −21.8 before intrusion to −77.9 W m^{-2} during intrusion and mean ΔF_{BOA} values from −123.6 to −149.0 W m^{-2} (Table A4.1). These results indicate that the Saharan dust intrusion caused a cooling effect in the atmosphere (Perrone and Bergamo, 2011), with a mean heating rate of −15.6 K day^{-1} during the dust event. Therefore, the Saharan intrusion influenced the radiative forcing in León, mainly decreasing the solar energy at surface. However, the energy in the atmosphere did not accumulate since the outgoing forcing at the top of the atmosphere was also intensified, losing much of the energy (lower values of ΔF_{ATM}). Besides, the optical properties during the event suggest also the change in absorbing capacities of the air mass, with an increase of *SSA* values (from 0.84 to 0.97 at 550 nm).

Concerning the Saharan dust event in 2017, the same pattern was observed, with the mean ΔF_{TOA} varying from −21.1 before intrusion to −84.1 W m^{-2} during intrusion and the mean ΔF_{BOA} from −52.1 to −164.9 W m^{-2} (Table A4.2 in Annex 4). A cooling effect was also observed with a mean heating rate of −12.4 K day^{-1} during intrusion, lower than mean values for "before" and "after" periods. The optical properties during the event, such as *SSA* and g values did not present a large change that could support by itself the stronger scattering radiative effect, but the large variation of AOT between the "before", "during" and "after" period could explain the strong radiative signature of this event.

According to AEMET data, the visibility and the solar radiation in León were affected during both Saharan dust outbreaks. In days without dust intrusions, the visibility in León typically ranges between 50 and 60 km. However, during the event of 2016, the visibility decreased to 30 km. In the event of 2017, the decrease of the visibility was more evident, dropping to 24 km on 23 February at 0000–0700 UTC and to 10 km at 0700–1300 UTC, when the intrusion was at its peak. The negative impact of both events on visibility is comparable with that reported by Alonso-Blanco et al. (2018) during two large wildfires at 70 km away from León city, causing a reduction in visibility from 78 km to 20 km. Regarding to solar radiation, during the day before the events, the direct total radiation was approximately 340 W m^{-2} in León, and the total daily diffuse radiation was about 20 W m^{-2}. During both Saharan dust intrusions, the direct total radiation decreases up to 71 W m^{-2} in 2016 and 140 W m^{-2} in 2017. Moreover, the total daily diffuse radiation increases up to 94 W m^{-2} and 87 W m^{-2} in 2016 and 2017, respectively. These results show that the contribution of solar diffuse radiation on global irradiance (direct + diffuse) increased (from 5% to 57% in 2016 and 38% in 2017) when the dust plume reached León city. Similar results were obtained by Antón et al. (2012), who reported that the solar diffuse radiation contributed for almost 60% of the global radiation during an extreme Saharan dust event detected in September 2007 in Granada (Spain).

7.4.4. Bioaerosol characterization

The dust intrusions were also reflected in the pollen monitoring carried out at the sampling point, which highlights the modification of the population of both biological and non-biological particles due to long-range transport. During the Saharan dust intrusion studied in 2016 (between 21 and 22 February), sand particles and pollen grains not typical of flowering plants in this period of the year in the province of León were identified: i.e. *Artemisia* (17–28 µm) (Fig. 7.12b) and

Daphne (18–23 µm). These pollen types are typical of the south of the Iberian Peninsula and the Mediterranean area, where they flourish in winter. Before and after the intrusion, a low concentration of pollen was detected with a predominance of *Cupressaceae*, *Corylus*, *Alnus* (13–18 µm) (Fig. 7.12a), and Poaceae (graminaceus). Other authors have reported the influence of the long-range transport in the presence of atypical pollen types and in the pollen concentration. Izquierdo et al. (2011) showed, for different long-range transport scenarios in summer of 1999 over Canary Island, Spain, the presence of several pollen types, such as *Artemisa*, *Olea*, *Quercus*, Poaceae, Cyperaceae, among others. In Córdoba, Spain, Cariñanos et al. (2004) identified pollen types which did not correspond to the local pollen species or whose flowering period occurs at different periods of the year, in samples of the dust intrusion of summer 1999. *Cannabis*, *Sambucus*, *Pinus*, *Cupressus*, *Quercus* and *Fraxinus* were among the pollen types identified by these researchers.

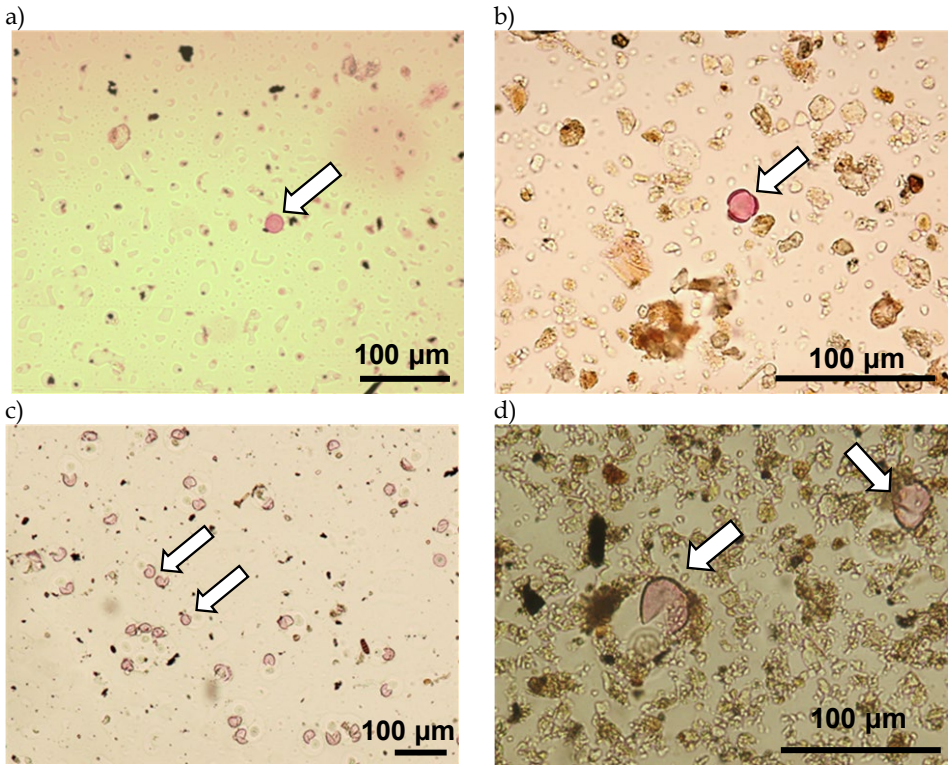

FIG. 7.12. Optical microscope images of pollen samples collected by the Hirst-type volumetric trap corresponding to a) 20/02/2016; b) 22/02/2016; c) 21/02/2017 and d) 23/02/2017 (a) and c) without dust intrusion and b) and d) under Sahara dust intrusion). The withe arrows indicate: a) *Corylus* b) *Artemisia* c) *Cupressaceae* [1] and Poaceae [2] pollen and d) *Cupressacea* pollen.

Unlike the 2016 event, in 2017 the presence of atypical pollen types in León was not observed (Fig. 7.12 c and d). However, on 23 February 2017, when the dust plume reached the north of the Iberian Peninsula, the *Corylus* concentration was about six times higher (60 pollen m^{-3}) than the maximum value reached in previous days (10 pollen m^{-3}). From 24 February, the *Corylus* concentration in the atmosphere began to decline until it completely disappeared. This behavior can be due to the trajectory of the air masses described in Fig. 7.3c, at 500 m level, that dragged large amounts of pollen emitted by the forests of the Cantabrian Mountains, located about 30 km north far from the city. Furthermore, the *Cupressaceae* pollen concentration decreased

considerably during the dust intrusion (from 269 to 72 pollen m^{-3}). The presence of this type of pollen is very important in the east and central peninsula during this season since its flowering occurs earlier than in the city of León. The highest concentration of this type of pollen in the previous days is probably due to the trajectories of the air masses described above.

7.4.5. Inhalable, thoracic, tracheobronchial and respirable fractions

Changes in the aerosol size distribution caused for the dust plumes result in different amounts of mass deposited in the distinct zones of the respiratory tract. The results showed highest values of inhaled mass of aerosols during the days in which the dust plume was more intense in both February 2016 and 2017 (58 ± 11 and 52 ± 29 μg m^{-3}, respectively). These values are comparable with those obtained during summer 2012 in León city (43 μg m^{-3}) (Oduber et al., 2018), when the Saharan dust intrusions are more frequents (Table 7.3). Furthermore, the mass fraction of particles that could reach the alveolar area was higher during the intrusion days, due to the presence of a greater number of particles in the atmosphere. Values of respirable fraction, when the maximum particle mass concentration was reached in 2016, were 102 and 134 μg m^{-3} in healthy adults and in high-risk populations, respectively. In 2017, this value reached 155 μg m^{-3} in both healthy adults and in high-risk populations, respectively.

TABLE 7.3. Inhalable, thoracic, tracheobronchial and respirable mass fractions (μg m^{-3}) in healthy adults and high-risk population (children, frail or sick people), and maximum mass fraction values for the two study periods. Values corresponding to the main dust outbreak days are in bold.

Date (Day)	Inhalable (μg m^{-3})	Thoracic (μg m^{-3})	Tracheobronchial (μg m^{-3})		Respirable (μg m^{-3})	
			Healthy Adult	High Risk	Healthy Adult	High Risk
February 2016						
20	18 ± 9	17 ± 8	3 ± 4	5 ± 4	14 ± 5	12 ± 4
21	32 ± 29	31 ± 28	4 ± 4	9 ± 9	27 ± 24	22 ± 19
22	58 ± 11	55 ± 8	6 ± 1	15 ± 2	49 ± 7	40 ± 6
23	17.5± 0.3	17.3 ± 0.5	1.5 ± 0.4	3.3 ± 0.4	15.8 ± 0.8	14.0 ± 0.8
Maximum (22, 1200 UTC)	156	153	19	51	134	102
February 2017						
21	10.0 ± 0.5	9.8 ± 0.2	0.6 ± 0.7	0.8 ± 0.9	9.2 ± 0.5	9.0 ± 0.6
22	17 ± 12	16 ± 12	2 ± 1	3 ± 2	14 ± 10	13 ± 10
23	52 ± 29	52 ± 29	1 ± 2	2 ± 3	51 ± 31	50 ± 32
24	14 ± 1	14 ± 1	4 ± 2	6 ± 3	10 ± 2	8 ± 4
Maximum (23, 1200 UTC)	155	155	0	0.01	155	155

7.5. CONCLUSIONS

Two unusual Saharan dust outbreaks arriving at León in February 2016 and 2017 were analyzed from a multidisciplinary perspective. In León city, the arrival of desert dust plumes resulted in the increase of the coarse fraction (Dp > 1 μm) and in the exceedance of the PM_{10} DLV, with daily concentrations of 52 μg m^{-3} in 2016 and 86 μg m^{-3} in 2017, values even higher than

those observed during summer Saharan dust intrusions of 2016 in the same city. Furthermore, a change in the biological material caused by long-range transport has been observed, evidenced by the presence of pollen grains not typical of flowering plants in this period in the province of León.

The rise in the iron concentration estimated from the aethalometer data is consistent with the high contribution of dust in both outbreaks, reaching values up to 5.73 and 7.38 μg m^{-3} in 2016 and 2017, respectively. These results were also supported by the chemical analysis of the teflon filters sampled during the African intrusion of 2017, with daily Fe concentrations of 1.9 μg m^{-3} from the PIXE technique and 2.0 μg m^{-3} from the aethalometer data. Furthermore, the dust contribution in the event of 2017 was evidenced through the increase of the concentrations of the main elements associated with mineral sources (calcium, aluminum, titanium and silica), reaching values higher than those observed in summer Saharan dust intrusions in León in 2016. The total mineral fraction reached 44% of PM_{10} mass during the dust outbreak, while in the days before the dust intrusion, the mineral fraction reached mean values of 7%. It was also noted an increase in the SO_4^{2-}, NO_3^- and Cl^- concentrations during the Saharan dust intrusion.

During both dust events, the estimated mean aerosol radiative forcing values at the top and at the bottom of the atmosphere were of the same order. The presence of the dusty air masses decreased the incoming solar flux at the surface. The energy did not accumulate in the atmosphere as mean atmospheric radiative forcing estimations decreased between the "during", "before" and "after" periods. Consequently, the outgoing radiative fluxes at the top of the atmosphere were enhanced. The scattering optical properties at the origin of this cooling effect of the dust event were supported by the variation of the *SSA* values for the 2016 event, and by the large variation of the total amount of aerosol in the column, revealed through the AOT parameter evolution, for the 2017 event. The enhancement of the scattering property was also supported by the radiative surface measurements. Furthermore, on the 2016 event, AOD and extinction-related Ångström exponent showed clearly characteristics of desert aerosol, registering values of 1.1 and 0.05, respectively.

The impact on the respiratory tract regions of the high levels of particulate matter during both Saharan dust intrusions was estimated using the International Organization for Standardization. The highest values of inhaled mass of aerosols were 58 ± 11 and 52 ± 29 μg m^{-3}, during the 2016 and 2017 outbreaks, respectively, with values of respirable fraction of 102 and 134 μg m^{-3} in healthy adults and high-risk populations, respectively in 2016. In 2017, these values reached approximately 155 μg m^{-3} in healthy adults and high-risk populations. These concentrations are approximately 9 times the mean value recorded in days without dust intrusion, showing that these natural events can cause a negative impact on human health.

This kind of complete descriptive studies is essential not only for air quality and transport understandings but also for the subsequent implications on health and climate, two main targets of policy makers. An integrative approach should be performed through modeling exercises to go on understanding the dynamic, radiative, and transport feedback loops and their impact on air quality and health.

7.6. REFERENCES

Alastuey, A., Querol, X., Aas, W., Lucarelli, F., Pérez, N., Moreno, T., Cavalli, F., Areskoug, H., Balan, V., Catrambone, M., Ceburnis, D., Cerro, J.C., Conil, S., Gevorgyan, L., Hueglin, C., Imre, K., Jaffrezo, J.-L., Leeson, S.R., Mihalopoulos, N., Mitosinkova, M., O'Dowd, C.D., Pey, J., Putaud, J.-P., Riffault, V., Ripoll, A., Sciare, J., Sellegri, K., Spindler, G., Yttri, K.E., 2016. Geochemistry of PM_{10} over Europe during the EMEP intensive measurement periods in summer 2012 and winter 2013. Atmos. Chem. Phys. 16, 6107–6129. https://doi.org/10.5194/acp-16-6107-2016.

Alonso-Blanco, E., Castro, A., Calvo, A.I., Pont, V., Mallet, M., Fraile, R., 2018. Wildfire smoke plumes transport under a subsidence inversion: climate and health implications in a distant urban area. Sci. Total Environ. 619–620, 988–1002. https://doi.org/10.1016/j. scitotenv.2017.11.142.

Alves, C., Calvo, A.I., Marques, L., Castro, A., Nunes, T., Coz, E., Fraile, R., 2014. Particulate matter in the indoor and outdoor air of a gymnasium and a fronton. Environ. Sci. Pollut. Res. 21, 12390–12402. https://doi.org/10.1007/s11356-014-3168-1.

Alves, C.A., Lopes, D.J., Calvo, A.I., Evtyugina, M., Rocha, S., Nunes, T., 2015. Emissions from light-duty diesel and gasoline in-use vehicles measured on chassis dynamometer test cycles. Aerosol Air Qual. Res. 15, 99–116. https://doi.org/10.4209/aaqr.2014.01.0006.

Ansmann, A., Bösenberg, J., Chaikovsky, A., Comerón, A., Eckhardt, S., Eixmann, R., Freudenthaler, V., Ginoux, P., Komguem, L., Linné, H., Márquez, M.Á.L., Matthias, V., Mattis, I., Mitev, V., Müller, D., Music, S., Nickovic, S., Pelon, J., Sauvage, L., Sobolewsky, P., Srivastava, M.K., Stohl, A., Torres, O., Vaughan, G., Wandinger, U., Wiegner, M., 2003. Long-range transport of Saharan dust to northern Europe: the 11–16 October 2001 outbreak observed with EARLINET. J. Geophys. Res. Atmos. 108. https://doi.org/10.1029/2003JD003757.

Antón, M., Valenzuela, A., Cazorla, A., Gil, J.E., Fernández-Gálvez, J., Lyamani, H., Foyo-Moreno, I., Olmo, F.J., Alados-Arboledas, L., 2012. Global and diffuse shortwave irradiance during a strong desert dust episode at Granada (Spain). Atmos. Res. 118, 232–239. https://doi.org/10.1016/j.atmosres.2012.07.007.

Artíñano, B., Salvador, P., Alonso, D.G., Querol, X., Alastuey, A., 2003. Anthropogenic and natural influence on the PM_{10} and $PM_{2.5}$ aerosol in Madrid (Spain). Analysis of high concentration episodes. Environ. Pollut. 125, 453–465. https://doi.org/10.1016/ S0269-7491(03)00078-2.

Aymoz, G., Jaffrezo, J., Jacob, V., Colomb, A., George, C., 2004. Evolution of organic and inorganic components of aerosol during a Saharan dust episode observed in the French Alps. Atmos. Chem. Phys. 2499–2512.

Blanco-Alegre, C., Calvo, A.I., Coz, E., Castro, A., Oduber, F., Prévôt, A.S.H., Močnik, G., Fraile, R., 2019. Quantification of source specific black carbon scavenging using an aethalometer and a disdrometer. Environ. Pollut. 246, 336–345. https://doi.org/ 10.1016/j.envpol.2018.11.102.

Bond, T.C., 2001. Spectral dependence of visible light absorption by carbonaceous particles emitted from coal combustion. Geophys. Res. Lett. 28, 4075–4078. https://doi. org/10.1029/2001GL013652.

Cachorro, V.E., Toledano, C., Prats, N., Sorribas, M., Mogo, S., Berjón, A., Torres, B., Rodrigo, R., de la Rosa, J., De Frutos, A.M., 2008. The strongest desert dust intrusion mixed with smoke over the Iberian Peninsula registered with Sun photometry. J. Geophys. Res. 113, D14S04. doi:https://doi.org/10.1029/2007JD009582

Calvo, A.I., Pont, V., Castro, A., Mallet, M., Palencia, C., Roger, J.C., Dubuisson, P., Fraile, R., 2010. Radiative forcing of haze during a forest fire in Spain. J. Geophys. Res. 115, D08206. https://doi.org/10.1029/2009JD012172.

Calvo, A.I., Alves, C., Castro, A., Pont, V., Vicente, A.M., Fraile, R., 2013. Research on aerosol sources and chemical composition: past, current and emerging issues. Atmos. Res. 120–121, 1–28. https://doi.org/10.1016/j.atmosres.2012.09.021.

Caquineau, S., Gaudichet, A., Gomes, L., Magonthier, M.-C., Chatenet, B., 1998. Saharan dust: clay ratio as a relevant tracer to assess the origin of soil-derived aerosols. Geophys. Res. Lett. 25, 983–986. https://doi.org/10.1029/98GL00569.

Cariñanos, P., Galán, C., Alcázar, P., Domínguez, E., 2004. Analysis of the particles transported with dust-clouds reaching Cordoba, southwestern Spain. Arch. Environ. Contam. Toxicol. 46, 141–146. https://doi.org/10.1007/s00244-003-2273-9.

Castro, A., Alonso-Blanco, E., González-Colino, M., Calvo, A.I., Fernández-Raga, M., Fraile, R., 2010. Aerosol size distribution in precipitation events in León, Spain. Atmos. Res. 96, 421–435. https://doi.org/10.1016/j.atmosres.2010.01.014.

Castro, A., Calvo, A.I., Alves, C., Alonso-Blanco, E., Coz, E., Marques, L., Nunes, T., Fernández-Guisuraga, J.M., Fraile, R., 2015. Indoor aerosol size distributions in a gymnasium. Sci. Total Environ. 524–525, 178–186. https://doi.org/10.1016/j. scitotenv.2015.03.118.

Castro, A., Calvo, A.I., Blanco-Alegre, C., Oduber, F., Alves, C., Coz, E., Amato, F., Querol, X., Fraile, R., 2018. Impact of the wood combustion in an open fireplace on the air quality of a living room: estimation of the respirable fraction. Sci. Total Environ. 628–629, 169–176. https://doi.org/10.1016/j.scitotenv.2018.02.001.

Cazorla, A., Casquero-Vera, J.A., Román, R., Guerrero-Rascado, J.L., Toledano, C., Cachorro, V.E., Orza, J.A.G., Cancillo, M.L., Serrano, A., Titos, G., Pandolfi, M., Alastuey, A., Hanrieder, N., Alados-Arboledas, L., 2017. Near-real-time processing of a ceilometer network assisted with sun-photometer data: mnitoring a dust outbreak over the Iberian Peninsula. Atmos. Chem. Phys. 17, 11861–11876. https://doi.org/10.5194/acp- 2017-151.

Charron, A., Harrison, R.M., 2003. Primary particle formation from vehicle emissions during exhaust dilution in the roadside atmosphere. Atmos. Environ. 37, 4109–4119. https://doi.org/10.1016/S1352-2310(03)00510-7.

Córdoba-Jabonero, C., Sorribas, M., Guerrero-Rascado, J.L., Adame, J.A., Hernández, Y., Lyamani, H., Cachorro, V., Gil, M., Alados-Arboledas, L., Cuevas, E., de la Morena, B., 2011. Synergetic monitoring of Saharan dust plumes and potential impact on surface: a case study of dust transport from Canary Islands to Iberian Peninsula. Atmos. Chem. Phys. 11, 3067–3091. https://doi.org/10.5194/acp-11-3067-2011.

Coz, E., Gómez-Moreno, F.J., Pujadas, M., Casuccio, G.S., Lersch, T.L., Artíñano, B., 2009. Individual particle characteristics of North African dust under different long-range transport scenarios. Atmos. Environ. 43, 1850–1863. https://doi.org/10.1016/j. atmosenv.2008.12.045.

Coz, E., Gómez-Moreno, F.J., Casuccio, G.S., Artíñano, B., 2010. Variations on morphology and elemental composition of mineral dust particles from local, regional, and long-range transport meteorological scenarios. J. Geophys. Res. Atmos. 115, 1–12. https://doi.org/10.1029/2009JD012796.

Denjean, C., Cassola, F., Mazzino, A., Triquet, S., Chevaillier, S., Grand, N., Bourrianne, T., Momboisse, G., Sellegri, K., Schwarzenbock, A., Freney, E., Mallet, M., Formenti, P., 2016. Size distribution and optical properties of mineral dust aerosols transported in the western Mediterranean. Atmos. Chem. Phys. 16, 1081–1104. https://doi.org/ 10.5194/acp-16-1081-2016.

Dentener, F.J., Carmichael, G.R., Zhang, Y., Lelieveld, J., Crutzen, P.J., 1996. Role of mineral aerosol as a reactive surface in the global troposphere. J. Geophys. Res. Atmos. 101, 22869–22889. https://doi.org/10.1029/96JD01818.

Díaz, J., Linares, C., Carmona, R., Russo, A., Ortiz, C., Salvador, P., Trigo, R.M., 2017. Saharan dust intrusions in Spain: health impacts and associated synoptic conditions. Environ. Res. 156, 455–467. https://doi.org/10.1016/j.envres.2017.03.047.

Draxler, R., Rolph, G., 2012. Hysplit (Hybrid Single-Particle Lagrangian Integrated Trajectory). Silver Spring. NOAA Air Resour, Lab.

Dubuisson, P., Buriez, J.C., Fouquart, Y., 1996. High spectral resolution solar radiative transfer in absorbing and scattering media: application to the satellite simulation. J. Quant. Spectrosc. Radiat. Transf. 55, 103–126. https://doi.org/10.1016/0022-4073 (95)00134-4.

Dubuisson, P., Dessailly, D., Vesperini, M., Frouin, R., 2004. Water vapor retrieval over ocean using near-infrared radiometry. J. Geophys. Res. D Atmos. 109, 1–14. https:// doi.org/10.1029/2004JD004516.

Dunn, O.J., 1964. Multiple comparisons using rank sums. Technometrics 6, 241–252. https://doi.org/10.1080/00401706.1964.10490181.

Escudero, M., Querol, X., Ávila, A., Cuevas, E., 2007. Origin of the exceedances of the European daily PM limit value in regional background areas of Spain. Atmos. Environ. 41, 730–744. https://doi.org/10.1016/j.atmosenv.2006.09.014.

Estellés, V., Campanelli, M., Smyth, T.J., Utrillas, M.P., Martínez-Lozano, J.A., 2012. Evaluation of the new ESR network software for the retrieval of direct sun products from CIMEL CE318 and PREDE POM01 sun-sky radiometers. Atmos. Chem. Phys. 12, 11619–11630. https://doi.org/10.5194/acp-12-11619-2012.

Fialho, P., Freitas, M.C., Barata, F., Vieira, B., Hansen, A.D.A., Honrath, R.E., 2006. The Aethalometer calibration and determination of iron concentration in dust aerosols. J. Aerosol Sci. 37, 1497–1506. https://doi.org/10.1016/j.jaerosci.2006.03.002.

Fialho, P., Cerqueira, M., Pio, C., Cardoso, J., Nunes, T., Custódio, D., Alves, C., Almeida, S.M., Almeida-Silva, M., Reis, M., Rocha, F., 2014. The application of a multi-wavelength aethalometer to estimate iron dust and black carbon concentrations in the marine boundary

layer of Cape Verde. Atmos. Environ. 97, 136–143. https://doi.org/10.1016/j.atmosenv.2014.08.008.

Fubini, B., Otero Areán, C., 1999. Chemical aspects of the toxicity of inhaled mineral dusts. Chem. Soc. Rev. 28, 373–381. https://doi.org/10.1039/a805639k.

Galán Soldevilla, C., Cariñanos González, P., Alcázar Teno, P., Domínguez Vilches, E., 2007. Spanish Aerobiology Network (REA): Management and Quality Manual.

Galindo, N., Nicolás, J.F., Yubero, E., Caballero, S., Pastor, C., Crespo, J., 2008. Factors affecting levels of aerosol sulfate and nitrate on the Western Mediterranean coast. Atmos. Res. 88, 305–313. https://doi.org/10.1016/j.atmosres.2007.11.024.

Garrison, V.H., Foreman, W.T., Genualdi, S., Griffin, D.W., Kellogg, C.A., Majewski, M.S., Mohammed, A., Ramsubhag, A., Shinn, E.A., Simonich, S.L., Smith, G.W., 2006. Saharan dust – a carrier of persistent organic pollutants, metals and microbes to the Caribbean? Int. J. Trop. Biol. Conserv. 54, 9–21.

Glaccum, R.A., Prospero, J.M., 1980. Saharan aerosols over the tropical north Atlantic — mineralogy. Mar. Geol. 37, 295–321. https://doi.org/10.1016/0025-3227(80)90107-3.

Goudie, A.S., 2014. Desert dust and human health disorders. Environ. Int. 63, 101–113. https://doi.org/10.1016/j.envint.2013.10.011.

Griffin, D.W., 2007. Atmospheric movement of microorganisms in clouds of desert dust and implications for human health. Clin. Microbiol. Rev. 20, 459–477. https://doi.org/10.1128/CMR.00039-06.

Griffin, D.W., Kellogg, C.A., Shinn, E.A., 2001. Dust in the wind: long range transport of dust in the atmosphere and its implications for global public and ecosystem health. Glob. Chang. Hum. Health 2, 20–33.

Guerrero-Rascado, J.L., Olmo, F.J., Avilés-Rodríguez, I., Navas-Guzmán, F., Pérez-Ramírez, D., Lyamani, H., Alados Arboledas, L., 2009. Extreme Saharan dust event over the southern Iberian Peninsula in September 2007: active and passive remote sensing from surface and satellite. Atmos. Chem. Phys. 9, 8453–8469. https://doi.org/ 10.5194/acp-9-8453-2009.

Guerzoni, S., Molinaroli, E., Chester, R., 1997. Saharan dust inputs to the western Mediterranean Sea: depositional patterns, geochemistry and sedimentological implications. Deep. Res. II 44, 631–654.

Guieu, C., Bozec, Y., Blain, S., Ridame, C., Sarthou, G., Leblond, N., 2002. Impact of high Saharan dust inputs on dissolved iron concentrations in the Mediterranean Sea. Geophys. Res. Lett. 29, 17–1–17–4. doi:https://doi.org/10.1029/2001GL014454

Holben, B.N., Eck, T.F., Slutsker, I., Tanré, D., Buis, J.P., Setzer, A., Vermote, E., Reagan, J.A., Kaufman, Y.J., Nakajima, T., Lavenu, F., Jankowiak, I., Smirnov, A., 1998. AERONET-A federated instrument network and data archive for aerosol characterization. Remote Sens. Environ. 66, 1–16.

International Organization for Standardization, 1995. ISO 7708: 1995 Air quality -Particle size fraction definitions for health-related sampling. ISO Publications, 1st edition, 1995-04-01.

IPCC, 2014. Climate Change 2014: Impacts, Adaptation, and Vulnerability. Part A: Global and Sectoral Aspects. Contribution of Working Group II to the Fifth Assessment Report of the Intergovernmental Panel on Climate Change. Cambridge University Press, Cambridge.

Izquierdo, R., Belmonte, J., Avila, A., Alarcón, M., Cuevas, E., Alonso-Pérez, S., 2011. Source areas and long-range transport of pollen from continental land to Tenerife (Canary Islands). Int. J. Biometeorol. 55, 67–85. https://doi.org/10.1007/s00484-010-0309-1.

Jiménez, E., Linares, C., Martínez, D., Díaz, J., 2010. Role of Saharan dust in the relationship between particulate matter and short-term daily mortality among the elderly in Madrid (Spain). Sci. Total Environ. 408, 5729–5736. https://doi.org/10.1016/j. scitotenv.2010.08.049.

Kruskal, W.H., Wallis, W.A., 1952. Use of ranks in one-criterion variance analysis. J. Am. Stat. Assoc. 47, 583–621. https://doi.org/10.1080/01621459.1952.10483441.

Levin, E.J.T., McMeeking, G.R., Carrico, C.M., Mack, L.E., Kreidenweis, S.M., Wold, C.E., Moosmüller, H., Arnott, W.P., Hao, W.M., Collett, J.L., Malm, W.C., 2010. Biomass burning smoke aerosol properties measured during fire Laboratory at Missoula Experiments (FLAME). J. Geophys. Res. 115, D18210. https://doi.org/10.1029/ 2009JD013601.

Liao, H., Adams, P.J., Chung, S.H., Seinfeld, J.H., Mickley, L., Jacob, D., 2003. Interactions between tropospheric chemistry and aerosols in a unified general circulation model. J. Geophys. Res. 108, 4001. https://doi.org/10.1029/2001JD001260.

López-Villarrubia, E., Iñiguez, C., Peral, N., García, M.D., Ballester, F., 2012. Characterizing mortality effects of particulate matter size fractions in the two capital cities of the Canary Islands. Environ. Res. 112, 129–138. https://doi.org/10.1016/j. envres.2011.10.005.

Lucarelli, F., Chiari, M., Calzolai, G., Giannoni, M., Nava, S., Udisti, R., Severi, M., Querol, X., Amato, F., Alves, C., Eleftheriadis, K., 2015. The role of PIXE in the AIRUSE project "testing and development of air quality mitigation measures in Southern Europe." Nucl. Instrum. Methods Phys. Res., Sect. B 363, 92–98. doi:https://doi.org/10.1016/j. nimb.2015.08.023.

Lyamani, H., Valenzuela, A., Perez-Ramirez, D., Toledano, C., Granados-Muñoz, M.J., Olmo, F.J., Alados-Arboledas, L., 2015. Aerosol properties over the western Mediterranean basin: temporal and spatial variability. Atmos. Chem. Phys. 15, 2473–2486. https:// doi.org/10.5194/acp-15-2473-2015.

Morawska, L., Salthammer, T., 2003. Indoor Environment. Airborne Particles and Settled Dust. Wiley-VCH Verlag GmbH & Co. KGaA, Weinheim, Germany, Indoor Environment https://doi.org/10.1002/9783527610013.

Nicolás, J., Chiari, M., Crespo, J., Orellana, I.G., Lucarelli, F., Nava, S., Pastor, C., Yubero, E., 2008. Quantification of Saharan and local dust impact in an arid Mediterranean area by the positive matrix factorization (PMF) technique. Atmos. Environ. 42, 8872–8882. https://doi.org/10.1016/j.atmosenv.2008.09.018.

Oduber, F., Castro, A., Calvo, A.I., Blanco-Alegre, C., Alonso-Blanco, E., Belmonte, P., Fraile, R., 2018. Summer-autumn air pollution in León, Spain: changes in aerosol size distribution and expected effects on the respiratory tract. Air Qual. Atmos. Health 11, 505–520. https://doi.org/10.1007/s11869-018-0556-6.

Oduber, F., Calvo, A.I., Blanco-Alegre, C., Castro, A., Vega-Maray, A.M., Valencia-Barrera, R.M., Fernández-González, D., Fraile, R., 2019. Links between recent trends in airborne pollen concentration, meteorological parameters and air pollutants. Agric. For. Meteorol. 264, 16–26. https://doi.org/10.1016/j.agrformet.2018.09.023.

Olson, M.R., Victoria Garcia, M., Robinson, M.A., Van Rooy, P., Dietenberger, M.A., Bergin, M., Schauer, J.J., 2015. Investigation of black and brown carbon multiple-wavelength-dependent light absorption from biomass and fossil fuel combustion source emissions. J. Geophys. Res. Atmos. 120, 6682–6697. https://doi.org/10.1002/ 2014JD022970.

Oteros, J., Buters, J., Laven, G., Röseler, S., Wachter, R., Schmidt-Weber, C., Hofmann, F., 2017. Errors in determining the flow rate of Hirst-type pollen traps. Aerobiologia 33, 201–210. https://doi.org/10.1007/s10453-016-9467-x.

Perez, L., Tobias, A., Querol, X., Künzli, N., Pey, J., Alastuey, A., Viana, M., Valero, N., González-Cabré, M., Sunyer, J., 2008. Coarse particles from Saharan dust and daily mortality. Epidemiology 19, 800–807. https://doi.org/10.1097/ EDE.0b013e31818131cf.

Perrone, M.R., Bergamo, A., 2011. Direct radiative forcing during Sahara dust intrusions at a site in the Central Mediterranean: anthropogenic particle contribution. Atmos. Res. 101, 783–798. https://doi.org/10.1016/j.atmosres.2011.05.011.

Pio, C., Cerqueira, M., Harrison, R.M., Nunes, T., Mirante, F., Alves, C., Oliveira, C., Sanchez de la Campa, A., Artíñano, B., Matos, M., 2011. OC/EC ratio observations in Europe: rethinking the approach for apportionment between primary and secondary organic carbon. Atmos. Environ. 45, 6121–6132. https://doi.org/ 10.1016/j.atmosenv.2011.08.045.

Polymenakou, P.N., Mandalakis, M., Stephanou, E.G., Tselepides, A., 2007. Particle size distribution of airborne microorganisms and pathogens during an intense African dust event in the eastern Mediterranean. Environ. Health Perspect. 116, 292–296. https://doi.org/10.1289/ehp.10684.

Putaud, J.-P., Van Dingenen, R., Mangoni, M., Virkkula, A., Raes, F., Maring, H., Prospero, J.M., Swietlicki, E., Berg, O.H., Hillamo, R., Mäkelä, T., 2000. Chemical mass closure and assessment of the origin of the submicron aerosol in the marine boundary layer and the free troposphere at Tenerife during ACE-2. Tellus Ser. B Chem. Phys. Meteorol. 52, 141–168. https://doi.org/10.3402/tellusb.v52i2.16090.

Querol, X., Alastuey, A., Rodríguez, S., Viana, M.M., Artíñano, B., Salvador, P., Mantilla, E., do Santos, S.G., Patier, R.F., de La Rosa, J., de la Campa, A.S., Menéndez, M., Gil, J.J., 2004a. Levels of particulate matter in rural, urban and industrial sites in Spain. Sci. Total Environ. 334–335, 359–376. https://doi.org/10.1016/j.scitotenv.2004.04.036.

Querol, X., Alastuey, A., Ruiz, C.R., Artiñano, B., Hansson, H.C., Harrison, R.M., Buringh, E., ten Brink, H.M., Lutz, M., Bruckmann, P., Straehl, P., Schneider, J., 2004b. Speciation and origin of PM_{10} and $PM_{2.5}$ in selected European cities. Atmos. Environ. 38, 6547–6555. https://doi.org/10.1016/j.atmosenv.2004.08.037.

Querol, X., Alastuey, A., Pandolfi, M., Reche, C., Pérez, N., Minguillón, M.C., Moreno, T., Viana, M., Escudero, M., Orio, A., Pallarés, M., Reina, F., 2014. 2001–2012 trends on air quality in Spain. Sci. Total Environ. 490, 957–969. https://doi.org/10.1016/j. scitotenv.2014.05.074.

Rodríguez, S., Querol, X., Alastuey, A., Kallos, G., Kakaliagou, O., 2001. Saharan dust contributions to PM_{10} and TSP levels in southern and eastern Spain. Atmos. Environ. 35, 2433–2447. https://doi.org/10.1016/S1352-2310(00)00496-9.

Rolph, G., Stein, A., Stunder, B., 2017. Real-time Environmental Applications and Display sYstem: READY. Environ. Model. Softw. 95, 210–228. https://doi.org/10.1016/j. envsoft.2017.06.025.

Salvador, P., Artíñano, B., Molero, F., Viana, M., Pey, J., Alastuey, A., Querol, X., 2013. African dust contribution to ambient aerosol levels across central Spain: characterization of long-range transport episodes of desert dust. Atmos. Res. 127, 117–129. https://doi.org/10.1016/j.atmosres.2011.12.011.

Sandradewi, J., Prévôt, A.S.H., Szidat, S., Perron, N., Alfarra, M.R., Lanz, V.A., Weingartner, E., Baltensperger, U.R.S., 2008. Using aerosol light absorption measurements for the quantitative determination of wood burning and traffic emission contribution to particulate matter. Environ. Sci. Technol. https://doi.org/10.1021/es702253m.

Schütz, L., Sebert, M., 1987. Mineral aerosol and source identification. J. Aerosol Sci. 18, 1–10.

Sorribas, M., Adame, J.A., Andrews, E., Yela, M., 2017. An anomalous African dust event and its impact on aerosol radiative forcing on the Southwest Atlantic coast of Europe in February 2016. Sci. Total Environ. 583, 269–279. https://doi.org/10.1016/ j.scitotenv.2017.01.064.

Stafoggia, M., Zauli-Sajani, S., Pey, J., Samoli, E., Alessandrini, E., Basagaña, X., Cernigliaro, A., Chiusolo, M., Demaria, M., Díaz, J., Faustini, A., Katsouyanni, K., Kelessis, A.G., Linares, C., Marchesi, S., Medina, S., Pandolfi, P., Pérez, N., Querol, X., Randi, G., Ranzi, A., Tobias, A., Forastiere, F., 2015. Desert dust outbreaks in southern Europe: contribution to daily PM_{10} concentrations and short-term associations with mortality and hospital admissions. Environ. Health Perspect. 124, 413–419. https://doi.org/ 10.1289/ehp.1409164.

Stein, A.F., Draxler, R.R., Rolph, G.D., Stunder, B.J.B., Cohen, M.D., Ngan, F., 2015. NOAA's HYSPLIT atmospheric transport and dispersion modeling system. Bull. Am. Meteorol. Soc. 96, 2059–2077. https://doi.org/10.1175/BAMS-D-14-00110.1.

Struckmeier, C., Drewnick, F., Fachinger, F., Gobbi, G.P., Borrmann, S., 2016. Atmospheric aerosols in Rome, Italy: sources, dynamics and spatial variations during two seasons. Atmos. Chem. Phys. 16, 15277–15299. https://doi.org/10.5194/acp-16-15277-2016.

Takamura, T., Nakajima, T., 2004. Overview of SKYNET and its activities. J. Pure Appl. Opt. 37, 3303–3308.

Titos, G., Ealo, M., Pandolfi, M., Pérez, N., Sola, Y., Sicard, M., Comerón, A., Querol, X., Alastuey, A., 2017. Spatiotemporal evolution of a severe winter dust event in the western Mediterranean: aerosol optical and physical properties. J. Geophys. Res. Atmos. 122, 4052–4069. https://doi.org/10.1002/2016JD026252.

Tobías, A., Pérez, L., Díaz, J., Linares, C., Pey, J., Alastruey, A., Querol, X., 2011. Short-term effects of particulate matter on total mortality during Saharan dust outbreaks: a case-crossover analysis in Madrid (Spain). Sci. Total Environ. 412–413, 386–389. https://doi.org/10.1016/j.scitotenv.2011.10.027.

Tomadin, L., Cesari, G., Fuzzi, S., Lobietti, A., Mandrioli, P., Lenaz, R., Landuzzi, V., Mariotti, M., Mazzucotelli, A., Vannucci, R., 1989. Eolian dust collected in springtime (1979 and 1984 years)

at the seawater-air interface of the northern Red Sea. In: Leinen, M., Sarnthein, M. (Eds.), Paleoclimatology and Paleometeorology: Modern and Past Patterns of Global Atmospheric Transport. Springer Netherlands, Dordrecht, pp. 283–310 https://doi.org/10.1007/978-94-009-0995-3_12.

UNI 11108:2004, 2004. Air quality: Method for sampling and counting of airborne pollen grains and fungal spores.

Viana, M., Querol, X., Alastuey, A., Cuevas, E., Rodríguez, S., 2002. Influence of African dust on the levels of atmospheric particulates in the Canary Islands air quality network. Atmos. Environ. 36, 5861–5875. https://doi.org/10.1016/S1352-2310(02)00463-6.

Viana, M., Pey, J., Querol, X., Alastuey, A., de Leeuw, F., Lükewille, A., 2014. Natural sources of atmospheric aerosols influencing air quality across Europe. Sci. Total Environ. 472, 825–833. https://doi.org/10.1016/j.scitotenv.2013.11.140.

Wehner, B., Wiedensohler, A., 2002. Long term measurements of submicrometer urban aerosols: statistical analysis for correlations with meteorological conditions and trace gases. Atmos. Chem. Phys. Discuss. 2, 1699–1733. https://doi.org/10.5194/ acpd-2-1699-2002.

Weingartner, E., Saathoff, H., Schnaiter, M., Streit, N., Bitnar, B., Baltensperger, U., 2003. Absorption of light by soot particles: determination of the absorption coefficient by means of aethalometers. J. Aerosol Sci. 34, 1445–1463. https://doi.org/10.1016/ S0021-8502(03)00359-8.

Wiedensohler, A., Birmili, W., Nowak, A., Sonntag, A., Weinhold, K., Merkel, M., Wehner, B., Tuch, T., Pfeifer, S., Fiebig, M., Fjäraa, A.M., Asmi, E., Sellegri, K., Depuy, R., Venzac, H., Villani, P., Laj, P., Aalto, P., Ogren, J.A., Swietlicki, E., Williams, P., Roldin, P., Quincey, P., Hüglin, C., Fierz-Schmidhauser, R., Gysel, M., Weingartner, E., Riccobono, F., Santos, S., Grüning, C., Faloon, K., Beddows, D., Harrison, R., Monahan, C., Jennings, S.G., O'Dowd, C.D., Marinoni, A., Horn, H.-G., Keck, L., Jiang, J., Scheckman, J., McMurry, P.H., Deng, Z., Zhao, C.S., Moerman, M., Henzing, B., de Leeuw, G., Löschau, G., Bastian, S., 2012. Mobility particle size spectrometers: harmonization of technical standards and data structure to facilitate high quality long-term observations of atmospheric particle number size distributions. Atmos. Meas. Tech. 5, 657–685. https://doi.org/10.5194/amt-5-657-2012.

Yang, M., Howell, S.G., Zhuang, J., Huebert, B.J., 2009. Attribution of aerosol light absorption to black carbon, brown carbon, and dust in China - interpretations of atmospheric measurements during EAST-AIRE. Atmos. Chem. Phys. 9, 2035–2050. https://doi.org/10.5194/acp-9-2035-2009.

8

TOWARDS A MODEL FOR AEROSOL REMOVAL BY RAIN SCAVENGING: THE ROLE OF PHYSICAL-CHEMICAL CHARACTERISTICS OF RAINDROPS

Sent to Environmental Research, February 2020

8.1. INTRODUCTION

Over years, several authors have highlighted the negative impact of air pollutants on human health and the environment (Bernstein et al., 2004; Kampa and Castanas, 2008; Ren-Jian et al., 2012), especially in megacities (Lelieveld et al., 2015; Mage et al., 1996; Naddafi et al., 2012). Atmospheric wet deposition plays a crucial role in mitigating these negative effects, as it acts directly on the removal and transport of different pollutants and soluble gases from the atmosphere to the earth's surface (Keresztesi et al., 2017; Seinfeld and Pandis, 1998), through two main processes: in-cloud and below-cloud scavenging. Below-cloud scavenging depends on the characteristics of rainfall (raindrop size distribution and rainfall rate) and on the local/regional concentration of the particles and gases in the atmosphere and in-cloud processes involve both, the condensation of water vapor onto aerosols and the incorporation of gases by reactions in the aqueous phase (Celle-Jeanton et al., 2009; Xu et al., 2017).

The study of the chemical properties of rainwater, and of the concentration and composition of the aerosol, provides useful information on the emissions of pollutants, since it helps to identify the possible sources that contribute to rainwater chemistry, local and regional dispersion of pollutants and their impact on the ecosystem (Martins et al., 2019; Sanets and Chuduk, 2005; Zhang et al., 2007). The composition of rainwater depends on several factors, such as the local and long-range emissions sources, geography and meteorological conditions (Alastuey et al., 1999; Calvo et al., 2012; Jain et al., 2019; Knote et al., 2015; Mori et al., 2014).

The scavenging process of different species is affected by the intensity and volume of precipitation (Calvo et al., 2012; Custódio et al., 2014; Luan et al., 2019; Pan and Wang, 2015; Uchiyama et al., 2017). However, there are many other parameters involved in this process, such as concentration, size distribution and composition of atmospheric aerosol and raindrop size distribution (Blanco-Alegre et al., 2019, 2018; Fredericks and Saylor, 2019; Zikova and Zdimal, 2016). In recent years, several authors have proposed different models to explain the removal

process of aerosols by rain. For example, Olszowski and Ziembik (2018) presented a linear model for the reduction of PM_{10} mass concentrations, which includes the type of precipitation and the water vapor content in air. Moreover, Roy et al. (2019), proposed a linear model to predict the aerosol scavenging, based on the influence of rain rate and duration. In previous studies, carried out in León, Spain, the influence of the physical characteristics of precipitation on the total concentration of particles (Castro et al., 2010) and on the removal of black carbon (Blanco-Alegre et al., 2019), have already been reported. However, studies integrating the chemical properties of aerosol and precipitation and the physical properties of precipitation are scarce, underestimating the potential synergies between them. Studies involving the physical-chemical parameters of precipitation can provide valuable information to deepen the understanding of the process of aerosol removal by rainfall.

A one-year sampling campaign of aerosols and precipitation was carried out in León (NW Spain), with the objective of studying the influence of aerosol chemical composition and the physical characteristics of precipitation (from disdrometer data) on the physical-chemical properties of rainwater and, consequently, on the scavenging process of different species. With this information several models have been stablished to explain the removal process for different chemical species in the atmospheric air.

8.2. EXPERIMENTAL

8.2.1. Sampling instruments

The sampling campaign was carried out in León city, located in the NW of the Iberian Peninsula (42º 36′ N, 05º 35′ W and 838 m above sea level) (Fig. 8.1). León is mainly a residential city, with a population of 125,317 inhabitants (2017 report of the National Institute for Statistics www.ine.es) and characterized by the absence of large air-emitting industries and by a high contribution of air emissions from traffic and small-scale heating devices, especially during the cold months (Oduber et al., 2018).

FIG. 8.1. Location of León in the Iberian Peninsula.

The climate is continental type with Mediterranean influences. The winters are long and cold with daily mean temperatures of 5 °C, and summers are warm with mean temperatures of 20 °C. On average, there are 2624 sun hours, 78 rain days and 16 storm days per year, with frequent frosts in winter (74 frost days per year, on average), and a mean of 16 snow days. Summer droughts are very common, with sporadic storm events, often with hail (Fernández-Raga et al., 2017).

8.2.2. Materials and methods

8.2.2.1. PM_{10} and rainwater sampling

The sampling campaign was carried out between 9 March 2016 and 14 March 2017 on the roof of the Faculty of Veterinary Sciences of the University of León, located in a suburban area in the NE of the urban center. During the sampling period, a total of 74 rainwater samples and a total of 739 PM_{10} samples (369 quartz filters and 370 teflon filters) were collected. The filters and rainwater samples were collected every 24 h, starting at 1200 UTC every day.

The sampling of PM_{10} was carried out using a low volume sampler (TECORA, ECHOPM) equipped with 47 mm diameter teflon filters and using a high volume sampler (CAV-Mb) equipped with 150 mm diameter quartz filters. PM_{10} mass was determined by gravimetry, using an electronic semi-micro balance (Mettler Toledo, XPE105DR).

Rainwater samples were collected in glass bottles using a wet-only precipitation sampler (Eigenbrodt UNS 130/E). Conductivity and pH of precipitation samples were determined immediately after collection. Then, the water samples were filtered through a 15 mm diameter quartz filters in order to separate the insoluble and soluble fractions.

8.2.2.2. PM_{10} and rainwater analysis

The thermo-optical technique was used for the determination of organic and elemental carbon (OC and EC) of quartz filters of PM_{10}, and for the determination of water insoluble organic and elemental carbon (WIOC and WIEC) of the insoluble rainwater fraction, following the methodology described by Custódio et al. (2014) and Pio et al. (2011).

Teflon filters were used for the analysis of water-soluble inorganic ions by ionic chromatography, and for the determination of major trace elements, using PIXE technique (Particle-Induced X-ray Emission) (Lucarelli et al., 2015), following the methodology described by Oduber et al. (2019a).

The soluble fractions of rainwater samples were separated into two fractions; one of them was used for the determination of dissolved organic carbon (DOC) content. This analysis was carried out by combustion and infrared detection in a Total Organic Carbon Analyzer Shimadzu (TOC-VCPH). The other fraction was filtered through a 13 mm polyvinyl difluoride (PVDF) syringe filter with 0.2 μm pore size (Whatman™) and used for the determination of the water-soluble inorganic ions by ionic chromatography. The chromatographic analysis was performed on a Thermo Scientific DionexTM ICS-5000 equipment provided with an IonPac® CS16 column

(4 × 250 mm) and an IonPac® AS11 column (4 × 250 mm) for the analysis of cations (Li^+, Na^+, K^+, Ca^{2+}, Mg^{2+}, NH_4^+) and anions (F^-, Cl^-, SO_4^{2-}, NO_3^-, NO_2^-), respectively.

8.2.2.3. Disdrometer

The raindrop size spectrum was obtained with a laser disdrometer (Laser Precipitation Monitor, LPM) of Thies Clima, which registered drops between 0.125 and 8 mm in 22 drop size ranges, on a 1-minute basis (Fernández-Raga et al., 2009). From the data provided by the LPM, the following rainfall variables were obtained: precipitation intensity, accumulated precipitation, number of drops, volume swept by falling drops, mean and standard deviation of raindrop sizes.

8.2.2.4. Circulation weather types

In order to study the relationship between the precipitation and the weather type, a Circulation Weather Types (CWTs) classification, based on Lamb (1972), was carried out. Four indices associated with the direction and vorticity of geostrophic flow (southerly flow SF, westerly flow WF, southerly shear vorticity ZS and westerly shear vorticity ZW) have been calculated from the surface pressure in 16 grid points distributed over the Iberian Peninsula (Trigo and DaCamara, 2000). They have been used to establish each of the 26 different CWTs: i) 8 "pure" weather types, (N, S, E, W, NW, SW, SE and NE); ii) 2 "non-directional" (anticyclonic-A and cyclonic-C); iii) 16 "hybrid" types, as a result of the combination between "non-directional" and "pure" types: AN, ANE, ANW, AS, ASE, ASW, AE, AW and CN, CNE, CNW, CS, CSE, CSW, CE, CW. More information about this classification can be found in Blanco-Alegre et al. (2019), Fernandez-Raga et al. (2017) and Trigo and DaCamara (2000).

8.2.2.5. Statistical analysis

The statistical treatment has been carried out using SPSS software (IBM Statistics Software V. 24). The Kruskal-Wallis non-parametric test (Kruskal and Wallis, 1952) followed by Dunn test (Dunn, 1964), were applied to the data in order to identify statistically significant differences. The correlations were calculated using the nonparametric Pearson's rank correlation method. The principal component analysis (PCA) was performed, applying a matrix of Varimax rotated components to the studied species, in order to determinate a common origin. The application of an automatic linear modeling (IBM SPSS Statistics 24) by step-wise, with an entry probability of 0.05 was also used.

8.2.2.6. Additional data

Seasons have been defined as follows: *i*) winter: from 21 December to 20 March; *ii*) spring: from 21 March to 20 June; *iii*) summer: from 21 June to 20 September; and *iv*) autumn: from 21 September to 20 December. Weather information (temperature, wind and relative humidity) was obtained from a weather station installed in the sampling point. The origin of air masses during the study period was estimated by the HYSPLIT model (Draxler and Rolph, 2012; Rolph et al., 2017; Stein et al., 2015) through the determination of 3-day back trajectories (at 500, 1500 and 3000 m).

8.2.2.7. Volume-weighted mean precipitation concentrations

Volume-weighted mean concentrations (*VWM*, in μeq L^{-1}) of ionic species in rainwater have been calculated using Eq. (8.1):

$$VWM = (\sum_{i=1}^{N} C_i P_i) / \sum_{i=1}^{N} P_i \quad \text{Equation 8.1}$$

where *Ci* is the concentration of each species in μeq L^{-1}, *Pi* the precipitation amount for each precipitation event, and *N* the total number of precipitation events in each study period.

8.2.2.8. Neutralization factors and enrichment factors

Neutralization factors (*NF*, dimensionless) have been calculated following Eq. (8.2) (Kulshrestha et al., 1995):

$$NF_x = C_x / [C_{SO_4^{2-}} + C_{NO_3^-}] \quad \text{Equation 8.2}$$

where C_x is the concentration of the species of interest and $C_{SO_4^{2-}}$ and $C_{NO_3^-}$ are the concentrations of sulfate and nitrate in rainwater, respectively. All ion concentrations are expressed in μeq L^{-1}.

The enrichment factors (*EF*, dimensionless) were calculated for both the seawater and crustal material, according to Eq. (8.3) (Kulshrestha et al., 1996; Zhang et al., 2007):

$$EF = \frac{(C_x/C_r)_{sample}}{(C_x/C_r)_{crustal/seawater}} \quad \text{Equation 8.3}$$

where $(C_x/C_r)_{sample}$ is the ratio between the concentration of an element *x* and that of a reference element (*r*) in the sample. $(C_x/C_r)_{crustal/seawater}$ is the ratio between the same elements but considering the concentrations in the seawater or crustal material (Keene et al., 1986; Zhang et al., 2007).

In order to determine the best seawater tracer, the Mg^{2+}/Na^+ ratio was evaluated. A ratio higher than 0.227 indicates a crustal Mg^{2+} influence and a lower ratio suggests a crustal Na^+ origin (Jordan et al., 2003). In this study, the mean Mg^{2+}/Na^+ ratio was 0.713 and, according to this result, sodium was used as seawater reference element. Calcium was used as crustal reference, since it is a typical lithophylic element representative of the soil composition.

Besides, the source contribution of seawater and crustal was obtained as follows (Zhang et al., 2007):

$$Seawater\ fraction\ \% = 100(C_x/C_{Na^+})_{seawater} / (C_x/C_{Na^+})_{sample} \quad \text{Equation 8.4}$$

$$Crustal\ fraction\ \% = 100(C_x/C_{Ca^{2+}})_{crustal} / (C_x/C_{Ca^{2+}})_{sample} \quad \text{Equation 8.5}$$

8.2.2.9. Scavenging ratio

Scavenging ratios (*W*, dimensionless) were calculated according to Eq. 8.6 (Cheng and Zhang, 2017; He and Balasubramanian, 2008; Kasper-Giebl et al., 1999).

$$W = \frac{C_{rain}}{C_{air}} \times \frac{\rho_{air}}{\rho_w} \quad \text{Equation 8.6}$$

where, C_{rain} is the concentration, in mg L^{-1}, of each studied species in rainwater samples, and C_{air} is the concentration in μg m^{-3}, of the same species in the aerosol samples during the precipitation event. ρ_{air} and ρ_w are the densities of air (1.290 kg m^{-3}) and water (106 mg L^{-1}), respectively, at 20 °C and 1 atm.

Following Blanco-Alegre et al. (2019) and Cugerone et al. (2018), for the determination of *W*, the following considerations were taken into account:

a) Only events in which the rainfall duration covered more than 15% of the 24 hours of sampling were considered.

b) Rain events with a variation in wind speed greater than 2 m s^{-1} were excluded from the sample.

c) Due to aerosol samples were collected at 24-h intervals, it is assumed that the rainwater samples are representative of this sampling period.

8.2.2.10. Removal coefficients

Removal coefficients (ΔC_{rel}) were calculated as follows:

$$\Delta C_{rel} = \frac{\Delta C}{C_1} \times 100 = \frac{C_2 - C_1}{C_1} \times 100 \quad \text{Equation 8.7}$$

where C_2 and C_1 are the concentration of the studied species after and before the precipitation event, respectively. Consequently, a negative ΔC_{rel} indicates effective scavenging.

Besides the considerations above mentioned for *W* determination, ΔC_{rel}, was calculated as follows:

a) Two types of precipitation events were considered: *i*) a "24-h event", when the precipitation period covered more than 15% of the 24 hours of sampling and *ii*) a "full event", taking the precipitation event as the consecutive rain days, and considering that the event ended when there was a minimum of 48 hours without precipitation after collection of the last rainwater sample.

b) Aerosol concentrations before and after the precipitation event were obtained as a mean value, calculated from the concentrations 2 days before and 2 days after the event, respectively.

8.3. RESULTS AND DISCUSSIONS

8.3.1. Characterization of precipitation

During the sampling period, a total of 485 mm of precipitation, distributed in 118 days, was registered in León. This value is very close to the annual average precipitation, reported in León by the Spanish National Agency for Meteorology (AEMET in its Spanish acronym), of 515 mm. April was the month with more precipitation days (18 days) and more accumulated precipitation (112.4 mm), followed by February and May (Fig. 8.2a). Besides, July, August and September were the months with less rain days. The lowest accumulated precipitation of the entire campaign (3.7 mm) was registered in July.

The mean precipitation intensity, taking into account the individual precipitation events, was 0.8 mm h^{-1} in both spring and autumn, 1.7 mm h^{-1} in summer and 0.7 mm h^{-1} in winter. The longest precipitation episodes were recorded in spring, with a mean duration of 7 ± 5 days, and a maximum duration of 15 days, between 09 and 24 April 2016, although it only rained during 35% of the time period.

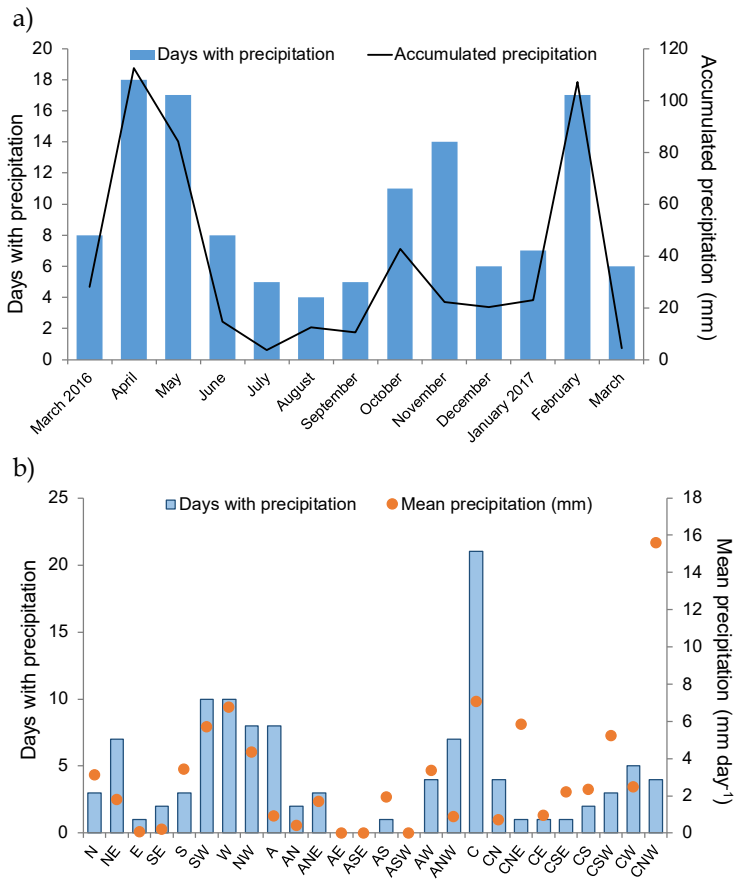

FIG. 8.2. a) Monthly evolution of days with precipitation and accumulated precipitation and b) days with precipitation and mean precipitation for each of the Circulation Weather Types.

The most frequent weather type during the rainy days was the cyclonic type (C) with 21 days (19% of the total), followed by westerly types SW and W, both with 10 days (9% each of the

total) (Fig. 8.2b). The weather types with more accumulated precipitation were: cyclonic (C) with 149 mm, westerly (W) with 68 mm and northwesterly cyclonic (CNW) with 62 mm. Regarding to the average daily precipitation volume, the type CNW showed the highest value with 15.6 mm day^{-1}, followed by C with 7.1 mm day^{-1} and *W* with 6.8 mm day^{-1}.

8.3.2. Rainwater chemical composition

8.3.2.1 Inorganic ions

During the sampling period, 74 rain samples, distributed in 31 precipitation events, were analyzed (Table 8.1). The season with more samples was winter, with 25 rainwater samples (in 23 precipitation events), although the season with more volume collected was spring. The season with less rainwater samples was summer, with 6.

TABLE 8.1. Annual and seasonal Volume-Weighted Mean (*VWM*) ion concentrations, Dissolved Organic Carbon (DOC), Water Insoluble Organic and Elemental Carbon (WIOC and WIEC, respectively) in rainwater.

	Annual	**Winter**	**Spring**	**Summer**	**Autumn**
Number of 24-h event types	31	8	9	4	10
Total precipitation (mm)	363	130	130	25	78
Number of rainwater samples collected	74	25	23	6	20
Volume collected (L)	16.64	5.63	6.68	0.48	3.85
VWM (μeq L^{-1})					
Na^+	6.64 ± 0.07	11.72 ± 0.11	3.35 ± 0.08	5.3 ± 0.3	5.2 ± 0.2
NH_4^+	21.5 ± 0.2	14.7 ± 0.2	24.5 ± 0.2	40 ± 2	20.7 ± 0.3
Mg^{2+}	3.19 ± 0.02	3.97 ± 0.03	2.09 ± 0.02	7.6 ± 0.2	2.50 ± 0.05
K^+	3.37 ± 0.01	3.02 ± 0.02	2.92 ± 0.02	5.21 ± 0.04	4.03 ± 0.03
Ca^{2+}	5.92 ± 0.11	8.80 ± 0.10	8.09 ± 0.10	35 ± 2	5.02 ± 0.08
Cl^-	9.43 ± 0.08	14.61 ± 0.12	6.67 ± 0.11	9.2 ± 0.3	6.6 ± 0.2
SO_4^{2-}	13.59 ± 0.08	14.62 ± 0.12	12.33 ± 0.10	20.2 ± 0.9	12.11 ± 0.15
NO_3^-	13.18 ± 0.09	10.52 ± 0.09	13.07 ± 0.11	27.0 ± 1.3	12.81 ± 0.11
VWM (mg L^{-1})					
DOC	1.554 ± 0.014	1.520 ± 0.011	0.685 ± 0.004	2.92 ± 0.15	2.57 ± 0.05
WIOC	0.234 ± 0.002	0.173 ± 0.002	0.225 ± 0.004	0.83 ± 0.02	0.1522 ± 0.0015
WIEC	0.0180 ± 0.0001	0.0157 ± 0.0002	0.0211 ± 0.0003	0.0192 ± 0.0003	0.0158 ± 0.0002

The inorganic content of rainwater (Table 8.1) reveals a predominance of NH_4^+, followed by SO_4^{2-} and NO_3^-. The statistical correlation between SO_4^{2-}, NO_3^- and NH_4^+ ($r > 0.9$, $p < 0.01$) and the source contribution indicate that nitrate and sulfate have a common origin, mainly anthropogenic (92.3 and 99.8%, respectively, Table A5.1 in Annex 5). These elements, related to secondary aerosol showed their highest concentrations during the AN, CN and NE weather types (above 30 μeq L^{-1} for SO_4^{2-}, 48 μeq L^{-1} for NO_3^- and 70 μeq L^{-1} for NH_4^+), all of them with a northern flow component. These high levels may be due to the presence of two major companies, a thermal

power plant and a cement factory about 30 km north of León. In addition, from the point of view of medium and long-range transport of pollutants, northeast is the direction where the air masses from industrial areas in Spain and Europe come from. Additionally, in summer the secondary photochemical reactions are more frequent and there is a low volume of precipitation, which can trigger the concentrations of SO_4^{2-}, NO_3^- and NH_4^+.

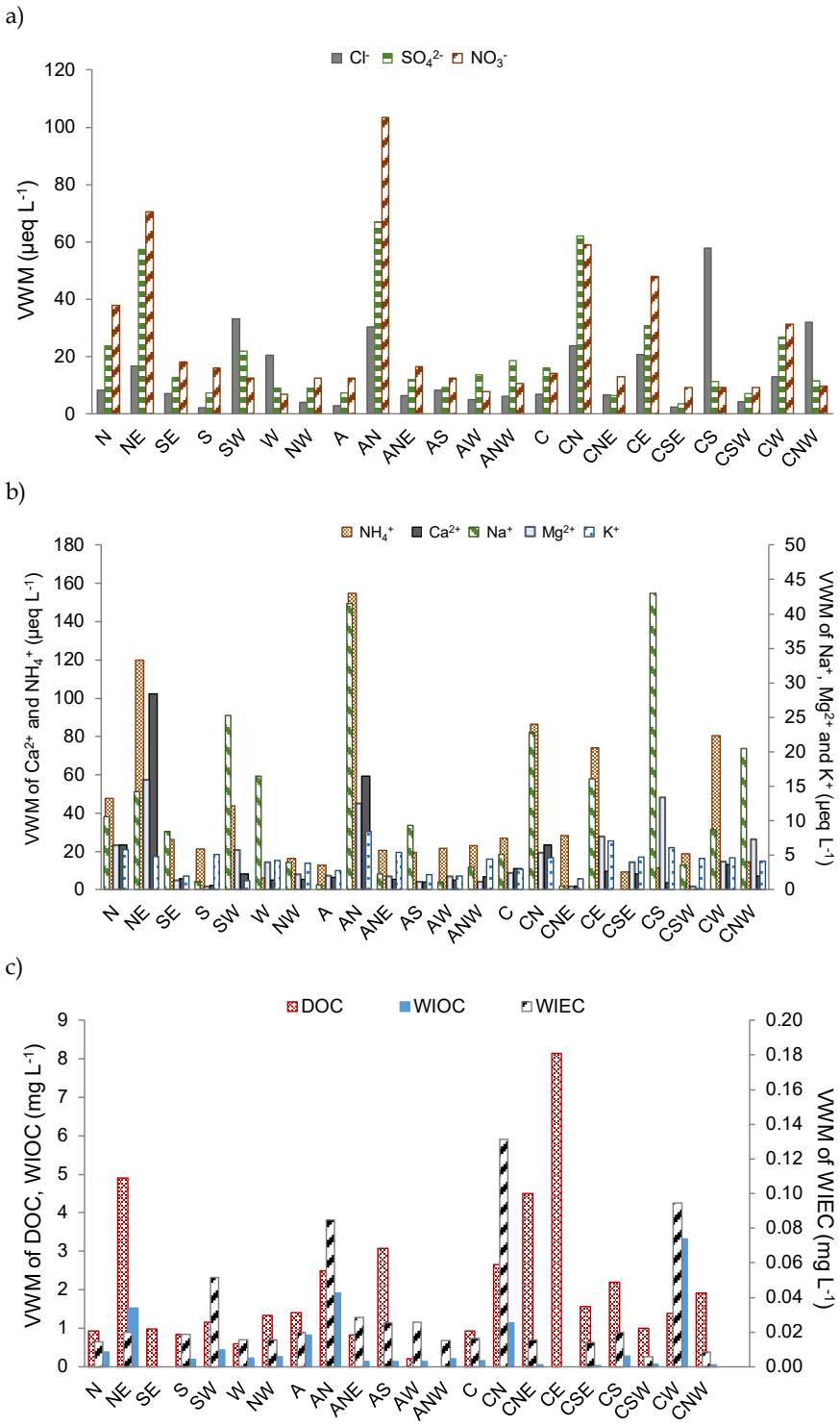

FIG. 8.3. Volume-Weighted Mean (*VWM*) for the different categories of Circulation Weather Types (CWT) for a) inorganic anions, b) inorganic cations and c) the carbonaceous fraction (DOC, WIOC, WIEC).

The highest *VWM* Na^+ and Cl^- concentrations were reached in winter, with 11.72 ± 0.11 and 14.61 ± 0.12 μeq L^{-1}, respectively (Table 8.1). Both the enrichment factor of 1.2 (Table A5.1 in Annex 5) and the significant correlation between these two ions (r = 0.91, p < 0.01), reflect the common marine origin. The highest *VWM* values of these sea-salt related elements, were recorded during the CS, CN, AN and SW weather types (Fig. 8.3a and 8.3b), reaching concentrations between 25 and 43 μeq L^{-1} for Na^+ and between 27 and 58 μeq L^{-1} for Cl^-.

High Ca^{2+} and Mg^{2+} concentrations were recorded in summer, reflecting the contribution from dust intrusion events which arrived at the Peninsula during warmer months, confirmed by the enrichment factor result (Table A5.1 in Annex 5). The highest potassium concentration is observed in summer, when there are frequent wildfires and African dust events in the Iberian Peninsula that could rise the K^+ values (Vicente et al., 2013). The highest volumetric concentrations of crustal-related elements, Ca^{2+} and Mg^{2+}, were observed in AN, CS and NE weather types, with *VWM* values ranging between 17 and 101 μeq L^{-1} for Ca^{2+} and between 12 and 16 μeq L^{-1} for Mg^{2+}; while the lowest *VWM* values were recorded mainly in the hybrid cyclonic types CNE and CSW, due to the significant dispersion of the contaminants in the cyclonic circulations and large periods of continuous precipitation.

8.3.2.2 Carbonaceous fraction

The organic carbonaceous fraction can be scavenged by wet deposition in two forms, soluble (DOC) and insoluble (WIOC) fractions. The contribution from DOC to the total organic fraction ranged between 71% and 82%, with the lowest contribution obtained in summer and the highest in autumn. However, in summer and autumn the DOC values are higher (Table 8.1). There is a significant correlation between DOC and the main crustal elements in summer and spring (r > 0.5, p < 0.05). In these seasons, the air masses coming mainly from the south, travel through large areas of forest until they reach León; therefore, the concentration of dissolved organic carbon could be partly related to the transport of biogenic material from the south of the Iberia Peninsula. Additionally, the highest photochemical activity during these seasons could also to contribute to the oxidation of volatile organic compounds (VOCs) into soluble organic particles. Between summer and spring there is also a high incidence of wildfires in the Iberian Peninsula (Alonso-Blanco et al., 2012; Alves et al., 2011; Vicente et al., 2013, 2012), that can emit large amount of water-soluble organic compounds (Alves et al., 2011), causing an increase in DOC concentrations. While in autumn, DOC concentrations could be affected by anthropogenic emissions from the use of domestic heating systems (Siudek et al., 2015). DOC values are higher for NE, CE and CNE weather types (Figure 8.3c), reaching concentrations up to 8 mg L^{-1}. Less than 3 km NE of the city of León there is a large mass of plants, which contributes a large amount of biogenic material and may be responsible for the increase in concentrations of dissolved organic carbon (Oduber et al., 2019b).

The significant correlation between WIEC and WIOC during winter and spring (r > 0.7, p < 0.01) may indicate a common origin (traffic and fossil fuel primary emissions) (Favez et al., 2008; Theodosi et al., 2010). Moreover, the highest WIOC concentrations were recorded for CW and AN weather types, while the highest WIEC were observed for CW, CN and AN weather types.

8.3.3. Acidic contribution

The individual pH values of rainwater ranged between 4.2 and 7.2 (Fig. 8.4a). The *VWM* pH of the entire campaign was 5.87 ± 0.02, while the mean annual conductivity was 27.0 ± 0.2 μS cm^{-1}, reflecting the low influence on precipitation of emissions from large industries and other local sources. The lowest conductivity (2.77 μS cm^{-1}, in 103 ml) and highest pH value (7.20, in 38 ml) were observed in May 2016 and February 2017 (Fig. 8.4b), respectively, after several days of continuous rain. The highest conductivity (164.90 μS cm^{-1}, in 27 ml) and lowest pH (4.23, in 304 ml) were registered during forest fire events that took place in Portugal between June and August 2016.

The Kruskal-Wallis test shows significant differences between pH values of spring rainwater samples and those of summer and autumn. Winter and spring are rainy seasons in León, which helps to clean the atmosphere. Consequently, an increase in the pH and a decrease in the conductivity of the rainwater can be observed when compared to other seasons. A reduction of the conductivity values due to the abundant rainfall was also observed by Zhang et al. (2007) in rainwater samples from southern China, indicating the dilution effect on the atmospheric pollution.

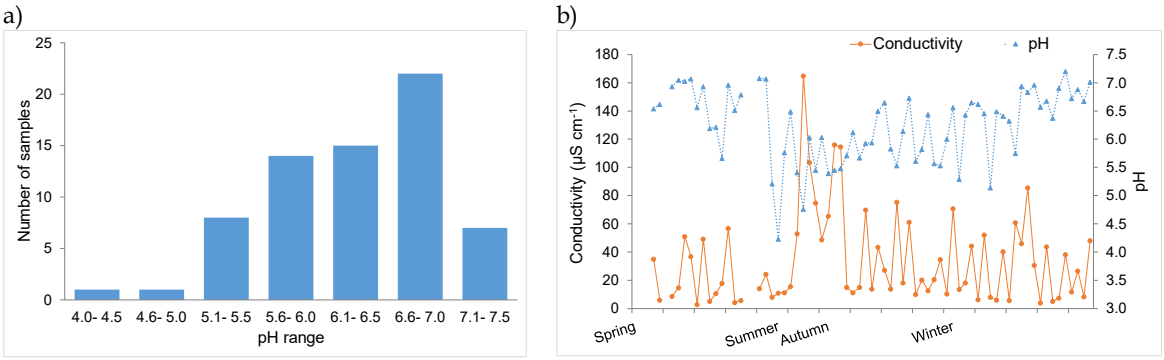

FIG. 8.4. a) Frequency distribution of pH and b) daily evolution of pH and conductivity of rainwater samples.

The highest neutralization factor was obtained by NH_4^+ with 0.8 ± 0.5, while the lowest *NF* was found for Mg_2^+ with 0.09 ± 0.09 (Table A5.2 in Annex 5). These results suggest that the crustal components neutralized a small fraction of the available acid in the precipitation and that ammonia plays an important role in the neutralization of the rainwater, as well Na^+, mainly in winter. Ca^{2+} shows statistically significant differences between the *NF* values of summer and the rest of the seasons, confirming the neutralizing effect of this crustal component when the dust contribution is greater. The high *NF* of Na^+ in winter (0.7 ± 0.8) could partly justify the high pH values observed in this season.

8.3.4. Scavenging ratios

The scavenging ratios (*W*) provide valuable information on the relationship between the concentration of the pollutants in rainwater and their concentrations in air. The scavenging ratios were higher in summer than in other seasons, except for Na^+, K^+, SO_4^{2-} and EC (Table 8.2). In León, convective phenomena are frequent in summer, which generally cause short and intense

precipitation events (Fernández-Raga et al., 2017). Kulshrestha et al. (2003, 2009) studied the relation between the aerosol size and duration of precipitation in below-scavenging processes, reporting that scavenging ratios increase with the increase of the precipitation intensity for species present in fine particles, such as NH_4^+, K^+ and NO_3^-. Moreover, the soil-derived coarse particles are also effectively scavenged due to the inertial impaction by raindrops through the rain columns.

TABLE 8.2. Seasonal scavenging ratios (*W*, dimensionless) for each analyzed species and mean seasonal precipitation intensity.

Season	Intensity (mm h^{-1})	*W* (×10^3)									
		Na^+	NH_4^+	Mg^{2+}	K^+	Ca^{2+}	Cl^-	SO_4^{2-}	NO_3^-	EC	DOC + WIOC
Winter	0.7 ± 0.9	178.9	108.3	183.1	31.6	106.2	60.0	51.5	24.6	0.034	1.6
Spring	0.8 ± 0.6	47.1	228.0	106.9	67.4	88.3	116.2	46.8	46.5	0.136	1.4
Summer	1.7 ± 1.5	88.3	290.9	823.4	59.3	231.7	1061.9	35.9	157.8	0.013	5.7
Autumn	0.8 ± 1.7	109.9	64.7	126.7	59.3	110.7	45.0	30.5	26.4	0.049	2.3

The scavenging ratio also depends on the particle sizes (Encinas et al., 2004; Jaffrezo and Colin, 1988). Ions related to marine and crustal sources (Na^+, Mg^{2+}, Cl^- and Ca^{2+}) show high *W* values, indicating that they could be scavenged more efficiently than ions mainly bound to the fine fraction, such as the anthropogenic ions (NO_3^-, SO_4^{2-} and NH_4^+) and K^+, which showed lower *W* values. However, NH_4^+ exhibited one of the highest scavenging ratios in spring and summer. The composition of the rainwater is determined by the scavenging process of both gases and particles, thus, the scavenging ratios can be overestimated for some species such as Cl^-, $NO3^-$, SO_4^{2-} and NH_4^+, due to the incorporation to the rain droplets of the gases HNO_3, HCl, SO_2 and NH_3, especially in spring and summer, when the formation of secondary aerosols is favored by the photochemical reactions. Kasper-Giebl et al. (1999) report that NO_3^- values in rainwater are predominantly due to gas-phase scavenging of HNO_3 (88-96%), while NH_4^+ in rainwater is formed between 49 and 79% by particulate NH_4^+.

8.4.5. Removal coefficients

The removal coefficient (ΔC_{rel}) allow us to infer information about the removal mechanism in the air, through the evolution of the concentration of pollutants before and after a precipitation event. Principal component analysis (PCA) was performed by applying a matrix of Varimax rotated components to the studied species. Three main groups were extracted (Tables. A5.4 and A5.5 in Annex 5), according to their common origin: a) Al, Si, Ca, Ti, Fe, Mg, Mn and K as crustal elements; b) Na and Cl as marine elements and c) NH_4^+, SO_4^{2-}, NO_3^- as secondary aerosol. Episodes of high aerosol emissions (dust intrusion, biomass combustion and sulfate episodes) causing an extreme increase in concentrations during the precipitation event were excluded from the database for the calculation of removal coefficients, since they are not representative for this study.

The results show that, in general, the removal coefficients of almost all studied species present negative values (Fig. 8.5), indicating that precipitation helps to reduce the concentrations

of all these species in the atmosphere. When comparing the monthly removal coefficient of the 24 h events with those of the full events (Fig. 8.5a and 8.5b), it is observed that scavenging is more efficient when the precipitation event is longer, increasing the ΔC_{rel} by 82%, on average. Olszowski (2014) reported that rainfalls with six hours of duration are 3.5 times more effective than similar intensity rainfalls with half an hour of duration in removing PM_{10}.

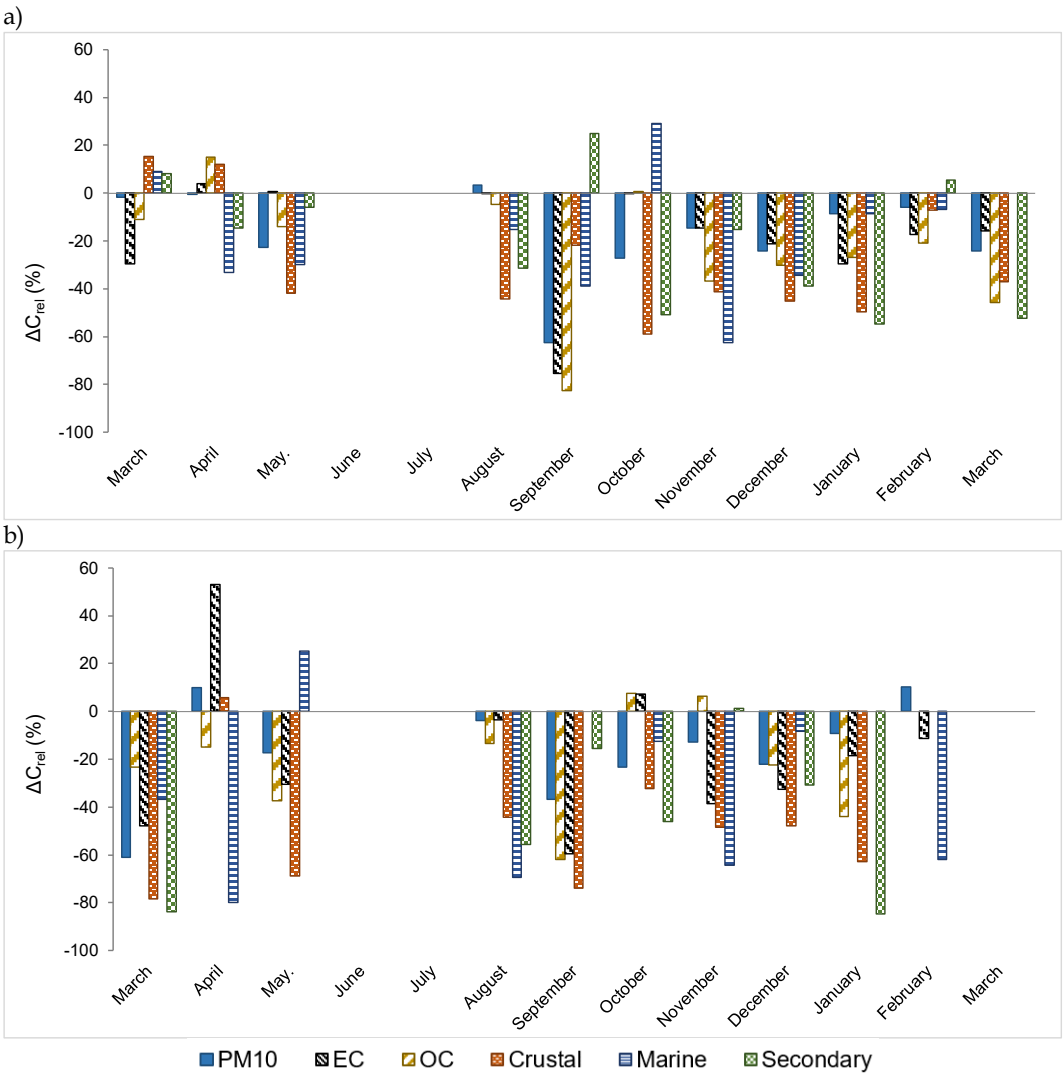

FIG. 8.5. Monthly evolution of removal coefficients (ΔC_{rel}) of particulate matter (PM_{10}), carbon fractions (EC and OC), crustal elements (Al, Si, Ca, Ti, Fe, Mg, Mn and K), marine elements (Na and Cl), secondary aerosol (NH_4^+, SO_4^{2-}, NO_3^-), for a) 24-h rainwater samples and b) full events of precipitation.

The effect of the precipitation intensity and duration on the removal coefficient is shown in Fig. 8.6. In general, intensities between 0.5 and 0.8 mm h^{-1} showed an increase in the removal coefficient for long time periods (> 20 hours of rain). Intensities higher than 0.9 mm h^{-1} show maxima ΔC at short periods of time (between 4 and 6 hours). Olszowski (2014) observed that rains with intensities greater than 4 mm h^{-1} are approximately 35% more effective in removing PM from the air than precipitations with intensities lower than 0.5 mm h^{-1}, suggesting that PM_{10} concentrations increase much faster after a light rain event. Similar results were also reported by

Castro et al. (2010) in a study carried out in León, Spain, in spring 2005, when it was observed that with intensities over 3.2 mm h^{-1}, there was an intense washout and the number of both small and large particles decreased significantly. However, low rain intensities (< 0.5 mm h^{-1}) showed high removal coefficients in a period between 7 and 9 hours, except for crustal-related elements, and an increase of ΔC in long periods for the elements related to secondary aerosols. These results, as well as those reported by Kulshrestha et al. (2009), suggest that short-duration and high-intensity rain events effectively remove coarse mode particles, such as particles related to crustal and marine sources, probably by a process of below-cloud scavenging, while rain of low intensity, but with longer duration, is more effective in removing fine particles.

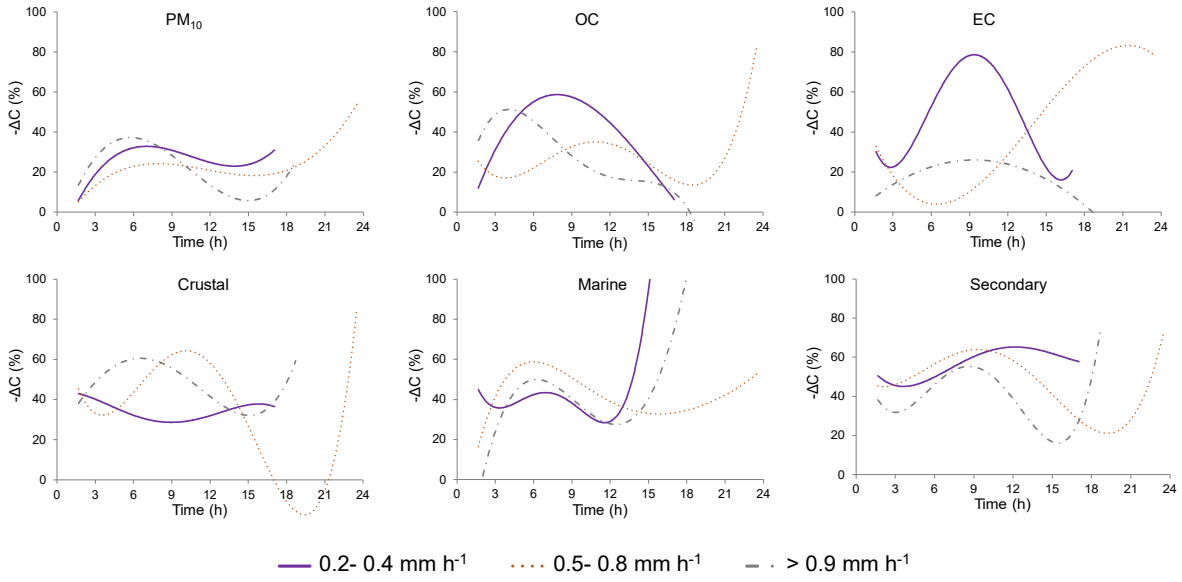

FIG. 8.6. Evolution of the removal coefficient with the duration of the daily precipitation event as a function of the rain intensity and for PM_{10}, carbonaceous fraction (OC and EC), crustal, marine and secondary aerosols.

8.4.6. Linear predictive models for rain scavenging and for chemical properties of rainwater

Linear models have been built from the data obtained for each studied species in each event. The application of automatic linear modeling (IBM SPSS Statistics 24) by step-wise, with an entry probability of 0.05, was used. Table 8.3 only shows the dependent and independent variables and the statistically significant coefficients ($p < 0.05$) used to construct the multi-linear models. The statistically significant models for the prediction of rainwater chemical characteristic were: a) concentrations in rainwater of WIOC, DOC, WIEC, SO_4^{2-} and NO_3^-, b) mass in rainwater of Ca^{2+}, SO_4^{2-}, c) scavenging ratios (W) of NO_3^-, and d) removal coefficients (ΔC) during 24h events and ΔC during full events for PM_{10}, OC, EC, crustal, marine and secondary aerosol.

Previously, the Pearson correlations were calculated between rainwater concentrations, W and ΔC with the following independent variables:

- Chemical aerosol properties: the concentration in air of each species before precipitation (C_1).

- Physical parameters of precipitation: event duration, time with precipitation during the daily sampling period of aerosol (t), accumulated precipitation (Prec.), mean rainfall intensity (Intensity), mean raindrop size (D_{size}), sum of volume swept by falling drops (V_{swept}), total number of drops (N_{drops}). Besides, the time without rain between two precipitation events (t_{before}) has been included.

The multi-linear models observed in table 8.5, were constructed as:

$$y_j = \sum \alpha_{ij} X_{ij} + \beta_{ij} \qquad \text{Equation 8.8}$$

where subscript j= 1 to 18 refers to the dependent variables (Table 8.3): rainwater concentrations, W and ΔC. αij is the coefficient of the linear model for each independent variable (i) for each j, i=1 to 6, and β is the intercept.

The results show that:

- The amount of DOC and water-soluble ions in rain samples, Ca^{2+}, SO_4^{2-}, NO_3^-, increases with the volume swept by the drops that fall, probably due to the high solubility in water of these compounds, so that a greater volume of precipitation or total number of drops, favors the elimination of these species.

- A negative dependence between V_{swept} and water-insoluble elemental carbon (WIEC) was observed, while the water-insoluble organic carbon (WIOC) is dependent of the raindrop diameter and the time between two precipitation events. Scavenging of insoluble species can be more affected by the inertial impact of the raindrops through the columns of rain. This behavior was also described by Blanco-Alegre et al. (2019), who deduced a multi-linear model to estimate the black carbon scavenging by rain.

- In general, the decrease in the concentration of PM_{10}, OC, EC, crustal, marine and secondary related aerosols after a precipitation event is affected by the concentration of each species before the event. The negative coefficient in all cases shows that the higher the concentration before the precipitation event, the more efficient the elimination process.

- The ΔC of the 24-hour events showed positive coefficients for the time elapsed between two consecutive precipitation events, while the ΔC for full events show a negative dependence with the percentage of time with precipitation during the sampling period. Therefore, the scavenging of pollutants is more efficient with prolonged and continuous precipitation events. These results are consistent with those observed by Castro et al. (2010) in the study carried out in León, Spain, in the spring of 2005. They observed that with rain intensities lower than 0.6 mm h^{-1}, the time it took for the number of particles to regain values similar to the initial number registered before the precipitation event was about 2 h.

- The model for the scavenging ratio (W) was significant only for NO_3^-, depending on the time between two rain events and their concentration in the aerosol before the rain event. This is consistent with the inverse relationship of W and C_{air} (Eq. 8.6).

TABLE 8.3. Coefficients of multi-linear regression models for rainwater concentration of each species (C_{rain}), scavenging ratios (W) and removal coefficients (ΔC).

y_j	β_j (mg L^{-1})	Chemical aerosol properties	Physical precipitation parameters					R^2
		C_1 (μg m^{-3})	t (%)	Intensity (mm h^{-1})	D_{size} (mm)	V_{swept} (mm^3 m^{-3})	t_{befoe} (min)	
		α_{1j} (m^3 mg μg^{-1} L^{-1})	α_{2j} (mg L^{-1} %$^{-1}$)	α_{3j} (mg h L^{-1} mm^{-1})	α_{4j} (mg L^{-1} mm^{-1})	α_{5j} (mg m^{-3} L^{-1} mm^{-3})	α_{6j} (mg L^{-1} min^{-1})	
C_{rain} (mg L^{-1})								
WIOC	-1.40				2.82×10^{-5}		4.71	0.31
DOC	1.51						2.88×10^{-4}	0.36
WIEC	0.06					-1.30×10^{-9}		0.29
SO_4^{2-}	2.44			3.22				0.30
NO_3^-	3.79					1.30×10^{-7}	-0.00019	0.29
	β_j (mg)	α_{1j} (m^3 mg μg^{-1})	α_{2j} (mg %$^{-1}$)	α_{3j} (mg h mm^{-1})	α_{4j} (mg mm^{-1})	α_{5j} (mg m^{-3} mm^{-3})	α_{6j} (mg min^{-1})	
Mass in rainwater (mg)								
Ca^{2+}	-2.20					2.27×10^{-7}		0.37
SO_4^{2-}	-1.73					1.81×10^{-7}		0.41
	β_j	α_{1j} (m^3 μg^{-1})	α_{2j} (%$^{-1}$)	α_{3j} (h mm^{-1})	α_{4j} (mm^{-1})	α_{5j} (m^{-3} mm^{-3})	α_{6j} (min^{-1})	
W (dimensionless)								
NO_3^-	4.99×10^4	-2.00×10^4					4.99	0.50
	β_j (μg m^{-3})	α_{1j}	α_{2j} (μg m^{-3} %$^{-1}$)	α_{3j} (μg h m^{-3} mm^{-1})	α_{4j} (μg m^{-3} mm^{-1})	α_{5j} (μg m^{-3} m^{-3} mm^{-3})	α_{6j} (μg m^{-3} min^{-1})	
ΔC (24-h event) (μg m^{-3})								
PM_{10}	7.79	-0.53						0.50
OC	1.12	-0.85					4.50×10^{-5}	0.80
EC	0.55	-0.99					7.50×10^{-6}	0.80
Crustal	0.09	-0.90		0.13		-5.94×10^{-9}	5.40×10^{-6}	0.70
Marine	0.15	-0.57						0.29
Secondary	0.35	-0.88					3.81×10^{-5}	0.80
	β_j (μg m^{-3})	α_{1j}	α_{2j} (μg m^{-3} %$^{-1}$)	α_{3j} (μg h m^{-3} mm^{-1})	α_{4j} (μg m^{-3} mm^{-1})	α_{5j} (μg m^{-3} m^{-3} mm^{-3})	α_{6j} (μg m^{-3} min^{-1})	
ΔC (full event) (μg m^{-3})								
PM_{10}	19.16		-0.77					0.56
OC	3.57	-0.54	-0.08					0.82
Crustal	0.27	-0.64	-0.007					0.73
Secondary	2.60	-1.02	-0.05					0.84

8.5. CONCLUSIONS

A one-year sampling campaign was carried out between March 2016 and March 2017, in order to characterize the below cloud scavenging process and establish linear models showing the influence of the physical parameters of raindrops and the chemical properties of aerosols on the removal of atmospheric pollutants. A total of 363 mm of precipitation were recorded during the entire sampling period, April being the month with more days of precipitation and more accumulated rainwater and July the month with fewer days and less accumulated rainfall.

The chemistry of the rainwater sampled provided evidence on the influence of anthropogenic sources and long-range transport phenomena on rainfall in León. In winter, the high values of Na^+ and Cl^- in the rainwater composition show the contribution from marine sources. These species arrived at León in the air masses from the Atlantic and are related to CS, CN, AN and SW weather types. This source could also explain the high values of pH in the precipitation sampled in winter season. Moreover, summer precipitation is characterized by high concentrations of elements from crustal and anthropogenic sources, mainly related to air masses from North Africa and AN, CS and NE weather types. The mean pH and conductivity of the rainwater were 5.87 and 27.0 $\mu S\ cm^{-1}$, respectively, indicating the low influence of large industries and other local anthropogenic sources in León, and suggesting that the crustal components and ammonia play an important role in the neutralization of rainwater. The carbonaceous fraction was dominated by DOC, showing the lowest values in summer and the highest in winter. In summer, the dissolved organic carbon concentrations could be related to the transport of biogenic material from the south of the Iberian Peninsula, and secondary organic carbon production, while in winter they could be linked to traffic and fossil fuel primary emissions and biomass burning for heating proposes.

Scavenging ratios and removal coefficients showed that below-cloud scavenging is in general an effective process to remove air pollutants in León. Linear models for the prediction of the chemical composition of rainwater, scavenging ratio and removal coefficients were constructed. The results showed that only the amount of the water-soluble ions in rainwater, Ca^{2+}, SO_4^{2-}, NO_3^-, increases with the volume swept by the drops, while the concentration of water insoluble organic and elemental carbon is affected by raindrop diameter and swept volume, respectively. The removal coefficients (ΔC) are affected by the air concentration of each species before precipitation, for the duration of the precipitation event and for the elapsed time between two events.

The results confirm the influence of physicochemical properties of the rain and the chemical properties of the aerosols in the elimination of atmospheric pollutants. This work represents a further step in the study of the mechanisms of elimination of air pollutants, proving that simple models can allow a first approach to the calculation of the efficiency of removal of pollutants by rain in a region, taking into account not only the chemical characteristics of the precipitation, but also its physical properties, which represent a scarce studied field.

8.6. REFERENCES

Alastuey, A., Querol, X., Chaves, A., Ruiz, C.R., Carratala, A., Lopez-Soler, A., 1999. Bulk deposition in a rural area located around a large coal-fired power station, northeast Spain. Environ. Pollut. 106, 359–367. doi:10.1016/S0269-7491(99)00103-7

Alonso-Blanco, E., Calvo, A.I., Fraile, R., Castro, A., 2012. The Influence of Wildfires on Aerosol Size Distributions in Rural Areas. Sci. World J. 2012, 1–13. doi:10.1100/2012/735697

Alves, C.A., Lopes, D.J., Calvo, A.I., Evtyugina, M., Rocha, S., Nunes, T., 2015. Emissions from Light-Duty Diesel and Gasoline in-use Vehicles Measured on Chassis Dynamometer Test Cycles. Aerosol Air Qual. Res. 15, 99–116. doi:10.4209/aaqr.2014.01.0006

Alves, C.A., Vicente, A., Monteiro, C., Gonçalves, C., Evtyugina, M., Pio, C., 2011. Emission of trace gases and organic components in smoke particles from a wildfire in a mixed-evergreen forest in Portugal. Sci. Total Environ. 409, 1466–1475. doi:10.1016/j.scitotenv.2010.12.025

Arsene, C., Olariu, R.I., Mihalopoulos, N., 2007. Chemical composition of rainwater in the northeastern Romania, Iasi region (2003–2006). Atmos. Environ. 41, 9452–9467. doi:10.1016/j.atmosenv.2007.08.046

Bernstein, J.A., Alexis, N., Barnes, C., Bernstein, I.L., Nel, A., Peden, D., Diaz-Sanchez, D., Tarlo, S.M., Williams, P.B., Bernstein, J.A., 2004. Health effects of air pollution. J. Allergy Clin. Immunol. 114, 1116–1123. doi:10.1016/j.jaci.2004.08.030

Blanco-Alegre, C., Calvo, A.I., Coz, E., Castro, A., Oduber, F., Prévôt, A.S.H., Močnik, G., Fraile, R., 2019. Quantification of source specific black carbon scavenging using an aethalometer and a disdrometer. Environ. Pollut. 246, 336–345. doi:10.1016/j.envpol.2018.11.102

Blanco-Alegre, C., Castro, A., Calvo, A.I., Oduber, F., Alonso-Blanco, E., Fernández-González, D., Valencia-Barrera, R.M., Vega-Maray, A.M., Fraile, R., 2018. Below-cloud scavenging of fine and coarse aerosol particles by rain: The role of raindrop size. Q. J. R. Meteorol. Soc. 144, 2715–2726. doi:10.1002/qj.3399

Calvo, A.I., Pont, V., Olmo, F.J., Castro, A., Alados-Arboledas, L., Vicente, A.M., Fernández-Raga, M., Fraile, R., 2012. Air Masses and Weather Types: A Useful Tool for Characterizing Precipitation Chemistry and Wet Deposition. Aerosol Air Qual. Res. 12, 856–878. doi:10.4209/aaqr.2012.03.0068

Castro, A., Alonso-Blanco, E., González-Colino, M., Calvo, A.I., Fernández-Raga, M., Fraile, R., 2010. Aerosol size distribution in precipitation events in León, Spain. Atmos. Res. 96, 421–435. doi:10.1016/j.atmosres.2010.01.014

Celle-Jeanton, H., Travi, Y., Loÿe-Pilot, M.-D., Huneau, F., Bertrand, G., 2009. Rainwater chemistry at a Mediterranean inland station (Avignon, France): Local contribution versus long-range supply. Atmos. Res. 91, 118–126. doi:10.1016/j.atmosres.2008.06.003

Cheng, I., Zhang, L., 2017. Long-term air concentrations, wet deposition, and scavenging ratios of inorganic ions, HNO3, and SO2 and assessment of aerosol and precipitation acidity at Canadian rural locations. Atmos. Chem. Phys. 17, 4711–4730. doi:10.5194/acp-17-4711-2017

Cugerone, K., De Michele, C., Ghezzi, A., Gianelle, V., 2018. Aerosol removal due to precipitation and wind forcings in Milan urban area. J. Hydrol. 556, 1256–1262. doi:10.1016/j.jhydrol.2017.06.033

Custódio, D., Cerqueira, M., Fialho, P., Nunes, T., Pio, C., Henriques, D., 2014. Wet deposition of particulate carbon to the Central North Atlantic Ocean. Sci. Total Environ. 496, 92–99. doi:10.1016/j.scitotenv.2014.06.103

Draxler, R., Rolph, G., 2012. Hysplit (Hybrid Single-Particle Lagrangian Integrated Trajectory). Silver Spring. NOAA Air Resour. Lab.

Dunn, O.J., 1964. Multiple Comparisons Using Rank Sums. Technometrics 6, 241–252. doi:10.1080/00401706.1964.10490181

Encinas, D., Calzada, I., Casado, H., 2004. Scavenging Ratios in an Urban Area in the Spanish Basque Country. Aerosol Sci. Technol. 38, 685–691. doi:10.1080/02786820490460716

Favez, O., Cachier, H., Sciare, J., Alfaro, S.C., El-Araby, T.M., Harhash, M.A., Abdelwahab, M.M., 2008. Seasonality of major aerosol species and their transformations in Cairo megacity. Atmos. Environ. 42, 1503–1516. doi:10.1016/j.atmosenv.2007.10.081

Fernández-Raga, M., Castro, A., Marcos, E., Palencia, C., Fraile, R., 2017. Weather types and rainfall microstructure in Leon, Spain. Int. J. Climatol. 37, 1834–1842. doi:10.1002/joc.4816

Fernández-Raga, M., Castro, A., Palencia, C., Calvo, A.I., Fraile, R., 2009. Rain events on 22 October 2006 in León (Spain): Drop size spectra. Atmos. Res. 93, 619–635. doi:10.1016/j.atmosres.2008.09.035

Fredericks, S., Saylor, J.R., 2019. Experimental study of drop shape and wake effects on particle scavenging for non-evaporating drops using ultrasonic levitation. J. Aerosol Sci. 127, 1–17. doi:10.1016/j.jaerosci.2018.10.001

He, J., Balasubramanian, R., 2008. Rain-aerosol coupling in the tropical atmosphere of Southeast Asia: distribution and scavenging ratios of major ionic species. J. Atmos. Chem. 60, 205–220. doi:10.1007/s10874-008-9118-x

Jaffrezo, J.-L., Colin, J.-L., 1988. Rain-aerosol coupling in urban area: Scavenging ratio measurement and identification of some transfer processes. Atmos. Environ. 22, 929–935. doi:10.1016/0004-6981(88)90270-3

Jain, C.D., Madhavan, B.L., Ratnam, M.V., 2019. Source apportionment of rainwater chemical composition to investigate the transport of lower atmospheric pollutants to the UTLS region. Environ. Pollut. 248, 166–174. doi:10.1016/j.envpol.2019.02.007

Jordan, C.E., Dibb, J.E., Anderson, B.E., Fuelberg, H.E., 2003. Uptake of nitrate and sulfate on dust aerosols during TRACE-P. J. Geophys. Res. Atmos. 108, 1–10. doi:10.1029/2002jd003101

Kampa, M., Castanas, E., 2008. Human health effects of air pollution. Environ. Pollut. 151, 362–367. doi:10.1016/j.envpol.2007.06.012

Kasper-Giebl, A., Kalina, M.F., Puxbaum, H., 1999. Scavenging ratios for sulfate, ammonium and nitrate determined at Mt. Sonnblick (3106m a.s.l.). Atmos. Environ. 33, 895–906. doi:10.1016/S1352-2310(98)00279-9

Keene, W.C., Pszenny, A.A.P., Galloway, J.N., Hawley, M.E., 1986. Sea-salt corrections and interpretation of constituent ratios in marine precipitation. J. Geophys. Res. 91, 6647. doi:10.1029/JD091iD06p06647

Keresztesi, Á., Korodi, A., Boga, R., Petres, S., Ghita, G., Ilie, M., 2017. Chemical characteristics of wet precipitation in the Eastern Carpathians, Romania. Ecoterra 14, 52–59.

Knote, C., Hodzic, A., Jimenez, J.L., 2015. The effect of dry and wet deposition of condensable vapors on secondary organic aerosols concentrations over the continental US. Atmos. Chem. Phys. 15, 1–18. doi:10.5194/acp-15-1-2015

Kruskal, W.H., Wallis, W.A., 1952. Use of Ranks in One-Criterion Variance Analysis. J. Am. Stat. Assoc. 47, 583–621. doi:10.1080/01621459.1952.10483441

Kulshrestha, U.C., Kulshrestha, M.J., Sekar, R., Sastry, G.S.R., Vairamani, M., 2003. Chemical characteristics of rainwater at an urban site of south-central India. Atmos. Environ. 37, 3019–3026. doi:10.1016/S1352-2310(03)00266-8

Kulshrestha, U.C., Reddy, L.A.K., Satyanarayana, J., Kulshrestha, M.J., 2009. Real-time wet scavenging of major chemical constituents of aerosols and role of rain intensity in Indian region. Atmos. Environ. 43, 5123–5127. doi:10.1016/j.atmosenv.2009.07.025

Kulshrestha, U.C., Sarkar, A.K., Srivastava, S.S., Parashar, D.C., 1996. Investigation into atmospheric deposition through precipitation studies at New Delhi (India). Atmos. Environ. 30, 4149–4154. doi:10.1016/1352-2310(96)00034-9

Kulshrestha, U.C., Sarkar, A.K., Srivastava, S.S., Parashar, D.C., 1995. Wet-only and bulk deposition studies at New Delhi (India). Water, Air, Soil Pollut. 85, 2137–2142. doi:10.1007/BF01186150

Lamb, H.H., 1972. British Isles weather types and a register of daily sequence of circulation patterns, Geophysical Memoir, HMSO, London. Her Majesty's stationery office.

Lelieveld, J., Evans, J.S., Fnais, M., Giannadaki, D., Pozzer, A., 2015. The contribution of outdoor air pollution sources to premature mortality on a global scale. Nature 525, 367–371. doi:10.1038/nature15371

Luan, T., Guo, X., Zhang, T., Guo, L., 2019. Below-Cloud Aerosol Scavenging by Different-Intensity Rains in Beijing City. J. Meteorol. Res. 33, 126–137. doi:10.1007/s13351-019-8079-0

Lucarelli, F., Chiari, M., Calzolai, G., Giannoni, M., Nava, S., Udisti, R., Severi, M., Querol, X., Amato, F., Alves, C., Eleftheriadis, K., 2015. The role of PIXE in the AIRUSE project "testing and development of air quality mitigation measures in Southern Europe." Nucl. Instruments Methods Phys. Res. Sect. B Beam Interact. with Mater. Atoms 363, 92–98. doi:10.1016/j.nimb.2015.08.023

Mage, D., Ozolins, G., Peterson, P., Webster, A., Orthofer, R., Vandeweerd, V., Gwynne, M., 1996. Urban air pollution in the mega-cities of the world. Atmos. Environ. 30, 681–686.

Martins, E.H., Nogarotto, D.C., Mortatti, J., Pozza, S.A., 2019. Chemical composition of rainwater in an urban area of the southeast of Brazil. Atmos. Pollut. Res. 10, 520–530. doi:10.1016/j.apr.2018.10.003

Mori, T., Kondo, Y., Ohata, S., Moteki, N., Matsui, H., Oshima, N., Iwasaki, A., 2014. Wet deposition of black carbon at a remote site in the East China Sea. J. Geophys. Res. Atmos. 119, 10485–10498. doi:10.1002/2014JD022103

Naddafi, K., Hassanvand, M.S., Yunesian, M., Momeniha, F., Nabizadeh, R., Faridi, S., Gholampour, A., 2012. Health impact assessment of air pollution in megacity of Tehran, Iran. Iranian J. Environ. Health Sci. Eng. 9, 28. doi:10.1186/1735-2746-9-28

Oduber, F., Calvo, A.I., Blanco-Alegre, C., Castro, A., Nunes, T., Alves, C., Sorribas, M., Fernández-González, D., Vega-Maray, A.M., Valencia-Barrera, R.M., Lucarelli, F., Nava, S., Calzolai, G., Alonso-Blanco, E., Fraile, B., Fialho, P., Coz, E., Prevot, A.S.H., Pont, V., Fraile, R., 2019a. Unusual winter Saharan dust intrusions at Northwest Spain: Air quality, radiative and health impacts. Sci. Total Environ. 669, 213–228. doi:10.1016/j.scitotenv.2019.02.305

Oduber, F., Calvo, A.I., Blanco-Alegre, C., Castro, A., Vega-Maray, A.M., Valencia-Barrera, R.M., Fernández-González, D., Fraile, R., 2019b. Links between recent trends in airborne pollen concentration, meteorological parameters and air pollutants. Agric. For. Meteorol. 264, 16–26. doi:10.1016/j.agrformet.2018.09.023

Oduber, F., Castro, A., Calvo, A.I., Blanco-Alegre, C., Alonso-Blanco, E., Belmonte, P., Fraile, R., 2018. Summer-autumn air pollution in león, Spain: Changes in aerosol size distribution and expected effects on the respiratory tract. Air Qual. Atmos. Heal. 11, 505–520. doi:10.1007/s11869-018-0556-6

Olszowski, T., 2014. The efficiency of PM10 scavenging from troposphere as a function of type and duration of wet deposition, in: Fiore, S. (Ed.), 1st International Conference on Atmospheric Dust- DUST2014. pp. 393–398. doi:10.14644/dust.2014.064

Olszowski, T., Ziembik, Z., 2018. An alternative conception of PM10 concentration changes after short-term precipitation in urban environment. J. Aerosol Sci. 121, 21–30. doi:10.1016/j.jaerosci.2018.04.001

Pan, Y.P., Wang, Y.S., 2015. Atmospheric wet and dry deposition of trace elements at 10 sites in Northern China. Atmos. Chem. Phys. 15, 951–972. doi:10.5194/acp-15-951-2015

Pio, C., Cerqueira, M., Harrison, R.M., Nunes, T., Mirante, F., Alves, C., Oliveira, C., Sanchez de la Campa, A., Artíñano, B., Matos, M., 2011. OC/EC ratio observations in Europe: Re-thinking the approach for apportionment between primary and secondary organic carbon. Atmos. Environ. 45, 6121–6132. doi:10.1016/j.atmosenv.2011.08.045

Ren-Jian, Z., Kin-Fai, H., Zhen-Xing, S., 2012. The Role of Aerosol in Climate Change, the Environment, and Human Health. Atmos. Ocean. Sci. Lett. 5, 156–161. doi:10.1080/16742834.2012.11446983

Rolph, G., Stein, A., Stunder, B., 2017. Real-time Environmental Applications and Display sYstem: READY. Environ. Model. Softw. 95, 210–228. doi:10.1016/j.envsoft.2017.06.025

Roy, A., Chatterjee, A., Ghosh, A., Das, S.K., Ghosh, S.K., Raha, S., 2019. Below-cloud scavenging of size-segregated aerosols and its effect on rainwater acidity and nutrient deposition: A long-term (2009–2018) and real-time observation over eastern Himalaya. Sci. Total Environ. 674, 223–233. doi:10.1016/j.scitotenv.2019.04.165

Sanets, E. V., Chuduk, V.N., 2005. Sulphur atmospheric deposition in areas with different anthropogenic loads in Belarus. Atmos. Res. 77, 88–99. doi:10.1016/j.atmosres.2004.10.019

Seinfeld, J.H., Pandis, S.N., 1998. Atmospheric chemistry and physics: from air pollution to climate change. John Wiley & Sons.

Siudek, P., Frankowski, M., Siepak, J., 2015. Seasonal variations of dissolved organic carbon in precipitation over urban and forest sites in central Poland. Environ. Sci. Pollut. Res. 22, 11087–11096. doi:10.1007/s11356-015-4356-3

Stein, A.F., Draxler, R.R., Rolph, G.D., Stunder, B.J.B., Cohen, M.D., Ngan, F., 2015. NOAA's HYSPLIT Atmospheric Transport and Dispersion Modeling System. Bull. Am. Meteorol. Soc. 96, 2059–2077. doi:10.1175/BAMS-D-14-00110.1

Tang, A., Zhuang, G., Wang, Y., Yuan, H., Sun, Y., 2005. The chemistry of precipitation and its relation to aerosol in Beijing. Atmos. Environ. 39, 3397–3406. doi:10.1016/j.atmosenv.2005.02.001

Theodosi, C., Im, U., Bougiatioti, A., Zarmpas, P., Yenigun, O., Mihalopoulos, N., 2010. Aerosol chemical composition over Istanbul. Sci. Total Environ. 408, 2482–2491. doi:10.1016/j.scitotenv.2010.02.039

Trigo, R.M., DaCamara, C.C., 2000. Circulation weather types and their influence on the precipitation regime in Portugal. Int. J. Climatol. 20, 1559–1581. doi:10.1002/1097-0088(20001115)20:13<1559::AID-JOC555>3.0.CO;2-5

Uchiyama, R., Okochi, H., Katsumi, N., Ogata, H., 2017. The impact of air pollutants on rainwater chemistry during "urban-induced heavy rainfall" in downtown Tokyo, Japan. J. Geophys. Res. Atmos. 122, 6502–6519. doi:10.1002/2017JD026803

Vicente, A., Alves, C., Calvo, A.I., Fernandes, A.P., Nunes, T., Monteiro, C., Almeida, S.M., Pio, C., 2013. Emission factors and detailed chemical composition of smoke particles from the 2010 wildfire season. Atmos. Environ. 71, 295–303. doi:10.1016/j.atmosenv.2013.01.062

Vicente, A., Alves, C., Monteiro, C., Nunes, T., Mirante, F., Cerqueira, M., Calvo, A., Pio, C., 2012. Organic speciation of aerosols from wildfires in central Portugal during summer 2009. Atmos. Environ. 57, 186–196. doi:10.1016/j.atmosenv.2012.04.030

Xu, D., Ge, B., Wang, Z., Sun, Y., Chen, Y., Ji, D., Yang, T., Ma, Z., Cheng, N., Hao, J., Yao, X., 2017. Below-cloud wet scavenging of soluble inorganic ions by rain in Beijing during the summer of 2014. Environ. Pollut. 230, 963–973. doi:10.1016/j.envpol.2017.07.033

Zhang, M., Wang, S., Wu, F., Yuan, X., Zhang, Y., 2007. Chemical compositions of wet precipitation and anthropogenic influences at a developing urban site in southeastern China. Atmos. Res. 84, 311–322. doi:10.1016/j.atmosres.2006.09.003

Zikova, N., Zdimal, V., 2016. Precipitation scavenging of aerosol particles at a rural site in the Czech Republic. Tellus B Chem. Phys. Meteorol. 68, 27343. doi:10.3402/tellusb.v68.27343

9

CHEMICAL COMPOSITION OF RAINWATER UNDER TWO EVENTS OF AEROSOL TRANSPORT: A SAHARAN DUST OUTBREAK AND WILDFIRES

Sent to Science of the Total Environment, February 2020

9.1. INTRODUCTION

Rainwater plays an important role by removing aerosols and gases from the atmosphere (scavenging), and acts through two mechanisms: in-cloud scavenging (ICS) or rainout and below-cloud scavenging (BCS) or washout (Keresztesi et al., 2017; Seinfeld and Pandis, 2016). The first one requires the presence of aerosols playing the role of cloud condensation nuclei (CCN) inside the cloud droplets, while the second one consists in the washing out of aerosols by falling raindrops (Kajino and Aikawa, 2015). The pollutants of local anthropogenic origin are removed mainly in the initial fractions of rain, dominated by the washout process. Subsequent fractions have mainly a chemical composition attributed to transport events from different regions, characterized by rainout processes (Celle-Jeanton et al., 2009). Therefore, the chemical composition of rainwater can provide information on the local sources of pollutant emissions, as well as on the impact of long-range transport emissions (such as those from Saharan dust intrusions and biomass burning events) on the air quality of a specific location (Alastuey et al., 1999; Knote et al., 2015; Kopáček et al., 2016).

The BCS process of different chemical species is affected by the intensity and volume of rainfall (Custodio et al., 2014; Luan et al., 2019; Pan and Wang, 2015). Furthermore, the physical parameters of precipitation (raindrop size distribution and volume swept by raindrops) are also important factors influencing the scavenging process and can also determine the chemical composition of the rainwater (Blanco-Alegre et al., 2019, 2018; Fredericks and Saylor, 2019). Why is the raindrop size important? In an ideal model, as a raindrop is falling, it could collide with all the particles contained in the swept volume constituted by a cylinder of radius equal to the raindrop radius and length equal to the distance travelled by the raindrop.

Biomass burning releases a large amount of gases and particles into the atmosphere. Vicente et al. (2013) reported that during wildfires, CO and CO_2 are largely emitted, while the aerosol from this source contains organic carbon (OC), Na^+, NH_4^+, Cl^- and NO_3^- in the fine fraction and

K^+, Mg^{2+}, Ca^{2+} and SO_4^{2-} in the coarse fraction. Specifically, a large number of organic constituents such as phenolic compounds and their alteration products, acids, carbohydrates, levoglucosan and diterpenoids, were detected in aerosols from wildfires (Alves et al., 2011a; Vicente et al., 2012, 2011). When wildfires coincide with a rainfall event, their emissions can affect the chemistry of rainwater causing an increase in the concentration of organic acidic (e.g., $HCOO^-$, CH_3COO^-) and inorganic ions (SO_4^{2-}, Cl^-, NO_3^-, NH_4^+) (Bisht et al., 2015; Mimura et al., 2016; Sun et al., 2016). Besides, the incorporation into the drops of gaseous pollutants such as SO_x, NO_x and organic acids causes an acidifying effect on rainwater (Balasubramanian et al., 1999), which has detrimental effects on the aquatic and terrestrial ecosystems and an indirect negative effect on human health (Cathcart et al., 2016; Duan et al., 2016; Livingston, 2016; Rosborg and Nihlgård, 2018). Moreover, phenomena such as Saharan dust intrusions transport large amounts of mineral dust particles, characterized by high concentrations of Al, Ca, Ti, Si, Fe, SO_4^{2-}, NO_3^- and Cl^-, as well as high loads of biological material (pollen, spores and fungi), which entails an increase in the organic carbon concentration of aerosols (Oduber et al., 2019). Several authors have studied the impact of Saharan dust outbreaks on the chemical composition of rainwater, showing that dust intrusions can rise the concentration of Na^+, Ca^{2+}, K^+, Mg^{2+} and SO_4^{2-}, and cause an alkalization of rainwater due to the $CaCO_3$ content in airborne dust (Anil et al., 2017; Escudero et al., 2005; Morales-Baquero et al., 2013).

Every year, due to the high temperatures and low rainfall registered in summer, a considerable area of the north and west of the Iberian Peninsula is often affected by wildfires that can last several days (Alonso-Blanco et al., 2012; Alves et al., 2011a; Vicente et al., 2013, 2012). Fernández-Raga et al. (2017) reported that in León (NW, Spain), in summer, mainly short-duration storms occur. In these latitudes, convective phenomena in this season generally causes short and intense rainfall events, most of them lasting only 5 minutes. Furthermore, the Iberian Peninsula is often affected by Saharan dust intrusions, due to the proximity to the emitting sources (Alastuey et al., 2016; Escudero et al., 2007; Querol et al., 2014). However, African dust outbreaks do not usually reach the north of Spain, much less during winter, and when this happens, the episodes tend to last less than 4 days (Oduber et al., 2019; Querol et al., 2004). Escudero et al. (2005) reported that, in eastern Iberia, on average, during 3% of the days of the year, wet deposition occurs simultaneously with an African dust outbreak, being February one of the months with less mean number of days with this type of episodes (mean of 0.4 days) and May the month with more (mean of 2.9 days).

The combination of the study of the characteristics of the aerosol and the precipitation can constitute a key tool in the understanding of the scavenging processes. To our knowledge, there are very few studies that try to combine both aspects. Therefore, we set out to study the organic and inorganic compounds present in rainwater and atmospheric aerosol before, during and after rainfall. Thus, the main aim of this work is to study the impact on rainwater chemical composition, collected in León, Spain, during AERORAIN project, of the two most outstanding events recorded with specific characteristics linked to the sources of the pollutants: *i*) an episode of massive wildfires that occurred in the western Iberian Peninsula in August 2016; and *ii*) a Saharan dust intrusion that reached northern Spain in February 2017.

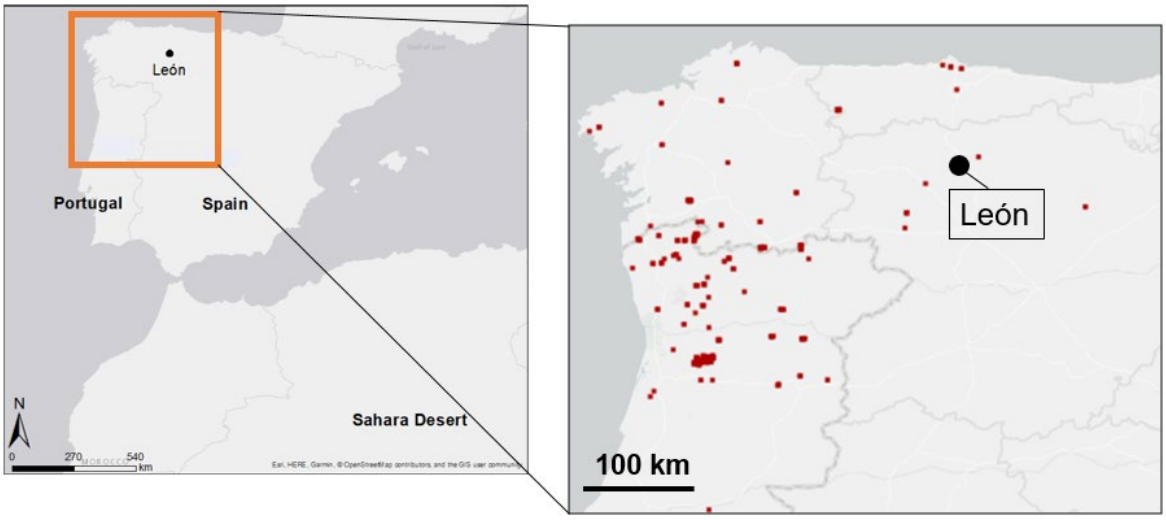

FIG. 9.1. Map of the Iberian Peninsula and location of León and Sahara Desert (left). Active wildfires between 14 and 15 August 2016 (right), in the NW of the peninsula, indicated by red points (map and data from NASA Fire Information for Resource Management System, FIRMS).

9.2. METHODOLOGY

9.2.1. Sampling site

The sampling campaign was carried out in León city, Spain, at NW of the Iberian Peninsula (42º 36′ N, 05º 35′ W and 838 m a.s.l) (Fig. 9.1). In León, the climate is continental type with influence of the Mediterranean climate. Winters are cold and long, with average temperature of 5 ºC and a mean accumulate precipitation of 150 mm, while summers are warm with an average temperature of 20 ºC and mean accumulate precipitations of 73 mm (Castro et al., 2010). During summer, droughts are very common, although there are sporadic storms, often with hail (Fernández-Raga et al., 2017). The sampling site is located in a suburban area at NE of the city center of León, characterized by the absence of large emitting industries and a certain contribution from biomass burning and fossil fuels sources, due to the high traffic flow in the vicinity and the use of domestic heating devices in nearby towns during the colder months (Blanco-Alegre et al., 2019; Oduber et al., 2018).

9.2.2. Study events

This study focuses on two specific rain events, which occurred in León and that were influenced by the arrival of atmospheric pollutants from two different sources: *i*) wildfires that took place between 14 and 15 August 2016, in northern Portugal (about 250 km from León) and in northwest Spain (approximately 100 to 200 km far from León) and *ii*) a Saharan dust intrusion, coming from a distance of approximately between 1200 and 2000 km (Fig. 9.1), which reached León between 12 and 13 February 2017. These two rain episodes represent the extremes on pH values recorded during the one-year sampling campaign. The rainwater fractions collected and the sampling days for both events are detailed in Table 9.1:

Table 9.1. Rainwater fractions, sampling dates and total volume sampled of each fraction.

Rainwater fraction	Event	Rainwater sampling date	Volume sampled (ml)
F_1	Wildfires	15 August 2016	27.3
P_1	Saharan dust intrusion	11 February 2017	31.7
P_2		12 February 2017	66.0
P_3		13 February 2017	1456.7
P_4		14 February 2017	54.6

9.2.3. PM_{10} and rainwater sampling

The samples used in this study belong to the one-year sampling campaign (between May 2016 and May 2017), part of the AERORAIN research project, in which samples of aerosols and rainwater were collected every 24 hours, starting at 1200 UTC every day.

For the PM_{10} sampling, a low volume sampler (TECORA, ECHOPM), equipped with 47 mm diameter Teflon filters and a high-volume sampler (CAV-Mb), equipped with 150 mm diameter quartz filters, were used. PM_{10} mass was determined by gravimetry, using an electronic semi-microbalance (Mettler Toledo, XPE105DR).

The rainwater was collected in glass bottles using a wet-only precipitation sampler (Eigenbrodt UNS 130/E). The conductivity and pH of the rain samples were determined immediately after being collected with a pH and conductivity meter (Hach, HQ 40d multi). The rain samples were filtered through a 15 mm diameter quartz filters in order to separate the insoluble and soluble matter.

All quartz fiber filters used in this work were pre-baked at 600 ^{o}C for 6 h in order to remove interfering carbonaceous material. Furthermore, some tests were carried out by filtering milli-Q water through blank filters in order to know the concentrations of ions that could be released by these filters. This background was subtracted from the concentrations registered in the filters used to filter rainwater.

9.2.4. PM_{10} and rainwater analysis

Quartz filters of both aerosols and water insoluble fraction of rain samples were used for the determination of organic and elemental carbon (OC and EC, respectively), by using the thermal-optical system developed by the University of Aveiro (Portugal) and following the procedure described by Alves et al. (2015) and Pio et al. (2011). Besides, PM_{10} quartz filters were used for the determination of levoglucosan and other sugars, taking a portion equal to 1/10 of the total filter area and extracting the soluble compounds with 3 ml of ultra-pure Milli-Q water by ultrasonic agitation, followed by filtration with a 0.2 μm pore size PTFE syringe filter into glass vials. The analysis was carried out in a Thermo Scientific DionexTM ICS-5000 ion Chromatograph, equipped with a CarboPac® PA-1 (2 × 250 mm) column, and a mobile phase of diluted sodium hydroxide (NaOH), using the methodology based on Caseiro et al. (2007) and Piazzalunga et al. (2010), with a multi-step gradient condition.

Teflon filters were cut into two equal portions. One of them was used for the determination of the major trace elements by PIXE (Particle-Induced X-ray Emission), following the methodology described by Lucarelli et al. (2015). The second portion was extracted with 6 ml ultra-pure Milli-Q water in ultrasonic agitation, and filtered with a 0.2 μm pore size PTFE syringe filter into glass vials for the analysis of inorganic water soluble ions: Na^+, K^+, NH_4^+, Mg^{2+}, Ca^{2+}, Cl^-, F^-, SO_4^{2-} and NO_3^-. The determination of water soluble ions of both aerosols and rain samples was carried out in a Thermo Scientific DionexTM ICS-5000 ion Chromatograph, equipped with an IonPac® CS16 (4 × 250 mm) column, with a solution of 30 mM of methanesulphonic (MSA) as eluent for cations, and an IonPac® AS11 (4 × 250 mm) column, with a solution of 30 mM of potassium hydroxide (KOH) as eluent for analysis of anions. The Dissolved Organic Carbon (DOC) content was determined by combustion and infrared detection in a Total Organic Carbon Analyzer Shimadzu (TOC-V CPH).

The following analytical checks were carried out: *i*) a duplicate analysis was carried out every 10 samples, *ii*) the extraction and analysis of blank filters were carried out, *iii*) the detection and quantification limits were determined from the blank filters, *iv*) every 10 or 15 samples a known standard was analyzed to check the quantification.

Furthermore, quality control for the entire database was verified for each rainfall sample by calculating the ion balance. The difference between the sum of cations and the sum of anions (including alkalinity) can be taken to indicate the sum of organic acids. In the wildfires rain event, the difference between the sum of cations and the sum of anions was equal to 120 μeq L^{-1}. In the Saharan dust intrusion, this difference was 15 μeq L^{-1} for P_1, 66.4 for P_2, 1.6 for P_3 and 4.8 for P_4.

9.2.5. Circulation Weather Types and meteorological parameters

A classification of Circulation Weather Types (CWTs) was carried out based on Lamb (1972). The direction and vorticity of the geostrophic flow, obtained for 16 grid points distributed over and around the Iberian Peninsula (Trigo and DaCamara, 2000), allowed to establish 26 different CWTs: eight known as "pure" weather types (N, S, E, W, NW, SW, SE and NE), two so-called "non-directional" (anticyclonic (A) and cyclonic (C)), and sixteen weather types so-called as "hybrid" types, as a result of the combination between "non-directional" and "pure" types (AN, ANE, ANW, AS, ASE, ASW, AE, AW and CN, CNE, CNW, CS, CSE, CSW, CE, CW).

Weather information in the sampling area was obtained with a weather station, which provided information on temperature, wind and relative humidity. Precipitation was measured with a laser disdrometer (Laser Precipitation Monitor, LPM) on a 1-minute basis. Furthermore, the origin of air masses was interpreted by the determination of daily back trajectories (at 500, 1500 and 3000 m agl) using the HYSPLIT model (Draxler and Rolph, 2012; Rolph et al., 2017; Stein et al., 2015).

9.2.6. Calculations

In order to characterize the rain samples and events, volume-weighted mean precipitation concentrations (*VWM*), neutralization factors (*NF*) and source contributions were determined.

VWM (in μeq L^{-1} and mg L^{-1}) of species in rainwater was calculated as follows:

$$VWM = (\sum_{i=1}^{N} C_i P_i) / \sum_{i=1}^{N} P_i \quad \text{Equation 9.1}$$

where, C_i is the concentration of each species in μeq L^{-1} for ions and in mg L^{-1} (for carbonaceous fraction), P_i the precipitation amount for each precipitation event in mm, and N the total number of precipitation events in each study period.

NF have been calculated following Eq. 9.2 (Kulshrestha et al., 1995), where C_x, is the concentration of the cation of interest, $C_{SO_4^{2-}}$ and $C_{NO_3^-}$ are the concentrations of the sulfate and nitrate anions, respectively, all in μeq L^{-1}.

$$NF_x = C_x / [C_{SO_4^{2-}} + C_{NO_3^-}] \quad \text{Equation 9.2}$$

Source contributions were calculated taking into account the enrichment factors (*EF*) values, which were calculated for both the seawater and crustal material, according to Eq. 3 and 4 (Kulshrestha et al., 1996; Zhang et al., 2007), where ($C_x/C_{r\ sample}$) is the ratio between the concentration of an element *X* and that of a reference element (*r*) in the sample. ($C_x/C_{r\ crustal}$) and ($C_x/C_{r\ seawater}$) are the ratios between the same elements considering the reference concentrations in the crustal material or seawater, respectively (Keene et al., 1986; Zhang et al., 2007). In this study, sodium was used as seawater reference element and calcium as crustal reference. The Mg^{2+}/Na^+ ratio was evaluated in order to determine the best tracer for seawater. According to Jordan et al. (2003) a ratio greater than 0.227 suggests a marine origin of Na^+. In this study, the Mg^{2+}/Na^+ ratio was greater than 0.7 for both studied events and, according to this result, sodium was used as the reference element for seawater. Regarding the crustal tracer, there is no specific rule for the choice of a crustal reference element, except that it must not be affected by anthropogenic factors. Ca^{2+} is widely used as a reference for continental emissions or terrestrial crust (Calvo et al., 2012; Khan et al., 2018; Martins et al., 2019; Zhang et al., 2007), as its composition in the soil is hardly changed. The abundance of Ca2+ in the Earth's crust was taken from Taylor (1964) and Zhang et al. (2007).

$$EF = \frac{(C_x/C_r)_{sample}}{(C_x/C_r)_{crustal}} \quad \text{Equation 9.3}$$

$$EF = \frac{(C_x/C_r)_{sample}}{(C_x/C_r)_{seawater}} \quad \text{Equation 9.4}$$

The source contribution of seawater and crustal fractions was obtained according to Eq. 9.5 and 9.6, respectively (Zhang et al., 2007):

$$Seawater\ fraction\ \% = 100(C_x/C_{Na^+})_{seawater} / (C_x/C_{Na^+})_{sample} \quad \text{Equation 9.5}$$

$$Crustal\ fraction\ \% = 100(C_x/C_{Ca^{2+}})_{crustal} / (C_x/C_{Ca^{2+}})_{sample} \quad \text{Equation 9.6}$$

Assuming that seawater and crust are the main natural sources, the anthropogenic fraction is defined as:

$$Anthropogenic\ fraction\ \% = 100 - (Crustal\ fraction + Seawater\ fraction) \quad \text{Equation 9.7}$$

9.3. RESULTS AND DISCUSSIONS

9.3.1. Biomass burning event

9.3.1.1. Meteorological conditions

Summer of 2016 was characterized as a very hot and dry season in the Iberian Peninsula. In León, the mean daily temperature for this season was 20 ± 4 ºC, reaching on 8 August a maximum of 35 ºC and a minimum relative humidity of 32%. The accumulated precipitation registered during summer was 21.54 mm, with a maximum on August with 11.48 mm. The Ministry of Agriculture, Food and the Environment (MAPAMA, in Spanish acronym) reported that August was a month with average temperatures throughout the Spanish territory of 1.3 ºC above the average normal value and 75% less precipitation than the average normal value for this period. These meteorological conditions favored the occurrence of forest fires in the Iberian Peninsula, especially in northern Portugal and northwest Spain. According to the MAPAMA Annual Report (2016), 3 biomass burning episodes may have affected the particle levels in northern Spain in August 2016: *i*) between days 13 and 17, *ii*) on day 19, and *iii*) between days 26 and 27. In addition, the Institute of Conservation of Nature and Forest of the Government of Portugal reported that in August 2016, a total of 116,885 ha had been burned throughout the territory of Portugal.

On 14 August 2016, the NAAP images show high smoke concentrations at the north of the Peninsula caused by wildfires, while the HYSPLIT model evidenced the influx of air masses at 500, 1500 and 3000 m, from the west of the Peninsula, confirming the arrival of smoke plumes in León (Fig. 9.2).

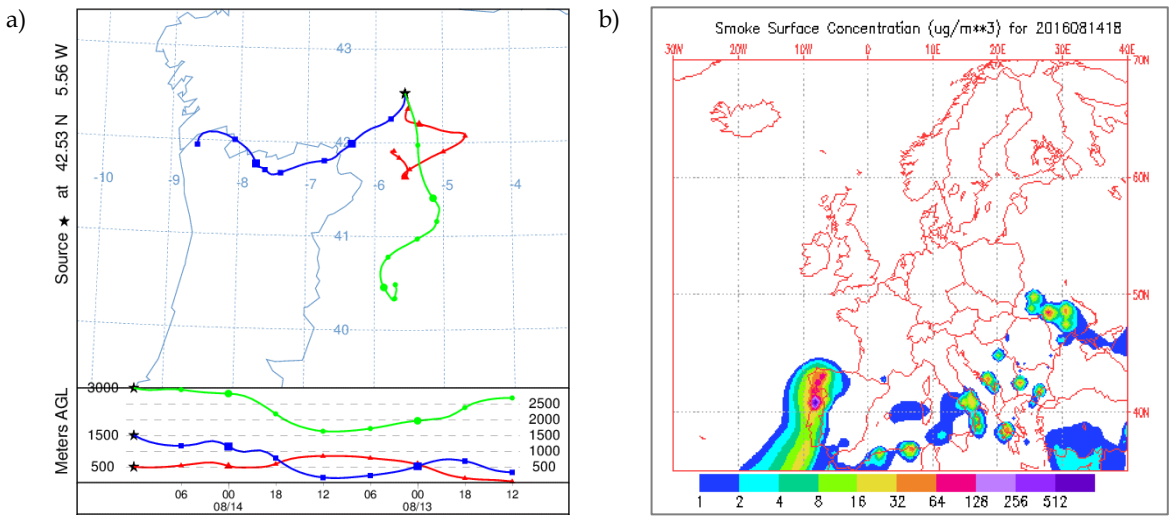

FIG. 9.2. a) HYSPLIT back trajectories at 500, 1500 and 3000 m agl and b) NAAPs images of smoke concentration on 14 August 2016.

TABLE 9.2. PM_{10}, elemental and organic carbon, potassium and levoglucosan concentrations in air (in μg m^{-3}) on day 14 August and the mean values in days without biomass burning events (days between 01 and 30 May 2016).

	14 August 2016	**Days without biomass burning**
PM_{10}	26	20 ± 4
EC	0.7	0.4 ± 0.2
OC	3.4	1.9 ± 0.6
K	0.20	0.10 ± 0.04
Levoglucosan	0.005	0.001 ± 0.002

9.3.1.2. Aerosol chemical composition

The contribution from biomass burning emissions to the aerosol burden in León was also confirmed by the increase in the aerosol concentration. Thus, PM_{10} daily concentration increased from 19 μg m 3 on 13 August to 26 μg m 3 on 14 August, while the main biomass burning tracers, K and levoglucosan (Vicente and Alves, 2018), showed an increase of 25 and 71%, respectively, and the carbonaceous fraction (EC + OC) showed an increase of 42% (Table 9.2).

9.3.1.3. Rainwater samples chemical composition

Although the rainfall was scarce in the summer of 2016, between 14 and 15 August, a rain event took place coinciding with the wildfires described above. The rain event began on 14 August at approximately 2300 UTC, and ended on 15 August at approximately 0400 UTC, recording an accumulated precipitation of 3.72 mm and a mean intensity of 1.28 mm h^{-1}. On 15 August between 0400 UTC and 0500 UTC, a total of 3.09 mm of rainfall were recorded (Fig. 9.3), with an intensity of 4.4 mm h^{-1}. Castro et al. (2010) reported that precipitation intensities above 3.2 mm h^{-1} produce effective washout of fine and coarse particles. Besides, Kulshrestha et al. (2009) showed that short period rains of high intensity effectively remove relatively coarse mode particles possibly by below-cloud scavenging process. Moreover, Alastuey et al. (2001) reported an exponential decreasing behavior throughout the precipitation event for most ions and that between 40 and 80% of the wet-only deposition of major ions takes place during the first 2 mm.

The volume swept by raindrops during this period was mainly due to drops with sizes greater than 2 mm, while for the lower precipitation intensity (about 0.3 mm h^{-1}) it was due to drop sizes less than 2 mm. Blanco-Alegre et al. (2019, 2018) showed that higher volume swept by drops caused a more effective scavenging on particles between 0.12 and 0.19 μm, and there was a significant correlation between the scavenging efficiency of black carbon particles and the number of drops with diameters between 0.375 and 2.5 nm. Therefore, this precipitation event could have been responsible for removing pollutants from the atmosphere through the washout process.

The chemical composition of rainwater showed high NH_4^+, Ca^{2+}, SO_4^{2-} and NO_3^- concentrations (153.15 μeq L^{-1}, 128.54 μeq L^{-1}, 65.19 μeq L^{-1} and 121.17 μeq L^{-1}, respectively), compared to those obtained in rain samples collected on days 8, 10, 12, 28, 29 and 30 May 2016 (Fig. 9.4), when, according to MAPAMA and the NAAP images (not shown here), there was no influence from forest fire emissions.

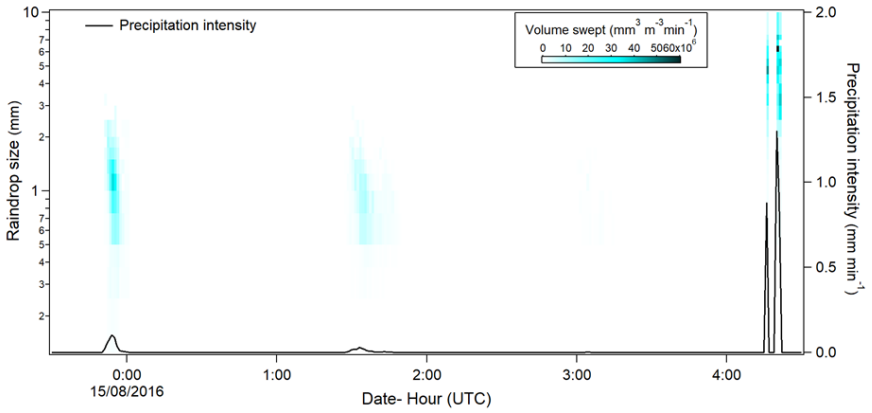

FIG. 9.3. Evolution of precipitation intensity (black line) and volume swept by the raindrops of each size interval (colour scale), between 14 and 15 August 2016.

The high concentrations of SO_4^{2-}, NO_3^- and NH_4^+ are probably the result of nucleation of the components transported by the air masses impacted by the biomass burning. Vicente et al. (2013) reported the presence of these ions in aerosol samples collected in the smoke plumes from wildfires that occurred in Portugal. The high content of these ions in rainwater could be due to the below-cloud scavenging of aerosols and in-cloud processes (Balasubramanian et al., 1999). Cachier and Ducret (1991) that studied the impact of biomass burning emissions on rainwater collected at remote site in the Northern Congo, showed that the biomass-burning particles may act as CCN, playing an important role in cloud formation. Furthermore, Pio et al. (2008) found a correlation between diacids with K^+ and SO_4^{2-} concentrations in aerosol samples from Aveiro, Portugal, during 2003 summer intense forest fire period, showing the in-cloud secondary formation of dicarboxylic species and SO_4^{2-} from CCN derived from biomass burning.

As expected, a high conductivity value was obtained (164.9 µS cm^{-1}) due to the high concentrations of ions, while the VWM conductivity was 31.2 ± 0.1 µS cm^{-1} in the rain samples of May 2016.

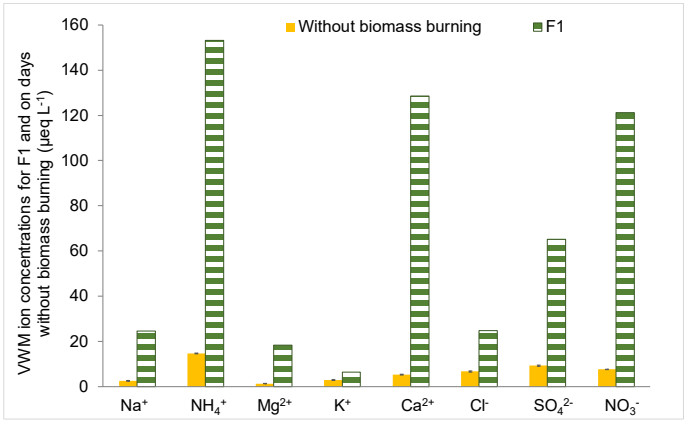

FIG. 9.4. Ion concentrations of rainwater fraction collected on 15 August 2016 (F_1) and on days without biomass burning influence (days 8, 10, 12, 28, 29 and 30 May 2016).

The inorganic ions of the rain samples of May 2016 have source contributions similar to those obtained for F_1. Thus, the anthropogenic contributions for sulfate were of 92% (F_1) and 96%

(samples of May 2016), and for nitrate of 100% and 99.86% for the same rain samples; while Ca^{2+}, Mg^{2+} and K^{+} mainly have a crustal origin (crustal fraction higher than 65%) and Cl^{-} has a marine origin with a seawater fraction of 98-100% (Table 9.3). High values of sulfate and nitrate in the atmosphere are usually related to secondary photochemical reactions that are more frequent in summer. Also, during the combustion of biomass, the SO_4^{2-} values can be related to the adsorption of SO_2 on black carbon particles through a catalytic effect, which promotes a very fast gas-to-particle conversion of SO_2 to sulfate (Alves et al., 2011b). K^{+}, Ca^{2+} and Mg^{2+} from crustal sources may originate in dust resuspension processes in the proximities of the sampling location.

With regard to the carbonaceous fraction of the rainwater sample F_1, DOC and WIOC values were 14.7 and 1.7 mg L^{-1}, respectively, while in days without biomass burning the *VWM* for DOC and WIOC were 1.2 ± 2.6 and 0.274 ± 0.01 mg L^{-1}, respectively. The carbonaceous content in rainwater is related to the emission of many organic compounds during the biomass burning and with the amount of rainfall during the event. Cerqueira et al. (2010) reported DOC values between 0.2 and 1.5 mg L^{-1} in European background sites not influenced by biomass burning events, while Godoy-Silva et al. (2017) documented values between 0.2 and 60 mg L^{-1} in a tropical agro-industrial region of São Paulo, which is frequently affected by biomass burning events. Moreover, Pan et al. (2010) described a negative correlation between DOC concentrations and the amount of precipitation in a study carried out in northern China during the summer, when coal emissions from domestic use are insignificant, indicating that the OC tend to be effectively washed out (below-cloud scavenging) during the initial period of precipitation.

TABLE 9.3. Source contributions (seawater, crustal and anthropogenic) for inorganic ions in rainwater fraction F_1 collected on 15 August 2016 (with biomass burning) and on May 2016 (without biomass burning).

	Seawater fraction (%)	**Crustal fraction (%)**	**Anthropogenic fraction (%)**
F_1			
K^{+}	9	91	-
Mg^{2+}	30	70	-
Ca^{2+}	1	99	-
Cl^{-}	98	2	-
SO_4^{2-}	5	4	92
NO_3^{-}	-	-	100
Without biomass burning			
K^{+}	30 ± 32	70 ± 29	-
Mg^{2+}	35 ± 34	65 ± 31	-
Ca^{2+}	4 ± 1	96 ± 1	-
Cl^{-}	99.7 ± 0.2	0.3 ± 0.1	-
SO_4^{2-}	3 ± 4	1.2 ± 0.6	96 ± 4
NO_3^{-}		0.14 ± 0.06	99.86 ± 0.06

9.3.1.4. Acidic contribution

Previous studies have established that precipitation in a clean atmosphere has a weakly acidic pH, with a reference value ranging from 5.0 to 5.6, so that rainwater samples with pH values lower than 5.0 are considered acid rain (Charlson and Rodhe, 1982). In the present study, the rain sample F_1, had an acidic pH of 4.8, whereas the rain samples of May 2016 showed a *VWM*

pH of 6.7 ± 1, showing that wildfire emissions had an acidification effect on the precipitation of 15 August 2016. Taking into account the main inorganic soluble ions, an excess of cations was observed in relation to anions. The unbalanced ratio ($\sum$ cations/ $\sum$ anions = 1.6) is enhanced when H+ is added. This acidity can be explained by the contribution of organic species released during fire events. In F_1, the highest neutralization factor was obtained by NH_4^+ (0.8), followed by Ca^{2+} (0.7), indicating that calcium and ammonium could prevent the acidification of the rainwater. The cation/anion unbalance suggests that the acidic pH is likely due to the contribution of acidic organic species, which is in accordance with the high DOC value. Balasubramanian et al. (1999) observed high concentrations of organic acids and HCl, in rainwater collected during the dry season in Indonesia, mainly due to the incorporation of gases and particles from biomass burning emissions, causing acidic pH values. Alves et al. (2011) reported that dicarboxylic acids and related compounds, such as the glycolic, lactic, hydroxybutyric and levulinic acids were the most abundant compounds in smoke particles from the plume of a wildfire that took place in Portugal. These results reflect the importance of the contribution from organic acid compounds to the pH of the rainwater.

9.3.2. African dust intrusion event

9.3.2.1. Meteorological conditions

The daily average temperature recorded in the sampling site during February 2017 was 6 ± 4 ºC, and the average relative humidity was 71 ± 7%. However, during the second week of the month, there was a change in weather conditions and maximum temperatures increased to 9 ºC (11 February) and 13 ºC (15 February). The annual report of 2016, issued by MAPAMA, on the events that could have affected the air quality in Spain, reported that on 12 February 2017, northern Spain was affected by the arrival of a Sahara dust intrusion. The 2-day back trajectories provided by the HYSPLIT model confirmed the arrival of air masses coming from North Africa to the North of Iberian Peninsula, during this day (Fig. 9.5a). The NAAP model shows that the dust load from the Sahara reached León on 12 February at approximately 1200 UTC (Fig. 9.5b), and remained until 13 February at approximately 1200 UTC. It is important to mention that Saharan dust outbreaks in winter are not common in the north of Spain.

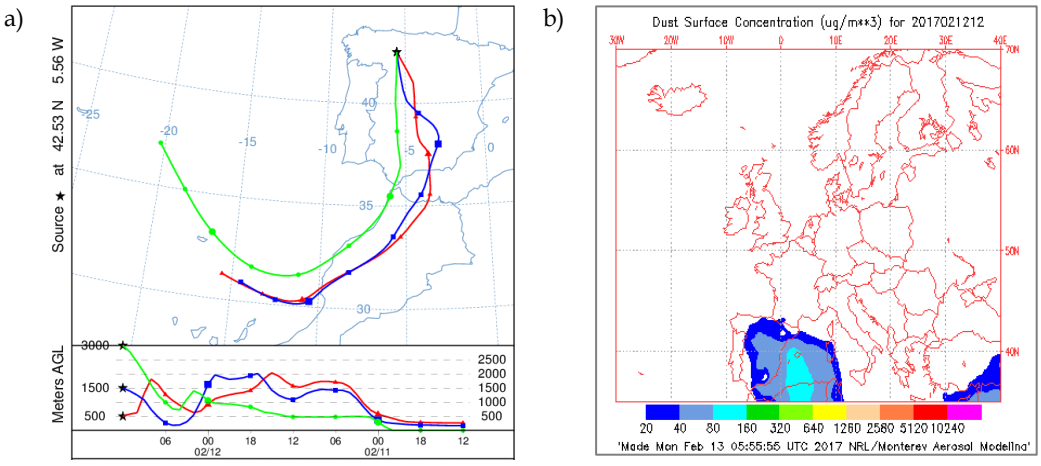

FIG. 9.5. a) HYSPLIT back trajectories at 500, 1500 and 3000 m agl and b) NAAP image of dust concentration, both on 12 February 2017 at 1200 UTC.

TABLE 9.4. PM_{10}, silicon, aluminum, calcium, titanium, magnesium, iron and sucrose concentrations in air (in μg m^{-3}) on 13 February 2017 and the mean values in days without dust intrusion in León (days between 01 and 11 February 2017).

	13 February 2017	**Days without dust intrusion**
PM_{10}	33	25 ± 3
Si	2.9	0.16 ± 0.12
Al	1.58	0.07 ± 0.06
Ca	1.25	0.14 ± 0.06
Ti	0.081	0.005 ± 0.003
Mg	0.38	0.09 ± 0.05
Fe	0.82	0.11 ± 0.06
Sucrose	0.0024	0.0009 ± 0.0002

9.3.2.2. Aerosol chemical composition

The increase recorded in the PM_{10} concentration, from 20 to 33 μg m^{-3}, and in the concentration of the main mineral elements (an increase greater than 300% for Si, Al and Ca), in aerosol samples collected between 12 and 13 February 2017, evidence the arrival of a dust cloud coming from the Sahara to León (Table 9.4). The high values of Si, Al and Ca are an indicator of dust of Saharan origin, due to the presence of minerals such as quartz (SiO_2), dolomite ($(CaMgCO_3)_2$), kaolinite ($Al_2Si_2O_5(OH)_4$) and calcite ($CaCO_3$) (Avila et al., 1997; Formenti et al., 2003).

9.3.2.3. Rainwater samples chemical composition

The arrival of the Saharan dust intrusion, between 12 and 13 February 2017, coincided with a precipitation event, which began on 11 February at 0300 UTC and ended on 14 February 2017 at 1700 UTC. During these 4 days, an accumulated precipitation of 20.46 mm was registered, with a mean intensity of 0.53 mm h^{-1}. Given that precipitation lasted four days, a total of four daily rainwater fractions (P_1, P_2, P_3 and P_4) were collected as Table 9.1 shows. The days with less accumulated precipitation were 11 and 14 February, with 0.95 and 0.98 mm, respectively (Fig. 9.6), while 13 February was the day with more accumulated precipitation and higher mean intensity (14.18 mm and 1.18 mm h^{-1}). In all cases, the volume swept by rain was mainly due to raindrops smaller than 2 mm. In the study carried out by Castro et al. (2010) in León, Spain, the results showed that with precipitation intensities lower than 0.6 mm h^{-1} the aerosol size distribution regains its initial values approximately 2 h after the precipitation. Moreover, Kulshrestha et al. (2009) reported that a low-intensity rain that lasts a couple of hours is responsible for the removal of fine particles.

The rain sample collected on 11 February (P_1), shows a chemical composition with high values of NH_4^+ (74 μeq L^{-1}), SO_4^{2-} (41 μeq L^{-1}) and NO_3^- (31 μeq L^{-1}) (Fig. 9.7). The pollutants related to local anthropogenic origin such as SO_4^{2-} and NO_3^-, are removed mainly in the initial fractions of rain through the washout process (Celle-Jeanton et al., 2009). Thus, the chemical composition of P_1 could reflect the impact of fossil fuel combustion emissions on rainwater. Besides, between 10 and 11 February, the air masses coming from the Atlantic transported aerosols loaded with

marine particles. This fact was reflected on the source contribution of P_1, where 91% of Cl^- is related to marine origin (Table 9.5) and in the Cl^-/Na^+ ratio of 1.3, value very close to that reported for seawater origin (1.2) (Keene et al., 1986).

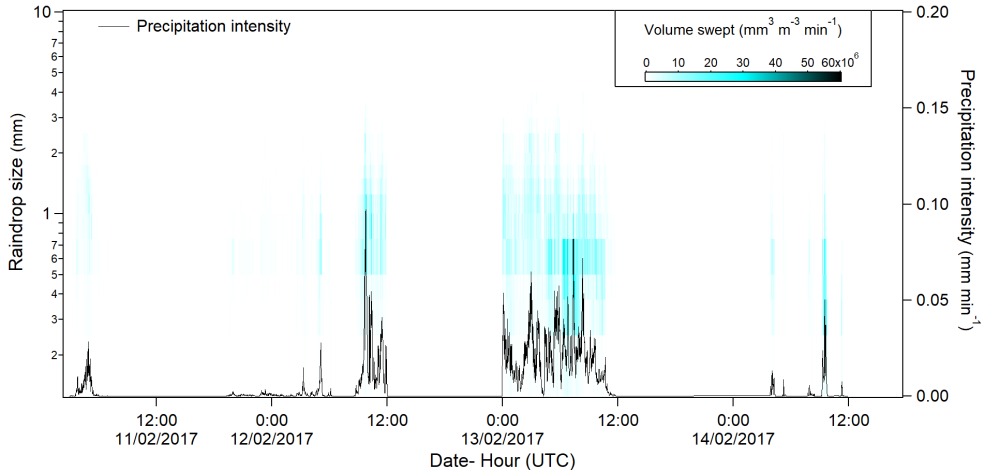

FIG. 9.6. Evolution of precipitation intensity (black line) and volume swept by the raindrops of each size interval (colour scale), between 11 and 14 February 2017.

TABLE 9.5. Source contributions (seawater, crustal and anthropogenic) in % for inorganic ions in rainwater fractions collected on days 11 (P_1), 12 (P_2), 13 (P_3) and 14 (P_4) February 2017.

Rainwater sample	K^+	Mg^{2+}	Ca^{2+}	Cl^-	SO_4^{2-}	NO_3^-
Seawater fraction (%)						
P_1	5	47	7	91	6	-
P_2	21	40	1	82	7	-
P_3	14	28	2	85	3	
P_4	41	12	17	100	18	-
Crustal fraction (%)						
P_1	69	53	93	-	0.6	-
P_2	79	60	99	0.9	4.4	0.6
P_3	86	72	98	0.6	1.2	0.3
P_4	59	88	83	-	0.7	-
Anthropogenic fraction (%)						
P_1	26	-	-	9	93	100
P_2	-	-	-	16.9	89	99
P_3	-	-	-	14.6	96	99.7
P_4	-	-	-	-	81	100

On 11 and 12 February the weather types were hybrid cyclonic CE and pure cyclonic (C), respectively, and the air masses came from North Africa, keeping this scenario until 13 February, consistent with the observation that, between January and June, the dust transport from Africa is mainly caused by cyclonic activity over the west and south of the Peninsula (Rodríguez et al., 2001). The chemical composition of the precipitation was very influenced by the new atmospheric

conditions of this event. The concentration of crustal elements, Ca^{2+} and Mg^{2+}, reached maximum values of 96 and 13 µeq L^{-1}, respectively, on 12 February (Fig. 9.7).

The high content of Ca^{2+} and Mg^{2+} of mineral origin in P_2 may be due to the fact that these ions are incorporated into the cloud during the transport of the air masses (rainout mechanism) (Rodrigo et al., 2003). In addition, mineral dust can act as a surface of pollutant reaction for anthropogenic contaminants (Krueger et al., 2004), which can be reflected in the increase in the concentrations of sulphate and chloride of anthropogenic origin (Fig. 9.7).

The crustal influence was observed on 12 and 13 February, in the increase on the crustal contribution of K^+ (79 and 86%, respectively) and SO_4^{2-} (4.4 and 1.2%, respectively) (Table 9.5). Avila et al. (1997) reported that red rains (rain with reddish silt residues) are enriched in K about 3 times more than non-red rains. Furthermore, during this type of events, the raindrops with dust content would incorporate the anthropogenic pollutants, NO_3^-, NH_4^+ and SO_4^{2-}, as they fall (washout) (Rodrigo et al., 2003).

On 14 February, the HYSPLIT back-trajectories showed air masses coming from the Atlantic. The weather type was SW, which is characterized by humid air masses loaded with marine salts from the Atlantic Ocean. These changes were evidenced in the chemical composition of the rain sample P_4. The fraction of rainwater collected between day 13 in the afternoon and day 14 in the morning (P_4) shows a decrease in the crustal element (Ca^{2+}) concentrations and an increase in the seawater elements (Na^+ and Cl^-) concentrations compared to previous days (Fig. 9.7). The fact that air masses changed their path (Atlantic instead of African) is the most probable explanation of a lowering of the crustal element concentrations in rain. Similar results were observed by Avila and Alarcón (1999), in the studies carried out in Montseny (Spain), about air masses coming from the Atlantic and the Mediterranean. Source contribution showed a seawater influence on the precipitation composition (Table 9.5), which was confirmed by the Cl-/Na+ ratio of 0.9.

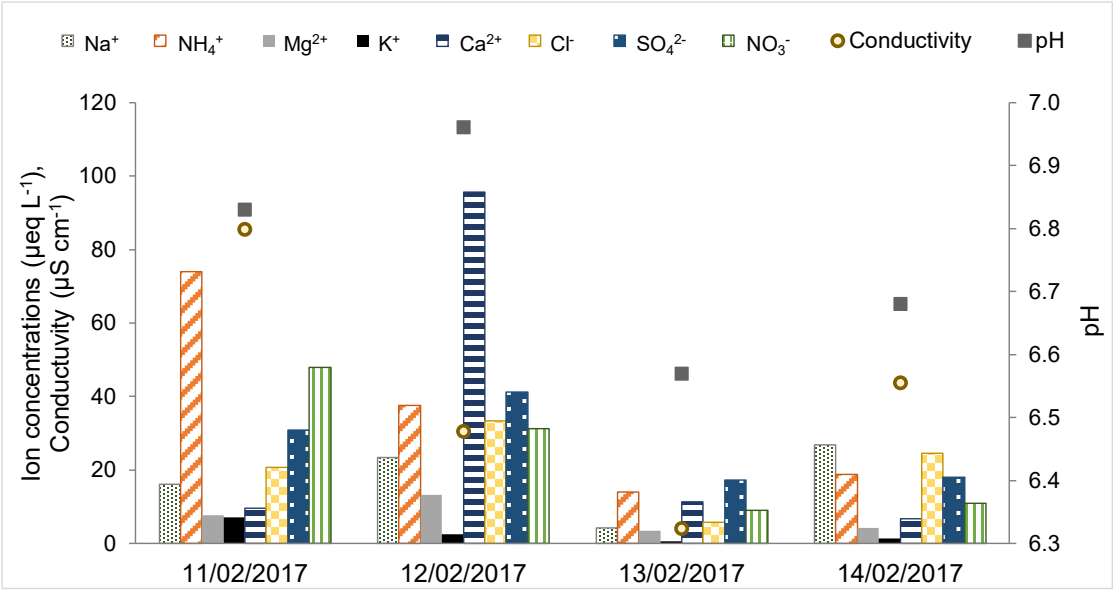

FIG. 9.7. Evolution of ion concentrations, pH and conductivity of each rainwater fractions collected between 11 and 14 February 2017.

TABLE 9.6. Dissolved organic carbon (DOC), water insoluble organic and elemental carbon (WIOC and WIEC, respectively) for rainwater fractions collected on days 11 (P_1), 12 (P_2), 13 (P_3) and 14 (P_4) February 2017.

	P_1	**P_2**	**P_3**	**P_4**
Concentration in rainwater (mg L^{-1})				
DOC	1.41	1.75	1.69	0.40
WIOC	-	0.41	0.14	0.07
WIEC	-	0.03	0.01	0.02

During the dust intrusion, both DOC and WIOC in rain sample P_2 also showed an increase of 24% and 100%, respectively, as compared to P_1 (Table 9.6), reflecting an enhancement in the air concentration of organic species. Between 12 and 13 February, the airborne concentration of sucrose was 3 times higher than those observed in the days before the dust intrusion (Table 9.4). Sucrose is a sugar associated to pollen and plants (Bieleski, 1995; Medeiros et al., 2006); thus, the increase in the sucrose concentration may be related to the transport of bioaerosols, mixed with the local contribution from domestic heating device emissions.

9.3.2.4. Alkaline contribution

The rainwater fraction collected on 12 February had the highest pH value of the event (7.0) (Fig. 9.7). Rainfall samples affected by African events usually show pH values higher than 6 and Ca^{2+} concentrations higher than 80 µeq L^{-1}, as a result of the dissolution of the calcite in the dust carried by the air masses from North Africa (Avila et al., 1998, 1997; Avila and Alarcón, 1999; Calvo et al., 2012, 2010; Camarero and Catalan, 1996; Escudero et al., 2005; Izquierdo et al., 2012; Morales-Baquero et al., 2013). On days before and after the dust intrusion (P_1 and P_4), ammonium was the main component that helped neutralize the rainwater (*NF* of 0.9 for P_1 and 0.6 for P_4). During the dust outbreak, calcium played an important role in neutralizing rainwater acidic components (*NF* of 1.3 for P_2 and 0.4 for P_3). Therefore, the high Ca^{2+} concentration during the dust outbreak, was the main responsible for the alkaline pH value. Moreover, the conductivity values decreased from 86 µS cm^{-1} (P_1) to 4.0 µS cm^{-1} (P_3), as the precipitation event has evolved. Celle-Jeanton et al. (2009) observed that during a rain event, the initial fraction of the rainwater mainly had a chemical composition characteristic of local anthropogenic sources, while the subsequent fractions were influenced by transport events from different regions. Thus, the observed decrease in pH and conductivity values, the decrease in ion concentrations, and the change in the chemical composition of the P_3 and P_4 fractions, could be associated with the change in the air masses.

9.4. CONCLUSIONS

This study shows the impact that caused several wildfires that occurred in summer 2016 and a Saharan dust intrusion event in winter 2017, on rainwater chemistry in León.

The wildfires that took place in northern Portugal and northwest Spain in August 2016 affected the air quality of León causing an increase in the PM_{10} concentration and in the levoglucosan, K, EC and OC values. Coinciding with these wildfires, on 14 August 2016, a

precipitation event was registered in León. The rainwater chemistry was affected by the biomass burning aerosols, which was reflected in the high concentrations of SO_4^{2-} (65.19 μeq L^{-1}) and NO_3^- (121.17 μeq L^{-1}) of a main anthropogenic origin, in the high values of NH_4^+ (153.15 μeq L^{-1}), and in the high DOC (14.7 mg L^{-1}) and WIOC (1.7 mg L^{-1}) concentrations, due to the contribution of several organic compounds emitted by wildfires. The impact of biomass burning emissions on the acidity of rainwater was also observed, probably caused by a high concentration of acidic organic species, which is mirrored in the pH value of 4.8 of the rain sample.

A second precipitation event, which began on 11 February 2017 and was sampled in four sequential rain fractions, P_1, P_2, P_3 and P_4, allowed to study the effects of local and long-range transport emissions on precipitation in León, as well as to assess the scavenging effect of the rain in the atmosphere. The fraction of rainwater collected the first day (P_1), reflected the local anthropogenic contribution of the aerosol, typical of winter in León, with high concentrations of NH_4^+, SO_4^{2-} and NO_3^-. On 12 February, a Saharan dust intrusion reached the north of the Peninsula, causing an increase in the PM_{10} and in the Ca, Si, Al, Ti, Mg and Fe air concentrations, and affecting the chemical composition of the rainwater P_2, with an increase in the Ca^{2+} (>800%), Mg^{2+} (71%), Cl^- (62%), and SO_4^{2-} (33%) concentrations. A small mineral input of SO_4^{2-}, a typical anthropogenic element, into rainwater was also observed during dust outbreaks. The input of crustal elements to the atmosphere, especially Ca^{2+}, helped neutralize the rainwater, causing pH values higher than 6.5. Furthermore, during the Saharan dust outbreak, an increase in DOC values in rainwater was observed, due to a mixed contribution from dust and local anthropogenic emissions. Once the dust intrusion leaved the north of the Peninsula, the composition of the rainwater revealed a mixture of marine constituents together with local anthropogenic emissions, with a 100% of the Cl^- content from seawater source and a 100% of the NO_3^- from anthropogenic source.

The results showed that the rainwater composition is strongly affected by both local and long-range transport aerosol events. The amount and intensity of precipitation, as well as drop size and volume swept by raindrops (a function of size and terminal velocity of raindrops), are also important factors to consider when studying precipitation-air pollutants interaction. Precipitation plays a crucial role in mitigating the negative impact of atmospheric pollutants on human health and the environment. The study of the influence of pollutant emissions on the chemical properties of rainwater provides useful information, which makes it possible to assess their impact on ecosystems and human health.

9.5. REFERENCES

Alastuey, A., Querol, X., Aas, W., Lucarelli, F., Pérez, N., Moreno, T., Cavalli, F., Areskoug, H., Balan, V., Catrambone, M., Ceburnis, D., Cerro, J.C., Conil, S., Gevorgyan, L., Hueglin, C., Imre, K., Jaffrezo, J.-L., Leeson, S.R., Mihalopoulos, N., Mitosinkova, M., Dowd, C.D., Pey, J., Putaud, J.-P., Riffault, V., Ripoll, A., Sciare, J., Sellegri, K., Spindler, G., Yttri, K.E., 2016. Geochemistry of PM10 over Europe during the EMEP intensive measurement periods in summer 2012 and winter 2013. Atmos. Chem. Phys. 16, 6107–6129. doi:10.5194/acp-16-6107-2016

Alastuey, A., Querol, X., Chaves, A., Lopez-Soler, A., Carmen, R.R., 2001. Wet-only sequential deposition in a rural area in north-eastern Spain. Tellus B Chem. Phys. Meteorol. 53, 40–52. doi:10.3402/tellusb.v53i1.16535

Alastuey, A., Querol, X., Chaves, A., Ruiz, C.R., Carratala, A., Lopez-Soler, A., 1999. Bulk deposition in a rural area located around a large coal-fired power station, northeast Spain. Environ. Pollut. 106, 359–367. doi:10.1016/S0269-7491(99)00103-7

Alonso-Blanco, E., Calvo, A.I., Fraile, R., Castro, A., 2012. The Influence of Wildfires on Aerosol Size Distributions in Rural Areas. Sci. World J. 2012, 1–13. doi:10.1100/2012/735697

Alves, C.A., Lopes, D.J., Calvo, A.I., Evtyugina, M., Rocha, S., Nunes, T., 2015. Emissions from Light-Duty Diesel and Gasoline in-use Vehicles Measured on Chassis Dynamometer Test Cycles. Aerosol Air Qual. Res. 15, 99–116. doi:10.4209/aaqr.2014.01.0006

Alves, C.A., Vicente, A., Monteiro, C., Gonçalves, C., Evtyugina, M., Pio, C., 2011a. Emission of trace gases and organic components in smoke particles from a wildfire in a mixed-evergreen forest in Portugal. Sci. Total Environ. 409, 1466–1475. doi:10.1016/j.scitotenv.2010.12.025

Alves, C.A., Vicente, A., Nunes, T., Gonçalves, C., Fernandes, A.P., Mirante, F., Tarelho, L., Sánchez de la Campa, A.M., Querol, X., Caseiro, A., Monteiro, C., Evtyugina, M., Pio, C., 2011b. Summer 2009 wildfires in Portugal: Emission of trace gases and aerosol composition. Atmos. Environ. 45, 641–649. doi:10.1016/j.atmosenv.2010.10.031

Anil, I., Alagha, O., Karaca, F., 2017. Effects of transport patterns on chemical composition of sequential rain samples: trajectory clustering and principal component analysis approach. Air Qual. Atmos. Heal. 10, 1193–1206. doi:10.1007/s11869-017-0504-x

Avila, A., Alarcón, M., 1999. Relationship between precipitation chemistry and meteorological situations at a rural site in NE Spain. Atmos. Environ. 33, 1663–1677. doi:10.1016/S1352-2310(98)00341-0

Avila, A., Alarcón, M., Queralt, I., 1998. The chemical composition of dust transported in red rains - Its contribution to the biogeochemical cycle of a Holm Oak Forest in Catalonia (Spain). Atmos. Environ. doi:10.1016/S1352-2310(97)00286-0

Avila, A., Queralt-Mitjans, I., Alarcón, M., 1997. Mineralogical composition of African dust delivered by red rains over northeastern Spain. J. Geophys. Res. Atmos. 102, 21977–21996. doi:10.1029/97JD00485

Balasubramanian, R., Victor, T., Begum, R., 1999. Impact of biomass burning on rainwater acidity and composition in Singapore. J. Geophys. Res. Atmos. 104, 26881–26890. doi:10.1029/1999JD900247

Bieleski, R.L., 1995. Onset of Phloem Export from Senescent Petals of Daylily. Plant Physiol. 109, 557–565. doi:10.1104/pp.109.2.557

Bisht, D.S., Tiwari, S., Srivastava, A.K., Singh, J. V., Singh, B.P., Srivastava, M.K., 2015. High concentration of acidic species in rainwater at Varanasi in the Indo-Gangetic Plains, India. Nat. Hazards 75, 2985–3003. doi:10.1007/s11069-014-1473-0

Blanco-Alegre, C., Calvo, A.I., Coz, E., Castro, A., Oduber, F., Prévôt, A.S.H., Močnik, G., Fraile, R., 2019. Quantification of source specific black carbon scavenging using an aethalometer and a disdrometer. Environ. Pollut. 246, 336–345. doi:10.1016/j.envpol.2018.11.102

Blanco-Alegre, C., Castro, A., Calvo, A.I., Oduber, F., Alonso-Blanco, E., Fernández-González, D., Valencia-Barrera, R.M., Vega-Maray, A.M., Fraile, R., 2018. Below-cloud scavenging of fine and coarse aerosol particles by rain: The role of raindrop size. Q. J. R. Meteorol. Soc. 144, 2715–2726. doi:10.1002/qj.3399

Cachier, H., Ducret, J., 1991. Influence of biomass burning on equatorial African rains. Nature 352, 228–230. doi:10.1038/352228a0

Calvo, A.I., Olmo, F.J., Lyamani, H., Alados-Arboledas, L., Castro, A., Fernández-Raga, M., Fraile, R., 2010. Chemical composition of wet precipitation at the background EMEP station in Víznar (Granada, Spain) (2002–2006). Atmos. Res. 96, 408–420. doi:10.1016/j.atmosres.2010.01.013

Calvo, A.I., Pont, V., Olmo, F.J., Castro, A., Alados-Arboledas, L., Vicente, A.M., Fernández-Raga, M., Fraile, R., 2012. Air Masses and Weather Types: A Useful Tool for Characterizing Precipitation Chemistry and Wet Deposition. Aerosol Air Qual. Res. 12, 856–878. doi:10.4209/aaqr.2012.03.0068

Camarero, L., Catalan, J., 1996. Variability in the chemistry of precipitation in the Pyrenees (northeastern Spain): Dominance of storm origin and lack of altitude influence. J. Geophys. Res. Atmos. doi:10.1029/96jd01816

Caseiro, A., Marr, I.L., Claeys, M., Kasper-Giebl, A., Puxbaum, H., Pio, C.A., 2007. Determination of saccharides in atmospheric aerosol using anion-exchange high-performance liquid chromatography and pulsed-amperometric detection. J. Chromatogr. A 1171, 37–45. doi:10.1016/j.chroma.2007.09.038

Castro, A., Alonso-Blanco, E., González-Colino, M., Calvo, A.I., Fernández-Raga, M., Fraile, R., 2010. Aerosol size distribution in precipitation events in León, Spain. Atmos. Res. 96, 421–435. doi:10.1016/j.atmosres.2010.01.014

Cathcart, H., Aherne, J., Jeffries, D.S., Scott, K.A., 2016. Critical loads of acidity for 90,000 lakes in northern Saskatchewan: A novel approach for mapping regional sensitivity to acidic deposition. Atmos. Environ. 146, 290–299. doi:10.1016/j.atmosenv.2016.08.048

Celle-Jeanton, H., Travi, Y., Loÿe-Pilot, M.-D., Huneau, F., Bertrand, G., 2009. Rainwater chemistry at a Mediterranean inland station (Avignon, France): Local contribution versus long-range supply. Atmos. Res. 91, 118–126. doi:10.1016/j.atmosres.2008.06.003

Cerqueira, M., Pio, C., Legrand, M., Puxbaum, H., Kasper-Giebl, A., Afonso, J., Preunkert, S., Gelencsér, A., Fialho, P., 2010. Particulate carbon in precipitation at European background sites. J. Aerosol Sci. 41, 51–61. doi:10.1016/j.jaerosci.2009.08.002

Charlson, R.J., Rodhe, H., 1982. Factors controlling the acidity of natural rainwater. Nature 295, 683–685. doi:10.1038/295683a0

Custódio, D., Cerqueira, M., Fialho, P., Nunes, T., Pio, C., Henriques, D., 2014. Wet deposition of particulate carbon to the Central North Atlantic Ocean. Sci. Total Environ. 496, 92–99. doi:10.1016/j.scitotenv.2014.06.103

Draxler, R., Rolph, G., 2012. Hysplit (Hybrid Single-Particle Lagrangian Integrated Trajectory). Silver Spring. NOAA Air Resour. Lab.

Duan, L., Yu, Q., Zhang, Q., Wang, Z., Pan, Y., Larssen, T., Tang, J., Mulder, J., 2016. Acid deposition in Asia: Emissions, deposition, and ecosystem effects. Atmos. Environ. 146, 55–69. doi:10.1016/j.atmosenv.2016.07.018

Escudero, M., Castillo, S., Querol, X., Avila, A., Alarcón, M., Viana, M.M., Alastuey, A., Cuevas, E., Rodríguez, S., 2005. Wet and dry African dust episodes over eastern Spain. J. Geophys. Res. 110, D18S08. doi:10.1029/2004JD004731

Escudero, M., Querol, X., Ávila, A., Cuevas, E., 2007. Origin of the exceedances of the European daily PM limit value in regional background areas of Spain. Atmos. Environ. 41, 730–744. doi:10.1016/j.atmosenv.2006.09.014

Fernández-Raga, M., Castro, A., Marcos, E., Palencia, C., Fraile, R., 2017. Weather types and rainfall microstructure in Leon, Spain. Int. J. Climatol. 37, 1834–1842. doi:10.1002/joc.4816

Formenti, P., Elbert, W., Maenhaut, W., Haywood, J., Andreae, M.O., 2003. Chemical composition of mineral dust aerosol during the Saharan Dust Experiment (SHADE) airborne campaign in the Cape Verde region, September 2000. J. Geophys. Res. 108, 8576. doi:10.1029/2002JD002648

Fredericks, S., Saylor, J.R., 2019. Experimental study of drop shape and wake effects on particle scavenging for non-evaporating drops using ultrasonic levitation. J. Aerosol Sci. 127, 1–17. doi:10.1016/j.jaerosci.2018.10.001

Galloway, J.N., Likens, G.E., Keene, W.C., Miller, J.M., 1982. The composition of precipitation in remote areas of the world. J. Geophys. Res. doi:10.1029/JC087iC11p08771

Godoy-Silva, D., Nogueira, R.F.P., Campos, M.L.A.M., 2017. A 13-year study of dissolved organic carbon in rainwater of an agro-industrial region of São Paulo state (Brazil) heavily impacted by biomass burning. Sci. Total Environ. 609, 476–483. doi:10.1016/j.scitotenv.2017.07.145

Izquierdo, R., Avila, A., Alarcón, M., 2012. Trajectory statistical analysis of atmospheric transport patterns and trends in precipitation chemistry of a rural site in NE Spain in 1984-2009. Atmos. Environ. 61, 400–408. doi:10.1016/j.atmosenv.2012.07.060

Jordan, C.E., Dibb, J.E., Anderson, B.E., Fuelberg, H.E., 2003. Uptake of nitrate and sulfate on dust aerosols during TRACE-P. J. Geophys. Res. Atmos. 108, 1–10. doi:10.1029/2002jd003101

Kajino, M., Aikawa, M., 2015. A model validation study of the washout/rainout contribution of sulfate and nitrate in wet deposition compared with precipitation chemistry data in Japan. Atmos. Environ. 117, 124–134. doi:10.1016/j.atmosenv.2015.06.042

Keene, W.C., Pszenny, A.A.P., Galloway, J.N., Hawley, M.E., 1986. Sea-salt corrections and interpretation of constituent ratios in marine precipitation. J. Geophys. Res. 91, 6647. doi:10.1029/JD091iD06p06647

Keresztesi, Á., Korodi, A., Boga, R., Petres, S., Ghita, G., Ilie, M., 2017. Chemical characteristics of wet precipitation in the Eastern Carpathians, Romania. Ecoterra 14, 52–59.

Khan, M.F., Maulud, K.N.A., Latif, M.T., Chung, J.X., Amil, N., Alias, A., Nadzir, M.S.M., Sahani, M., Mohammad, M., Jahaya, M.F., Hassan, H., Jeba, F., Tahir, N.M., Abdullah, S.M.S., 2018. Physicochemical factors and their potential sources inferred from long-term rainfall

measurements at an urban and a remote rural site in tropical areas. Sci. Total Environ. 613–614, 1401–1416. doi:10.1016/j.scitotenv.2017.08.025

Knote, C., Hodzic, A., Jimenez, J.L., 2015. The effect of dry and wet deposition of condensable vapors on secondary organic aerosols concentrations over the continental US. Atmos. Chem. Phys. 15, 1–18. doi:10.5194/acp-15-1-2015

Kopáček, J., Hejzlar, J., Krám, P., Oulehle, F., Posch, M., 2016. Effect of industrial dust on precipitation chemistry in the Czech Republic (Central Europe) from 1850 to 2013. Water Res. 103, 30–37. doi:10.1016/j.watres.2016.07.017

Krueger, B.J., Grassian, V.H., Cowin, J.P., Laskin, A., 2004. Heterogeneous chemistry of individual mineral dust particles from different dust source regions: The importance of particle mineralogy. Atmos. Environ. 38, 6253–6261. doi:10.1016/j.atmosenv.2004.07.010

Kulshrestha, U.C., Reddy, L.A.K., Satyanarayana, J., Kulshrestha, M.J., 2009. Real-time wet scavenging of major chemical constituents of aerosols and role of rain intensity in Indian region. Atmos. Environ. 43, 5123–5127. doi:10.1016/j.atmosenv.2009.07.025

Kulshrestha, U.C., Sarkar, A.K., Srivastava, S.S., Parashar, D.C., 1996. Investigation into atmospheric deposition through precipitation studies at New Delhi (India). Atmos. Environ. 30, 4149–4154. doi:10.1016/1352-2310(96)00034-9

Kulshrestha, U.C., Sarkar, A.K., Srivastava, S.S., Parashar, D.C., 1995. Wet-only and bulk deposition studies at New Delhi (India). Water, Air, Soil Pollut. 85, 2137–2142. doi:10.1007/BF01186150

Lamb, H.H., 1972. British Isles weather types and a register of daily sequence of circulation patterns, Geophysical Memoir, HMSO, London. Her Majesty's stationery office.

Livingston, R.A., 2016. Acid rain attack on outdoor sculpture in perspective. Atmos. Environ. 146, 332–345. doi:10.1016/j.atmosenv.2016.08.029

Luan, T., Guo, X., Zhang, T., Guo, L., 2019. Below-Cloud Aerosol Scavenging by Different-Intensity Rains in Beijing City. J. Meteorol. Res. 33, 126–137. doi:10.1007/s13351-019-8079-0

Lucarelli, F., Chiari, M., Calzolai, G., Giannoni, M., Nava, S., Udisti, R., Severi, M., Querol, X., Amato, F., Alves, C., Eleftheriadis, K., 2015. The role of PIXE in the AIRUSE project "testing and development of air quality mitigation measures in Southern Europe." Nucl. Instruments Methods Phys. Res. Sect. B Beam Interact. with Mater. Atoms 363, 92–98. doi:10.1016/j.nimb.2015.08.023

Martins, E.H., Nogarotto, D.C., Mortatti, J., Pozza, S.A., 2019. Chemical composition of rainwater in an urban area of the southeast of Brazil. Atmos. Pollut. Res. 10, 520–530. doi:10.1016/j.apr.2018.10.003

Medeiros, P.M., Conte, M.H., Weber, J.C., Simoneit, B.R.T., 2006. Sugars as source indicators of biogenic organic carbon in aerosols collected above the Howland Experimental Forest, Maine. Atmos. Environ. 40, 1694–1705. doi:10.1016/j.atmosenv.2005.11.001

Mimura, A.M.S., Almeida, J.M., Vaz, F.A.S., de Oliveira, M.A.L., Ferreira, C.C.M., Silva, J.C.J., 2016. Chemical composition monitoring of tropical rainwater during an atypical dry year. Atmos. Res. 169, 391–399. doi:10.1016/j.atmosres.2015.11.001

Morales-Baquero, R., Pulido-Villena, E., Reche, I., 2013. Chemical signature of Saharan dust on dry and wet atmospheric deposition in the south-western Mediterranean region. Tellus B Chem. Phys. Meteorol. 65, 18720. doi:10.3402/tellusb.v65i0.18720

Oduber, F., Calvo, A.I., Blanco-Alegre, C., Castro, A., Nunes, T., Alves, C., Sorribas, M., Fernández-González, D., Vega-Maray, A.M., Valencia-Barrera, R.M., Lucarelli, F., Nava, S., Calzolai, G., Alonso-Blanco, E., Fraile, B., Fialho, P., Coz, E., Prevot, A.S.H., Pont, V., Fraile, R., 2019. Unusual winter Saharan dust intrusions at Northwest Spain: Air quality, radiative and health impacts. Sci. Total Environ. 669, 213–228. doi:10.1016/j.scitotenv.2019.02.305

Oduber, F., Castro, A., Calvo, A.I., Blanco-Alegre, C., Alonso-Blanco, E., Belmonte, P., Fraile, R., 2018. Summer-autumn air pollution in león, Spain: Changes in aerosol size distribution and expected effects on the respiratory tract. Air Qual. Atmos. Heal. 11, 505–520. doi:10.1007/s11869-018-0556-6

Pan, Y., Wang, Yuesi, Xin, J., Tang, G., Song, T., Wang, Yinghong, Li, X., Wu, F., 2010. Study on dissolved organic carbon in precipitation in Northern China. Atmos. Environ. 44, 2350–2357. doi:10.1016/j.atmosenv.2010.03.033

Pan, Y.P., Wang, Y.S., 2015. Atmospheric wet and dry deposition of trace elements at 10 sites in Northern China. Atmos. Chem. Phys. 15, 951–972. doi:10.5194/acp-15-951-2015

Piazzalunga, A., Fermo, P., Bernardoni, V., Vecchi, R., Valli, G., de Gregorio, M.A., 2010. A simplified method for levoglucosan quantification in wintertime atmospheric particulate matter by high performance anion-exchange chromatography coupled with pulsed amperometric detection. Int. J. Environ. Anal. Chem. doi:10.1080/03067310903023619

Pio, C., Cerqueira, M., Harrison, R.M., Nunes, T., Mirante, F., Alves, C., Oliveira, C., Sanchez de la Campa, A., Artíñano, B., Matos, M., 2011. OC/EC ratio observations in Europe: Re-thinking the approach for apportionment between primary and secondary organic carbon. Atmos. Environ. 45, 6121–6132. doi:10.1016/j.atmosenv.2011.08.045

Pio, C.A., Legrand, M., Alves, C.A., Oliveira, T., Afonso, J., Caseiro, A., Puxbaum, H., Sanchez-Ochoa, A., Gelencsér, A., 2008. Chemical composition of atmospheric aerosols during the 2003 summer intense forest fire period. Atmos. Environ. 42, 7530–7543. doi:10.1016/j.atmosenv.2008.05.032

Querol, X., Alastuey, A., Pandolfi, M., Reche, C., Pérez, N., Minguillón, M.C., Moreno, T., Viana, M., Escudero, M., Orio, A., Pallarés, M., Reina, F., 2014. 2001–2012 trends on air quality in Spain. Sci. Total Environ. 490, 957–969. doi:10.1016/j.scitotenv.2014.05.074

Querol, X., Alastuey, A., Rodríguez, S., Viana, M.M., Artíñano, B., Salvador, P., Mantilla, E., do Santos, S.G., Patier, R.F., de La Rosa, J., de la Campa, A.S., Menéndez, M., Gil, J.J., 2004. Levels of particulate matter in rural, urban and industrial sites in Spain. Sci. Total Environ. 334–335, 359–376. doi:10.1016/j.scitotenv.2004.04.036

Rodrigo, A., Àvila, A., Rodà, F., 2003. The chemistry of precipitation, throughfall and stemflow in two holm oak (Quercus ilex L.) forests under a contrasted pollution environment in NE Spain. Sci. Total Environ. 305, 195–205. doi:10.1016/S0048-9697(02)00470-9

Rodríguez, S., Querol, X., Alastuey, A., Kallos, G., Kakaliagou, O., 2001. Saharan dust contributions to PM10 and TSP levels in Southern and Eastern Spain. Atmos. Environ. 35, 2433–2447. doi:10.1016/S1352-2310(00)00496-9

Rolph, G., Stein, A., Stunder, B., 2017. Real-time Environmental Applications and Display sYstem: READY. Environ. Model. Softw. 95, 210–228. doi:10.1016/j.envsoft.2017.06.025

Rosborg, I., Nihlgård, B., 2018. Health Consequences of Acid Rain in South West Sweden. J. Geosci. Environ. Prot. 06, 126–142. doi:10.4236/gep.2018.62009

Seinfeld, J.H., Pandis, S.N., 2016. Atmospheric Chemistry and Physics: From Air Pollution to Climate Change, 3rd ed. John Wiley & Sons.

Stein, A.F., Draxler, R.R., Rolph, G.D., Stunder, B.J.B., Cohen, M.D., Ngan, F., 2015. NOAA's HYSPLIT Atmospheric Transport and Dispersion Modeling System. Bull. Am. Meteorol. Soc. 96, 2059–2077. doi:10.1175/BAMS-D-14-00110.1

Sun, X., Wang, Y., Li, H., Yang, X., Sun, L., Wang, X., Wang, T., Wang, W., 2016. Organic acids in cloud water and rainwater at a mountain site in acid rain areas of South China. Environ. Sci. Pollut. Res. 23, 9529–9539. doi:10.1007/s11356-016-6038-1

Taylor, S.R., 1964. Abundance of chemical elements in the continental crust: a new table. Geochim. Cosmochim. Acta 28, 1273–1285. doi:10.1016/0016-7037(64)90129-2

Trigo, R.M., DaCamara, C.C., 2000. Circulation weather types and their influence on the precipitation regime in Portugal. Int. J. Climatol. 20, 1559–1581. doi:10.1002/1097-0088(20001115)20:13<1559::AID-JOC555>3.0.CO;2-5

Vicente, A., Alves, C., Calvo, A.I., Fernandes, A.P., Nunes, T., Monteiro, C., Almeida, S.M., Pio, C., 2013. Emission factors and detailed chemical composition of smoke particles from the 2010 wildfire season. Atmos. Environ. 71, 295–303. doi:10.1016/j.atmosenv.2013.01.062

Vicente, A., Alves, C., Monteiro, C., Nunes, T., Mirante, F., Cerqueira, M., Calvo, A., Pio, C., 2012. Organic speciation of aerosols from wildfires in central Portugal during summer 2009. Atmos. Environ. 57, 186–196. doi:10.1016/j.atmosenv.2012.04.030

Vicente, A., Alves, C., Monteiro, C., Nunes, T., Mirante, F., Evtyugina, M., Cerqueira, M., Pio, C., 2011. Measurement of trace gases and organic compounds in the smoke plume from a wildfire in Penedono (central Portugal). Atmos. Environ. 45, 5172–5182. doi:10.1016/j.atmosenv.2011.06.021

Vicente, E.D., Alves, C.A., 2018. An overview of particulate emissions from residential biomass combustion. Atmos. Res. 199, 159–185. doi:10.1016/j.atmosres.2017.08.027

Zhang, M., Wang, S., Wu, F., Yuan, X., Zhang, Y., 2007. Chemical compositions of wet precipitation and anthropogenic influences at a developing urban site in southeastern China. Atmos. Res. 84, 311–322. doi:10.1016/j.atmosres.2006.09.003

10

CONCLUSIONES Y PERSPECTIVAS

10.1. CONCLUSIONES

Este capítulo resume las conclusiones principales de este trabajo en función de los objetivos centrales planteados en el Capítulo 1.

En el primer objetivo se planteaba estudiar la evolución temporal de la concentración de contaminantes atmosféricos en la ciudad de León (España), así como su correlación con la concentración de algunos pólenes alergénicos y con ciertos parámetros meteorológicos. Las conclusiones generales relacionadas con este objetivo son:

- Se ha observado una tendencia decreciente en la concentración de los contaminantes atmosféricos estudiados (CO, NO, NO_2, SO_2, O_3 y PM_{10}) en la ciudad de León, desde el año 1997 hasta el 2016, probablemente causada por las medidas de mitigación implementadas en los diferentes sectores: industrial, transporte y energía.

- El índice polínico estacional (SPIn) del tipo polínico *Fraxinus* mostró una correlación negativa significativa con los contaminantes atmosféricos estudiados antes del período de floración. Por otra parte, el SPIn del tipo polínico Poaceae mostró una correlación significativa con la precipitación antes y durante el período de floración. La duración de la estación polínica principal (MPS) del *Fraxinus* está correlacionada positiva y significativamente con la temperatura, la humedad relativa y la precipitación durante el período de floración. La duración de la MPS del Poaceae está correlacionada positivamente con la temperatura mínima durante el período de floración, mientras que la del *Populus* muestra una correlación negativa con dicha temperatura.

Con el segundo objetivo se pretendía determinar la contribución de las principales fuentes de emisión de partículas biogénicas y no biogénicas, mediante la caracterización química del PM_{10} en León. Como conclusiones generales hemos establecido que:

- La concentración media anual de PM_{10} en la ciudad de León fue 23 ± 8 μg m^{-3}. La concentración media anual de la fracción carbonosa, que representa la fracción másica mayoritaria con un 21

± 7% del PM_{10}, fue de 2.4 ± 1.3 μg m^{-3} de OC, 0.7 ± 0.4 μg m^{-3} de EC. La concentración media anual de azúcares en el aerosol fue 64 ± 108 ng m^{-3}, lo que representa el 0.3% del PM_{10}.

- El modelo de Factorización de Matriz Positiva (PMF) permitió distinguir 6 fuentes de emisión de aerosoles en León: el tráfico (29% del PM_{10}), la sal marina envejecida (26% del PM_{10}), el aerosol secundario (16% del PM_{10}), las fuentes minerales (13% del PM_{10}), el aerosol marino (7% del PM_{10}) y la quema de biomasa (3% del PM_{10}). Las fuentes de tráfico y de aerosol secundario mostraron la mayor contribución al PM_{10} en los tipos de tiempo ciclónico híbridos CE, CS y CSE. Los tipos de tiempo anticiclónicos A, AN y ANE exhibieron altas contribuciones de aerosoles secundarios (15%), sal marina envejecida (20%) y fuentes minerales (17%), mientras que los tipos del norte N y NW presentaron las mayores contribuciones del factor mineral (23 y 27%, respectivamente).

- Utilizando los resultados obtenidos con el PMF y los parámetros de los tipos de tiempo asociados al flujo geostrófico (SF, WF, ZS y ZW), se construyeron modelos de regresión multilineal que permitieron determinar la contribución de cada factor al PM_{10}. El factor marino mostró una dependencia positiva con WF, demostrando que las masas de aire del oeste son responsables del transporte de sales marinas desde el océano Atlántico hasta León. Los factores de aerosoles secundarios y de tráfico mostraron correlaciones positivas con SF, debido a la contribución de las emisiones antropogénicas del centro de la ciudad y de otras ciudades situadas al sur de León. En el caso de la sal marina envejecida, la correlación negativa con ZS confirmó que este factor se ve favorecido principalmente por las situaciones anticiclónicas. Las correlaciones del factor mineral, negativas con SF y positivas con ZS, sugieren que las emisiones de la fábrica de cemento de La Robla, ubicada al norte de la ciudad de León, son una importante fuente de aerosol mineral. El factor de combustión de biomasa no mostró ninguna relación con el flujo geostrófico, probablemente porque se trata de una fuente más local.

- En primavera, cuando se producen altos niveles de actividad metabólica de las plantas y aumentan las temperaturas, los azúcares glucosa, sacarosa, 2-metil-eritritol, manitol, arabitol e inositol, están relacionados con la concentración de polen en la atmósfera. Sin embargo, las concentraciones de glucosa y la arabinosa en el aire también pueden estar relacionados con las emisiones de la quema de biomasa, por lo que no son buenos trazadores de los niveles de polen en el aire. Por otra parte, en otoño, el arabitol, el sorbitol y el adonitol pueden ser utilizados como trazadores de la espora fúngica *Alternaria*. Durante los días de lluvia, el alérgeno Alt a 1 y el manitol están correlacionados con la *Alternaria*, por lo que son trazadores de esta espora fúngica.

- En otoño, el levoglucosano, el manosano, el galactosano, la arabinosa, la fructosa y la glucosa, están relacionados con el K (trazador de quema de biomasa), el NO_3^- y el OC. El manosano y el levoglucosano están correlacionados con EC, OC, Cu, Zn, Se, Pb, V y Ni (característicos de tráfico y de combustión de combustibles fósiles). El manosano también se correlaciona con el As (trazador de combustión de carbón). Así pues, la elección de estos anhídridos como marcadores de la quema de biomasa durante la estación fría, puede estar sobreestimando la contribución de esa fuente, debido a la aportación de otras fuentes antropogénicas.

- La precipitación puede provocar un aumento de la concentración de glucosa y sacarosa, debido a que la rotura de las partículas de polen hidratado libera los azúcares unidos a los fragmentos más pequeños. La precipitación también incrementa la concentración de arabitol (trazador de esporas fúngicas aerotransportadas), probablemente porque es capaz de disparar los mecanismos de liberación activa y pasiva de esporas fúngicas. El crecimiento de la concentración de glucosa después de la lluvia está correlacionado positiva y significativamente con la intensidad media de las precipitaciones, el volumen barrido por las gotas de lluvia y el tamaño medio de gota. Además, la cantidad de gotas mayores de 3 mm también correlaciona con el incremento de la concentración de glucosa. Este hecho podría sugerir que el tamaño de la gota de lluvia puede marcar un umbral que divide ambos procesos: el lavado y la liberación de los azúcares.

Las conclusiones principales relacionadas con el tercer objetivo, que pretendía analizar el impacto en la calidad del aire de la ciudad de León, en dos casos particulares de contaminación, uno de origen natural (intrusiones de polvo sahariano) y otro de origen antrópico (tráfico), son:

- Las intrusiones de polvo sahariano que tuvieron lugar en febrero del año 2016 y del año 2017, causaron un incremento en la concentración de las partículas de la moda gruesa (D_p > 1 μm) y la superación del valor límite diario de PM_{10}, con 52 μg m^{-3} en 2016 y 86 μg m^{-3} en 2017. Además, se evidenció un cambio en el material biológico, con la presencia de pólenes que no son típicos de León durante el periodo de estudio. Los valores de las fracciones másicas alcanzaron valores máximos de 156 μg m^{-3} en el evento de 2016 y 155 μg m^{-3} en el de 2017 para la fracción inhalable, y de 102-134 μg m^{-3} en el de 2016 y de 155 μg m^{-3} en el de 2017 para la fracción respirable; valores nueve veces superiores a los obtenidos durante los días sin intrusiones de polvo en León.

- Los forzamientos radiativos atmosféricos indican que las dos intrusiones de polvo sahariano invernales causaron un efecto de enfriamiento en la atmósfera, con valores de ratio media estimada de -15.6 K $día^{-1}$ y -12.4 K $día^{-1}$ en los eventos de los años 2016 y 2017, respectivamente. El incremento de los valores del albedo de dispersión simple (SSA) y del espesor óptico de los aerosoles (AOD) durante las intrusiones de polvo, muestra el efecto de *scattering* de estos eventos.

- El número de partículas se incrementa de 1000 ± 600 partículas cm^{-3} en agosto a 1500 ± 1000 partículas cm^{-3} en octubre durante la transición verano-otoño, debido a la intensificación del tráfico después de las vacaciones de verano, a una menor dispersión causada por la baja altura de la capa de mezcla y al inicio del uso de las calefacciones. La fracción respirable del material particulado alcanzó el valor más alto en septiembre y octubre, con 12 μg m^{-3}, mientras que, en los días laborables el máximo fue observado durante las horas de mayor flujo de vehículos, entre las 0600 y las 1000 UTC, con 15 μg m^{-3} y entre las 1700 y las 2000 UTC, con 12 μg m^{-3}.

El cuarto objetivo planteaba examinar la influencia de la composición química de los aerosoles y de las características físicas de la precipitación, en las propiedades físico-químicas del agua de lluvia. Las conclusiones más relevantes, relacionadas con este objetivo son:

- De forma general, el *scavenging* de los contaminantes atmosféricos es más eficiente con eventos de precipitación prolongados y continuos. La concentración en el agua de lluvia de los iones

solubles en agua, Ca^{2+}, SO_4^{2-} y NO_3^-, y del carbono orgánico disuelto (DOC) se incrementa con el volumen barrido por las gotas de agua. Sin embargo, la concentración de las especies de carbono elemental (WIEC) y carbono orgánico (WIOC) insolubles en agua son dependientes del tamaño de la gota, ya que el *scavenging* de estas especies probablemente se ve afectado por el impacto inercial de las gotas a través de la columna de agua.

- El agua de lluvia recogida en León bajo la influencia de las emisiones procedentes de los incendios forestales masivos que tuvieron lugar al norte de la Península Ibérica en agosto de 2016, registró un pH de 4.8, siendo el valor medio anual del pH de la precipitación en León de 5.87 ± 0.02. Este valor tan bajo probablemente se debe a la presencia de una alta concentración de especies orgánicas en el aerosol. Las altas concentraciones en el agua de lluvia de NH_4^+ (153 μeq L^{-1}), SO_4^{2-} (65 μeq L^{-1}), NO_3^- (121 μeq L^{-1}), DOC (15 mg L^{-1}) y WIOC (2 mg L^{-1}), reflejaron la influencia de los aerosoles provenientes de la quema de biomasa en la precipitación.

- La composición química del agua de lluvia, correspondiente al evento de precipitación que tuvo lugar entre los días 11 y 14 de febrero de 2017, se vio afectada por la intrusión de polvo sahariano que afectó a León el 12 de febrero, causando un incremento en las concentraciones de los iones Ca^{2+} (> 800%), Mg^{2+} (71%), Cl^- (62%) y SO_4^{2-} (33%), con respecto al día anterior. Además, se observó un incremento en el pH del agua de lluvia hasta un valor de 7.0, debido al efecto de neutralización del Ca^{2+} sobre los componentes ácidos.

10.2. PERSPECTIVAS

Para concluir esta tesis doctoral, en esta sección se exponen las posibles aplicaciones del trabajo presentado y, en base a los resultados obtenidos, una serie de posibles investigaciones futuras que podrían aportar resultados interesantes en el campo de estudio de los aerosoles, así como de la interacción aerosol-precipitación.

Los aerosoles biogénicos y no biogénicos desempeñan un papel importante en la salud humana y en los procesos atmosféricos. Los resultados presentados en esta memoria aportan una información valiosa que puede ayudar al establecimiento de diferentes medidas para la mitigación de la contaminación del medioambiente y para reducir el impacto de los contaminantes atmosféricos en la salud humana. Asimismo, este trabajo ofrece una mejor comprensión de las complicadas interacciones existentes entre la biósfera, la atmósfera y la litósfera.

A lo largo de la memoria se han presentado una serie de resultados que podrían ser útiles para otros investigadores que trabajan con modelos atmosféricos de transporte de contaminantes a escala local o regional. Por ejemplo, la combinación de los modelos de PMF y los tipos de tiempo, e incluso la introducción de otras variables como la concentración de los azúcares en el aerosol, puede ser una herramienta útil en el análisis local de la distribución de las fuentes, permitiendo una mejor comprensión de la influencia de los diferentes mecanismos de evolución y transporte de los aerosoles y su comportamiento a diferentes escalas. Continuando con esta línea de investigación, en los estudios futuros interesaría centrar la atención en el análisis de las fuentes de emisión de otras fracciones del material particulado como el $PM_{2.5}$ y el PM_1, y su relación con los parámetros meteorológicos. De igual forma, la monitorización continua de las partículas

ultrafinas con el SMPS, es crucial para la identificación de los procesos de nucleación, lo que resulta clave en el estudio de los procesos de formación de partículas.

En cuanto al estudio de los azúcares, su interacción con otras partículas bióticas o abióticas, puede aumentar los síntomas de las alergias respiratorias, por lo que la descripción detallada de de dichas partículas y de sus fuentes de emisión podría ayudar en el establecimiento de medidas que reduzcan el impacto de los aerosoles en la salud humana. El estudio de la relación de los azúcares con trazadores (biológicos y no biológicos) y con las condiciones meteorológicas, es un instrumento útil para conocer el origen de estos compuestos orgánicos presentes en el aerosol atmosférico. Por otra parte, los resultados obtenidos en esta memoria presentan la posibilidad de averiguar bajo qué condiciones ambientales pueden usarse ciertos azúcares como marcadores de fuentes de aerosol.

Debido al creciente interés en el campo de los bioaerosoles, consideramos de gran importancia la profundización de ciertos aspectos relacionados con este tipo de aerosoles. Resulta interesante realizar un estudio a largo plazo de las variaciones estacionales de la concentración de polen, esporas de hongos y diversos alérgenos en el aire y su relación con la concentración de azúcares en PM_{10}, $PM_{2.5}$ y PM_1. Dicho estudio se podría complementar con la medida continua del bioaerosol, utilizando un espectrómetro WIBS (del inglés *Wideband Integrated Bioaerosol Spectrometer*), que permite la identificación y cuantificación de los grupos específicos de bacterias, hongos o polen a través del análisis de las huellas de fluorescencia proporcionadas por este equipo. Además, la determinación de bioaerosoles en el agua de lluvia, permitiría ahondar en la influencia de la precipitación en sus procesos de emisión, transporte y eliminación. A partir de los resultados obtenidos y recogidos en esta memoria, se hace necesario estudiar en profundidad la interacción de los azúcares presentes en el aerosol atmosférico con los parámetros físicos de la precipitación, para discernir entre las características de la lluvia que causan la liberación de estos compuestos y las que producen el lavado efectivo de los mismos.

Los procesos de combustión (la quema de restos de cosechas de diferentes cultivos, la quema de carbón y de otros combustibles fósiles en maquinaria e instalaciones industriales, así como en sistemas de calefacción y agua caliente, entre otros), expulsan a la atmósfera grandes cantidades de contaminantes. Estas prácticas, lejos de ser un problema local, repercuten en la calidad del medioambiente a nivel global, por lo que consideramos necesario realizar trabajos de investigación que permitan ahondar en las emisiones causadas por dichos procesos.

El carbono negro (BC) es uno de los contaminantes emitidos por los procesos de combustión. La identificación de las fuentes específicas del BC no es tarea sencilla, y los modelos actuales permiten estimar principalmente, la contribución de la quema de biomasa y de la combustión de combustibles fósiles a la concentración de carbono negro. Sin embargo, la emisión de carbono negro por la combustión específica del carbón, especialmente en países como China donde esta práctica se ha convertido en una de las actividades más contaminantes, sigue siendo un serio problema a nivel mundial. Por ello se hace necesaria la implementación de una metodología que posibilite la obtención en tiempo real de la contribución de la quema de carbón al BC total. Siguiendo con esta línea de investigación, el uso de otros instrumentos altamente sensibles como el fotómetro SP2-XR, que mide directamente el carbono negro de las partículas individuales a través de la incandescencia láser y de la dispersión de la luz por las partículas,

podría ser utilizado para discernir entre las fuentes del BC. Por otra parte, el SP2-XR aporta información sobre la distribución de tamaños del BC, lo que permite el estudio de la influencia de los distintos tamaños de gota en la eliminación de las partículas de BC.

Precisamente el estudio de la interacción precipitación-aerosol son esenciales, ya que la precipitación juega un papel crucial en la mitigación del impacto negativo de los contaminantes atmosféricos en la salud humana y en el medioambiente. Los resultados presentados en este trabajo contribuyen al estudio de los mecanismos de eliminación, demostrando que los modelos simples permiten el cálculo de la eficiencia de la eliminación de contaminantes por la precipitación, teniendo en cuenta las características químicas del aerosol y las propiedades físico-químicas de la precipitación. Sin embargo, es necesario profundizar en la influencia de las propiedades físico-químicas de la lluvia en el lavado del aerosol, a través de la identificación de los tamaños de gota más eficientes en el lavado de los diferentes contaminantes (biogénicos y no biogénicos). Esto resultaría clave en el desarrollo de otros trabajos, centrados en la generación de gotas de agua que puedan ser utilizadas en zonas de elevada concentración de contaminantes para reducir los niveles de contaminación. Asimismo, el análisis del impacto de la deposición húmeda y seca del material particulado en los ecosistemas sería otra sugerente línea de trabajo.

Los aerosoles y las nubes repercuten en los flujos radiativos y modulan el clima, por lo que es indispensable realizar mediciones más amplias y precisas que permitan comprender mejor estas complejas interacciones climáticas. Llevar a cabo un estudio de las propiedades ópticas de los aerosoles a través del fotómetro CIMEL, ubicado en el mismo punto de muestreo de los aerosoles, permitiría obtener información más precisa sobre el forzamiento radiativo en distintos eventos de contaminación local. De igual forma, se sugiere realizar el estudio del forzamiento radiativo local en distintos escenarios meteorológicos como antes y después de un evento de precipitación.

Finalmente, consideramos de gran importancia la integración de los estudios antes mencionados con una investigación más profunda relacionada con la salud, como podrían ser los estudios epidemiológicos en colaboración con las instituciones sanitarias. Además de los efectos perjudiciales en la salud humana y en los ecosistemas, es importante realizar también una valoración sobre el impacto económico de la contaminación atmosférica, atendiendo al importante deterioro del patrimonio arquitectónico que ocasiona.

CONCLUSIONS AND PERSPECTIVES

10.1. CONCLUSIONS

This chapter summarizes the main conclusions of this work in terms of the central objectives set out in Chapter 1.

The first objective was to study the temporal evolution of the concentration of atmospheric pollutants in León city (Spain), as well as its correlation with the concentration of some allergenic pollens and with certain meteorological parameters. The general conclusions related to this objective are:

- A decreasing trend has been observed in the concentration of the studied atmospheric pollutants (CO, NO, NO_2, SO_2, O_3 and PM_{10}) in León city, from 1997 to 2016, probably caused by the mitigation measures implemented in the different sectors: industrial, transport and energy.

- The seasonal pollen index (SPIn) of the *Fraxinus* pollen type showed a significant negative correlation with the air pollutants studied before the flowering period. Moreover, the SPIn of the Poaceae pollen type showed a significant correlation with precipitation before and during the flowering period. The duration of the *Fraxinus* main pollen season (MPS) is positively and significantly correlated with temperature, relative humidity and precipitation during the flowering period. The duration of the Poaceae MPS is positively correlated with minimum temperature during the flowering period, while that of *Populus* shows a negative correlation with minimum temperature.

The second objective was to determine the contribution of the main emission sources of biogenic and non-biogenic particles, through the chemical characterization of PM_{10} in León. As general conclusions we have established that:

- The PM_{10} annual mean concentration in León city was 23 ± 8 μg m^{-3}. The annual mean concentration of the carbonaceous fraction, which represents the majority mass fraction with 21 ± 7% of PM_{10}, was 2.4 ± 1.3 μg m^{-3} of OC, 0.7 ± 0.4 μg m^{-3} of EC. The annual mean

concentration of sugar compounds in the aerosol was 64 ± 108 ng m^{-3}, representing 0.3% of PM_{10}.

- The Positive Matrix Factorization (PMF) model allowed the identification of 6 sources of aerosol emissions in León: traffic (29% of PM_{10}), aged sea salt (26% of PM_{10}), secondary aerosol (16% of PM_{10}), mineral sources (13% of PM_{10}), marine aerosol (7% of PM_{10}) and biomass burning (3% of PM_{10}). Traffic and secondary aerosol sources showed the largest contribution to PM_{10} in the hybrid cyclonic weather types CE, CS and CSE. The anticyclonic weather types A, AN and ANE showed high contributions of secondary aerosols (15%), aged sea salt (20%) and mineral sources (17%), while the northern N and NW types showed the highest contributions of the mineral factor (23 and 27%, respectively).

- Using the results obtained with the PMF model and the parameters from the weather types associated to the geostrophic flows (SF, WF, ZS and ZW), multi-linear regression models were built to determine the contribution of each factor to PM_{10}. The marine factor showed a positive dependence with WF, demonstrating that the air masses from west are responsible for the transport of sea salts from the Atlantic Ocean to León. The secondary aerosol and traffic factors showed positive correlations with SF, due to the contribution of anthropogenic emissions from the city centre and other cities located south of León. In the case of aged sea salt, the negative correlation with ZS confirmed that this factor is mainly favoured by anticyclonic situations. The correlations of the mineral factor, negative with SF and positive with ZS, suggest that emissions from the La Robla cement factory, located to the north of León city, are an important source of mineral aerosol. The biomass combustion factor did not show any relationship with geostrophic flow, probably because it is a more local source.

- In spring, when high levels of metabolic activity of plants occurs and temperatures increase, the sugar compounds glucose, sucrose, 2-methyl-erythritol, mannitol, arabitol and inositol are related to the pollen concentration in the atmosphere. However, glucose and arabinose concentrations in the air can also be related to biomass burning emissions, so they are not good tracers of pollen levels in the air. Furthermore, in autumn, arabitol, sorbitol and adonitol can be used as tracers of the *Alternaria* fungal spore. During rainy days, Alt a 1 allergen and mannitol are correlated with *Alternaria*, so they are tracers of this fungal spore.

- In autumn, levoglucosan, mannosan, galactosan, arabinose, fructose and glucose are related to K (biomass burning tracer), NO_3^- and OC. Mannosan and levoglucosan are correlated with EC, OC, Cu, Zn, Se, Pb, V and Ni (characteristic of traffic and fossil fuel combustion). Mannosan also correlates with As (coal combustion tracer). Thus, the choice of these anhydrides as markers of biomass burning during the cold season may be overestimating the contribution of that source, due to the contribution of other anthropogenic sources.

- Precipitation can cause an increase in glucose and sucrose concentration, due to the fact that the breakage of the hydrated pollen particles releases the sugars linked to the smaller fragments. Precipitation also increases the arabitol concentration (airborne fungal spore tracer), probably because it is able to trigger both active and passive fungal spore release mechanisms. The growth of glucose concentration after rainfall is positively and significantly correlated with mean rainfall intensity, raindrop swept volume and mean droplet size. In

addition, the number of drops larger than 3 mm also correlates with the increase in glucose concentration. This fact might suggest that the size of the raindrop may mark a threshold dividing both processes: the washing and the release of this sugar compound.

The main conclusions related to the third objective, which aimed to analyse the impact on air quality in León city, in two particular cases of pollution, one of natural origin (Saharan dust intrusions) and the other of anthropic origin (traffic), are:

- The Saharan dust intrusions that took place in February 2016 and 2017 caused an increase in the concentration of coarse-mode particles (D_p > 1 μm) and the exceeding of the PM_{10} daily limit value, with 52 μg m^{-3} in 2016 and 86 μg m^{-3} in 2017. In addition, a change in biological material was evident, with the presence of pollens that are not typical from León during the study period. The values of the mass fractions reached maximum values of 156 μg m^{-3} in the 2016 event and 155 μg m^{-3} in 2017 for the inhalable fraction, and 102-134 μg m^{-3} in 2016 and 155 μg m^{-3} in 2017 for the respirable fraction; values nine times higher than those obtained during the days without dust intrusions in León.

- Atmospheric radiative forcing indicates that the two winter Saharan dust intrusions caused a cooling effect in the atmosphere, with estimated average ratio values of -15.6 K day^{-1} and -12.4 K day^{-1} in the events of the years 2016 and 2017, respectively. The increase in single-scattered albedo (SSA) and aerosol optical depth (AOD) values during the dust intrusions shows the scattering effect of these events.

- The number of particles increases from 1000 ± 600 particles cm^{-3} in August to 1500 ± 1000 particles cm^{-3} in October during the summer-autumn transition, due to the intensification of traffic after the summer holidays, to a lower dispersion caused by the low height of the mixing layer and to the beginning of the use of the heater devices. The respirable fraction of the particulate matter reached its highest value in September and October, with 12 μg m^{-3}, while on working days the maximum was observed during the hours of greatest vehicle flow, between 0600 and 1000 UTC, with 15 μg m^{-3} and between 1700 and 2000 UTC, with 12 μg m^{-3}.

The fourth objective proposed to examine the influence of the aerosol chemical composition and the physical characteristics of precipitation on the physical-chemical properties of rainwater. The most relevant conclusions related to this objective are:

- In general, wet scavenging of air pollutants is more efficient with prolonged and continuous precipitation events. The concentration of water-soluble ions, Ca^{2+}, SO_4^{2-} and NO_3^-, and dissolved organic carbon (DOC) in rainwater increases with the volume swept by the raindrops. However, the concentration of the water-insoluble elemental carbon (WIEC) and organic carbon (WIOC) species are dependent on the raindrop size, as the scavenging of these species is probably affected by the inertial impact of the droplets through the water column.

- The rainwater sampled in León under the influence of the emissions from the massive forest fires that took place in the north of the Iberian Peninsula in August 2016, registered a pH of 4.8, while the pH annual mean value of the precipitation in León was 5.87 ± 0.02. This low value is probably due to the presence of a high concentration of organic species in the aerosol. The high concentrations in rainwater of NH_4^+ (153 μeq L^{-1}), SO_4^{2-} (65 μeq L^{-1}), NO_3^- (121

μeq L^{-1}), DOC (15 mg L^{-1}) and WIOC (2 mg L^{-1}), reflected the influence of aerosols from biomass burning on precipitation.

- The rainwater chemical composition, corresponding to the precipitation event registered between 11 and 14 February 2017, was affected by the intrusion of Saharan dust that reached to León on 12 February, causing an increase in the concentrations of Ca^{2+} (> 800%), Mg^{2+} (71%), Cl^- (62%) and SO_4^{2-} (33%), with respect to the previous day. In addition, an increase in the pH of rainwater to 7.0 was observed, due to the neutralizing effect of Ca^{2+} on the acidic components.

10.2. PERSPECTIVES

To conclude this doctoral thesis, this section presents the possible applications of the work presented and, based on the results obtained, a series of possible future investigations that could provide interesting results in the field of study of aerosols, as well as aerosol-precipitation interaction.

Biogenic and non-biogenic aerosols play an important role in human health and atmospheric processes. The results presented in this work provide valuable information that can help to establish different measures for the mitigation of environmental pollution and to reduce the impact of air pollutants on human health. Furthermore, this work offers a better understanding of the complicated interactions between the biosphere, the atmosphere and the lithosphere.

Throughout this work, a series of results have been presented that could be useful for other researchers working with atmospheric models of pollutant transport on a local or regional scale. For example, the combination of PMF models and weather types, and even the introduction of other variables such as the sugar compound concentrations in the aerosol, can be a useful tool in the local analysis of the distribution of sources, allowing a better understanding of the influence of the different mechanisms of evolution and transport of aerosols and their behaviour at different scales. Continuing with this line of research, future studies should focus on the analysis of emission sources of other particulate matter fractions such as $PM_{2.5}$ and PM_1, and their relationship with meteorological parameters. Similarly, continuous monitoring of ultrafine particles with SMPS is crucial for the identification of nucleation processes, which is key in the study of particle formation processes.

Regarding the study of sugar compounds, their interaction with other biotic or abiotic particles can increase the symptoms of respiratory allergies, so a detailed description of these particles and their emission sources could help in the establishment of measures to reduce the impact of aerosols on human health. The study of the relationship of sugar compounds with tracers (biological and non-biological) and with meteorological parameters is a useful tool to know the origin of these organic compounds present in the atmospheric aerosol. Moreover, the results obtained in this study present the possibility of finding out under which environmental conditions certain sugar compounds can be used as aerosol source markers.

Due to the growing interest in the field of bioaerosols, we consider of great importance to deepen certain aspects related to this type of aerosols. It is interesting to carry out a long-term study of the seasonal variations in the concentration of pollen, fungal spores and various allergens in the air and their relationship with the concentration of sugar compounds in PM_{10}, $PM_{2.5}$ and PM_1. This study could be complemented with the continuous measurement of bioaerosol, using a Wideband Integrated Bioaerosol Spectrometer (WIBS), which allows the identification and quantification of specific groups of bacteria, fungi or pollen through the analysis of the fluorescence footprints provided by this equipment. In addition, the determination of bioaerosols in rainwater would allow to deepen the influence of the precipitation on their emission, transport and removal processes. Based on the results obtained and collected in this work, it is necessary to study in depth the interaction of the sugar compounds present in the atmospheric aerosol with the physical parameters of precipitation, in order to discern between the characteristics of rain that cause the release of these compounds and those that produce the effective scavenging of them.

Combustion processes (the burning of crop residues from different crops, the coal burning and other fossil fuels in machinery and industrial installations, as well as in heating and hot water systems, among others), release large amounts of pollutants into the atmosphere. These practices, far from being a local problem, have an impact on the environment quality at a global scale, which is why we feel it is crucial to conduct some research works to study in depth the emissions caused by these processes.

Black carbon (BC) is one of the pollutants emitted by combustion processes. The identification of specific sources of BC is not a simple task, and current models allow to estimate mainly the contribution of biomass burning and fossil fuel combustion to the black carbon concentration. However, the emission of black carbon from specific coal combustion, especially in countries such as China where this practice has become one of the most polluting activities, remains a serious concern worldwide. For this reason, it is necessary to implement a methodology to obtain in real time the contribution of coal burning to the total CB. Following this line of research, the use of other highly sensitive instruments such as the SP2-XR photometer, which directly measures the black carbon of individual particles through laser incandescence and light scattering by the particles, could be used to discern between the sources of BC. On the other hand, the SP2-XR provides information on the BC size distribution, which allows the study of the influence of different drop sizes on the removal of BC particles.

Indeed, the study of the precipitation-aerosol interaction is essential, since precipitation plays a crucial role in mitigating the negative impact of air pollutants on human health and the environment. The results presented in this work contribute to the study of removal mechanisms, demonstrating that simple models allow the calculation of the efficiency of pollutant removal by precipitation, considering the chemical characteristics of the aerosol and the physico-chemical properties of precipitation. However, it is necessary to go deeper into the influence of the physical-chemical properties of rain on aerosol scavenging, through the identification of the most efficient drop sizes in the scavenging of different pollutants (biogenic and non-biogenic). This would be key in the development of future work, focused on the generation of water droplets that can be released in areas of high concentration of pollutants to reduce pollution levels. Also, the

analysis of the impact of wet and dry deposition of particulate matter on ecosystems would be an exciting line of research

Aerosols and clouds influence the radiative fluxes and modulate climate, so it is essential to make more extensive and accurate measurements for a better understanding of these complex climate interactions. Carrying out a study of the optical properties of aerosols using the CIMEL photometer, located at the same sampling point as the aerosols, would supply more precise information on radiative forcing at different local contamination events. Similarly, we also suggest a deeper study of local radiative forcing under different meteorological scenarios such as before and after a precipitation event.

Finally, we consider of great importance the integration of the above-mentioned studies with a more in-depth research related to health, as epidemiological studies in collaboration with health institutions. Besides the harmful effects on human health and ecosystems, it is also important to carry out an assessment of the economic impact of air pollution, considering the significant deterioration of the architectural heritage caused.

Annex 1

SUPPLEMENTARY MATERIAL OF CHAPTER 3

This annex contains information related to the evolution of pollutant emissions from different sectors in Spain from 1997 to 2014. Then, the evolution of energy production and consumption in the province of León from 1998 to 2014 is presented. The last section includes a description of the trends in air pollutant concentrations in León city, focusing on road transport, public electricity and industrial activity. This information completes the study presented in Chapter 3.

A.1.1. PRODUCTION AND CONSUMPTION OF ENERGY AND EMISSIONS ASSOCIATED

A.1.1.1. Evolution of pollutant emissions from different sectors in Spain

Before focusing on León, it is useful to have a global view of the evolution of emissions generated by different sectors on a national level in order to establish a comparison between the local and the national scenario. During the study period, Spain registered changes in the emission levels of air pollutants (Fig. A1.1). It is important to describe the annual national emission evolution in order to find similarities with those observed in León.

The statistical analysis of the long-term trends of the emissions in Spain shows:

- A high and statistically significant reduction in the CO emissions from road traffic (-6.66% year^{-1}). However, there is a statistically significant increase in the emissions from public electricity (4.97% year^{-1}).

- A significant reduction of the NO_x emissions from road transport with a -2.57% year^{-1} in the period of 1997 to 2014 in Spain. However, the decrease in NO_x is not statistically significant when the trend was observed in other sectors like industry or public electricity (-1.52 and -2.58% year^{-1}, respectively).

- An important decrease in PM_{10} emissions from public electricity and road transport (-5.59 and -3.14% year^{-1}, respectively).

- An important decrease of SO_2 emissions from industrial, public electricity and especially transport sources (-4.44, -4.44 and -9.85% year^{-1}, respectively).

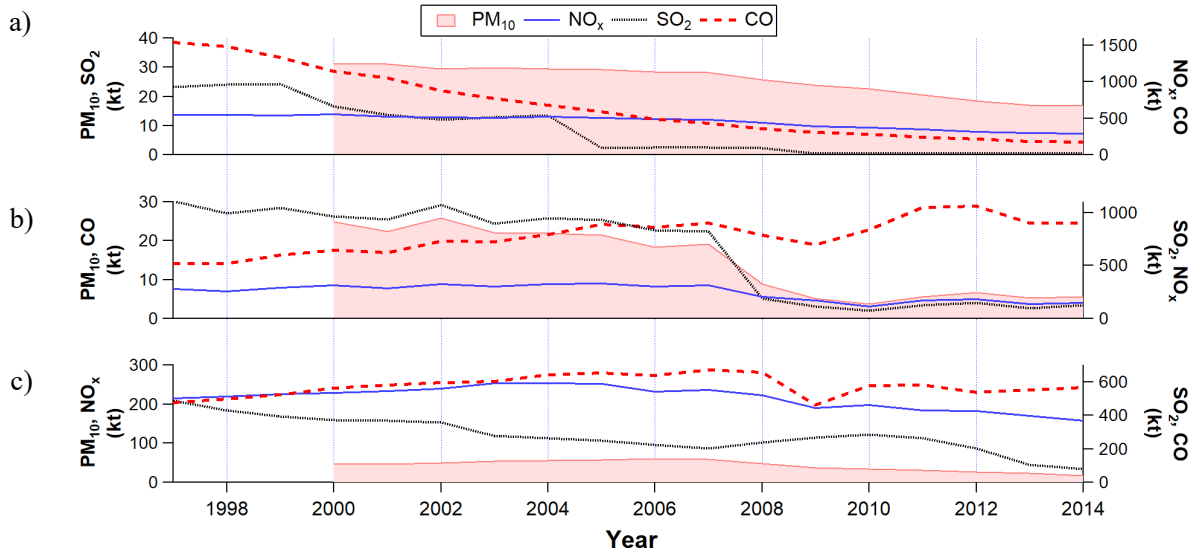

FIG. A1.1. Evolution of Spanish national emissions of CO, NO_x, PM_{10} and SO_2 from a) industrial, b) public electricity and c) road transport sectors (data from MAGRAMA).

A.1.1.2. Evolution of energy production and consumption in León

The data from the regional government Junta de Castilla y León shows that in the period 1998 to 2014 there were several changes in the production and consumption of energy in the province of León (www.energia.jcyl.es) which may have influenced the pollutant levels. Figure A1.2 shows this evolution for the fossil fuel, liquefied petroleum gas (LPG), natural gas and electric energy consumption. The evolution of the primary energy production is also shown.

The Junta de Castilla y León (www.estadistica.jcyl.es) reports that in 2008 the main sources of energy for domestic heating systems in the province of León were diesel (37.1%), gas (30.0%), electricity (9.6%) and others (27.7%). In the "others" category, 4.7% of the homes used coal and 5.1% wood. Fig. A1.2 shows that the production of primary energy from coal has decreased by 83% and the hydraulic and wind energies have experienced a very important increase (48 and 847%, respectively). Moreover, the consumption of electric energy registered an increase, both in domestic and industrial sectors (38 and 11%, respectively). The consumption of natural gas has soared by more than 600%.

LPG and fossil fuel consumption shows a very important decrease in the period from 1998 to 2014. In particular, the consumption of propane and butane decreased by 64 and 44% respectively, and that of gasoline and fuel oil by 50 and 94%, respectively, while the consumption of diesel increased by 8% in the same period.

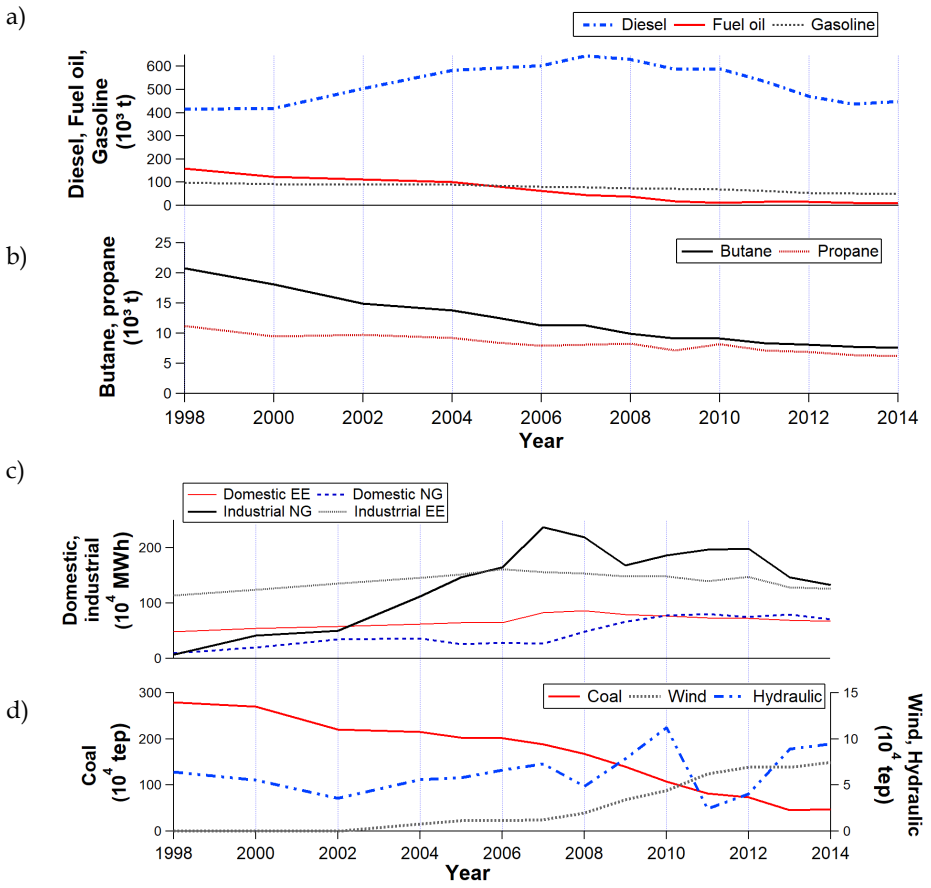

FIG. A1.2. Evolution of the production and consumption of energy and fuel in the province of León (data from the website of the Junta de Castilla y León): a) Fossil fuel consumption (fuel oil, gasoline and diesel), b) LPG consumption (butane and propane), c) Natural gas consumption (NG) and electric energy (EE) consumption for domestic and industrial use, d) Primary energy production (coal, wind and hydraulic).

A.1.2.TRENDS IN AIR POLLUTANT CONCENTRATIONS

- **Road transport**

Authors like Querol et al. (2014) show that in different cities of Spain the implementation of measures like Euro standards and the progressive transition from fossil fuel to bio-fuels in vehicles are responsible for the reduction in CO, PM and SO_2 emission levels. Euro standards, applied to individual and collective transport vehicles, were created in 1992 in order to regulate emissions from road traffic. From 1992 (Euro 1), the standard has been modified, including Euro 2 (1996), Euro 3 (2000), Euro 4 (2005), Euro 5 (2009) and, more recently, Euro 6 (2014). These standards have forced manufacturers to develop new exhaust pipe systems, such as Exhaust Gas Recirculation valves (EGR) or urea catalysts to meet the emission limits. Studies carried out by Tzamkiozis et al. (2010) in three diesel passenger cars and by Fontaras et al. (2014) in thirteen Euro 5 passenger cars, show that the implementation of these regulations leads to a decrease in CO, NO and PM_{10} emissions from road transport. Similar results were also reported by Alves et al. (2015a, 2015b), in the study of the emissions from several diesel and petrol vehicles, with a decrease in CO and NO_x emissions for both, with the implementation of Euro standards 3, 4 and 5.

On the other hand, the road transport with diesel engines is largely responsible for NO and NO_2 emissions, and the high decrease in the trend observed may be due to the diverse actions taken by the local government for the reduction in road traffic through the promotion of electrical and hybrid vehicles and of public transport. Soret et al. (2014) observed in Barcelona and Madrid, Spain, a reduction of 11% and 17%, respectively, of the total NO_x emissions due to the implementation of electric vehicles in these cities.

The reduction in the NO_x emissions is probably the cause of the decrease in O_3 levels in the city of León. The O_3 concentration may depend on Volatile Organic Compounds (VOC) and/or on NO_x concentrations. The VOC/NO_x ratio drops a hint on the dependence of the O_3 concentrations on VOC or NO_x concentrations. If this ratio is low, this means that the NO_X concentration is high, and O_3 concentrations depend mainly on VOC concentration. As a consequence, there is no clear relationship between the NO_x and O_3 concentration trends (Querol et al., 2014; Santurtún et al., 2015; Sicard et al., 2016, 2013). However, in León the opposite occurs, probably due to an increase in the VOC/NO_x ratios, which makes O_3 levels depend on NO_x concentrations.

- **Public electricity**

The policies implemented by the international, national and local governments have achieved positive results in reducing emissions from this sector. The marked decrease in the SO_2, CO and PM_{10} concentrations observed in the station León1 is consistent with the decrease in emissions from public electricity. This is also in accordance with a decrease in energy production by coal and an increase in renewable energies in the past decade in León and in the rest of Spain (Montoya et al., 2014). Besides, the increase in domestic natural gas consumption in León causes a decrease in the emissions of air pollutants, especially CO, SO_2 and PM_{10}, from heating systems in residential areas.

- **Industrial**

Karagulian et al. (2015) described the industrial sector as a heterogeneous category which includes emissions from industries like power plants (oil and coal combustion) and emissions from other types of industries (ceramic, metallurgic, pharmaceutical, petrochemical, etc.). León is characterized by the absence of large industries, so the main sources in this sector are the emissions from a coal power plant in La Robla, which is located 22.5 km to the north of León, and from a series of small industries located around the city. The data published by the Environmental Statement of the power plant in La Robla (www.medioambiente.jcyl.es) shows that from 2001 to 2015 there was a significant decrease in the emissions of the SO_x (-83%), NO_x (-49%) and PM (-35%) due to the implementation of several measures like i) the installation of the desulphurization plant for the reduction of SO_2, ii) low NO_x burners and over combustion air systems that inhibit the formation of NO_x, and iii) control systems of electrostatic precipitators for the reduction of atmospheric particles from combustion.

A.1.3.REFERENCES

Alves, C.A., Barbosa, C., Rocha, S., Calvo, A., Nunes, T., Cerqueira, M., Pio, C., Karanasiou, A.,

Querol, X., 2015a. Elements and polycyclic aromatic hydrocarbons in exhaust particles emitted by light-duty vehicles. Environ. Sci. Pollut. Res. 22, 11526–11542. doi:10.1007/s11356-015-4394-x

Alves, C.A., Lopes, D.J., Calvo, A.I., Evtyugina, M., Rocha, S., Nunes, T., 2015b. Emissions from Light-Duty Diesel and Gasoline in-use Vehicles Measured on Chassis Dynamometer Test Cycles. Aerosol Air Qual. Res. 15, 99–116. doi:10.4209/aaqr.2014.01.0006

Fontaras, G., Franco, V., Dilara, P., Martini, G., Manfredi, U., 2014. Development and review of Euro 5 passenger car emission factors based on experimental results over various driving cycles. Sci. Total Environ. 468–469, 1034–1042. doi:10.1016/j.scitotenv.2013.09.043

Karagulian, F., Belis, C.A., Dora, C.F.C., Prüss-Ustün, A.M., Bonjour, S., Adair-Rohani, H., Amann, M., 2015. Contributions to cities' ambient particulate matter (PM): A systematic review of local source contributions at global level. Atmos. Environ. 120, 475–483. doi:10.1016/j.atmosenv.2015.08.087

Montoya, F.G., Aguilera, M.J., Manzano-Agugliaro, F., 2014. Renewable energy production in Spain: A review. Renew. Sustain. Energy Rev. 33, 509–531. doi:10.1016/j.rser.2014.01.091

Querol, X., Alastuey, A., Pandolfi, M., Reche, C., Pérez, N., Minguillón, M.C., Moreno, T., Viana, M., Escudero, M., Orio, A., Pallarés, M., Reina, F., 2014. 2001–2012 trends on air quality in Spain. Sci. Total Environ. 490, 957–969. doi:10.1016/j.scitotenv.2014.05.074

Santurtún, A., González-Hidalgo, J.C., Sanchez-Lorenzo, A., Zarrabeitia, M.T., 2015. Surface ozone concentration trends and its relationship with weather types in Spain (2001–2010). Atmos. Environ. 101, 10–22. doi:10.1016/j.atmosenv.2014.11.005

Sicard, P., De Marco, A., Troussier, F., Renou, C., Vas, N., Paoletti, E., 2013. Decrease in surface ozone concentrations at Mediterranean remote sites and increase in the cities. Atmos. Environ. 79, 705–715. doi:10.1016/j.atmosenv.2013.07.042

Sicard, P., Serra, R., Rossello, P., 2016. Spatiotemporal trends in ground-level ozone concentrations and metrics in France over the time period 1999–2012. Environ. Res. 149, 122–144. doi:10.1016/j.envres.2016.05.014

Soret, A., Guevara, M., Baldasano, J.M., 2014. The potential impacts of electric vehicles on air quality in the urban areas of Barcelona and Madrid (Spain). Atmos. Environ. 99, 51–63. doi:10.1016/j.atmosenv.2014.09.048

Tzamkiozis, T., Ntziachristos, L., Samaras, Z., 2010. Diesel passenger car PM emissions: From Euro 1 to Euro 4 with particle filter. Atmos. Environ. 44, 909–916. doi:10.1016/j.atmosenv.2009.12.003

Annex 2

SUPPLEMENTARY MATERIAL OF CHAPTER 4

This Annex contains information related to the study presented in Chapter 4, such as the description of the weather types, the evolution of PM_{10} and its main components over the sampling period and the PMF factor profiles obtained in the sampling area. A brief description of the location of the main sources is given in the following section. Finally, this annex includes some statistical information on the linear models described in the results of Chapter 4.

TABLE A2.1. Original weather types CWTs, with 2 pure types controlled by geostrophic vorticity (A and C), 8 directional types, 16 hybrid types (Source: Fernández-Raga et al., 2017; Trigo and DaCamara, 2000).

Lamb's weather types							
Pure		**Directional types**		**Cyclonic hybrid**		**Anticyclonic hybrid**	
C	Cyclonic	NE	Northeasterly	CNE	Cyclonic northeasterly	ANE	Anticyclonic northeasterly
A	Anticyclonic	E	Easterly	CE	Cyclonic easterly	AE	Anticyclonic easterly
		SE	Southeasterly	CSE	Cyclonic southeasterly	ASE	Anticyclonic southeasterly
		S	Southerly	CS	Cyclonic southerly	AS	Anticyclonic southerly
		SW	Southwesterly	CSW	Cyclonic southwesterly	ASW	Anticyclonic southwesterly
		W	Westerly	CW	Cyclonic westerly	AW	Anticyclonic westerly
		NW	Northwesterly	CNW	Cyclonic northwesterly	ANW	Anticyclonic northwesterly
		N	Northerly	CN	Cyclonic northerly	AN	Anticyclonic northerly

TABLE A2.2. Annual and seasonal mean concentrations of PM_{10} (in µg/m³) and its major components.

Species	Annual	Winter	Spring	Summer	Autumn
PM_{10}	23 ± 8	25 ± 9	19 ± 6	24 ± 8	25 ± 7
POM	4 ± 2	4 ± 2	3 ± 2	4 ± 2	4 ± 2
OC	2.4 ± 1.3	2.7 ± 1.5	1.9 ± 1.0	2.4 ± 1.1	2.5 ± 1.3
EC	0.7 ± 0.4	0.9 ± 0.5	0.7 ± 0.3	0.6 ± 0.4	0.8 ± 0.4
NH_4^+	0.6 ± 0.6	0.7 ± 0.8	0.6 ± 0.5	0.5 ± 0.3	0.6 ± 0.6
SO_4^{2-}	1.2 ± 0.9	0.9 ± 0.9	1.1 ± 0.8	1.6 ± 0.9	1.2 ± 0.8
NO_3^-	0.9 ± 1.0	1.3 ± 1.5	0.7 ± 0.7	0.6 ± 0.3	1.1 ± 1.0
Al	0.3 ± 0.3	0.2 ± 0.4	0.13 ± 0.11	0.4 ± 0.4	0.2 ± 0.2
Ca	0.2 ± 0.2	0.2 ± 0.3	0.16 ± 0.11	0.4 ± 0.2	0.2 ± 0.2
Cl	0.3 ± 0.3	0.5 ± 0.4	0.2 ± 0.3	0.07 ± 0.12	0.2 ± 0.3
Fe	0.2 ± 0.2	0.2 ± 0.2	0.14 ± 0.08	0.3 ± 0.2	0.25 ± 0.14
K	0.17 ± 0.12	0.20 ± 0.14	0.10 ± 0.05	0.19 ± 0.14	0.18 ± 0.10
Mg	0.06 ± 0.06	0.06 ± 0.08	0.05 ± 0.03	0.08 ± 0.06	0.05 ± 0.03
Na	0.2 ± 0.2	0.3 ± 0.3	0.2 ± 0.2	0.17 ± 0.14	0.2 ± 0.2
Si	0.6 ± 0.6	0.4 ± 0.8	0.3 ± 0.3	0.9 ± 0.7	0.6 ± 0.4
Ti	0.01 ± 0.02	0.01± 0.02	0.007 ± 0.006	0.02 ± 0.02	0.012 ± 0.009
Levoglucosan	0.02 ± 0.01	0.02 ± 0.02	0.013 ± 0.014	0.008 ± 0.008	0.02 ± 0.03

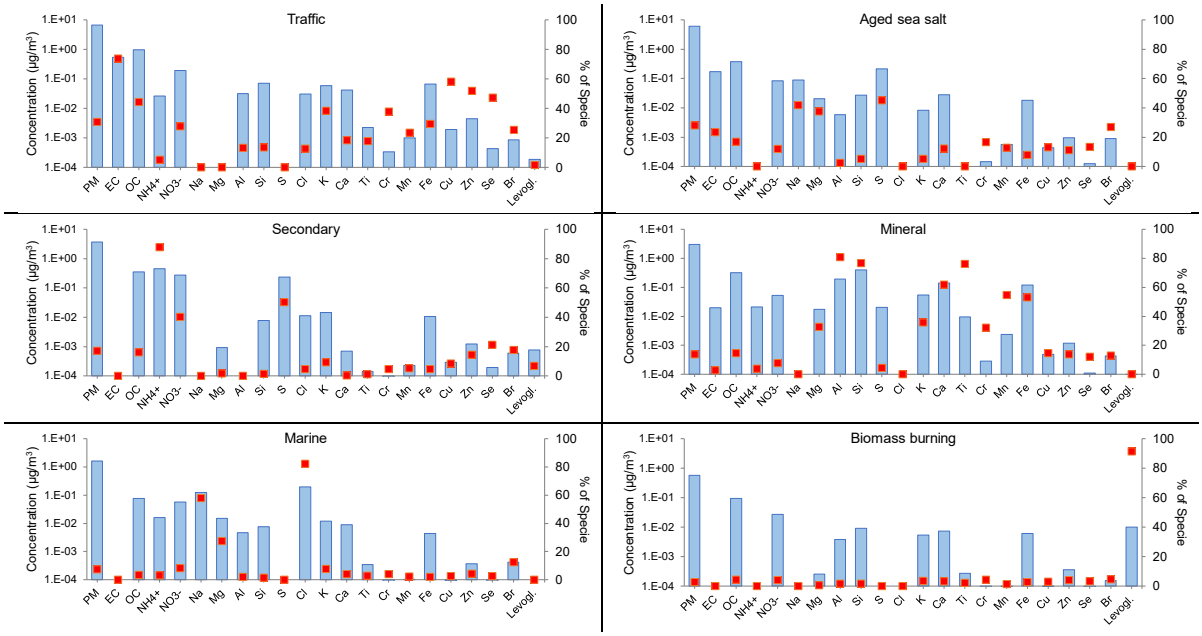

FIG. A2.1. PMF factor profiles obtained in the sampling area of León: traffic, aged sea salt, secondary, mineral, marine and biomass burning. Blue bars show the mean concentration of the species and red points show the percentage of each species in each factor.

TABLE A2.3. Mean concentrations for each CWT.

CWT	PM_{10}	OC	EC	NH_4^+	SO_4^{2-}	NO_3^-	Al	Ca	Cl	Fe	K	Mg	Na	Si	Ti	Levoglucosan
A	23 ± 7	2.3 ± 1	0.7 ± 0.4	0.5 ± 0.3	1.6 ± 0.8	0.7 ± 0.6	0.3 ± 0.3	0.25 ± 0.16	0.2 ± 0.3	0.2 ± 0.2	0.15 ± 0.1	0.07 ± 0.05	0.2 ± 0.2	0.6 ± 0.6	0.014 ± 0.014	0.011 ± 0.013
AE	20 ± 1	1.7 ± 0.7	0.8 ± 0.3	0.1 ± 0.1	0.8 ± 0.5	0.33 ± 0.1	0.22 ± 0.10	0.28 ± 0.13	0.1 ± 0.2	0.24 ± 0.06	0.12 ± 0.02	0.032 ± 0.005	0.10 ± 0.08	0.5 ± 0.2	0.011 ± 0.004	0.0042 ± 0.0005
AN	24 ± 9	2.3 ± 1.2	0.6 ± 0.3	0.5 ± 0.4	1.6 ± 1.1	0.6 ± 0.3	0.3 ± 0.3	0.2 ± 0.2	0.1 ± 0.2	0.2 ± 0.2	0.18 ± 0.16	0.07 ± 0.05	0.18 ± 0.13	0.6 ± 0.6	0.015 ± 0.014	0.012 ± 0.012
ANE	21 ± 7	1.5 ± 0.5	0.5 ± 0.2	0.6 ± 0.4	1.6 ± 0.7	0.7 ± 0.4	0.3 ± 0.4	0.2 ± 0.2	0.1 ± 0.2	0.2 ± 0.2	0.12 ± 0.1	0.06 ± 0.06	0.2 ± 0.2	0.5 ± 0.8	0.01 ± 0.02	0.007 ± 0.006
ANW	21 ± 7	1.9 ± 1.0	0.6 ± 0.2	0.4 ± 0.4	1.0 ± 0.6	0.8 ± 0.8	0.2 ± 0.2	0.17 ± 0.10	0.3 ± 0.3	0.17 ± 0.11	0.14 ± 0.07	0.06 ± 0.04	0.3 ± 0.2	0.4 ± 0.3	0.009 ± 0.008	0.02 ± 0.02
AS	15	2.2	0.6	0.5	0.7	0.8	0.06	0.06	0.1	0.1	0.11	0.05	0.2	0.5	0.004	0.005
AW	18 ± 3	1.9 ± 0.5	0.6 ± 0.4	0.25 ± 0.11	0.6 ± 0.4	0.5 ± 0.2	0.11 ± 0.13	0.10 ± 0.07	0.5 ± 0.6	0.1 ± 0.07	0.10 ± 0.03	0.07 ± 0.04	0.4 ± 0.3	0.2 ± 0.2	0.006 ± 0.006	0.019
C	23 ± 7	2.4 ± 1.3	0.8 ± 0.4	0.5 ± 0.5	0.9 ± 0.8	1.0 ± 0.8	0.2 ± 0.3	0.3 ± 0.3	0.3 ± 0.4	0.2 ± 0.2	0.18 ± 0.11	0.07 ± 0.06	0.3 ± 0.3	0.5 ± 0.6	0.01 ± 0.02	0.013 ± 0.012
CE	28 ± 5	3.1 ± 0.7	1.0 ± 0.3	1.7 ± 1.5	2 ± 2	2 ± 2	0.2 ± 0.13	0.21 ± 0.14	0.4 ± 0.3	0.24 ± 0.09	0.23 ± 0.06	0.04 ± 0.02	0.2 ± 0.2	0.7 ± 0.7	0.011 ± 0.006	0.012 ± 0.006
CN	24 ± 8	3.2 ± 1.5	1.1 ± 0.7	0.6 ± 0.3	0.9 ± 0.3	1.1 ± 0.7	0.3 ± 0.2	0.29 ± 0.13	0.3 ± 0.2	0.29 ± 0.13	0.3 ± 0.2	0.06 ± 0.02	0.2 ± 0.2	0.6 ± 0.4	0.016 ± 0.010	0.010 ± 0.005
CNE	25 ± 7	2.2 ± 1.1	0.9 ± 0.7	0.7 ± 0.8	1.0 ± 0.6	1.4 ± 1.7	0.24 ± 0.14	0.25 ± 0.11	0.2 ± 0.2	0.23 ± 0.09	0.16 ± 0.07	0.04 ± 0.02	0.16 ± 0.12	0.5 ± 0.3	0.014 ± 0.008	0.016 ± 0.011
CNW	19 ± 5	1.4 ± 0.6	0.6 ± 0.2	0.3 ± 0.4	0.5 ± 0.3	0.3 ± 0.2	0.12 ± 0.15	0.13 ± 0.12	0.23 ± 0.15	0.10 ± 0.08	0.10 ± 0.05	0.05 ± 0.02	0.21 ± 0.10	0.3 ± 0.3	0.006 ± 0.006	0.001
CS	33 ± 9	3.9 ± 1.0	1.3 ± 0.3	1.4 ± 0.8	1.3 ± 0.6	3 ± 2	0.3 ± 0.2	0.23 ± 0.13	0.5 ± 0.2	0.3 ± 0.2	0.30 ± 0.09	0.05 ± 0.03	0.18 ± 0.10	0.7 ± 0.4	0.016 ± 0.011	0.03 ± 0.03
CSE	30 ± 6	3.5 ± 1.2	1.2 ± 0.7	0.9 ± 0.7	1.2 ± 1.0	1.4 ± 1.0	0.18 ± 0.15	0.23 ± 0.13	0.4 ± 0.3	0.28 ± 0.14	0.23 ± 0.11	0.04 ± 0.02	0.21 ± 0.15	0.4 ± 0.3	0.011 ± 0.007	0.02 ± 0.02
CSW	25 ± 6	2.9 ± 1.0	0.8 ± 0.3	0.5 ± 0.2	0.8 ± 0.2	1.0 ± 0.5	0.3 ± 0.2	0.2 ± 0.2	0.4 ± 0.3	0.3 ± 0.2	0.19 ± 0.09	0.07 ± 0.03	0.3 ± 0.2	0.5 ± 0.4	0.013 ± 0.011	0.014 ± 0.008
CW	21 ± 6	2.1 ± 1.6	0.7 ± 0.2	0.4 ± 0.2	0.7 ± 0.3	0.8 ± 0.5	0.13 ± 0.1	0.15 ± 0.09	0.5 ± 0.6	0.14 ± 0.08	0.17 ± 0.10	0.07 ± 0.05	0.4 ± 0.4	0.3 ± 0.2	0.008 ± 0.006	0.03 ± 0.03
E	22 ± 5	2.1 ± 0.6	0.6 ± 0.3	0.4 ± 0.2	0.9 ± 0.3	0.7 ± 0.3	0.2 ± 0.09	0.24 ± 0.09	0.3 ± 0.4	0.22 ± 0.06	0.13 ± 0.03	0.06 ± 0.03	0.3 ± 0.2	0.5 ± 0.2	0.011 ± 0.005	0.01 ± 0.02
N	25 ± 9	2.7 ± 1.3	0.8 ± 0.3	0.5 ± 0.4	1.5 ± 0.9	0.8 ± 0.5	0.4 ± 0.6	0.4 ± 0.4	0.1 ± 0.2	0.3 ± 0.3	0.19 ± 0.15	0.07 ± 0.11	0.16 ± 0.07	0.8 ± 1.1	0.02 ± 0.04	0.01 ± 0.02
NE	21 ± 7	1.9 ± 0.8	0.6 ± 0.3	0.5 ± 0.5	1.4 ± 0.9	0.6 ± 0.5	0.3 ± 0.2	0.3 ± 0.2	0.1 ± 0.2	0.21 ± 0.12	0.13 ± 0.08	0.06 ± 0.04	0.2 ± 0.2	0.6 ± 0.5	0.013 ± 0.010	0.02 ± 0.02
NW	27 ± 13	3 ± 1.5	1.0 ± 0.4	0.4 ± 0.5	1.2 ± 0.9	1.0 ± 1.1	0.5 ± 0.7	0.4 ± 0.4	0.2 ± 0.2	0.4 ± 0.4	0.2 ± 0.2	0.10 ± 0.10	0.19 ± 0.09	1.0 ± 1.3	0.03 ± 0.03	0.01 ± 0.01
S	31 ± 9	3 ± 2	0.8±0.4	1.4 ± 0.9	1.6 ± 0.9	3 ± 2	0.16 ± 0.09	0.21 ± 0.11	0.3 ± 0.2	0.23 ± 0.09	0.22 ± 0.13	0.043 ± 0.013	0.17 ± 0.06	0.4 ± 0.2	0.008 ± 0.004	0.05 ± 0.07
SE	21 ± 6	2.4 ± 1.1	0.8 ± 0.4	0.38 ± 0.11	0.5 ± 0.2	0.6 ± 0.4	0.18 ± 0.14	0.20 ± 0.13	0.1 ± 0.2	0.23 ± 0.14	0.14 ± 0.07	0.04 ± 0.02	0.11 ± 0.07	0.4 ± 0.3	0.011 ± 0.007	0.03 ± 0.03
SW	22 ± 9	2 ± 2	0.7 ± 0.4	0.7 ± 0.4	0. 5± 0.3	1.0 ± 1.0	0.11 ± 0.16	0.2 ± 0.2	0.4 ± 0.3	0.15 ± 0.14	0.2 ± 0.2	0.05 ± 0.02	0.3 ± 0.2	0.3 ± 0.3	0.009 ± 0.011	0.015 ± 0.012
W	21 ± 5	2.0 ± 0.6	0.7 ± 0.2	0.3 ± 0.3	0.8 ± 0.5	0.7 ± 0.4	0.15 ± 0.16	0.16 ± 0.09	0.5 ± 0.6	0.15 ± 0.12	0.14 ± 0.05	0.007 ± 0.04	0.4 ± 0.4	0.4 ± 0.4	0.008 ± 0.008	0.01 ± 0.02

A.2.1. Location of the main sources

Figure A2.2 depicts the daily source contributions as a function of wind speed and direction of particulate matter in León city for each source. Polar plot shows, in general, an increase in the concentration with the wind speed. Yu et al. (2004) and Carslaw et al. (2006) described that pollutants emitted from sources far from the sampling site or at higher altitudes, need high wind speeds to be transported to the monitoring site.

The main source contributing to traffic and biomass burning factors is in the first quadrant, where the ring road and the neighboring towns are located (Fig. 4.1). Biomass burning emissions are mainly due to the use of domestic heating devices, while traffic source is dominated by exhaust emissions from road traffic, but there may be some overlap in emissions from heating appliances. The aged sea salt polar plot shows higher concentrations with increasing distance to the receptor, suggesting long-range transport (Carslaw et al., 2006). The Saharan dust and/or the sea salt aerosols that are transported to León city, can suffer oxidative processes by reacting with anthropogenic emissions produced in the city center. Thus, the highest concentration for the sea salt aged factor is located to the third quadrant. Mineral polar plots show a decrease in concentration with increasing wind speed, suggesting sources with greatest impact in stagnant atmospheric conditions.

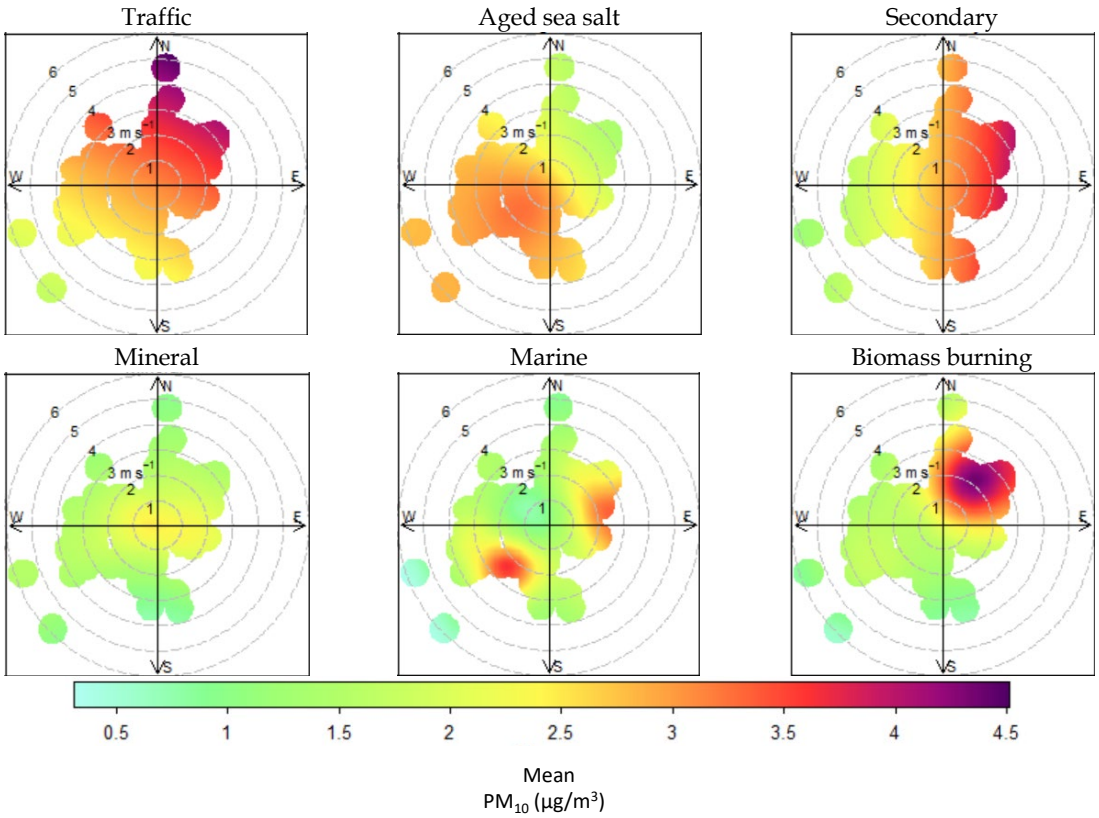

FIG. A2.2. Polar plots of daily particulate matter source contributions as a function of wind speed and direction in León (concentrations: biomass burning × 5, Traffic × 0.5 and Aged sea salt × 0.7).

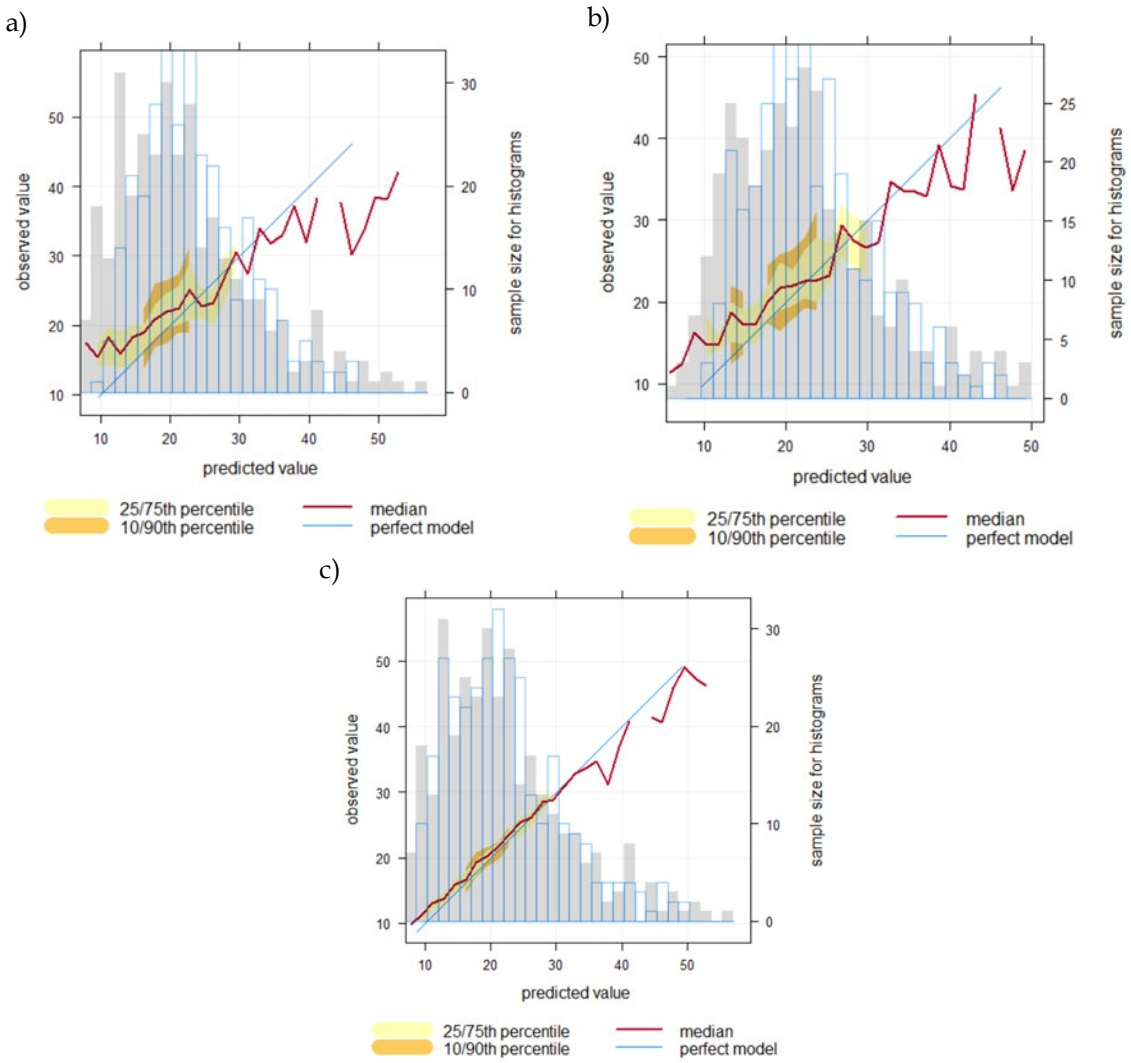

FIG. A2.3. Linear models for: a) PM_{10} observed vs predicted with linear models, b) PM_{10} observed vs predicted with PMF models and c) PM_{10} predicted with PMF vs predicted with linear models. The blue line shows the results for a perfect model, the red line shows the median value of the predictions and the shading shows the predicted quantile intervals, i.e. the 25/75th and the 10/90th.

A.2.2.REFERENCES

Carslaw, D.C., Beevers, S.D., Ropkins, K., Bell, M.C., 2006. Detecting and quantifying aircraft and other on-airport contributions to ambient nitrogen oxides in the vicinity of a large international airport. Atmos. Environ. 40, 5424–5434. doi:10.1016/j.atmosenv.2006.04.062

Fernández-Raga, M., Castro, A., Marcos, E., Palencia, C., Fraile, R., 2017. Weather types and rainfall microstructure in Leon, Spain. Int. J. Climatol. 37, 1834–1842. doi:10.1002/joc.4816

Trigo, R.M., DaCamara, C.C., 2000. Circulation weather types and their influence on the precipitation regime in Portugal. Int. J. Climatol. 20, 1559–1581. doi:10.1002/1097-0088(20001115)20:13<1559:AID-JOC555>3.0.CO;2-5

Yu, K.N., Cheung, Y.P., Cheung, T., Henry, R.C., 2004. Identifying the impact of large urban airports on local air quality by nonparametric regression. Atmos. Environ. 38, 4501–4507. doi:10.1016/j.atmosenv.2004.05.034

Annex 3

SUPPLEMENTARY MATERIAL OF CHAPTER 5

This annex contains the supplementary material corresponding to Chapter 5, which includes information about the location of the sampling site (Fig. A3.1), and mean annual and seasonal concentrations of the studied sugar compounds (Fig. A3.2 and Table A3.2). Additionally, Table A3.1 gives information about the sources of different sugar compounds.

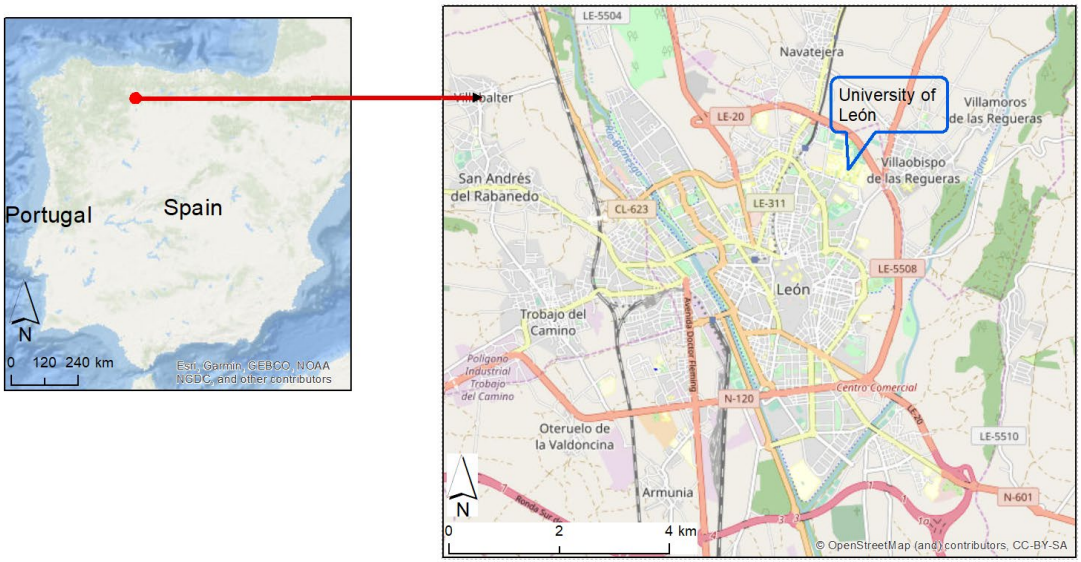

FIG A3.1. Map of the Iberian Peninsula and location of the province of León (left). Location of the sampling site (right).

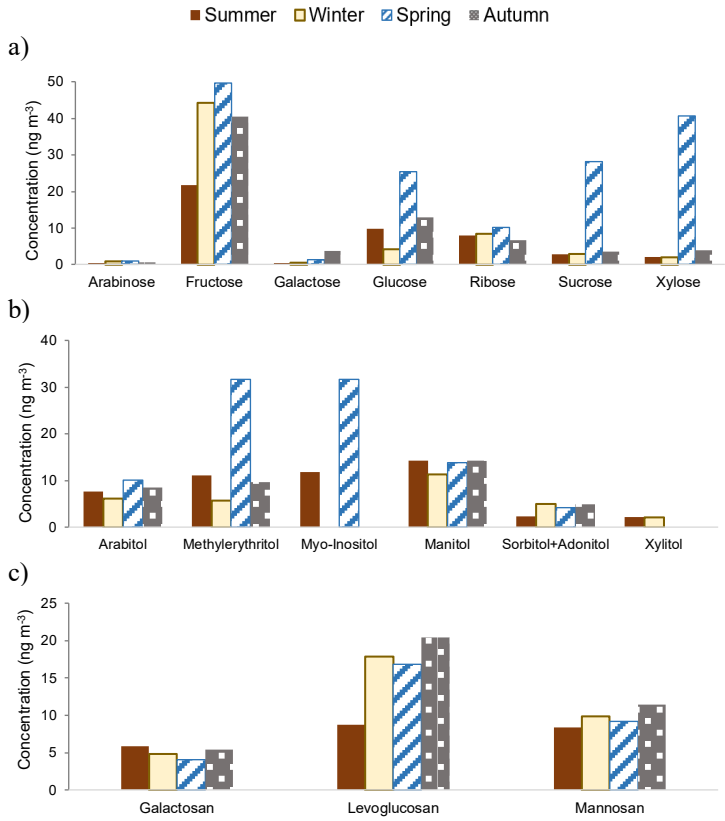

FIG A3.2. Mean seasonal concentrations of a) saccharides, b) alcohol-saccharides, c) anhydrosaccharides.

TABLE A3.1. Sugar compounds commonly found in atmospheric aerosols and their sources (Adapted from Caseiro et al., 2007).

Compounds	Source	Reference
Saccharides		
Arabinose	Lichens, non-woody tissues	(Dahlman et al., 2003; Medeiros et al., 2006)
Fructose	Soil biota, pollen	(Dahlman et al., 2003; Simoneit et al., 2004)
Galactose	Soil biota, non-woody tissues	(Medeiros et al., 2006; Simoneit et al., 2004)
Glucose	Fungi, soil biota, biomass burning, pollen	(Dahlman et al., 2003; Medeiros et al., 2006; Simoneit et al., 2004)
Ribose	Biomass burning, soil biota	(Vicente et al., 2013, 2012, 2011)
Sucrose	Soil biota, pollen	(Medeiros et al., 2006; Simoneit et al., 2004)
Xylose	Soil biota	(Simoneit et al., 2004)
Alcohol-saccharides		
Arabitol	Lichens, Bacterium, fungal spores, soil biota	(Liu et al., 2016; Medeiros et al., 2006)
2-methylerythritol	Soil biota	(Dahlman et al., 2003; Simoneit et al., 2004)
Myo-inositol	Soil biota	(Simoneit et al., 2004)
Mannitol	Lichens, Fungal spores, soil biota	(Dahlman et al., 2003; Martin et al., 1988; Simoneit et al., 2004)
Sorbitol	Bacteria, soil biota	(Dahlman et al., 2003; Loos et al., 1994; Simoneit et al., 2004)
Xylitol	Soil biota	(Simoneit et al., 2004)
Anhydrosaccharides		
Galactosan		
Levoglucosan	Biomass burning	(Simoneit et al., 2004, 1999)
Mannosan		

TABLE A3.2. Annual and seasonal mean sugar compound concentrations (minimum- maximum), in ng m^{-3}, determined during the sampling campaign.

	Annual	**Spring**	**Summer**	**Autumn**	**Winter**
Saccharides					
Arabinose	0.8 ± 0.8 (0.2 - 5)	1.08 ± 1.14 (0.26 - 5.11)	0.5 ± 0.2 (0.2 - 0.9)	0.7 ± 0.4 (0.3 - 2)	0.9 ± 0.5 (0.2 - 2)
Fructose	39 ± 56 (5 - 407)	50 ± 77 (5 - 407)	22 ± 19 (5 - 90)	40 ± 23 (7 - 80)	44 ± 38 (5 - 138)
Galactose	1.5 ± 1.5 (0.5 - 7)	1.4 ± 0.8 (0.6 - 3.9)	0.5	4 ± 3 (0.5 - 7)	0.6
Glucose	13 ± 32 (0.8 - 371)	25 ± 42 (2 - 274)	10 ± 40 (1.2 - 371)	13 ± 22 (1.3 - 189)	4 ± 4 (0.8 - 24)
Ribose	9 ± 10 (0.5 - 65)	10 ± 12 (2 - 65)	8 ± 8 (0.8 - 30)	7 ± 7 (0.5 - 22)	8 ± 7 (0.9 - 27)
Sucrose	15 ± 33 (1.2 - 161)	28 ± 44 (1.2 - 160.8)	2.8 ± 1.7 (1.3 - 9)	4 ± 4 (1.5 - 15)	2.9 ± 1.8 (1.5 - 8)
Xylose	9 ± 18 (1.3 - 71)	41 ± 30 (10 - 71)	2.2	4 ± 3 (1.5 - 9)	2.1 ± 0.8 (1.3 - 4)
Alcohol-saccharide					
Arabitol	8 ± 5 (4 - 32)	10 ± 7 (4 - 32)	8 ± 3 (4 - 19)	8 ± 6 (4 - 28)	6 ± 2 (4 - 9)
2- Methylerythritol	27 ± 22 (6 - 75)	32 ± 23 (6 - 75)	11 ± 2 (9 - 13)	10	6
Myo-inositol	27 ± 18 (6 - 61)	32 ± 18 (6 - 61)	12 ± 4 (7 - 16)	B.D.L.	B.D.L.
Mannitol	13 ± 9 (2 - 73)	14 ± 10 (2 - 57)	14 ± 6 (5 - 37)	14 ± 9 (3 - 53)	11 ± 12 (2 - 73)
Sorbitol+Adonitol	5 ± 3 (2 - 10)	4 ± 2 (2 - 6)	2.4	5 ± 3 (2 - 10)	5 ± 2 (2 - 8)
Xylitol	2.12 ± 0.10 (1.9 - 2.2)	B.D.L	2.16 ± 0.05 (2.1 - 2.2)	B.D.L.	2.10 ± 0.11 (1.9 - 2.2)
Anhydrosaccharide					
Galactosan	5 ± 3 (2 - 19)	4 ± 2 (1.9 - 8.5)	6 ± 3 (2 - 10)	5 ± 4 (2 - 19)	5 ± 3 (2 - 14)
Levoglucosan	17 ± 23 (3 - 214)	17 ± 16 (3 - 73)	9 ± 7 (3 - 36)	20 ± 33 (3 - 214)	18 ± 20 (3 - 91)
Mannosan	10 ± 6 (5 - 35)	9 ± 3 (7 - 15)	8 ± 4 (5 - 17)	11 ± 8 (5 - 35)	10 ± 6 (5 - 35)
Total (n = 327)	64 (1.3 - 1052)	122 (9 - 1052)	45 (7 - 396)	56 (1.3 - 404)	41 (1.4 - 303)

B.D.L.= Value below the detection limit

A.3.1.REFERENCES

Caseiro, A., Marr, I.L., Claeys, M., Kasper-Giebl, A., Puxbaum, H., Pio, C.A., 2007. Determination of saccharides in atmospheric aerosol using anion-exchange high-performance liquid chromatography and pulsed-amperometric detection. J. Chromatogr. A 1171, 37–45. doi:10.1016/j.chroma.2007.09.038

Dahlman, L., Persson, J., Näsholm, T., Palmqvist, K., 2003. Carbon and nitrogen distribution in the green algal lichens Hypogymnia physodes and Platismatia glauca in relation to nutrient supply. Planta 217, 41–48. doi:10.1007/s00425-003-0977-8

Liu, X., Du, Z., Cheng, Y., Liang, L., Engling, G., Duan, F., He, K., 2016. Seasonal variations and source estimation of saccharides in atmospheric particulate matter in Beijing, China. Chemosphere 150, 365–377. doi:10.1016/j.chemosphere.2016.02.002

Loos, H., Kramer, R., Sahm, H., Sprenger, G.A., 1994. Sorbitol promotes growth of Zymomonas mobilis in environments with high concentrations of sugar: Evidence for a physiological function of glucose- fructose oxidoreductase in osmoprotection. J. Bacteriol. 176, 7688–7693. doi:10.1128/jb.176.24.7688-7693.1994

Martin, F., Ramstedt, M., Söderhäll, K., Canet, D., 1988. Carbohydrate and Amino Acid Metabolism in the Ectomycorrhizal Ascomycete Sphaerosporella brunnea during Glucose Utilization. Plant Physiol. 86, 935–940. doi:10.1104/pp.86.3.935

Medeiros, P.M., Conte, M.H., Weber, J.C., Simoneit, B.R.T., 2006. Sugars as source indicators of biogenic organic carbon in aerosols collected above the Howland Experimental Forest, Maine. Atmos. Environ. 40, 1694–1705. doi:10.1016/j.atmosenv.2005.11.001

Simoneit, B.R.T., Elias, V.O., Kobayashi, M., Kawamura, K., Rushdi, A.I., Medeiros, P.M., Rogge, W.F., Didyk, B.M., 2004. Sugars Dominant Water-Soluble Organic Compounds in Soils and Characterization as Tracers in Atmospheric Particulate Matter. Environ. Sci. Technol. 38, 5939–5949. doi:10.1021/es0403099

Simoneit, B.R.T., Schauer, J.J., Nolte, C.G., Oros, D.R., Elias, V.O., Fraser, M.P., Rogge, W.F., Cass, G.R., 1999. Levoglucosan, a tracer for cellulose in biomass burning and atmospheric particles. Atmos. Environ. 33, 173–182.

Vicente, A., Alves, C., Calvo, A.I., Fernandes, A.P., Nunes, T., Monteiro, C., Almeida, S.M., Pio, C., 2013. Emission factors and detailed chemical composition of smoke particles from the 2010 wildfire season. Atmos. Environ. 71, 295–303. doi:10.1016/j.atmosenv.2013.01.062

Vicente, A., Alves, C., Monteiro, C., Nunes, T., Mirante, F., Cerqueira, M., Calvo, A., Pio, C., 2012. Organic speciation of aerosols from wildfires in central Portugal during summer 2009. Atmos. Environ. 57, 186–196. doi:10.1016/j.atmosenv.2012.04.030

Vicente, A., Alves, C., Monteiro, C., Nunes, T., Mirante, F., Evtyugina, M., Cerqueira, M., Pio, C., 2011. Measurement of trace gases and organic compounds in the smoke plume from a wildfire in Penedono (central Portugal). Atmos. Environ. 45, 5172–5182. doi:10.1016/j.atmosenv.2011.06.021

Annex 4

SUPPLEMENTARY MATERIAL OF CHAPTER 7

This annex contains the radiative forcing estimated and the optical properties data recorded during the Saharan dusts intrusions that affected León city in winter 2016 (Table A4.1) and 2017 (Table A4.1). Both dust outbreaks were studied in detail in Chapter 7.

TABLE A4.1. Radiative forcing on surface (ΔF_{BOA}), for the surface + atmosphere system (ΔF_{TOA}) and atmospheric radiative forcing (ΔF_{ATM}), during Saharan intrusion in winter 2016 and optical properties, single scattering albedo (*SSA*), asymmetry parameter (*g*), aerosol optical depth (*AOD*), along the event.

Date & Time	ΔF_{BOA} (W m^{-2})	ΔF_{TOA} (W m^{-2})	ΔF_{ATM} (W m^{-2})	K day^{-1} caused by aerosol	PBL (m)	*SSA* 400 nm	*SSA* 550 nm	*SSA* 850 nm	*g* 400 nm	*g* 550 nm	*g* 850 nm	*AOD*
19/02 06:00	-122.6	-16.3	106.4	-7.5	0	0.86	0.86	0.85	0.72	0.69	0.64	0.48
19/02 09:00	-122.9	-16.0	106.8	-7.4	89	0.86	0.86	0.85	0.72	0.70	0.65	0.48
19/02 12:00	-123.4	-15.6	107.7	-17.0	530	0.85	0.86	0.85	0.72	0.69	0.65	0.48
19/02 15:00	-125.0	-14.8	110.2	-17.3	674	0.85	0.86	0.85	0.72	0.70	0.65	0.49
19/02 18:00	-124.7	-15.2	109.5	-7.6	37	0.85	0.86	0.85	0.72	0.70	0.65	0.49
20/02 06:00	-128.2	-26.3	101.8	-21.5	36	0.84	0.84	0.84	0.72	0.70	0.67	0.47
20/02 09:00	-120.2	-27.2	92.9	-15.2	68	0.85	0.85	0.84	0.71	0.69	0.65	0.47
20/02 12:00	-125.7	-26.0	99.7	-15.8	260	0.84	0.84	0.84	0.72	0.70	0.67	0.48
20/02 15:00	-116.5	-29.0	87.5	-14.5	347	0.86	0.86	0.84	0.70	0.68	0.62	0.47
20/02 18:00	-126.9	-31.7	95.2	-15.3	0	0.86	0.86	0.85	0.72	0.69	0.64	0.47
21/02 06:00	-110.4	-56.3	54.0	-7.9	37	0.96	0.96	0.97	0.67	0.65	0.63	0.62
21/02 09:00	-111.1	-57.0	54.1	-7.8	122	0.96	0.97	0.97	0.67	0.66	0.64	0.62
21/02 12:00	-142.4	-73.9	68.5	-10.2	395	0.96	0.97	0.97	0.68	0.66	0.62	1.04
21/02 15:00	-211.5	-108.8	102.6	-14.2	844	0.97	0.97	0.97	0.68	0.66	0.61	2.22
21/02 18:00	-206.5	-109.9	96.6	-15.6	33	0.97	0.97	0.97	0.69	0.66	0.60	2.22
22/02 06:00	-167.7	-87.6	80.1	-12.7	35	0.97	0.97	0.97	0.68	0.66	0.62	1.37
22/0209:00	-166.7	-88.0	78.8	-12.8	87	0.97	0.97	0.97	0.68	0.66	0.62	1.37
22/02 12:00	-130.7	-69.5	61.2	-8.6	702	0.97	0.97	0.97	0.68	0.66	0.62	0.90
22/02 15:00	-116.8	-62.0	54.8	-7.9	1014	0.97	0.97	0.97	0.68	0.66	0.61	0.82
22/02 18:00	-126.2	-65.7	60.5	-9.3	50	0.97	0.97	0.97	0.68	0.67	0.63	0.82
23/02 06:00	-133.7	-29.1	104.6	-18.5	39	0.85	0.86	0.86	0.73	0.70	0.66	0.55
23/02 09:00	-131.2	-29.7	101.6	-17.6	117	0.86	0.86	0.86	0.73	0.70	0.66	0.55
23/02 12:00	-131.5	-29.8	101.7	-17.3	466	0.86	0.87	0.86	0.73	0.71	0.66	0.55
23/02 15:00	-152.2	-31.2	121.0	-19.1	714	0.81	0.83	0.85	0.74	0.73	0.71	0.53
23/02 18:00	-124.0	-27.5	96.5	-16.7	34	0.85	0.86	0.86	0.73	0.71	0.67	0.49
24/02 06:00	-127.5	-14.2	113.3	-8.0	83.41	0.85	0.86	0.86	0.74	0.72	0.68	0.49
24/02 09:00	-124.3	-14.3	110.0	-20.9	276.2	0.85	0.87	0.87	0.74	0.72	0.68	0.49
24/02 12:00	-129.1	-12.0	117.1	-22.5	555.9	0.84	0.85	0.86	0.74	0.73	0.70	0.49
24/02 15:00	-128.3	-12.6	115.7	-24.1	507.3	0.84	0.85	0.86	0.74	0.72	0.69	0.49

24/02 18:00	-121.6	-14.9	106.7	-21.8	365.6	0.86	0.86	0.86	0.73	0.71	0.66	0.49
25/02 06:00	-127.5	-14.2	113.3	-8.0	75.41	0.86	0.87	0.86	0.73	0.70	0.64	0.49
25/02 09:00	-123.8	-15.3	108.5	-7.7	187.4	0.85	0.86	0.86	0.72	0.70	0.66	0.49
25/02 12:00	-126.8	-14.4	112.4	-18.0	797.4	0.84	0.86	0.86	0.73	0.71	0.68	0.49
25/02 15:00	-125.5	-14.1	111.3	-7.8	744.7	0.85	0.86	0.86	0.73	0.71	0.67	0.49
25/02 18:00	-125.2	-14.2	110.9	-17.9	78.3	0.85	0.86	0.86	0.73	0.71	0.67	0.49

TABLE A4.2. Radiative forcing on surface (ΔF_{BOA}), for the surface + atmosphere system (ΔF_{TOA}) and atmospheric radiative forcing (ΔF_{ATM}), during Saharan intrusion in winter 2017 and optical properties, single scattering Albedo (*SSA*), asymmetry parameter (*g*), aerosol optical depth (*AOD*), along the event.

Date & Time	ΔF_{BOA} **(W m^{-2})**	ΔF_{TOA} **(W m^{-2})**	ΔF_{ATM} **(W m^{-2})**	**K day^{-1} caused by aerosol**	**PBL (m)**	***SSA* 400 nm**	***SSA* 550 nm**	***SSA* 850 nm**	***g* 400 nm**	***g* 550 nm**	***g* 850 nm**	***AOD***
20/02 06:00	-66	-26.8	39.2	-4.0	22	0.96	0.96	0.96	0.71	0.69	0.62	0.30
20/02 09:00	-56.1	-22.5	33.6	-4.3	586	0.96	0.97	0.96	0.71	0.69	0.62	0.20
20/02 12:00	-55.4	-22.3	33.1	-4.2	832	0.96	0.97	0.96	0.72	0.71	0.65	0.20
20/02 15:00	-46	-17.1	28.9	-3.3	24	0.96	0.96	0.96	0.72	0.71	0.67	0.10
20/02 18:00	-45.7	-17.3	28.4	-3.6	916	0.96	0.96	0.96	0.72	0.70	0.65	0.10
21/02 06:00	-45.5	-16.9	28.6	-3.4	37	0.96	0.97	0.96	0.72	0.69	0.62	0.10
21/02 09:00	-43.8	-16.5	27.3	-3.5	613	0.96	0.97	0.96	0.71	0.69	0.63	0.10
21/02 12:00	-41.8	-15.5	26.3	-3.4	925	0.96	0.96	0.96	0.71	0.69	0.65	0.10
21/02 15:00	-42.6	-15.7	26.9	-3.3	0	0.96	0.96	0.96	0.71	0.69	0.63	0.10
21/02 18:00	-42.4	-16	26.4	-3.4	914	0.96	0.96	0.96	0.71	0.69	0.64	0.10
22/02 06:00	-42.6	-16.3	26.3	-3.3	20	0.98	0.98	0.98	0.70	0.68	0.63	0.10
22/0209:00	-63.4	-28.9	34.5	-4.5	374	0.98	0.98	0.98	0.71	0.68	0.62	0.30
22/02 12:00	-58.5	-26	32.5	-4.2	490	0.98	0.98	0.98	0.72	0.70	0.66	0.20
22/02 15:00	-65.4	-29	36.4	-3.8	19	0.98	0.98	0.97	0.70	0.68	0.62	0.30
22/02 18:00	-65.8	-29.9	35.9	-4.5	911	0.98	0.98	0.98	0.71	0.69	0.64	0.30
23/02 06:00	-159.8	-80.6	79.3	-6.1	27	0.98	0.98	0.97	0.71	0.69	0.61	1.50
23/02 09:00	-166.1	-84	82.1	-12.4	484	0.97	0.98	0.98	0.71	0.70	0.65	1.50
23/02 12:00	-160.2	-83.5	76.6	-9.9	771	0.98	0.98	0.97	0.71	0.68	0.61	1.50
23/02 15:00	-169.6	-84.5	85.2	-6.4	72	0.98	0.98	0.98	0.72	0.70	0.65	1.60
23/02 18:00	-169	-87.3	81.7	-10.9	907	0.98	0.98	0.98	0.71	0.69	0.64	1.60
24/02 06:00	-162.7	-82.4	80.3	-6.2	97	0.98	0.98	0.97	0.71	0.68	0.60	1.60
24/02 09:00	-166.7	-86.1	80.6	-10.4	931	0.98	0.98	0.98	0.71	0.69	0.63	1.60
24/02 12:00	-65.5	-26.7	38.8	-5.1	952	0.96	0.96	0.96	0.70	0.69	0.64	0.20
24/02 15:00	-58.6	-23	35.6	-3.8	23	0.96	0.96	0.96	0.70	0.68	0.63	0.20
24/02 18:00	-57.8	-23.1	34.7	-4.5	913	0.96	0.96	0.96	0.71	0.68	0.60	0.20
25/02 06:00	-57.7	-22.6	35.2	-3.8	34	0.96	0.97	0.96	0.72	0.70	0.64	0.20
25/02 09:00	-42.5	-15.3	27.2	-3.5	420	0.96	0.96	0.96	0.71	0.69	0.63	0.10
25/02 12:00	-41.7	-15	26.7	-3.4	624	0.96	0.96	0.96	0.71	0.68	0.63	0.10
25/02 15:00	-40.2	-14.1	26.1	-3.3	32	0.96	0.96	0.96	0.71	0.68	0.62	0.00
25/02 18:00	-41	-14.1	26.9	-3.4	911	0.97	0.96	0.95	0.69	0.64	0.54	0.00

Annex 5

SUPPLEMENTARY MATERIAL OF CHAPTER 8

This annex contains the histograms of the number of samples per time duration of the precipitation event (Fig. A5.1) collected during the one-year sampling campaign carried out in León (Spain) from March 2016 to March 2017. Furthermore, the seawater and crustal ratios, enrichment factors (EF) and source contributions (seawater and crustal) for inorganic ions in rainwater during this period are presented (Tables A5.1, A5.2). The information included in the last three tables (Tables A5.3, A5.4) shows the results of two statistical methods (Pearson correlation and principal component analysis) applied to the data obtained during the sampling campaign. This supplementary material completes the study addressed in Chapter 8.

TABLE A5.1. Seawater and crustal ratios, Enrichment Factors (*EF*) and source contributions (seawater and crustal) for inorganic ions in rainwater during the sampling campaign.

	K^+	Mg^{2+}	Ca^{2+}	Cl^-	SO_4^{2-}	NO_3^-
Seawater ratios (Keene et al., 1986)	0.022	0.227	0.044	1.167	0.121	-
$(C_x/C_{Na^+})_{sample}$	0.487	0.478	1.561	1.432	2.008	1.305
$EF_{seawater}$	22.1	2.1	35.5	1.2	16.1	-
Crustal ratios (Zhang et al., 2007)	0.504	0.561	-	0.0031	0.0188	0.0021
$(C_x/C_{Ca^{2+}})_{sample}$	0.312	0.306	-	0.918	1.286	1.305
$EF_{crustal}$	0.6	0.5	-	296.0	68.4	621.5
Seawater fraction (%)	4.5	47.5	2.8	81.0	6.2	-
Crustal fraction (%)	95.5	52.5	97.2	0.3	1.5	0.2
Anthropogenic fraction (%)	-	-	-	18.7	92.3	99.8

TABLE A5.2. Seasonal neutralization factor (*NF*) for each analyzed species.

Season	*NF*				
	Na^+	NH_4^+	Mg^{2+}	K^+	Ca^{2+}
Winter	0.7 ± 0.8	0.8 ± 0.5	0.2 ± 0.2	0.12 ± 0.14	0.3 ± 0.3
Spring	0.2 ± 0.4	1.0 ± 0.4	0.09 ± 0.09	0.13 ± 0.11	0.3 ± 0.3
Summer	0.14 ± 0.15	0.7 ± 0.3	0.19 ± 0.12	0.20 ± 0.17	0.6 ± 0.2
Autumn	0.2 ± 0.5	0.9 ± 0.3	0.10 ± 0.14	0.14 ± 0.12	0.21 ± 0.15
Annual	0.4 ± 0.6	0.8 ± 0.4	0.13 ± 0.16	0.14 ± 0.13	0.3 ± 0.3

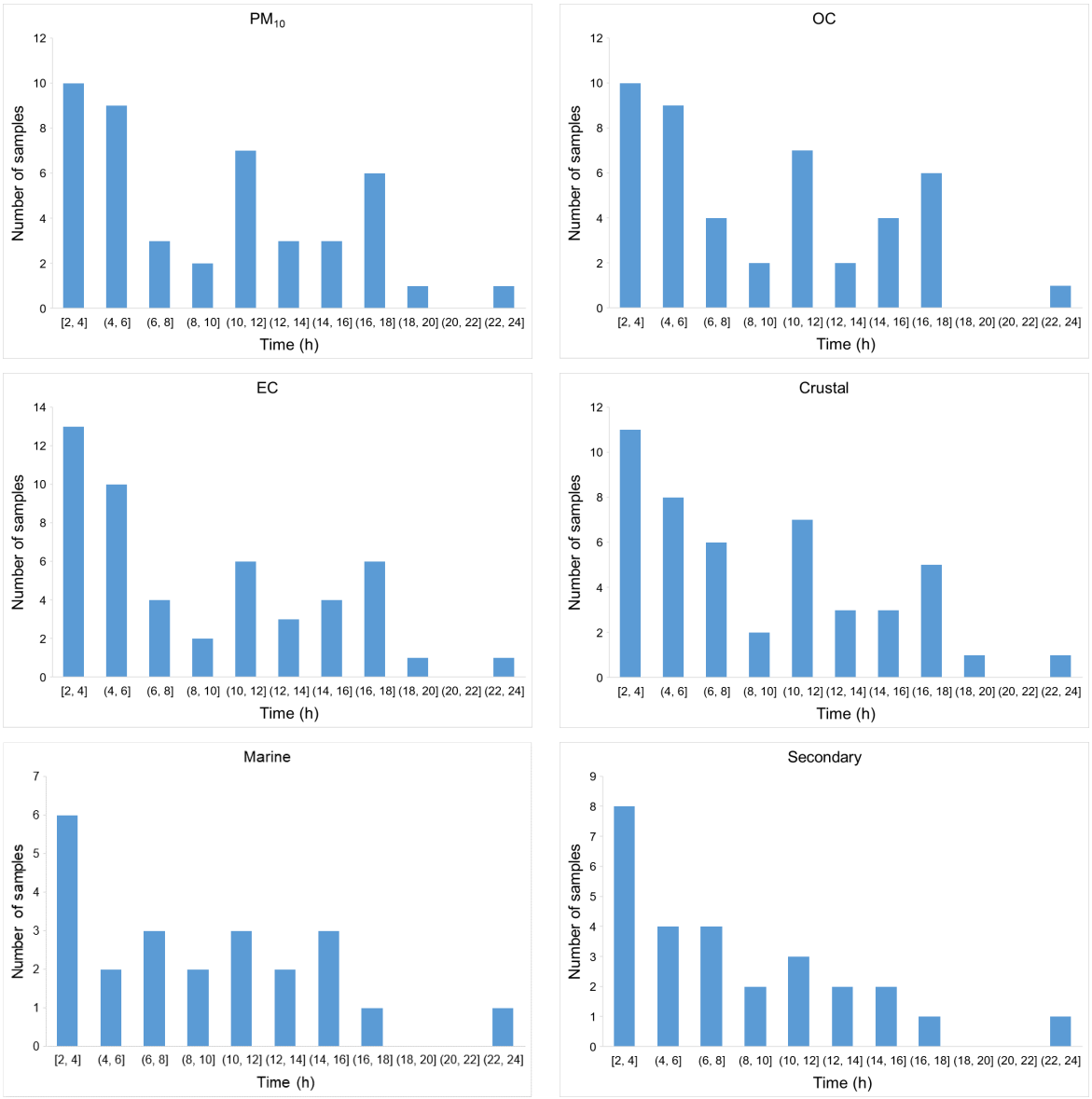

FIG. A5.1. Histograms of the number of samples per time duration of the precipitation event.

TABLE A5.3. Pearson correlation coefficients (*r*) for ionic species of wet-only precipitation during the sampling period.

	Na^+	**NH_4^+**	**Mg^{2+}**	**K^+**	**Ca^{2+}**	**Cl^-**	**SO_4^{2-}**	**NO_3^-**	**DOC**	**WIOC**
Winter										
NH_4^+	-0.087									
Mg^{2+}	**0.708****	-0.021								
K^+	0.270	0.280	0.348							
Ca^{2+}	0.229	0.240	**0.612****	0.022						
Cl^-	**0.910****	-0.071	**0.832****	0.301	0.290					
SO_4^{2-}	0.163	**0.862****	0.341	0.347	**0.489***	0.235				
NO_3^-	0.114	**0.772****	0.088	**0.428***	0.339	-0.057	**0.717****			
DOC	0.123	0.259	0.040	0.170	-0.014	0.127	0.271	0.217		
WIOC	0.124	**0.634****	0.220	0.290	0.373	0.133	**0.795****	**0.645****	0.169	
WIEC	0.052	**0.688****	0.138	0.381	0.319	0.061	**0.856****	**0.709****	0.291	**0.915****
Spring										
NH_4^+	**0.474***									
Mg^{2+}	**0.412***	**0.624****								
K^+	0.027	**0.469***	**0.477***							
Ca^{2+}	0.258	**0.717****	**0.818****	**0.499****						
Cl^-	**0.668****	**0.535****	**0.749****	0.159	**0.473***					
SO_4^{2-}	**0.582****	**0.797****	**0.649****	**0.500****	**0.700****	**0.412***				
NO_3^-	**0.395***	**0.850****	**0.570****	**0.562****	**0.682****	**0.387***	**0.684****			
DOC	**0.556****	**0.887****	**0.502***	0.299	**0.650****	0.366	**0.841****	**0.837****		
WIOC	0.268	**0.454***	**0.384***	0.310	0.291	0.332	0.254	**0.583****	**0.733****	
WIEC	**0.543****	**0.623****	**0.588****	0.266	**0.478***	**0.675****	**0.412***	**0.730****	**0.705****	**0.731****
Summer										
NH_4^+	**0.935****									
Mg^{2+}	0.708	**0.883***								
K^+	0.708	0.627	0.669							
Ca^{2+}	0.705	**0.890***	**0.995****	0.614						
Cl^-	**0.893***	**0.963****	**0.936****	0.762	**0.932****					
SO_4^{2-}	0.797	**0.958****	**0.944****	0.510	**0.961****	**0.931****				
NO_3^-	**0.932****	**0.981****	**0.880***	0.677	**0.892***	**0.980****	**0.934****			
DOC	0.619	**0.814***	**0.913***	0.477	**0.944****	**0.871***	**0.905***	**0.861***		
WIOC	0.607	**0.837***	**0.975****	0.501	**0.985****	**0.878***	**0.945****	**0.831***	**0.947****	
WIEC	**-0.852***	-0.782	-0.523	-0.478	-0.551	-0.766	-0.653	**-0.843***	-0.635	-0.493
Autumn										
NH_4^+	-0.225									
Mg^{2+}	**0.716****	0.071								
K^+	0.186	0.103	**0.536***							
Ca^{2+}	-0.045	**0.513***	0.251	0.221						
Cl^-	**0.967****	-0.086	**0.800****	0.280	-0.018					
SO_4^{2-}	-0.105	**0.929****	0.217	0.346	**0.644****	0.034				
NO_3^-	-0.159	**0.859****	0.149	0.132	**0.765****	-0.095	**0.847****			
DOC	-0.173	0.007	-0.265	-0.157	-0.194	-0.201	-0.133	-0.084		
WIOC	0.201	-0.391	0.110	0.010	-0.105	0.176	-0.305	-0.393	-0.106	
WIEC	0.176	0.262	0.142	-0.091	0.505*	0.192	0.350	0.193	-0.005	-0.017

* Significant at 0.05

** Significant at 0.01

TABLE A5.4. Rotated Component Matrix and Total variance explained by the Principal Component Analysis (PCA).

Specie	**Component**		
	1	**2**	**3**
NH_4^+	-0.025	**0.972**	-0.037
NO_3^-	0.028	**0.888**	0.145
SO_4^{2-}	0.260	**0.685**	-0.231
Na	-0.016	-0.113	**0.951**
Mg	**0.862**	-0.075	0.357
Al	**0.983**	0.006	-0.101
Si	**0.955**	0.126	-0.124
Cl	-0.065	0.062	**0.965**
K	**0.775**	0.362	0.083
Ca	**0.947**	0.014	-0.054
Ti	**0.984**	0.018	-0.051
Mn	**0.960**	0.133	-0.125
Fe	**0.964**	0.114	-0.058
Sums of rotation of charges squared			
Total	7.012	2.403	2.095
% Variance	53.941	18.485	16.115
% Accumulated	53.941	72.425	88.541